DIET, DISEASE, AND DEATH IN MEDIEVAL ROMANIA

A Dissertation Presented for the
Doctor of Philosophy
Degree
The University of Tennessee, Knoxville

Jenna Mackenzie Spears Watson
August 2024

Copyright © 2024 by Jenna Mackenzie Spears Watson
All rights reserved.

ACKNOWLEDGEMENTS

There are so many people to thank and not enough words to adequately express my gratitude. First, thank you to my dissertation committee, Drs. Amy Mundorff, Anneke Janzen, Dawnie Wolfe Steadman, and Thomas Crist. Amy, I could not have asked for a better committee chair and mentor throughout my time at UT Knoxville. Thank you for always being willing to talk things through and push me to be the best anthropologist and person I can be. Anneke, thank you for teaching me everything you know about isotopes, training me on sampling, and providing your expertise to this project. Dawnie, thank you for your support and for challenging me to think about the "why". Tom, thank you for running the best field school there is and telling me to learn to teach gross anatomy. It is advice I took to heart. Your support and encouragement are part of why I am here today.

Next, I would like to thank Drs. Steven Lautzenheiser, Derek Boyd and Haley Horbaly. Steven, thank you for your support, encouragement, endless vent sessions, and being a fantastic teaching partner and mentor. Derek, thank you for being such a good friend, mentor, and colleague. You very much did the work of a committee member and deserve all the praise. You will be a fantastic mentor to your future students. They will be lucky to have you. Your friendship, guidance, and support have kept me going (as well as our video game and Taco Bell nights). Fit buddies for life. Haley, thank you for being so supportive, and always willing to give me honest advice and provide perspective in difficult times. Your friendship has kept me sane in so many ways and I will always be grateful to you for getting me hooked on Formula 1. Your friendship has meant the world to me, and you have had a significant impact on the anthropologist and person I want to be. Derek and Haley, you both paved the way for me in so many ways and provided a guiding light when I needed it most.

To my colleagues at the FRIA, Dr. Mihai Constantinescu, Dr. Andrei Soficaru, and Costin Sendroiu, thank you for allowing me to use the collections at the FRIA, supporting me in this research, and making Romania feel like home. I couldn't ask for better research collaborators and friends.

Thank you to my parents, Steve and Liz, and my sister Megan. Your unwavering support and love have seen me through everything, and I wouldn't have survived without you. To my fiancé and partner, Clark, you have been with me from day one and I couldn't have asked for a more supportive and loving partner than you. Thank you for trusting me, believing in me, and supporting me. There were many nights I wouldn't have eaten a hot meal if you hadn't cooked for me. I love you. To whatever end.

Brigid and Taylor (aka Pain and Panic), thank you for being such supportive and fun carrel mates. I will miss our late nights in the carrels and trash TV nights. Your friendship has been one of the highlights of my graduate school experience. Liz, Helen, Rachel, Elizabeth, and JD, thank you for being the best group of friends a person could ask for. Our many get-togethers to chat, watch TV, and eat takeout got me through many long weeks. To my book-loving gang, Liz, Helen, Rachel, and Taylor, chatting about books and our Sundays at Fable Hollow Bookshoppe have been a bright spot in my life this past year. I will miss our Fable Hollow Sundays dearly. I love you all. Until the darkness claims us. Taylor Swift and Sarah J. Maas, your music and books have seen me through this past year.

I would like to thank the funders that made this research possible, the College of Arts and Sciences, the Center for Global Engagement, the Department of Anthropology, and the Fulbright U.S. Student program. Also, thank you to the individuals buried at Suceava, Cnejilor Palace, and Schitișor who were studied for this research. I hope that your lives and the information you left

behind in your bones will help your descendants and others around the world live better lives. It is a privilege to be a part of making that possible.

Finally, I dedicate this dissertation to my grandfather, McGehee (Mac) Harrod Spears, affectionately known by his grandchildren as Nana Mac. He was never able to complete his PhD in Economics but believed strongly in educating women. He instilled the value of education in his three daughters and required them each to pursue a college education. As a result, my mother earned her bachelor's degree from the University of Tennessee Knoxville and eventually a Doctor of Audiology degree from A.T. Still University. She and my father instilled these same values in me and fostered a lifelong love of learning and an appreciation for the power of knowledge. Thank you, Nana Mac. I know you would be happy someone in the family finally finished a doctorate. I like to think you would be proud.

ABSTRACT

During the Late Medieval and Early Modern period Romania was made up of three principalities: Transylvania, Wallachia, and Moldavia. Wallachia and Moldavia experienced periodic rule by the Ottoman Turkish Empire between the 14^{th} – 19^{th} centuries and were feudal agricultural societies with landed nobility, peasants, and slaves. A long history of imperial occupation and feudalism widened social, economic, and political gaps between the classes, which may have resulted in differential access to food resources or intensified pre-existing barriers to resources. Lower-status individuals likely had more exposure to environmental and occupational hazards and limited access to adequate nutrition leading to differential health outcomes between privileged and marginalized groups along the lines of age, sex, and social status.

This research explored how age, sex, social class, and diet influenced patterns of stress and frailty in human populations using skeletal assemblages from three sites in northeast Romania dating between the 14^{th} and 18^{th} centuries: Suceava, Palatul Cnejilor and Schitişor. This research used bioarchaeological methods, historical sources, archaeological context, and carbon and nitrogen stable isotope analysis to 1) determine patterns of skeletal stress in these populations, 2) explore the dietary composition of these populations, and 3) assess how dietary isotopes, age, sex, and social status influenced patterns of non-specific skeletal stress. I hypothesized that there would be a difference in lesion frequencies between sexes and social classes, individuals were consuming a majority C_3 diet with some C_4 inputs with dietary differences between sexes and social status, and given age, sex, and social status, dietary composition will play an important role in experiences of physiological stress. The findings of this dissertation suggest that there were no significant differences in experiences of stress

between males and females or sites, nor any significant mortality bias for any of the non-specific stress lesions. However, there were significant dietary differences between lower-status (Palatul Cnejilor and Schitişor) and higher-status sites (Suceava) with lower-status sites consuming more C_4 crops, which also corresponds to higher frequencies of dental disease at these sites. This suggests either social status or some other aspect of living at these sites was predictive of experiencing dental disease.

TABLE OF CONTENTS

CHAPTER ONE: INTRODUCTION 1

Research Objectives and Study Design 4

Questions and Hypotheses 5
Question 1: What physiological stressors did people experience? 5
Question 2: What did they eat? 7
Question 3: Considering demographic factors (age, sex, and site) from questions 1 and 2, how did diet influence patterns of skeletal stress in these populations? 9

Dissertation Organization 9

CHAPTER TWO: HISTORICAL AND SITE BACKGROUND 13

Chapter Overview 13

The Origins of Late Medieval-Early Modern Romania: A Crossroads of East and West 13
The Dacians and The Romans: 2nd Century BCE to the 4thCentury CE 16
The Bulgarian, Byzantine, Hungarian, and Ottoman Empires: 8th – 17th Centuries CE 17
The Austrian Empire and Phanariot Rule: 17th – 18th Centuries CE 20

Romanian Feudalism: Social Class and Roma Slavery in Medieval Romania 21

Exploring Stress and Diet in the Romanian Principalities 22

Site Background 24
Suceava Fortress (Cetatea de Scuan a Sucevei) 24
Palatul Cnejilor (Cnejilor Palace) 35
Schitișor 37

History of the Francisc I. Rainer Institute of Anthropology (FRIA) 40

CHAPTER THREE: BIOARCHAEOLOGICAL THEORETICAL FRAMEWORK 45

Chapter Overview 45

What is Stress and What is Health? 46

The Osteological Paradox 48
Demographic Non-Stationarity 49
Selective Mortality and Hidden Heterogeneity in Risks 50

Responses to the Osteological Paradox and Implications for Bioarchaeology Research 51

Skeletal Biology of Bone Remodeling, Inflammation, and Stress 54
Bone Remodeling 54
The Role of Molecular Signaling Pathways in Bone Remodeling: Wnt β-Catenin and RANK/RANKL/OPG Pathways 55
Bone Remodeling and Inflammation 57
The Physiological Stress Response 58

Skeletal Biology and the Meaning of Non-Specific Stress Lesions 60
Periosteal New Bone Formation (PNBF) 60

Porotic Lesions of the Skull: Cribra orbitalia and porotic hyperostosis 62
Dental Disease: Dental Caries, Abscesses, and Periodontal Disease (PD) 65
Biocultural Theory 68
CHAPTER FOUR: ISOTOPE ECOLOGY OF CARBON AND NITROGEN STABLE ISOTOPES 71
Chapter Overview 71
What are Stable Isotopes? 71
Isotopic Fractionation: Equilibrium and Kinetic Fractionation 72
Calculation of the Fractionation Factor and Enrichment 73
Measuring and Reporting Isotopic Composition: The Delta (δ) Value 75
Carbon Isotopes in Plants 76
C_3, C_4, and Crassulacean Acid Metabolism (CAM) Photosynthesis: Variation in Plant $\delta^{13}C$ Values 76
C_3 Photosynthesis 77
C_4 Photosynthesis 80
Crassulacean Acid Metabolism (CAM) Photosynthesis 81
Carbon Isotopes in Aquatic Ecosystems 82
Nitrogen Isotopes in Plants and Soil Systems 84
The Nitrogen Cycle in Soil Systems 84
Nitrogen Assimilation in Plants 86
Intra and Inter-Plant Variation and Nitrogen Fractionation 86
The Impact of Human Agricultural Activity on Soil Nitrogen 88
Carbon and Nitrogen Isotopes in Humans and Animals: You Are What You Eat 89
Nitrogen Isotope Sources and Trophic Level Enrichment 90
Nitrogen Isotopes and Nutritional Stress 92
Carbon Isotopes in Human Tissues: Bioapatite vs. Collagen 93
Sources of Carbon and Nitrogen in Romania 95
Multi-isotope Approaches to the Study of Human Diet and Health 98
Exploring Human Diet, Social Status, and Health with Carbon and Nitrogen Stable Isotopes 98
CHAPTER FIVE: MATERIALS AND METHODS 102
Chapter Overview 102
Individuals Analyzed and Sampled 102
Skeletal Demography and Paleopathology 102
Assigning Unique Identifiers and Inventory 102
Age-at-Death Estimation 104
Non-Metric and Metric Sex Estimation 105
Skeletal Pathology: Non-specific indicators of stress and dental pathology 106
Periosteal New Bone Formation (PNBF) 107

Porotic Lesions of the Skull (porotic hyperostosis and cribra orbitalia) 110
Dental Pathology: Caries, Abscesses, and Periodontal Disease 113
Statistical Analyses: Skeletal Data 118
Frequencies and Tests of Association 118
Intra-observer Error 120
Stable Isotope Sampling 120
Sampling Protocol: Femora and Ribs 120
Bone Collagen Pre-treatment and Analysis for Carbon and Nitrogen Stable Isotopes 122
Bone Collagen Pre-treatment 124
Bone Collagen Analysis 127
Statistical Analyses: Stable Isotope Data 129
Bayesian Model: Skeletal and Isotopic Data 129
Bayesian Logistic Regression 129
Model Description. 132
Model Selection. 134
Data Management 136
CHAPTER SIX: RESULTS 138
Chapter Introduction 138
Sample Demography 138
Intraobserver Error 139
Tests of Difference and Association for Age and Sex 141
Age-at-Death 141
Biological Sex 141
Patterns of Skeletal Stress 142
PNBF 142
Preservation 142
Raw Lesion Frequencies. 142
Tests of Difference and Association. 143
PH 145
Preservation 145
Raw Lesion Frequencies. 145
Tests of Difference and Association. 147
CO 148
Preservation 148
Raw Lesion Frequencies. 148
Tests of Difference and Association. 148
Caries 150
Preservation 150
Raw Lesion Frequencies. 151
Tests of Difference and Association. 151
Abscesses 153

Preservation. 153
Raw Lesion Frequencies. 153
Tests of Difference and Association. 154
PD 156
Preservation. 156
Raw Lesion Frequencies. 156
Tests of Difference and Association. 157
Diet 159
Carbon Isotopes 159
Descriptive Statistics. 159
Tests of Difference and Association. 162
Nitrogen Isotopes 163
Descriptive Statistics. 163
Tests of Difference and Association. 165
Carbon and Nitrogen Covariation 166
Bayesian Models for Stress and Diet 171
PNBF and Femur $\delta^{13}C$ and $\delta^{15}N$ values 171
Model Description. 171
Model Selection. 173
Model Summary 175
PNBF and Rib $\delta^{13}C$ and $\delta^{15}N$ values 181
Model Description. 181
Model Selection. 181
Model Summary 184
PH and Femur $\delta^{13}C$ and $\delta^{15}N$ values 189
Model Description. 189
Model Selection. 189
Model Summary 189
PH and Rib $\delta^{13}C$ and $\delta^{15}N$ values 196
Model Description. 196
Model Selection. 196
Model Summary 199
CO and Femur $\delta^{13}C$ and $\delta^{15}N$ values 199
Model Description. 199
Model Selection. 204
Model Summary 204
CO and Rib $\delta^{13}C$ and $\delta^{15}N$ values 211
Model Description. 211
Model Selection. 211
Model Summary 213
Caries and Femur $\delta^{13}C$ and $\delta^{15}N$ values 219
Model Description. 219
Model Selection. 219
Model Summary 219

Caries and Rib $\delta^{13}C$ and $\delta^{15}N$ values 225
Model Description. 225
Model Selection. 225
Model Summary 230
Abscesses and Femur $\delta^{13}C$ and $\delta^{15}N$ values 233
Model Description. 233
Model Selection. 233
Model Summary 238
Abscesses and Rib $\delta^{13}C$ and $\delta^{15}N$ values 238
Model Description. 238
Model Selection. 238
Model Summary 242
PD and Femur $\delta^{13}C$ and $\delta^{15}N$ values 248
Model Description. 248
Model Selection. 248
Model Summary 248
PD and Rib $\delta^{13}C$ and $\delta^{15}N$ values 253
Model Description. 253
Model Selection. 253
Model Summary 256
Post Hoc Analysis: Kaplan-Meier Survival Curves 262
PNBF 262
PH 262
CO 264
Caries 264
Abscesses 264
PD 267
CHAPTER SEVEN: DISCUSSION 269
Dietary Composition 270
C_3 versus C_4 Animal Protein Consumption 272
Terrestrial versus Aquatic Protein Consumption 275
C_3 vs C_4 Plant Protein Consumption 276
C_3 and C_4 Sources in the Bulk Diet versus Protein 279
Suceava 280
Palatul Cnejilor and Schitişor 282
Differences in Dietary Composition: Social Status or Temporal Change? 283
Patterns of Skeletal Stress and Dental Disease 286
Demography 287
Non-Specific Stress Lesions and Dental Disease 287
Non-Specific Stress in Medieval Romania 290
Dental Disease in Medieval Romania 291
Diet, Demography, and Skeletal Stress 293
Burial Site as Predictors for Dental Caries? 293

Diet and Nutritional Stress 296
CHAPTER EIGHT: CONCLUSION 299
Limitations and Future Research 300
Sample Size 301
Site Dates, Historical Background, and Baseline Isotopic Data 302
Role of Migration: Demographic Non-Stationarity and Hidden Heterogeneity in Frailty 303
Modeling the Relationship between Isotopes and Pathology 305
Additional Future Research 308
Broader Impacts and Final Reflections 309
REFERENCES 312
APPENDIX ONE: TESTS OF DIFFERENCE AND ASSOCIATION 335
APPENDIX TWO: CARBON AND NITROGEN STABLE ISOTOPE DATA SET AND BIPLOTS 359
APPENDIX THREE: BAYESIAN MODEL FITS AND MARGINAL EFFECTS PLOTS 385
APPENDIX FOUR: SURVIVAL TABLES 401
APPENDIX FIVE: ENAMEL CARBON STABLE ISOTOPE DATA, STANDARDS, AND METHODS 403
Pretreatment Protocol 406
Analysis and Standards 407
VITA 408

LIST OF TABLES

Table 5.1. Study sites with location, number of individuals, dates, context, and probable social class of individuals buried at each site. 103

Table 5.2. PNBF Scores for Buikstra and Ubelaker (1994) and Steckel et al. (2006) 108

Table 5.3. Scores for porotic hyperostosis from Buikstra and Ubelaker (1994) and Steckel et al. (2006) 112

Table 5.4. Scores for cribra orbitalia from Buikstra and Ubelaker (1994) and Steckel et al. (2006) 112

Table 5.5. Scores for dental caries from Buikstra and Ubelaker (1994) and Steckel et al. (2006) 116

Table 5.6. Scores for dental abscesses from Buikstra and Ubelaker (1994) and Steckel et al. (2006) 116

Table 5.7. Scores for periodontal disease (PD) from Steckel et al. (2006) and Ogden (2008) 119

Table 5.8. Meanings for the outcome (y) and predictor β variables of the Bayesian Logistic Regression equation 133

Table 5.9. Seven Bayesian logistic regression models used for each lesion type and femur $\delta^{13}C$ and $\delta^{15}N$ values and different combinations of predictor variables. Model selection was performed to see which model was most parsimonious given the data. 135

Table 5.10. Seven Bayesian logistic regression models used for each lesion type and rib $\delta^{13}C$ and $\delta^{15}N$ values and different combinations of predictor variables. Model selection was performed to see which model was most parsimonious given the data. 135

Table 6.1. Total individuals and % of total sample for each site and sex. 140

Table 6.2. Average age of individuals from each site and sex. 140

Table 6.3. Mean age-at-death for individuals with and without PNBF by site and sex. 144

Table 6.4. Number of individuals, mean age, and standard deviation for presence/absence of PH for each site and sex. 146

Table 6.5. Number of individuals, mean age, and standard deviation for presence/absence of CO for each site and sex. 149

Table 6.6. Number of individuals, mean age, and standard deviation for presence/absence of caries for each site and sex. 152

Table 6.7. Number of individuals, mean age, and standard deviation for presence/absence of abscesses for each site. 155

Table 6.8. Number of individuals, mean age, and standard deviation for presence/absence of PD for each site and sex. 158

Table 6.9. Mean, standard deviation, and variance for femur and rib $\delta^{13}C$ values. 160

Table 6.10. Mean and standard deviations of femur and rib $\delta^{13}C$ values for males and females. 160

Table 6.11. Mean and standard deviations of femur and rib $\delta^{13}C$ values for each site. 160

Table 6.12. Mean femur and rib $\delta^{13}C$ and $\delta^{15}N$ values for those with and without PNBF. 160

Table 6.13. Mean femur and rib $\delta^{13}C$ and $\delta^{15}N$ values for those with and without PH. 160

Table 6.14. Mean femur and rib $\delta^{13}C$ and $\delta^{15}N$ values for those with and without CO. 161

Table 6.15. Mean femur and rib $\delta^{13}C$ and $\delta^{15}N$ values for those with and without caries. 161

Table 6.16. Mean femur and rib $\delta^{13}C$ and $\delta^{15}N$ values for those with and without abscesses. . 161

Table 6.17. Mean femur and rib $\delta^{13}C$ and $\delta^{15}N$ values for those with and without PD. 161

Table 6.18. Mean, standard deviation, and variance for femur and rib $\delta^{15}N$ values. 164

Table 6.19. Mean and standard deviations of femur and rib $\delta^{15}N$ values for males and females. 164

Table 6.20. Mean and standard deviations of femur and rib $\delta^{15}N$ values for each site. 164

Table 6.21. 12 Bayesian logistic regression models for each lesion type and femur and rib carbon and nitrogen isotope values. 172

Table 6.22. Log odds estimate, error, 95% Credibility Interval, Rhat values, and Bulk and Tail ESS for the full model. 174

Table 6.23. LOOIC values for each model fit. 174

Table 6.24. The log odds estimate, 95% Credibility Interval, Rhat, and Bulk and Tail ESS for fit7 (the intercept). 174

Table 6.25. The log odds estimate, 95% Credibility Interval, Rhat, and Bulk and Tail ESS for fit5. 176

Table 6.26. Odds Ratios and 95% Credibility Interval for fit5. 180

Table 6.27. Log odds estimate, error, 95% Credibility Interval, Rhat values, and Bulk and Tail ESS for the full model. 182

Table 6.28. LOOIC values for each model fit. 182

Table 6.29. The log odds estimate, 95% Credibility Interval, Rhat values, and Bulk and Tail ESS for fit7. 182

Table 6.30. The log odds estimate, 95% Credibility Interval, Rhat values, and Bulk and Tail ESS for fit5. 183

Table 6.31. Odds Ratios and 95% Credibility Interval for fit5. 188

Table 6.32. Log odds estimate, error, 95% Credibility Interval, Rhat values, and Bulk and Tail ESS for the full model. 190

Table 6.33. LOOIC values for each model fit. 190

Table 6.34. The log odds estimate, 95% Credibility Interval, Rhat values, and Bulk and Tail ESS for fit7. 190

Table 6.35. The log odds estimate, 95% Credibility Interval, Rhat values, and Bulk and Tail ESS for fit5. 191

Table 6.36. Odds Ratios and 95% Credibility Interval for fit5. 195

Table 6.37. Log odds estimate, error, 95% Credibility Interval, Rhat values, and Bulk and Tail ESS for the full model. 197

Table 6.38. LOOIC values for each model fit. 197

Table 6.39. The log odds estimate, 95% Credibility Interval, Rhat values, and Bulk and Tail ESS for fit7. 197

Table 6.40. The log odds estimate, 95% Credibility Interval, Rhat values, and Bulk and Tail ESS for fit5. 198

Table 6.41. Odds Ratios and 95% Credibility Interval for fit5. 203

Table 6.42. Log odds estimate, error, 95% Credibility Interval, Rhat values, and Bulk and Tail ESS for the full model. 205

Table 6.43. LOOIC values for each model fit. 205

Table 6.44. The log odds estimate, 95% Credibility Interval, Rhat values, and Bulk and Tail ESS for fit7. 205

Table 6.45. The log odds estimate, 95% Credibility Interval, Rhat values, and Bulk and Tail ESS for fit5. 206

Table 6.46. Odds Ratios and 95% Credibility Interval for fit5. 210

Table 6.47. Log odds estimate, error, 95% Credibility Interval, Rhat values, and Bulk and Tail ESS for the full model. 212

Table 6.48. LOOIC values for each model fit. 212

Table 6.49. The log odds estimate, 95% Credibility Interval, Rhat values, and Bulk and Tail ESS for fit7. 214

Table 6.50. The log odds estimate, 95% Credibility Interval, Rhat values, and Bulk and Tail ESS for fit5. 214

Table 6.51. Odds Ratios and 95% Credibility Interval for fit5. 218

Table 6.52. Log odds estimate, error, 95% Credibility Interval, Rhat values, and Bulk and Tail ESS for the full model. 220

Table 6.53. LOOIC values for each model fit. 220

Table 6.54. The log odds estimate, 95% Credibility Interval, Rhat values, and Bulk and Tail ESS for fit5. 220

Table 6.55. Odds Ratios and 95% Credibility Interval for fit5. 224

Table 6.56. Log odds estimate, error, 95% Credibility Interval, Rhat values, and Bulk and Tail ESS for the full model. 226

Table 6.57. LOOIC values for each model fit. 226

Table 6.58. The log odds estimate, 95% Credibility Interval, Rhat values, and Bulk and Tail ESS for fit7. 226

Table 6.59. The log odds estimate, 95% Credibility Interval, Rhat values, and Bulk and Tail ESS for fit4. 227

Table 6.60. Odds Ratios and 95% Credibility Interval for fit4. 232

Table 6.61. Log odds estimate, error, 95% Credibility Interval, Rhat values, and Bulk and Tail ESS for the full model. 234

Table 6.62. LOOIC values for each model fit. 235

Table 6.63. The log odds estimate, 95% Credibility Interval, Rhat values, and Bulk and Tail ESS for fit7. 235

Table 6.64. The log odds estimate, 95% Credibility Interval, Rhat values, and Bulk and Tail ESS for fit5. 235

Table 6.65. Odds Ratios and 95% Credibility Interval for fit5. 240

Table 6.66. Log odds estimate, error, 95% Credibility Interval, Rhat values, and Bulk and Tail ESS for the full model. 241

Table 6.67. LOOIC values for each model fit. 243

Table 6.68. The log odds estimate, 95% Credibility Interval, Rhat values, and Bulk and Tail ESS for fit7. 243

Table 6.69. The log odds estimate, 95% Credibility Interval, Rhat values, and Bulk and Tail ESS for fit5. 243

Table 6.70. Odds Ratios and 95% Credibility Interval for fit5. 247

Table 6.71. Log odds estimate, error, 95% Credibility Interval, Rhat values, and Bulk and Tail ESS for full model. 249

Table 6.72. LOOIC values for each model fit. 249

Table 6.73. The log odds estimate, 95% Credibility Interval, Rhat values, and Bulk and Tail ESS for fit7. 249

Table 6.74. The log odds estimate, 95% Credibility Interval, Rhat values, and Bulk and Tail ESS for fit5. 250

Table 6.75. Odds Ratios and 95% Credibility Interval for fit5. 255

Table 6.76. Log odds estimate, error, 95% Credibility Interval, Rhat values, and Bulk and Tail ESS for the full model. 255

Table 6.77. LOOIC values for each model fit. 255

Table 6.78. The log odds estimate, 95% Credibility Interval, Rhat values, and Bulk and Tail ESS for fit7. 257

Table 6.79. The log odds estimate, 95% Credibility Interval, Rhat values, and Bulk and Tail ESS for fit5. 257

Table 6.80. Odds Ratios and 95% Credibility Interval for fit5. 261

Table 7.1. Full Bayesian logistic regression models and best-fit model selected. The only model that selected Site as a predictor is highlighted in grey. 294

Table A.1. Carbon and nitrogen stable isotope data set for all adult rib samples. Asterice* indicates samples with a C:N > 3.6 suggesting an unreliable value due to diagenesis. 359

Table A.2. Carbon and nitrogen stable isotope data set for all adult femur samples. Asterice* indicates samples with a C:N > 3.6 suggesting an unreliable value due to diagenesis. 363

Table A.3. All seven model fits for PNBF using different combinations of predictor variables and only femur carbon and nitrogen isotope values. 385

Table A.4. All seven model fits for PNBF using different combinations of predictor variables and only rib carbon and nitrogen isotope values. 385

Table A.5. All seven model fits for PH using different combinations of predictor variables and only femur carbon and nitrogen isotope values. 385

Table A.6. All seven model fits for PH using different combinations of predictor variables and only rib carbon and nitrogen isotope values. 386

Table A.7. All seven model fits for CO using different combinations of predictor variables and only femur carbon and nitrogen isotope values. 386

Table A.8. All seven model fits for CO using different combinations of predictor variables and only rib carbon and nitrogen isotope values. 386

Table A.9. All seven model fits for caries using different combinations of predictor variables and only femur carbon and nitrogen isotope values. 387

Table A.10. All seven model fits for caries using different combinations of predictor variables and only rib carbon and nitrogen isotope values. 387

Table A.11. All seven model fits for abscesses using different combinations of predictor variables and only femur carbon and nitrogen isotope values. 387

Table A.12. All seven model fits for abscesses using different combinations of predictor variables and only rib carbon and nitrogen isotope values. 388

Table A.13. All seven model fits for PD using different combinations of predictor variables and only femur carbon and nitrogen isotope values. 388

Table A.14. All seven model fits for PD using different combinations of predictor variables and only rib carbon and nitrogen isotope values. 388

Table A.15. Carbon stable isotope data of bone collagen and enamel apatite. 403

LIST OF FIGURES

Figure 2.1. The middle and lower Danube River Basin contributing to Romania's southern border with Bulgaria and part of Serbia. 15

Figure 2.2. The Ottoman Empire 16th century (Encyclopedia Britannica). Red square indicates the Romanian Principalities. 18

Figure 2.3. The three Romanian principalities of Transylvania, Wallachia, and Moldavia c. 1600 CE (Treptow et al. 1997). 19

Figure 2.4. Locations of the three study sites: Suceava (red), Schitișor (orange), and Palatul Cnejilor (purple). 25

Figure 2.5. Figure of the excavation plans at Suceava showing its location relative to the river. 1) Suceava Fortress, 2) plateau in front of the Fortress, 3) Cemetery (Mitrea B. et al. 1955). 26

Figure 2.6. Suceava fortress (2022). White line demarcates where the original fortress ends and reconstructions begins (everything above line). Photographed by J. Watson 2022. 27

Figure 2.7. Remains of trenches dug as part of the cemetery excavation at Suceava called "Field of Ditches" (photographed by J. Watson 2022) 29

Figure 2.8. General ecavation plan of Suceava. The orange box indicates location of the cemetery that was excavated "Cimitir feudal (Feudal Cemetery)" (Nestor et al. 1959). 30

Figure 2.9. Top: Photograph of a burial covered in layers of flagstone. Bottom: Higher status vault graves made of bricks and mortar (Mitrea and Nestor 1953). 32

Figure 2.10. Top: Cemetery excavation map from 1952 showing locations and orientations of the graves (Mitrea and Nestor 1953). Bottom: Cemetery excavation maps for 1952, 1953, and 1954 field seasons (Mitrea B. et al. 1955). 33

Figure 2.11. Left: Drawings of buttons, rings, and earrings found in graves at Suceava (Batariuc 1993). Right: Drawings of earrings dating to the 15th century found in graves at Suceava (Mitrea and Nestor 1953). 34

Figure 2.12. Remains of the fortress towers (photographed by J. Watson 2022). 38

Figure 2.13. Rebuilt church that sits within the remains of Palatul Cnejilor (photographed by J. Watson 2022). 39

Figure 2.14. Cemetery excavation map for Schitișor (Zaharia and Zaharia 2003). The church (Biserica) is in the middle with burials extending to the north, south, and east around it. 41

Figure 2.15. House and small associated structure that now occupy the excavation site (photographed by J. Watson 2022). 42

Figure 5.1. Three activity stages for PNBF on the tibia: (A) active, (B), sclerotic, and (C) mixed. 109

Figure 5.2. Two types of PNBF observed in two tibiae: (A) Diffuse lamellar PNBF possibly associated with biomechanical stress and (B) discrete patch of sclerotic PNBF with clear signs of healing and bridging. 111

Figure 5.3. (A) Active cribra orbitalia and (B) porotic hyperostosis 114

Figure 5.4. Dental caries on a left mandibular first molar (LM_1) 115

Figure 5.5. Dental abscess at the right maxillary first premolar (PM^3). Partial tooth root is still present. 117

Figure 5.6. Rib with sample taken from shaft (red arrow) preserving the sternal rib end. 123

Figure 5.7. Yellow-brown discoloration of hydrochloric acid from humic acids during demineralization of rib samples. 125

Figure 5.8. First sodium hydroxide treatment of a rib sample. 126

Figure 5.9. Filtering gelatinized sample with an Ezee-filter™ to isolate the supernatant prior to freeze-drying. 128

Figure 6.1. $\delta^{13}C$ and $\delta^{15}N$ values for femur collagen by sex with 95% confidence ellipses. Males are purple and females are green. 167

Figure 6.2. $\delta^{13}C$ and $\delta^{15}N$ values for rib collagen by sex with 95% confidence ellipses. Males are purple and females are green. 168

Figure 6.3. $\delta^{13}C$ and $\delta^{15}N$ values for femur collagen by site with 95% confidence ellipses. Teal =Palatul Cnejilor, orange=Schitișor, and purple= Suceava. 169

Figure 6.4. $\delta^{13}C$ and $\delta^{15}N$ values for rib collagen by site with 95% confidence ellipses. Teal =Palatul Cnejilor, orange=Schitișor, and purple= Suceava. 170

Figure 6.5. Posterior parameter distribution of the fit5 (PNBF~Age+Sex) model parameters and Hamilton Monte Carlo (HMC) chains. The posterior distributions on the left describe the log odds of presenting with PNBF based on the predictor variables in the models. The central tendency of the distribution reflects the most credible value for the log odds of presenting with PNBF, with less credible values distributed towards the tails. On the right, the HMC chains are healthy and recovered similar values at each of the 40,000 random walks of the posterior parameter space indicating reliable posterior parameter distributions given the data. 177

Figure 6.6. Autocorrelation plots for each fit5 (PNBF~Age+Sex) parameter by HMC chain with flat priors. There is negligible autocorrelation. When predictor variables are correlated with each other, the sequential HMC samples from the posterior parameter space are correlated. This results in a slower HMC simulation and thus a less efficient exploration of the posterior parameter space. 178

Figure 6.7. Density (left) and histogram (right) charts showing the posterior draws of the probability of presenting with PNBF based on fit5 (PNBF~Age+Sex). Dark lines represent the mean and flat priors used. Light blue lines are the random draws from the posterior parameter space. They symmetrical distribution of the light blue lines around the mean suggests the model converged. 179

Figure 6.8. Posterior parameter distribution of the fit5 (PNBF~Age+Sex) model parameters and HMC chains. 185

Figure 6.9. Autocorrelation plots for each fit5 (PNBF~Age+Sex) parameter by HMC chain with flat priors that suggest negligible autocorrelation. 186

Figure 6.10. Density (left) and histogram (right) charts showing the posterior draws of the probability of presenting with PNBF based on fit 5 (PNBF~Age+Sex). Dark lines represent the mean and flat priors used. Light blue lines are the random draws from posterior parameter space. The symmetrical distribution of the light blue lines around the mean suggests the model converged. 187

Figure 6.11. Posterior parameter distribution of the fit5 (PH~Age+Sex) model parameters and HMC chains. 192

Figure 6.12. Autocorrelation plots for each fit5 (PH~Age+Sex) parameter by HMC chain with flat priors that suggest negligible autocorrelation. 193

Figure 6.13. Density (left) and histogram (right) charts showing the posterior draws of the probability of presenting with PH based on fit5 (PH~Age+Sex). Dark lines represent the mean and flat priors used. Light blue lines are the random draws from the posterior parameter space. The symmetrical distribution of the light blue lines around the mean suggests the model converged. 194

Figure 6.14. Posterior parameter distribution of the fit5 (PH~Age+Sex) model parameters and HMC chains. 200

Figure 6.15. Autocorrelation plots for each fit5 (PH~Age+Sex) parameter by HMC chain with flat priors that suggest negligible autocorrelation. 201

Figure 6.16. Density (left) and histogram (right) charts showing the posterior draws of the probability of presenting with PH based on fit5 (PH~Age+Sex). Dark lines represent the mean and flat priors used. Light blue lines are the random draws from the posterior parameter space. The symmetrical distribution of the light blue lines around the mean suggests the model converged. 202

Figure 6.17. Posterior parameter distribution of the fit5 (CO~Age+Sex) model parameters and HMC chains. 207

Figure 6.18. Autocorrelation plots for each fit5 (CO~Age+Sex) parameter by HMC chain with flat priors that suggest negligible autocorrelation. 208

Figure 6.19. Density (left) and histogram (right) charts showing the posterior draws of the probability of presenting with CO based on the fit5 (CO~Age+Sex). Dark lines represent the mean and flat priors used. Light blue lines are the random draws from the posterior parameter space. The symmetrical distribution of the light blue lines around the mean suggests the model converged. 209

Figure 6.20. Posterior parameter distribution of the fit5 (CO~Age+Sex) model parameters and HMC chains. 215

Figure 6.21. Autocorrelation plots for each fit5 (CO~Age+Sex) parameter by HMC chain with flat priors that suggest negligible autocorrelation. 216

Figure 6.22. Density (left) and histogram (right) charts showing the posterior draws of the probability of presenting with CO based on fit5 (CO~Age+Sex). Dark lines represent the mean and flat priors used. Light blue lines are the random draws from the posterior parameter space.

The symmetrical distribution of the light blue lines around the mean suggests the model converged. 217

Figure 6.23. Posterior parameter distribution of the fit5 (Caries~Age+Sex) model parameters and HMC chains. 221

Figure 6.24. Autocorrelation lots for each fit5 (Caries~Age+Sex) parameter by HMC chain with flat priors that suggest negligible autocorrelation. 222

Figure 6.25. Density (left) and histogram (right) charts showing the posterior draws of the probability of presenting with caries based on fit5 (Caries~Age+Sex). Dark lines represent the mean and flat priors used. Light blue lines are the random draws from the posterior parameter space. The symmetrical distribution of the light blue lines around the mean suggests the model converged. 223

Figure 6.26. Posterior parameter distribution of the fit4 (Caries~Age+Sex+Site) model parameters and HMC chains. 228

Figure 6.27. Autocorrelation plots for each fit4 (Caries~Age+Sex+Site) parameter by HMC chain with flat priors that suggest negligible autocorrelation. 229

Figure 6.28. Density (left) and histogram (right) charts showing the posterior draws of the probability of presenting with caries based on fit4 (Caries~Age+Sex+Site). Dark lines represent the mean and flat priors used. Light blue lines are the random draws from the posterior parameter space. The symmetrical distribution of the light blue lines around the mean suggests the model converged. 231

Figure 6.29. Posterior parameter distribution of the fit5 (Abscesses~Age+Sex) model parameters and HMC chains. 236

Figure 6.30. Autocorrelation plots for each fit5 (Abscesses~Age+Sex) parameter by HMC chain with flat priors that suggest negligible autocorrelation. 237

Figure 6.31. Density (left) and histogram (right) charts showing the posterior draws of the probability of presenting with abscesses based on fit5 (Abscesses~Age+Sex). Dark lines represent the mean and flat priors used. Light blue lines are the random draws from the posterior parameter space. The symmetrical distribution of the light blue lines around the mean suggests the model converged. 239

Figure 6.32. Posterior parameter distribution for the fit5 (Abscesses~Age+Sex) model parameters and HMC chains. 244

Figure 6.33. Autocorrelation plots for each fit5 (Abscesses~Age+Sex) parameter by HMC chain with flat priors that suggest negligible autocorrelation. 245

Figure 6.34. Density (left) and histogram (right) charts showing the posterior draws of the probability of presenting with abscesses based on fit5 (Abscesses~Age+Sex). Dark lines represent the mean and flat priors used. Light blue lines are the random draws from the posterior parameter space. The symmetrical distribution of the light blue lines around the mean suggests the model converged. 246

Figure 6.35. Posterior parameter distribution of the fit5 (PD~Age+Sex) model parameters and HMC chains. 251

Figure 6.36. Autocorrelation plots for each fit5 (PD~Age+Sex) parameter by HMC chains with plat priors that suggest negligible autocorrelation. 252

Figure 6.37. Density (left) and histogram (right) charts showing the posterior draws of the probability of presenting with abscesses based on fit5 (PD~Age+Sex). Dark lines represent the mean and flat priors used. Light blue lines are the random draws from the posterior parameter space. The symmetrical distribution of the light blue lines around the mean suggests the model converged. 254

Figure 6.38. Posterior parameter distribution of the fit5 (PD~Age+Sex) model parameters and HMC chains. 258

Figure 6.39. Autocorrelation plots for each fit5 (PD~Age+Sex) parameter by HMC chain with flat priors that suggest negligible autocorrelation. 259

Figure 6.40. Density (left) and histogram (right) charts showing the posterior draws of the probability of presenting with abscesses based on fit5 (PD~Age+Sex). Dark lines represent the mean and flat priors used. Light blue lines are the random draws from the posterior parameter space. The symmetrical distribution of the light blue lines around the mean suggests the model converged. 260

Figure 6.41. Kaplan-Meier survival functions for individuals with and without PNBF. 263

Figure 6.42. Kaplan-Meier survival functions for individuals with and without PH. 263

Figure 6.43. Kaplan-Meier survival functions for individuals with and without CO. 265

Figure 6.44. Kaplan-Meier survival functions for individuals with and without caries. 265

Figure 6.45. Kaplan-Meier survival functions for individuals with and without abscesses. 266

Figure 6.46. Kaplan-Meier survival functions for individuals with and without PD. 268

Figure 7.1. Biplot of $\delta^{13}C$ and $\delta^{15}N$ values for femur collagen by site. 271

Figure 7.2. Scatter plot of faunal $\delta^{13}C$ and $\delta^{15}N$ collagen values from two medieval sites in north-central Poland, and human collagen (light purple) from Suceava, Palatul Cnejilor, and Schitişor. 273

Figure 7.3. Human $\delta^{13}C$ and $\delta^{15}N$ collagen values with average $\delta^{13}C$ values for archaeological wheat (solid yellow line) and rye (solid green line). Dashed lines indicate the +5‰ diet to collagen enrichment for wheat (yellow) and rye (green). 277

Figure 7.4. Biplot of $\delta^{13}C$ and $\delta^{15}N$ human collagen values with the solid red line indicating the cut off for a C_3 versus C_4 diet. 278

Figure 7.5. Scatter plot of human $\delta^{13}C$ apatite and collagen values plotted against C_3 and C_4 protein regression lines calculated from rat $\delta^{13}C$ collagen and apatite values by Froehle et al. (2010). 281

Figure 7.6. Diagram illustrating the relationship between diet and dental caries with effect modification from social status. 297

Figure A.1. ANOVA with Scheffe's post hoc for differences in age structure between sites. Palatul Cnejilor (1), Schitișor (2), Suceava (3). 335

Figure A.2. Results of the Pearson Chi-Square Test for biological sex and site. 335
Figure A.3. Bar chart of the number of males and females at each site. 336
Figure A.4. Pearson Chi-Square Test for PNBF and preservation. 336
Figure A.5. Bar chart of presence/absence of PNBF by preservation. 337
Figure A.6. Levene's Test for Equality of Variances for PNBF and age-at-death. 337
Figure A.7. Pearson Chi-Square Test for PNBF and biological sex. 337
Figure A.8. Bar chart of presence/absence of PNBF for males and females. 338
Figure A.9. Pearson Chi-Square Test for PNBF and site 338
Figure A.10. Bar chart of presence/absence of PNBF for each site 339
Figure A.11. Pearson Chi-Square Test for PH and preservation. 339
Figure A.12. Bar chart of presence/absence of PH by preservation. 340
Figure A.13. Levene's Test for Equality of Variances for PH and age-at-death. 340
Figure A.14. Pearson Chi-Square Test for PH and biological sex. 340
Figure A.15. Bar chart of presence/absence of PH for males and females. 341
Figure A.16. Pearson Chi-Square Test for PH and site. 341
Figure A.17. Bar chart of presence/absence of PH for each site. 342
Figure A.18. Pearson Chi-Square Test for CO and preservation. 342
Figure A.19. Bar chart of presence/absence of CO by preservation. 343
Figure A.20. Levene's Test for Equality of Variances for CO and age-at-death. 343
Figure A.21. Pearson Chi-Square Test for biological sex and CO. 343
Figure A.22. Bar chart of presence/absence of CO for males and females. 344
Figure A.23. Pearson Chi-Square Test for CO and site. 344
Figure A.24. Bar chart of presence/absence of CO for each site. 345
Figure A.25. Pearson Chi-Square Test for caries and preservation. 345
Figure A.26. Bar chart of presence/absence of caries by preservation. 346
Figure A.27. Levene's Test for Equality of Variances for caries and age-at-death. 346
Figure A.28. Pearson Chi-Square Test for biological sex and caries. 346
Figure A.29. Bar chart of presence/absence of caries for males and females 347
Figure A.30. Pearson Chi-Square Test for caries and site. 347
Figure A.31. Bar chart of presence/absence of caries for each site. 348
Figure A.32. Pearson Chi-Square Test for abscesses and preservation. 348
Figure A.33. Bar chart of presence/absence of abscesses by preservation. 349

Figure A.34. Levene's Test for Equality of Variances for abscesses and age-at-death. 349
Figure A.35. Pearson Chi-Square Test for biological sex and abscesses. 349
Figure A.36. Bar chart of presence/absence of abscesses for males and females. 350
Figure A.37. Pearson Chi-Square Test for abscesses and site. 350
Figure A.38. Bar chart of presence/absence of abscesses for each site. 351
Figure A.39. Pearson Chi-Square Test for PD and preservation. 351
Figure A.40. Bar chart of presence/absence of PD by preservation. 352
Figure A.41. Levene's Test for Equality of Variances for PD and age-at-death. 352
Figure A.42. Pearson Chi-Square Test for biological sex and PD. 352
Figure A.43. Bar chart of presence/absence of PD for males and females. 353
Figure A.44. Pearson Chi-Square Test for PD and site. 353
Figure A.45. Bar chart of presence/absence of PD for each site. 354
Figure A.46. Descriptive statistics for $\delta^{13}C$ femur values for males and females. 354
Figure A.47. Levene's Test for Equality of Variances for $\delta^{13}C$ femur values and sex. 354
Figure A.48. Descriptive statistics for $\delta^{13}C$ rib values for males and females. 355
Figure A.49. Levene's Test for Equality of Variances for $\delta^{13}C$ rib and sex. 355
Figure A.50. One-Way ANOVA for $\delta^{13}C$ femur values and site. 355
Figure A.51. ANOVA with Scheffe's post hoc for differences in $\delta^{13}C$ femur values between sites. 355
Figure A.52. One-Way ANOVA for $\delta^{13}C$ rib values and site. 356
Figure A.53. ANOVA with Scheffe's post hoc for differences in $\delta^{13}C$ rib values between sites. 356
Figure A.54. Descriptive statistics for $\delta^{15}N$ femur values for males and females. 356
Figure A.55. Levene's Test for Equality of Variances for $\delta^{15}N$ femur values and sex. 356
Figure A.56. Descriptive statistics for $\delta^{15}N$ rib values for males and females. 357
Figure A.57. Levene's Test for Equality of Variances for $\delta^{15}N$ rib values and sex. 357
Figure A.58. One-Way ANOVA for $\delta^{15}N$ femur values and site. 357
Figure A.59. ANOVA with Scheffe's post hoc for differences in $\delta^{15}N$ femur values between sites. 357
Figure A.60. One-Way ANOVA for $\delta^{15}N$ rib values and site. 358
Figure A.61. ANOVA with Scheffe's post hoc for differences in $\delta^{15}N$ rib values between sites. 358

Figure A.62. $\delta^{13}C$ and $\delta^{15}N$ femur values for individuals that are absent (0), present (1), and unobservable (2) for PNBF with 95% confidence ellipses. 367

Figure A.63. $\delta^{13}C$ and $\delta^{15}N$ femur values those absent (0), present (1), and unobservable (2) for PNBF by site and sex with 95% confidence ellipses. 367

Figure A.64. $\delta^{13}C$ and $\delta^{15}N$ femur values for individuals that are absent (0), present (1), and unobservable (2) for PH with 95% confidence ellipses. 368

Figure A.65. $\delta^{13}C$ and $\delta^{15}N$ femur values for individuals that are absent (0), present (1), and unobservable (2) for PH by site with 95% confidence ellipses. 368

Figure A.66. $\delta^{13}C$ and $\delta^{15}N$ femur values for individuals that are absent (0), present (1), and unobservable (2) for PH by sex with 95% confidence ellipses. 369

Figure A.67. $\delta^{13}C$ and $\delta^{15}N$ femur values for individuals that are absent (0), present (1), and unobservable (2) for CO with 95% confidence ellipses. 369

Figure A.68. $\delta^{13}C$ and $\delta^{15}N$ femur values for individuals that are absent (0), present (1), and unobservable (2) for CO by site with 95% confidence ellipses. 370

Figure A.69. $\delta^{13}C$ and $\delta^{15}N$ femur values for individuals that are absent (0), present (1), and unobservable (2) for CO by sex with 95% confidence ellipses. 370

Figure A.70. $\delta^{13}C$ and $\delta^{15}N$ femur values for individuals that are absent (0), present (1), and unobservable (2) for caries with 95% confidence ellipses. 371

Figure A.71. $\delta^{13}C$ and $\delta^{15}N$ femur values for individuals that are absent (0), present (1), and unobservable (2) for caries by site with 95% confidence ellipses. 371

Figure A.72. $\delta^{13}C$ and $\delta^{15}N$ femur values for individuals that are absent (0), present (1), and unobservable (2) for caries by sex with 95% confidence ellipses. 372

Figure A.73. $\delta^{13}C$ and $\delta^{15}N$ femur values for individuals that are absent (0), present (1), and unobservable (2) for abscesses with 95% confidence ellipses. 372

Figure A.74. $\delta^{13}C$ and $\delta^{15}N$ femur values for individuals that are absent (0), present (1), and unobservable (2) for abscesses by site with 95% confidence ellipses. 373

Figure A.75. $\delta^{13}C$ and $\delta^{15}N$ femur values for individuals that are absent (0), present (1), and unobservable (2) for abscesses by sex with 95% confidence ellipses. 373

Figure A.76. $\delta^{13}C$ and $\delta^{15}N$ femur values for individuals that are absent (0), present (1), and unobservable (2) for PD with 95% confidence ellipses. 374

Figure A.77. $\delta^{13}C$ and $\delta^{15}N$ femur values for individuals that are absent (0), present (1), and unobservable (2) for PD by site with 95% confidence ellipses. 374

Figure A.78. $\delta^{13}C$ and $\delta^{15}N$ femur values for individuals that are absent (0), present (1), and unobservable (2) for PD by sex with 95% confidence ellipses. 375

Figure A.79. $\delta^{13}C$ and $\delta^{15}N$ rib values for individuals that are absent (0), present (1), and unobservable (2) for PNBF with 95% confidence ellipses. 376

Figure A.80. $\delta^{13}C$ and $\delta^{15}N$ rib values for individuals that are absent (0), present (1), and unobservable (2) for PNBF by site with 95% confidence ellipses. 376

Figure A.81. $\delta^{13}C$ and $\delta^{15}N$ rib values for individuals that are absent (0), present (1), and unobservable (2) for PNBF by sex with 95% confidence ellipses..... 377

Figure A.82. $\delta^{13}C$ and $\delta^{15}N$ rib values for individuals that are absent (0), present (1), and unobservable (2) for PH with 95% confidence ellipses..... 377

Figure A.83. $\delta^{13}C$ and $\delta^{15}N$ rib values for individuals that are absent (0), present (1), and unobservable (2) for PH by site with 95% confidence ellipses. 378

Figure A.84. $\delta^{13}C$ and $\delta^{15}N$ rib values for individuals that are absent (0), present (1), and unobservable (2) for PH by sex with 95% confidence ellipses. 378

Figure A.85. $\delta^{13}C$ and $\delta^{15}N$ rib values for individuals that are absent (0), present (1), and unobservable (2) for CO with 95% confidence ellipses. 379

Figure A.86. $\delta^{13}C$ and $\delta^{15}N$ rib values for individuals that are absent (0), present (1), and unobservable (2) for CO by site with 95% confidence ellipses..... 379

Figure A.87. $\delta^{13}C$ and $\delta^{15}N$ rib values for individuals that are absent (0), present (1), and unobservable (2) for CO by sex with 95% confidence ellipses. 380

Figure A.88. $\delta^{13}C$ and $\delta^{15}N$ rib values for individuals that are absent (0), present (1), and unobservable (2) for caries with 95% confidence ellipses..... 380

Figure A.89. $\delta^{13}C$ and $\delta^{15}N$ rib values for individuals that are absent (0), present (1), and unobservable (2) for caries by site with 95% confidence ellipses. 381

Figure A.90. $\delta^{13}C$ and $\delta^{15}N$ rib values for individuals that are absent (0), present (1), and unobservable (2) for caries by sex with 95% confidence ellipses. 381

Figure A.91. $\delta^{13}C$ and $\delta^{15}N$ rib values for individuals that are absent (0), present (1), and unobservable (2) for abscesses with 95% confidence ellipses..... 382

Figure A.92. $\delta^{13}C$ and $\delta^{15}N$ rib values for individuals that are absent (0), present (1), and unobservable (2) for abscesses by site with 95% confidence ellipses..... 382

Figure A.93. $\delta^{13}C$ and $\delta^{15}N$ rib values for individuals that are absent (0), present (1), and unobservable (2) for abscesses by sex with 95% confidence ellipses. 383

Figure A.94. $\delta^{13}C$ and $\delta^{15}N$ rib values for individuals that are absent (0), present (1), and unobservable (2) for PD with 95% confidence ellipses..... 383

Figure A.95. $\delta^{13}C$ and $\delta^{15}N$ rib values for individuals that are absent (0), present (1), and unobservable (2) for PD by site with 95% confidence ellipses. 384

Figure A.96. $\delta^{13}C$ and $\delta^{15}N$ rib values for individuals that are absent (0), present (1), and unobservable (2) for PD by sex with 95% confidence ellipses. 384

Figure A.97. Marginal effect of sex on PNBF frequency for femur $\delta^{13}C$ and $\delta^{15}N$ values..... 389

Figure A.98. Marginal effect of age on PNBF frequency for femur $\delta^{13}C$ and $\delta^{15}N$ values..... 389

Figure A.99. Marginal effect of sex on PNBF frequency for rib $\delta^{13}C$ and $\delta^{15}N$ values. 390
Figure A.100. Marginal effect of age on PNBF frequency for rib $\delta^{13}C$ and $\delta^{15}N$ values. 390
Figure A.101. Marginal effect of sex on PH frequency for femur $\delta^{13}C$ and $\delta^{15}N$ values. 391
Figure A.102. Marginal effect of age on PH frequency for femur $\delta^{13}C$ and $\delta^{15}N$ values. 391
Figure A.103. Marginal effect of sex on PH frequency for rib $\delta^{13}C$ and $\delta^{15}N$ values. 392
Figure A.104. Marginal effect of age on PH frequency for rib $\delta^{13}C$ and $\delta^{15}N$ values. 392
Figure A.105. Marginal effect of sex on CO frequency for femur $\delta^{13}C$ and $\delta^{15}N$ values. 393
Figure A.106. Marginal effect of age on CO frequency for femur $\delta^{13}C$ and $\delta^{15}N$ values. 393
Figure A.107. Marginal effect of sex on CO frequency for rib $\delta^{13}C$ and $\delta^{15}N$ values. 394
Figure A.108. Marginal effect of age on CO frequency for rib $\delta^{13}C$ and $\delta^{15}N$ values. 394
Figure A.109. Marginal effect of sex on caries frequency for femur $\delta^{13}C$ and $\delta^{15}N$ values..... 395
Figure A.110. Marginal effect of age on caries frequency for femur $\delta^{13}C$ and $\delta^{15}N$ values. 395
Figure A.111. Marginal effect of sex on caries frequency for rib $\delta^{13}C$ and $\delta^{15}N$ values. 396
Figure A.112. Marginal effect of age on caries frequency for rib $\delta^{13}C$ and $\delta^{15}N$ values. 396
Figure A.113. Marginal effect of sex on abscesses frequency for femur $\delta^{13}C$ and $\delta^{15}N$ values. 397
Figure A.114. Marginal effect of age on abscesses frequency for femur $\delta^{13}C$ and $\delta^{15}N$ values. 397
Figure A.115. Marginal effect of sex on abscesses frequency for rib $\delta^{13}C$ and $\delta^{15}N$ values..... 398
Figure A.116. Marginal effect of age on abscesses frequency for rib $\delta^{13}C$ and $\delta^{15}N$ values. ... 398
Figure A.117. Marginal effect of sex on PD frequency for femur $\delta^{13}C$ and $\delta^{15}N$ values. 399
Figure A.118. Marginal effect of age on PD frequency for femur $\delta^{13}C$ and $\delta^{15}N$ values. 399
Figure A.119. Marginal effect of sex on PD frequency for rib $\delta^{13}C$ and $\delta^{15}N$ values. 400
Figure A.120. Marginal effect of age on PD frequency for rib $\delta^{13}C$ and $\delta^{15}N$ values. 400
Figure A.121. Mean and median survival estimates for individuals with and without PNBF. . 401
Figure A.122. Mean and median survival estimates for individuals with and without PH. 401
Figure A.123. Mean and median survival estimates for individuals with and without CO. 401
Figure A.124. Mean and median survival estimates for individuals with and without caries. .. 401
Figure A.125. Mean and median survival estimates for individuals with and without abscesses. 402
Figure A.126. Mean and median survival estimates for individuals with and without PD. 402

CHAPTER ONE: INTRODUCTION

Today, Romania is home to a diverse population composed of Romanian, Hungarian, Romani, Ukrainian, and German ethnic groups. The roots of this diversity extend back to the Roman conquest and subsequent occupation of Dacia (modern Romania) in the early 2nd century CE. Romania's proximity to both Central Europe and Western Asia made it the nexus for competing empires such as the Byzantine, Ottoman, Hungarian, and Russian Empires from the 2nd through the 18th centuries, which brought extensive trade and significant population movement into the region (Hitchins 2014b). A long history of imperial occupation and feudalism widened social, economic, and political gaps between the classes. This disparity among classes may have resulted in differential access to resources or intensified pre-existing barriers to resources. Lower status individuals likely had more exposure to environmental and occupational hazards and limited access to adequate nutrition leading to differential health outcomes between privileged and marginalized groups along the lines of age, sex, and social class. The exact consequences of centuries of social stratification, slavery, and imperial occupation on health during the Late Medieval and Early Modern periods (14th – 18th centuries CE) in Romania are not known.

There have been few studies that explore diet, sex, social status, and health in early to late medieval Eastern and Central Europe (Jílková et al. 2019; Kaupová et al. 2018; Knipper et al. 2015; Vidal-Ronchas et al. 2019) and even fewer that have addressed these questions in Romania or utilized stable isotope methods. Voas and colleagues (2021) explored childhood diet and weaning in early modern Transylvania using carbon and nitrogen stable isotope analysis of bone collagen and tooth dentin. Excavations of burials from this region of Transylvania, a Hungarian

diaspora known as the Székelyföld or Székely land, by Dr. Jonathan Bethard from the University of South Florida are underway. Initial carbon and nitrogen stable isotope analyses which shows a pure C_3 diet, likely from wheat consumption (communication with Dr. Jonathan Bethard March 22, 2024). Additionally, another study of a late medieval (14^{th}-17^{th} C) cemetery in southern Romania showed a predominantly C_3 and terrestrial protein diet of the three individuals analyzed for stable isotopes (Palincaş et al. 2019), but none of these studies address sex-based dietary differences or differences based on social status**.** Otherwise, the bulk of studies on dietary reconstruction using stable isotope analysis have focused on neighboring countries like Hungary, Czech Republic, Croatia, and Poland and much earlier time periods such as the middle-late bronze age and 5^{th}-6^{th} centuries AD (Gugora et al. 2018; Martinoia et al. 2021; Plecerová et al. 2020; Reitsema et al. 2013).

In modern-day Romania, the urban-rural divide and regional disparities in poverty, income, education, health, and nutrition are not new to the modern era. Rather, they are systemic issues that have deep roots in historical processes of occupation, slavery, and social stratification experienced during the medieval period. Some of these processes continued into the modern era with the rise of the Communist State in 1947, resulting in economic inequality, violence, and policies that directly influenced access to food and healthcare. While communisms' effect on health is more immediate and visible, the roots of modern health disparities extend deep into Romanian history. Exploring how factors like age, sex, social status, and access to nutritional resources impacted human health in Romania's past has the potential to provide a historically informed perspective of how these processes continue to play out in Romania today. This knowledge can be leveraged to address unequal access to resources and health disparities that affect Romanians today, and potentially address these issues globally.

Bioarchaeologists are uniquely positioned to study the effects of demography, social status, and diet on health in past populations. The application of biogeochemical methods like stable isotope analysis adds a suite of new tools and methods that can complement and enhance macroscopic skeletal data and help bioarchaeologists begin to unravel the hidden heterogeneity in frailty, stress, and diet that was present in past populations and the complex relationship between social, cultural, environmental, and intrinsic biological factors and human health outcomes and experiences over the life course.

In the absence of thorough historical records, botanical and/or faunal remains, and other archaeological evidence of food procurement and processing, it is difficult to reconstruct what people were eating and how this may have differed across social classes, between sexes, or changed over the life course. Stable isotope analysis of human tissues makes it possible to see how humans were interacting with their environment at an atomic level by looking at the ratios or relative abundance of elements like carbon and nitrogen that were routed from the food an individual consumed to various body tissues. While several factors mediate how these heavier and lighter isotopes of different elements are partitioned to various tissues, the resulting stable isotope values (measured in per mil ‰) are very informative for understanding different components of the diet, and what type of plant and animal resources were being consumed by past peoples.

Research that explores factors like age, sex, diet, and social class, and their role in experiences of physiological stress can provide temporal depth and nuance to our understanding of how these processes continue to affect human health today, and potentially inform public and global health policy aimed at addressing health disparities.

In this dissertation, I aim to explore questions about skeletal stress, demography, and dietary composition within the theoretical framework of isotope ecology and biocultural theory by combining standard methods for bioarchaeological and paleopathological analyses of human skeletal remains and archaeological and historical evidence with stable carbon and nitrogen isotope analysis. I use a Bayesian modeling approach to determine which variables (age, sex, social status, or isotopic indicators of diet) are predictive of individuals exhibiting skeletal stress lesions.

Research Objectives and Study Design

To explore the relationship between diet, social status, and stress in Late Medieval – Early Modern Romania I examined human skeletal assemblages excavated from three sites in Northeast Romania: Suceava, Palatul Cnejilor, and Schitișor, all housed at the Francisc I. Rainer Institute of Anthropology in Bucharest, Romania. The objectives of this research are to 1) document the frequency of non-specific stress lesions in these populations to understand the overall burden of physiological stress, 2) determine the demographic makeup of the sites by estimating age-at-death and biological sex using features of the cranium and pelvis, 3) reconstruct dietary composition using carbon and nitrogen stable isotope analysis of bone collagen, and 4) to utilize this combination of skeletal, archaeological, historical, and isotope data to understand how age, sex, social status, and diet influenced patterns of stress in these populations.

Using flat priors, I combined information about social status from archaeological site reports, frequencies of non-specific stress lesions, age-at-death, biological sex, and carbon and nitrogen stable isotope data to perform Bayesian model selection for a Bayesian logistic

regression model that included the variables that were the best predictors for the probability of presenting with a stress lesion.

Questions and Hypotheses

This dissertation focuses on three major research questions and associated hypotheses. I use a combination of frequentist methods (ANOVAs, t-tests, and chi-squares) to test these hypotheses and identify associations or differences between the variables, and identify any interesting patterns in the data. However, to get at how an individual's age, sex, social status, and diet affected their health experience, specifically physiological stress as understood by skeletal lesions, I employed a Bayesian logistic regression with a model selection approach to determine which combination of these variables best predicts the odds of an individual having a stress lesion.

Question 1: What physiological stressors did people experience?

This research was largely exploratory as no previous anthropological or bioarchaeological analyses have been done on the skeletal remains excavated from Suceava, Palatul Cnejilor, and Schitișor. So, the first question asks, *what physiological stressors did people at this time in Romania's history experience, as understood by skeletal stress lesions, and how were those stressors distributed amongst individuals based on biological sex and social status* (as understood by historical and archaeological evidence from each site). *I hypothesize that individuals at this time experienced a variety of different physiological stressors as indicated by the presence of non-specific stress lesions and dental disease.*

There is a lack of substantial historical knowledge of this region and time, specifically about how health experiences differed between males and females. Most research into this question focuses on Western Europe (in particular medieval London) (DeWitte 2010; Godde et

al. 2020; Walter et al. 2016; Yaussy et al. 2016) and the literature presents conflicting results about whether males or females are more likely to present with stress lesions due to the complexity of how social, cultural, and environmental factors intersect with an individual's biology to shape health experiences and how this is further mediated by sex. In a black death cemetery population from medieval England, researchers found that excess mortality associated with skeletal stress lesions was higher for males than females (DeWitte 2010), while females in medieval England had a higher frequency of dental caries (Walter et al. 2016). Conversely, modern clinical research (while mostly based on animal models) has shown that there are sex differences in immunocompetence due to sex hormones that have been shown to affect immune responses and drive differential immune responses between males and females. However, differences in immunocompetence between males and females can change throughout life due to reproduction status and hormone fluctuations. Thus, whether males or females are more impacted by certain diseases or are more vulnerable to certain stressors will change depending on the exposure, age, etc. (Klein and Flanagan 2016; Zuckerman and Crandall 2019). Since understanding differential health experiences and outcomes between males and females is complex in living populations, it becomes even more so when studying skeletal assemblages, but it follows that males and females would not have been affected by stressors in the same way, with some individuals being more or less buffered against physiological stress due to social, cultural, and innate biological factors. Thus, *I hypothesize that there will be a difference in physiological stress experiences between the sexes, but given the lack of contextual information, I cannot predict the directionality of this difference i.e. which sex will be more affected.*

Using the burial sites as a proxy for social status, historical and archaeological evidence suggests Suceava had predominantly high-status individuals, Schitișor had predominantly low-

status individuals, and Palatul Cnejilor had a mix of high-status, low-status, and monastic individuals. Bioarchaeological research on the medieval period has identified health differentials by social status (Curto et al. 2019; DeWitte 2014). Therefore, *I hypothesize that there will be a difference in physiological stress experiences between sites, with individuals from low-status sites experiencing a greater burden of stress than individuals at high status sites.*

Question 2: What did they eat?

While there is historical documentation of the types of food sources people in Moldavia had access to during the late medieval-early modern period, there has been no previous research on these specific sites or this region of Romania that used a stable isotope approach to dietary reconstruction, thus what diet looked like at this time is not well understood. My second question asks, *what protein sources (plant and animal) were people at Suceava, Palatul Cnejilor, and Schitișor eating?* Based on historical information about the plant sources available, *I hypothesize that Romanians were consuming a majority C_3 plant diet (wheat, barley, oats, spelt, and rye), with some C_4 inputs due to the availability of millet and eventually maize by the early 18th century.* Based on historical sources, poultry, pork, and beef were commonly consumed along with some freshwater fish and possibly marine fish, so *I hypothesize that nitrogen isotopes will reflect a mostly terrestrial protein diet from livestock with possibly some aquatic protein sources as well.*

This research seeks to understand what people were eating, and how access to and consumption of food resources varied based on sex and social status. While some literature has shown males in medieval Europe may have had more access to protein and higher quality protein (Gugora et al. 2018), there is no literature specific to medieval Romania that has looked at sex-based dietary differences, so *I hypothesize that there will be dietary differences between sexes*

(as seen in carbon and nitrogen stable isotope values), but I cannot predict how these differences will be distributed between males and females in terms of their isotopic values.

Based on the historical and archaeological evidence available for the three study sites, the social status of individuals at each site is heterogenous but roughly divides between more high-status individuals at Suceava and more low-status individuals at Palatul Cnejilor and Schitișor. More specifically, based on grave goods and burial style, it was determined that Suceava likely contained members of the nobility and palace rulers as well as merchants and soldiers, Palatul Cnejilor likely also contained high-status nobility, but also lower-status peasants, and some monastic individuals. Schitișor, located less than two miles from Palatul Cnejilor contained mostly peasants and monastic individuals.

As previously mentioned, bioarchaeological and modern epidemiological research has shown that diet and access to food resources are often driven by social status/class, thus the types of plant and animal protein sources the people at these sites ate and had access to likely differed. The consumption of millet (a C_4 crop) in Europe has historically been associated with lower-status diets, with C_3 crops like wheat being more accessible to higher-status individuals (Gugora et al. 2018). Maize, another C_4 crop, was introduced to Romania in the late 17th century and quickly became the main food source for peasants, with wheat being consumed by the ruling classes (Georgescu 1991b; Rüsz Fogarasi 2009; Székely 2018; Tița 2006). Using burial site as a proxy for social status due to a lack of individual-level social status data, *I hypothesize that dietary composition (as understood by carbon and nitrogen stable isotope values) will be associated with burial site and there will be significant differences in diet (and thus carbon and nitrogen stable isotope values) between the sites with higher social status individuals and sites with lower social status individuals.*

Question 3: Considering demographic factors (age, sex, and site) from questions 1 and 2, how did diet influence patterns of skeletal stress in these populations?

Bringing age, sex, site, and diet from the first two research questions, the third research question seeks to understand how all these factors ultimately influenced experiences of physiological stress and how stress patterned in the populations at each site. So, put more simply my final question asks *how did diet affect pathology?* Research has shown that proper nutrition and nourishment over the life course is crucial for immunocompetence and being able to mount a robust immune response to biological stressors (Calder and Jackson 2000; Morgan 1997; Scrimshaw and SanGiovanni 1997). Bioarchaeological research has shown too much of foods high in simple carbohydrates and sugars lead to worse outcomes for dental health, while diets insufficient in essential vitamins and minerals lead to metabolic diseases like rickets and scurvy that have a direct impact on the juvenile and adult skeleton. There is no reason to expect that this relationship between nutrition and health will be different from the documented experience of so many other human populations across the world and through time. Thus, *I hypothesize that diet impacted patterns of physiological stress and dental diseases. By using a Bayesian model that incorporates demographic factors, the model selection process employed by Bayesian modeling will allow me to consider multiple demographic factors along with diet in predicting skeletal stress, and what that can tell us about experiences of physiological stress in these populations.*

Dissertation Organization

Chapter two provides a review of the historical background of this study as well as background on the archaeological context of the study sites. The first section reviews Romania's history beginning with the Dacians and Romans in the 2nd century and ending with the Austrian Empire in the 17th and 18th centuries. The second section outlines Romania's feudal system and

its effects on social class. The third section reviews the food sources that would have been accessible to people at this time and the ways stable isotope analysis can elucidate dietary composition. The fourth section reviews the archaeology of each of the study sites, specifically their geographical location, excavations, grave goods recovered, and who was buried at these sites. The final section provides a brief historical overview of the Francisc I. Rainer Institute of Anthropology (FRIA) where the skeletal assemblages used in this research are curated.

Chapter three discusses the theoretical orientation for understanding skeletal stress and health: the osteological paradox (OP). The tenets of the theory are reviewed as well as how bioarchaeology has incorporated the OP into studies of past human morbidity and mortality. The second section provides a review of the skeletal biology of bone remodeling and stress and the molecular signaling pathways that govern the stress response and its effect on bone. The third section discusses the skeletal biology of the non-specific stress lesions analyzed in this study, and the final section discusses biocultural theory and how our understanding of bone biology and stress can be combined with historical, archaeological, and isotopic data to gain a more holistic understanding of human health from the past.

Chapter four begins by reviewing what stable isotopes are, how they are measured and reported, and how isotopes move through environmental and biological systems. The second section outlines carbon isotopes in plants by reviewing the three different photosynthetic pathways used by plants and how this affects carbon isotope fractionation in plant tissues. The third section reviews nitrogen isotopes in plant-soil systems and possible human impacts on nitrogen isotopes in these systems. The fourth section reviews carbon and nitrogen isotopes in humans and animals and discusses how nitrogen isotopes move up the food chain, are affected by different environmental conditions, and how these effects can be understood from human and

animal tissues. The fifth section discusses the sources of carbon and nitrogen in Romania, specifically what plant and animal resources would have been available to individuals in Late Medieval-Early Modern Romania. This chapter concludes with a discussion of the literature that has used multi-isotope approaches to studying diet and health in past human populations.

Chapter five outlines the material and methods used in this study. The first section reviews the sample composition and size. The second section outlines the methods for age-at-death and biological sex estimation. The third section outlines the methods for scoring and documenting non-specific skeletal stress lesions. The fourth section discusses the statistical approach for the skeletal data, specifically tests of association and difference and intraobserver error. The fifth section outlines the sampling protocol for femora and rib samples taken for carbon and nitrogen stable isotope analysis. The sixth section outlines the protocol for bone collagen pre-treatment and stable isotope analysis. The seventh section outlines the statistical approach for the stable isotope data. The final section outlines the Bayesian model approach combining the skeletal and isotopic data to understand their predictive value for skeletal stress lesions.

Chapter six presents the results of this study. The first section reviews the demography of these study sites and the intraobserver analysis for age-at-death and biological sex estimation. The second section focuses on the first research question, *what physiological stresses did people experience?* and reports descriptive statistics of skeletal preservation and raw lesion frequencies for age, sex, and site and tests of association and difference for age, sex, and site for each lesion type. The second section focuses on the second research question, *what did people eat?* and reports descriptive statistics and tests of difference for carbon and nitrogen isotope data by sex and site. It also presents the biplots of carbon and nitrogen isotope values by sex and site. The

third section focuses on the third research question *how did diet affect pathology?* and reports the description, selection, and summary of Bayesian logistic regression models for predicting the odds of presenting with a lesion given age, sex, site, carbon, and nitrogen stable isotopes. This section also reports the Kaplan-Meier survival for age-at-death and lesion type.

Chapter seven discusses the results of this study. This chapter is divided into sections based on the three main research questions. The first section discusses the results of the descriptive statistics and tests of difference and association for stress lesions of childhood (PH and CO) and adulthood (PNBF), including dental disease. The second section discusses the stable isotope results and what they say about dietary composition at these study sites. The third section discusses the results of the Bayesian model selection and which predictor variables were relatively more meaningful for predicting the presence/absence of each lesion type. Significant differences in $\delta^{13}C$ values and site, and the selection of Site as a predictor variable for dental caries are discussed.

Chapter eight presents the conclusions of this study by first summarizing the major findings of this research, the major limitations and future directions for this research, and concludes with the broader impacts of this research.

CHAPTER TWO: HISTORICAL AND SITE BACKGROUND

Chapter Overview

This chapter discusses the history of Romania and its origins as a modern nation-state, beginning with a discussion of Romania's geographical context in southeastern Europe, and the importance of the Danube River for human movement throughout history. Next, the periods from the Dacian Kingdom in the 2nd century BCE, the periodic occupation and/or rule by the Roman, Bulgarian, and Byzantine Empires for more than a millennium, and eventual occupation by the Hungarian, Ottoman, and Austrian Empires in the late medieval-early modern period is discussed. These periods of Romania's history are covered to highlight the deep history of human mobility in Romania and its possible root causes, and the military, political, social, and cultural consequences of this mobility. The second section discusses the Romanian feudal system that characterized late medieval-early modern Romania and divided individuals into strict social categories that determined their role in society and access to various resources. The third section discusses Romanian culture, cuisine, society, politics, and religion, and the various social, cultural, and health consequences of social status and diet. The role of stable isotope analysis into bioarchaeological studies is also discussed, specifically how its incorporation can provide insight into stress, disease, diet, and even social status at an individual level which can then help identify trends at the population level. The final section provides background and archaeological context for the three cemetery collections that were analyzed, as well as background on the Francisc I. Rainer Institute of Anthropology (FRIA), where the collections are currently curated.

The Origins of Late Medieval-Early Modern Romania: A Crossroads of East and West

The modern nation-state of Romania is situated at the geographical and cultural crossroads of southeastern/central Europe, and western Asia. This is due to both its geographical

proximity to these regions and its long history of occupation by eastern and western powers resulting in both eastern and western influences on the politics, language, culture, cuisine, and religion of Romania and the Balkan region. The geography and natural landscape of Romania also makes it an interesting region to study human mobility and migration through time. Romania contains the Carpathian Mountains, the Carpathian or Pannonian Basin, and the Lower Danube River Basin, which makes up Romania's southern border with Bulgaria and part of Serbia (Figure 2.1).

The Danube River stretches from western Germany to the eastern coast of Romania where it empties into the Black Sea and forms the Danube Delta. The Danube is a major waterway that permitted trade, travel, and military movement into and out of the Balkan region from the earliest historic human settlements in the area, including the Dacians and Romans. Southeastern Europe, and Romania in particular, saw the movement and convergence of human groups during the 1st century CE during the Roman Empire, and into the early modern period (17th – 18th centuries). The region lay squarely in the path of traders, migrants, military forces from the Ottoman, Polish, Russian, and Hungarian empires, as well as nomadic groups from western and central Asia and northern Europe resulting in a culturally diverse population that formed during continuous occupation and rule by Roman, Bulgarian, Byzantine (Eastern Roman), Hungarian and Ottoman empires (Hitchins 2014b).

The Danube was also an important waterway in prehistory. The climatic and archaeological record of the early Upper Paleolithic in the Carpathian Basin shows that modern humans from southeast Europe entered the Carpathian Basin and moved into central Europe via the Danube River catchment. The Danube River also served as a corridor for the spread of



Figure 2.1. The middle and lower Danube River Basin contributing to Romania's southern border with Bulgaria and part of Serbia.

agriculture and Neolithic farmers from southwest Asia and western Anatolia (modern Turkey) during the Mesolithic-Neolithic transition (Borić and Price 2013; Chu 2018; Dobos et al. 2010). The Danube River catchment is also hypothesized to have served as a route into Europe for some of the earliest anatomically modern humans who migrated from Africa (Chu 2018).

The long history of population movement aided by the Danube River makes Romania a microcosm of the political, cultural, and social environment of southeastern Europe and the Balkans throughout modern history. The historical and geographic context of Romania is crucial to understanding how Romania came to be as it is today, but also how it came to be three separate principalities (Transylvania, Wallachia, and Moldavia) ruled by the Hungarian and Ottoman Empires during the late medieval-early modern period.

The Dacians and The Romans: 2nd Century BCE to the 4thCentury CE

While there is archaeological evidence that humans have inhabited what is now Romania since the Upper Paleolithic (Chu 2018; Dobos et al. 2010), the earliest written record of people in the area of present day Romania, Republic of Moldova, and northern Bulgaria were the Dacians, recorded by Herodotus in Book IV of his *Histories*. The height of the Dacian Kingdom was from 82 and 44 BCE. The Dacians were eventually defeated by the Roman Emperor Trajan in 106 CE. Dacia was colonized by Roman citizens, eventually becoming a Roman province that exported gold and silver mined from the Carpathian Mountains and saw the beginnings of a proto-Romanian language (Burns 2003). After several successful attacks by the Carpi, a free Dacian tribe, and the Goths, an ethnic group from the eastern region of modern Romania, Ukraine, and Republic of Moldova, the Romans withdrew from Dacia around 271 CE (Hitchins 2014a).

During the early medieval period (4th century CE), several nomadic and semi-nomadic tribes (Huns, Avars, Bulgars, and Gepids) from Central Asia, Eurasia, the Pontic-Caspian steppe

(a region north of the Black and Caspian seas), and Germany invaded Transylvania (northwest region of modern-day Romania) and ruled this region until the 8th century CE (Hitchins 2014a).

The Bulgarian, Byzantine, Hungarian, and Ottoman Empires: 8th – 17th Centuries CE

The First Bulgarian Empire was formed in 681 CE after it defeated the Byzantine army led by Constantine IV and would remain the dominant power in the region until its defeat by the Byzantines in 1018 CE (Hitchens 2014). In 1185 CE the Second Bulgarian Empire was formed, becoming the cultural center of the Slavic world, and was a highly stratified society divided into clergy, nobility, and peasantry controlled by feudal lords or central authorities, a common social organization in the medieval world. The Second Bulgarian Empire continued to be a dominant power until the 13th century when they were weakened by the invasions of the Mongols, Byzantines, Hungarians, and Serbs. They were ultimately defeated in the late 14th century by the Ottoman Empire, which would remain the dominant imperial power for the next 500 years encompassing parts of the Middle East, North Africa, and southeast Europe, including Romania (Figure 2.2). After the collapse of the Second Bulgarian Empire, what emerged in Romania were three principalities, each ruled by a voivod (prince/ruler): Transylvania, Wallachia, and Moldavia. Wallachia and Moldavia were bordered by the Ottoman Empire to the south and east (Figure 2.3) and experienced periods of Ottoman rule punctuated by periods of independence under Vlad III in the mid-15th century. The principalities were briefly unified under Mihai the Brave in 1600 until his death the same year. The three principalities again fell under Ottoman suzerainty by the early 17th century, which meant they were vassal states that retained limited internal autonomy but ceded control over foreign relations to the Sultan of the Ottoman

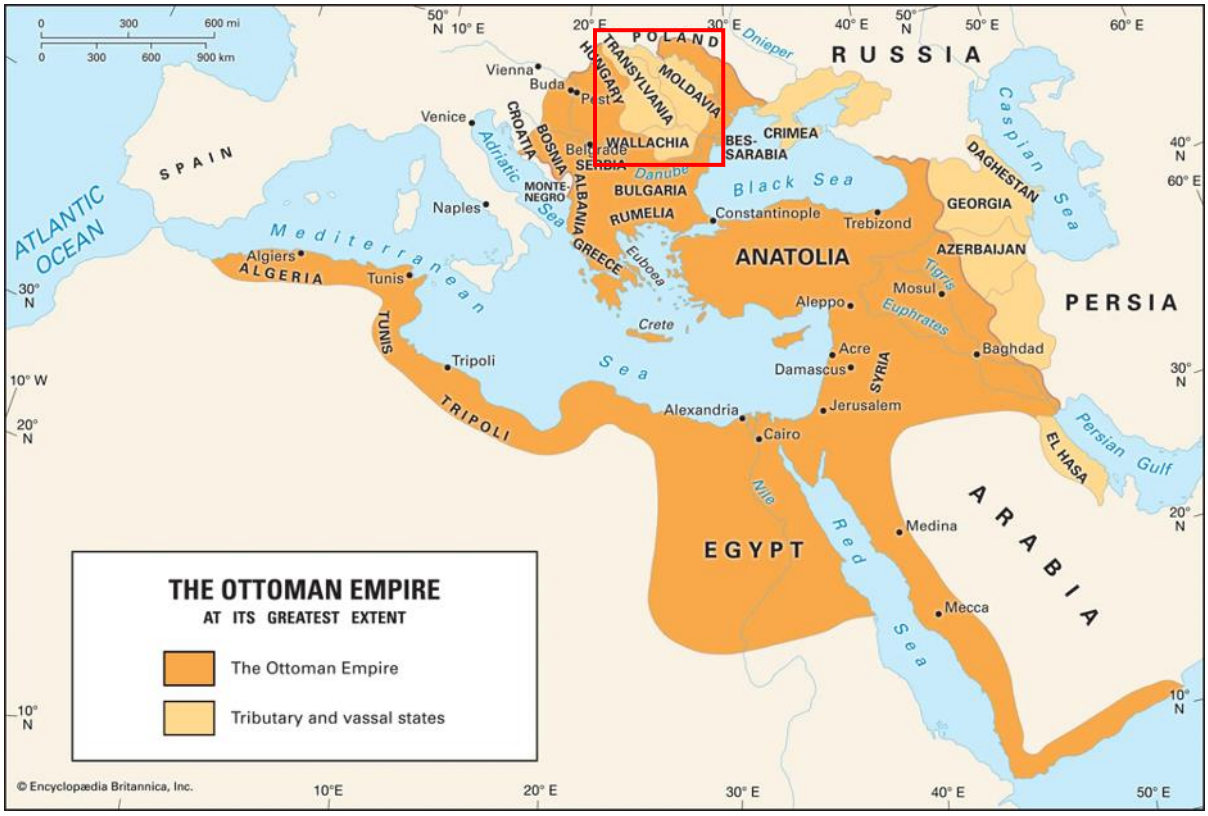


Figure 2.2. The Ottoman Empire 16th century (Encyclopedia Britannica). Red square indicates the Romanian Principalities.



Figure 2.3. The three Romanian principalities of Transylvania, Wallachia, and Moldavia c. 1600 CE (Treptow et al. 1997).

Empire (Hitchins 2014a). While Wallachia and Moldavia were periodically under Ottoman suzerainty, Transylvania came under Hungarian control between the 10th and 13th centuries, eventually becoming part of the Kingdom of Hungary, experiencing a wave of Saxon settlers from central and western Europe. Transylvania remained a part of the Kingdom of Hungary until its collapse in the 16th century, and Transylvania briefly became an independent principality before falling under Ottoman suzerainty as well (Hitchins 2014a).

The Austrian Empire and Phanariot Rule: 17th – 18th Centuries CE

By the end of the 17th century, the Austrian Empire had gained control of Transylvania, while Wallachia and Moldavia experienced continued attacks from the Turks, Tatars, Poles, Hungarians, and Cossacks. During this period both principalities saw the emergence of a lesser noble class due to the land grants made to boyars (members of the Romanian nobility) in exchange for military service. These land grants resulted in the encroachment on peasant lands, higher taxes, and worsening quality of life for peasants leading to frequent revolts against feudal lords (Djuvara 1995; Hitchins 2014a). By the beginning of the 18th century Romania had moved into the Phanariot period. This was a period from 1715 to 1821 when the central authority of the Ottoman Empire, the Porte, appointed members of the Greek merchant class that resided in the Phanar district of Constantinople (modern day Istanbul) to political and administrative positions in Romania as a means of re-establishing Ottoman control in Wallachia and Moldavia. The result was the erosion of traditional institutions and political instability in the principalities, which was further exacerbated by clashes between the Austrian, Ottoman, and Russian Empires leaving Moldavia, Wallachia, and Transylvania often caught in the middle (Georgescu 1991b; Iordachi 2020).

Wallachia and Moldavia would not unite until 1859 when Alexandru Ioan Cuza was voted the ruling prince of Wallachia and Moldavia. He implemented major reforms that would pave the way for a modern Romania, including land reform in 1864 that abolished feudalism. His successor was a Prussian prince, Karl of Hohenzollern-Sigmaringen (1866-1881), who was appointed by Parliament and later become the first King of Romania, King Carol I (1881-1914). Under his rule, all three principalities gained independence from the Ottoman Empire during the Russo-Turkish War (1877-1878) and Romania gained formal recognition as a Kingdom in 1881 (Hitchens 2014).

Romanian Feudalism: Social Class and Roma Slavery in Medieval Romania

Romania has a long history of social stratification with society divided into wealthy noble classes and peasants as far back as the First and Second Bulgarian Empires. Throughout the medieval period, Romania adopted its own form of feudalism characterized by a privileged ruling class of princes and boyars, impoverished free peasants, and Roma slaves.

Romania was (and still is) a mostly rural country, and during the late medieval period was a predominantly agrarian society with peasants performing most of the agricultural work (Hitchins 2014a). The Roma (singular Rom, meaning "man" in the Romani language) are a Romani-speaking nomadic ethnic group thought to have originated in India (Achim 2004a; Georgescu 1991b). The first written records of the Roma in Romania date to 1385 CE in Wallachia and 1400 CE in Moldavia, aligning with the first documentation of Roma slavery in the 14th century. The Tatar (Mongol) invasion in 1241 CE, which brought the Roma to Romania as slaves, may be the origin of their slavery in the Romanian principalities. When the Tatars withdrew in the 14th century, the Roma were acquired by the Romanians who continued to enslave them (Achim 2004b).

The Roma migration route is not known, but linguistic and philological studies have shown the Romani language is part of the Indo-European language family and similar to Sanskrit suggesting the Romani may have originated in India and migrated across Europe over several centuries, possibly between the 9th and 14th centuries. By looking at other Indo-European languages and words that are also present in the Romania language, a possible Romani migration route was reconstructed that went through Persia, Armenia, Asia Minor, the Greek Isles and Byzantine Empire, and eventually into the Balkan peninsula including Bulgaria, Serbia, and Romania (Achim 2004a).

More Roma from Bulgaria and Serbia arrived in Romania in the 15th century after Bulgaria and Serbia fell to the Ottomans (Achim 2004b; Beck 1989). In medieval Romanian society Roma slaves were their own social category representing the lowest of the subjugated classes, ranking below peasants due to their status as property with no legal status. Slavery of the Roma would continue until it was abolished in the mid-19th century (Achim 2004b).

Exploring Stress and Diet in the Romanian Principalities

The medieval and early modern periods brought not only people, but culture, religion, language, goods and resources, politics, ideas, even pathogens such as syphilis, which was first documented in Transylvania in 1501 and possibly brought to Romania by Austrian and Russian armies (Radu et al. 2016). Due to Romania's proximity to both eastern and western empires and cultural influences, Romania was very much a part of the Eastern Orthodox world and drew from the Byzantines in its legal and political structures, but western influences were also present in the Romanian language, which is derived from Latin, and their Roman ancestry. One only has to look at Romania today to see the eastern influences that remain in Romanian cuisine, language, architecture, etc. and the western influences in its current religious and political institutions: for

example, Romania is a majority Christian Orthodox nation and after the fall of communism in 1989 Romania became a parliamentary democratic republic following centuries of rule by the Ottoman Empire, an Islamic Caliphate ruled by a Sultan, followed by a monarchy in the late 19th/early 20th century.

Health is a complicated subject in living people but becomes even more complicated when studying the dead due to paradoxical issues inherent in trying to reconstruct individual and population level health and disease processes from skeletal remains (a can of worms I will open in the next chapter). Incorporating molecular and biogeochemical methods, like stable isotope analysis, into bioarchaeological research can provide valuable data on how a person was interacting with their environment during life, such as the plant and animal protein sources consumed, the water sources they drank, adult nutritional stress, nutritional history during infancy, and even region-of-origin and geographic mobility between childhood and adulthood.

The ratios of different isotopes of carbon and nitrogen in human bones can tell a more detailed story of an individual's life-course and the way their biology intersected and interacted with their environment. Combining stable isotope data with traditional types of macroscopic data collected from the skeleton (age-at-death, biological sex, and skeletal pathologies) can provide possible explanations for why some individuals had skeletal lesions (nutritional stress), what about their life history, and intrinsic factors (age, sex) made their probability of having lesions higher or lower, and what the life history of an individual can tell us about health, disease, and access to resources in the wider population they were a part of (Reitsema and Holder 2018).

By taking a biocultural approach in northeast Romania and combining isotopic evidence of dietary composition with demographic, historical, and pathological data, a more complete picture of health and stress for individuals living in Moldavia during the late medieval-early

modern period can emerge. Thus, as discussed in the introduction, I am exploring the questions about what stressors people were experiencing and what people were eating at this time in Romania's history, with the hypothesis that patterns of stress and diet will differ between sexes, and social classes.

Site Background

The three sites analyzed for this research are Suceava Fortress, Palatul Cnejilor (Cnejilor Palace), and Schitișor. Suceava Fortress is in the historic region of Bucovina, an area on the northern slopes of the Carpathian Mountains that today encompasses both Romania and Ukraine and sits in the plains along the northeast stretch of the Carpathian Mountains. About 72 linear kilometers (45 miles) to the southwest, in the northern stretch of the Carpathian Mountains, is Palatul Cnejilor and its nearby village of Schitișor. Both are located in the historic region of Moldavia in Neamț County in the modern town of Ceahlău (Figure 2.4). All three sites are in what was the Principality of Moldavia during the late medieval-early modern period when the cemeteries were in use until it was unified with Wallachia in 1859.

Suceava Fortress (Cetatea de Scuan a Sucevei)

Suceava Fortress is located on a plateau overlooking the Suceava River, which served as a major trade route, and this position gave it significant strategic advantage against Tatar and Turkish invaders (Figure 2.5). The first evidence of human habitation on the plateau dates to the Eneolithic (5000 – 3000 BC), with evidence of habitation continuing through the Bronze Age, Dacian period (2nd century BC), the early medieval/late migration period (8-10th century CE) and into the late medieval-early modern period (13th – 18th centuries CE). Habitation continued into the modern period and is still present today, along with what is left of the original fortress (Batariuc 1993) (Figure 2.6). Suceava Fortress was first excavated between 1895-1904 by Karl

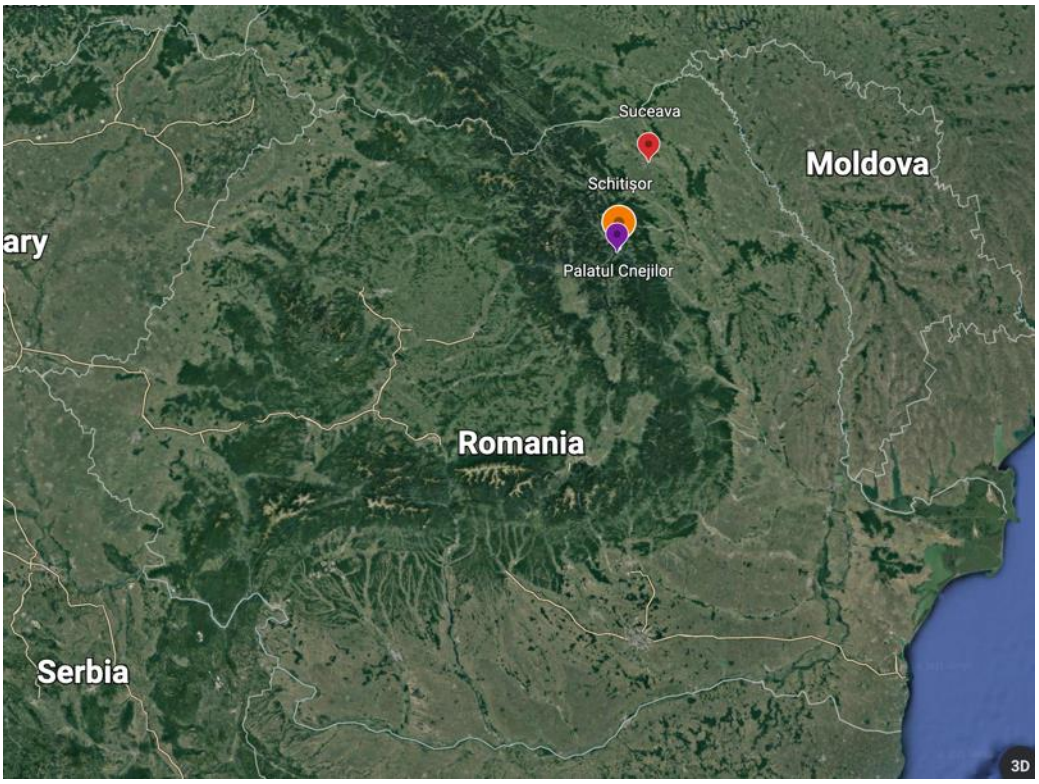


Figure 2.4. Locations of the three study sites: Suceava (red), Schitișor (orange), and Palatul Cnejilor (purple).

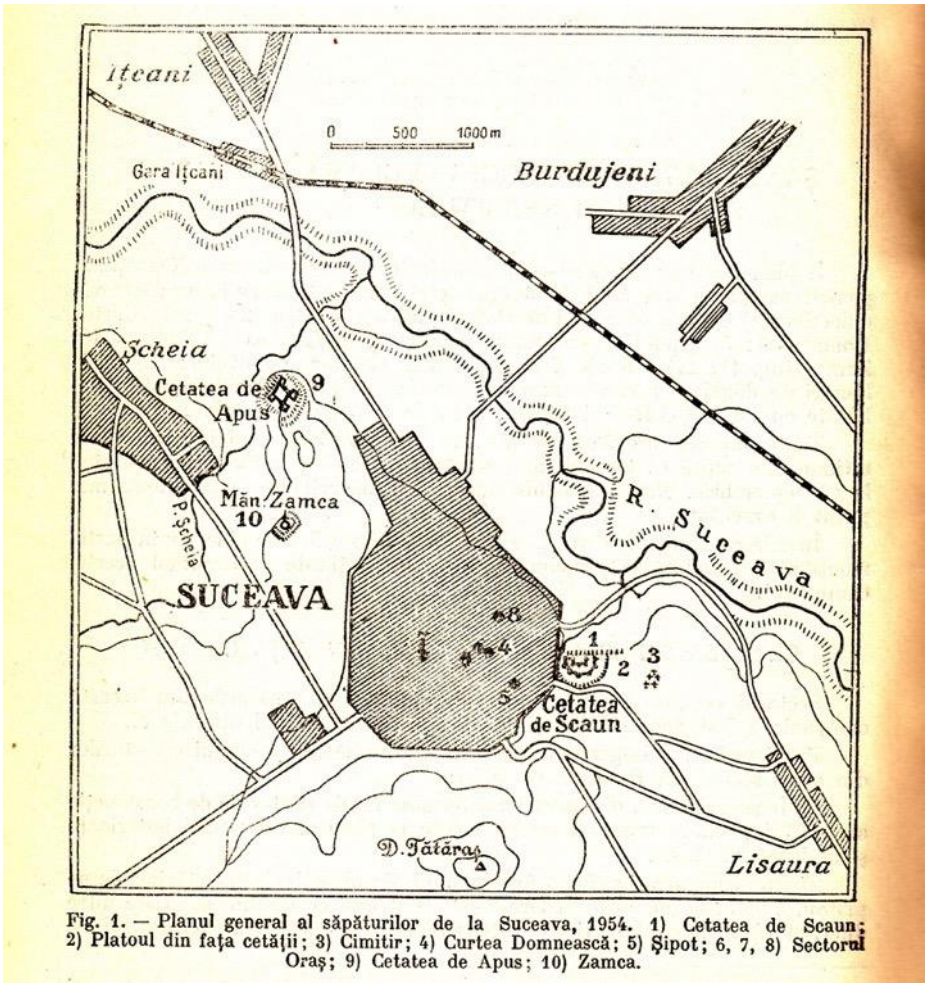


Fig. 1. — Planul general al săpăturilor de la Suceava, 1954. 1) Cetatea de Scaun; 2) Platoul din faţa cetăţii; 3) Cimitir; 4) Curtea Domnească; 5) Şipot; 6, 7, 8) Sectorul Oraş; 9) Cetatea de Apus; 10) Zamca.

Figure 2.5. Figure of the excavation plans at Suceava showing its location relative to the river. 1) Suceava Fortress, 2) plateau in front of the Fortress, 3) Cemetery (Mitrea B. et al. 1955).



Figure 2.6. Suceava fortress (2022). White line demarcates where the original fortress ends and reconstructions begins (everything above line). Photographed by J. Watson 2022.

Romstorfer. These excavations lead to the discovery of the foundations of a church and three graves. The associated cemetery on the southeastern side of the citadel was plowed, resulting in the name "Field of Ditches", which may have resulted in the disturbance of several graves, but it is thought the graves were deep enough to avoid significant disturbance (Figure 2.7). Excavations were resumed in 1951 by Ion Nestor. In 1952 Nestor began excavating the Field of Ditches and between 1953-1955 they excavated a medieval cemetery found in the east and southeast portions of the plateau (Figure 2.8). Nestor also reopened the church foundations and discovered evidence of two churches, one that was likely made of wood and dates to the 15th century. Traces of fire were present suggesting it was burned, possibly during the Polish siege of 1497 that was likely the cause of the destruction of other buildings on the plateau as well. The other chapel, which was made of river stone and mortar, was likely in use until the 17th century, and the largest density of graves was found around this chapel (Batariuc 1993).

The earliest coins found date to the 14th century during the reign of Petru I (Peter I) from 1375 to 1391 and the latest coins date to 1526 (16th century) during the reign of Ludovic II (Louis II) of Hungary (1516-1526). The chapel's destruction and the end of the cemetery's use likely came with the Turkish Siege in the summer of 1538 when Sultan Soliman lead the Ottoman Army in a siege attack of the citadel. At this time, the ruler was Petru Rareș (1527-1538 and 1541-1546) and Moldavia was under Ottoman suzerainty. The dates of the coins and the date of the Turkish siege put the timeframe for the cemetery between 1375-1538 CE (14th – 16th centuries CE). It is thought that the Turks, who were Muslim, banned Christian burials and possibly desecrated the site and destroyed the church and nearby buildings (Batariuc 1993).

Four types of grave constructions were documented during the excavations that are thought to correspond to the social status of the person buried. Most graves were rectangular or



Figure 2.7. Remains of trenches dug as part of the cemetery excavation at Suceava called “Field of Ditches” (photographed by J. Watson 2022)

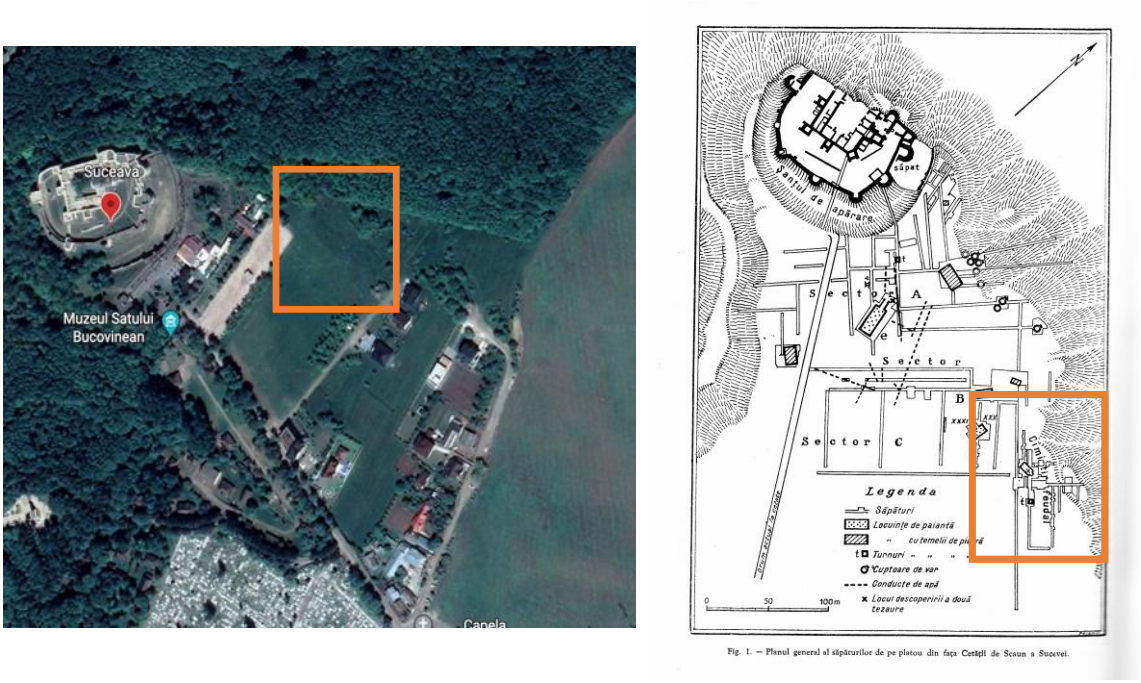


Fig. 1. — Planul general al săpăturilor de pe platou din fața Cetății de Scaun a Sucevei.

Figure 2.8. General ecavation plan of Suceava. The orange box indicates location of the cemetery that was excavated "*Cimitir feudal* (Feudal Cemetery)" (Nestor et al. 1959).

oval pit graves at a depth ranging from 0.50-1.20 meters, with most graves being 0.80 meters deep. These would have been for lower status individuals, likely peasants living around the fortress. Graves that indicated higher status, such as merchants or nobility, were either pit graves covered in multiple layers of flagstone which served to mark the place of burial, or the margins were lined with brick or flagstone. The fourth burial style was vault graves made of brick and mortar with an arched roof that contained a wood coffin. These likely contained high status individuals like the boyars (nobles) and rulers of the court (Figure 2.9). It is not fully understood why, but reburials were also a common practice in the medieval period, usually found in pit graves and often resulting in two or more individuals being reburied together (Batariuc 1993).

All burials followed the Christian practice of the time, which consisted of orienting the individuals with the head to west and feet to the east, and arms bent at the elbows with hands placed on the abdomen or the chest (Figure 2.10). Most of the burials had traces of trapezoid shaped coffins made of wood, with remnants of charcoal found under the coffin. This was related to the use of burning charcoal or incense in a censer, a common practice in Christian funerals. The remains of the charcoal are then placed in the bottom of the grave before the individual is placed inside. Many graves also contained coins, fragments of clothing, buttons, silver, bronze, or wooden crosses, and jewelry including silver, plated gold, or amber earrings and rings, as well as beads that were likely a necklace based on their location near an individual's neck (Figure 2.11). When coins were found they were usually in a bag or tied together with hemp and placed in the individual's left hand. The presence of silk cloth fragments and gold jewelry indicated the presence of a higher status individual in the burial. A typical medieval cemetery would have consisted of graves in rows with children usually buried in a separate area since they were not

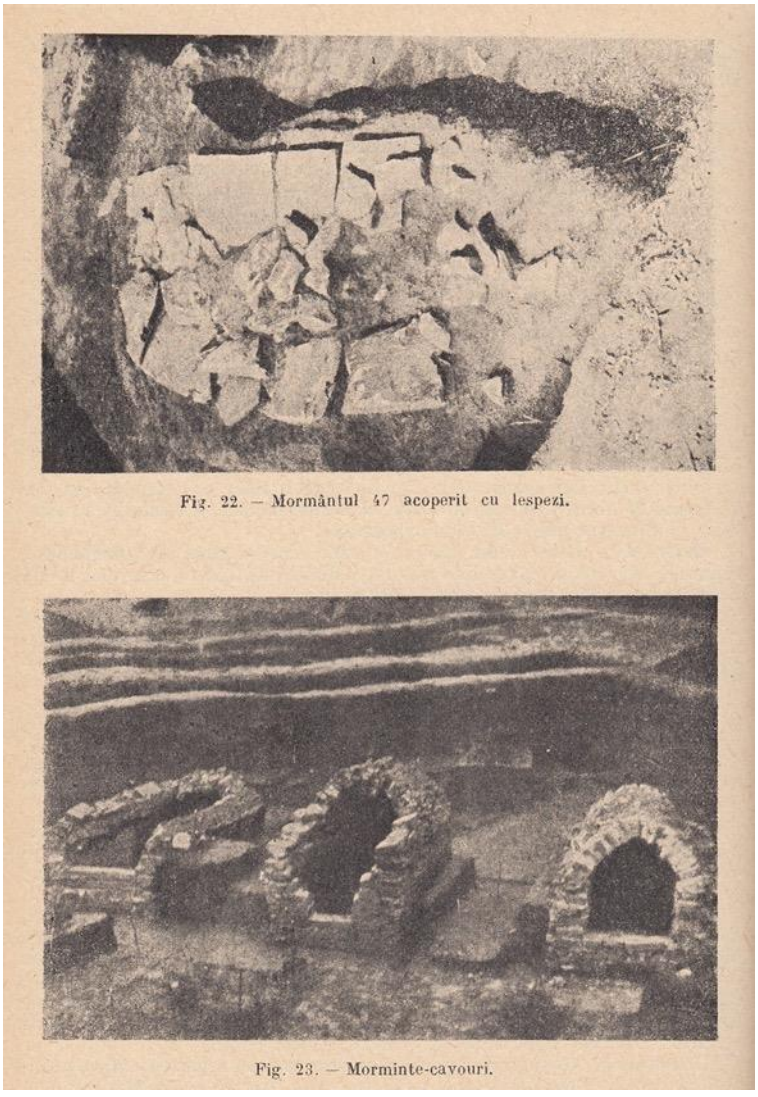
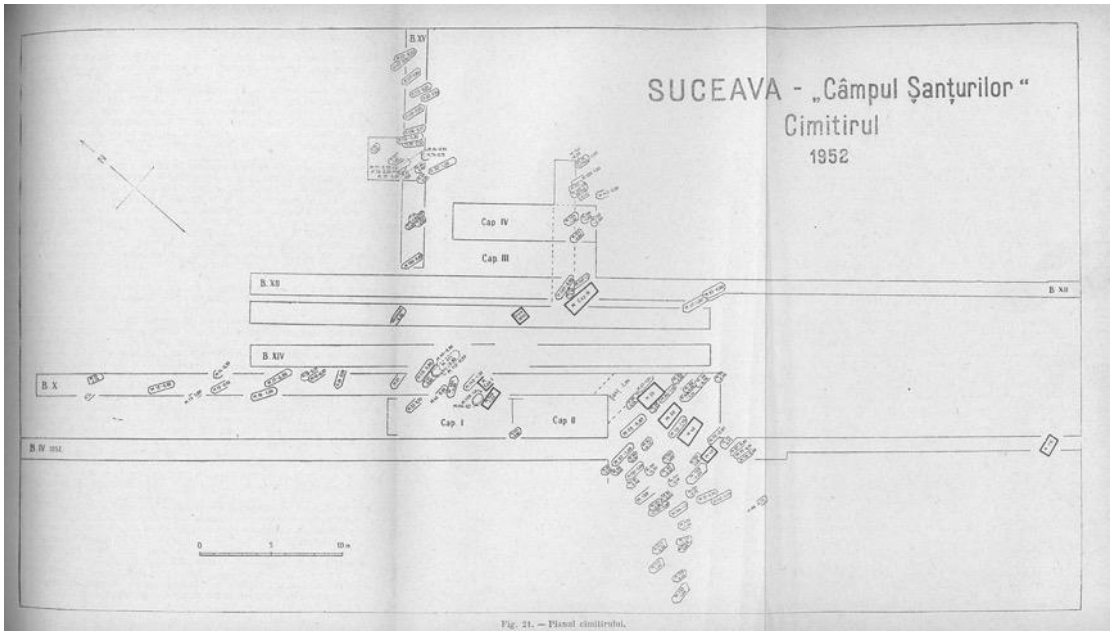


Fig. 22. — Mormântul 47 acoperit cu lespezi.

Fig. 23. — Morminte-cavouri.

Figure 2.9. Top: Photograph of a burial covered in layers of flagstone. Bottom: Higher status vault graves made of bricks and mortar (Mitrea and Nestor 1953).



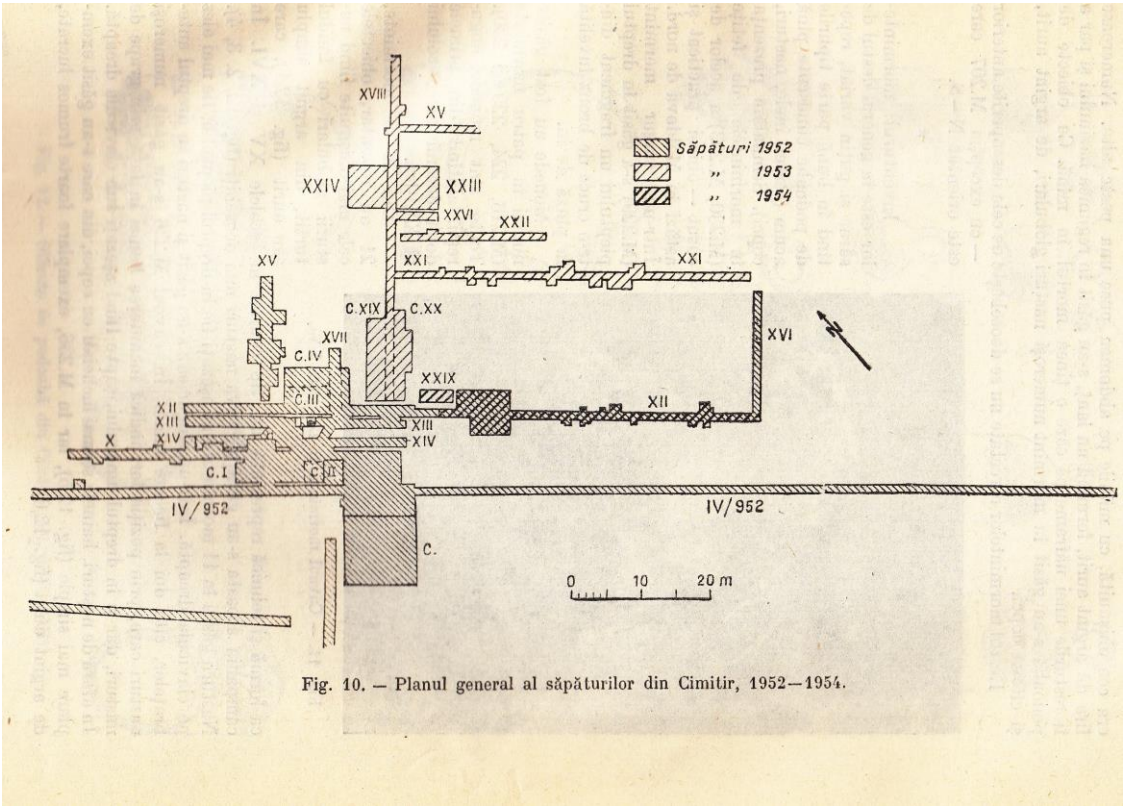


Fig. 10. — Planul general al săpăturilor din Cimitir, 1952—1954.

Figure 2.10. Top: Cemetery excavation map from 1952 showing locations and orientations of the graves (Mitrea and Nestor 1953). Bottom: Cemetery excavation maps for 1952, 1953, and 1954 field seasons (Mitrea B. et al. 1955).

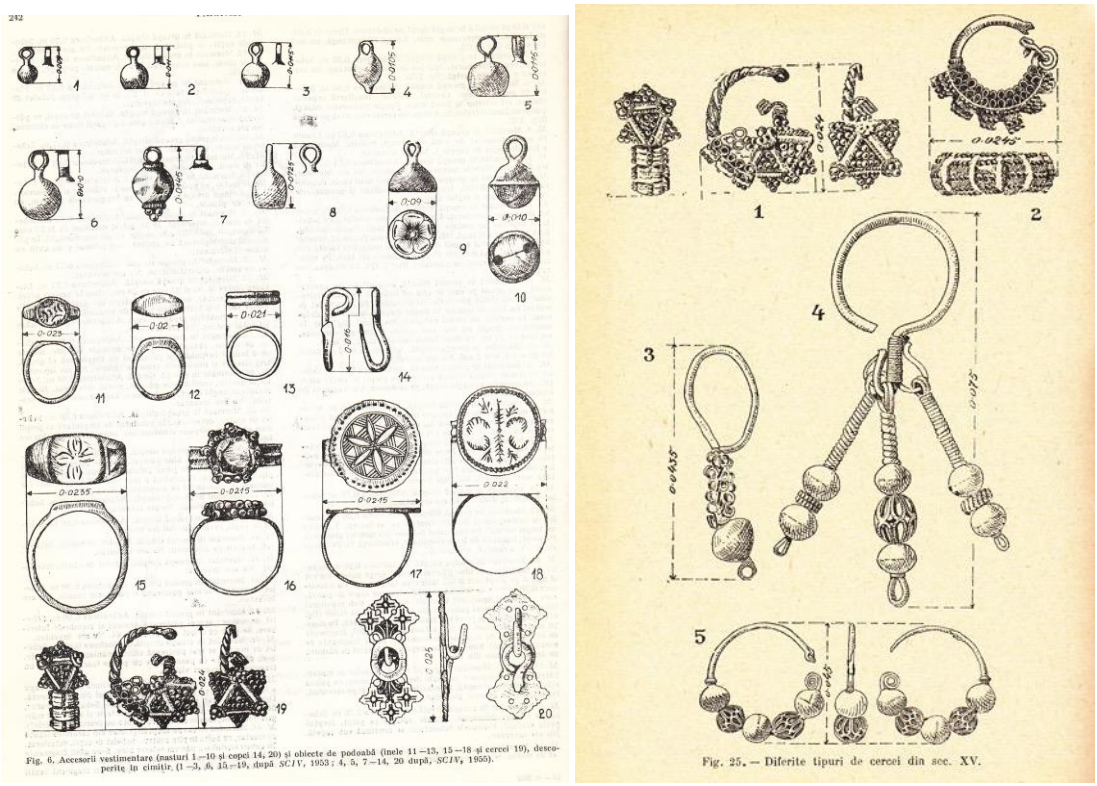


Fig. 6. Accesorii vestimentare (nasturi 1—10 și copci 14, 20) și obiecte de podoabă (inele 11—13, 15—18 și cercei 19), descoperite în cimitir. (1—3, 6, 15—19, după *SCIV*, 1953; 4, 5, 7—14, 20 după, *SCIV*, 1955).

Fig. 25. — Diferite tipuri de cercei din sec. XV.

Figure 2.11. Left: Drawings of buttons, rings, and earrings found in graves at Suceava (Batariuc 1993). Right: Drawings of earrings dating to the 15th century found in graves at Suceava (Mitrea and Nestor 1953).

baptized. However, this typical pattern is not seen at Suceava. Instead, several areas of the cemetery had two to three burials on top of each other, possibly due to space limitations. Both adults and juveniles were recovered from the graves, and at the time of excavation it was estimated that 43% of the cemetery was subadults (Batariuc 1993).

The fortress itself was likely inhabited by the ruler or "voivod" of Moldavia, members of the princely court who were part of the boyar class (the nobility), as well as soldiers who guarded the fortress. Evidence of houses, ovens, and ceramic, metal, and mason workshops were excavated directly outside the fortress which suggested the presence of merchants and craftsmen who served the princely court and produced brick, stonework, ceramic, metal goods, etc. (Nestor et al. 1957).

There were likely also settlements of peasants in the areas surrounding the fortress who were buried in the cemetery. The presence of women and children suggests the cemetery was not limited to only higher status individuals or soldiers stationed at the fortress. Overall, the grave goods and grave styles all indicate that most of the individuals buried in this cemetery were of modest to low social status. However, a few higher status individuals like merchants, craftsmen, and palace rulers were present based on the use of flagstone in some burials and the presence of brick vault burials (Batariuc 1993).

Palatul Cnejilor (Cnejilor Palace)

Cnejilor Palace consists of a fortified palace, much like Suceava, with a church inside its walls in the northern stretch of the Carpathian Mountains. Like Suceava, it also sits in a strategic location atop a plateau with the River Schit (pronounced *skit*) running to the east placing it in a strategic position for defending against attacks. The site and cemetery were excavated between 1956-1958 by Gheorghe Diaconu from the Institute of Archaeology in Bucharest. The oldest

evidence of medieval habitation was dated to the 17th century CE and the most recent to the 19th century CE. The church was built in 1639 by Gheorghe Coci who was the brother of the ruler of Moldavia at the time, Vasile Lupu (1634-1653). The walls of the church were 1.2 meters thick and small windows in the bell tower made it possible to point muskets outside to oncoming attackers, suggesting the church also had a defensive purpose. This was a common way for churches associated with defensive fortresses to be built as attacks from Tatars, Poles, and the Ottomans were common (Diaconu 2003).

Palatul Cnejilor consisted of stone walls with four towers, one in each corner, with paths along the top of each wall that allowed soldiers to move around and patrol. In total the fortress was 3000 square meters and likely required at least 200 soldiers to defend it. On the east and southern parts of the fortress were small houses covered with adobe (usually a mixture of clay or earth and water) typical of monk houses that date to the 17th century. According to Diaconu (2003), evidence of ovens that were used for iron working as well as for firing ceramics were also found near the fortress suggesting the presence of a small market that likely produced ceramics and metal goods, several of which were recovered in the excavations including fire pokers, knives, keys, and fire tongs. Bronze, copper, and silver tools were also found near the church and according to Diaconu (2003) were likely ceremonial. Evidence of woodworking and stone mason shops were also recovered.

Like Suceava, Palatul Cnejilor would have had blacksmiths, masons, ceramicists, and other trades people who produced all the goods needed by the fortress and the church. Also recovered from the site of the fortress were pieces of glazed pottery with patterns consistent with pottery from the Baltic or North Sea region, and Anatolia. This suggests the presence of trade

with these regions, and these goods likely were imported to the nearby cities of Suceava or Iasi and then transported to Palatul Cnejilor (Diaconu 2003).

In 1672 after the construction of the church and adobe houses, there was a fire that burned the houses that according to Diaconu (2003) was likely from a Tatar attack. As a result, an outer fortification wall and then more houses were constructed. While the fortress itself was likely a summer home for the Moldavian ruler, the church was used continuously and the monks would have lived there year-round, as well as the secular individuals living nearby. The graves excavated from the cemetery around the church belonged to monks as well as the secular/common people living around the fortress. The graves of secular individuals contained bronze rings, bronze or bone buttons, and small bells were often found in subadult burials. Monk burials had fewer grave goods and bricks were often placed under their heads. While there is no documentation of the grave styles at Palatul Cnejilor, they were likely the typical grave style of the time, which was pit graves at least one meter deep. There is no documentation of vault graves, like those found in Suceava that indicate noble individuals, but graves with richer inventories were excavated that suggest higher status individuals, possible palace rulers (Diaconu 2003). In 1820, the church was rebuilt and today only ruins of the north and west towers of the fortress remain. The church is still present within the ruins of the fortress and in use by the local community (Figures 2.12-2.13).

Schitișor

Schitișor (pronounced *Skit-ee-shore*) was a small hermitage (village) about 1.88 kilometers (1.17 miles) from Cnejilor Palace. Salvage excavations between 1956-1957 found two small houses, one dating to the 17th century and the other dating to the early 19th century, and a church. The houses consisted of a stone foundation, and wooden walls sealed with adobe



Figure 2.12. Remains of the fortress towers (photographed by J. Watson 2022).



Figure 2.13. Rebuilt church that sits within the remains of Palatul Cnejilor (photographed by J. Watson 2022).

on the outside. The remains of a stove were found in one house along with decorative tiles that typically were placed around the outside of the stove. It is thought that some tiles may have been imported from Transylvania while some tiles and other ceramics were produced at Cnejilor Palace, suggesting Schitișor had a close association with Cnejilor Palace. Hungarian coins were also found suggesting trade between nearby Hungarian controlled Transylvania and Schitișor and Cnejilor Palace. Evidence of fire as well as arrow heads were found during the excavations of the houses, suggesting they may have been destroyed in an attack. According to Zaharia and Zaharia (2003), these houses likely belonged to peasants who were directly connected to the small church and relied on Cnejilor Palace for various goods (Zaharia and Zaharia 2003).

The church itself was made of wood and had a cemetery. Archaeologists recovered 61 graves from this cemetery, 11 of which were dated to the 17th century and the remaining 50 to the 18th/early 19th century based on coins and ceramics recovered from the site (Figure 2.14). The graves were oval/rectangular pits placed in parallel rows, grouped around the church. The depths were between 0.45 to 1.0 meter in depth. Four graves had clay bricks inside, which is usually indicative of a monk or nun burial. Individuals were buried according to the Christian tradition, laying supine and oriented West-East with the hands placed on the abdomen or chest. Today, only a small house remains where the original houses, church, and cemetery were located (Figure 2.15) (Zaharia and Zaharia 2003).

History of the Francisc I. Rainer Institute of Anthropology (FRIA)

The Francisc I. Rainer Institute of Anthropology of the Romanian Academy currently houses one of the largest human osteological collections in Europe. Francisc Rainer was born in 1874 and served as the director of the Institute of Anatomy and Embryology at the Medical School in Bucharest, Romania as well as a professor of anatomy from 1920 until his retirement

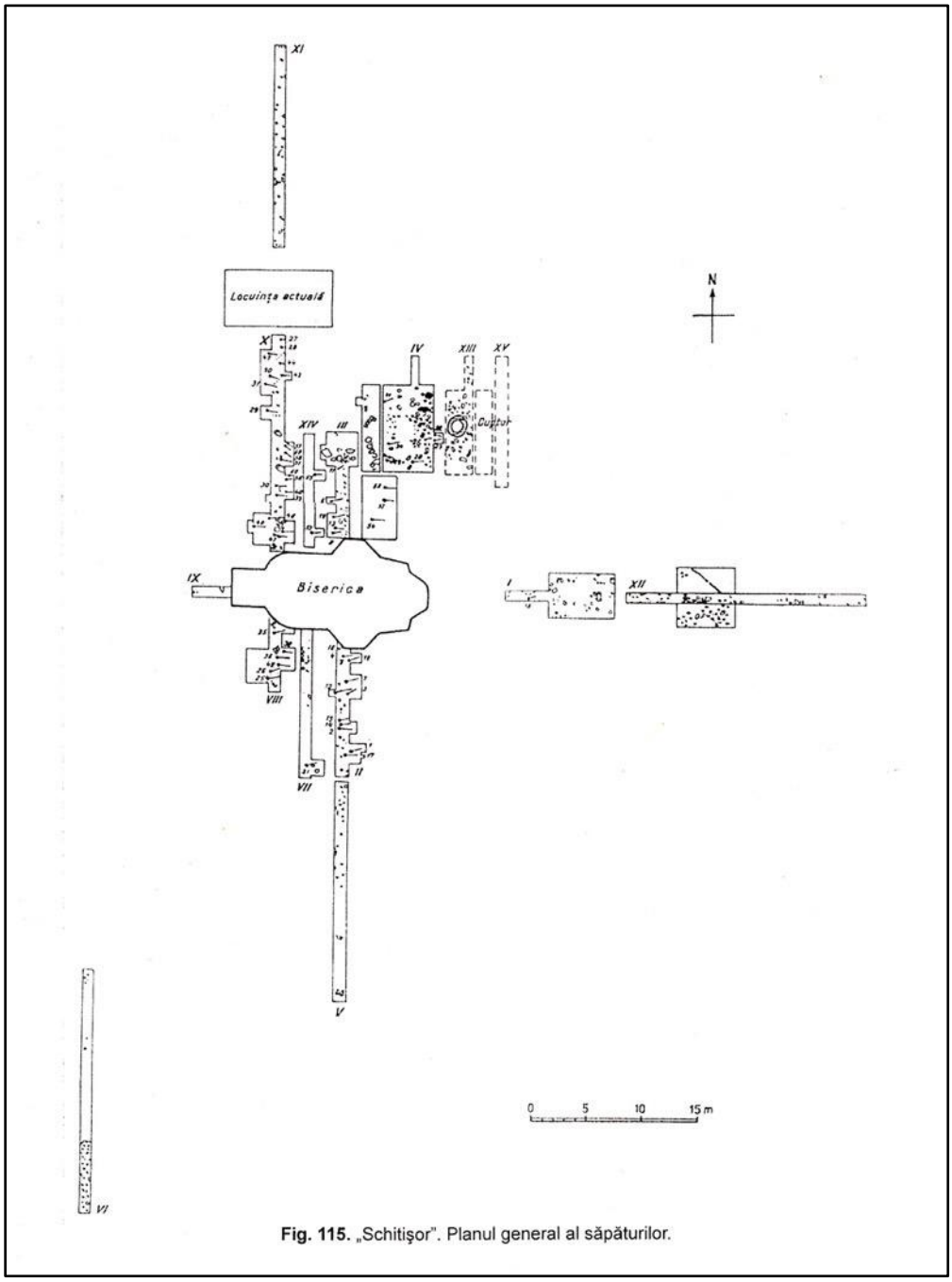


Fig. 115. „Schitişor". Planul general al săpăturilor.

Figure 2.14. Cemetery excavation map for Schitișor (Zaharia and Zaharia 2003). The church (*Biserica*) is in the middle with burials extending to the north, south, and east around it.



Figure 2.15. House and small associated structure that now occupy the excavation site (photographed by J. Watson 2022).

in 1940. Rainer amassed a large collection of human skeletal remains during his tenure, procured primarily from cadavers used for dissection at the medical school. Prior to his tenure in 1919, Paul Petrini, the head of the Anatomy Museum of the Medical School at the University of Bucharest, sought to create a new institution that would focus on growing an osteological collection to continue anthropological research, specifically racial studies. After World War I Romania was a newly unified nation state and thus there was a lot of interest in using scientific fields like anthropology to create a biological basis for Romanian ethnicity and nationality, a goal not dissimilar to the racial science of the United States that sought to find biological differences between White and Black people (Ion 2011).

Petrini's institute was not brought to fruition until Rainer's tenure as director of the Institute of Anatomy. Since 1900 Rainer had collected osteological material that he used in anatomy instruction and the majority of his collection was amassed between 1931-1940 with the rest collected in the 1950s. This resulted in the creation of the Institute of Anthropology in 1937, which was separate from the Institute of Anatomy, but part of the University of Bucharest. As of 1940 the collection was comprised of 4000 crania and 600 bone histology samples. Now, the collection contains 6800 crania of which 3585 have been inventoried. The data recorded for these skulls includes age, sex, ethnicity, pathology, cause of death and profession, and half of the crania are of known individuals. The crania are from bodies that were acquired from 33 hospital and morgues in Bucharest and used for anatomical dissection with the crania later retained for anthropological and anatomical study. Like the Terry and Hamann-Todd collections in the United States, these individuals were mostly poor and thus were likely given to the medical school because their remains were unclaimed and there is no record of their consent for donation (Ion 2011).

The occupations recorded for these individuals include workers, peasants, servants, and housewives, as well as individuals that were classified as “beggars”, “prostitutes”, and “vagrants”. Most causes of death were chronic and infectious disease like tuberculosis, pneumonia, and cardiovascular disease, as well as dementia, suicide, and execution. 93% were classified as “Romanian” and 235 individuals belonged to ethnic minority groups that were present in Romania during this time including Germans, Hungarians, Jews, Roma, and Turks (Ion 2011).

In addition to the modern collection of crania, the Rainer Institute now houses remains excavated from archaeological sites including prehistoric sites from the Iron and Bronze Ages, as well as late medieval and early modern sites. Many of these sites, including the sites analyzed for this research were excavated in the 1950s, during the Communist rule in Romania. Human remains were not always of interest to or the focus on the archaeologists excavating these sites. As a result, the remains were curated at the Rainer Institute but were not analyzed right away, as was the case with Suceava, Palatul Cnejilor, and Schitișor which remained curated at the Rainer Institute since the mid 1950s until my analysis in 2021 and 2022.

CHAPTER THREE: BIOARCHAEOLOGICAL THEORETICAL FRAMEWORK

Chapter Overview

In this chapter, I discuss the theoretical orientation of this research for understanding skeletal stress, health, and the external social and environmental factors that intersect with biology to create differential health experiences and stress patterns in past populations. In the first part of the chapter, I discuss the concepts of stress and health as they are studied and understood in bioarchaeology and how the introduction of a theoretical paradigm by Wood and colleagues (1992), the Osteological Paradox, reframed how paleopathologists and bioarchaeologists interpret skeletal lesions and what they mean for studies of past health. I summarize responses to the Osteological Paradox and how it has (or has not) been operationalized in bioarchaeological research over the past 30 years.

In the second part of the chapter, I discuss the biomolecular underpinnings of bone remodeling, inflammation, and the body's stress response, and how these processes affect the skeleton in ways that bioarchaeologists can study. I then summarize each of the lesions analyzed for this research, periosteal new bone formation (PNBF), porotic lesions of the skull (porotic hyperostosis and cribra orbitalia), and dental disease (caries, abscesses, and periodontitis), how they are formed, and how they help bioarchaeologists better understand the inflammatory process and physiological stress. I end this chapter with a discussion of biocultural theory, specifically how it provides a theoretical framework for combining multiple lines of evidence, to understand human behavior in the past and how it is used to understand health in late medieval-early modern Romania.

What is Stress and What is Health?

One of the main goals of contemporary paleopathology is to understand how stress is embodied in the human skeleton and the correct interpretation of stress markers to reconstruct the health of past people. As a result, any discussion of these goals and where the field stands in terms of its ability to achieve these goals must begin with the (dreaded) question, what is stress? This naturally begs another question, what is health? The terms "stress" and "health" are often used in the bioarchaeological and paleopathological literature. They are broad and vague terms that are often used interchangeably, but it is important to discuss how we as bioarchaeologists define stress and health.

Health, as defined by the World Health Organization (WHO) is physical, mental, and social well-being, and is not simply the absence of stress or disease (World Health Organization 2023). However, I think most people would include the absence of disease, injury, mental illness, and stress in their definition of health. Essentially, health is the absence of any stressors. However, this definition makes it nearly impossible for anyone to qualify as "healthy". In terms of understanding health in archaeological populations, mental health, many diseases, and completely healed past injuries are impossible to see in the skeleton, further complicating the goal of assessing the "health" of past populations from their skeletal remains.

The human physiological stress response is a reaction to an external or internal stressor, such as a pathogen, that affects the various mechanisms that work to maintain homeostasis in the human body, resulting in a homeostatic imbalance. Stress as a concept in bioarchaeology has been around since the 1970s, but studies of stress in past populations were mostly typological. Goodman and colleagues (1984) developed an ecological model of stress for bioarchaeological studies. This model addresses how cultural buffering systems and intrinsic biological factors of

each individual produce significant variability within a population in how people resist or succumb to stress, and how individuals can respond to homeostatic imbalance, often at the expense of energy and resources to crucial body systems necessary for growth, reproduction, and long-term health (Goodman et al. 1984; Temple and Goodman 2014). Our understanding of stress has expanded beyond just the physiological mechanisms that govern the stress response in humans and the extensively studied stressors in bioarchaeological contexts like pathogens (viruses, bacteria, and parasites), metabolic diseases (rickets, scurvy), and cancer (primary bone neoplasms and metastatic cancer) (Temple and Goodman 2014). Now, it is understood in bioarchaeological research that stressors can also be from environmental, social, and psychological factors like food insecurity and malnutrition, climate change, recurrent physical injury, emotional stress, displacement, migration, discrimination, racism, and sexism (Dent et al. 2020; Temple 2019). There are myriad ways these stressors can affect an individual on a biological and epigenetic level by triggering a physiological stress response resulting in real biological consequences for an individual's health.

This idea that individuals will vary in their ability to meet and overcome the effects of stress due to intrinsic biological factors, as well as external factors like cultural buffering systems, prompts the need for a more complex definition of health. Rather than the absence of stress and its effects, health is the ability of an individual to produce a robust physiological stress response to an external stressor, survive that stress response, and then return to homeostasis (Temple and Goodman 2014; Wilson 2014). For bioarchaeologists who study stress and health in human skeletal remains, this means that neither individuals with lesions nor without lesions are inherently unhealthy nor healthy, one of the key tenants of the Osteological Paradox (OP) (Wood et al. 1992) and demands the field move beyond typological labels of "health" or "unhealthy"

and instead accept that it is possible for two seemingly conflicting facts to be true at once, that a person is both stressed and healthy, and to consider and hold seemingly conflicting ideas at once when drawing conclusions about past human health based on skeletal remains. This sort of reevaluation of stress and health, and how we interpret and draw meaning from skeletal lesions is exactly what Wood and colleagues were calling upon paleopathologists and bioarchaeologists to do with the publication of their seminal paper introducing a new theoretical framework called The Osteological Paradox (Wood et al. 1992).

The Osteological Paradox

The main goal of paleopathology and paleodemography is to be able to accurately measure and interpret health differences in past populations, to understand population-level changes in health across time and space, and to understand how humans have adapted to these health challenges. Early paleopathological studies focused on describing lesions on an individual level rather than looking at population-level patterns, and there was an assumption that calculating lesion frequencies or mean age-at-death was reflective of the health of that population: more lesions and lower age-at-death meant worse health and likely an increase in certain conditions that caused the observed lesions (Wood et al. 1992). The inherent bias in studying past populations and their health from a collection of often partial skeletons of individuals who are dead (and died for a reason) was recognized and spurred conversation about the issues and limits of age estimation, life tables, and how well skeletal lesions represent population-level patterns of stress and health (Wood et al. 1992).

Bringing together the dialogue and scholarship surrounding these issues in paleopathology, paleodemography, and bioarchaeology, Wood and colleagues (1992) published *The Osteological Paradox: Problems of Inferring Prehistoric Health from Skeletal Samples*. This

article introduced a new theoretical paradigm that addressed three major biases present when studying the health and demography of past populations from skeletal remains. The authors called for reconsideration of how we interpret skeletal lesions and urged the field beyond typological approaches. These three biases are collectively referred to as the Osteological Paradox and are demographic non-stationarity, selective mortality, and hidden heterogeneity in risk of death (Wood et al. 1992).

Demographic Non-Stationarity

A population in a stationary state is characterized by zero migration, constant age-specific fertility and mortality, and zero growth (birth and death rates in equilibrium). This is not a realistic state for any human population and most populations are non-stationary: people move in and out via migration, birth and death rates are not equal, and age-specific mortality is not constant across all individuals. In non-stationary populations, age-at-death distributions are more sensitive to changes in fertility, not changes in mortality. As a result, small changes in fertility (an increased birth rate) will have a much larger effect on that population's age-at-death distribution (Sattenspiel and Harpending 1983).

For example, in a population with high fertility and a high birth rate, there will be an influx of young individuals into the population, driving down the mean age of the population. Skeletal assemblages that bioarchaeologists study come from cemetery sites and are made up of individuals who were selectively removed from that population (death). Due to high fertility, the population whose dead created a future skeletal assemblage has a lower mean age-at-death, not because people were dying younger, but because there were simply more young people in the population due to high fertility. As a result, this lowers the average age-at-death of the skeletal assemblage making it seem like more young people were dying, when in fact the skeletal

assemblage simply represents a population with high fertility. The opposite is true for populations with low fertility. Fewer births drive up the mean age of the population, which also drives up the mean age-at-death of the individuals who die, making it appear as if people were living longer when in fact fertility was low (Sattenspiel and Harpending 1983; Wood et al. 1992).

Selective Mortality and Hidden Heterogeneity in Risks

Selective mortality and hidden heterogeneity in risks are interrelated as selection does not act on homogenous populations. Selective mortality is a concept that describes the bias present in all skeletal samples – everyone in the sample is dead. Skeletal samples represent those from all age cohorts who were selected out of the larger population by death and represent those of each age with the highest age-specific risk of death. This can result in an overrepresentation of lesions that increase one's risk of death at each age, making it appear as if the prevalence of these lesions in the larger population was high. Hidden heterogeneity describes the fact that populations from which skeletal samples are derived are comprised of individuals with different disease risks and health histories and thus varying levels of underlying frailty (i.e. susceptibility to disease and death). Not everyone in a population has the same age-specific risk of death. This heterogeneity provides something for selective mortality to act on, which ultimately produces the skeletal assemblages that bioarchaeologists study (Wood et al. 1992).

As a result of these three biases, in particular hidden heterogeneity and selective mortality, it is very difficult to extrapolate population-level data about frailty from a skeletal sample as it cannot be assumed that no lesion equals healthy, or lesions equal not healthy. Rather, because only some disease processes leave evidence on the skeleton and can take years or decades to develop, not everyone who has a disease that can produce skeletal lesions will

necessarily have skeletal evidence of that disease. Those without lesions could represent individuals who died without disease (low frailty), or those who were the frailest and had an acute disease process that caused them to die quickly before any skeletal changes could occur. Individuals with lesions could also represent the frailest individuals who died while experiencing an active disease process or who survived a disease process long enough for lesions to form, and if there is evidence of healing, survived long enough to begin to recover, representing the least frail in the population. This creates a paradox that makes simply calculating lesion prevalence and extrapolating that to the larger population problematic as it ignores the biases inherent in skeletal samples and assumes that lesions always equal poor health (Wood et al. 1992).

While lesions can certainly mean poor health, as previously explained, the OP allows for a reframing of our interpretations of lesions and how we think about stress and health. The OP makes it possible to think about stress and health in a more nuanced way and allows bioarchaeologists to accept that a person with stress lesions can not only be healthy but could represent the "healthiest" or least frail individual in a sample (Wood et al. 1992).

Responses to the Osteological Paradox and Implications for Bioarchaeology Research

After the OPs publication in 1992, it received a polarizing response. While some responses agreed and recognized Wood and colleagues' argument as well reasoned with important implications for the field of paleopathology, several respondents pointed out gaps in their argument or exceptions to the OP. In his reply, Cohen pointed out that conclusions about population health from skeletal assemblages do not rely simply on skeletal lesions, but rather use data from multiple sources. He cites the example of increased infection as a result of the rise of sedentary, agricultural populations, a trend not just supported by the skeletal evidence but by epidemiological and ethnographic data (Wood et al. 1992). Wilkinson pointed out that the idea

that “better health makes for worse skeletons” (Wood et al. 1992:356) may not be an accurate statement for certain disease processes like treponemal disease or leprosy, which leave distinctive lesions on the bone and if contracted by an individual, can lead to severe disease and death, and arguably much worse health (Wood et al. 1992).

Despite the Osteological Paradox and its varied responses, the subsequent 30 years have not produced a significant amount of research directly interrogating its tenets. DeWitte and Stojanowski (2015) reviewed the effects of the Osteological Paradox on the fields of bioarchaeology and paleopathology and how well the research produced in the 20 years after its publication has engaged with Wood and colleagues’ call to action. DeWitte and Stojanowski found that most papers that had cited Wood and colleagues in the last 20 years used the Osteological Paradox as a discussion point to address possible limitations in their study or as an interpretative framework for their results. Several studies did engage with Wood and colleagues’ call to directly address the OP in their research design. For example, using samples from populations with known chronologies and non-complex social structures, applying biomolecular approaches to understand the genetic and epigenetic underpinnings of various diseases, and exploring the etiology and physiology of skeletal lesions (DeWitte and Stojanowski 2015; Wilson 2014).

DeWitte and Stojanowski put forth several recommendations for future bioarchaeological and paleopathological research, including better connections between modern clinical research and paleopathology to better engage with the pathophysiology of skeletal lesions and understand the sources of frailty in a population (DeWitte and Stojanowski 2015). This is especially the case for non-specific stress lesions like periosteal new bone formation (PNBF), porotic lesions of the skull (cribra orbitalia and porotic hyperostosis), periodontal disease, and dental caries and

abscesses that cannot be attributed to one disease process but have been shown to be informative about mortality risk and frailty (DeWitte and Stojanowski 2015). Advances in ancient biomolecular research and their application to paleopathological research also have the potential to help researchers interrogate the Osteological Paradox. For example, DeWitte and Stojanowski highlight the utility of ancient DNA analysis to identify specific microbes in skeletal samples, genetic analysis that can identify genes specific to a disease and make an individual more susceptible to disease, and stable isotope analysis that can identify sources of heterogeneity in a population such as migrants and dietary variation (DeWitte and Stojanowski 2015).

While the purpose of this dissertation is not to directly interrogate the OP, it is moving beyond simple documentation of lesions on skeletal remains and instead documenting patterns of physiological stress and incorporating biogeochemical methods to identify possible sources of heterogeneity in these medieval Romanian populations that would otherwise not be visible. Specifically, the presence of migrant or non-local individuals and dietary composition and how it varies by age, sex, migrant status, class, and site. Migration, dietary composition, and who had access to what resources are sources of hidden heterogeneity that may have had a significant influence on the age-specific risk of death and who presents with skeletal lesions in this sample. Additionally, diseases may affect how isotopes from food and water are taken up by the body's digestive system and the fractionation of those isotopes as they are routed to various body tissues, resulting in another source of hidden heterogeneity in a population (DeWitte and Stojanowski 2015). Isotopic data interpretation should always be considered within the context of historical and archaeological data. This context is important for interpreting stable isotope data from human tissues, determining what conclusions can be drawn about diet, migration, and

health, and beginning to disentangle the many sources of hidden heterogeneity in a population from which a skeletal assemblage is derived.

Skeletal Biology of Bone Remodeling, Inflammation, and Stress

The shift in paleopathology toward understanding the underlying pathophysiology and biochemistry of skeletal lesions and bone-immune system interactions provides a promising avenue for addressing and interrogating the OP in paleopathology and bioarchaeology research. The fields of skeletal biology and osteoimmunology are contributing significantly to our understanding of physiological stress and the cascading effect it has on various organ systems, the delicate homeostatic balance our body must maintain, and ultimately its effect on bone remodeling (Crespo 2021; Dent et al. 2020; Klaus 2014).

Bone Remodeling

Bone remodeling is an essential and ongoing process that allows the skeleton to maintain itself. Bone remodeling involves the coupled action of osteoclasts and osteoblasts with osteoclasts resorbing bone and osteoblasts depositing new bony matrix. Remodeling occurs throughout life, but not uniformly across the skeleton, and is carried out within a Basic Multicellular Unit (BMU), a temporary group of cells on a specific part of the bone. The remodeling process consists of activation, resorption, reversal, and formation phases that can be condensed into a three-phase bone remodeling cycle: initiation, transition, and termination (Matsuo and Irie 2008). It is triggered in response to increased or decreased mechanical loading, the need to repair microcracks in bone from mechanical loading or injury, low blood calcium levels, and hormonal changes (Matsuo and Irie 2008).

In the initiation phase, osteoclast precursors are recruited to the BMU. Osteoclasts are derived from hematopoietic stem cells, which are stem cells that also give rise to blood cells, and

share the same precursor cell as macrophages, which are cells crucial to the immune system. During the initiation phase, differentiation and activation of osteoclasts occurs, as well as maintenance of bone resorption which can last for as long as three weeks (Matsuo and Irie 2008).

During the transition phase, bone resorption is inhibited and osteoclasts undergo apoptosis (cell death). From mesenchymal stem cells (MSCs), osteoprogenitor cells differentiate into pre-osteoblasts, osteoblasts, bone lining cells, and eventually osteocytes. Osteoblasts are recruited to the remodeling site and differentiate, and the resorption site is prepared for bone deposition by the macrophage-like cells. Osteocytes are mature osteoblasts that are embedded in the bony matrix and act as mechanosensors that moderate bone deposition and bone resorption in response to mechanical loading. The final phase, the termination phase, is when osteoid (new bone) is laid down by osteoblasts. This is often very soft, disorganized bone that will eventually mineralize, a process that can last three months and ends in quiescence, a period when new osteons are formed and osteoblasts become osteocytes, bone lining cells, or undergo apoptosis (Bradley et al. 2018; Matsuo and Irie 2008).

The Role of Molecular Signaling Pathways in Bone Remodeling: Wnt β-Catenin and RANK/RANKL/OPG Pathways

These three phases of bone remodeling and the coupled action of osteoblasts and osteoclasts are contingent upon the interaction of osteoclast and osteoblast precursors through two signaling pathways that control osteoclast and osteoblast differentiation and either promote or inhibit bone resorption and deposition. The Wingless-related integration site (Wnt) β-Catenin mediation canonical pathway (the Wnt pathway) controls osteoblastogenesis and osteoblast differentiation and commits MSCs to the osteoblast lineage. This occurs when Wnt ligands bind to receptors LRP5/6 (low density lipoprotein-related receptor 5 and 6) and FZD (Frizzled). This

activates the Disheveled (DSH) protein and results in the destruction of the β-catenin destruction complex. The destruction of this complex prevents β-catenin from being phosphorylated so that it can build up in the cytoplasm of the cell and be translocated to the nucleus where it facilitates Wnt signaling and the transcription factors responsible for osteoblast differentiation and ultimately bone formation (Bradley et al. 2018; Crespo 2021; Maeda et al. 2019; Matsuo and Irie 2008).

The receptor activator of nuclear factor $\kappa\beta$ /RANK Ligand/Osteoprotegerin (RANK/RANKL/OPG) pathway is responsible for osteoclastogenesis through the binding of RANKL, a protein secreted by osteoblasts, and monocyte colony stimulating Factor (M-CSF), a cytokine, to the RANK and CSFR receptors on pre-osteoclasts and trigger this differentiation into osteoclasts (Matsuo and Irie 2008; Takayanagi 2018). Both RANK/RANKL/OPG and the Wnt β-Catenin pathways can be suppressed by osteocytes and osteoblasts, as well as immune factors like cytokines (small proteins secreted by immune cells that are crucial to cell signaling). Osteocytes and osteoblasts produce OPG which acts as a decoy receptor for RANK, blocking the RANKL/RANK pathway and preventing osteoclastogenesis and bone destruction. Osteocytes also produce sclerostin and the cytokine, Tumor Necrosis Factor–alpha (TNFα). TNF produces the protein Dickkopf-1 (DKK-1) which along with sclerostin both block the binding of Wnt ligands preventing osteoblast differentiation and inhibiting bone formation (Houschyar et al. 2019). This means that osteoblasts ultimately control and are crucial for bone turnover as they can start or stop osteoclast differentiation, as well as being responsible for bone formation. However, pro-inflammatory cytokines like TNFα can block the Wnt pathway and stop bone formation, while also upregulating RANK/RANKL resulting in increased bone destruction (Crespo 2021; Hankenson et al. 2015). Additionally, immune T-cells can also express RANKL

allowing them to bind to the RANK receptor on pre-osteoclast cells and induce osteoclast differentiation (Bradley et al. 2018; Crespo 2021; Houschyar et al. 2019; Kong et al. 1999; Matsuo and Irie 2008).

In homeostasis, both signaling pathways and the interactions between osteoclasts and osteoblasts/osteocytes are crucial for controlling bone remodeling needed to maintain the health and integrity of the skeleton. However, disease, chronic inflammation, or trauma can throw this delicate balance off, resulting in too much bone formation or too much bone resorption producing lesions on the bone indicative of a physiological stress response or disease process (Crespo 2021; Maeda et al. 2019).

Bone Remodeling and Inflammation

Inflammation is one of the primary ways the immune system responds to pathogens, injury, or other stressors and initiates healing. Acute inflammation at the site of tissue injury or infection recruits various immune cells like monocytes, macrophages, and lymphocytes. These cells release pro- and anti-inflammatory cytokines that activate signaling pathways that mediate the inflammatory response, either inhibiting or facilitating inflammation to ultimately return to homeostasis. Too little inflammation risks leaving antigens at the site of injury or infection worsening the infection and inhibiting healing. Too much inflammation over an extended period can cause tissue damage due to cytotoxins released by immune cells that can destroy healthy cells when left unchecked. This can be seen in bone and soft tissue damage at the site of a bone fracture or an infection like osteomyelitis (Chen et al. 2018; Crespo 2021).

Chronic inflammatory diseases can occur when the inflammatory response becomes unbalanced, and more pro-inflammatory cytokines are produced resulting in a “spill over” effect where the inflammatory response is no longer contained to the site of injury or infection and

enters systemic circulation resulting in a hyper inflammatory state throughout the entire body. This has been shown to lead to tissue damage, organ failure, immune system dysregulation, and bone destruction. TNFα is one of the main pro-inflammatory cytokines that is involved in this spillover. As previously discussed, TNFα is a cytokine capable of inhibiting the Wnt pathway and stopping bone formation while also upregulating the RANK/RANKL pathway increasing osteoclast differentiation. A hyper-inflammatory state due to excess pro-inflammatory cytokines like TNFα can have serious impacts on bone remodeling and lead to excessive bone destruction (Crespo 2021; Matsuo and Irie 2008).

As these signaling pathways show, the immune system and the skeleton are interconnected with significant crosstalk occurring, resulting in the formation of skeletal lesions. As previously discussed, osteoclasts are derived from macrophages/monocyte lineage cells of hematopoietic stem cell origin and are formed from the same lineage as immune cells and share many cytokines, like TNFα (Berger et al. 2020; Crespo 2021; Qin et al. 2020). Cytokines released as part of the immune response can influence the differentiation of bone cells crucial to bone remodeling making the skeleton and the immune system intrinsically linked in ways that make the study of both key to fields like bioarchaeology and paleopathology (Berger et al. 2020; Crespo 2021). Osteoimmunology is a field that studies this interplay between bones and the immune system and can offer important insights into the ways the immune system and the inflammatory response affect the skeleton and provide additional explanatory frameworks for skeletal lesions seen in the archaeological record (Berger et al. 2020; Crespo 2021).

The Physiological Stress Response

As previously discussed, the stress response in the human body can be caused by both physical factors (injury, disease, nutritional stress) and environmental/social factors (climate

change, food insecurity and discrimination) that elicit a neuroendocrine stress response that involves the autonomic nervous system (sympathetic nervous system), the central nervous system, the immune system, and the Hypothalamic-Pituitary-Adrenal-Axis (HPA-axis) (Dent et al. 2020; Temple and Goodman 2014). When the body experiences a stressor, the HPA-axis is activated to release glucocorticoids like cortisol in the bloodstream, the autonomic nervous system produces adrenaline and noradrenaline, and the central nervous system produces substance P, a neuropeptide. Cortisol, adrenaline, and noradrenaline block the production of pro-inflammatory cytokines that inhibit the immune response and make an individual more susceptible to infection. Substance P activates the production of pro-inflammatory cytokines so combined with the immune response inhibiting effects of the HPA-axis and the autonomic nervous system, this can create a dysregulated inflammatory reaction (Dent et al. 2020; Temple and Goodman 2014).

The stress response serves an important function in our evolutionary history because it is a mechanism we evolved to ensure short-term survival (Temple and Goodman 2014). Our body's stress response prepares our body to respond to a stressor, such as a physical threat through the fight, flight, or freeze reactions. The activation of the sympathetic nervous system and release of cortisol and adrenaline into systemic circulation results in increased heart rate and blood flow to limb muscles for running, pupil dilatation for better vision, and the cessation of digestion and other bodily functions that are energetically costly. In the short term, an acute stress response is not harmful. However, when this stress response is continuously induced due to social factors like threats of violence, discrimination, racism, food insecurity, chronic disease, or anxiety, an individual is now experiencing chronic stress leading to decreased immune response and chronic inflammation that can result in increased susceptibility to disease. How chronic physiological

stress affects each individual will vary as a result of genetics and various environmental factors that shape each individual's unique response to stressors, but the body's inability to differentiate stress from an illness or injury and stress from social factors that are often chronic rather than acute means that our stress response, when left unchecked, can wreak havoc on various body systems leading to chronic health issues. The consequences of this homeostatic imbalance can, in some cases, be observed directly on the skeleton in the form of blastic (bone deposition), lytic (bone resorption), or mixed lesions on the bone surface that provide insight into the stress experiences in past peoples (Crespo 2021; Dent et al. 2020; Klaus 2014).

Ultimately the goal of studying stress in bioarchaeology, and of this research, is to understand how the stressors people in late medieval Romania were experiencing from aspects of their environment like diet and experiences of mobility, and social structures like class stratification, interacted with their biology. How did these factors either provide a buffer against stressors or inhibit an individual's ability to either mount an effective stress response or trigger a chronic inflammatory state and how did this shape patterns of stress and frailty in these groups? (Klaus 2014).

Skeletal Biology and the Meaning of Non-Specific Stress Lesions

Periosteal New Bone Formation (PNBF)

Periosteal new bone formation (PNBF), or periostitis, is a common skeletal lesion found in the archaeological record, most commonly on the long bones especially the tibiae (Weston 2008). PNBF is the result of inflammation of the periosteum, a thin fibrous connective tissue layer that adheres to the surfaces of all bones. This can be the result of trauma, neoplasms, infection, metabolic disease, etc. (Buikstra 2019; Chen et al. 2018; Klaus 2014; Weston 2008, 2012). The periosteum consists of two layers, a thick outer fibrous layer and a thin inner layer

called the cambium that is in contact with the bone surface. The cambium is vascularized and full of osteogenic cells that can differentiate into osteoblasts and chondrocytes (Ito et al. 2001; Klaus 2014). When the bone and surrounding periosteum experience some form of stress, such as a fracture, the presence of these osteogenic cells is crucial for fracture repair and healing. The initial inflammatory response recruits pro-inflammatory cytokines and macrophages and initiates the differentiation of these osteogenic cells into chondrocytes and osteoblasts via the Wnt β-Catenin pathway that begin laying down new osteoid matrix and cartilage to form an initial soft callus at the fracture site (Ito et al. 2001; Klaus 2014).

For other kinds of perturbations to the periosteum (soft tissue trauma, infection, metabolic disease, nutritional stress) the osteogenic cells in the cambium layer differentiate into mature osteoblasts and begin to lay down woven bone, creating patches of raised, disorganized, reactive bone that is characteristic of periosteal lesions (Ito et al. 2001; Klaus 2014). In cases of infection that produce a long-term chronic inflammatory response, leukocytes, neutrophils, and fibroblasts are recruited to the infection site. As a result of these cells fighting off a pathogen, often bacterial infections due to *Staphylococcus aureus*, pus is produced which builds up between the bone and the cambium causing tearing in the periosteum and triggering further inflammation that results in more reactive new bone formation (Klaus 2014).

PNBF is non-specific since it can manifest as the result of a variety of stressors, but has historically been viewed as an indication that an individual was experiencing a physiological assault at the time of death (Klaus 2014; Weston 2008, 2012). However, the documentation of the healing stage of periosteal lesions provides further insight into how active this assault was and has been used to interrogate the Osteological Paradox to see if different healing stages of PNBF are associated with different levels of individual frailty and survivability (DeWitte 2014).

This was tested by DeWitte (2014) in a Black Death cemetery population in London. Those with active lesions had the lowest survivorship across all age groups while those with healed lesions had the highest survivorship across age groups. So while the presence of periosteal lesions indicates that individuals were experiencing some sort of physiological stress, the healing stage is important for interpreting levels of frailty and provides support for the idea proposed by Wood and colleagues (1992) that those with lesions were likely robust enough to survive a physiological stressor long enough to develop a lesion and those with healing lesions are the least frail as they were recovering from the stressor at the time of their death (DeWitte 2014; Wood et al. 1992).

Porotic Lesions of the Skull: Cribra orbitalia and porotic hyperostosis

Porotic hyperostosis (PH) is an area of micro or macroporosity on the surface of the cranial vault, most commonly on the parietal, occipital, and frontal bones, while *cribra orbitalia* (CO) is also micro or macroporosity localized to one or both orbital roofs (Walker et al. 2009). Both conditions are of particular interest to bioarchaeologists and paleopathologists because they are two of the most common skeletal lesions found in archaeological populations. While thought to be the result of nutritional stress, the cause of PH and CO is debated due to these lesions being non-specific, meaning they are not the result of one specific disease process, but rather the result of several possible stressors (nutritional, trauma, disease, etc.) (McIlvaine 2015; Walker et al. 2009). The mechanism and etiology of PH and CO have been the subject of much debate and our understanding of the cause of these lesions has evolved as the field of skeletal biology has advanced our understanding of bone remodeling and the pathophysiology of various skeletal lesions, and this research has been incorporated into bioarchaeology (Klaus 2014; Walker et al. 2009).

Expansion of the diploe of the skull in response to marrow hypertrophy was thought to be due to anemia, scurvy, and other metabolic. Iron deficiency anemia (IDA) was the accepted cause of this marrow hypertrophy and subsequent resorption of the outer table of the cranial bones resulting in porotic lesions (Ortner 2003). Walker (2009) argued that anemias do cause premature apoptosis of red blood cells (RBCs) and increased erythropoiesis (RBC production) in the bone marrow leading to marrow hypertrophy, but this does not match the pathophysiology of IDA and its effects on RBC production. Rather, Walker argues that severe iron deficiency would inhibit the synthesis of hemoglobin and the formation and maturation of RBCs leading to reduced RBC production and would not lead to marrow hypertrophy (Walker et al. 2009). Additionally, IDA is characterized by inadequate RBC production, not RBC destruction (hemolysis). Hemolysis is triggered when the body has sufficient iron stores to be able to sustain erythropoiesis, and the response is to increase RBC production causing marrow hypertrophy. This is not the case in IDA.

Instead, Walker argues that megaloblastic (B12 and folic acid deficiencies) and hemolytic anemias (thalassemia and sickle cell disease) are more likely etiologies for PH because of premature RBC destruction, in the case of hemolytic anemias, or ineffective erythropoiesis, in the case of megaloblastic anemias, resulting in a feedback cycle of increased RBC leading to marrow hypertrophy (Walker et al. 2009). CO, on the other hand, is likely not the result of diploic expansion due to marrow hypertrophy but is more likely caused by subperiosteal bleeding as a result of scurvy or rickets, which are caused by severe deficiencies in vitamin C and D. Additionally, it is more commonly observed in children, which may be due to the fact that the periosteum of the orbital roof is less firmly attached in children and is more vascularized, so scurvy from severe Vitamin C deficiency that compromises the integrity of connective tissue

could lead to subperiosteal inflammation and bleeding of the orbits leading to CO. While active CO is observed in adults, it is not known how long it takes CO to remodel and its presence in adults is often thought to reflect childhood stress that was survived and may not always be a stressor that the individual was experiencing at the time of death (Pilloud and Schwitalla 2020). However, like PH, IDA does not fully explain CO, and it is likely the result of multiple co-occurring nutritional deficiencies, of which children have historically been at higher risk (Walker et al. 2009).

In response to Walker's argument that IDA does not cause PH, Oxenham and Cavill (2010) argue that the clinical literature supports the hypothesis that a lack of iron does not inhibit RBC production, rather RBC production increases. This results in RBCs with insufficient hemoglobin which triggers hemolysis. IDA does produce an increase in RBCs, but it is ineffective erythropoiesis that causes marrow hyperplasia. Oxenham and Cavills' position is further supported by clinical findings that show RBC counts for people with IDA, genetic anemias and non-anemic individuals have significant overlap. The authors argue that while blood cell count may be low in IDA due to hemoglobin-deficient RBCs being destroyed, this is only after an increase in the production of ineffective RBCs causing marrow hypertrophy, so IDA can lead to PH and should not be completely ruled out as an etiology for PH (Oxenham and Cavill 2010).

McIlvain (2015) also argues that IDA should not be dismissed as a possible etiology of PH, because of the possibility of IDA cooccurring with other anemias resulting in the effects being masked. McIlvain argues that if IDA does inhibit RBC production then dismissing IDA as a cause of PH could result in hidden heterogeneity. Iron and vitamin B12 deficiency are both caused by a lack of animal protein in the diet and/or sanitation problems leading to diarrheal

disease and parasitic infection and commonly co-occur in human populations. It is possible that if IDA is inhibiting RBC production and marrow hypertrophy, then it is suppressing the development of PH despite a co-occurring B12 deficiency that is stimulating RBC production and marrow hypertrophy. In these cases of co-occurrence, the megaloblastic anemia could be masked by the effects of IDA resulting in no skeletal lesions in stressed individuals and hidden heterogeneity in nutritional deficiencies (McIlvaine 2015).

Additionally, McIlvain (2015) argues that PH may be a sign of an adaptive response in populations that experience high pathogen loads that cause IDA. For individuals who survive those infections, they may have PH because they lived long enough to survive an infectious pathogen and IDA, and are some of the least frail individuals in the population. This highlights the complexity of not only understanding the etiologies of skeletal lesions but also what the presence of these lesions mean for patterns of frailty in a population and understanding stress and health in past peoples (McIlvaine 2015).

Dental Disease: Dental Caries, Abscesses, and Periodontal Disease (PD)

Dental caries are caused by the demineralization of the enamel, dentine, and cementum by organic acids that are produced by oral bacteria fermenting carbohydrates consumed as part of the diet, especially in diets high in sugars and starches (Hillson 1996). Dental caries may present as small opaque spots that can eventually progress to a cavity in the enamel surface. These can occur on the tooth crown, the occlusal surface being common, as well as the tooth root, and are most commonly found on the molars (Hillson 1996). Cavities on the tooth crown can progress to the enamel dentine junction (EDJ). If a cavity progresses through the dentine and into the pulp chamber, bacteria can invade the pulp chamber and lead to inflammation of the periapical tissues

around the tooth root and alveoli, or even enter the bloodstream leading to systemic infection (Hillson 1996).

Inflammatory lesions, like abscesses, can also develop and are either chronic or acute. These lesions usually involve the presence of immune cells, like lymphocytes and phagocytes, which fight off a bacterial infection that triggers the inflammatory reaction. This response produces pus, a mixture of dead tissue and cell debris, that increases pressure and pushes the tooth up into the alveolar bone causing severe pain. The build-up of pus in the alveolar bone or pulp chamber can cut off the blood supply and kill the pulp. If this continues and becomes a chronic inflammatory reaction, the bone will continue to remodel and create a chamber around the infection. This chronic inflammation affects all parts of the tooth and alveolar bone and can lead to bone loss. This bone loss can create a large abscess in the bone around a tooth root in the mandible or maxilla, or periapical abscesses that form around the apex of the tooth root and result in bone loss that exposes the tooth root through the maxillary or mandibular bone (Hillson 1996).

Periodontal disease (PD) or periodontitis is the result of inflammation of the periodontal tissues. Usually, the micro-organisms that reside in the mouth are kept in check by the anti-bacterial properties of the saliva and the gingiva which protects underlying tissues. However, when an imbalance occurs that the body's immune system cannot fight off it can lead to inflammation of the gingiva called gingivitis, and if it progresses to the underlying periodontal tissues it becomes periodontitis. If the inflammation progresses it can affect the periodontal ligament, which exposes the tooth root, and eventually the tooth root becomes detached from the alveolar bone leading to resorption of the alveolar bone. In advanced cases, the alveolar bone can resorb to such an extreme degree that the tooth falls out (Hillson 1996).

While dental disease is often studied in the context of diet and the transition to higher carbohydrate starcher food sources, like maize, it does represent an inflammatory state due to an imbalance of oral micro-flora and the body's immune response. Dent and colleagues have hypothesized that chronic systemic inflammation, like from chronic PD or abscesses, can cause a shift in homeostasis affecting the balance of immune system function and resulting in immune dysregulation. They looked at food insecurity and chronic PD in a modern population and found that the stress of food insecurity (unpredictable or uncertain access to food) caused a depressed immune response and greater susceptibility to PD. PD upregulated immune activity leading to a dysregulated immune response (Dent et al. 2020). As a result, the inflammatory cytokines at the site of PD, can "spill over" into systemic circulation leading to chronic inflammation that can then lead to bone lesions in other areas of the body not involved in the original PD infection (Crespo 2021; Dent et al. 2020). Crespo (2021) calls this a "hyper-inflammatory state" that may affect the immune response to future stressors. For bioarchaeologists, this inflammatory response can be visible in skeletal remains as chronic PD. Its activation of the immune system brings in T-cells and pro-inflammatory cytokines like TNFα, which activate the RANK/RANKL/OPG pathway resulting in lytic lesions and bony destruction of the alveoli, as well as increased remodeling seen in periosteal lesions throughout the skeleton (Crespo 2021). While it may not be possible to diagnose a hyper-inflammatory state through skeletal lesions alone, this hypothesis shows that dental disease is not only informative for studying dietary changes and oral health, but when it co-occurs with PNBF it may be an additional indicator of physiological stress and suggestive of a spillover effect causing systemic effects throughout the skeleton manifesting as multiple stress lesions (Crespo 2021).

Biocultural Theory

The biocultural approach is a theoretical framework commonly used in bioarchaeology that combines the biological and evolutionary history of humans and social, cultural, and environmental factors that interact with human biology to understand how human behavior and health have changed over time (Cheverko et al. 2021; Zuckerman and Armelagos 2011). The biocultural approach moved anthropology, particularly biological anthropology, beyond the typological, racialized approaches of the early 19th century, a phenomenon that has been attributed to the field's origins in biology and the focus on discrete biological categories, and a lack of concern or interest in the historical or archaeological context of human remains (Armelagos et al. 1982; Buikstra 2006; Zuckerman and Armelagos 2011). Rather than counting lesions or trying to quantify physical differences between groups, the biocultural approach has made it possible to explore more nuanced questions about how biology and culture interact to affect human adaptation, health, and behavior in the past, which can ultimately inform our understanding of how these interactions continue to play out today.

The biocultural approach takes into consideration multiple lines of evidence for reconstructing the human past and acknowledging the complex ways human biology and the environment interact and how this shapes population health over time and space. This approach has been employed by many recent bioarchaeological studies (Allen et al. 2020; Beck et al. 2021; Curto et al. 2019; Marcu Istrate and Diana 2017; Pilloud and Schwitalla 2020; Redfern et al. 2018; Voas et al. 2021). For example, a biocultural approach to the study of past human health and disease combines biological data (skeletal biology, lesions, age, sex) with cultural factors like social status, economic status, ethnicity, religion, migration status, etc. obtained from archaeological, ethnographic, and/or historical sources to understand how humans interacted

with their environment and how these interactions produced patterns of stress and disease over space and time. A biocultural approach will consider exposures and stressors present in an individual's environment (pathogens, environmental change, differential access to resources, occupation, violence, etc.) and how those interact with both cultural buffering systems and individual intrinsic factors like immunocompetence and genetics to produce patterns of stress within and/or between populations (Cheverko et al. 2021).

The development and application of biomolecular methods such as aDNA, paleo proteomics, and stable isotope analysis to bioarchaeology have provided additional lines of evidence to incorporate into bioarchaeological studies. These methods make it possible to understand how humans interact with their environment at a molecular level. Dietary composition, nutritional stress, culinary practices, weaning, and migration can all be explored with these methods. This dissertation employs stable isotope analysis of bone collagen and tooth enamel to look at both dietary composition and mobility. Using a biocultural approach, this dissertation will combine biological data (age-at-death, biological sex, and skeletal pathology) and biogeochemical data from carbon, nitrogen, oxygen, and strontium isotopes with the archaeological and historical context of the cemetery sites and the time period in which these individuals lived.

The combination of biological, archaeological, and historical data will allow me to contextualize the biological data. The individuals in this sample lived during a period of Romania's history when society was strictly stratified and was experiencing periodic control and invasion by the Ottoman Turkish army. The resulting political changes, violence, and differential access to resources shaped the biology of these individuals in complex ways. As discussed earlier in this chapter, studying human health from the dead creates a set of paradoxes for

bioarchaeologists and requires us to move beyond basic lesion frequencies and rethink the meaning of skeletal lesions (Wood et al. 1992). Skeletal remains and lesions only tell a part of the story, but with the addition of other evidence; archaeological evidence, historical context, and the atoms of various elements taken up by a person's bones and teeth throughout their life, a more complete and nuanced picture of stress and frailty in populations can emerge.

CHAPTER FOUR: ISOTOPE ECOLOGY OF CARBON AND NITROGEN STABLE ISOTOPES

Chapter Overview

In this chapter, I will provide a review of what stable isotopes are, how isotopic ratios are measured and reported, how isotopes are fractionated, and how fractionation and the resulting enrichment in the heavy or the light isotope is quantified. With the necessary background information, the isotope ecology of the two isotopes utilized in this research (carbon and nitrogen) will be discussed. This includes how these isotopes move from the atmosphere into the biosphere and are incorporated into various biological and chemical systems that make it possible to reconstruct diet and geographic movement of past peoples.

This chapter will also discuss the types of plant and animal food sources that would have been available to individuals in Moldavia during the 14^{th} – 18^{th} century based on historical documentation of agriculture, animal husbandry, and common foods consumed during this time that should be visible isotopically in bone collagen. Finally, this chapter provides a review of the relevant literature that have used multi-isotope approaches to answer questions about past human diet, as well as studies that have combined stable isotopes with demographic data, skeletal pathology, and historical and archaeological documentation to explore stress and disease in past populations and attempt to disentangle the relationship between skeletal lesions, diet, and health.

What are Stable Isotopes?

Isotopes are atoms of the same element with the same number of protons but differ in their number of neutrons, resulting in a different atomic mass. This difference in mass is denoted as a superscript before the element abbreviation (i.e. ^{13}C). Isotopes may be stable or radioactive. Stable isotopes do not undergo radioactive decay. For example, carbon isotopes ^{12}C and ^{13}C are

stable and do not undergo radioactive decay whereas ^{14}C is unstable and does undergo radioactive decay. However, some isotopes are radiogenic, meaning they are the result of radioactive decay of another isotope. For example, ^{87}Sr is the result of the radioactive decay of rubidium-87 (^{87}Rb). Isotopes of an element that have an extra neutron (or two) are considered the "heavy" isotope due to their greater atomic mass. For example, carbon's stable isotopes are ^{12}C, and ^{13}C. ^{13}C is the heavier stable isotope because it possesses 7 neutrons, in contrast to ^{12}C's six neutrons (Sharp 2007; Sulzman 2007).

Isotopes of an element are not present in equal abundances; the heavy isotopes are less abundant. For example, the abundance of ^{13}C versus ^{12}C is 1.108% versus 98.892%. For nitrogen, the abundance of the heavier isotope ^{15}N is 0.365% compared to the lighter isotope, ^{14}N, which is 99.635% (Sulzman 2007).

Isotopic Fractionation: Equilibrium and Kinetic Fractionation

Isotopes of an element will undergo the same chemical, physical, and biological processes, like Photosynthesis, but due to their differences in mass they will undergo these reactions at different rates, and this will affect how these isotopes are partitioned or sorted during different phases of these reactions.

The isotopic sorting is called fractionation. Light isotopes like carbon, nitrogen, oxygen, and hydrogen have large degrees of fractionation because of the large mass difference between isotopes of these elements. For example, the mass difference between ^{13}C and ^{12}C is 8.3%. Heavy isotopes, like strontium, have a much smaller mass difference (1% between ^{87}Sr and ^{86}Sr) so the reaction rates between ^{87}Sr (atomic mass = 86.9 Da) and ^{86}Sr (atomic mass = 85.9 Da) are similar and less fractionation that occurs.

There are three types of fractionation, nuclear spin, equilibrium and kinetic, but only equilibrium and kinetic will be discussed. Equilibrium fractionation is the sorting of isotopes between two substances or phases in a closed system. Equilibrium fractionation must obey conservation of mass, meaning the number of atoms of each isotope is fixed. The heavier isotope will accumulate where the molecular bonds are strongest, which is usually in the denser phase with the largest molecular mass. Equilibrium fractionation decreases with increasing temperature, so the degree of fractionation is greater at lower temperatures (Sharp 2007; Sulzman 2007).

Kinetic fractionation occurs in contexts in which reactions or processes are unidirectional and cannot be reversed. Strength of the molecular bonds and velocity are important, and the lighter isotope will go faster in kinetic fractionation. As a result, the product tends to be depleted in the heavier isotope and enriched in the lighter isotope, while the substrate is enriched in the heavier isotope and depleted in the lighter isotope. Examples include evaporation in an open system, diffusion, and enzymatic reactions. In the case of water evaporation, the lighter isotope (^{16}O) will evaporate more quickly than the heavier isotope (^{18}O). Thus, as the evaporation process progresses, ^{16}O will accumulate in the water vapor (the product), while the water puddle (substrate) will have a greater concentration of ^{18}O (Sharp 2007; Sulzman 2007). Enrichment occurs as a result of the fractionation process. After isotopic sorting via fractionation, the product will be either enriched ($\varepsilon > 0$) or depleted ($\varepsilon < 0$) in the heavy isotope.

Calculation of the Fractionation Factor and Enrichment

Fractionation is quantified by calculating the fractionation factor (α), which shows the degree of fractionation between the product (A) and the substrate (B) and is calculated as the

ratio of the heavy/light isotope in the product (R_A) divided by the ratio of the heavy/light isotope in the substrate (R_B):

$$\alpha_{A-B} = \frac{R_A}{R_B}$$

To put this in δ values, the equation is:

$$\alpha_{A-B} = \frac{1000 + \delta_A}{1000 + \delta_B}$$

α is a function of temperature, so values of α are only meaningful when temperature is specified. If α is greater than 1, then the product is enriched in the heavier isotope relative to the substrate. (Sharp 2007; Sulzman 2007).

Another fractionation calculation is for discrimination, which is the degree to which a process avoids or discriminates against the heavy isotope. This is indicated by Δ, which is a good approximation of α. Δ can be calculated by subtracting the δ value of the substrate (B) from the delta value of the product (A):

$$\Delta_{A-B} = \delta_A - \delta_B$$

These calculations are important in studies that seek to understand how heavy isotopes are discriminated against as they move from the environment into human and animal tissues (Sharp 2007; Sulzman 2007).

$\Delta_{A\text{-}B}$ is a good approximation of the fractionation ($10^3 \ln \alpha$) when the δ values of the two substances and Δ are less than 10. When either are greater than 10, $10^3 \ln \alpha$ should be calculated.

$$\Delta_{A-B} \approx 10^3 \ln \alpha_{A-B}$$

The enrichment factor (ε) is the result of the fractionation process. After isotopic sorting via fractionation, the product will be either enriched or depleted in the heavy isotope. The enrichment factor of a product and substrate is calculated as:

$$\varepsilon_{A/B} = (\alpha - 1) * 1000$$

If ε is greater than 0 then a product is enriched in the heavy isotope relative to the substrate and if ε is less than 0 the product is depleted in the heavy isotope relative to the substrate (Sharp 2007; Sulzman 2007).

Measuring and Reporting Isotopic Composition: The Delta* (δ) *Value

The ratio of the heavy isotope to the light isotope is denoted by R. However, differences in R between materials, such as plants, are so small that the isotopic composition of a material is reported relative to an internationally recognized standard using the delta (δ) value in the units per mil (‰) (parts per thousand) (Sharp 2007; Sulzman 2007). The δ value is a ratio of a ratio and it is calculated using the following formula:

$$\delta(‰) = \left(\frac{R_{sample} - R_{standard})}{R_{standard}}\right) * 1000$$

R_{sample} is the ratio of the heavy to the light isotope in the sample, $R_{standard}$ is the ratio of the heavy to the light isotope in the international standard, and the value is multiplied by 1000 to get the δ value in the units per mil (‰). A δ value that is positive indicates that the ratio of the heavy to the light isotope is higher in the sample than in the standard, and a δ value that is negative indicates that the ratio of the heavy to the light isotope is higher in the standard than in the sample (Sharp 2007; Sulzman 2007).

The original standard used for reporting $\delta^{13}C$ and $\delta^{18}O$ values of carbonates was from an Upper Cretaceous specimen, *Belemnitella americana,* called PeeDee Belemnite (PDB). As the

sample has been depleted new samples, PDB II and PDB III, have been prepared and calibrated against the original PDB standard. For nitrogen, the reference standard is atmospheric nitrogen or AIR as it is constant across Earth (Sharp 2007).

Carbon Isotopes in Plants

C_3, C_4, and Crassulacean Acid Metabolism (CAM) Photosynthesis: Variation in Plant $\delta^{13}C$ Values

Carbon isotopes are useful for reconstructing the diets of animals and humans due to the ways carbon isotopes fractionate differently in plants that use different photosynthetic pathways, and then how carbon isotopes fractionate between plant and animal/human tissues. There are a couple of factors that influence how much ^{13}C a plant can uptake. The first is the source of carbon dioxide (CO_2). CO_2 from the atmosphere is diffused through plants' stomata. Today, the $\delta^{13}C$ value of atmospheric CO_2 is about -8‰. In pre-industrial times the $\delta^{13}C$ value of atmospheric CO_2 was about -6.5‰. Today's lower $\delta^{13}C$ value is due to the burning of ^{13}C-depleted fossil fuels since the early 19th century. As a result, there is variation in $\delta^{13}C$ values between modern (post-19th century) and archaeological materials and a correction of 1.5‰ must be applied when comparing archaeological and modern materials (O'Leary 1988). Second, plants will always have less ^{13}C than atmospheric CO_2 because of discrimination against ^{13}C that occurs during CO_2 uptake. In all plants, CO_2 diffuses through pores on the leaves called stomata. These pores can open to allow CO_2 to diffuse into the leaf or close during hot/dry periods to limit water loss. CO_2 diffusion is a kinetic fractionation process and thus there is some initial discrimination against ^{13}C at this step (4.4‰) due to it being the heavier isotope and thus forms stronger bonds and diffuses slower than ^{12}C (O'Leary 1981; O'Leary 1988). This discrimination occurs in all plants regardless of the photosynthetic pathway used.

Once the CO_2 has dissolved in the sap of the plant cell and diffuses into the chloroplast, the next step (also kinetic fractionation) is the fixing of carbon into the plant tissues via a process called carboxylation. The carboxylation step is what determines a plant's $\delta^{13}C$ value as this is where the main isotope fractionation occurs and is an irreversible step in plant photosynthesis There are three photosynthetic pathways found in plants that determine how those plants take in CO_2 from the atmosphere and create oxygen and energy in the form of sugar: the C_3, C_4, and CAM photosynthetic pathways. How those plants fix CO_2 in their tissues is what differentiates the three photosynthetic pathways, and drives the differences in $\delta^{13}C$ values between plants that use those pathways.

C_3 Photosynthesis

Terrestrial plants using the C_3 photosynthetic pathway include trees, shrubs, and cool-season/high-elevation grasses. C_3 plants also include commonly consumed staple crops such as wheat, rice, soy, oats, barley, and rye. In C_3 plants, fixation of the carbon atoms from CO_2, which is catalyzed by ribulose bisphosphate carboxylase/oxygenase, or RuBisCo. RuBisCo combines with atmospheric CO_2 brought into the leaf through the stomata and fixes the carbon into the plant tissues and produces a 3-carbon sugar called phosphoglycerate (PGA) (hence the term C_3 photosynthesis). The products, Adenosine Triphosphate (ATP) and Nicotinamide Adenine Dinucleotide Phosphate Hydrogen (NADPH), are used in the reduction phase to reduce PGA and synthesize the sugar Glyceraldehyde-3-Phosphate (G3P), which furthers plant metabolism and regenerates ribulose bisphosphate (RuBP), the CO_2 acceptor, so that they cycle can begin again (O'Leary 1988).

However, C_3 photosynthesis is inefficient. RuBisCo can only fix 3-10 molecules of CO_2 per second per molecule of enzyme and thus is the rate limiting factor of the Calvin Cycle in C_3

photosynthesis. This slow carboxylation rate also causes some CO_2 to leak back out of the plant through the stomata. Additionally, C_3 plants do not do well in hot/dry environments and experience a process called photorespiration. Photorespiration occurs in conditions where atmospheric CO_2 is low or the plant stomata are closed to prevent water loss in dry environments. Eventually CO_2 concentrations become so low that RuBisCo, which is already inefficient at grabbing CO_2, will begin to grab O_2 and fix it to RuBP, producing one PGA and phosphoglycolate. RuBisCo will catalyze the oxygenation RuBP and the continued metabolism of phosphoglycolate results in the release of CO_2 from the plant i.e., photorespiration. This is energy expensive, wasteful, and reduces the efficiency of the plant's photosynthetic process and is why C_3 plants do not do well in hot or dry environments (O'Leary 1988).

Stomatal diffusion rate and carboxylation are the two most crucial steps in carbon isotope fractionation in photosynthesis. Carboxylation is the limiting factor in C_3 photosynthesis, so with low stomatal resistance fractionation is 28‰ with a predicted leaf $\delta^{13}C$ value of -36‰ and with high stomatal resistance fractionation is 4.4‰ with a predicted leaf $\delta^{13}C$ value of -12‰. Diffusion and carboxylation are the limiting factors in fractionation so C_3 plants have delta values that cluster around -28‰ (O'Leary 1988).

There is a wide range of $\delta^{13}C$ values observed in C_3 plants and this is driven by various environmental factors that affect how CO_2 diffuses into the plant and the isotopic composition of that CO_2. The major factors driving this variation are water-use efficiency and the Canopy Effect. The concept of water-use efficiency describes a plants ability to control water loss while still fixing carbon into their tissues via photosynthesis. As a result, this effects discrimination against ^{13}C thus causing variation in plant $\delta^{13}C$ values. For example, during dry periods plants will close their stomata to limit water loss. This causes intercellular CO_2 concentrations to drop

and the plant to discriminate against ^{13}C less and thus fix more of it into its tissues causing leaf $\delta^{13}C$ values to increase. When water-use efficiency is high during low precipitation periods $\delta^{13}C$ values are higher. During wet periods with plenty of precipitation, plants will open their stomata as there is less risk of significant water loss. This increases intercellular CO_2 concentrations to increase and more discrimination against ^{13}C causing leaf $\delta^{13}C$ values to be lower (Farquhar et al. 1989; Petrík et al. 2023).

The canopy effect describes the effect on plant $\delta^{13}C$ values in a forested environment. Plants growing below the forest canopy in a low light environment will have lower $\delta^{13}C$ values. This is because CO_2 concentrations are higher under the canopy due to CO_2 that is respired by decomposing organic material, bacteria, and other microorganisms in the soil. This respired CO_2 is also enriched in ^{12}C, thus the plants growing under the canopy are taking in and fixing ^{12}C enriched CO_2 thus lowering their $\delta^{13}C$ values. Additionally, rates of photosynthesis will be faster at the top of the canopy where there is more sunlight, but this also means more water loss causing plants to close their stomata and decrease discrimination against ^{13}C. At the bottom of the canopy there is less light and more humidity, so plant stomata stay open for longer. Animals, like ruminant herbivores, that graze on ^{13}C depleted plants growing under the canopy will also have lower $\delta^{13}C$ collagen values accounting for diet to collagen (5‰) or enamel (14.1‰) enrichment (Tieszen 1991; Winner et al. 2004). Both water-use efficiency and the canopy effect are sources of variation in C_3 plant $\delta^{13}C$ values that can then affect the $\delta^{13}C$ values of animal and human collagen and are important for interpretations of animal and human diet.

C_4 Photosynthesis

C_3 plants evolved when atmospheric CO_2 was much higher than it is today. Over the last 30 million years there has been a drop in atmospheric CO_2 and an increase in atmospheric O_2, which has led to the evolution of plants with a photosynthetic pathway that is adapted to a CO_2-poor environment, as well as warmer climates, preventing photorespiration from occurring and increasing water-use efficiency. This is the C_4 photosynthetic pathway.

C_4 photosynthesis (aka Hatch-Slack pathway) has a specialized anatomy called Krantz Anatomy that isolates RuBisCo and the C_3 photosynthetic Calvin Cycle to an interior layer of cells called the Bundle Sheath Cells (BSC). The bundle sheath cells are separate from a layer of mesophyll cells where CO_2 enters the leaf via the stomata and the initial carboxylation step occurs. In the mesophyll cells is Phosphenolpyruvate (PEP) carboxylase, an enzyme that catalyzes carbon fixation. PEP carboxylase combines with CO_2, which is converted to HCO_{3-} (Bicarbonate), and converted to oxaloacetate, a 4-acid carbon. Oxaloacetate is transformed into Malate/malic acid and diffuses from the mesophyll layer to the bundle sheath cells. This 4-carbon acid is then decarboxylated and broken back down into PEP and CO_2. PEP effectively acts as a CO_2 pump moving CO_2 from the mesophyll into the bundle sheath cells and increasing the CO_2 concentration. This results in CO_2 concentrations in the chloroplast of C_4 plants that are greater than C_3 plants. PEP then returns to the mesophyll to start the carbon fixing process again, while the CO_2 enters the Calvin Cycle, which occurs in the bundle sheath cells the same way it occurs in C_3 plants. However, since CO_2 concentrations are much higher in the BSC, there is a greater CO_2/O_2 ratio which means RuBisCo has plenty of CO_2 to fix and effectively eliminates photorespiration (O'Leary 1988).

In C_4 plants, diffusion and carboxylation of PEP are important to isotope fractionation. Discrimination against ^{13}C associated with PEP carboxylase is much lower than in C_3 plants (2.0‰). The fixing of carbon by RuBisCo via the Calvin Cycle is isolated from where CO_2 enters the leaf, thus the effects of the large fractionation associated with RuBisCo (29‰) are not seen in C_4 plants. Instead, the PEP carboxylation phase in the mesophyll cells is irreversible and drives the $\delta^{13}C$ values of the plant. Diffusion of CO_2 through the stomata is the main limiting factor in C_4 photosynthesis, resulting in a predicted leaf $\delta^{13}C$ value of -12‰ (atmospheric CO_2 = -8‰, ε_t = 4.4 ‰ (fractionation of ^{13}C associated with diffusion of CO_2 through stomata)), with actual observed values around -14‰ (O'Leary 1988). $\delta^{13}C$ values for C_4 plants range between -10 and -14‰, which is a much tighter range than seen in C_3 plants. This is because fractionation associated with PEP carboxylase is -5.7‰, much lower than the fractionation for RuBisCo in C_3 plants (28‰). This is because Bicarbonate is enriched in ^{13}C relative to CO_2 and PEP carboxylase does not discriminate against ^{13}C as much as RuBisCo resulting in much higher $\delta^{13}C$ values and less variation in C_4 plants.

Crassulacean Acid Metabolism (CAM) Photosynthesis

A third type of photosynthesis is Crassulacean Acid Metabolism (CAM), which is used by plants like succulents and cacti in desert environments. Like C_4 photosynthesis, CAM photosynthesis also separates the carboxylation step from RuBisCo, but rather than a spatial separation, CAM plants temporally separate these steps. CAM plants will open their stomata at night when it is cooler to avoid water loss and use PEP carboxylase to capture the carbon from the CO_2 that diffuses through the stomata. During the night, PEP carboxylase converts to oxaloacetate and then to malic acid which accumulates overnight. In the morning, the stomata close and the malic acid is decarboxylated creating CO_2, which is then fixed into the plant tissues

by RuBisCo. By keeping the stomata closed and by temporally separating the carboxylation process from RuBisCo, CAM plants prevent CO_2 from leaking out of the stomata and preventing photorespiration from occurring (O'Leary 1988). Most CAM plants have $\delta^{13}C$ values that fall between -10 and -20‰ (Cerling et al. 1997; O'Leary 1988).

The different carboxylation reactions in C_3, C_4 and CAM photosynthesis means that plants that use these different photosynthetic pathways discriminate against ^{13}C differently. This results in different ranges of delta values for C_3 ($\delta^{13}C = -26.7 \pm 2.3$‰), C_4 ($\delta^{13}C = -12.5 \pm 1.1$‰) and CAM plants ($\delta^{13}C = -10$ to -20‰) (Cerling et al. 1997). Variation in CAM plant $\delta^{13}C$ values is driven by when CAM plants open their stomata. If the stomata are open during the day they engage in C_3 photosynthesis resulting in low $\delta^{13}C$ values similar to those seen in C_3 plants. However, when CAM plants open their stomata only at night, they will have $\delta^{13}C$ values similar to those seen in C_4 plants. This is because at night they use PEP carboxylase to capture carbon and convert to oxaloacetate and malic acid, and the decarboxylation of malic acid into CO_2 and the fixing of carbon by RuBisCo does not occur until daytime.

Because of the different $\delta^{13}C$ value ranges between these three photosynthetic pathways, the isotopic composition of plants not only makes it possible to identify which photosynthetic pathway it uses, but also to look at how the carbon isotopes in these plants move up the food chain and are routed to various tissues, allowing the C_3 and C_4 plant component of human and animal diets to be reconstructed.

Carbon Isotopes in Aquatic Ecosystems

Plants in aquatic ecosystems have a much larger range of $\delta^{13}C$ values than terrestrial plants with some species having values as low as -50‰ (Keeley and Sandquist 1992). Aquatic

plants get their carbon from dissolved inorganic carbon. Carbon dioxide is soluble in water and can then convert to different inorganic forms: free CO_2, carbonic acid, bicarbonate, and carbonate. The abundance of each form is largely based on the pH and temperature of the water with more free CO_2 in low pH water, more bicarbonate in neutral water, and more carbonate in more basic water, and in colder water CO_2 is more soluble than in warmer water. The wide range of $\delta^{13}C$ values has less to do with the photosynthetic pathway used and more to do with diffusive resistance in the aquatic environment, the species of carbon used, and the $\delta^{13}C$ value of dissolved inorganic carbon (Fry and Sherr 1989; Keeley and Sandquist 1992).

Aquatic plants can get carbon via either diffusion or carbon concentrating mechanisms, and biochemical processes through active bicarbonate influx or through CAM and C_4 photosynthetic pathways. Diffusion is the simplest way for plants to get carbon and will affect the fractionation of carbon isotopes. The thickness of the boundary layer (the area around the leaf) influences how quickly CO_2 and energy can be exchanged between the leaf and the water. In stagnant waters with a thick boundary layer, diffusion is slower and thus there is less discrimination against ^{13}C resulting in higher $\delta^{13}C$ values. In fast moving waters with a thin boundary layer, diffusion is much faster leading to greater discrimination against ^{13}C and thus higher $\delta^{13}C$ values. Additionally, the $\delta^{13}C$ values of aquatic plants is affected by which species of carbon is used. For example, plants that use bicarbonate have higher $\delta^{13}C$ values than plants that use CO_2 (Fry and Sherr 1989; Keeley and Sandquist 1992). This variation in how aquatic plants take in CO_2 and the effects of temperature and pH on CO_2 concentration influence the fractionation of carbon isotopes. This results in aquatic plants with a wide range of $\delta^{13}C$ values, often with very low values. As a result, the fish consuming these plants or other fish will also have lower $\delta^{13}C$ values.

Nitrogen Isotopes in Plants and Soil Systems

Nitrogen isotopes are useful for understanding human diet, specifically the protein sources consumed. However, to understand nitrogen isotopes in human tissue we first must understand the sources of variation of $\delta^{15}N$ values in the environment.

The two stable isotopes of nitrogen are ^{15}N and ^{14}N. As noted earlier, the $\delta^{15}N$ value of nitrogen isotopes in soil, plants, animals, etc. Inorganic nitrogen gas (N_2) makes up 78% of the earth's atmospheric gases and thus is very abundant. However, N_2 is not biologically available to plants and thus must be converted into other forms of nitrogen, such as ammonium or nitrate. The various steps in the nitrogen cycle that convert nitrogen to different forms contribute to variation in $\delta^{15}N$ values between soil and plants as well as between different plants. Thus, plant tissue $\delta^{15}N$ values do not necessarily reflect soil $\delta^{15}N$ values (Evans 2007; Pardo and Nadelhoffer 2009).

The Nitrogen Cycle in Soil Systems

Plants primarily take up nitrogen in the forms of ammonium (NH_{4+}) and nitrate (NO_{3-}), which are inorganic forms of nitrogen, as well as amino acids. Atmospheric nitrogen that gets fixed into soil must first be converted into these usable forms. This can be done in a few ways. Mineralization, which includes ammonification and nitrification, are processes that involve the decomposition or oxidation of nitrogen in decaying organic matter into accessible forms for plants. Ammonification occurs when nitrogen-fixing bacteria or fungi in the soil break down decomposing organic plant or animal matter and convert it back to ammonium. Ammonification can result in a fractionation of 0-5‰. Additionally, volatilization of ammonium (gaseous loss) from soil can result in discriminations as high as 40 ‰ (Evans 2007). Through the process of nitrification, nitrifying bacteria in the soil can also oxidate ammonium and convert it to nitrite

(NO_{2}-). Nitrification can result in a fractionation of 15‰ to 35‰. A secondary oxidation can occur that further converts nitrite into nitrate, also a bioavailable form of inorganic nitrogen. Through a process called immobilization, nitrate can be converted back to N_2 by anaerobic denitrifying bacteria, which is then released back into the atmosphere as N_2 gas (Evans 2007; Evans 2001; Pardo and Nadelhoffer 2009).

Areas with high amounts of precipitation have increased microbial activity and thus increased nitrogen fixation in the soil and thus lower $\delta^{15}N$ values. Arid areas may experience volatilization, leaching, and denitrification. Volatilization is the loss of nitrogen through the conversion of ammonium into ammonia gas which is then released into the atmosphere (Evans 2007). Arid environments also mean the soil cannot retain nitrate, so leaching of nitrate out of the soil with water occurs, but the rate of leaching depends on soil drainage, rainfall amounts, the amount of nitrate originally present in the soul, and crop uptake of nitrate. Arid environments also experience nitrogen loss through denitrification, the conversion of nitrate into nitric oxide (NO), nitrous oxide (N_2O), and inorganic nitrogen gas. This leads to higher plant $\delta^{15}N$ values due to the preferential loss of ^{14}N leaving the soil enriched in ^{15}N (Evans 2007). Individuals who live in arid environments can also have elevated $\delta^{15}N$ values due to consumption of these ^{15}N enriched plants or animals. Having plants with elevated $\delta^{15}N$ due to aridity increases the $\delta^{15}N$ value baseline resulting in animals and human with elevated $\delta^{15}N$ values.

In forested environments, litterfall is another key part of the nitrogen cycle as microorganisms that break down dead organic matter from plants (also animals and microbes), nitrogen is released as dissolved organic matter which is then mineralized into forms that are accessible to plants (Zhu et al. 2015). Soil $\delta^{15}N$ values have been shown to be affected by temperature, with warmer climates being characterized by higher $\delta^{15}N$ values than colder

climates, which is related to greater water loss in warmer climates which, as discussed above, leads to soil that is enriched in ^{15}N (Pardo et al. 2006; Szpak 2014).

Nitrogen Assimilation in Plants

Plants take up nitrogen in the form of ammonium or nitrate in a process called assimilation. The basic steps of nitrogen uptake are 1) nitrogen is taken up from the soil 2) nitrogen is translocated to the site of assimilation, and 3) assimilation of inorganic nitrogen to organic nitrogen occurs (Evans 2007; Evans 2001).

Assimilation of ammonium occurs in the root through the Glutamine Synthetase-Glutamate Synthase (GS-GOGAT) pathway. The assimilation of nitrate occurs in the roots or shoots (leaves) through the Nitrate Reductase-Nitrite Reductase pathway. The assimilation of nitrate results in ammonium so then that ammonium enters the GS-GOGAT pathway to assimilate into the plant (Evans 2007; Evans 2001).

Intra and Inter-Plant Variation and Nitrogen Fractionation

When plants uptake inorganic nitrogen in either the form of ammonium or nitrate, very little discrimination occurs, and it enters a pool of nitrogen inside the plant cell that then gets assimilated into the plant via the GS-GOGAT or Nitrate Reductase-Nitrite Reductase pathway. Both pathways discriminate against ^{15}N, about 15‰ for Nitrate Reductase and 17‰ for Glutamine Synthetase, which results in the nitrogen pool inside the cell being enriched in ^{15}N relative to both the nitrogen outside of the plant and the organic nitrogen produced by the assimilation process (Evans 2001). The organic nitrogen that was assimilated into the plant tissues is depleted in ^{15}N resulting in plant tissues having a more negative $\delta^{15}N$ value relative to the nitrogen that was taken up from the soil (Evans 2001). However, when external nitrogen concentrations are low plants will not discriminate against the heavier isotope thus reducing

isotopic fractionation, and the resulting $\delta^{15}N$ value of the plant will be similar to the external nitrogen source in the soil (Evans 2001).

Intra-plant variation in nitrogen isotope values occurs due to the two assimilation pathways used for the two types of inorganic nitrogen that plants uptake. Ammonium is taken up at the root and assimilated at the root in one event. Nitrate, however, is taken up at the root but can be assimilated at either the root or leaf. When nitrate is assimilated at the root, the Nitrate Reductase-Nitrite Reductase pathway discriminates against ^{15}N and leaves behind a pool nitrate that is enriched in ^{15}N. The unassimilated, ^{15}N enriched nitrate is then available for assimilation in the leaves of the plant, giving the leaves a pool of nitrate with a higher $\delta^{15}N$ value than the roots, resulting in leaves that have $\delta^{15}N$ values higher than the $\delta^{15}N$ values of the roots. Experiments with two plant species, *Brassica campestris* and *Lycopersicon esculentum* show that $\delta^{15}N$ values of leaves from *Brassica* (10.6‰) were more enriched than the root $\delta^{15}N$ (4.9‰) (Evans 2001).

Mycorrhizae are mutualistic fungi that partner with plant roots and provide nitrogen to plants. Mycorrhizae will provide most of the nitrogen when soil inorganic nitrogen is low. However, these associations between plants and mycorrhizae cause plant $\delta^{15}N$ values to be lower due to retention of ^{15}N by the fungi. Studies have shown that plant $\delta^{15}N$ values can differ from mycorrhizae by between 8‰ and 12‰ (Hobbie and Hobbie 2006; Pardo and Nadelhoffer 2009). The most likely cause is fractionation that occurs during the transfer for nitrogen from the mycorrhizae to the plant's roots (Hobbie and Hobbie 2006; Pardo and Nadelhoffer 2009).

Differences in nitrogen isotopic composition can also vary between plants, especially plants of different species due to differences in plant physiology, genetic differences, and the form of inorganic nitrogen that is preferentially assimilated. Differences in environmental

conditions can also impact the $\delta^{15}N$ values of plants and soil. However, due to the many variables that can affect the $\delta^{15}N$ values of plants and soil, whether from the assimilation pathway used, the concentration of inorganic nitrogen in the soil, wet versus arid environments, or the presence of certain fungi, plant $\delta^{15}N$ values are not reliable tracers of nitrogen sources in an environment and there is still much to be learned about nitrogen isotope fractionation in plant and soil systems. What is understood of nitrogen isotope ecology will help in studies of how these isotopes move through the food chain into animals and humans, but other factors such as human activity need to also be considered when interpreting plant and human stable nitrogen isotope values.

Plant $\delta^{15}N$ values are not necessarily reflective of soil $\delta^{15}N$ values because of discrimination against ^{15}N that occurs during ammonification and nitrification. These processes result in plants having more negative $\delta^{15}N$ values than the soil they grow in. Nitrogen is often the limiting factor in plant growth. Thus, there is greater discrimination against ^{15}N with increasing amounts of nitrate in the soil (Evans 2001).

The Impact of Human Agricultural Activity on Soil Nitrogen

Of importance to archaeologists are some of the agriculture practices humans used in the past that can impact nitrogen isotope fractionation in soil and plants and thus effect our ability to reconstruct past land and animal management practices, subsistence strategies, and human and animal diet. This includes the use of animal fertilizer (manure), burning (swiddening), and tillage.

The use of animal manure as fertilizer, whether by collecting and storing manure to be spread over fields or deposited by grazing animals, introduces nitrogen to the soil. The $\delta^{15}N$

value of manure is often higher than the $\delta^{15}N$ value of the soil, and usually results in the $\delta^{15}N$ value of the plant being higher than the soil as well. The type of manure used, the amount applied, and whether the manure was stored for a period of time before being used will also impact the plant's $\delta^{15}N$ value. Different animals have manure with different nitrogen isotopic compositions due to physiological differences between animal species and how they excrete nitrogen waste. Cattle manure tends to have the lowest $\delta^{15}N$ values while pigs have the highest. Storing manure for long periods of time results in nitrogen loss through the volatilization of ammonium into ammonia gas and denitrification. These processes result in ^{15}N depleted products, leaving the manure enriched in ^{15}N. If this manure is then used as fertilizer, it will result in plants with higher $\delta^{15}N$ values (Choi et al. 2002; Fraser et al. 2011; Szpak 2014).

Variation within and between plants will still exist since the introduction of fertilizers will impact how nitrogen is transformed into different forms of nitrogen (both usable and not usable to plants), and how much nitrogen is lost through volatilization or denitrification. Also, the amount of mineralized nitrogen in the fertilizer (and thus usable to plants) will differ depending on the animal and thus affect how much of the nitrogen is accessible for plant uptake (Bogaard et al. 2007; Choi et al. 2002; Fraser et al. 2011; Szpak 2014).

Carbon and Nitrogen Isotopes in Humans and Animals: You Are What You Eat

The ecology of carbon and nitrogen stable isotopes in plant-soil systems and the various environmental factors that can affect isotope discrimination in these systems (whether human driven or not) that were discussed above are foundational to understanding how those isotopes move through trophic levels and ultimately affect the isotopic composition of human tissues. Humans cultivate plants for food, consume those plants or use them as fodder for livestock, and then consume that livestock. Humans also hunt wild game and fish or trap for freshwater and

marine food sources. How carbon and nitrogen isotopes then get routed to various tissues are important for interpreting carbon and nitrogen stable isotope values of human tissues in archaeological research.

Nitrogen Isotope Sources and Trophic Level Enrichment

Nitrogen isotopes in all animals, including humans, are almost entirely supplied by dietary protein, thus nitrogen stable isotopes can provide insight into the degree to which people relied on terrestrial and/or aquatic sources of protein in their diet. There is a stepwise increase of 3-5‰ in $\delta^{15}N$ values of bone collagen at each trophic level, resulting in herbivores exhibiting lower $\delta^{15}N$ values than omnivores or carnivores (Bocherens and Drucker 2003; Deniro and Epstein 1981; Michener and Kaufmnan 2007; Minagawa and Wada 1984). Nitrogen stable isotopes can also be used to identify marine and terrestrial resources in diet. Freshwater fish have higher $\delta^{15}N$ values than terrestrial mammals (8-11‰) and anadromous marine fish, like sturgeon, have higher $\delta^{15}N$ values than freshwater fish and terrestrial mammals (Bocherens et al. 2007; Knudson et al. 2012; Linderholm and Kjellström 2011).

This trophic level enrichment is not entirely understood, but is thought to be the result of the isotopic composition of what an animal consumes combined with the isotopic fractionation associated with the physiological processes of incorporating what they consume into their body tissues and excreting the waste products (Ben-David and Flaherty 2012; Deniro and Epstein 1981). However, many factors mediate the incorporation of dietary isotopes into animal tissues such as age, nutritional status, trophic position, macronutrients present in the diet, etc. These factors can affect the diet to tissue fractionation factor (Ben-David and Flaherty 2012).

Animals excrete nitrogen waste in a few different ways. Fish and amphibians excrete ammonia; birds, and insects excrete uric acid; and mammals and some frogs excrete urea. This

production of nitrogen waste is the result of amino acid catabolism. When protein is consumed, amino acids are used to build muscle and collagen. This involves either removing amino acids from a molecule (deamination) or moving amino acid groups to a ketoacid to form new amino acids (transamination). In these processes, ^{14}N is preferentially taken up into urea because the molecular bonds with ^{14}N are easier to break. This leaves the body tissues enriched in ^{15}N. Once that ^{15}N enriched tissue is consumed by another animal higher up the food web, fractionation occurs again as those nitrogen atoms are routed to collagen or muscle tissue in the body, and nitrogen waste is excreted (Ambrose 1991; Sponheimer et al. 2003).

How nitrogen is routed to body tissues also varies between herbivores and carnivores. Herbivores are generally eating a protein-poor diet and thus whatever protein is consumed is used for collagen synthesis and very little is excreted as waste to maintain mass balance. Instead, most nitrogen is lost through the shedding of hair, milk, enzymes, and gut wall. This results in lower diet to tissue fractionation and thus less ^{15}N enrichment of body tissues. Carnivores, on the other hand, are consuming a high protein diet to meet energy and protein needs, and consume more protein and nitrogen than needed to maintain body tissues and nitrogen mass balance. Carnivores will shed excess nitrogen through their urine with ^{14}N being preferentially lost leading to a greater diet to tissue fractionation and larger ^{15}N enrichment of body tissues (Koch 2007).

It was previously thought that some arid-adapted species had elevated tissue $\delta^{15}N$ values due to metabolic processes like the recycling of urea due to low-protein diets. However, experimental studies have also shown that animals consuming plants in arid environments have elevated bone collagen $\delta^{15}N$ values not because of metabolism, but because of the elevated $\delta^{15}N$ values of the plants they are consuming (Murphy and Bowman 2006; Sealy et al. 1987). This is

also likely the case for humans living in arid environments, as the plants available for consumption are going to be enriched in ^{15}N due to nitrogen volatilization of the soil and loss of ^{14}N.

However, trophic enrichment is not the same within or between species or trophic levels, and even specialized animals do not have a diet that is consistent in isotope ratios or macronutrients. Animals, including humans, often switch dietary sources based on what is available in a given season or area where they are living and these changes in diet are not immediately reflected in their tissues. Tissue turnover takes time and thus changes in the isotopic composition or macronutrients of dietary sources will not be reflected for weeks or months (Ben-David and Flaherty 2012). This is all to say that while we have a growing understanding of how isotopes move through a food web – from dietary inputs to animal tissues to waste – and the many factors (macronutrient, age, health, omnivorous, herbivorous, or carnivorous diet) that influence diet to tissue isotope fractionation, tracing isotopes through a trophic position is complicated and still not fully understood. However, it is our best tool for reconstructing ancient food webs, the diets of long extinct species, and the foodways and dietary composition of past human groups.

Nitrogen Isotopes and Nutritional Stress

Often, organisms are not at a steady state, particularly during periods of nutritional stress/starvation and gestation. Each of these states represent anabolic and catabolic states. Studies have shown that during pregnancy, women are in an anabolic state if they are getting adequate nitrogen inputs from diet, and the process of building proteins (for themselves and the fetus) puts them in nitrogen balance (Fuller et al. 2004). During breastfeeding, infants have higher $\delta^{15}N$ values compared to the mother due to the trophic level enrichment from consuming

the mother's bodily tissues i.e. breast milk. Studies showed a wide range in ^{15}N enrichments in breastfed infants, between 1.7‰ and 2.8‰ with a gradual decline in $\delta^{15}N$ values as other foods are introduced during the weaning process (Fuller et al. 2006). Severe nutritional stress, like starvation, is a catabolic state where the body will begin to break down its own tissues (muscle) to get the nitrogen it needs to synthesize proteins. As a result, the body tissues become enriched in ^{15}N and the $\delta^{15}N$ value of body tissue increases. Thus, very high $\delta^{15}N$ values could indicate starvation rather than high protein consumption, but further evidence and proper context needs to be considered along with the isotopic data to determine if starvation is a possible explanation (Fuller et al. 2004, 2005).

Carbon Isotopes in Human Tissues: Bioapatite vs. Collagen

In contrast to nitrogen isotopes, carbon isotopes can come from animal protein as well as carbohydrates and fats. Therefore, how carbon atoms are routed from dietary sources into tissues differs according to the tissue in question. Ambrose and Norr (1993) demonstrated through controlled feeding experiments that carbon in body proteins (bone collagen) is derived mainly from protein sources. Carbon in bone carbonate is reflective of the whole diet (including protein, carbohydrates, and lipids) (Koch et al. 1994; Turner Tomaszewicz et al. 2015).

These tissues are reflective of the animal and plant food sources being consumed with different diet to tissue spacings for carbonate versus collagen and for herbivores and carnivores. For carnivores, diet to muscle tissue spacing is +1.1‰ (Roth and Hobson 2000), and Ambrose and Norr (1993) found a diet to bone collagen spacing of -2.2‰ to +9.6‰ for rats. For herbivores and humans consuming plants, the diet to bone collagen spacing is +4.8‰ ± 0.5‰, while humans or carnivores consuming animals having a spacing of 1‰ (Ambrose and Norr 1993; Bocherens and Drucker 2003; Fernandes et al. 2015). In controlled feeding experiments,

Ambrose and Norr fed rats a pure C_3 diet and the $\delta^{13}C$ value of bone carbonate was +9.5‰ relative to the diet suggesting that carbon atoms in bone carbonate represent the whole diet (Ambrose and Norr 1993). Diet to apatite (enamel) spacings are much larger, about +14.1‰ for ruminants and ~ +9‰ for humans (Cerling and Harris 1999).

Different tissue types also tell us different things about an individual's diet (whole diet versus protein) as discussed above, but also due to different tissues forming at different times or having different rates of turnover, the stable isotope values of different tissues also represent specific time periods in an individual's life. Dental enamel is made up almost entirely of hydroxyapatite (bioapatite), a calcium phosphate mineral that contains both carbonate ions and phosphate ions, and begins forming *in utero* and continues until early adolescence. Thus, it incorporates isotopes from food and water sources during this period of development. Once dental enamel is fully developed, it does not remodel and thus preserves the isotopic signature of the childhood environment (Bentley 2006; Budd et al. 2000; Hillson 1996). Bone is made up of both organic (collagen) and inorganic (hydroxyapatite) components and continuously remodels throughout an individual's life. There is some variability in turnover rates between different bones and between cortical and cancellous bone with cortical bone remodeling at a slower rate than cancellous. Thus, the isotopic composition of bone will represent an isotopic average over different periods, as much as the last two decades of life to as little as the last several years of life. Given these differences between how enamel and bone tissue grow, are maintained throughout life, and are preserved archaeologically, the types of isotopic information that can be gained from these tissues is different and should be a factor in choosing which tissues to sample (Bentley 2006; Bentley et al. 2002; Redfern et al. 2019).

Sources of Carbon and Nitrogen in Romania

When reconstructing human dietary composition, the sources of carbon and nitrogen in the diet must be considered along with how they may be reflected in bone tissue. In Romania during the 14th – 18th centuries common cereal crops included wheat, barley, rye, spelt, buckwheat, oats, and millet (Székely 2018; Tița 2006); except for millet, these crops all utilize the C_3 photosynthetic pathway. Millet is a hardy, high yield crop possibly first introduced to central and eastern Europe in the Late Neolithic to Early Bronze Age, and widely cultivated by the Middle to Late Bronze Age (Adamson 2004; Nesbitt and Summers 1988; Tafuri et al. 2009; Ventresca Miller and Makarewicz 2019). Its consumption in Europe has historically been associated with lower status diets, with C_3 crops like wheat being more accessible to higher status individuals (Gugora et al. 2018; Tafuri et al. 2009). Maize, a C_4 crop, was introduced to Romania in the late 17th century and quickly became the main food source for peasants, with wheat being consumed by the ruling classes (Georgescu 1991b; Rüsz Fogarasi 2009; Székely 2018; Tița 2006). A variety of fruits and vegetables—all C_3— were also grown in Moldavia and nearby principalities, including onions, leeks, garlic, legumes, cabbage, beetroot, parsley, cucumbers, stone fruits, apples, pears, quinces, grapes, melons, and chestnuts (Székely 2018; Tița 2006).

Not only are most of the domesticated staple crops C_3 plants, but Romania lies in the temperate zone that is hospitable to C_3 vegetation – spruce and beech forests in the mountains, oak and beach in the high hills, and poplar, willow, and alder trees in the low hills and floodplains – and thus much of the wild vegetation are C_3 plants. Just south of Romania are southern European countries like Bulgaria, Italy, Greece, as well as Turkey that are in the subtropical zone where more C_4 plants would grow (Ministry of Environment and Forests 2010).

Sources of animal protein in Romania during this same period would have included livestock such as pigs, cattle, sheep, goats, and chickens. Dairy products from cow and sheep's milk as well as butter and cheeses were also commonly consumed and also sold in local markets or exported throughout the Ottoman Empire (Székely 2018). Freshwater fishes were also a food source as the Danube River and the rivers that feed it contained sturgeon, carp, trout, mudminnows, and catfish (Székely 2018).

While no baseline faunal carbon or nitrogen stable isotope data exists for Romania's medieval or early modern period, faunal data from similar time periods and regions has been collected. In early medieval Bavaria (Germany), Hakenbeck and colleagues (2010) analyzed bone collagen from cattle (*Bos taurus)*, pig (*Sus*), sheep/goat (caprines), and horse (*Equus caballus*) remains, as well as wild game including red deer (*Cervus elaphus*) and unidentified canids. The domestic and wild (deer) terrestrial herbivores all had $\delta^{13}C$ values between -23.3 and -20.6‰ and $\delta^{15}N$ values between 3.9 and 11.6‰, consistent with terrestrial herbivores consuming a primarily C_3 diet in a temperate climate. A few animals with higher nitrogen values (>10‰) were possibly still weaning (Hakenbeck et al. 2010; Schoeninger and DeNiro 1984). The wild canids had $\delta^{15}N$ values that were consistent with a carnivorous diet ranging from 9.9 to 11.2‰. In medieval (12^{th}-13^{th} century) Poland, Reitsema and colleagues (2013) analyzed fish and domestic livestock (cow, sheep, chicken, and pig) bone collagen. For fish, the average $\delta^{15}N$ value was 9.5 ± 2.2‰ and the average $\delta^{13}C$ value was -21.9 ± 5.7‰. For domestic livestock. The average $\delta^{15}N$ value was 7.6 ± 1.2‰ and the average $\delta^{13}C$ value was -20.6 ± 1.1‰. These values are consistent with animals foddered on primarily C_3 plants, with the exception of one cow that was possibly foddered on millet (Reitsema et al. 2013). Gugora and colleagues (2018) found similar results in medieval (13^{th} century) Hungary with two faunal samples associated with

human burials that had $\delta^{13}C$ values of -15.7‰ and -22.1‰ and $\delta^{15}N$ values of 9.6‰ and 11.1‰ (Gugora et al. 2018). While not specific to Romania, these data come from livestock living at similar times and in neighboring regions with similar climates to Romania and thus will be informative for understanding carbon and nitrogen stable isotope values from bone collagen at the study sites.

Understanding what plant and animal protein sources were being consumed not only provides valuable insight into dietary composition and available food sources in the past, but when examined along with demographic data on a population (age and sex), skeletal stress lesions, and historical/archaeological evidence of social class we can begin to understand how factors like age, sex, and social status influenced access to food resources. Carbon and nitrogen stable isotope analysis makes it possible to explore dietary composition directly from human tissues in addition to historical and archaeological evidence. Additionally, we can begin to understand how these factors and diet affected the probability that an individual would exhibit skeletal stress lesions and what this says about individual and population level stress and health during this time.

In the principality of Moldavia and the three study sites, consumption of mostly C_3 (wheat, oats, barley, and rye) and some C_4 (millet and maize after the 17th C) food sources is expected, with millet being the staple of the peasant class and the higher classes like princes and nobles having more access to meat and dairy products. This difference would potentially manifest isotopically in the form of higher $\delta^{15}N$ values and more negative $\delta^{13}C$ values of bone collagen in high-status individuals, and higher $\delta^{13}C$ values and lower $\delta^{15}N$ values in those of lower social status. Combined with other historical and archaeological evidence, a person's social position may be able to be ascertained using this multi-isotope approach.

Multi-isotope Approaches to the Study of Human Diet and Health

Studies of human diet and health in the United Kingdom and Scandinavia have used various isotopes to explore questions about dietary composition, nutritional stress and famine, and patterns of infectious disease and skeletal stress. These approaches show how a multi-isotope approach along with archaeological, historical, and skeletal data yields more robust conclusions and helps to address some of the potential confounding factors that single isotope approaches introduce.

Exploring Human Diet, Social Status, and Health with Carbon and Nitrogen Stable Isotopes

It is well documented that an individual's social status in society, combined with other factors like age, sex, religion, etc. can impact access to resources and produce differential health outcomes (DeWitte 2014; Wilson 2014). In medieval Europe, diet and social status and sex have been found to be linked due to the different access to food resources, especially animal protein between higher and lower social status individuals and sex-based divisions of labor with males usually engaging in more physically demanding labor (Gugora et al. 2018; Richards et al. 2006). Multi-isotope and multi-method approaches combined with pathological data makes it possible to see these impacts of social identity on health and dietary composition.

In Sweden, Linderholm and Kjellström (2011) used sulfur, carbon, and nitrogen stable isotope analysis to investigate mobility, diet, and social status of individuals with leprosy. They found that carbon and nitrogen isotope composition of bone collagen did not significantly differ between those with and without evidence of leprosy. The $\delta^{15}N$ and $\delta^{13}C$ values suggested that both groups were consuming freshwater fish as well as terrestrial protein sources. However, burial position did suggest different treatment of those with leprosy in death. Homogenous

isotope results between groups and differential mortuary treatment shows that isotope results alone cannot elucidate the ways that different groups were treated in the past.

Carbon and nitrogen stable isotopes have been used to investigate diet and how it relates to health, nutritional stress, and social status as indicated by skeletal remains and burial treatment. In the U.K., carbon and nitrogen stable isotopes combined with historical and pathological data has allowed researchers to improve our understanding of the health consequences of famine and how it manifests in the skeleton. The results showed that non-famine burials had higher $\delta^{15}N$ values than famine burials and thus the isotope results were more indicative of dietary differences between famine and attritional burials with attritional burials consuming higher trophic level protein, in this case freshwater fish (Walter et al. 2020). Studying human health, diet, and mobility in the past is complex, and this study highlights the need for multiple lines of evidence (skeletal lesions, stable isotopes, archaeological, and historical documentation) to disentangle the relationship between diet, social status, and health. How these factors manifest on the skeleton both macroscopically and at the molecular level is a process mediated by a variety of complex extrinsic factors (culture, politics, environment) and intrinsic factors (individual metabolism, hormones, immunogenicity, genetics, disease burden, age, sex, etc.).

Multi-isotope approaches combined with pathological data have also made it possible to further disentangle the association between diet and indicators of stress or disease, mortality risk and diet, and whether isotopic fluctuations in certain tissues over time are due to dietary change or nutritional stress (Curto et al. 2019; Redfern et al. 2019; Walter et al. 2020). All the previously discussed studies have demonstrated the utility of a multi-isotope and multi-discipline approach in a variety of contexts for addressing questions about diet and health in the past and how to

begin to disentangle the many factors that influence patterns of stress and frailty in past human populations.

In Romania, studies have explored human diet and health from the Paleolithic and Bronze Age periods in Transylvania and the Carpathian Basin, as well as neighboring countries including Bulgaria, Hungary, and Ukraine (Beck et al. 2021; Gerling 2015a, 2015b; Gerling et al. 2012; Gerling and Ciugudean 2013; Ventresca Miller et al. 2021), but there is a lack of studies looking at health and diet in Romania's medieval period. Voas and colleagues (2021) used carbon and nitrogen stable isotopes of dentin and bone collagen of non-adults from the Carpathian Mountain basin of Transylvania to investigate weaning practices and diet composition of infants and children in the Early Modern period. Palincaş and colleagues (2019) found that some individuals from a 14^{th} – 17^{th} century cemetery site in southern Romania were consuming a C_3 and terrestrial animal protein diet, while one individual seemed to be consuming a more C_4 heavy diet suggesting they either came from a region of Romania where millet was cultivated or were consuming animals foddered on C_4 plants. This is in contrast to a Hungarian Székely site in Transylvania where preliminary carbon and nitrogen stable isotope analysis has shown a pure C_3 diet, which is consistent with what is understood about the diets of Hungarian diaspora populations being predominantly wheat (Personal communication with Dr. Jon Bethard, 2022). Overall, the medieval period in Romania, and eastern Europe more broadly, has a distinct lack of studies using multi-isotope approaches that explore diet and health.

Carbon stable isotopes are a useful tool for identifying the presence of C_3 and C_4 plant consumption at these sites, and how consumption of these plants may vary by age, sex, site, and social status. Nitrogen stable isotope analysis of collagen is useful for identifying animal protein consumption. Together, carbon and nitrogen stable isotope analysis of collagen can elucidate

terrestrial and aquatic protein sources being consumed in northeast Romania during the late medieval-early modern period.

CHAPTER FIVE: MATERIALS AND METHODS

Chapter Overview

In this chapter, I describe the materials and methods used in data collection and analyses. It includes information on the sites and skeletal collections and methods used for skeletal analyses of age, sex, and non-specific stress lesions. The second half of the chapter details the methods for stable isotope sampling of bone, sample preparation, pretreatment, and analyses. I conclude the chapter outlining statistical analyses of skeletal data and isotopic data, and data management and long-term curation of data.

Individuals Analyzed and Sampled

The individuals analyzed in this study were excavated from three cemetery sites in the region of Moldavia in northeast Romania: Suceava, Palatul Cnejilor (Cnejilor Palace), and Schitișor (Table 5.1). The human remains recovered from these excavations (1951-58) are currently curated at the Francisc I. Rainer Institute of Anthropology (FRIA) of the Romanian Academy in Bucharest, Romania. A total of 232 individuals (adults and subadults) were available for analysis (Suceava = 161, Palatul Cnejilor = 43, and Schitișor = 28). Eight individuals had to be eliminated due to poor preservation or commingling. 224 individuals were sufficiently preserved for analysis (Suceava = 155, Palatul Cnejilor = 42, and Schitișor = 27). For stable isotope sampling, 189 individuals had sufficiently preserved ribs and/or femora for sampling.

Skeletal Demography and Paleopathology

Assigning Unique Identifiers and Inventory

All individuals in the sample were assigned a unique individual identification (ID) name that consisted of the abbreviated site name (SUC = Suceava, PC = Palatul Cnejilor, SCHIT =

Table 5.1. Study sites with location, number of individuals, dates, context, and probable social class of individuals buried at each site.

Site Name	Location	No. of Individuals	Dates in Use	Social Class of Cemetery Population
Suceava	Cemetery located on a plateau called Câmpul Santurilor (Field of Ditches) on eastern side of Suceava Citadel	161	1375-1526/1538 CE	Presence of low-quality silver jewelry and simple pit graves indicates low-middle social status for most individuals. Some brick-and-mortar vault burials were present with jewelry and clothing suggesting higher status individuals, possible members of the royal court.
Schitișor	Cemetery with two small houses and a church in the village of Schit.	28	Late 16th – early 19th C. CE	Presence of clay bricks in some graves suggests burials of monks and nuns. House style suggest peasants resided at this site as well.
Palatul Cnejilor (Cnejilor Palace)	Fortified enclosure on a plateau. Four towers, a church and cemetery inside. Small houses built nearby.	43	17th – 18th C. CE	Cemetery contained monks and secular individuals. Some grave inventories suggest the presence of Palace rulers as well.

Schitișor), the context information (sector, trench and/or feature numbers), and grave number all separated by underscores (SITE_CONTEXT_GRAVE#). A database created in FileMaker Pro 19 (Claris International Inc.) was used to document all skeletal and isotopic data collected.

Prior to analysis, a photograph was taken of the box label that included the individual ID, which made sorting of photographs later more efficient. Each skeleton was laid out in anatomical position for inventory, and overview photographs were taken to have a visual record of which elements were present.

The percent (%) complete for each bone was documented (0-25%, 36-50%, 51-75%, or 76-100%) per Buikstra and Ubelaker (1994). Only the number of left and right ribs, carpals, tarsals, metacarpals, metatarsals, and phalanges was recorded. The number of cervical, thoracic, and lumbar vertebrae were recorded. A dental inventory was performed to document which teeth were present, and which were absent antemortem, postmortem, or completely unobservable.

Age-at-Death Estimation

Age-at-death was estimated using Transition Analysis 2 (TA2) (Boldsen et al. 2002). Transition Analysis uses features of the pelvis (pubic symphysis and auricular surface) and cranial sutures to estimate age-at-death. Up to 19 traits on the pelvis and skull are scored on a numerical scale according to the instructions from Data Collection Procedures for Forensic Skeletal Material 2.0 (Langley et al. 2016) and those scores are then entered into the ADBOU 2.1.046 age estimation software program using the white reference population which provides maximum likelihood curves and point estimates of the individual's age (Boldsen et al. 2016). This method is designed for fragmentary remains that may not have all the features present or preserved sufficiently for scoring, while avoiding issues of age mimicry and broad age ranges for older individuals (Boldsen et al. 2002).

Tooth eruption, specifically the presence or absence of third molars, and/or sternal rib ends (Hartnett 2010) were used to estimate age for individuals that did not have any preserved cranial sutures, pubic symphyses, or auricular surfaces. If sternal rib ends or third molars were not present, then fusion of the epiphyses was used to determine if the individual was an adult, and if so then age was listed as unknown. The age of subadult individuals was estimated by comparing the tooth eruption pattern to the tooth eruption diagrams in Schaefer et al. (2009). Epiphysial fusion age ranges from Buikstra and Ubelaker (1994) were used if there was no maxillary or mandibular dentition present.

Non-Metric and Metric Sex Estimation

Sex estimation was conducted using both non-metric and metric sex estimation methods. Non-metric methods included both cranial traits (Walker 2008) and traits of the pubic symphysis (Kenyhercz et al. 2017; Klales et al. 2012). Non-metric methods were used when sufficiently preserved cranial and/or pelvic traits were present. The metric method consisted of humeral and/or femoral head maximum diameter measurements (millimeters) using sliding calipers and employing regression formulae and sectioning points for the American White reference population (Spradley and Jantz 2011).

Present and sufficiently preserved traits of the skull were scored according to Walker (2008) and scores were entered into the logistic regression equations for cranial sex estimation. The trait combination with the highest probability was used for the final sex estimate for the skull. Present and sufficiently preserved pubic symphyses were scored according to Klales et al. (2012) and those scores were entered into the Kenyhercz et al. (2017) recalibrated linear regression formulas.

If both the skull and pelvis were present and scorable, but the Walker (2008) and Klales et al. (2012) methods did not agree, then the final sex estimation was based on the pelvis. When the pelvic and cranial traits did not agree, femoral and humeral head measurements were taken as an additional data point, but the final sex estimation was based on the pelvis. If there was no pelvis or cranium and only femoral and humeral head measurements were possible, then the final sex estimation was based on these measurements. However, if the measurements were right on the sectioning point, then the sex was considered intermediate. Sex was listed as undetermined in cases where pelvic and cranial scores produced probabilities below 70% (for example 60% probability male, 40% probability female), or when only a skull was present, and the scores produced probabilities below 70%. If an individual had no skull, pelvis, or preserved femoral and/or humeral heads then, if possible, other univariate metrics from Spradley and Jantz (2011) that had an accuracy of at least 70% were taken. Preservation usually made it possible to take the femoral transverse subtrochanteric breadth (accuracy = 0.69) (but only if no other measurement was available) or femoral transverse diameter (accuracy = 0.71). If these other univariate metrics were not possible, then sex was listed as undetermined. The overall preservation of these collections usually precluded maximum breadth or length measurements of long bones, which would have been preferable due to higher accuracy rates (Spradley and Jantz 2011).

Skeletal Pathology: Non-specific indicators of stress and dental pathology

The non-specific indicators of stress and dental pathology documented and analyzed for this collection include periosteal new bone formation (PNBF), porotic lesions of the skull (*porotic hyperostosis* and *cribra orbitalia*), caries, abscesses, and periodontal disease.

Periosteal New Bone Formation (PNBF)

PNBF was scored for all the long bones of the upper limb (scapula, humerus, radius, and ulna) and the lower limb (femur, tibia, and fibula). Each bone was first given a cortical bone preservation score from McKinley (2004) to document the preservation of the cortical surface and to justify scores of "unobservable" for bones where most or all the cortical surface was eroded and thus not scorable for PNBF. Scoring methods from both Buikstra and Ubelaker (1994) and Steckel et al. (2006) were used to score each bone for the presence of PNBF, as well as the state of activity/healing (Table 5.2). If the cortical surface was eroded on more than half of a bone surface, the bone was not present or less than 25% of the bone was present, then a score of "unobservable" was given.

Scoring for PNBF with both the Buikstra and Ubelaker (1994) method and the Steckel et al. (2006) method allowed cases of osteomyelitis and fractures to be differentiated from non-specific PNBF, as well as further describe each lesion's state of activity (active, sclerotic, and mixed) (Figure 5.1). However, scores using Buikstra and Ubelaker (1994) were preferentially used.

In addition to these scores, the section and aspect of the bone affected, extent of involvement (<1/3, 1/3-2/3, >2/3), and distribution of the lesions (focal, multifocal, diffuse) was documented along with a brief description. The breadth and length measurements were taken for discrete lesions. Lesions were photographed using a Canon EOS Rebel T3i digital camera. The image numbers were recorded in that individual's record in the Filemaker Pro database. For each individual, an overall conclusion of the presence or absence of PNBF and healing state was documented.

Table 5.2. PNBF Scores for Buikstra and Ubelaker (1994) and Steckel et al. (2006)

Buikstra and Ubelaker (1994)	Steckel et al. (2006)
Active (woven)	No osteoperiostitis present
Sclerotic (healing)	Markedly accentuated longitudinal striations
Mixed (active and sclerotic)	Slight, discrete patch(es) of reactive bone involving less than one quarter of the long bone surface
Absent	Moderate involvement of the periosteum, but less than one-half (1/2) of the long bone surface
Unobservable	Extensive periosteal reaction involving over half (>1/2) of the diaphysis, with cortical expansion, pronounced deformation
	Osteomyelitis (infection involving most of the diaphysis with cloaca)
	Osteoperiostitis associated with a fracture



Figure 5.1. Three activity stages for PNBF on the tibia: (A) active, (B), sclerotic, and (C) mixed.

For example, if PNBF was present on at least one bone, then the overall conclusion was "present" and if the lesion(s) were both sclerotic and active then the healing conclusion for that individual would be "mixed". Incidental pathological findings for conditions like osteoarthritis (OA), diffuse idiopathic skeletal hyperostosis (DISH), myositis ossificans, fractures, etc. were noted in that individual's record and photographed.

Most individuals in this collection presented with distinct striations on the femora and tibiae that often covered the entire diaphysis and most aspects of the bone. This was distinct from the diffuse or focal areas of sclerotic PNBF observed in some individuals. Communication with one of the author's committee members revealed this to be commonly seen in archaeological populations and may be the effect of biomechanical stress, especially in individuals who lived in rough terrain or who were physically active (personal communication, D. Steadman).

To differentiate these cases from the focal or diffuse patches of sclerotic PNBF that were found in this sample, a separate score of "present", "absent", or "unobservable" was given for "diffuse lamellar PNBF" and the bone section, aspect, and extent was documented (Figure 5.2). This was only scored on the bones of the lower limb, as it was not observed on the bones of the upper limb.

Porotic Lesions of the Skull (porotic hyperostosis and cribra orbitalia)

Porotic lesions of the skull were documented on the frontal, occipital, and parietal bones (*porotic hyperostosis*) as well as on the orbital roofs (*cribra orbitalia*) according to Buikstra and Ubelaker (1994) and Steckel et al. (2006) (Tables 5.3-5.4). Each bone was first given a cortical preservation score (McKinley 2004) and percent (%) complete score. If the cortical surface had



Figure 5.2. Two types of PNBF observed in two tibiae: (A) Diffuse lamellar PNBF possibly associated with biomechanical stress and (B) discrete patch of sclerotic PNBF with clear signs of healing and bridging.

Table 5.3. Scores for *porotic hyperostosis* from Buikstra and Ubelaker (1994) and Steckel et al. (2006)

Buikstra and Ubelaker (1994)	Steckel et al. (2006)
Absent	Absent
Indistinct porosity	Fine foramina cluster (<1 cm2)
True porosity	Small and/or large foramina (>1 cm2)
Coalescing pores	Unobservable
Coalescing pores with expansive change	
Unobservable	

Table 5.4. Scores for *cribra orbitalia* from Buikstra and Ubelaker (1994) and Steckel et al. (2006)

Buikstra and Ubelaker (1994)	Steckel et al. (2006)
Unobservable	No orbits present/unobservable
Absent	Absent with at least one orbit present
Indistinct porosity	Cluster of fine foramina (</= 1 cm2)
True porosity	Substantial area (>1 cm2) covered by small/large foramina with tendency to cluster
Coalescing pores	
Coalescing pores with expansive changes	

extensive taphonomic damage that prevented it from being reliably scored, or if the bone was not present then it was scored as unobservable. For *porotic hyperostosis* (PH), Buikstra and Ubelaker (1994) score the bones of the cranial vault (parietals, occipital, and frontal), and Steckel et al. (2006) score only the parietal bones (with at least one parietal present) so both methods were used, especially if an individual had parietal, occipital, and frontal bones present. If lesion(s) were present then the location, lesion activity, and lesion number and description were documented, and an overall conclusion about the presence or absence and healing state of PH was documented. *Cribra orbitalia* (CO) was scored on the orbital roofs, and the lesion activity, description, and overall presence/absence conclusion were also documented (Figure 5.3).

Dental Pathology: Caries, Abscesses, and Periodontal Disease

Each tooth was analyzed for the presence of dental caries. Caries were scored according to Buikstra and Ubelaker (1994). This method scores caries present on each tooth surface, on the cementoenamel junction (CEJ), the root, pulp exposure, and very large caries (Figure 5.4). If multiple scores described a carious lesion i.e., a caries that is on the buccal surface and CEJ, then all the scores that applied were documented and the total number of carious lesions were recorded.

In accordance with Steckel et al. (2006), the total number of erupted tooth positions, total erupted permanent teeth (or deciduous for juveniles), total caries on permanent teeth, and total teeth lost premortem were documented (Table 5.5). An overall conclusion of the presence or absence of caries for each individual was also documented.

The total number of dental abscesses was recorded according to Steckel et al. (2006). Each tooth was scored according to Buikstra and Ubelaker (1994) (Figure 5.5) (Table 5.6). If the maxilla or mandible were not present, part of either bone was missing, or there was extensive

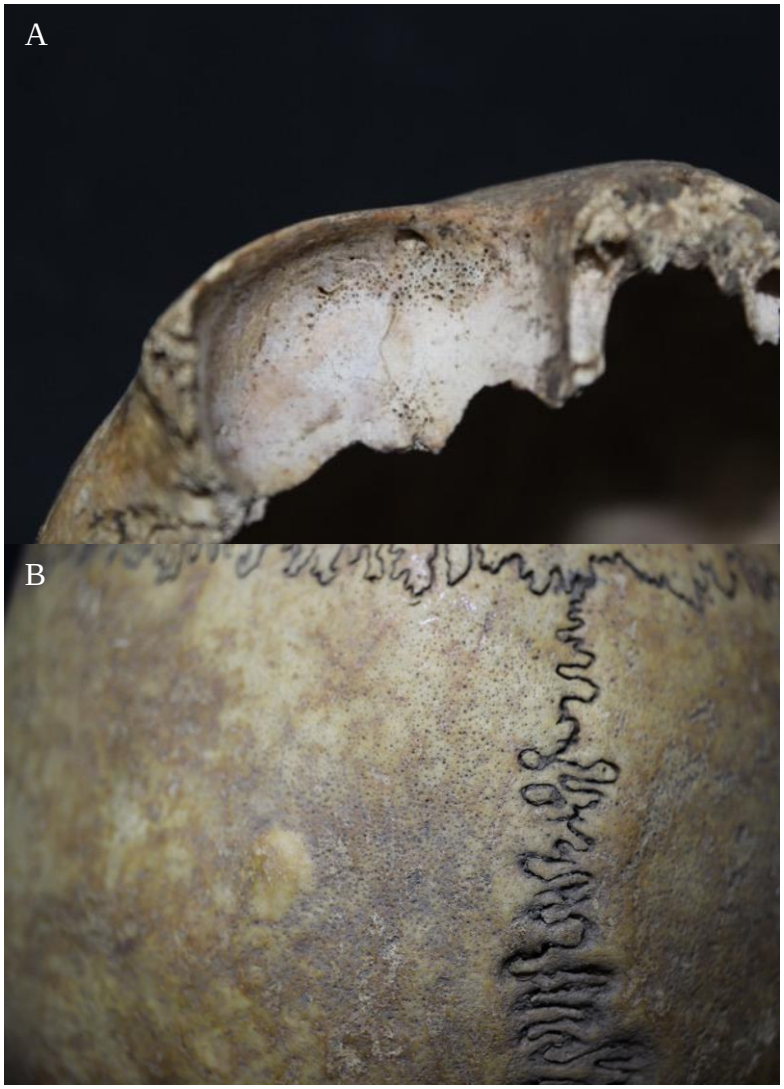


Figure 5.3. (A) Active *cribra orbitalia* and (B) *porotic hyperostosis*



Figure 5.4. Dental caries on a left mandibular first molar (LM_1)

Table 5.5. Scores for dental caries from Buikstra and Ubelaker (1994) and Steckel et al. (2006)

Buikstra and Ubelaker (1994)	Steckel et al. (2006)
No caries present	Total erupted tooth positions
Occlusal surface	Total erupted permanent teeth
Interproximal surface	Total caries permanent teeth
Smooth surfaces (buccal, labial, lingual)	Total teeth lost premortem
Cervical (CEJ except interproximal regions)	
Root caries (below CEJ)	
Large caries	
Non-carious pulp exposure	
Tooth absent/unobservable	

Table 5.6. Scores for dental abscesses from Buikstra and Ubelaker (1994) and Steckel et al. (2006)

Buikstra and Ubelaker (1994)	Steckel et al. (2006)
Absent	Total erupted tooth positions
Buccal or labial alveolar channel	Total erupted permanent teeth
Lingual perforation	Total caries permanent teeth
Tooth not present/unobservable	Total teeth lost premortem
	Total abscesses



Figure 5.5. Dental abscess at the right maxillary first premolar (PM^3). Partial tooth root is still present.

erosion and postmortem damage to all or part of the maxilla or mandible then those tooth positions were scored as unobservable Periodontal disease (PD) was scored according to Steckel et al. (2006), which scores the left mandibular second molar (right if not present), and Ogden (2008) (Table 5.7), which scores the mandibular and maxillary posterior teeth (premolars and molars) on both the left and right. A conclusion about the presence or absence of PD was documented for each individual.

Statistical Analyses: Skeletal Data

Frequencies and Tests of Association

To begin to explore the data, frequency pivot tables were created in Excel to assess the number of individuals and the number of individuals with lesions by each site, biological sex, age category (18-25, 26-35, 36-45, and 45+), and preservation. To understand the age structure across sites, a one-way ANOVA was run in SPSS (v.29.0.2.0(20)) (IBM Corp 2023). A one-way ANOVA (Analysis of Variance) is a test to determine if the means of two groups are significantly different. A one-way ANOVA of age and site was run to look for significant differences in age structure across the three study sites.

To understand the sex structure between sites a Chi-Square test was run in SPSS (v.29.0.2.0(20)) (IBM Corp 2023). Unlike a t-test, a Chi-Square test does not require continuous data and can determine if there is an association between two categorical variables. Lesion frequencies were also compared by biological sex, site, age, and level of preservation. For continuous variables (age) an independent samples t-test was run in SPSS (v.29.0.2.0(20)). Independent samples t-tests for age and each lesion type were run to determine if there was a significant difference between mean age-at-death and lesion type. For categorical variables (sex,

Table 5.7. Scores for periodontal disease (PD) from Steckel et al. (2006) and Ogden (2008)

Steckel et al. (2006)	Ogden (2008)
No periodontitis	No periodontitis
Beginning to moderate periodontitis	Mild periodontitis
Moderate periodontitis	Moderate periodontitis
Severe periodontitis	Severe periodontitis
Margin not available	Unobservable (alveoli missing)

site, and level of preservation), Chi-Square tests were run to test for associations between all the lesion types and biological sex, site, and skeletal preservation.

Intra-observer Error

Intra-observer error was assessed for age-at-death and biological sex estimates. To look at mean differences between TA2 age estimates a paired samples t-test was run in SPSS (v.29.0.2.0(20)). For the categorical variable, sex, Cohen's Kappa was calculated. Cohen's Kappa quantifies how well two observers agree in their classification of variables into categories. In this case, classifying individuals as either male or female.

Stable Isotope Sampling

Bone from the ribs and femora were sampled for carbon and nitrogen stable isotope analysis. Sampling occurred at the Francisc I. Rainer Institute of Anthropology in Bucharest, Romania.

Sampling Protocol: Femora and Ribs

All individuals that had both femora and ribs present were sampled (n=189). Samples were taken from the femur shaft and rib shaft. Sampling from both the femur and rib was done to capture intra-individual variability in bone collagen carbon and nitrogen stable isotope values because of different remodeling rates between skeletal elements. If an individual did not have ribs present, then only a femur sample was taken, and vice versa. An additional rib sample (0.5-2.0 grams) was taken from 60 individuals (Palatul Cnejilor = 10, Schitișor = 10, Suceava = 40). This was initially done when samples were going to be analyzed at the University of Bucharest (UB) Stable Isotope Laboratory to look at inter-lab variation. However, samples were not analyzed at UB, so these 60 samples served as a pilot dataset. The second rib sample and femur samples were also analyzed as part of the larger dataset. All bone samples were analyzed at the

University of Tennessee Knoxville, Department of Earth, Environment, and Planetary Sciences (EEPS) Stable Isotope Laboratory.

Prior to sampling, the femur and rib were photographed to document the presence and appearance of the bone before destructive analysis. In addition to the Individual ID, each individual was assigned a skeleton number, which was assigned based on the order in which individuals were sampled. So, the first individual sampled is skeleton #1 and then each successive individual was assigned a skeleton number in numerical order. Every sample taken from an individual (femur, rib, or enamel) was given a unique sample name consisting of the abbreviated site name, "rib" or "femur", and that individual's skeleton number (i.e., SUC_Rib_#1 and SUC_Femur_#1). The assignment of a skeleton number to each individual allows for simple tracking of multiple samples for each individual. For example, if skeleton #1 had rib, femur, second molar, and third molar sampled, then the skeleton number (#1) is present in each sample name making it simple to tell which bone and tooth samples belong to that individual.

Each sample was placed in a 15 mL centrifuge tube for storage until stable isotope analysis could be performed, and each tube was labeled with the sample name. The sample name, Individual ID, rib side/#, femur side/aspect, sample weight (g), sample date, photo numbers, and notes were recorded in a notebook, Excel spreadsheet, and in the FileMaker Pro database.

For consistency, femur samples were taken from the anterior aspect of the proximal third of the right femur. This approach was taken to avoid features like the *linea aspera* on the posterior aspect, as well as to preserve the midshaft for future research that may require midshaft maximum circumference or diameter measurements. In cases where an individual did not have a

right femur present or it was not sufficiently preserved, the sample was taken from the left. If there was pathology present on the anterior proximal third of the femur, then the sample was taken from another part of the diaphysis that was free of any pathology to preserve the lesions present. Rib samples were taken from the rib shaft (Figure 5.6). Ribs were selected based on the preservation and quality of cortical bone. Heavily eroded ribs were avoided and if the sternal rib end was present then that feature was left intact to preserve the ability of future researchers to use this feature for age estimation. Ribs with pathology present were also avoided to preserve the lesion(s) for future research.

Samples were taken with a hand-held drill and a 19 mm dentistry-grade diamond disc drill bit. At least 0.5 g were taken from the ribs and femora, with most samples ranging between 0.5 – 2.0 g to ensure sufficient collagen for stable isotope analysis. Each bone sample was washed using distilled water and a toothbrush to remove bone dust and residual dirt and left to dry for 24 hours in open air before the samples were placed in 15 mL centrifuge tubes. The drill bit was washed with distilled water and a toothbrush and dried with a Kimwipe delicate task wiper between each sample. The rib and femur were photographed to document the sample location and the bones were returned to their box. These weights were confirmed with a scale and recorded in the sample log spreadsheet and FileMaker Pro database.

Bone Collagen Pre-treatment and Analysis for Carbon and Nitrogen Stable Isotopes

A total of 332 femur and rib samples were pre-treated and analyzed for carbon and nitrogen stable isotope analysis of bone collagen. Bone collagen pre-treatment occurred at the University of Tennessee in the Zooarchaeology Laboratory in the Department of Anthropology and stable isotope analysis occurred in the Department of Earth, Environment, and Planetary Sciences (EEPS) Stable Isotope Laboratory.



Figure 5.6. Rib with sample taken from shaft (red arrow) preserving the sternal rib end.

Bone Collagen Pre-treatment

The protocol used for bone collagen extraction is based on the protocol described by Richards and Hedges (1999). Prior to collagen extraction, final "pre-extraction" weights in g were taken of each bone sample. Samples were then placed in glass culture tubes labeled with the sample ID and each tube was filled with 8 mL of 0.6 M HCl. Samples were refrigerated at 5°C for one week. After 1 week the first acid change was done. Acid was pipetted out of each tube and 8 mL of new 0.6 M HCl was added to each tube. After the initial acid change, acid changes occurred every three days until demineralization was complete, which was indicated by the samples being soft and pliable. Rib samples were sufficiently demineralized after about two weeks, while femur samples were ready after three to four weeks.

During demineralization of the 60 pilot samples, the acid turned a yellow-brown color a few days after the acid was added (Figure 5.7). The discoloration was due to the presence of humic acids. Humic acids are contaminants that leach into bone from the burial environment and may affect carbon and nitrogen stable isotope values. To eliminate any effects on the stable isotope values of the bone collagen for the remaining samples, once demineralization was complete and before gelatinization, each sample was treated with sodium hydroxide (NaOH) based on the protocol in Szpak et al. (2017). Each sample was rinsed three times with ultra-purified water from a Elga Purelab Flex water purification system to remove all HCl. Next, each sample was treated with 10 mL of 0.1 M NaOH at room temperature for 20 minutes (Figure 5.8). This protocol was repeated until the solution was clear. Once the humic acids had been removed, each sample was gelatinized. First, each sample was rinsed three times with ultra-



Figure 5.7. Yellow-brown discoloration of hydrochloric acid from humic acids during demineralization of rib samples.

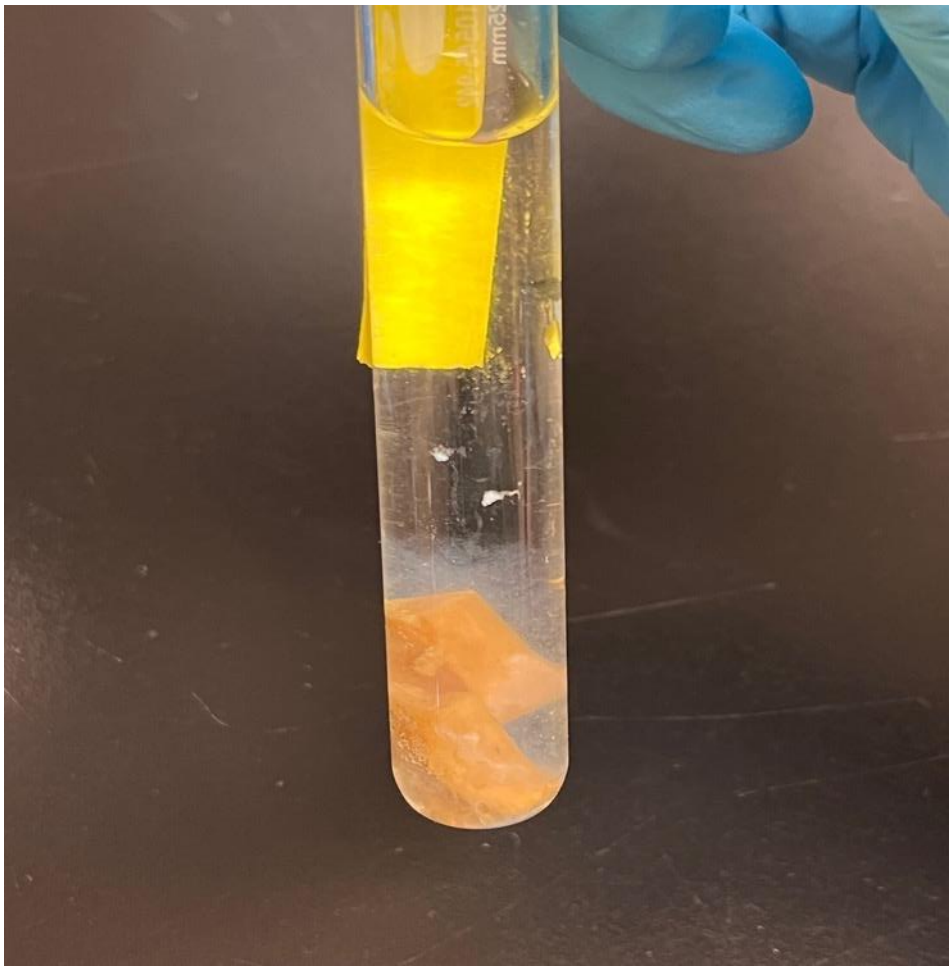


Figure 5.8. First sodium hydroxide treatment of a rib sample.

purified water and 10 mL of 0.001 M HCl (pH 3) was added to each sample. The samples were then placed in a laboratory heating and drying oven at 75 ˚C for 48 hours.

Once gelatinization was complete, each sample was filtered with an Ezee-filter ™ separator to isolate the supernatant containing collagen proteins (Figure 5.9). The filtered supernatant was then poured into a pre-labeled and weighed 15 mL centrifuge tube and frozen overnight in a -27 °C freezer, and then samples were freeze-dried.

Bone Collagen Analysis

Between 0.9 and 1.4 mg of collagen was weighed out using a microbalance and placed in a tin capsule for analysis. Each sample was then analyzed for $\delta^{13}C$, $\delta^{15}N$, %C and %N on a Thermo-Finnigan Delta mass spectrometer in the Department of Earth and Planetary Sciences Stable Isotope Laboratory. Every 12 samples, three in-house standards were used, UT729, acetCost, and LGlu4510, and samples were corrected to these standards. Isotopic ratios ($\delta^{13}C$ and $\delta^{15}N$) of these in-house standards were calibrated against two international standards, USGS40 and USGS41 with $\delta^{13}C$ values of -26.39‰ and 37.63‰, respectively, and $\delta^{15}N$ values of -4.52‰ and 47.57‰, respectively. Across 29 runs, the in-house standard UT729 yielded a mean $\delta^{13}C$ value of -12.99‰ ± 0.2 (expected value -12.97‰), and a mean $\delta^{15}N$ value of -3.66‰ ± 0.2 (expected value -3.67‰). The in-house standard acetCost yielded a mean $\delta^{13}C$ value of -33.95‰ ± 0.2 (expected value -33.95‰), and a mean $\delta^{15}N$ value of -0.85‰ ± 0.2 (expected value -0.86‰). The in-house standard LGlu4510 yielded a mean $\delta^{13}C$ value of -9.79‰ ± 0.3 (expected value -9.81‰), and a mean $\delta^{15}N$ value of 44.98‰ ± 0.1 (expected value 44.97‰). All isotopic results were scale normalized to the expected values of the in-house standards.

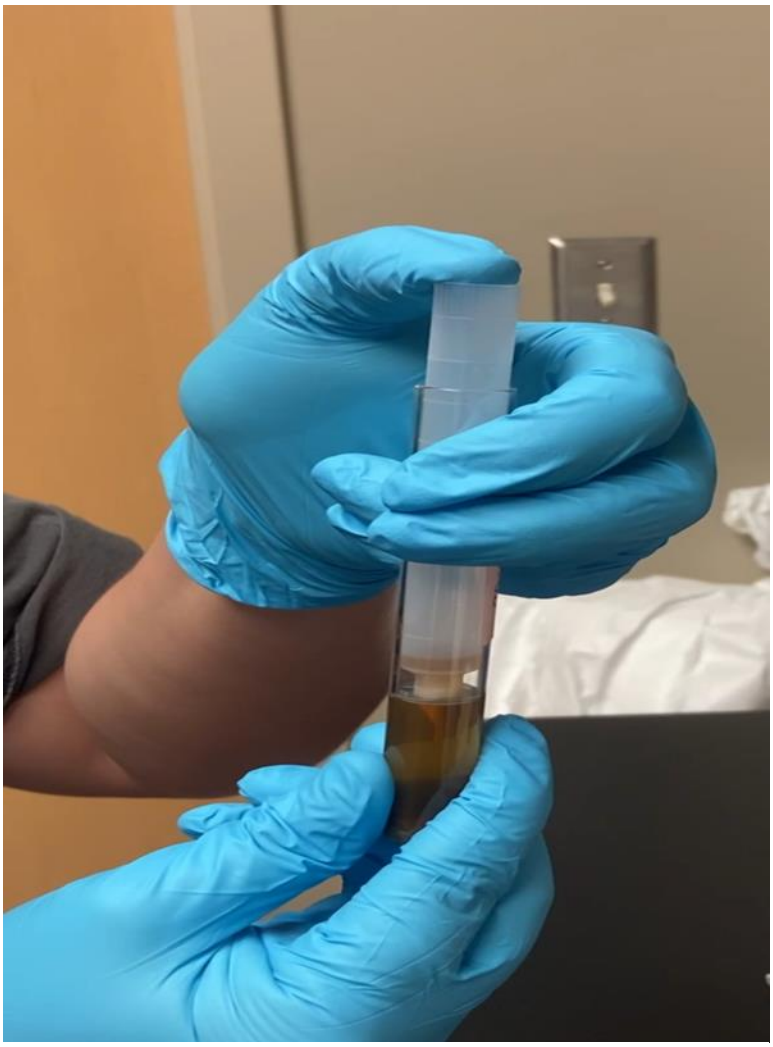


Figure 5.9. Filtering gelatinized sample with an Ezee-filter™ to isolate the supernatant prior to freeze-drying.

Stable isotope ratios of bone collagen were reported as delta (δ) values relative to an international standard. For carbon ratios in collagen this was Vienna Pee Dee Belemnite (VPDB) and for nitrogen isotope ratios in collagen this is air. Values are reported using the (‰) notation, where δ(‰) = (Rsample/Rstandard)-1, and R is the heavy/light isotope ratio for a particular element.

Statistical Analyses: Stable Isotope Data

To begin exploring the isotope data, descriptive statistics (means and variances) for each isotope were calculated in Excel pivot tables, as well as descriptive statistics for each isotope by site and biological sex. To look at the spatial patterns in the isotope data, biplots of $\delta^{13}C$ and $\delta^{15}N$ values of femur and rib collagen were created in RStudio (v. 2023.12.1+402). $\delta^{13}C$ and $\delta^{15}N$ values of femur and rib collagen were plotted by sex, site, and pathology.

To look at associations between stable isotope values and sex and site, and pathology, ANOVAs and t-tests were performed in SPSS (v.29.0.2.0(20)) (IBM Corp 2023). Since more than two sites are being compared, a one-way ANOVA was performed to test the association between $\delta^{13}C$ and $\delta^{15}N$ values for femora and ribs and each of the three study sites. Sex and pathology(presence/absence) had two categories each so independent samples t-tests were performed to look at the association between $\delta^{13}C$ and $\delta^{15}N$ values of femora and rib collagen and sex and each lesion type.

Bayesian Model: Skeletal and Isotopic Data

Bayesian Logistic Regression

In frequentist methods, logistic regressions produce a single slope of the data and rely on null hypothesis testing and p-values to indicate the probability of getting the test statistic result if

the null hypothesis is correct (there is no difference between samples). If the p-value is less than 0.05 this is considered a significant result meaning the test statistic is highly unlikely if the null hypothesis is true, or the result is unlikely to have occurred by chance. The confidence interval (CI), usually set at 90% or 95%, reflects how confident the test is that the true mean of the data falls within the CI.

Bayesian methods take prior knowledge (the prior probability), which is what you expect to find based on an existing data set, and combines that with new data (the likelihood) to produced adjusted beliefs about the data (the posterior probability) (Kruschke 2015). This is illustrated with Bayes' Theorem:

$$P(A|B) = \frac{P(B|A) \times P(A)}{P(B)}$$

Where P(A|B) is the posterior probability, P(B|A) is the probability of event B occurring given event A (the likelihood), P(A) is the prior (informed or uninformed), and P(B) is the probability of the new data. Instead of analyzing data in terms of significance and confidence that the true mean of a slope is contained with a 95% confidence interval, Bayesian methods focus on credibility, plausibility, and probability (McElreath 2018).

In preparation for building a Bayesian logistic regression model, a two sample Kolmogorov-Smirnov (KS) test was performed in SPSS (v.29.0.2.0(20)) (IBM Corp 2023) using my isotope data and a human bone collagen carbon and nitrogen stable isotope data set from Transylvania, Romania provided by Dr. Jonathan Bethard. The KS test is a nonparametric method for evaluating the differences between two distributions. This was done to evaluate Bethard's data set as an informed prior for Bayesian analysis. For a Bayesian approach, it is ideal to have an informed prior. Since Bethard's data was from a similar period and a region close to

the study sites analyzed in this dissertation, it has the potential to be a useful prior for the Bayesian models. However, the distributions of isotope values between my and Bethard's sites were significantly different. Thus, Bethard's data was not useful as an informed prior, and since no other suitable data sets exist that could be used as an informed prior, I used a flat or uninformed prior. Since it is impossible to estimate the probability of obtaining my data as they are (P(B)), the posterior probability (P(A|B)) was set as proportional to the likelihood (P(B|A)) times the prior (P(A)):

$$P(A|B) \propto P(B|A) \times P(A)$$

As a result, the posterior probability becomes a compromise between the prior (P(A)) and the likelihood (P(B|A)). This means if the prior is too strong it will reduce the impact of the likelihood and if the prior is too weak it will increase the impact of the likelihood. Since a flat prior was selected for this analysis, the outcome will be sensitive to the likelihood not the prior. However, despite this, the results are not reduced to a simple likelihood. A flat prior is still a prior and an acceptable solution for a Bayesian analysis, if not ideal, as the analysis and results are within the Bayesian theoretical framework and use Markov Chain Montecarlo (MCMC) to explore and recover the posterior parameter space (Kruschke 2015).

The MCMC in a Bayesian model does not just create a single slope of the data, as is the case with frequentist methods. Instead, it replicates this process 40,000 times to fully explore the data landscape and create a distribution of slopes based on the data. This allows a Bayesian model to reflect possible different relationships between the variables and to estimate how plausible and credible different outcomes are. So, of the 40,000 different slopes produced from the data, Bayesian models produce a credibility interval to tell you which of the 40,000 is the most plausible and credible. A Bayesian logistic regression begins with a prior belief (informed

or uninformed/flat) about the distribution of the data and calculates the slope of each predictor (independent) variable to produce a posterior distribution, rather than a point estimate, of the outcome variable slopes. Essentially, given these variables what is the probability of a specific outcome, and which slope for the outcome of interest is the most credible?

Model Description. Twelve Bayesian logistic regression models with flat priors (as no appropriate *a priori* data were available) were built in RStudio (v. 2023.12.1+402) using the brms and Rstan packages (Bürkner 2017): six models with each lesion type (PNBF, PH, CO, Caries, Abscesses, and PD) as the outcome of interest and age, sex, site, and diet (femur δ^{13}C and δ^{15}N values) as the predictor variables, and six models for each lesion type as the outcome of interest and age, sex, and site, and diet (rib δ^{13}C and δ^{15}N values) as the predictor variables. The basic formula for a Bayesian logistic regression model is:

$$y = \beta_0 + \beta_1 X_i + \beta_2 X_i + \beta_3 X_i + \beta_4 X_i + \beta_5 X_i + \in$$

Where y is the dependent variable, β_0 is the intercept slope, and β_1 is the beta coefficient (slope) for each independent variable and X_i is the independent (predictor) variable. The full Bayesian logistic regression model for femur carbon and nitrogen is:

$$y = \beta_0 + \beta_1 Age_i + \beta_2 Sex_i + \beta_3 Site_i + \beta_4 \delta^{13} CFemur_i + \beta_5 \delta^{15} NFemur_i + \in$$

rib carbon and nitrogen is:

$$y = \beta_0 + \beta_1 Age_i + \beta_2 Sex_i + \beta_3 Site_i + \beta_4 \delta^{13} CRib_i + \beta_5 \delta^{15} NRib_i + \in$$

In these models, y is the lesion outcome (presence/absence) which is categorical, sex and site predictor variables are categorical, and age and diet (δ^{13}C and δ^{15}N) variables are scaler (Table 5.8). Given a flat prior distribution, these models calculate the slope and value of each predictor variable to produce the log odds of an individual presenting with a lesion given the predictor

Table 5.8. Meanings for the outcome (y) and predictor (β) variables of the Bayesian Logistic Regression equation

Symbol	Meaning
y	Presence/Absence of Lesion (categorical)
β_0	Intercept (Sample Mean~)
$\beta_1 Age_i$	Slope for Age-at-Death (scalar)
$\beta_2 Sex_i$	Slope for Biological Sex (categorical)
$\beta_3 Sample_i$	Slope for Skeletal Sample/Site (categorical)
$\beta_4 \delta^{13} CFemur_i$	Slope for δ^{13}C Femur (scalar)
$\beta_5 \delta^{15} NFemur_i$	Slope for δ^{15}N Femur (scalar)
$\beta_4 \delta^{13} CRib_i$	Slope for δ^{13}C Rib (scalar)
$\beta_5 \delta^{15} NRib_i$	Slope for δ^{15}N Rib (scalar)
$\in$	Error

variables. Log odds can then be converted to an Odds Ratio (OR) which is the probability of an event occurring over the probability of an event not occurring, and then the probability (P) of the outcome of interest can be calculated from the OR (P = OR/1+OR). While no statistically significant difference was found between rib and femur $\delta^{13}C$ and $\delta^{15}N$ values, femur and rib isotope values were separated to see if one was a better predictor of lesions than the other and because these bones represent different times in an individual's life.

Model Selection. After each model was built, the model was fitted to the data using the brms package in R which uses a Hamilton Monte Carlo (HMC) simulation to sample the posterior distribution using random walks (Bürkner 2017). Brms code in R Studio instructed the program to fit the model to the specific data set using a Bernoulli distribution and logit function to produce the log odds of the outcome of interest, using four Markov Chains, and 40,000 iterations.

The chains are what will explore the data landscape through the random walks and 40,000 is how many times the chains will indicate a change in the elevation of the data. More iterations mean more nuance in how the data is mapped. Once complete, the Rhat statistic indicates whether each of the four chains converged (Gelman and Rubin 1992). An Rhat greater than 1.1 indicates the chains did not converge and a greater number of random walks of the posterior distribution is needed.

Once the full model was fitted to the data, several other models were built and fitted using different combinations of predictor variables (Table 5.9 and 5.10). Model selection was performed to determine which combination of predictor variables are the most parsimonious (explanatory) for each lesion type. Posterior distributions for each best-fit model were produced.

Table 5.9. Seven Bayesian logistic regression models used for each lesion type and femur $\delta^{13}C$ and $\delta^{15}N$ values and different combinations of predictor variables. Model selection was performed to see which model was most parsimonious given the data.

Femur Collagen	
Mod (Full Model)	Lesion~Age+Sex+Site+δ^{13}CFemur+δ^{15}NFemur
Mod2	Lesion~Age+Sex+Site+δ^{13}CFemur
Mod3	Lesion~Age+Sex+Site+δ^{15}NFemur
Mod4	Lesion~Age+Sex+Site
Mod5	Lesion~Age+Sex
Mod6	Lesion~Age+Site
Mod7 (Intercept)	Lesion~1

Table 5.10. Seven Bayesian logistic regression models used for each lesion type and rib $\delta^{13}C$ and $\delta^{15}N$ values and different combinations of predictor variables. Model selection was performed to see which model was most parsimonious given the data.

Rib Collagen	
Mod (Full Model)	Lesion~Age+Sex+Site+δ^{13}CRib+δ^{15}NRib
Mod2	Lesion~Age+Sex+Site+δ^{13}CRib
Mod3	Lesion~Age+Sex+Site+δ^{15}NRib
Mod4	Lesion~Age+Sex+Site
Mod5	Lesion~Age+Sex
Mod6	Lesion~Age+Site
Mod7 (Intercept)	Lesion~1

Finally, basic Kaplan-Meier Survival curves for each lesion type by age-at-death were produced in SPSS (v.29.0.2.0(20)) to look at differential survivability across lesion types.

Data Management

The FileMaker Pro database, Excel spreadsheet sample logs, QGIS files, and photographs were all saved to a password-protected Dropbox account and backed-up on a two Terabyte (TB) external hard drive. Folders were created for each site and within each site's folder, a separate folder was created for each individual, labeled with the Individual ID. During the skeletal analysis phase of data collection, photographs and the summary report from that individual's record in the FileMaker Pro database were saved to these folders. At the end of each day, photographs were uploaded and sorted into each individual's folder in Dropbox, but the original image files were retained on the camera's memory card.

Photographs retained the original photo number, and the photo numbers of all photographs associated with each individual were recorded in that individual's record in the database. At the end of each week, the folders for all the individuals analyzed that week, containing the summary reports and photographs, were copied to the external hard drive, along with the FileMaker Pro database file, and an exported Excel file of the FileMaker Pro database.

During the isotope sampling (bone and enamel) phase of data collection, photographs were uploaded and sorted into each individual's file in Dropbox and copied to the external hard drive at the end of each day. The photo numbers for all photographs associated with each individual that was sampled (before and after sample photos) were recorded in that individual's record in the database. The bone and tooth sampling log Excel spreadsheets were also saved daily to Dropbox and to the external hard drive. All the information recorded for each sample in the notebook and spreadsheet were also recorded in the FileMaker Pro database. All photographs

were retained on the camera's memory card. Plant sample logs were recorded in a notebook and an Excel spreadsheet, which was saved to Dropbox and the external hard drive. The waypoints for each sample and the QGIS maps containing the sample locations were also saved to Dropbox and the external hard drive.

CHAPTER SIX: RESULTS

Chapter Introduction

This chapter presents the results of this study. The first section, *Sample Demography,* reports the sample demography including sample size by site, biological sex, and age-at-death. Intraobserver error for biological sex and age-at-death estimates is also reported, along with tests of difference (ANOVA) and association (chi-squares) for biological sex and age-at-death at each site. The second section, *Patterns of Skeletal Stress,* reports skeletal preservation data, lesion frequencies, and tests of difference (Independent samples t-tests) and association (chi-square) for preservation, biological sex, age-at-death, and site for each lesion type. The third section, *Diet,* reports descriptive statistics and tests of difference and association (Independent t-tests and one-way ANOVA) for femur and rib carbon and nitrogen stable isotope values for biological sex and site, as well as carbon and nitrogen biplots for biological sex and site. The fourth section, *Bayesian Models for Stress and Diet,* reports the results of the 12 Bayesian logistic regression models performed including model description, selection, and summary to see which of the predictor variables are most informative for each lesion type. The final section, *Post Hoc Analysis,* reports the results of *post hoc* Kaplan-Meier survival curves.

Sample Demography

In total, 232 individuals were available for analysis (159 adults and 73 subadults). Eight individuals had to be eliminated due to poor preservation and commingling, leaving 224 individuals available for analysis. The scope and questions of this research focus on adults, with juveniles providing the opportunity to ask additional questions about health and diet over the life course as part of future research projects. Thus, only skeletal and isotopic data from adult individuals is included in the results of this research. In total, data from 159 adult individuals

across three study sites were available for analysis. Of these individuals, 23.90% (38/159) were from Palatul Cnejilor, 16.35% (26/159) were from Schitișor, and 59.75% (95/156) were from Suceava. Males comprised 45.28% (72/159) of the sample and females comprised 41.51% (66/159), with the remaining individuals either scoring intermediate between male and female or undetermined sex due to preservation issues **(**Table 6.1). The mean age-at-death of the entire sample was 48.60 years (*sd* = 22.40 years). The average age of individuals from each site and males and females are presented in Table 6.2.

Intraobserver Error

To evaluate intraobserver error for age-at-death and biological sex estimation, I re-examined the first 60 individuals, which came from Palatul Cnejilor and Schitișor. The first 60 individuals were selected because this was the first time I conducted TA2 scoring and so the first 60 would be where the most errors are likely to occur before I became more comfortable with the method. Anyone who could not be assessed for age-at-death or sex due to poor preservation, juveniles who were too young to be estimated with TA2, and anyone with a sex estimate of intermediate or indeterminate were excluded from the intraobserver analysis. This left 50 individuals for intraobserver statistical analyses. To evaluate intraobserver agreement in sex estimates, a Cohen's Kappa was calculated. Findings indicated excellent agreement between first and second observations (κ = 0.955, 95% CI = 0.867-1.000).

For age-at-death a paired samples t-test was performed. The t-test showed a significant difference between the first and second observations (p = 0.009). However, the mean difference is 5.19 years. Given that the prediction intervals provided by the TA2 method often include 10-20 years, a difference of 5.19 years is not biologically meaningful in this context.

Table 6.1. Total individuals and % of total sample for each site and sex.

Site	Total Individuals	% of Total Sample
Palatul Cnejilor	38	23.90%
Schitișor	26	16.35%
Suceava	95	59.75%
Sex		
Female	66	41.51%
Male	72	45.28%

Table 6.2. Average age of individuals from each site and sex.

Site	Avg. Age
Palatul Cnejilor	57.2
Schitișor	54.8
Suceava	43.4
Sex	
Female	45.3
Male	49.1

Tests of Difference and Association for Age and Sex

Both ANOVA and Pearson chi-square tests (Appendix One) were performed to test for differences and associations between the age-at-death and biological sex demographics of the three study sites. Significant results would suggest a significant difference in age or sex structure between these sites and problematize inter-site comparisons of lesion frequencies and diet.

Age-at-Death

To explore the age structure of each site and determine whether significant differences in age structure exist between the sites a one-way ANOVA with a Scheffe's post-hoc test was performed. All individuals with a TA2 point age estimate were included in the analysis for Palatul Cnejilor (n=33), Schitișor (n=23), and Suceava (n=82). The results of the ANOVA suggest a significant mean difference between groups ($F = 5.348$, $df = 2$, $p = 0.006$). The results of Scheffe's post hoc test suggest no significant difference in age structure between Schitișor and Palatul Cnejilor ($p = 0.919$) or Schitișor and Suceava ($p = 0.113$). Scheffe's post hoc test suggests a significant difference in age structure does exist between Palatul Cnejilor and Suceava ($p = 0.015$) (Figure A.1). The mean difference in age-at-death between Palatul Cnejilor (1) and Suceava (3) is 12.75 years. The mean age-at-death at Palatul Cnejilor is 57.18, at Schitișor it is 54.84, and at Suceava it is 44.43. Given these mean ages-at-death, a mean difference of 12.75 years between Palatul Cnejilor and Suceava is not biologically meaningful.

Biological Sex

To explore the biological sex structure of these sites and test for significant differences in the demography of males and females at these sites, a Pearson chi-square test was performed. All individuals with male ($n = 72$) or female ($n = 63$) sex estimates were included in the analysis.

The Pearson chi-square test showed no association between biological sex and site (df = 2, p = 0.111) suggesting that these sites have similar demography in terms of sex (Figure A.2-A.3).

Patterns of Skeletal Stress

This section reports the preservation, raw lesion frequencies, and tests of difference and association for preservation (Appendix One), age, biological sex, and site for each lesion type: periosteal new bone formation (PNBF), porotic hyperostosis (PH), cribra orbitalia (CO), caries, abscesses, and periodontal disease (PD). While data was collected on adults and subadult individuals, the analysis focused on the adult individuals (n=159) from all three study sites.

PNBF

Preservation. Of the 159 adults analyzed, 78% (124/159) had at least one upper limb, lower limb, or scapulae present and observable for PNBF. The mean age-at-death of individuals with at least one observable long bone is 46.7 years, and 49.2 years for individuals that did not have at least one long bone observable for PNBF.

Raw Lesion Frequencies. Of the 124 individuals that had at least one long bone or scapulae present and observable, 27.42% (34/124) presented with a lesion. By site, Suceava has the highest PNBF frequency (29.85% or 20/67), followed by Schitișor (25.0% or 6/24), and Palatul Cnejilor (24.24% or 8/33). By sex, males have a higher PNBF frequency (32.79% or 20/61) than females (25.45% or 14/55). Among those at Suceava, 29.63% of males (8/27) and 32.43% of females (12/37) presented with PNBF. Among those at Schitișor, 30.77% of males (4/13) and 18.18% of females (2/11) presented with PNBF. Among those at Palatul Cnejilor, 38.10% of males (8/21) and 0% of females presented with PNBF. PNBF is more frequent amongst those ages 18-25 at the time of death (40.91% or 9/22), and the least frequent amongst those between the ages of 36-45 (21.43% or 3/14) followed closely by those over the age of 45

(21.82% (12/55). The mean age-at-death of those with lesions is 42.9 years and for those without lesions is 50.4 years. Descriptive statistics for mean age-at-death for those with and without PNBF lesions by site and sex are listed in Table 6.3.

Tests of Difference and Association. To look at associations between the level of preservation (Good, Fair, or Poor) and PNBF, a Pearson chi-square test was performed. All individuals from each site that were scored as present or absent for PNBF were included in the analysis (n=124). The Pearson chi-square test showed no association between preservation and PNBF (df = 2, p = 0.061) (Figures A.4-A.5). Thus, there is no significant taphonomic bias in the sample for PNBF.

To look for significant differences between mean age-at-death and the presence or absence of PNBF, an independent samples t-test was performed. A Levene's test for equal variances was computed as well to adjust estimates of t-values based on adherence to or violation of the assumption of equal variances between groups. All individuals who had a point age estimate and were scored as present or absent for PNBF were included in the analysis (n=113). The mean age-at-death for those with lesions is 42.92 years and for those without lesions is 50.11 years. The results of Levene's test for equal variances suggest that equal variances can be assumed (F = 0.160, p = 0.690). There is no significant difference in the mean age-at-death between those with PNBF and those without PNBF (t = 1.619, df = 111, p = 0.108) (Figure A.6).

To look at associations between biological sex and PNBF, a Pearson chi-square test was performed. All individuals with male or female sex estimates that were scored as present or absent for PNBF were included in the analysis (n = 116). The Pearson chi-square test showed no association between biological sex and PNBF (df = 1, p = 0.386) (Figures A.7-A.8).

Table 6.3. Mean age-at-death for individuals with and without PNBF by site and sex.

	PNBF Absent			PNBF Present		
Variable	**n**	**Mean Age**	***sd***	**n**	**Mean Age**	***sd***
Site						
Palatul Cnejilor	25	56.15	17.71	8	56.36	20.21
Schitișor	18	59.03	18.40	6	36.64	18.86
Suceava	47	44.23	21.83	20	39.26	22.23
Sex						
Female	41	47.42	21.08	14	43.87	25.66
Male	41	52.16	20.88	20	42.37	20.10

To look at associations between the site where an individual was buried (as a proxy for social status) and PNBF, a Pearson chi-square test was performed. All individuals from each site that were scored as present or absent for PNBF were included in the analysis (n = 124). The Pearson chi-square test showed no association between site and PNBF (df = 2, p = 0.804) (Figures A.9-A.10).

PH

Preservation. Of the 159 adults analyzed, 59.12% (94/159) had either a frontal or parietal bone that was observable to assess for PH. The mean age-at-death of individuals with either a frontal or parietal bone is 41.9 years, and 56.8 years for individuals who did not have sufficiently preserved cranial bones for observation of PH.

Raw Lesion Frequencies. Of the 94 individuals who had at least one parietal or frontal bone present and observable, 19.15% (18/94) presented with a lesion. By site, Suceava has the highest PH frequency (20.34% or 12/59), followed by Schitișor (17.65% or 3/17), and Palatul Cnejilor (16.67% or 3/18). By sex, males have a higher PH frequency (22.92% or 11/48) than females (13.16% or 5/38). Among those at Suceava, 29.17% of males (7/24) and 10.71% of females (3/28) presented with PH. Among those at Schitișor, 9.09% of males (1/11) and 33.33% of females (2/6) presented with PH. Among those at Palatul Cnejilor, 23.08% of males (3/13) and 0.00% of females presented with PH. PH is more frequent amongst those ages 18-25 at the time of death (28.57% or 6/21), and the least frequent amongst those 45+ (14.71% or 5/34), followed closely by 26-35 (15.0% or 3/20). The mean age-at-death of those with PH lesions is 38.59 and for those without PH lesions is 45.22. Descriptive statistics for mean age-at-death for those with and without PH lesions by site and sex are listed in Table 6.4.

Table 6.4. Number of individuals, mean age, and standard deviation for presence/absence of PH for each site and sex.

	PH Absent			PH Present		
Variable	**n**	**Mean Age**	***sd***	**n**	**Mean Age**	***sd***
Site						
Palatul Cnejilor	15	49.13	17.47	3	47.27	20.96
Schitișor	14	52.50	20.20	3	49.90	20.82
Suceava	47	41.39	21.20	12	33.14	20.08
Sex						
Female	33	40.83	19.60	5	34.72	24.90
Male	37	47.99	20.77	11	36.98	16.61

Tests of Difference and Association. To look at associations between the level of preservation (Good, Fair, or Poor) and PH, a Pearson chi-square test was performed. All individuals from each site that were scored as present or absent for PH were included in the analysis (n=94). The Pearson chi-square test showed no association between preservation and PH (df = 2, p = 0.089) **(**Figures A.11-A.12). Thus, there is no significant taphonomic bias in the sample for PH.

To look for significant differences between mean age-at-death and the presence or absence of PH, an independent samples t-test was performed. A Levene's test for equal variances was computed as well to adjust estimates of t-values based on adherence to or violation of the assumption of equal variances between groups. All individuals who had a point age estimate and were scored as present or absent for PH were included in the analysis (n=87). The mean age-at-death for those with PH is 41.32 years and 45.56 years for those without PH. The results of Levene's test for equal variances suggest that equal variances can be assumed (F = 0.461, p = 0.499). There is no significant difference in the mean age-at-death between those with PH and those without PH (t = 0.769, df = 85, p = 0.444) (Figure A.13).

To look at associations between biological sex and PH, a Pearson chi-square test was performed. All individuals with male or female sex estimates that were scored as present or absent for PH were included in the analysis (n = 83). The Pearson Chi-Square test showed no association between biological sex and PH (df = 1, p = 0.179) (Figures A.14-A.15).

To look at associations between the site where an individual was buried and PH, a Pearson chi-square test was performed. All individuals from each site that were scored as present or absent for PH were included in the analysis (n = 94). The Pearson chi-square test showed no association between site and PH (df = 2, p = 0.954) (Figures A.16-A.17).

CO

Preservation. Of the 159 adults analyzed, 63.52% (101/159) had at least one orbit present and observable to assess for CO. The mean age-at-death of individuals with at least one orbit present is 41.9 years, and 59.9 years for individuals who did not have at least one frontal or parietal bone preserved for observation of CO.

Raw Lesion Frequencies. Of the 101 individuals who had at least one orbit present and observable, 9.90% (10/101) presented with a lesion. By site, Palatul Cnejilor has the highest CO frequency (11.11% or 2/18), followed by Suceava (10.61% or 7/66), and Schitișor (5.88% or 1/17)). By sex, females have a higher CO frequency (13.95% or 6/43) than males (7.84% or 4/51). Among those at Suceava, 10.71% of males (3/28) and 12.50% of females (4/32) presented with CO. Among those at Schitișor, 0.0% of males and 14.29% of females (1/7) presented with CO. Among those at Palatul Cnejilor, 7.69% of males (1/13) and 25.0% of females (1/4) presented with CO. CO was more frequent amongst those ages 18-25 at the time of death (12.5% or 3/24), and the least frequent amongst those between 36-45 (7.14% or 1/14), followed closely by 45+ (7.89% or 3/38). The mean age-at-death of those with lesions is 39.68 and for those without lesions is 44.09. Descriptive statistics for mean age-at-death for those with and without CO lesions by site and sex are listed in Table 6.5.

Tests of Difference and Association. To look at associations between the level of preservation (Good, Fair, or Poor) and CO, a Pearson chi-square test was performed. All individuals from each site that were scored as present or absent for CO were included in the analysis (n=98). The Pearson chi-square test showed no association between preservation and CO (df = 2, p = 0.133) **(**Figures A.18-A.19). Thus, there is no significant taphonomic bias in the sample for CO.

Table 6.5. Number of individuals, mean age, and standard deviation for presence/absence of CO for each site and sex.

	CO Absent			CO Present		
Variable	**n**	**Mean Age**	***sd***	**n**	**Mean Age**	***sd***
Site						
Palatul Cnejilor	16	49.09	18.47	2	42.40	13.58
Schitișor	16	52.17	20.86	1	81.00	-
Suceava	59	40.28	21.25	7	31.88	20.73
Sex						
Female	37	39.64	19.74	6	38.64	27.67
Male	47	46.01	21.37	4	40.98	21.18

To look for significant differences between mean age-at-death and the presence or absence of CO, an independent samples t-test was performed. A Levene's test for equal variances was computed as well to adjust estimates of t-values based on adherence to or violation of the assumption of equal variances between groups. All individuals who had a point age estimate and were scored as present or absent for CO were included in the analysis (n=94). The mean age-at-death for those with CO is 41.06 years and for those without is 45.3 years. The results of Levene's test for equal variances suggest that equal variances can be assumed ($F = 0.008$, $p = 0.927$). There is no significant difference in the mean age-at-death between those with CO and those without CO ($t = 0.592$, $df = 92$, $p = 0.555$) (Figure A.20).

To look at associations between biological sex and CO, a Pearson chi-square test was performed. All individuals with male or female sex estimates that were scored as present or absent for CO were included in the analysis (n = 91). The Pearson Chi-Square test showed no association between biological sex and CO ($df = 1$, $p = 0.279$) (Figures A.21-A.22).

To look at associations between the site where an individual was buried and CO, a Pearson chi-square test was performed. All individuals from each site that were scored as present or absent for CO were included in the analysis (n = 98). The Pearson chi-square test showed no association between site and CO ($df = 2$, $p = 0.811$) (Figures A.23-A.24).

Caries

Preservation. Of the 159 adults analyzed, 67.92% (108/159) had at least one tooth present and observable for dental caries. The mean age-at-death of individuals with at least one tooth present was 44.9 years, and 58.2 years for individuals who did not have at least one tooth preserved for observation of caries.

Raw Lesion Frequencies. Of the 108 individuals who had at least one tooth present and observable, 38.89% (42/108) presented with a carious lesion. By site, Schitișor had the highest caries frequency (60.0% or 12/20), followed by Palatul Cnejilor (41.18% or 7/17), and Suceava (32.39% or 23/71). By sex, males have a higher caries frequency (50.0% or 24/48) than females (31.25% or 15/48). Among those at Suceava, 39.29% of males (11/28) and 27.27% of females (9/33) presented with caries. Among those at Schitișor, 77.78% of males (7/9) and 50.0% of females (5/10) presented with caries. Among those at Palatul Cnejilor, 54.55% of males (6/11) and 20.0% of females (1/5) presented with caries. Caries were more frequent among those aged 45+ (48.78% or 20/41) and the least frequent among those between 36-45 (21.43% or 20/41). The mean age-at-death of those with caries is 46.29 and for those without caries is 43.54. Descriptive statistics for mean age-at-death for those with and without caries by site and sex are listed in Table 6.6.

Tests of Difference and Association. To look at associations between the level of preservation (Good, Fair, or Poor) and caries, a Pearson chi-square test was performed. All individuals from each site that were scored as present or absent for caries were included in the analysis (n=105). The Pearson Chi-Square test showed no association between preservation and caries (df = 2, p = 0.861) **(**Figures A.25-A.26). Thus, there is no significant taphonomic bias in the sample for caries.

To look for significant differences between mean age-at-death and the presence or absence of caries, an independent samples t-test was performed. A Levene's test for equal variances was computed as well to adjust estimates of t-values based on adherence to or violation of the assumption of equal variances between groups. All individuals who had a

Table 6.6. Number of individuals, mean age, and standard deviation for presence/absence of caries for each site and sex.

	Caries Absent			Caries Present		
Variable	**n**	**Mean Age**	***sd***	**n**	**Mean Age**	***sd***
Site						
Palatul Cnejilor	10	53.74	18.32	7	48.94	21.57
Schitișor	8	59.80	21.60	12	49.16	20.24
Suceava	48	38.28	21.48	23	43.76	22.97
Sex						
Female	33	40.74	22.11	15	39.61	20.59
Male	24	43.58	21.90	24	47.61	20.89

point age estimate and were scored as present or absent for caries were included in the analysis (n=97). The mean age-at-death for those with caries is 47.41 years and for those without lesions is 44.48 years. The results of Levene's test for equal variances suggest that equal variances can be assumed ($F = 0.007$, $p = 0.933$). There is no significant difference in the mean age-at-death between those with caries and those without caries ($t = -0.670$, $df = 95$, $p = 0.504$) (Figure A.27).

To look at associations between biological sex and caries, a Pearson chi-square test was performed. All individuals with male or female sex estimates that were scored as present or absent for caries were included in the analysis (n = 93). The Pearson Chi-Square test showed no association between biological sex and caries ($df = 1$, $p = 0.064$) (Figures A.28-A.29).

To look at associations between the site where an individual was buried and caries, a Pearson chi-square test was performed. All individuals from each site that were scored as present or absent for caries were included in the analysis (n = 105). The Pearson chi-square test showed no association between site and caries ($df = 2$, $p = 0.082$) (Figures A.30-A.31).

Abscesses

Preservation. Of the 159 adults analyzed, 71.07% (113/159) had at least a partial mandible or maxilla present and observable to assess for abscesses. The mean age-at-death of individuals with at least a partial mandible or maxilla was 44.5 years, and 58.4 years for individuals who did not have a partial mandible or maxilla preserved for observation of abscesses.

Raw Lesion Frequencies. Of the 113 individuals who had at least a partial mandible or maxilla present and observable, 24.78% (28/113) presented with an abscess. By site, Palatul Cnejilor had the highest abscess frequency (29.41% or 5/17), followed by Suceava (24.66% or 18/73), and Schitișor (21.74% or 5/23). By sex, males have a higher abscess frequency (32.69%

or 17/52) than females (20.83% or 10/48). Among those at Suceava, 28.57% of males (8/28) and 25.71% of females (9/35) presented with abscesses. Among those at Schitișor, 33.33% of males (4/12) and 10.0% of females (1/10) presented with abscesses. Among those at Palatul Cnejilor, 41.67% of males (5/12) and 0% of females (0/3) presented with abscesses. Abscesses were more frequent among those aged 36-45 (53.33% or 8/15) and the least frequent among those between 18-25 years (15.38% or 4/26). The mean age-at-death of those with abscesses is 43.19 years and for those without is 45.86 years. Descriptive statistics for mean age-at-death for those with and without abscesses by site and sex are listed in Table 6.7.

Tests of Difference and Association. To look at associations between the level of preservation (Good, Fair, or Poor) and abscesses, a Pearson chi-square test was performed. All individuals from each site that were scored as present or absent for abscesses were included in the analysis (n=110). The Pearson Chi-Square test showed no association between preservation and abscesses (df = 2, p = 0.306) **(**Figures A.32-A.33). Thus, there is no significant taphonomic bias in the sample for abscesses.

To look for significant differences between mean age-at-death and the presence or absence of abscesses, an independent samples t-test was performed. A Levene's test for equal variances was computed as well to adjust estimates of t-values based on adherence to or violation of the assumption of equal variances between groups. All individuals who had a point age estimate and were scored as present or absent for caries were included in the analysis (n=101). The mean age-at-death for those with abscesses is 44.22 years and for those without is 46.77 years. The results of the Levene's test for equal variances suggest that equal variances could not be assumed (F = 15.410, p = <.001). There was no significant difference in the mean age-at-death between those with abscesses and those without abscesses (t = 0.618, df = 61.259,

Table 6.7. Number of individuals, mean age, and standard deviation for presence/absence of abscesses for each site.

	Abscesses Absent			Abscesses Present		
Variable	**n**	**Mean Age**	***sd***	**n**	**Mean Age**	***sd***
Site						
Palatul Cnejilor	12	57.00	19.07	5	35.52	2.01
Schitișor	18	54.06	22.31	5	52.66	12.31
Suceava	55	40.17	22.97	18	42.68	19.82
Sex						
Female	38	40.27	21.50	10	42.65	21.96
Male	35	47.35	23.50	17	43.82	15.15

p= 0.539) (Figure A.34).

To look at associations between biological sex and abscesses, a Pearson chi-square test was performed. All individuals with male or female sex estimates that were scored as present or absent for abscesses were included in the analysis (n = 97). The Pearson Chi-Square test showed no association between biological sex and abscesses (df = 1, p = 0.159) (Figures A.35-A.36).

To look at associations between the site where an individual was buried and abscesses, a Pearson chi-square test was performed. All individuals from each site that were scored as present or absent for abscesses were included in the analysis (n = 110). The Pearson chi-square test showed no association between site and abscesses (df = 2, p = 0.853) (Figures A.37-A.38).

PD

Preservation. Of the 159 adults analyzed, 62.89% (100/159) had at least one-half of the posterior alveoli of the mandible or maxilla present and observable to assess for PD. The mean age-at-death of individuals with at least one-half of the posterior alveoli of the mandible or maxilla present was 45.2 years, and 57.4 years for individuals who did not have posterior alveoli preserved for observation of PD.

Raw Lesion Frequencies. Of the 100 individuals who had at least one-half of the posterior alveoli of the mandible or maxilla, 25.0% (25/100) presented with PD. By site, Palatul Cnejilor had the highest PD frequency (35.71% or 5/14), followed by Schitișor (29.41% or 5/17), and Suceava (21.74% or 15/69). By sex, males have a higher PD frequency (33.33% or 15/45) than females (20.93% or 9/43). Among those at Suceava, 33.33% of males (9/27) and 15.63% of females (5/32) presented with PD. Among those at Schitișor, 25.0% of males (2/8) and 37.50% of females (3/8) presented with PD. Among those at Palatul Cnejilor, 40.0% of males (4/10 and 33.33% of females (1/3) presented with PD. PD was more frequent among those ages 36-45

years (38.46% or 5/13) and the least frequent among those between 18-25 years (16.0% or 4/25). The mean age-at-death for those with PD is 48.47 and for those without is 41.96. Descriptive statistics for mean age-at-death for those with and without PD by site and sex are listed in Table 6.8.

Tests of Difference and Association. To look at associations between the level of preservation (Good, Fair, or Poor) and PD, a Pearson chi-square test was performed. All individuals from each site that were scored as present or absent for PD were included in the analysis (n=97). The Pearson chi-square test showed no association between preservation and PD ($df = 2$, $p = 0.066$) (Figures A.39-A.40). Thus, there is no significant taphonomic bias in the sample for PD.

To look for significant differences between mean age-at-death and the presence or absence of PD, an independent samples t-test was performed. A Levene's test for equal variances was computed as well to adjust estimates of t-values based on adherence to or violation of the assumption of equal variances between groups. All individuals who had a point age estimate and were scored as present or absent for PD were included in the analysis (n=88). The mean age-at-death for those with PD was 48.36 years and for those without was 43.45 years. The results of Levene's test for equal variances suggest that equal variances can be assumed ($F = 0.102$, $p = 0.750$). There was no significant difference in the mean-age-at death between those with PD and those without PD ($t = -0.983$, $df = 86$, $p = 0.328$) (Figure A.41).

To look at associations between biological sex and PD, a Pearson chi-square test was performed. All individuals with male or female sex estimates that were scored as present or

Table 6.8. Number of individuals, mean age, and standard deviation for presence/absence of PD for each site and sex.

	PD Absent			PD Present		
Variable	**n**	**Mean Age**	***sd***	**n**	**Mean Age**	***sd***
Site						
Palatul Cnejilor	9	45.30	19.15	5	53.62	19.34
Schitișor	12	47.95	22.84	5	64.42	17.47
Suceava	54	39.90	22.71	15	41.27	20.97
Sex						
Female	34	36.80	21.46	9	47.11	19.74
Male	30	44.21	21.64	15	47.09	22.33

absent for PD were included in the analysis (n = 85). The Pearson Chi-Square test showed no association between biological sex and PD (df = 1, p = 0.268) (Figures A.42-A.43).

To look at associations between the site where an individual was buried and PD, a Pearson chi-square test was performed. All individuals from each site that were scored as present or absent for PD were included in the analysis (n = 97). The Pearson chi-square test showed no association between site and PD (df = 2, p = 0.560) (Figures A.44-A.45).

Diet

Carbon Isotopes

All $\delta^{13}C$ values collagen for all adults, along with %C, and the carbon to nitrogen (C:N) ratios are provided in Appendix Two. The C:N ratio is to check for adequate collagen preservation which falls between 2.9 – 3.6 (Schoeninger and DeNiro 1984). Six rib samples and one femur sample had values >3.6 and thus were excluded from analysis.

Descriptive Statistics. The mean, standard deviation, and variance for femur (n = 132) and rib (n = 116) $\delta^{13}C$ values are listed in Tables 6.9. The mean $\delta^{13}C$ femur (n = 62) and rib (n = 55) values for males is -16.4‰ and -16.2‰, respectively and for females (n_{femur} = 58, n_{rib} = 52) is -17.4‰ and -17.5‰, respectively (Table 6.10). For all individuals at Palatul Cnejilor, the mean $\delta^{13}C$ femur value (n = 38) is -14.1‰ and the mean $\delta^{13}C$ rib value (n = 30) is -13.8‰ (Table 6.11). For all individuals at Schitișor, the mean $\delta^{13}C$ femur value (n = 24) is -15.8‰ and the mean $\delta^{13}C$ rib value (n = 24) is -15.8‰ (Table 6.11). For all individuals at Suceava, the mean $\delta^{13}C$ femur value (n = 70) is -18.6‰ and the mean $\delta^{13}C$ rib value (n = 62) is -18.8‰ (Table 6.11). Mean $\delta^{13}C$ femur and rib values for each lesion type are provided in Tables 6.12-6.17.

Table 6.9. Mean, standard deviation, and variance for femur and rib $\delta^{13}C$ values.

	n	Mean	*sd*	Var
Femur $\delta^{13}C$	132	-16.8	2.9	8.5
Rib $\delta^{13}C$	116	-16.9	3.0	9.1

Table 6.10. Mean and standard deviations of femur and rib $\delta^{13}C$ values for males and females.

Sex	n	Mean $\delta^{13}C$ Femur ‰	*sd* $\delta^{13}C$ Femur ‰	Mean $\delta^{13}C$ Rib ‰	*sd* $\delta^{13}C$ Rib ‰
Female	58	-17.4	2.6	-17.6	2.5
Male	62	-16.4	3.0	-16.2	3.3

Table 6.11. Mean and standard deviations of femur and rib $\delta^{13}C$ values for each site.

Site	n	Mean $\delta^{13}C$ Femur ‰	*sd* $\delta^{13}C$ Femur ‰	Mean $\delta^{13}C$ Rib ‰	*sd* $\delta^{13}C$ Rib ‰
Palatul Cnejilor	38	-14.1	2.5	-13.8	2.5
Schitișor	24	-15.8	3.4	-15.8	3.4
Suceava	70	-18.6	1.1	-18.8	1.0

Table 6.12. Mean femur and rib $\delta^{13}C$ and $\delta^{15}N$ values for those with and without PNBF.

PNBF	n	Mean $\delta^{13}C$ Femur ‰	Mean $\delta^{13}C$ Rib ‰	Mean $\delta^{15}N$ Femur ‰	Mean $\delta^{15}N$ Rib ‰
Absent	160	-16.7	-16.9	9.9	10.1
Present	57	-16.4	-16.3	10.2	10.3

Table 6.13. Mean femur and rib $\delta^{13}C$ and $\delta^{15}N$ values for those with and without PH.

PH	n	Mean $\delta^{13}C$ Femur ‰	Mean $\delta^{13}C$ Rib ‰	Mean $\delta^{15}N$ Femur ‰	Mean $\delta^{15}N$ Rib ‰
Absent	119	-16.9	-16.8	10.1	10.3
Present	22	-15.4	-16.0	9.3	10.3

Table 6.14. Mean femur and rib $\delta^{13}C$ and $\delta^{15}N$ values for those with and without CO.

CO	n	Mean $\delta^{13}C$ Femur ‰	Mean $\delta^{13}C$ Rib ‰	Mean $\delta^{15}N$ Femur ‰	Mean $\delta^{15}N$ Rib ‰
Absent	143	-17.0	-17.0	9.9	10.3
Present	11	-18.3	-17.9	1.0	10.1

Table 6.15. Mean femur and rib $\delta^{13}C$ and $\delta^{15}N$ values for those with and without caries.

Caries	n	Mean $\delta^{13}C$ Femur ‰	Mean $\delta^{13}C$ Rib ‰	Mean $\delta^{15}N$ Femur ‰	Mean $\delta^{15}N$ Rib ‰
Absent	100	-17.5	-17.6	10.0	10.2
Present	68	-16.3	-16.2	9.9	10.2

Table 6.16. Mean femur and rib $\delta^{13}C$ and $\delta^{15}N$ values for those with and without abscesses.

Abscesses	n	Mean $\delta^{13}C$ Femur ‰	Mean $\delta^{13}C$ Rib ‰	Mean $\delta^{15}N$ Femur ‰	Mean $\delta^{15}N$ Rib ‰
Absent	135	-16.9	-17.1	9.9	10.3
Present	42	-17.3	-17.0	10.1	10.3

Table 6.17. Mean femur and rib $\delta^{13}C$ and $\delta^{15}N$ values for those with and without PD.

PD	n	Mean $\delta^{13}C$ Femur ‰	Mean $\delta^{13}C$ Rib ‰	Mean $\delta^{15}N$ Femur ‰	Mean $\delta^{15}N$ Rib ‰
Absent	103	-17.3	-17.4	10.0	10.3
Present	48	-17.1	-17.3	1.0	10.3

Tests of Difference and Association. To look for associations between femur and rib carbon ($\delta^{13}C$) stable isotope values and biological sex and site, independent samples t-tests and a one-way ANOVA were performed. To look for significant differences in femur and rib $\delta^{13}C$ values and biological sex, independent samples t-tests were performed with a Levene's test for equal variances. For *sex and $\delta^{13}C$ femur values*, the results of the Levene's test for equal variances suggest that equal variances cannot be assumed (F = 5.558, p = 0.020). There is no significant difference in mean $\delta^{13}C$ femur values between males and females (t = 1.870, df = 116, p = 0.064) (Figure A.46-A.47). For *sex and $\delta^{13}C$ rib values*, the results of the Levene's test for equal variances suggest that equal variances cannot be assumed (F=11.882, p = <0.001). There is a significant difference in the mean $\delta^{13}C$ rib values between males and females (t = 2.358, df = 103, p = 0.020) (Figures A.48-A.49). However, despite this significant finding, the difference in $\delta^{13}C$ rib values between sexes is 1.4‰ which is not isotopically meaningful in terms of dietary differences between sexes.

To explore whether significant differences in rib and femur $\delta^{13}C$ values exist between the sites a one-way ANOVA with a Scheffe's post-hoc test was performed. For *$\delta^{13}C$ femur values*, the results of the ANOVA suggest a significant mean difference between the sites (F = 57.458, df = 2, p = <0.001) (Figure A.50). The results of the Scheffe's post hoc test suggest a significant mean difference in $\delta^{13}C$ femur values between Suceava and Palatul Cnejilor (p = <0.001) and Suceava and Schitișor (p = <0.001) **(**Figure A.51). Palatul Cnejilor has a mean $\delta^{13}C$ femur value 4.5‰ higher than Suceava. Schitișor has a mean $\delta^{13}C$ femur value 2.8‰ higher than Suceava. The results of the Scheffe's post hoc test suggest a significant mean difference in $\delta^{13}C$ femur

values between Palatul Cnejilor and Schitișor (p = 0.013). However, the mean difference is 1.7‰, which is not isotopically meaningful.

For *$\delta^{13}C$ rib values*, the results of the ANOVA suggest a significant mean difference between the sites (F = 59.3321, df = 2, p = <0.001) (Figure A.52). The results of the Scheffe's post hoc test suggest a significant mean difference in $\delta^{13}C$ rib values between Suceava and Palatul Cnejilor (p = <0.001), and Suceava and Schitișor (p = <0.001) (Figure A.53). Palatul Cnejilor has a mean $\delta^{13}C$ rib value 5.0‰ higher than Suceava. Schitișor has a mean $\delta^{13}C$ rib value 2.9‰ higher than Suceava. The results of the Scheffe's post hoc test suggest a significant mean difference in $\delta^{13}C$ rib values between Palatul Cnejilor and Schitișor (p = 0.003). The mean difference in $\delta^{13}C$ rib values between Palatul Cnejilor and Schitișor is 2.045‰, with Palatul Cnejilor having a mean $\delta^{13}C$ rib value of 2.045‰ higher than Schitișor.

Nitrogen Isotopes

All nitrogen stable isotope ($\delta^{15}N$) values for all adult individuals, along with %N, and the carbon to nitrogen (C:N) ratios are provided in Appendix Two.

Descriptive Statistics. The mean, standard deviation, and variance for femur (n = 132) and rib (n = 116) $\delta^{15}N$ values are listed in Table 6.18. The mean $\delta^{15}N$ femur (n = 62) and rib (n = 55) values for males are 10‰ and 10.3‰, respectively and for females (n_{femur} = 58, n_{rib} = 52) are 10.1‰ and 10.2‰, respectively (Table 6.19). For all individuals at Palatul Cnejilor, the mean $\delta^{15}N$ femur value (n = 38) is 9.5‰ and 9.6‰ for rib (n = 30) (Table 6.20). For all individuals at Schitișor, the mean $\delta^{15}N$ femur value (n = 25) is 9.5‰ and 9.6‰ for rib (n = 24) (Table 6.20). For all individuals at Suceava, the mean $\delta^{15}N$ femur value (n = 70) is 10.5‰ and

Table 6.18. Mean, standard deviation, and variance for femur and rib $\delta^{15}N$ values.

	n	Mean	*sd*	Var
Femur $\delta^{15}N$	132	10.0	0.9	0.8
Rib $\delta^{15}N$	116	10.2	0.9	0.8

Table 6.19. Mean and standard deviations of femur and rib $\delta^{15}N$ values for males and females.

Sex	n	Mean $\delta^{15}N$ Femur ‰	sd $\delta^{15}N$ Femur ‰	Mean $\delta^{15}N$ Rib ‰	sd $\delta^{15}N$ Rib ‰
Female	58	10.1	0.8	10.2	0.8
Male	62	10.0	1.0	10.3	0.9

Table 6.20. Mean and standard deviations of femur and rib $\delta^{15}N$ values for each site.

Site	n	Mean $\delta^{15}N$ Femur ‰	*sd* $\delta^{15}N$ Femur ‰	Mean $\delta^{15}N$ Rib ‰	*sd* of $\delta^{15}N$ Rib ‰
Palatul Cnejilor	38	9.5	0.6	9.6	0.6
Schitișor	24	9.5	0.6	9.6	0.6
Suceava	70	10.5	0.9	10.7	0.8

10.7‰ for rib (n = 62) (Table 6.20). See Tables 6.12-6.17 again for $\delta^{15}N$ femur and rib values for each lesion type.

Tests of Difference and Association. To look for associations between femur and rib nitrogen ($\delta^{15}N$) stable isotope values and biological sex and site, independent samples t-tests and a one-way ANOVA were performed. To look for significant differences in femur and rib $\delta^{15}N$ values and biological sex, independent samples t-tests were performed with a Levene's test for equal variances. For *sex and $\delta^{15}N$ femur values*, the results of the Levene's test for equal variances suggest that equal variances can be assumed (F = 2.055, p = 0.154). There was no significant difference in the mean $\delta^{15}N$ femur values between males and females (t = -0.394, df = 116, p = 0.694) (Figures A.54-55). For *sex and $\delta^{15}N$ rib values*, the results of the Levene's test for equal variances suggest that equal variance can be assumed (F = 3.107, p = 0.081). There was no significant difference in

the mean $\delta^{15}N$ rib values between males and females (t = 1.020, df = 103, p = 0.310) (Figures A.56-A.57).

To explore whether significant differences in rib and femur $\delta^{15}N$ values exist between the sites a one-way ANOVA with a Scheffe's post-hoc test was performed. For *$\delta^{15}N$ femur values*, the results of the ANOVA suggest a significant mean difference between the sites (F = 28.082, df = 2, p = <0.001) (Figure A.58). The results of the Scheffe's post hoc test suggest no significant mean difference in $\delta^{15}N$ femur values between Palatul Cnejilor and Schitișor (p = 0.887).

However, the Scheffe's post-hoc test does suggest a significant mean difference between Suceava and Palatul Cnejilor (p = <0.001) and Suceava and Schitișor (p = <0.001) (Figure A.59). The mean difference in $\delta^{15}N$ femur values between Suceava and Palatul Cnejilor is 1.1‰ and

between Suceava and Schitișor it is 1.0‰, neither of which are isotopically meaningful differences. For *$\delta^{15}N$ rib values*, the results of the ANOVA suggest a significant mean difference between the sites (F=37.207, df = 2, p = <0.001) (Figure A.60). The results of the Scheffe's post hoc test suggest no significant mean difference in the $\delta^{15}N$ rib values between Palatul Cnejilor and Schitișor (p = 1.0). The Scheffe's post hoc test does suggest a significant mean difference in $\delta^{15}N$ rib values between Suceava and Palatul Cnejilor (p = <0.001) and Suceava and Schitișor (p = <0.001) (Figure A.61). However, the mean difference between Suceava and Palatul Cnejilor and between Suceava and Schitișor is 1.1‰, neither of which is isotopically meaningful.

Carbon and Nitrogen Covariation

$\delta^{13}C$ and $\delta^{15}N$ values for rib and femur samples were plotted to show the relationship between carbon and nitrogen stable isotope values by sex and site, and by each lesion type. There was overlap for rib and femur carbon and nitrogen when plotted for each lesion type and these biplots are provided in Appendix Two. Figures 6.1 and 6.2 show $\delta^{13}C$ and $\delta^{15}N$ values for rib and femur collagen color-coded by sex. This biplot shows complete overlap of the 95% confidence ellipses. While there seems to be more males clustering in the area above -16‰ for $\delta^{13}C$ values (Males=25, Females =11) and 11‰ for $\delta^{15}N$ values (Males=12, Females=6), the points for males and females overlap showing no clear separation in $\delta^{13}C$ and $\delta^{15}N$ values between the sexes. Figures 6.3 and 6.4 show $\delta^{13}C$ and $\delta^{15}N$ values for rib and femur collagen color-coded by site. There are clear clusters in femur and rib $\delta^{13}C$ and $\delta^{15}N$ values for individuals from Suceava and individuals from Palatul Cnejilor and Schitișor. Individuals from Suceava have femur collagen $\delta^{13}C$ values that fall between ~ -17‰ and -21‰ and for femur $\delta^{15}N$ values only individuals from Suceava fall above 11.5‰, showing a clear cluster of

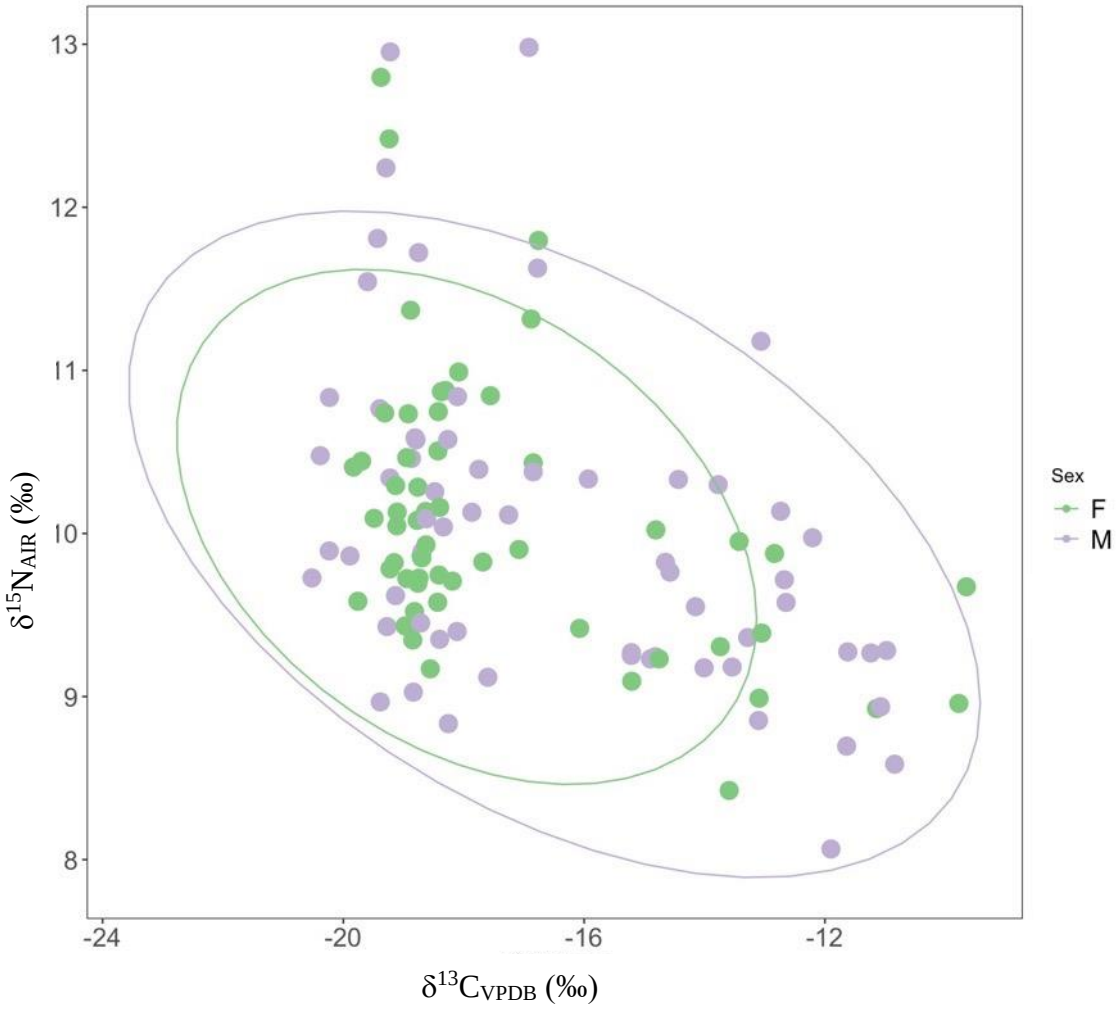


Figure 6.1. $\delta^{13}C$ and $\delta^{15}N$ values for femur collagen by sex with 95% confidence ellipses. Males are purple and females are green.

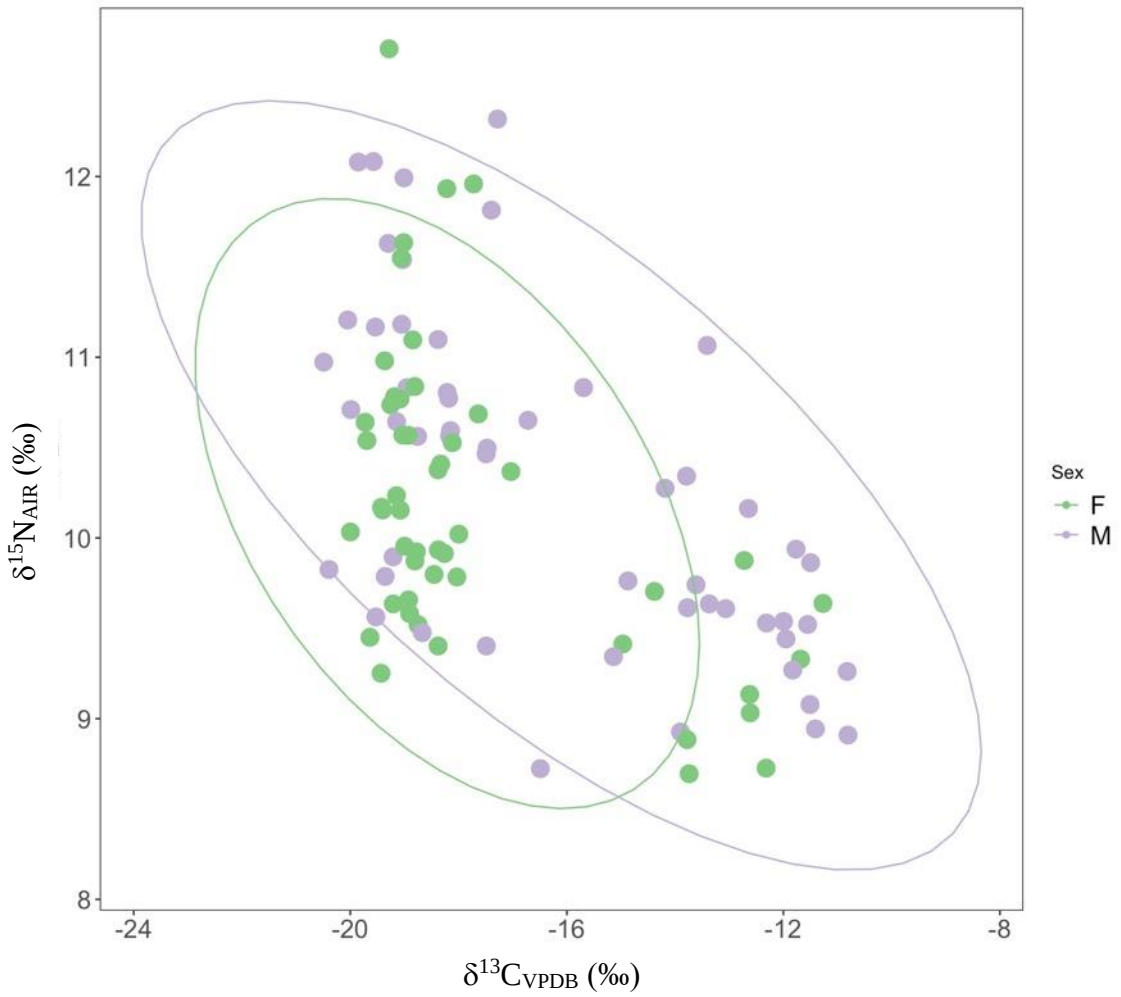


Figure 6.2. $\delta^{13}C$ and $\delta^{15}N$ values for rib collagen by sex with 95% confidence ellipses. Males are purple and females are green.

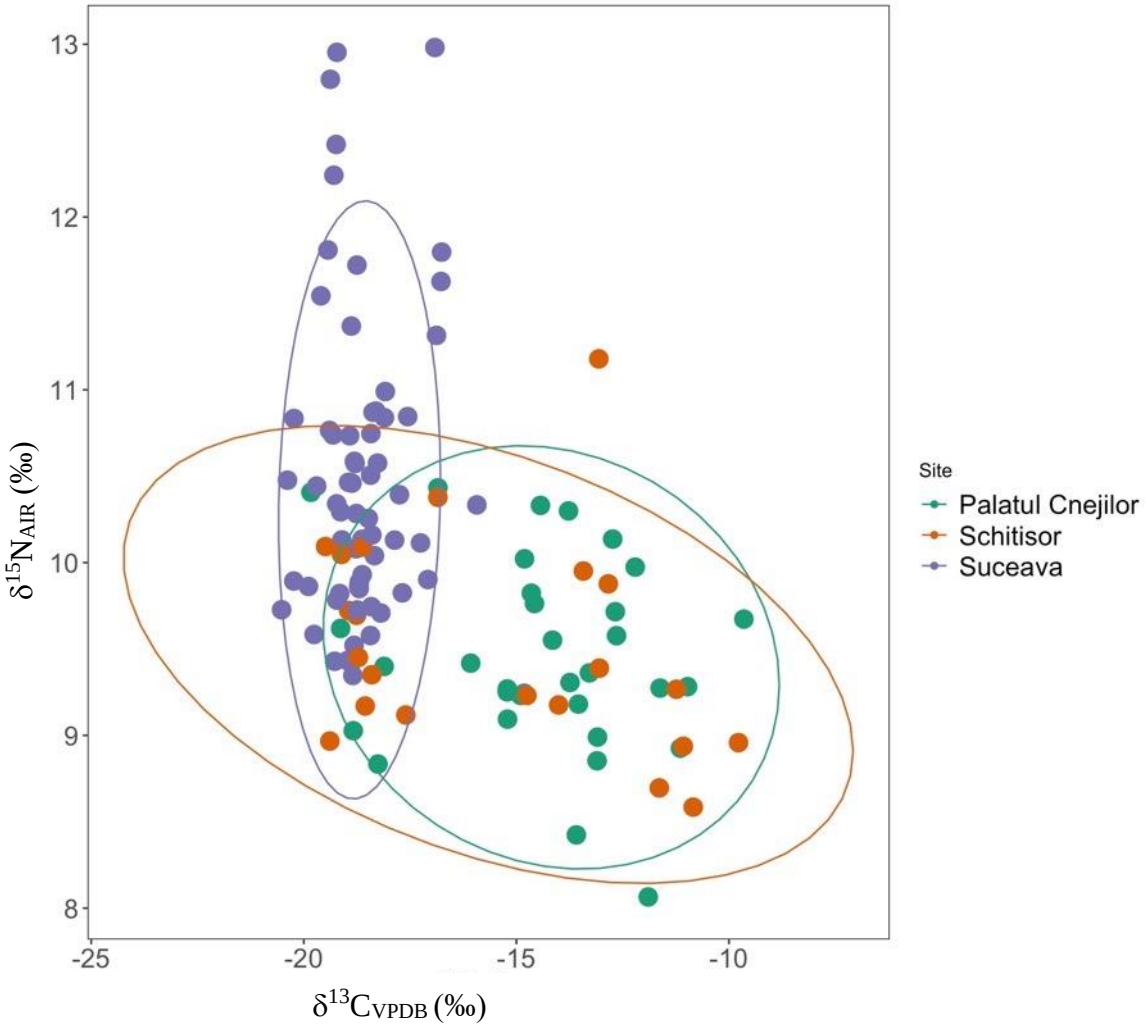


Figure 6.3. $\delta^{13}C$ and $\delta^{15}N$ values for femur collagen by site with 95% confidence ellipses. Teal =Palatul Cnejilor, orange=Schitișor, and purple= Suceava.

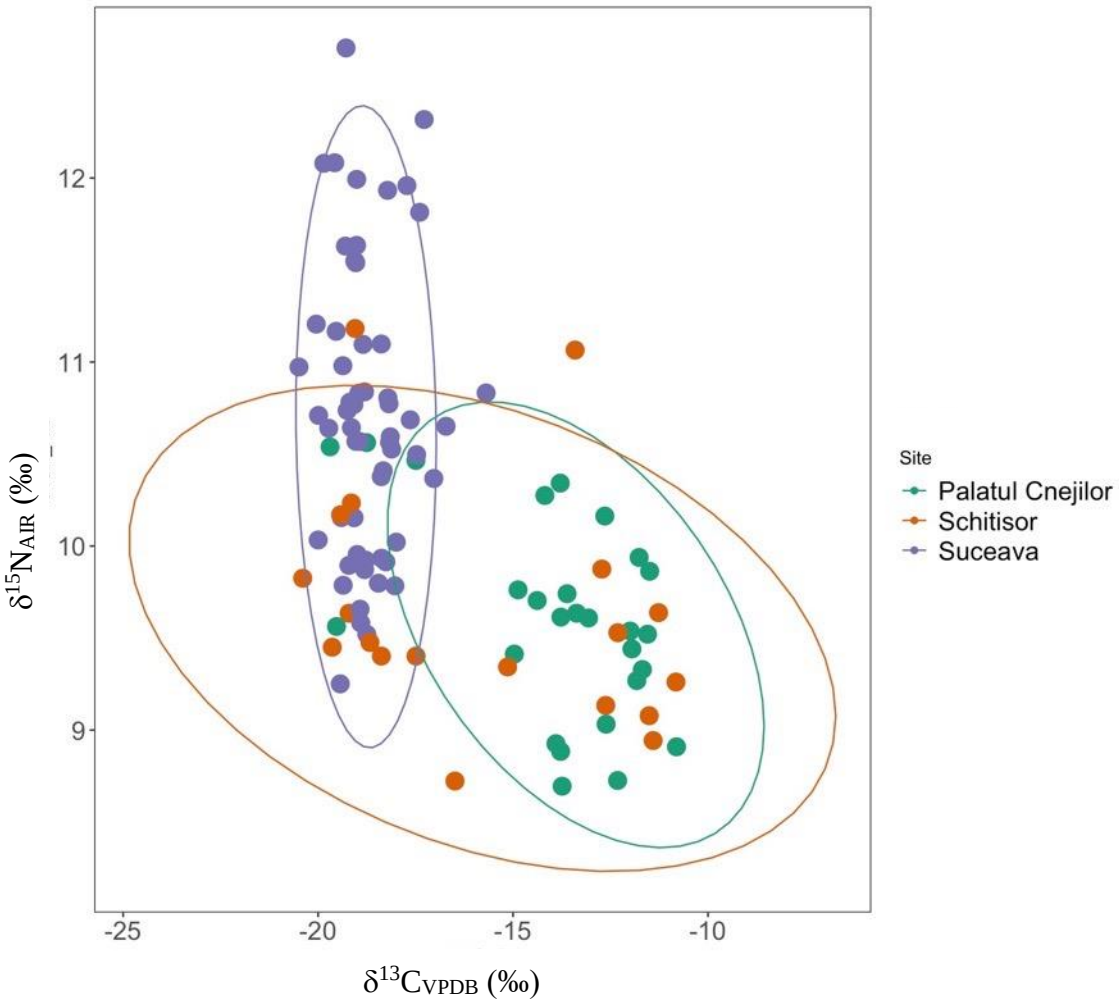


Figure 6.4. $\delta^{13}C$ and $\delta^{15}N$ values for rib collagen by site with 95% confidence ellipses. Teal =Palatul Cnejilor, orange=Schitișor, and purple= Suceava.

individuals from Suceava between 11.5‰ and 13‰ versus individuals from Palatul Cnejilor and Schitișor. For rib collagen only individuals from Suceava fall above 11‰ except for two individuals from Schitișor. For both femur and rib collagen $\delta^{13}C$ values, only individuals from Palatul Cnejilor and Schitișor fall above ~ -16‰ creating this distinct cluster along the x-axis for $\delta^{13}C$ values.

Bayesian Models for Stress and Diet

A 2-Sample Kolmogorov Smirvov (KS) Test was performed in SPSS (v.29.0.2.0(20)) to compare distributions between these data and Dr. Bethard's to see whether the isotope data are similar and whether Bethard's data could be used as an informed prior. The KS Test showed a significant difference in the distribution of stable isotope values for carbon and nitrogen between these two datasets ($p = <0.001$). Thus, Bethard's data cannot be used as prior information for any Bayesian models. Therefore, all Bayesian models reported below were run using flat or uninformed priors.

A total of 12 Bayesian models were created: Two models for each of the six lesions, one containing the femur carbon ($\delta^{13}C$) and nitrogen ($\delta^{15}N$) values and one containing the rib carbon ($\delta^{13}C$) and nitrogen ($\delta^{15}N$) values, and each containing age, sex, and site variables (Table 6.21). The following sections will describe these models, discuss model selection, and report the model that was the best fit for explaining the data.

PNBF and Femur $\delta^{13}C$ and $\delta^{15}N$ values

Model Description. The model for PNBF and femur carbon and nitrogen isotope values used flat priors (Table 6.21). PNBR (and all other lesion-type outcome variables) is Bernoulli distributed (a discrete probability distribution), biological sex and site are categorical variables,

Table 6.21. 12 Bayesian logistic regression models for each lesion type and femur and rib carbon and nitrogen isotope values.

Full Bayesian Logistic Regression Models
$PNBF \sim Age + Sex + Site + \delta^{13}C_{Femur} + \delta^{15}N_{Femur}$
$PNBF \sim Age + Sex + Site + \delta^{13}C_{Rib} + \delta^{15}N_{Rib}$
$PH \sim Age + Sex + Site + \delta^{13}C_{Femur} + \delta^{15}N_{Femur}$
$PH \sim Age + Sex + Site + \delta^{13}C_{Rib} + \delta^{15}N_{Rib}$
$CO \sim Age + Sex + Site + \delta^{13}C_{Femur} + \delta^{15}N_{Femur}$
$CO \sim Age + Sex + Site + \delta^{13}C_{Rib} + \delta^{15}N_{Rib}$
$Caries \sim Age + Sex + Site + \delta^{13}C_{Femur} + \delta^{15}N_{Femur}$
$Caries \sim Age + Sex + Site + \delta^{13}C_{Rib} + \delta^{15}N_{Rib}$
$Abscesses \sim Age + Sex + Site + \delta^{13}C_{Femur} + \delta^{15}N_{Femur}$
$Abscesses \sim Age + Sex + Site + \delta^{13}C_{Rib} + \delta^{15}N_{Rib}$
$PD \sim Age + Sex + Site + \delta^{13}C_{Femur} + \delta^{15}N_{Femur}$
$PD \sim Age + Sex + Site + \delta^{13}C_{Rib} + \delta^{15}N_{Rib}$

and age-at-death, $\delta^{13}C$ values, and $\delta^{15}N$ values are scalar variables. The full model summary is provided in Table 6.22. The first column contains all the model parameters/predictor variables, and the intercept is the mean of the sample before any predictor variables are considered. The Estimate column contains the slope of each parameter. The intercept slope is the overarching log odds of presenting with the outcome of interest (a lesion). The Rhat values for the full model are all less than 1.01 and the Bulk and Tail ESS (Effective Sample Sizes) are all around 10,000 or greater (the number of iterations out of 40,000 that do not contain outliers, thus the higher the number the better), which indicates that the model converged.

Model Selection. A series of model fits with flat priors and different combinations of predictor variables were created to see which predictor variables from the full model best explained the data and predicted the outcome of interest (presence or absence of a lesion). Tables of all model fits for each lesion type are provided in Appendix Three. Watanabe-Akaike information criteria (WAIC) were assigned to each model fit which then compared the fits of each model using the WAIC criterion (Watanabe 2010). For all model fits for PNBF and all other lesion types, the p WAIC values were too high so Leave One Out Information Criteria (LOOIC) were used for all model selection. WAIC and LOOIC are methods for estimating prediction accuracy from a fitted Bayesian model. The model fit with the lowest LOOIC value was selected as the best-fit model. Table 6.23 provides the LOOIC values for each model fit.

Model selection favored fitted model 7 (fit7) (PNBF~1) which is the intercept or naïve model (Table 6.24**)**. This intercept-only model estimates the mean of the data without consideration of any of the predictor variables of interest. That this model was favored suggests that the predictor variables included in this study do not influence the outcome in a predictable manner. Since the goal of this research is to better understand the ways in which these predictors

Table 6.22. Log odds estimate, error, 95% Credibility Interval, Rhat values, and Bulk and Tail ESS for the full model.

			95% Credibility Interval				
	Estimate	**Error**	**Lower**	**Upper**	**Rhat**	**Bulk ESS**	**Tail ESS**
Intercept	0.65	3.47	-6.11	7.53	1.00	134952	108325
Age	-0.02	0.01	-0.05	0.00	1.00	142245	100075
SexMale	0.64	0.54	-0.40	1.73	1.00	139002	100658
SiteSchitisor	-0.42	0.80	-2.05	1.13	1.00	131540	101021
SiteSuceava	0.75	0.92	-1.00	2.63	1.00	98601	91532
δ^{13}C Femur	0.25	0.13	0.00	0.53	1.00	110005	92508
δ^{15}N Femur	0.27	0.33	-0.38	0.92	1.00	134188	103661

Table 6.23. LOOIC values for each model fit.

Model fit	**elpd_diff**	**se_diff**	**elpd_loo**	**se_elpd_loo**	**p_loo**	**se_p_loo**	**looic**	**se_looic**
fit7	0.00	0.00	-57.53	4.91	1.01	0.12	**115.06**	9.83
fit5	-0.26	2.32	-57.79	5.49	3.26	0.49	**115.58**	10.97
fit2	-2.07	3.07	-59.60	5.93	6.73	1.08	**119.20**	11.86
fit6	-2.08	1.79	-59.61	5.46	4.46	0.66	**119.22**	10.91
fit4	-2.37	2.43	-59.90	5.73	5.44	0.78	**119.81**	11.46
fit	-2.93	3.28	-60.46	6.14	7.84	1.24	**120.92**	12.27
fit3	-3.40	2.52	-60.93	5.87	6.55	0.91	**121.85**	11.73

Table 6.24. The log odds estimate, 95% Credibility Interval, Rhat, and Bulk and Tail ESS for fit7 (the intercept).

			95% Credibility Interval				
	Estimate (log odds)	**Error**	**Lower**	**Upper**	**Rhat**	**Bulk ESS**	**Tail ESS**
Intercept	-1.11	0.23	-1.58	-0.67	1.00	55336	62704

influence the outcome of interest *relative to one another*, I decided to report the next-best (non-naïve) model, which in the case of PNBF was model 5 (fit5) (PNBF~Age+Sex). This same selection process was replicated for all models where the intercept-only version was favored. For fit5, the Rhat value is less than 1.01 and the Bulk and Tail ESS are greater than 10,000 which indicates that the model converged (Table 6.25). This is visually confirmed by the Hamilton Monte Carlo (HMC) Chains (Figure 6.5) and a lack of autocorrection between the chains (Figure 6.6). This supports the conclusion that the Markov chains effectively explored the posterior parameter space and produced a representative sample of the posterior probability distribution for the fit5 model.

Model Summary. Model fit5 included age and sex predictor variables. The posterior predictive checks confirm this and show that posterior draws for this model are distributed symmetrically around the mean (Figure 6.7). Table 6.26 provides the parameters, the ORs, and 95% Credibility Interval. The posterior distributions are depicted in Figure 6.5. Marginal effects plots are provided in Appendix Three.

Each parameter estimate represents a change in the log odds of presenting with PNBF given a change in the value associated with the predictor variable. A model parameter is considered probabilistically different from chance if the 95% Credibility Interval (CI) of its β coefficient does not contain zero (Kruschke 2015). The log odds estimate for each parameter was converted to an Odds Ratio (OR) by exponentiating the log odds value of each estimate. An OR >1 indicates an increased occurrence of an event, and an OR <1 indicates a decreased occurrence of an event. The increase or decrease in the odds of an occurrence is only meaningful if the 95% CI does not contain 1. For Estimates with ORs that have 95% CI that cross 1, there is no credible

Table 6.25. The log odds estimate, 95% Credibility Interval, Rhat, and Bulk and Tail ESS for fit5.

			95% Credibility Interval				
	Estimate (log odds)	**Error**	**Lower**	**Upper**	**Rhat**	**Bulk ESS**	**Tail ESS**
Intercept	-0.62	0.62	-1.86	0.58	1.00	160474	106629
Age	-0.02	0.01	-0.04	0.00	1.00	120145	99949
SexMale	0.65	0.50	-0.30	1.64	1.00	119035	100965

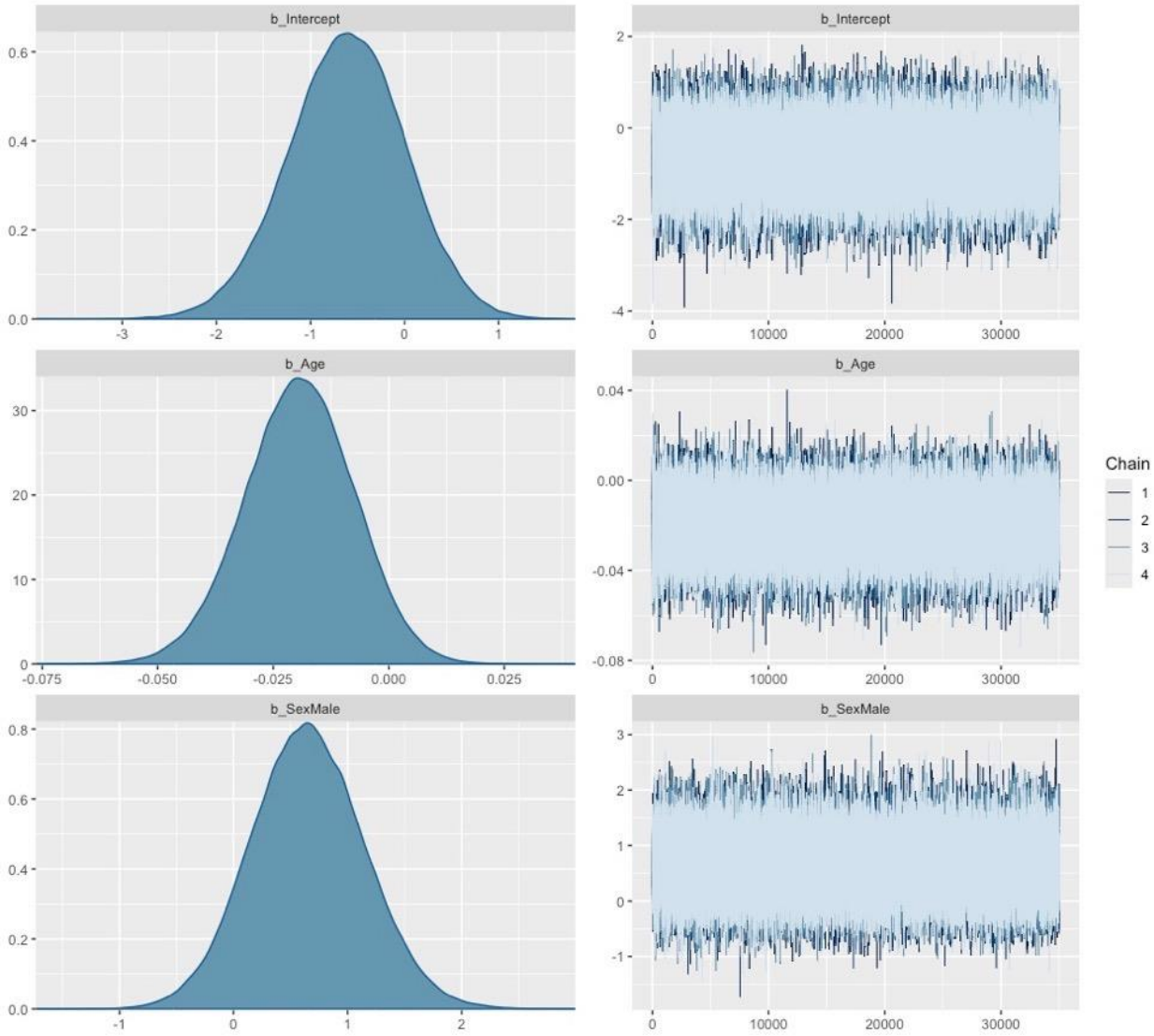


Figure 6.5. Posterior parameter distribution of the fit5 (PNBF~Age+Sex) model parameters and Hamilton Monte Carlo (HMC) chains. The posterior distributions on the left describe the log odds of presenting with PNBF based on the predictor variables in the models. The central tendency of the distribution reflects the most credible value for the log odds of presenting with PNBF, with less credible values distributed towards the tails. On the right, the HMC chains are healthy and recovered similar values at each of the 40,000 random walks of the posterior parameter space indicating reliable posterior parameter distributions given the data.

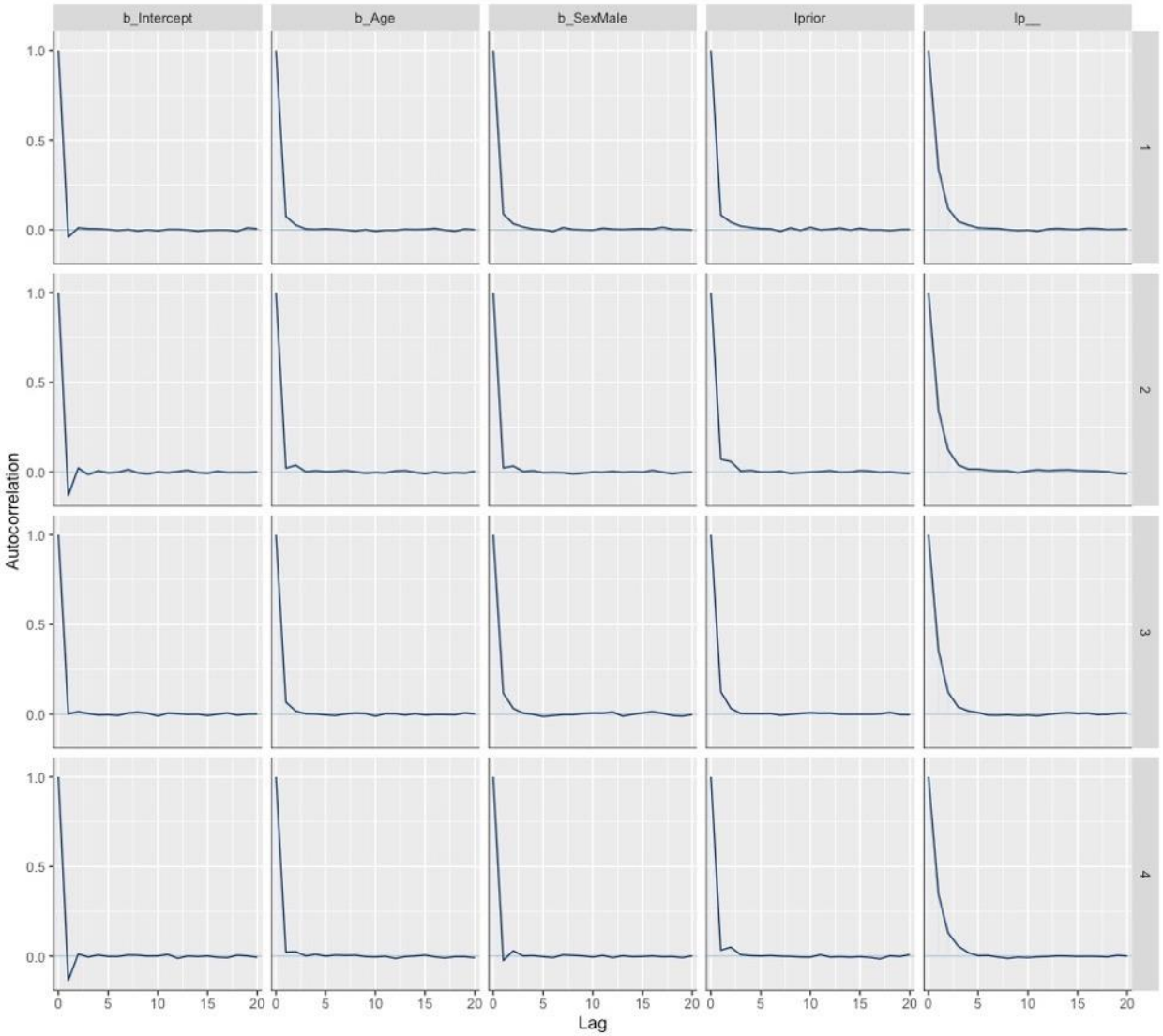


Figure 6.6. Autocorrelation plots for each fit5 (PNBF~Age+Sex) parameter by HMC chain with flat priors. There is negligible autocorrelation. When predictor variables are correlated with each other, the sequential HMC samples from the posterior parameter space are correlated. This results in a slower HMC simulation and thus a less efficient exploration of the posterior parameter space.

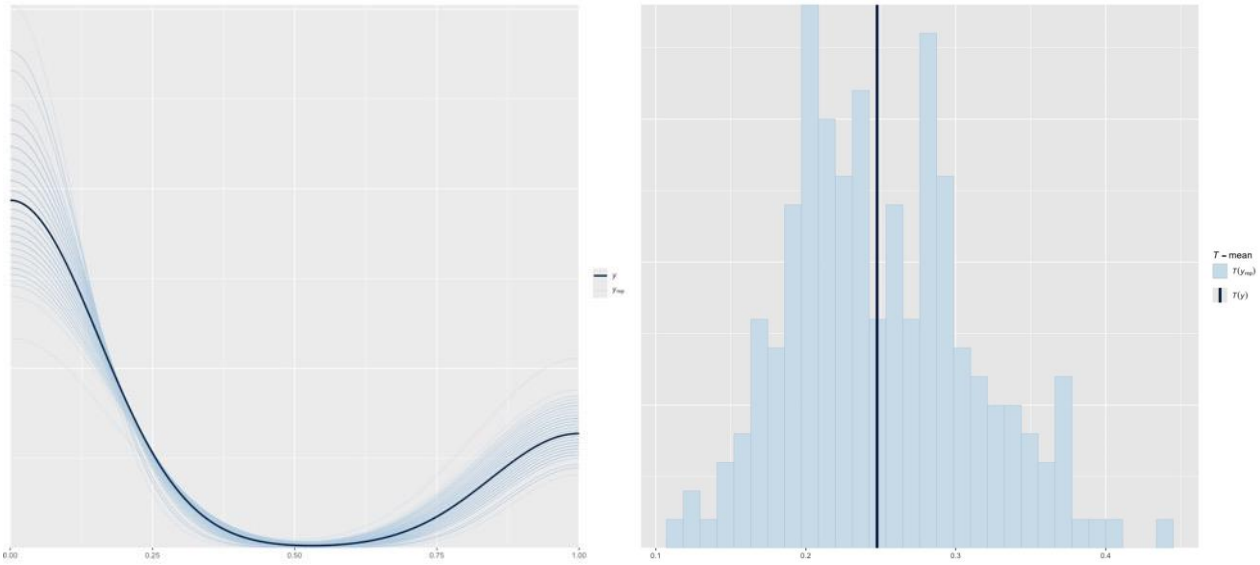


Figure 6.7. Density (left) and histogram (right) charts showing the posterior draws of the probability of presenting with PNBF based on fit5 (PNBF~Age+Sex). Dark lines represent the mean and flat priors used. Light blue lines are the random draws from the posterior parameter space. They symmetrical distribution of the light blue lines around the mean suggests the model converged.

Table 6.26. Odds Ratios and 95% Credibility Interval for fit5.

		95% Credibility Interval	
	Odds Ratio (OR)	**Lower**	**Upper**
Intercept	0.53	0.16	1.79
Age	0.98	0.96	1.0
SexMale	1.91	0.74	5.15

difference between groups. The probability (P) of an event occurring is calculated as P = OR/1+OR.

The log odds of presenting with PNBF were higher among males than females (log odds = 0.65, 95% CI = -0.30 – 1.64), and the odds of males presenting with PNBF are higher than the odds of females presenting with PNBF (OR = 1.91, 95% CI = 0.74 – 5.15), but it is not credibly different from chance. The probability of presenting with PNBF if male is 0.65 (OR/1+OR) or 65% compared to females (Table 6.26).

For the age parameter, with each year of life, there is a decrease in the log odds of presenting with PNBF (log odds = -0.02, 95% CI = -0.04 – 0.00), but it is not credibly different from chance (OR = 0.98, 95% CI = 0.96 – 1). The probability of presenting with PNBF increases by 49.5% with each year of age (Table 6.26).

PNBF and Rib $\delta^{13}C$ and $\delta^{15}N$ values

Model Description. The model for PNBF and rib carbon and nitrogen isotope ratios used flat priors (Table 6.21). The full model summary is provided in Table 6.27. The Rhat values are all less than 1.01 and the Bulk and Tail ESS are all around 10,000 or greater, which indicates that the model converged.

Model Selection. A series of model fits with flat priors and different combinations of predictor variables were created to see which predictor variables from the full model best explained the data and predicted the outcome of interest (presence or absence of a lesion). LOOIC were used for model selection. Table 6.28 provides the LOOIC values for each model fit. Model selection favored fit7 (PNBF~1) which is the intercept or naïve model (Table 6.29), so the next best-fit model, fit5 (PNBF~Age+Sex), is reported (Table 6.30). Fit5 Rhat values are less than 1.01 and the Bulk and Tail ESS are greater than 10,000 which indicates the model

Table 6.27. Log odds estimate, error, 95% Credibility Interval, Rhat values, and Bulk and Tail ESS for the full model.

			95% Credibility Interval				
	Estimate	**Error**	**Lower**	**Upper**	**Rhat**	**Bulk ESS**	**Tail ESS**
Intercept	0.09	4.28	-8.22	8.57	1.00	130971	106776
Age	-0.01	0.01	-0.04	0.01	1.00	143736	98803
SexMale	0.13	0.57	-0.98	1.25	1.00	134929	103537
SiteSchitisor	-0.15	0.83	-1.80	1.46	1.00	133089	99440
SiteSuceava	1.45	1.14	-0.63	3.84	1.00	90857	82378
δ^{13}C Rib	0.36	0.16	0.06	0.70	1.00	91983	82240
δ^{15}N Rib	0.43	0.43	-0.41	1.29	1.00	129098	101496

Table 6.28. LOOIC values for each model fit.

Model fit	**elpd_diff**	**se_diff**	**elpd_loo**	**se_elpd_loo**	**p_loo**	**se_p_loo**	**looic**	**se_looic**
fit7	0.00	0.00	-52.74	4.65	1.01	0.12	**105.48**	9.31
fit5	-1.69	1.32	-54.43	5.06	3.32	0.46	**108.86**	10.11
fit6	-2.87	1.29	-55.61	5.17	4.54	0.69	**111.22**	10.34
fit2	-3.23	3.39	-55.97	6.06	7.32	1.70	**111.94**	12.13
fit4	-3.81	1.49	-56.55	5.31	5.56	0.78	**113.10**	10.61
fit	-3.99	3.76	-56.73	6.35	8.51	1.86	**113.46**	12.70
fit3	4.92	1.58	-57.66	5.43	6.72	0.92	**115.32**	10.87

Table 6.29. The log odds estimate, 95% Credibility Interval, Rhat values, and Bulk and Tail ESS for fit7.

			95% Credibility Interval				
	Estimate	**Error**	**Lower**	**Upper**	**Rhat**	**Bulk ESS**	**Tail ESS**
Intercept	-1.10	0.24	-1.58	-0.64	1.00	51231	66930

Table 6.30. The log odds estimate, 95% Credibility Interval, Rhat values, and Bulk and Tail ESS for fit5.

			95% Credibility Interval				
	Estimate	**Error**	**Lower**	**Upper**	**Rhat**	**Bulk ESS**	**Tail ESS**
Intercept	-0.74	0.64	-2.03	0.49	1.00	157016	106751
Age	-0.01	0.01	-0.04	0.01	1.00	132215	103587
SexMale	0.27	0.50	-0.70	1.26	1.00	132756	105450

converged. This is visually confirmed by the Hamilton Monte Carlo (HMC) Chains (Figure 6.8) and no autocorrelation between the chains (Figure 6.9). This supports the conclusion that the Markov chains effectively explored the posterior parameter space and produced a representative sample of the posterior probability distribution for the fit5 model.

Model Summary. Model fit5 included age and sex predictor variables. The posterior predictive checks confirm this and show that posterior draws for this model are distributed symmetrically around the mean (Figure 6.10). Table 6.31 provides the parameters, the ORs, and 95% Credibility Interval. The posterior distributions for each estimate are depicted in Figure 6.8. Marginal effects plots are provided in Appendix Three.

Each parameter estimate represents a change in the log odds of presenting with PNBF given a change in the value associated with the predictor variable. The log odds of presenting with PNBF were higher among males than females (log odds = 0.27, 95% CI = -0.70 – 1.26), and the odds of males presenting with PNBF is higher than the odds of females presenting with PNBF (OR = 1.31, 95% CI = 0.49 – 3.52) but it is not credibly different from chance. The probability of males presenting with PNBF is 57% compared to females.

For age, with each year of life, there is a decrease in the log odds of presenting with PNBF (log odds = -0.01, 95% CI = -0.04 – 0.01), and the odds of presenting with PNBF slightly decreases for each year of age (OR = 0.99, 95% CI = 0.96 – 1.01), but it is not credibly different from chance. The probability of presenting with PNBF increases by 49.7% with each year of age.

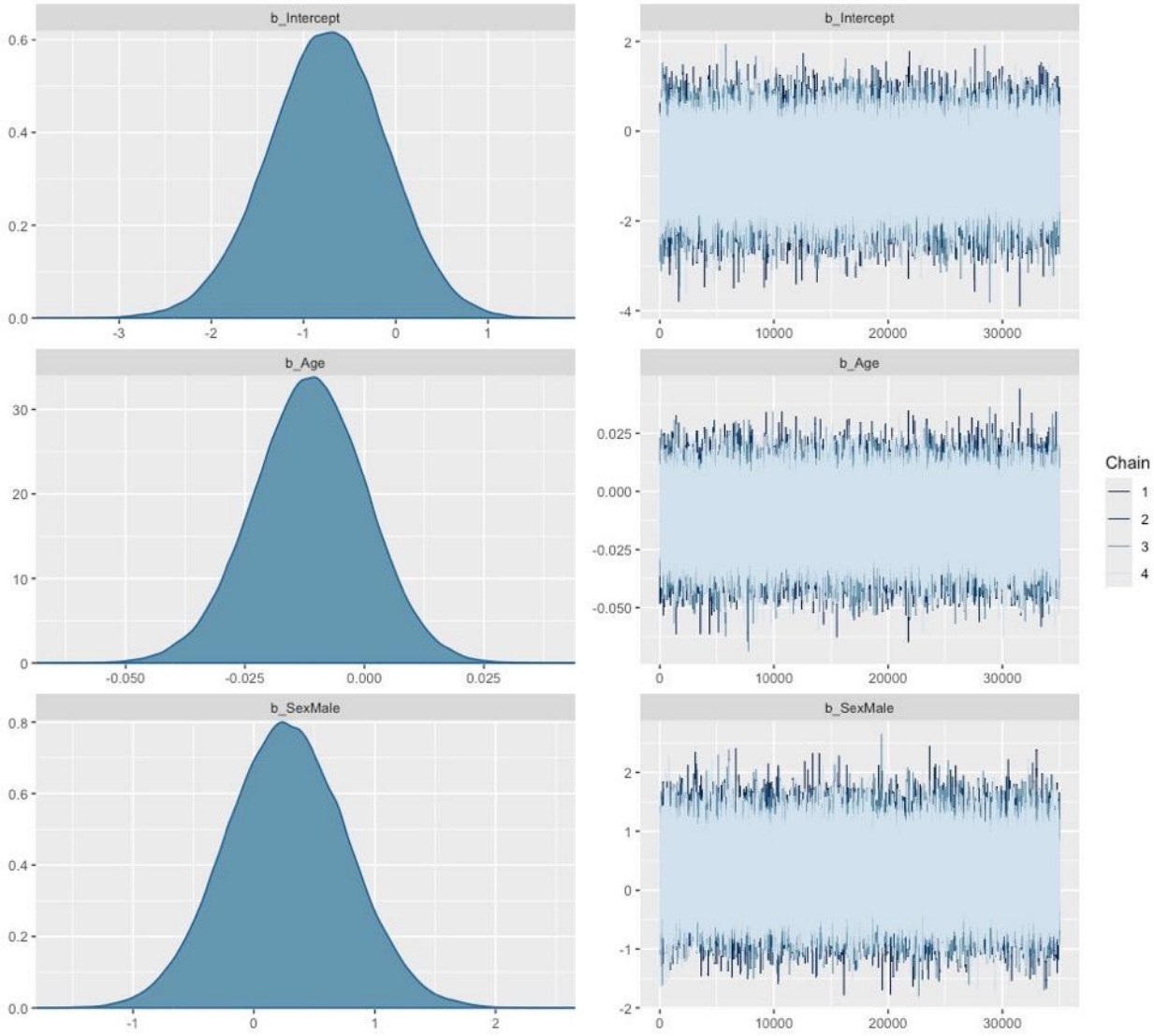


Figure 6.8. Posterior parameter distribution of the fit5 (PNBF~Age+Sex) model parameters and HMC chains.

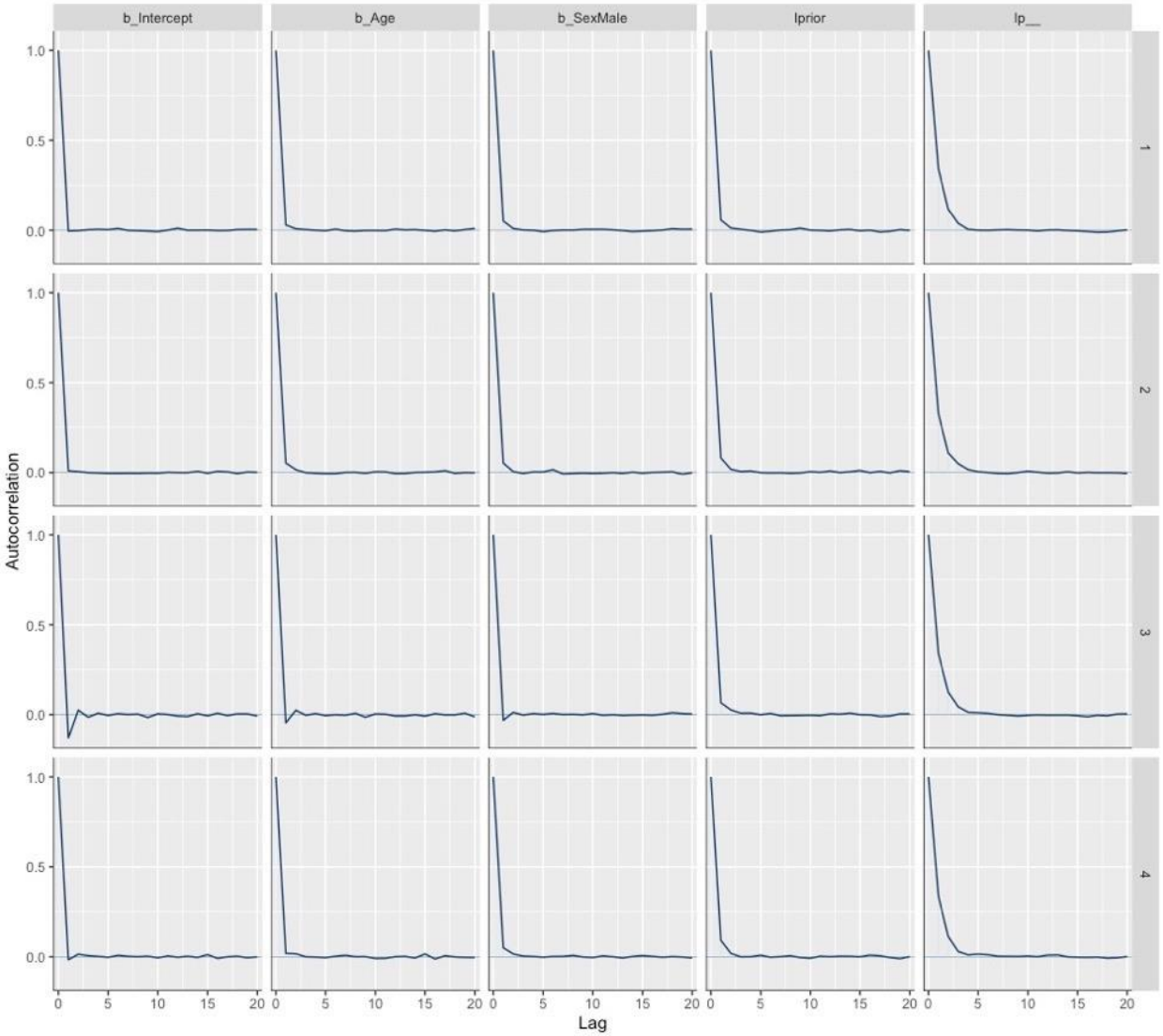


Figure 6.9. Autocorrelation plots for each fit5 (PNBF~Age+Sex) parameter by HMC chain with flat priors that suggest negligible autocorrelation.

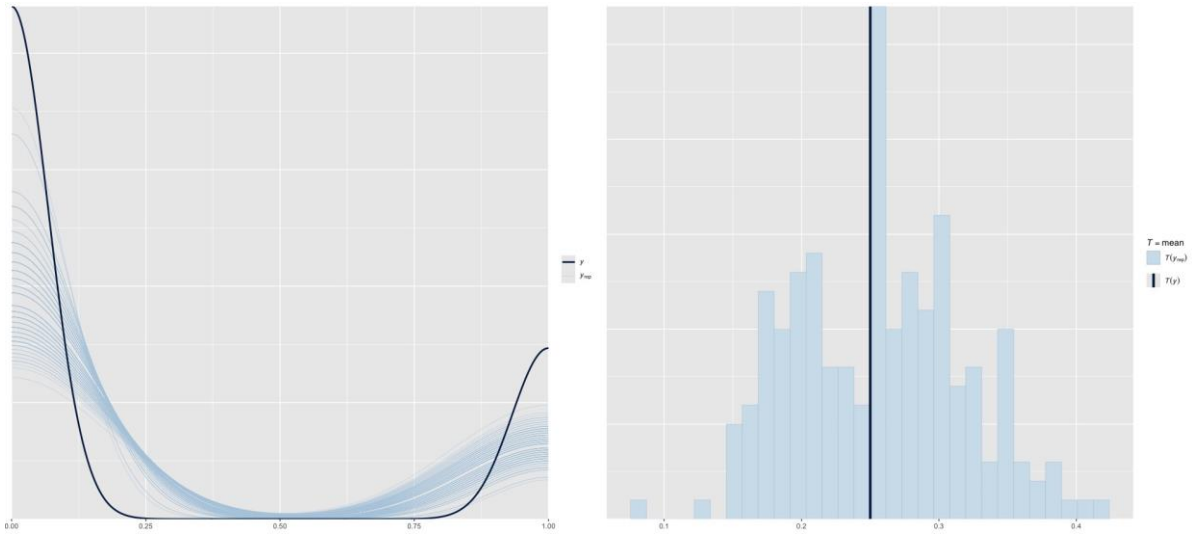


Figure 6.10. Density (left) and histogram (right) charts showing the posterior draws of the probability of presenting with PNBF based on fit 5 (PNBF~Age+Sex). Dark lines represent the mean and flat priors used. Light blue lines are the random draws from posterior parameter space. The symmetrical distribution of the light blue lines around the mean suggests the model converged.

Table 6.31. Odds Ratios and 95% Credibility Interval for fit5.

		95% Credibility Interval	
	Odds Ratio (OR)	**Lower**	**Upper**
Intercept	6.36	1.17	5.98
Age	0.99	0.96	1.01
SexMale	1.31	0.49	3.52

PH and Femur $\delta^{13}C$ and $\delta^{15}N$ values

Model Description. The model for PH and femur carbon and nitrogen isotope values used flat priors (Table 6.21). The full model summary is provided in Table 6.32. The Rhat values are all less than 1.01 and the Bulk and Tail ESS are all around 10,000 or greater, which indicates that the model converged.

Model Selection. A series of model fits with flat priors and different combinations of predictor variables were created to see which predictor variables from the full model best explained the data and predicted the outcome of interest (presence or absence of a lesion). LOOIC were used for model selection. Table 6.33 provides the LOOIC values for each. Model selection favored fit7 (PH~1) which is the intercept or naïve model (Table 6.34) so the next best-fit model, fit5 (PH~Age+Sex), is reported (Table 6.35). Fit5 Rhat values are less than 1.01 and the Bulk and Tail ESS are around or greater than 10,000 which indicates the model converged. This is visually confirmed by the Hamilton Monte Carlo (HMC) Chains (Figure 6.11) and no autocorrelation between the chains (Figure 6.12). This supports the conclusion that the Markov chains effectively explored the posterior parameter space and produced a representative sample of the posterior probability distribution for the fit5 model.

Model Summary. Model fit5 included age and sex predictor variables. The posterior predictive checks confirm this and show that posterior draws for this model are distributed symmetrically around the mean (Figure 6.13). Table 6.36 provides the parameters, the ORs, and 95% Credibility Interval. The posterior distributions for each estimate are depicted in Figure 6.11. Marginal effects plots are provided in Appendix Three.

Table 6.32. Log odds estimate, error, 95% Credibility Interval, Rhat values, and Bulk and Tail ESS for the full model.

			95% Credibility Interval				
	Estimate	**Error**	**Lower**	**Upper**	**Rhat**	**Bulk ESS**	**Tail ESS**
Intercept	13.47	6.39	1.79	26.79	1.00	109965	99089
Age	-0.01	0.02	-0.06	0.04	1.00	128319	94285
SexMale	1.91	1.02	0.06	4.08	1.00	109886	87473
SiteSchitisor	0.62	1.12	-1.55	2.86	1.00	121059	97854
SiteSuceava	1.71	1.39	-0.88	4.56	1.00	94613	88706
δ^{13}C Femur	0.04	0.19	-0.31	0.42	1.00	108994	90182
δ^{15}N Femur	-1.73	0.74	-3.31	-0.41	1.00	94817	86853

Table 6.33. LOOIC values for each model fit.

Model fit	**elpd_diff**	**se_diff**	**elpd_loo**	**se_elpd_loo**	**p_loo**	**se_p_loo**	**looic**	**se_looic**
fit7	0.00	0.00	-29.56	5.36	1.00	0.24	59.13	10.72
fit5	-0.82	2.43	-30.38	6.06	3.43	1.12	60.77	12.11
fit3	-1.56	4.34	-31.13	6.98	7.85	2.33	62.26	13.95
fit6	-3.26	1.12	-32.82	6.18	4.56	1.12	65.64	12.36
fit	-3.38	4.52	-32.95	7.37	9.77	2.79	65.89	14.74
fit4	-3.42	2.39	-32.99	6.52	6.22	1.71	65.97	13.04
fit2	-4.74	2.57	-34.30	6.80	8.11	2.22	68.60	13.61

Table 6.34. The log odds estimate, 95% Credibility Interval, Rhat values, and Bulk and Tail ESS for fit7.

			95% Credibility Interval				
	Estimate	**Error**	**Lower**	**Upper**	**Rhat**	**Bulk ESS**	**Tail ESS**
Intercept	-1.78	0.34	-2.48	-1.15	1.00	52981	59317

Table 6.35. The log odds estimate, 95% Credibility Interval, Rhat values, and Bulk and Tail ESS for fit5.

			95% Credibility Interval				
	Estimate	**Error**	**Lower**	**Upper**	**Rhat**	**Bulk ESS**	**Tail ESS**
Intercept	-2.65	1.08	-4.93	-0.69	1.00	90691	75547
Age	-0.01	0.02	-0.04	0.03	1.00	97112	87087
SexMale	1.53	0.89	-0.06	3.44	1.00	82763	71655

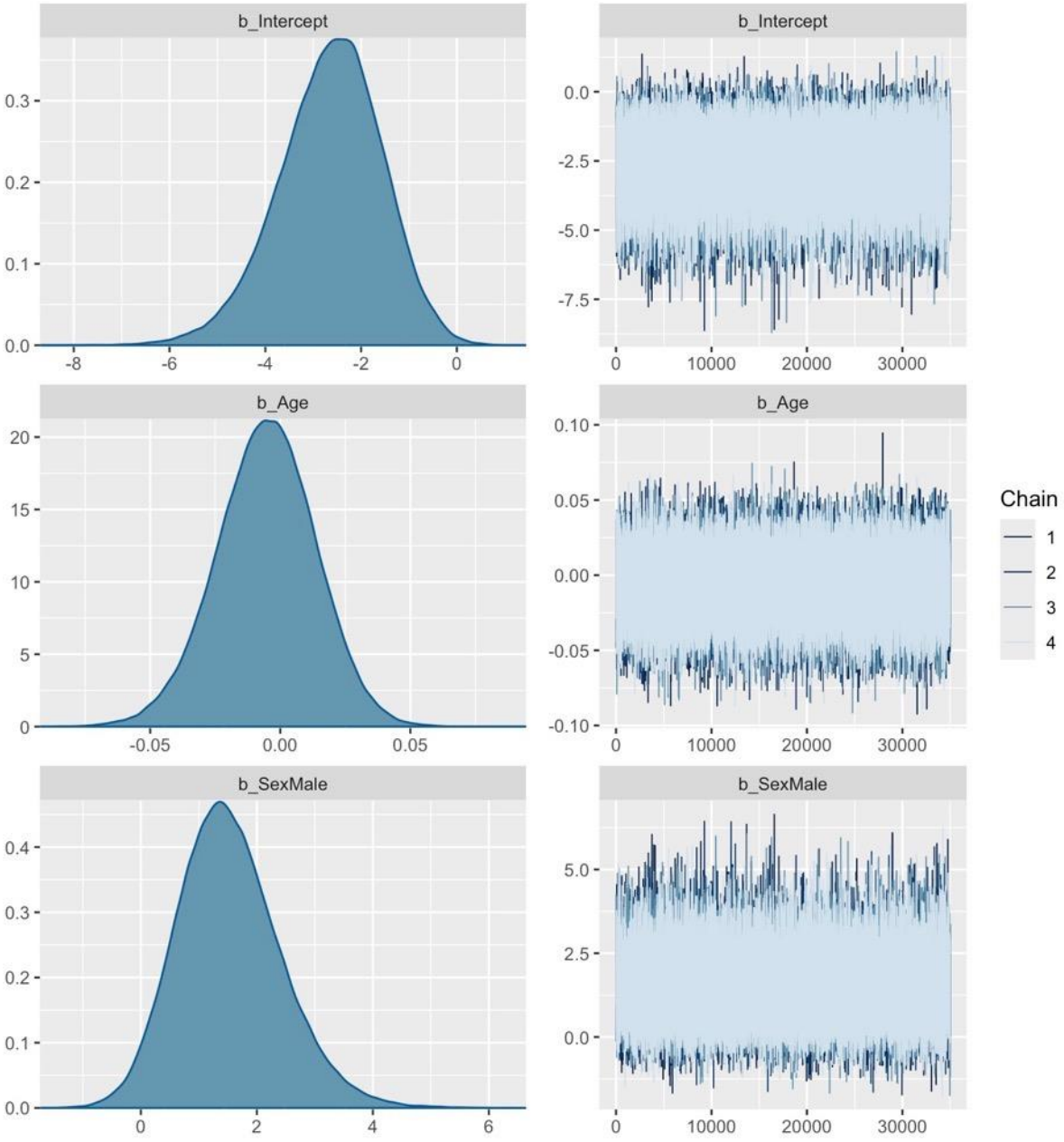


Figure 6.11. Posterior parameter distribution of the fit5 (PH~Age+Sex) model parameters and HMC chains.

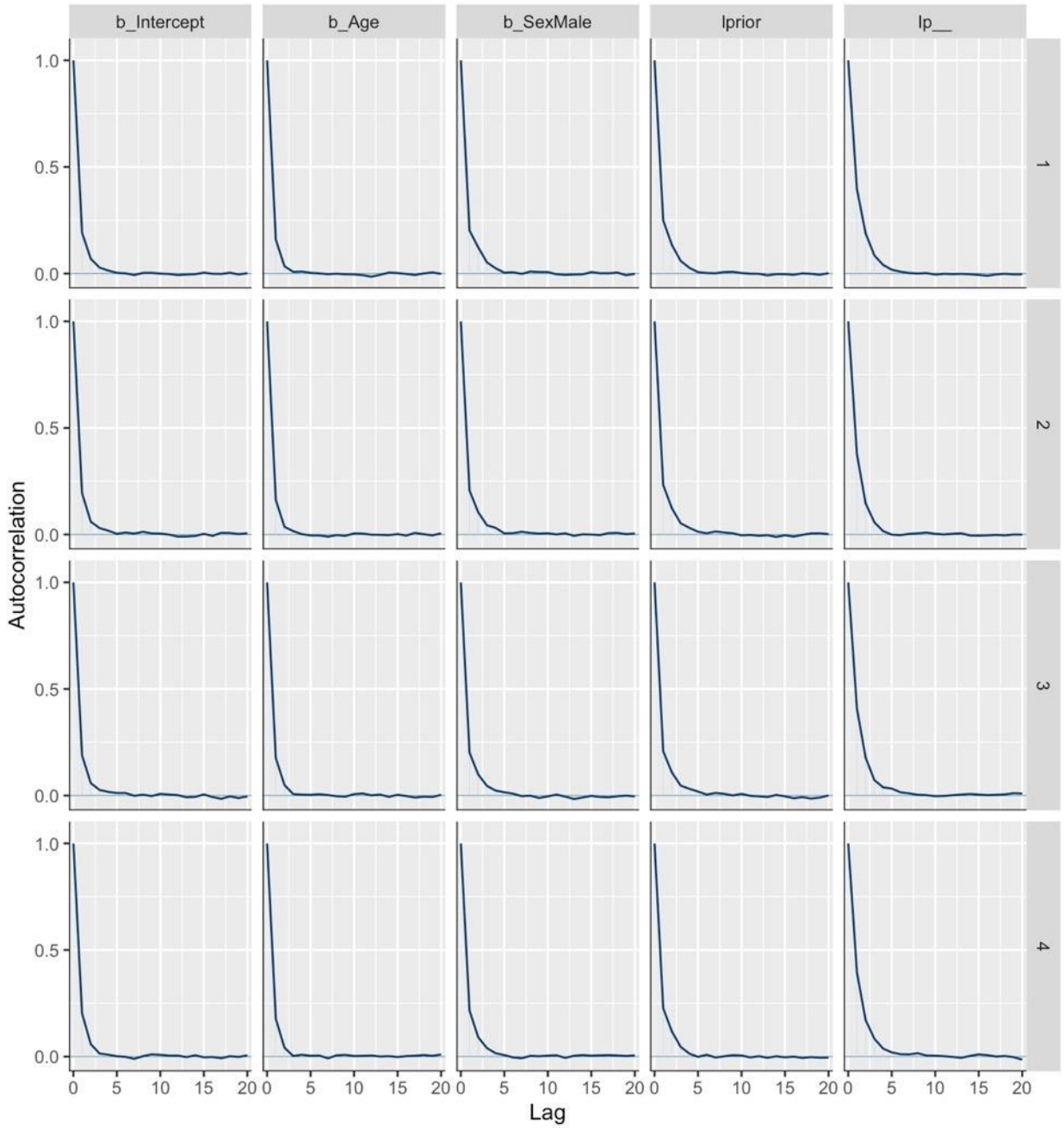


Figure 6.12. Autocorrelation plots for each fit5 (PH~Age+Sex) parameter by HMC chain with flat priors that suggest negligible autocorrelation.

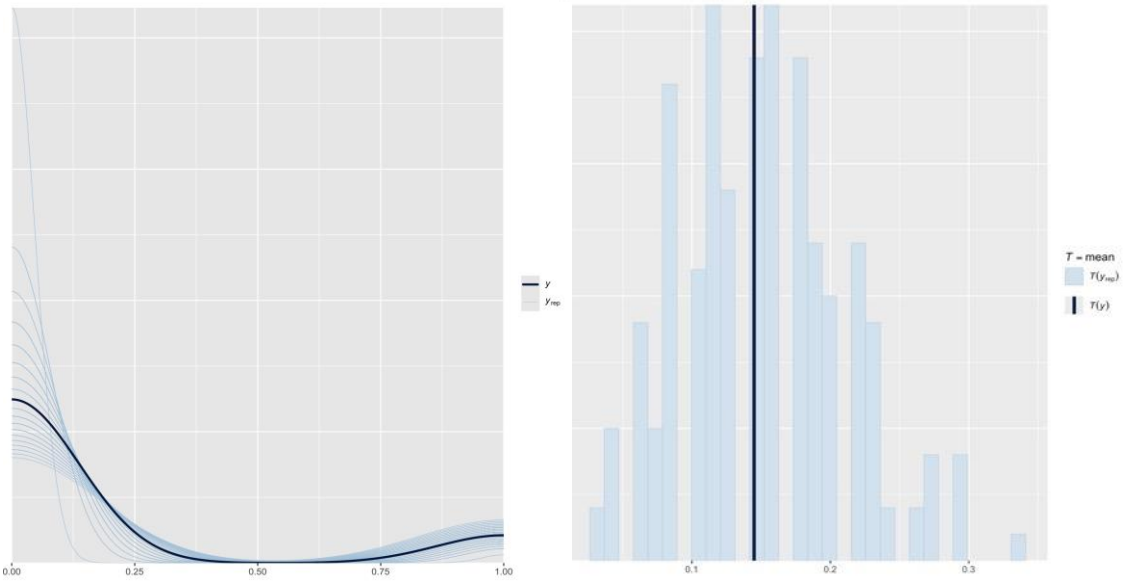


Figure 6.13. Density (left) and histogram (right) charts showing the posterior draws of the probability of presenting with PH based on fit5 (PH~Age+Sex). Dark lines represent the mean and flat priors used. Light blue lines are the random draws from the posterior parameter space. The symmetrical distribution of the light blue lines around the mean suggests the model converged.

Table 6.36. Odds Ratios and 95% Credibility Interval for fit5.

		95% Credibility Interval	
	Odds Ratio (OR)	**Lower**	**Upper**
Intercept	0.07	0.007	0.50
Age	0.99	0.96	1.03
SexMale	4.62	0.94	31.19

Each parameter estimate represents a change in the log odds of presenting with PH given a change in the value associated with the predictor variable. For age, with each year of life, there is a decrease in the log odds of presenting with PH (log odds = -0.01, 95% CI = -0.04 – 0.03), and the odds of presenting with PH slightly decreases for each year of age (OR = 0.99, 95% CI = 0.96 – 1.03), but it is not credibly different from chance. The probability of presenting with PH increases by 49.75% with each year of age.

By sex, the log odds of presenting with PH were higher among males than females (log odds = 1.53, 95% CI = -0.06 – 3.44), and the odds of males presenting with PH is higher than the odds of females presenting with PH (OR = 4.62, 95% CI = 0.94 – 31.19), but it is not credibly different from chance. The probability of males presenting with PH is 82.21%.

PH and Rib $\delta^{13}C$ and $\delta^{15}N$ values

Model Description. The model for PH and rib carbon and nitrogen isotope values used flat priors (Table 6.21). The full model summary is provided in Table 6.37. The Rhat values are all less than 1.01 and the Bulk and Tail ESS are all around 10,000 or greater, which indicates that the model converged.

Model Selection. A series of model fits with flat priors and different combinations of predictor variables were created to see which predictor variables from the full model best explained the data and predicted the outcome of interest (presence or absence of a lesion). LOOIC were used for model selection. Table 6.38 provides the LOOIC values for each. Model selection favored fit7 (PH~1) which is the intercept or naïve model (Table 6.39) so the next best-fit model, fit5 (PH~Age+Sex), is reported (Table 6.40). Fit5 Rhat values are less than 1.01 and the Bulk and Tail ESS are around or greater than 10,000, which indicates the model converged.

Table 6.37. Log odds estimate, error, 95% Credibility Interval, Rhat values, and Bulk and Tail ESS for the full model.

			95% Credibility Interval				
	Estimate	**Error**	**Lower**	**Upper**	**Rhat**	**Bulk ESS**	**Tail ESS**
Intercept	-0.79	5.55	-11.65	10.22	1.00	154499	107176
Age	-0.04	0.02	-0.09	0.00	1.00	132414	88500
SexMale	0.71	0.81	-0.83	2.34	1.00	140058	97162
SiteSchitisor	0.29	1.06	-1.80	2.39	1.00	141330	99866
SiteSuceava	0.74	1.43	-1.89	3.73	1.00	108836	88445
δ^{13}C Rib	0.24	0.21	-0.14	0.67	1.00	106114	85280
δ^{15}N Rib	0.37	0.59	-0.80	1.54	1.00	142028	100826

Table 6.38. LOOIC values for each model fit.

Model fit	**elpd_diff**	**se_diff**	**elpd_loo**	**se_elpd_loo**	**p_loo**	**se_p_loo**	**looic**	**se_looic**
fit7	0.00	0.00	-31.69	4.66	1.01	0.20	63.38	9.33
fit5	-0.62	2.88	-32.31	5.64	1.04	1.04	64.62	11.28
fit6	-2.25	2.19	-33.94	5.51	4.76	1.17	67.88	11.01
fit4	-3.16	3.07	-34.85	6.07	6.29	1.56	69.71	12.14
fit2	-4.57	3.25	-36.26	6.35	8.25	2.15	72.52	12.70
fit3	-4.85	3.29	-36.55	6.40	8.08	1.98	73.09	12.80
fit	-6.21	3.39	-37.91	6.56	10.11	2.45	75.81	13.13

Table 6.39. The log odds estimate, 95% Credibility Interval, Rhat values, and Bulk and Tail ESS for fit7.

			95% Credibility Interval				
	Estimate	**Error**	**Lower**	**Upper**	**Rhat**	**Bulk ESS**	**Tail ESS**
Intercept	-1.45	0.32	-2.11	-0.85	1.00	50007	53683

Table 6.40. The log odds estimate, 95% Credibility Interval, Rhat values, and Bulk and Tail ESS for fit5.

			95% Credibility Interval				
	Estimate	**Error**	**Lower**	**Upper**	**Rhat**	**Bulk ESS**	**Tail ESS**
Intercept	-0.62	0.87	-2.37	1.06	1.00	128772	99975
Age	-0.04	0.02	-0.08	0.00	1.00	90570	80754
SexMale	0.86	0.73	-0.52	2.35	1.00	97390	87639

This is visually confirmed by the Hamilton Monte Carlo (HMC) Chains (Figure 6.14) and no autocorrelation between the chains (Figure 6.15). This supports the conclusion that the Markov chains effectively explored the posterior parameter space and produced a representative sample of the posterior probability distribution for the fit5 model.

Model Summary. Model fit5 included age and sex predictor variables. The posterior predictive checks confirm this and show that posterior draws for this model are distributed symmetrically around the mean (Figure 6.16). Table 6.41 provides the parameters, the ORs, and 95% Credibility Interval. The posterior distributions for each estimate are depicted in Figure 6.14. Marginal effects plots are provided in Appendix Three.

Each parameter estimate represents a change in the log odds of presenting with PH given a change in the value associated with the predictor variable. For age, with each year of life, there is a decrease in the log odds of presenting with PH (log odds = -0.04, 95% CI = -0.08 – 0), and the odds of presenting with PH slightly decrease for each year of age (OR = 0.96, 95% CI = 0.92 – 1), but it is not credibly different from chance. The probability of presenting with PH increases 48.98% with each year of age.

By sex, the log odds of presenting with PH were higher among males than females (log odds = 0.86, 95% CI = -0.52 – 2.35), and the odds of males presenting with PH is higher than the odds of females presenting with PH (OR = 2.36, 95% CI = 0.59 – 10.48), but it is not credibly different from chance. The probability of males presenting with PH compared to females is 70.24%.

CO and Femur $\delta^{13}C$ and $\delta^{15}N$ values

Model Description. The model for CO and femur carbon and nitrogen isotope values used flat priors (Table 6.21).

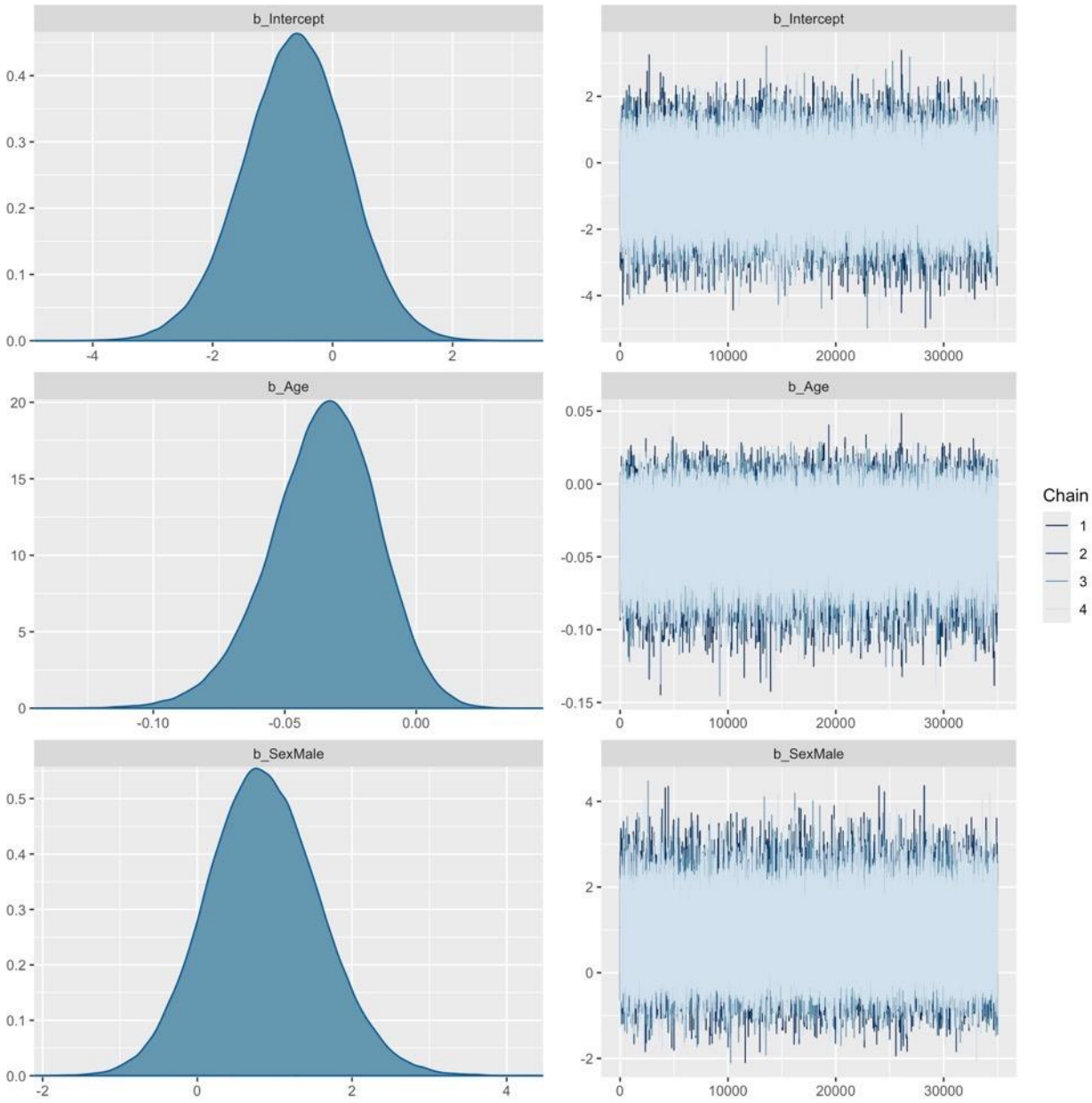


Figure 6.14. Posterior parameter distribution of the fit5 (PH~Age+Sex) model parameters and HMC chains.

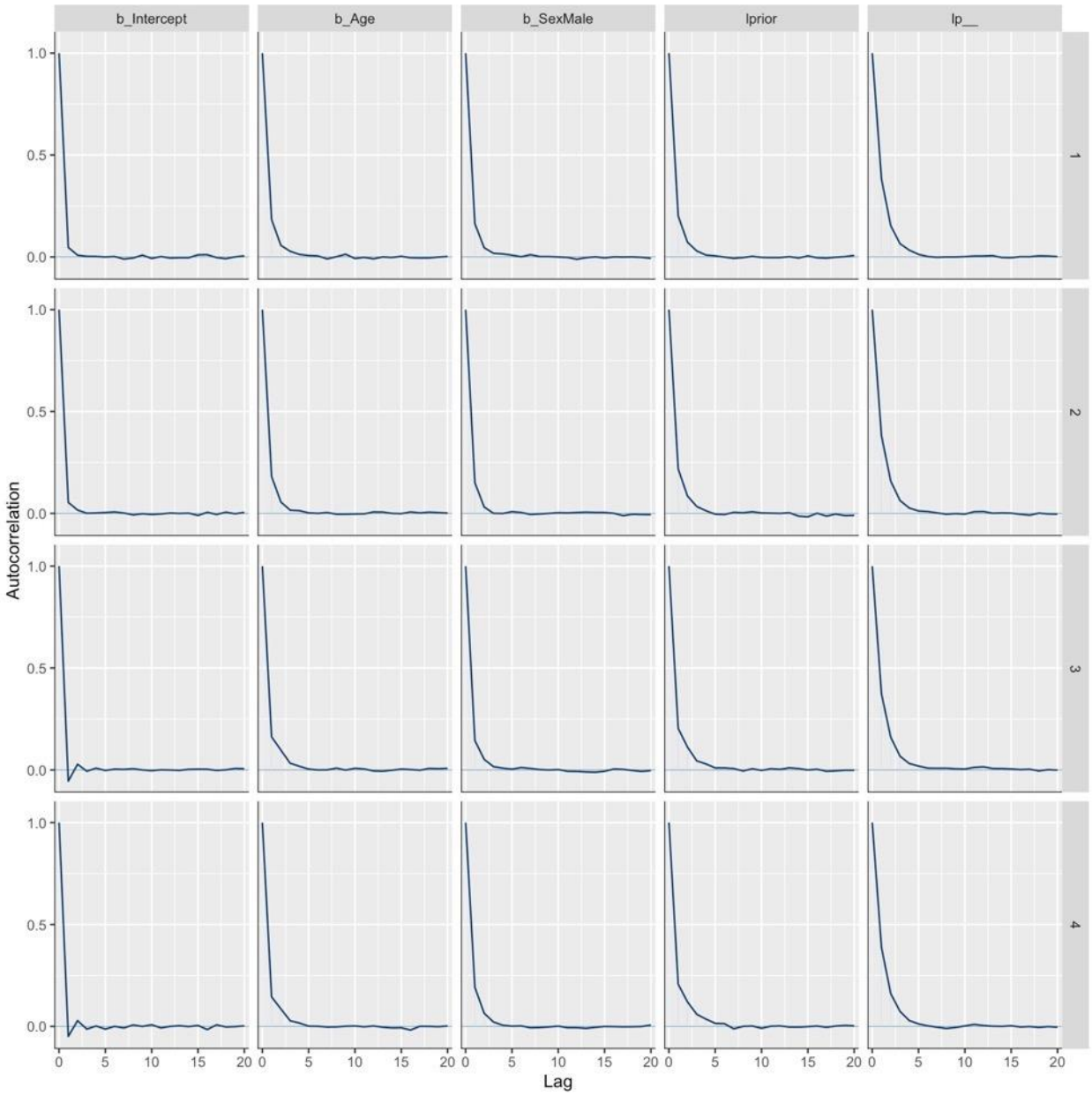


Figure 6.15. Autocorrelation plots for each fit5 (PH~Age+Sex) parameter by HMC chain with flat priors that suggest negligible autocorrelation.

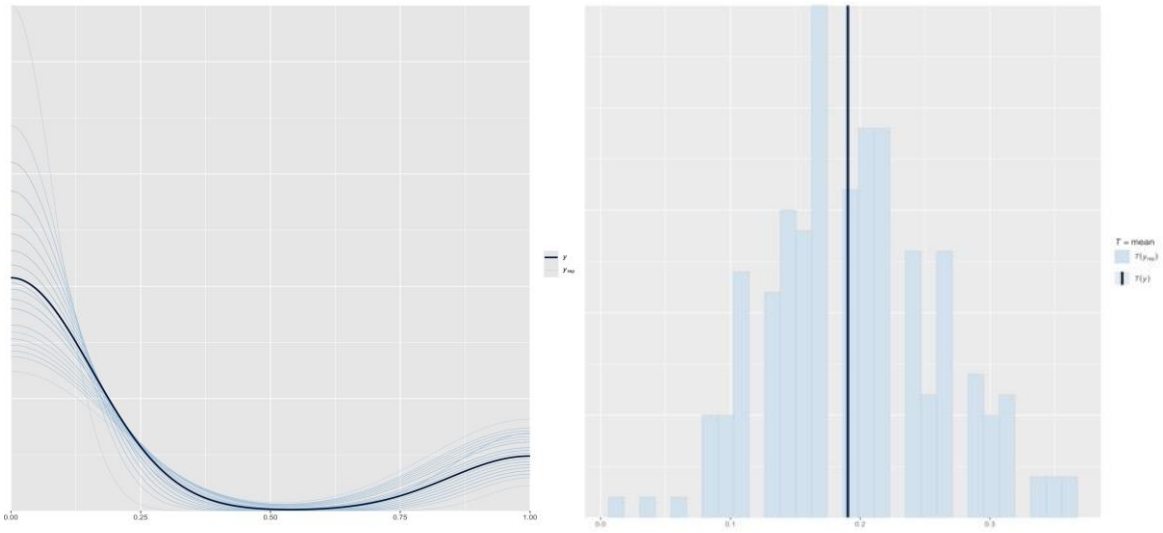


Figure 6.16. Density (left) and histogram (right) charts showing the posterior draws of the probability of presenting with PH based on fit5 (PH~Age+Sex). Dark lines represent the mean and flat priors used. Light blue lines are the random draws from the posterior parameter space. The symmetrical distribution of the light blue lines around the mean suggests the model converged.

Table 6.41. Odds Ratios and 95% Credibility Interval for fit5.

		95% Credibility Interval	
	Odds Ratio (OR)	**Lower**	**Upper**
Intercept	0.54	0.09	2.89
Age	0.96	0.92	1.0
SexMale	2.36	0.59	10.48

The full model summary is provided in Table 6.42. The Rhat values are all less than 1.01 and the Bulk and Tail ESS are all around 10,000, which indicates that the model converged.

Model Selection. A series of model fits with flat priors and different combinations of predictor variables were created to see which predictor variables from the full model best explained the data and predicted the outcome of interest (presence or absence of a lesion). LOOIC were used for model selection. The model fit with the lowest LOOIC value was selected as the best-fit model. For all model fits except fit5 and fit7 the Pareto *k* values were > 0.7. Pareto k diagnostics are used by the LOO package to monitor the sampling accuracy, and the result indicates that the model is not reliable, so only models fit5 and fit7 were successful. Table 6.43 provides the LOOIC values for each.

Model selection favored fit7 (CO~1) which is the intercept or naïve model (Table 6.44) and the next best-fit model is fit5 (CO~Age+Sex) (Table 6.45). The intercept model is only examined to evaluate the relative parsimony of the next best-fit model. Fit5 Rhat values are less than 1.01 and the Bulk and Tail ESS are greater than 10,000, which indicates the model converged. This is visually confirmed by the Hamilton Monte Carlo (HMC) Chains (Figure 6.17) and no autocorrelation between the chains (Figure 6.18). This supports the conclusion that the Markov chains effectively explored the posterior parameter space and produced a representative sample of the posterior probability distribution for the fit5 model.

Model Summary. Model fit5 included age and sex predictor variables. The posterior predictive checks confirm this and show that posterior draws for this model are distributed symmetrically around the mean (Figure 6.19). Table 6.46 provides the parameters, the ORs, and 95% Credibility Interval. The posterior distributions for each estimate are depicted in Figure 6.17. Marginal effects plots are provided in Appendix Three.

Table 6.42. Log odds estimate, error, 95% Credibility Interval, Rhat values, and Bulk and Tail ESS for the full model.

			95% Credibility Interval				
	Estimate	**Error**	**Lower**	**Upper**	**Rhat**	**Bulk ESS**	**Tail ESS**
Intercept	-12.23	8.44	-30.24	2.89	1.00	97934	90502
Age	0.02	0.03	-0.03	0.08	1.00	97675	94915
SexMale	-1.56	1.13	-3.96	0.52	1.00	90316	80771
SiteSchitisor	-2.72	1.89	-6.79	0.64	1.00	70803	74166
SiteSuceava	-2.53	1.56	-5.75	0.44	1.00	70974	78272
δ^{13}C Femur	-0.49	0.30	-1.15	0.03	1.00	77512	75446
δ^{15}N Femur	0.23	0.80	-1.38	1.79	1.00	97925	91656

Table 6.43. LOOIC values for each model fit.

Model fit	**elpd_diff**	**se_diff**	**elpd_loo**	**se_elpd_loo**	**p_loo**	**se_p_loo**	**looic**	**se_looic**
fit7	0.00	0.00	-22.03	6.02	1.03	0.37	44.06	12.04
fit5	-1.95	1.61	-23.98	6.88	3.83	1.46	47.97	13.76

Table 6.44. The log odds estimate, 95% Credibility Interval, Rhat values, and Bulk and Tail ESS for fit7.

			95% Credibility Interval				
	Estimate	**Error**	**Lower**	**Upper**	**Rhat**	**Bulk ESS**	**Tail ESS**
Intercept	-2.46	0.43	-3.37	-1.70	1.00	48638	53765

Table 6.45. The log odds estimate, 95% Credibility Interval, Rhat values, and Bulk and Tail ESS for fit5.

			95% Credibility Interval				
	Estimate	**Error**	**Lower**	**Upper**	**Rhat**	**Bulk ESS**	**Tail ESS**
Intercept	-2.68	1.10	-5.01	-0.67	1.00	107401	92126
Age	0.01	0.02	-0.03	0.06	1.00	93673	91702
SexMale	-1.13	0.98	-3.18	0.69	1.00	84612	75231

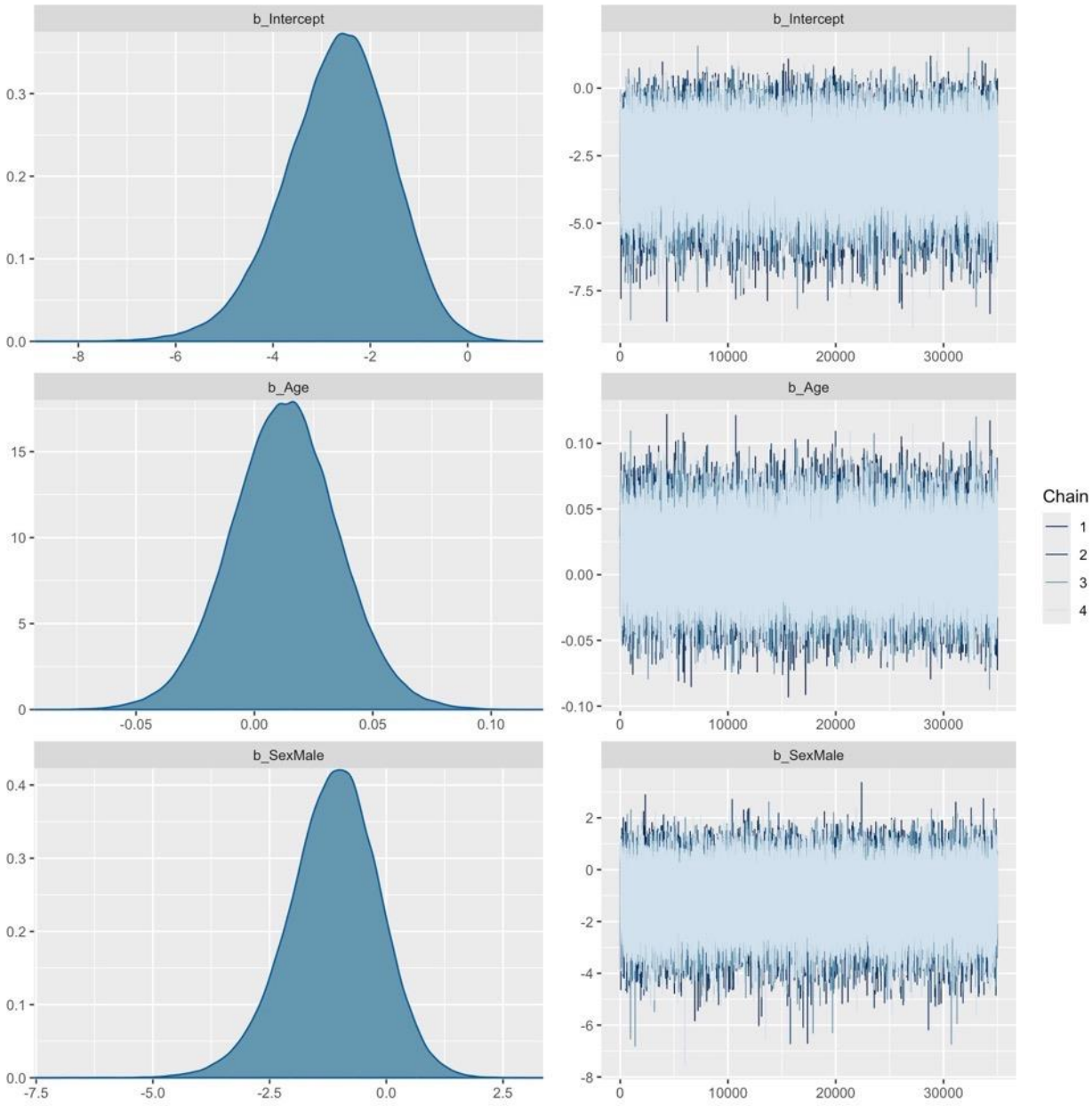


Figure 6.17. Posterior parameter distribution of the fit5 (CO~Age+Sex) model parameters and HMC chains.

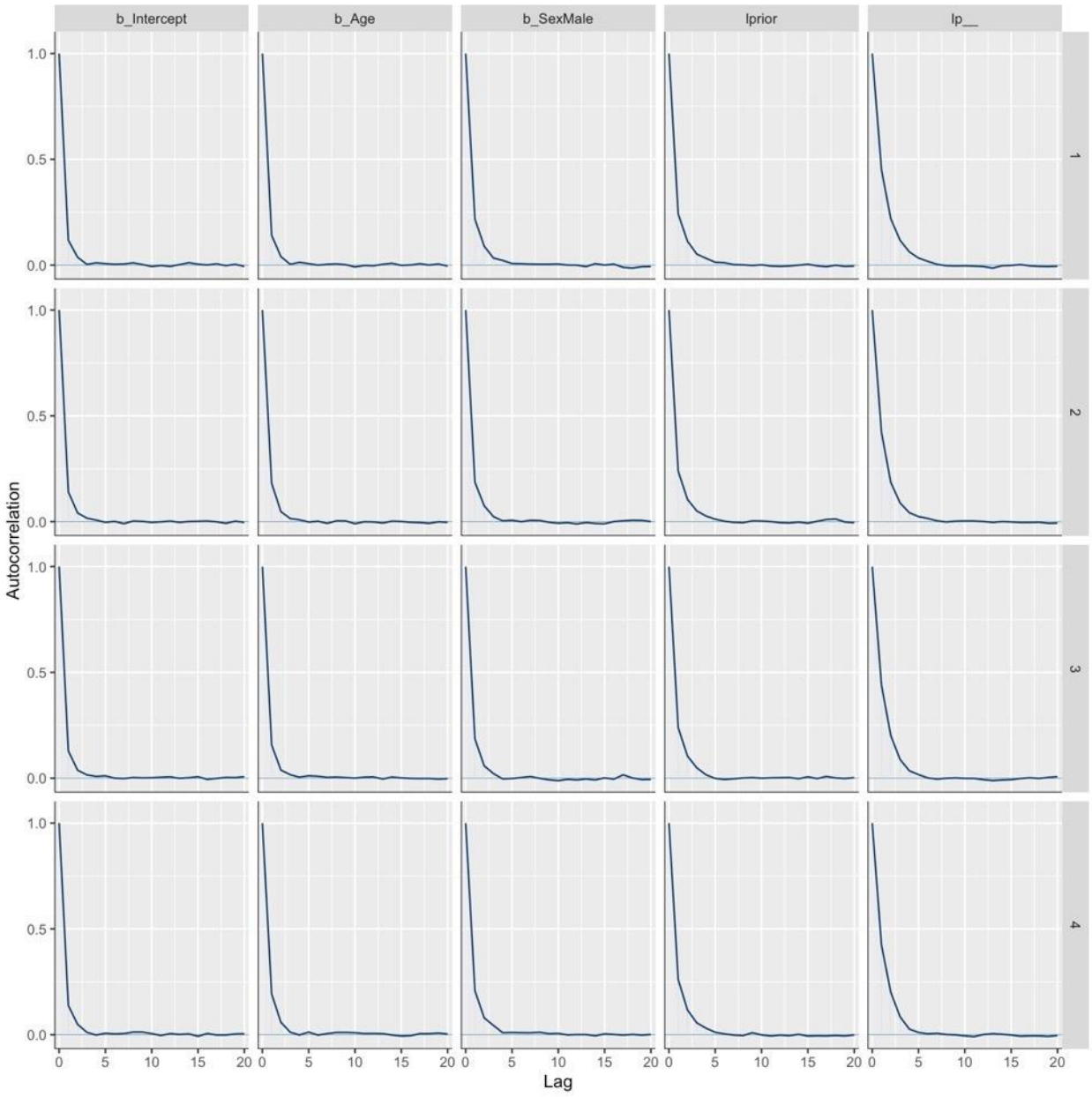


Figure 6.18. Autocorrelation plots for each fit5 (CO~Age+Sex) parameter by HMC chain with flat priors that suggest negligible autocorrelation.

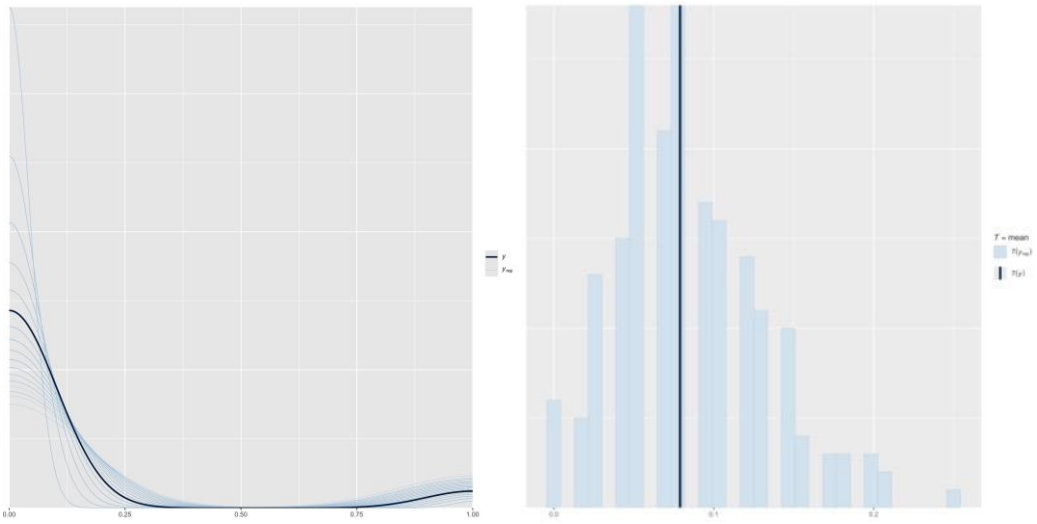


Figure 6.19. Density (left) and histogram (right) charts showing the posterior draws of the probability of presenting with CO based on the fit5 (CO~Age+Sex). Dark lines represent the mean and flat priors used. Light blue lines are the random draws from the posterior parameter space. The symmetrical distribution of the light blue lines around the mean suggests the model converged.

Table 6.46. Odds Ratios and 95% Credibility Interval for fit5.

		95% Credibility Interval	
	Odds Ratio (OR)	**Lower**	**Upper**
Intercept	0.07	0.007	0.51
Age	1.01	0.97	1.06
SexMale	0.32	0.04	1.99

Each parameter estimate represents a change in the log odds of presenting with CO given a change in the value associated with the predictor variable. For age, with each year of life, there is an increase in the log odds of presenting with CO (log odds = 0.01, 95% CI = -0.03 - 0.06), and the odds of presenting with CO slightly increase for each year of age (OR = 1.01, 95% CI = 0.97 – 1.06), but it is not credibly different from chance. The probability of presenting with CO increases 50.25% with each year of age.

By sex, the log odds of presenting with CO were lower among males than females (log odds = -1.13, 95% CI = -3.18 – .69), and males have a decreased odds of presenting with CO compared to females (OR = 0.323, 95% CI = 0.04 – 1.99), but it is not credibly different from chance. The probability of males presenting with CO compared to females is 24.41%.

CO and Rib $\delta^{13}C$ and $\delta^{15}N$ values

Model Description. The model for CO and rib carbon and nitrogen isotope values used flat priors (Table 6.21). The full model summary is provided in Table 6.47. The Rhat values are all less than 1.01 and the Bulk and Tail ESS are all greater than 10,000, which indicates that the model converged.

Model Selection. A series of model fits with flat priors and different combinations of predictor variables were created to see which predictor variables from the full model best explained the data and predicted the outcome of interest (presence or absence of a lesion). LOOIC were used for model selection. The model fit with the lowest LOOIC value was selected as the best-fit model. For all model fits except fit5 and fit7 the Pareto *k* values were > 0.7, so only models fit5 and fit7 were successful. Table 6.48 provides the LOOIC values for each.

Table 6.47. Log odds estimate, error, 95% Credibility Interval, Rhat values, and Bulk and Tail ESS for the full model.

			95% Credibility Interval				
	Estimate	**Error**	**Lower**	**Upper**	**Rhat**	**Bulk ESS**	**Tail ESS**
Intercept	-5.33	8.47	-22.17	11.29	1.00	119279	102004
Age	0.04	0.03	-0.02	0.10	1.00	85186	82684
SexMale	-1.05	1.28	-3.72	1.34	1.00	88093	81667
SiteSchitisor	-3.16	1.97	-7.41	0.31	1.00	62149	72469
SiteSuceava	-2.70	1.65	-6.11	0.42	1.00	64980	74722
δ^{13}C Rib	-0.42	0.27	-1.00	0.07	1.00	67829	78847
δ^{15}N Rib	-0.43	0.88	-2.24	1.20	1.00	89487	87491

Table 6.48. LOOIC values for each model fit.

Model fit	**elpd_diff**	**se_diff**	**elpd_loo**	**se_elpd_loo**	**p_loo**	**se_p_loo**	**looic**	**se_looic**
fit7	0.00	0.00	-18.97	5.76	1.02	0.40	37.94	11.52
fit5	-1.89	1.59	-20.86	6.64	3.60	1.46	41.73	13.28

Model selection favored fit7 (CO~1) which is the intercept or naïve model (Table 6.49) so the next best-fit model, fit5 (CO~Age+Sex), is reported (Table 6.50). Fit5 Rhat values are less than 1.01 and the Bulk and Tail ESS are greater than 10,000, which indicates the model converged. This is visually confirmed by the Hamilton Monte Carlo (HMC) Chains (Figure 6.20) and no autocorrelation between the chains (Figure 6.21). This supports the conclusion that the Markov chains effectively explored the posterior parameter space and produced a representative sample of the posterior probability distribution for the fit5 model.

Model Summary. Model fit5 included age and sex predictor variables. The posterior predictive checks confirm this and show that posterior draws for this model are distributed symmetrically around the mean (Figure 6.22). Table 6.51 provides the parameters, the ORs, and 95% Credibility Interval. The posterior distributions for each estimate are depicted in Figure 6.21. Marginal effects plots are provided in Appendix Three.

Each parameter estimate represents a change in the log odds of presenting with CO given a change in the value associated with the predictor variable. For age, with each year of life, there is an increase in the log odds of presenting with CO (log odds = 0.02, 95% CI = -0.02 - 0.07), and the odds of presenting with CO slightly increase for each year of age (OR = 1.02, 95% CI = 0.98– 1.07), but it is not credibly different from chance. The probability of presenting with CO increases 50.50% with each year of age.

By sex, the log odds of presenting with CO were lower among males than females (log odds = -0.69, 95% CI = -2.78 – 1.26), and males have a decreased odds of presenting with CO compared to females (OR = 0.50, 95% CI = 0.06 – 3.52), but it is not credibly different from chance. The probability of males presenting with CO compared to females is 33.4%.

Table 6.49. The log odds estimate, 95% Credibility Interval, Rhat values, and Bulk and Tail ESS for fit7.

			95% Credibility Interval				
	Estimate	**Error**	**Lower**	**Upper**	**Rhat**	**Bulk ESS**	**Tail ESS**
Intercept	-2.55	0.46	-3.55	-1.73	1.00	47397	51833

Table 6.50. The log odds estimate, 95% Credibility Interval, Rhat values, and Bulk and Tail ESS for fit5.

			95% Credibility Interval				
	Estimate	**Error**	**Lower**	**Upper**	**Rhat**	**Bulk ESS**	**Tail ESS**
Intercept	-3.54	1.32	-6.42	-1.22	1.00	90715	73923
Age	0.02	0.02	-0.02	0.07	1.00	93085	81744
SexMale	-0.69	1.02	-2.78	1.26	1.00	93631	78236

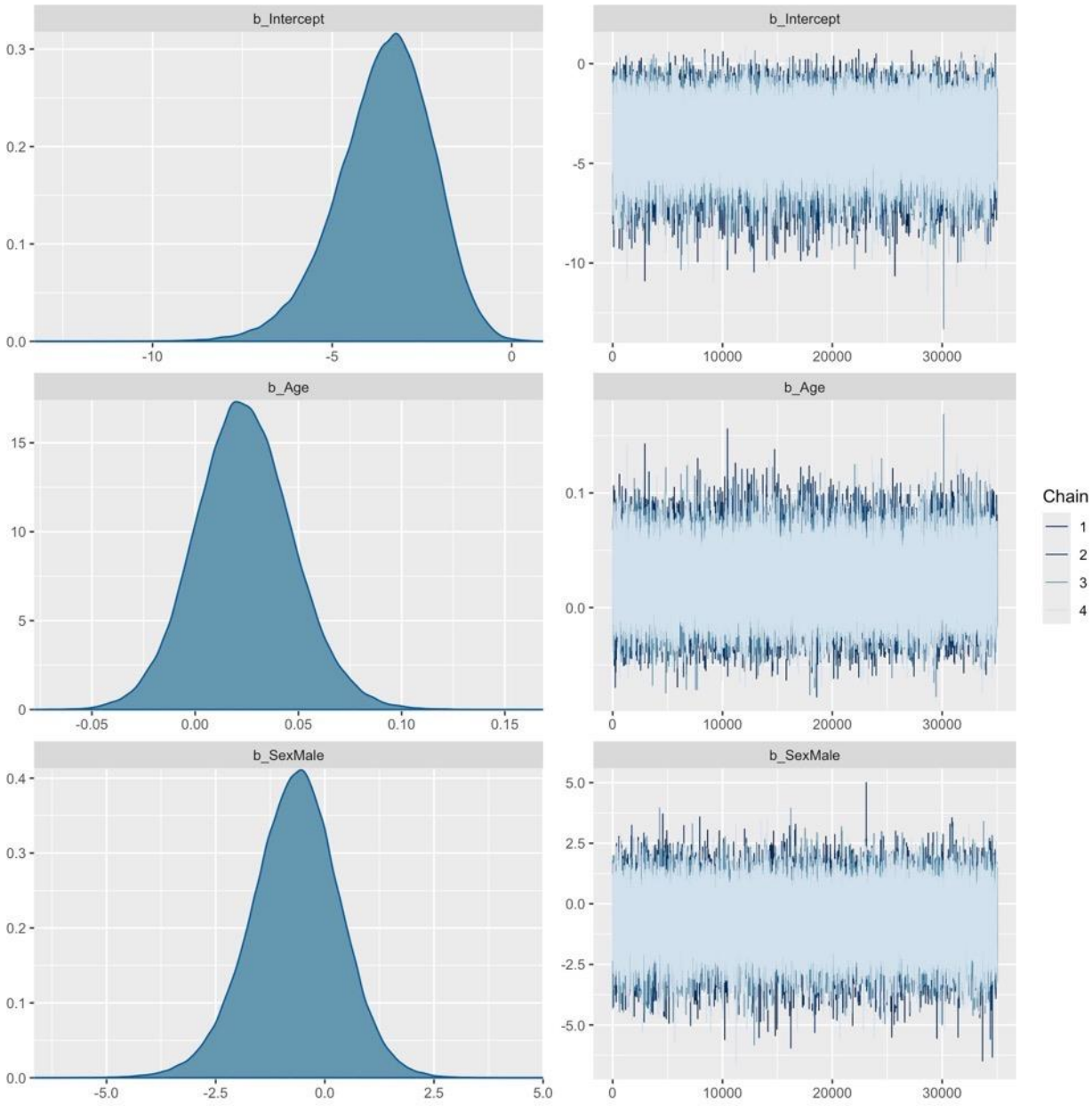


Figure 6.20. Posterior parameter distribution of the fit5 (CO~Age+Sex) model parameters and HMC chains.

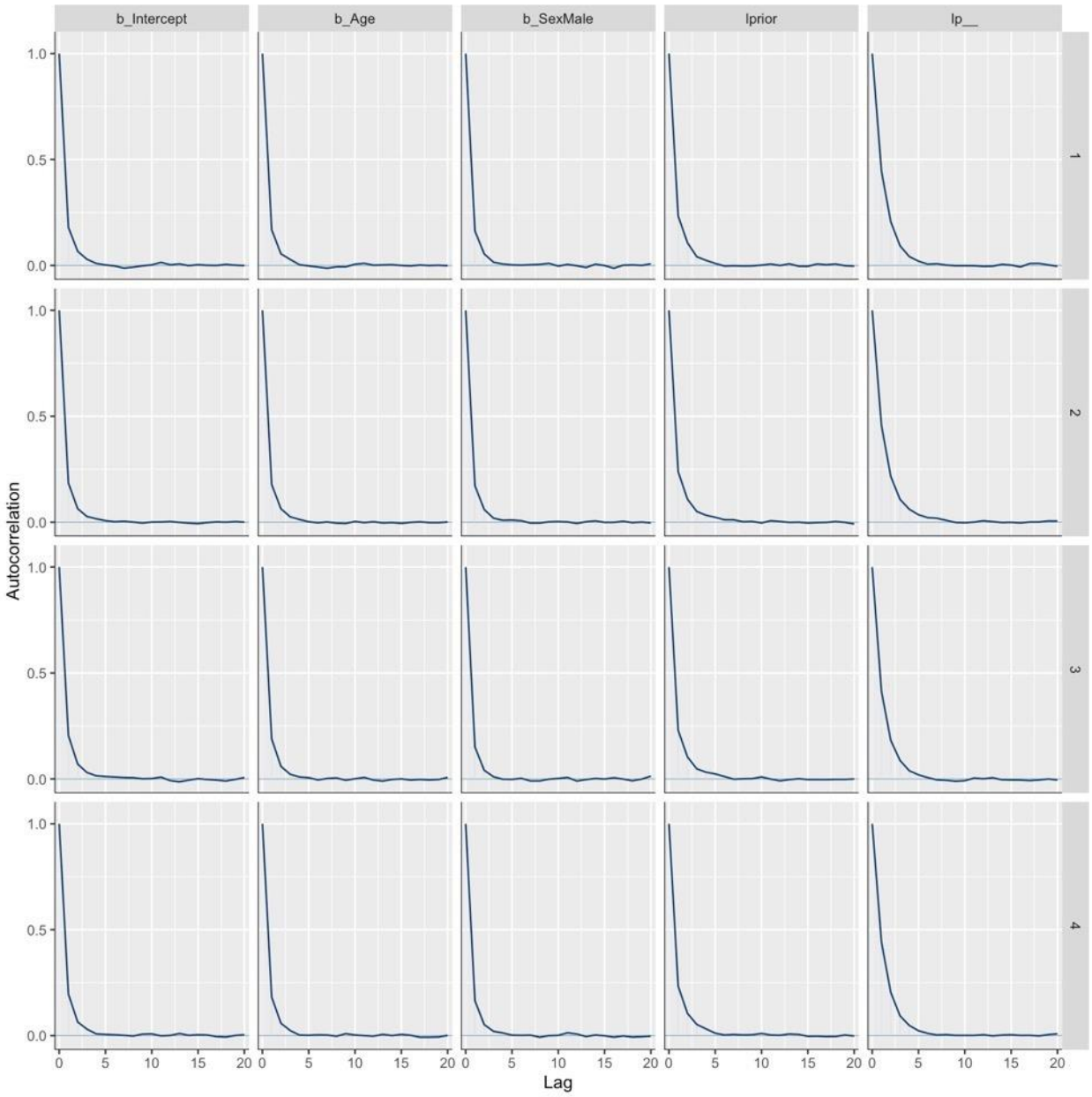


Figure 6.21. Autocorrelation plots for each fit5 (CO~Age+Sex) parameter by HMC chain with flat priors that suggest negligible autocorrelation.

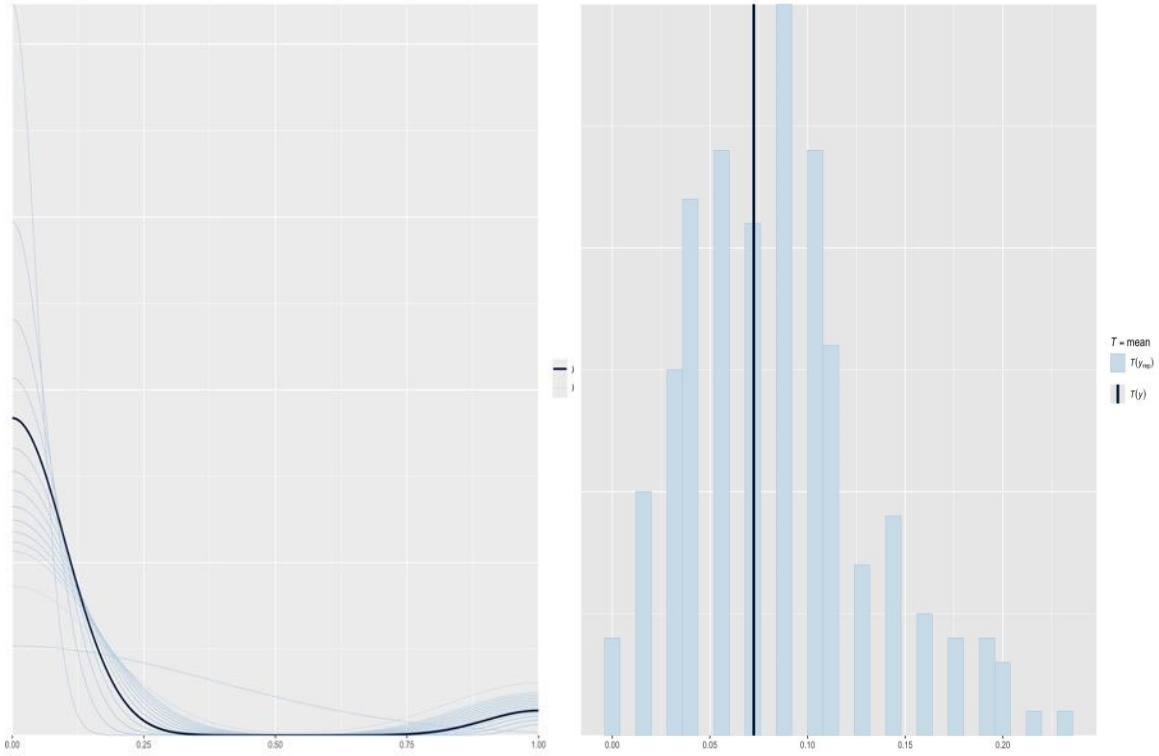


Figure 6.22. Density (left) and histogram (right) charts showing the posterior draws of the probability of presenting with CO based on fit5 (CO~Age+Sex). Dark lines represent the mean and flat priors used. Light blue lines are the random draws from the posterior parameter space. The symmetrical distribution of the light blue lines around the mean suggests the model converged.

Table 6.51. Odds Ratios and 95% Credibility Interval for fit5.

		95% Credibility Interval	
	Odds Ratio (OR)	**Lower**	**Upper**
Intercept	0.03	0.002	0.30
Age	1.02	0.98	1.07
SexMale	0.50	0.06	3.52

Caries and Femur $\delta^{13}C$ and $\delta^{15}N$ values

Model Description. The model for caries and femur carbon and nitrogen isotope values used flat priors (Table 6.21). The full model summary is provided in Table 6.52. The Rhat values are all less than 1.01 and the Bulk and Tail ESS are all greater than or around 10,000, which indicates that the model converged.

Model Selection. A series of model fits with flat priors and different combinations of predictor variables were created to see which predictor variables from the full model best explained the data and predicted the outcome of interest (presence or absence of a lesion). LOOIC were used for model selection. Table 6.53 provides the LOOIC values for each. Model selection favored fit5 (Caries~Age+Sex) (Table 6.54). Fit5 Rhat values are less than 1.01 and the Bulk and Tail ESS are greater than 10,000, which indicates the model converged. This is visually confirmed by the Hamilton Monte Carlo (HMC) Chains (Figure 6.23) and no autocorrelation between the chains (Figure 6.24). This supports the conclusion that the Markov chains effectively explored the posterior parameter space and produced a representative sample of the posterior probability distribution for the fit5 model.

Model Summary. Model fit5 included age and sex predictor variables. The posterior predictive checks confirm this and show that posterior draws for this model are distributed symmetrically around the mean (Figure 6.25). Table 6.55 provides the parameters, the ORs, and 95% Credibility Interval. The posterior distributions for each estimate are depicted in Figure 6.23. Marginal effects plots are provided in Appendix Three.

Each parameter estimate represents a change in the log odds of presenting with caries given a change in the value associated with the predictor variable. For age, with each year of life,

Table 6.52. Log odds estimate, error, 95% Credibility Interval, Rhat values, and Bulk and Tail ESS for the full model.

			95% Credibility Interval				
	Estimate	**Error**	**Lower**	**Upper**	**Rhat**	**Bulk ESS**	**Tail ESS**
Intercept	2.25	3.80	-5.06	9.84	1.00	122065	106550
Age	0.00	0.01	-0.02	0.03	1.00	141825	101239
SexMale	1.11	0.55	0.07	2.20	1.00	127961	102915
SiteSchitisor	1.67	0.90	-0.01	3.52	1.00	96572	96951
SiteSuceava	1.00	0.99	-0.86	3.01	1.00	84249	87256
δ^{13}C Femur	0.17	0.13	-0.07	0.44	1.00	104455	94617
δ^{15}N Femur	-0.11	0.37	-0.85	0.62	1.00	124288	102240

Table 6.53. LOOIC values for each model fit.

Model fit	**elpd_diff**	**se_diff**	**elpd_loo**	**se_elpd_loo**	**p_loo**	**se_p_loo**	**looic**	**se_looic**
fit5	0.00	0.00	-54.47	2.52	3.20	0.23	108.93	5.04
fit7	-0.19	2.35	-54.66	0.92	1.00	0.02	109.32	1.84
fit4	-0.64	2.15	-55.11	3.36	5.56	0.52	110.21	6.71
fit2	-1.14	2.89	-55.61	3.90	6.92	0.86	111.21	7.80
fit6	-1.68	2.95	-56.15	2.45	4.51	0.39	112.29	4.90
fit3	-1.86	2.31	-56.33	3.52	6.86	0.63	112.66	7.04
fit	-2.42	2.99	-56.88	4.03	8.22	0.95	113.77	8.06

Table 6.54. The log odds estimate, 95% Credibility Interval, Rhat values, and Bulk and Tail ESS for fit5.

			95% Credibility Interval				
	Estimate	**Error**	**Lower**	**Upper**	**Rhat**	**Bulk ESS**	**Tail ESS**
Intercept	-1.08	0.60	-2.28	0.07	1.00	140622	103564
Age	0.01	0.01	-0.01	0.03	1.00	128912	105962
SexMale	0.94	0.49	-0.00	1.91	1.00	128545	102013

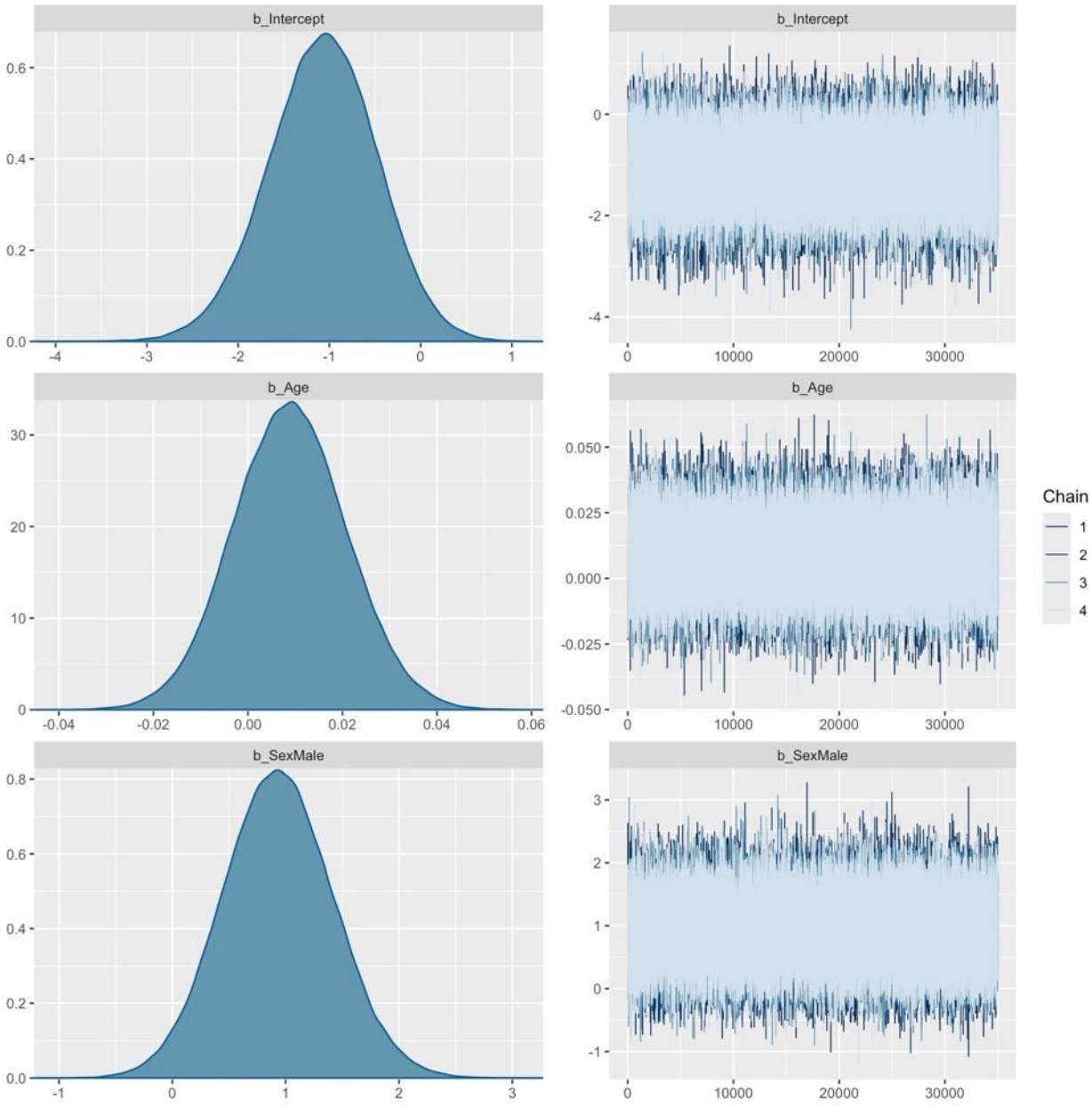


Figure 6.23. Posterior parameter distribution of the fit5 (Caries~Age+Sex) model parameters and HMC chains.

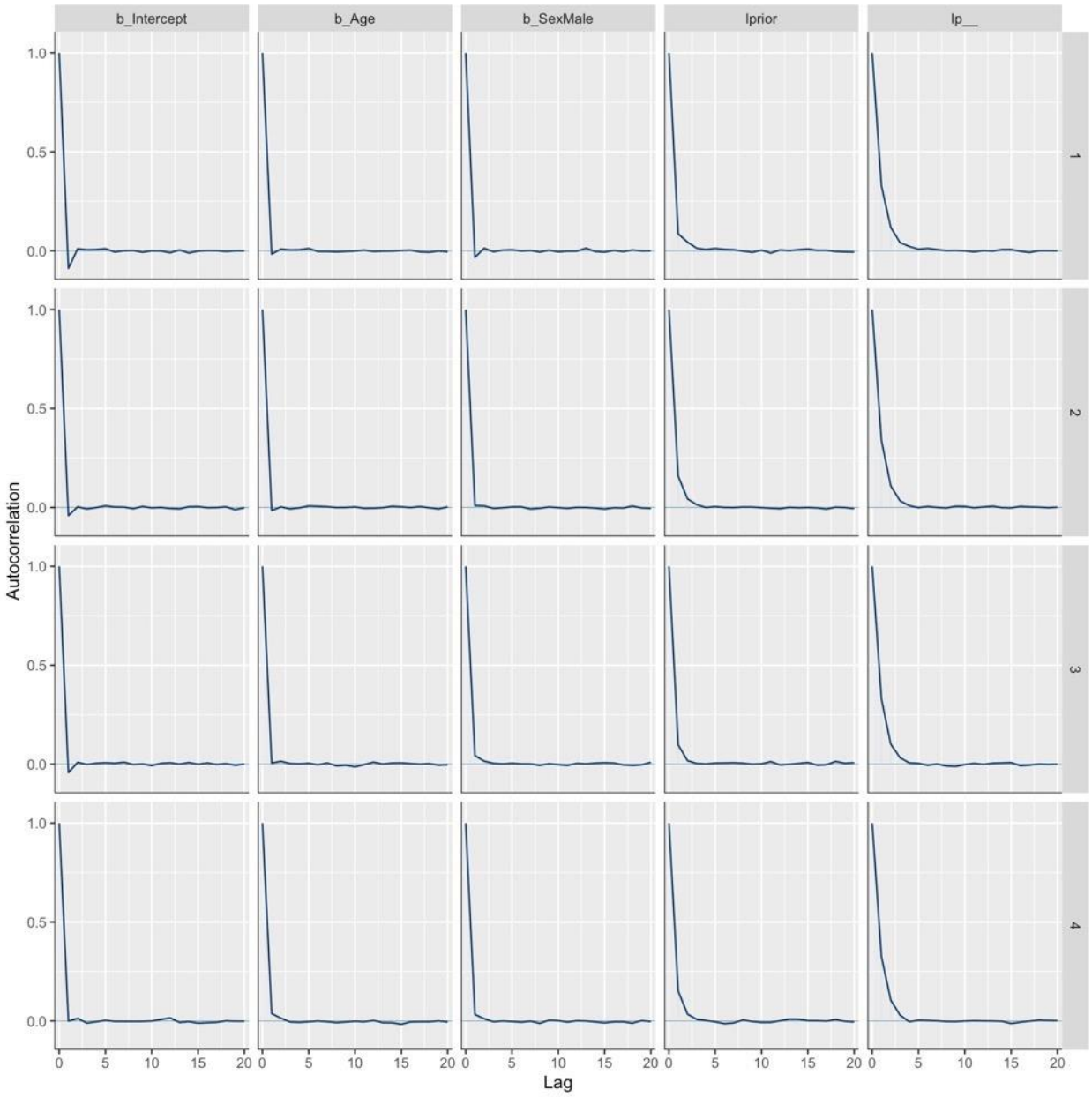


Figure 6.24. Autocorrelation lots for each fit5 (Caries~Age+Sex) parameter by HMC chain with flat priors that suggest negligible autocorrelation.

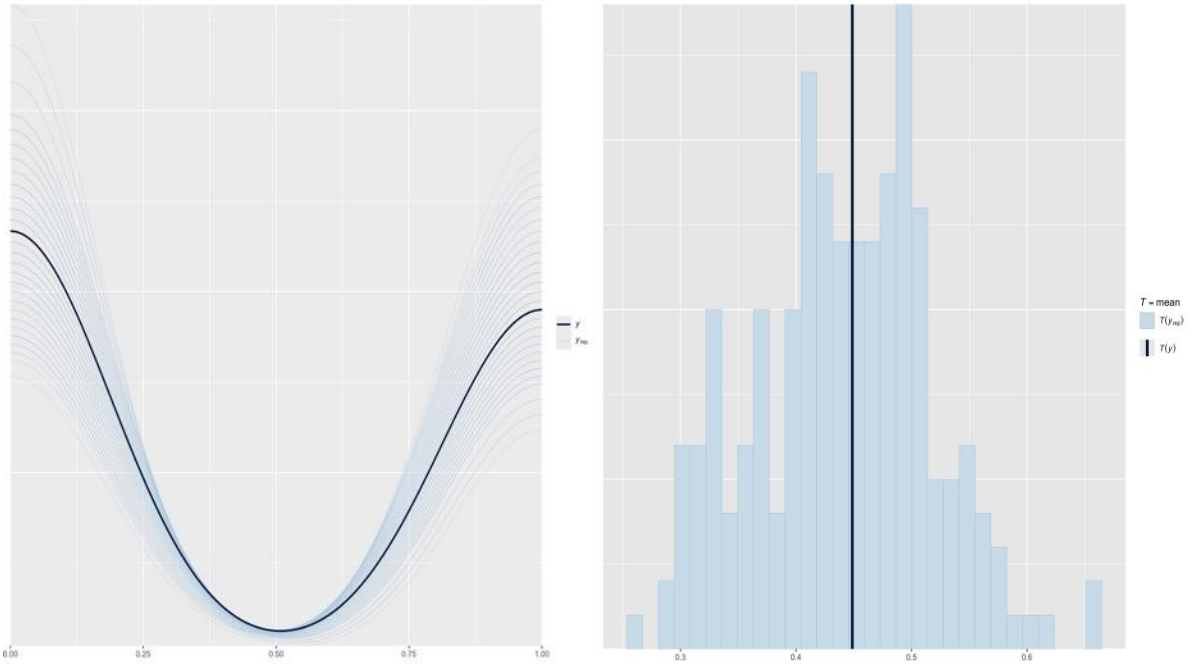


Figure 6.25. Density (left) and histogram (right) charts showing the posterior draws of the probability of presenting with caries based on fit5 (Caries~Age+Sex). Dark lines represent the mean and flat priors used. Light blue lines are the random draws from the posterior parameter space. The symmetrical distribution of the light blue lines around the mean suggests the model converged.

Table 6.55. Odds Ratios and 95% Credibility Interval for fit5.

		95% Credibility Interval	
	Odds Ratio (OR)	**Lower**	**Upper**
Intercept	0.34	0.10	1.07
Age	1.01	0.99	1.03
SexMale	2.56	1.0	6.75

there is an increase in the log odds of presenting with caries (log odds = 0.01, 95% CI = -0.01 - 0.03), and the odds of presenting with caries slightly increase for each year of age (OR = 1.01, 95% CI = 0.99– 1.03), but it is not credibly different from chance. The probability of presenting with Caries increases by 50.25% with each year of age.

By sex, the log odds of presenting with caries were higher among males than females (log odds = 0.94, 95% CI = -0.00 – 1.91), and males have increased odds of presenting with caries compared to females (OR = 2.56, 95% CI = 1.0 – 6.75), but it is not credibly different from chance. The probability of males presenting with caries compared to females is 71.91%.

Caries and Rib $\delta^{13}C$ and $\delta^{15}N$ values

Model Description. The model for caries and rib carbon and nitrogen isotope values used flat priors (Table 6.21). The full model summary is provided in Table 6.56. The Rhat values are all less than 1.01 and the Bulk and Tail ESS are all greater than 10,000, which indicates that the model converged.

Model Selection. A series of model fits with flat priors and different combinations of predictor variables were created to see which predictor variables from the full model best explained the data and predicted the outcome of interest (presence or absence of a lesion). LOOIC were used for model selection. Table 6.57 provides the LOOIC values for each. Model selection favored fit7 (Caries~1) which is the intercept or naïve model **(**Table 6.58) so the next best-fit model, fit4 (Caries~Age+Sex+Site), is reported (Table 6.59). Fit4 Rhat values are less than 1.01 and the Bulk and Tail ESS are greater than 10,000, which indicates the model converged. This is visually confirmed by the Hamilton Monte Carlo (HMC) Chains (Figure 6.26) and no autocorrelation between the chains (Figure 6.27). This supports the conclusion that the

Table 6.56. Log odds estimate, error, 95% Credibility Interval, Rhat values, and Bulk and Tail ESS for the full model.

			95% Credibility Interval				
	Estimate	**Error**	**Lower**	**Upper**	**Rhat**	**Bulk ESS**	**Tail ESS**
Intercept	-1.87	4.22	-10.20	6.39	1.00	125945	111194
Age	-0.00	0.01	-0.03	0.02	1.00	141657	103864
SexMale	0.79	0.58	-0.33	1.94	1.00	127951	106445
SiteSchitisor	1.89	0.94	0.15	3.82	1.00	92792	89443
SiteSuceava	0.55	1.03	-1.41	2.66	1.00	82055	84504
δ^{13}C Rib	0.26	0.14	0.00	0.55	1.00	91511	91252
δ^{15}N Rib	0.48	0.43	-0.37	1.34	1.00	116106	101019

Table 6.57. LOOIC values for each model fit.

Model fit	**elpd_diff**	**se_diff**	**elpd_loo**	**se_elpd_loo**	**p_loo**	**se_p_loo**	**looic**	**se_looic**
fit7	0.00	0.00	-50.78	1.31	1.01	0.04	101.56	2.63
fit4	-0.50	3.21	-51.28	3.46	5.58	0.53	102.56	6.93
fit5	-0.53	1.97	-51.31	2.37	3.17	0.22	102.62	4.74
fit2	-0.74	4.17	-51.52	4.34	7.19	1.06	103.03	8.68
fit6	-0.88	2.53	-51.65	2.86	4.44	0.40	103.31	5.72
fit	-1.62	4.46	-52.40	4.65	8.71	1.18	104.79	9.31
fit3	-1.75	3.39	-52.53	3.66	7.11	0.75	105.06	7.32

Table 6.58. The log odds estimate, 95% Credibility Interval, Rhat values, and Bulk and Tail ESS for fit7.

			95% Credibility Interval				
	Estimate	**Error**	**Lower**	**Upper**	**Rhat**	**Bulk ESS**	**Tail ESS**
Intercept	-0.30	0.24	-0.77	0.16	1.00	52214	73613

Table 6.59. The log odds estimate, 95% Credibility Interval, Rhat values, and Bulk and Tail ESS for fit4.

			95% Credibility Interval				
	Estimate	**Error**	**Lower**	**Upper**	**Rhat**	**Bulk ESS**	**Tail ESS**
Intercept	-0.85	0.92	-2.68	0.94	1.00	139073	104512
Age	-0.00	0.01	-0.03	0.02	1.00	165899	103508
SexMale	0.97	0.54	-0.07	2.04	1.00	153799	105042
SiteSchitisor	1.22	0.79	-0.29	2.81	1.00	133085	107728
SiteSuceava	-0.28	0.67	-1.60	1.04	1.00	129815	107601

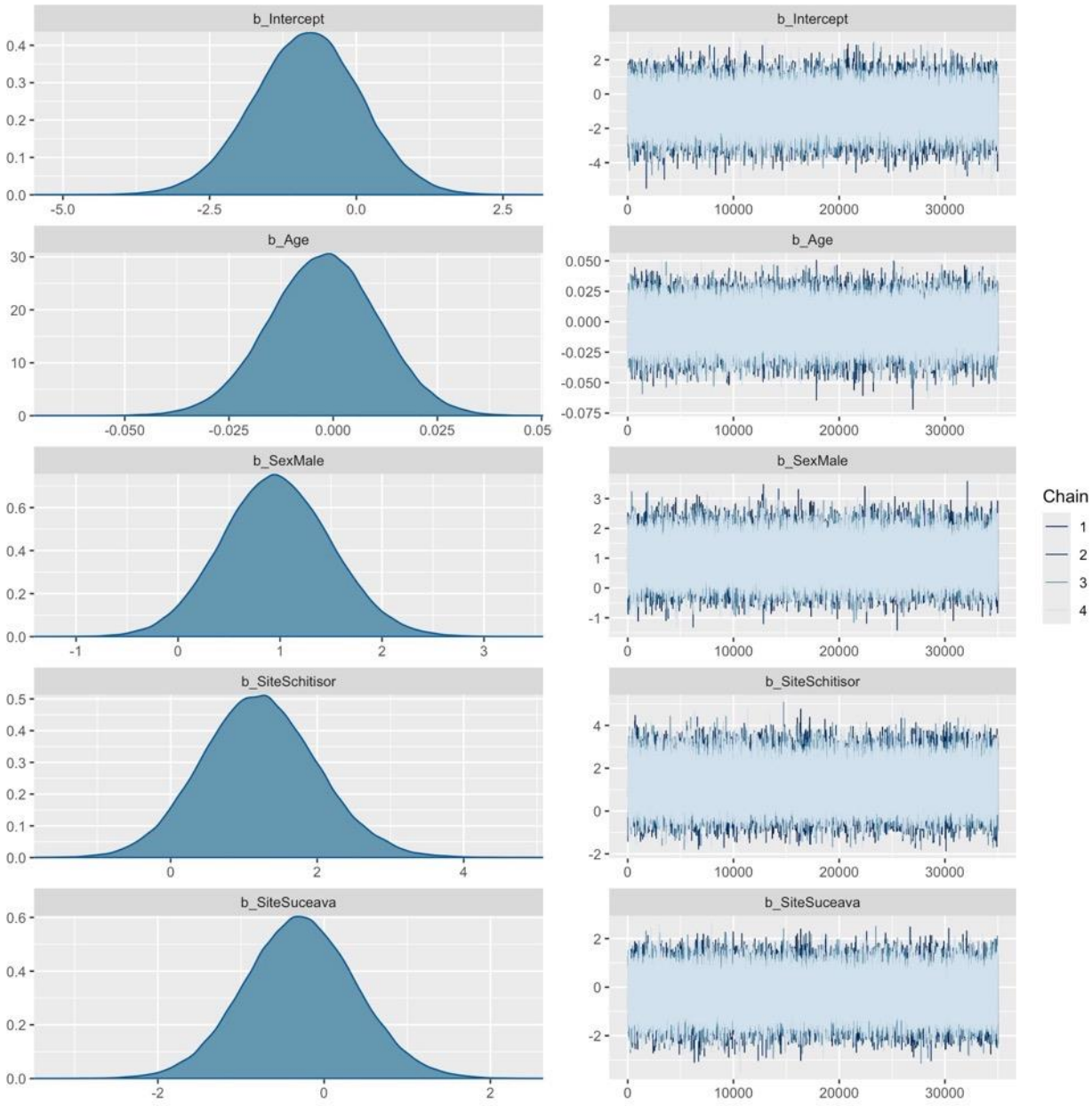


Figure 6.26. Posterior parameter distribution of the fit4 (Caries~Age+Sex+Site) model parameters and HMC chains.

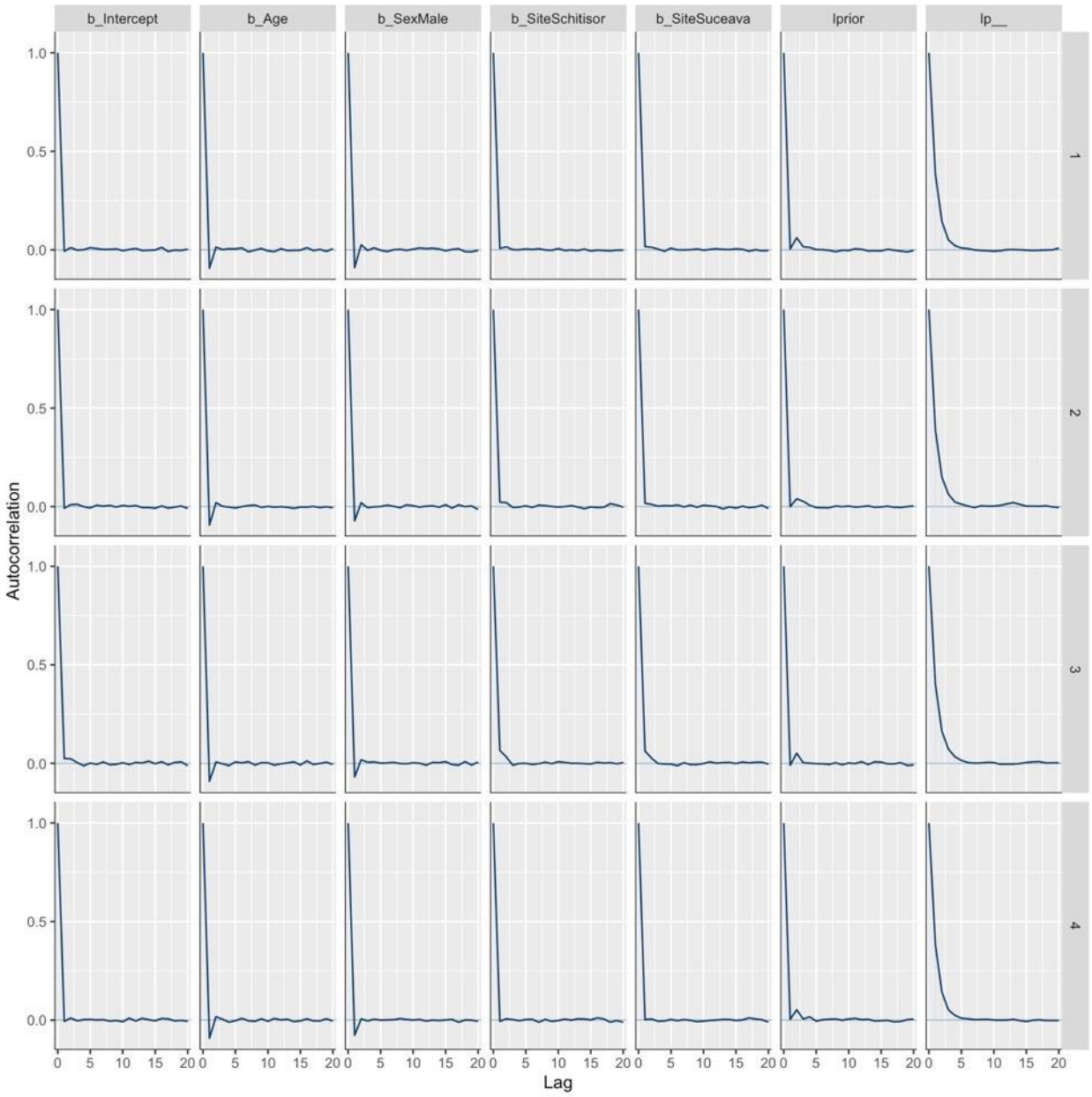


Figure 6.27. Autocorrelation plots for each fit4 (Caries~Age+Sex+Site) parameter by HMC chain with flat priors that suggest negligible autocorrelation.

Markov chains effectively explored the posterior parameter space and produced a representative sample of the posterior probability distribution for the fit4 model.

Model Summary. Model fit4 included age, sex, and site predictor variables. The posterior predictive checks confirm this and show that posterior draws for this model are distributed symmetrically around the mean (Figure 6.28). Table 6.60 provides the parameters, the ORs, and 95% Credibility Interval. The posterior distributions for each estimate are depicted in Figure 6.26. Marginal effects plots are provided in Appendix Three.

Each parameter estimate represents a change in the log odds of presenting with caries given a change in the value associated with the predictor variable. For age, with each year of life, there is no change in the log odds of presenting with caries (log odds = 0.0, 95% CI = -0.03 - 0.02), and the odds of presenting with caries do not change for each year of age (OR = 1.0, 95% CI = 0.97– 1.02), but it is not credibly different from chance. The probability of presenting with caries increases by 50% with each year of age.

By sex, the log odds of presenting with caries were higher among males than females (log odds = 0.97, 95% CI = -0.07 – 2.04), and males have increased odds of presenting with caries compared to females (OR = 2.64, 95% CI = 0.93 – 7.69), but it is not credibly different from chance. The probability of males presenting with caries compared to females is 72.51%.

By site, compared to someone from Palatul Cnejilor, an individual from Schitișor has an increased log odds of presenting with caries (log odds = 1.22, 95% CI = -0.29 – 2.81), and an individual from Schitișor has an increased odds of presenting with caries compared to someone from Palatul Cnejilor (OR = 3.38, 95% CI = 0.75 – 16.61), but it is not credibly different from chance. The probability of an individual from Schitișor presenting with caries is 77.17%. Compared to someone from Palatul Cnejilor, an individual from Suceava has a decreased log

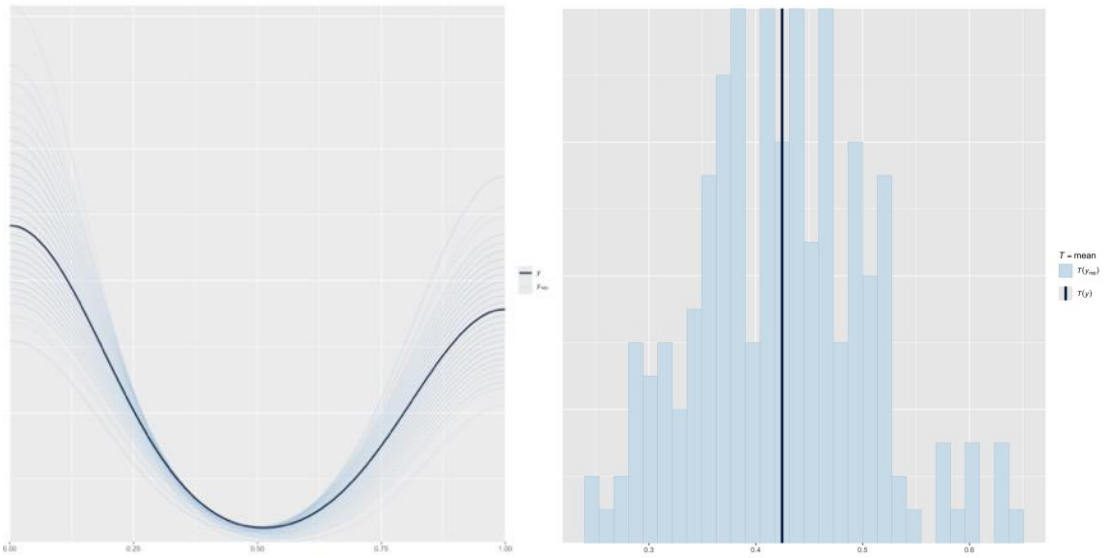


Figure 6.28. Density (left) and histogram (right) charts showing the posterior draws of the probability of presenting with caries based on fit4 (Caries~Age+Sex+Site). Dark lines represent the mean and flat priors used. Light blue lines are the random draws from the posterior parameter space. The symmetrical distribution of the light blue lines around the mean suggests the model converged.

Table 6.60. Odds Ratios and 95% Credibility Interval for fit4.

		95% Credibility Interval	
	Odds Ratio (OR)	**Lower**	**Upper**
Intercept	0.42	0.069	2.56
Age	1.0	0.97	1.02
SexMale	2.64	0.93	7.69
SiteSchitisor	3.39	0.75	16.61
SiteSuceava	0.76	0.20	2.83

odds of presenting with caries (log odds = -0.28, 95% CI = -1.60 – 1.04), and an individual from Suceava has a decreased odds of presenting with caries compared to someone from Palatul Cnejilor (OR = 0.76, 95% CI = 0.20 – 2.83), but it is not credibly different from chance. The probability of an individual from Suceava presenting with caries is 42.86%.

Abscesses and Femur $\delta^{13}C$ and $\delta^{15}N$ values

Model Description. The model for abscesses and femur carbon and nitrogen isotope values used flat priors (Table 6.21). The full model summary is provided in Table 6.61. The Rhat values are all less than 1.01 and the Bulk and Tail ESS are all greater than 10,000, which indicates that the model converged.

Model Selection. A series of model fits with flat priors and different combinations of predictor variables were created to see which predictor variables from the full model best explained the data and predicted the outcome of interest (presence or absence of a lesion). LOO criteria were used for model selection.

Table 6.62 provides the LOOIC values for each. Model selection favored fit7 (Abscesses~1) which is the intercept or naïve model (Table 6.63) so the next best-fit model, fit5 (Abscesses~Age+Sex), is reported (Table 6.64). Fit5 Rhat values are less than 1.01 and the Bulk and Tail ESS are greater than 10,000, which indicates the model converged. This is visually confirmed by the Hamilton Monte Carlo (HMC) Chains (Figure 6.29) and no autocorrelation between the chains (Figure 6.30). This supports the conclusion that the Markov chains effectively explored the posterior parameter space and produced a representative sample of the posterior probability distribution for the fit5 model.

Table 6.61. Log odds estimate, error, 95% Credibility Interval, Rhat values, and Bulk and Tail ESS for the full model.

			95% Credibility Interval				
	Estimate	**Error**	**Lower**	**Upper**	**Rhat**	**Bulk ESS**	**Tail ESS**
Intercept	-5.00	4.12	-13.23	2.95	1.00	136216	110120
Age	-0.01	0.01	-0.04	0.02	1.00	160976	105646
SexMale	0.55	0.59	-0.59	1.73	1.00	140466	106098
SiteSchitisor	-0.85	0.90	-2.66	0.88	1.00	107215	102656
SiteSuceava	-0.95	0.97	-2.87	0.95	1.00	85450	98301
δ^{13}C Femur	-0.10	0.13	-0.37	0.16	1.00	113902	100911
δ^{15}N Femur	0.30	0.40	-0.48	1.08	1.00	140829	107307

Table 6.62. LOOIC values for each model fit.

Model fit	elpd_diff	se_diff	elpd_loo	se_elpd_loo	p_loo	se_p_loo	looic	se_looic
fit7	0.00	0.00	-47.65	4.31	1.00	0.12	95.30	8.61
fit5	-1.36	1.45	-49.01	4.68	3.02	0.42	98.01	9.36
fit6	-2.81	1.30	-50.46	4.81	4.22	0.60	100.92	9.62
fit4	-3.49	1.78	-51.15	5.02	5.35	0.73	102.29	10.04
fit3	-4.41	2.04	-52.06	5.15	6.63	0.86	104.13	10.30
fit2	-4.50	2.18	-52.15	5.26	6.61	1.00	104.31	10.53
fit	-5.62	2.42	-53.27	5.41	8.04	1.17	106.53	10.82

Table 6.63. The log odds estimate, 95% Credibility Interval, Rhat values, and Bulk and Tail ESS for fit7.

			95% Credibility Interval				
	Estimate	**Error**	**Lower**	**Upper**	**Rhat**	**Bulk ESS**	**Tail ESS**
Intercept	-1.07	0.25	-1.58	-0.59	1.00	54566	59224

Table 6.64. The log odds estimate, 95% Credibility Interval, Rhat values, and Bulk and Tail ESS for fit5.

			95% Credibility Interval				
	Estimate	**Error**	**Lower**	**Upper**	**Rhat**	**Bulk ESS**	**Tail ESS**
Intercept	-1.02	0.65	-2.34	0.22	1.00	147313	101278
Age	-0.01	0.01	-0.04	0.02	1.00	121985	103261
SexMale	0.62	0.54	-0.43	1.70	1.00	116843	99862

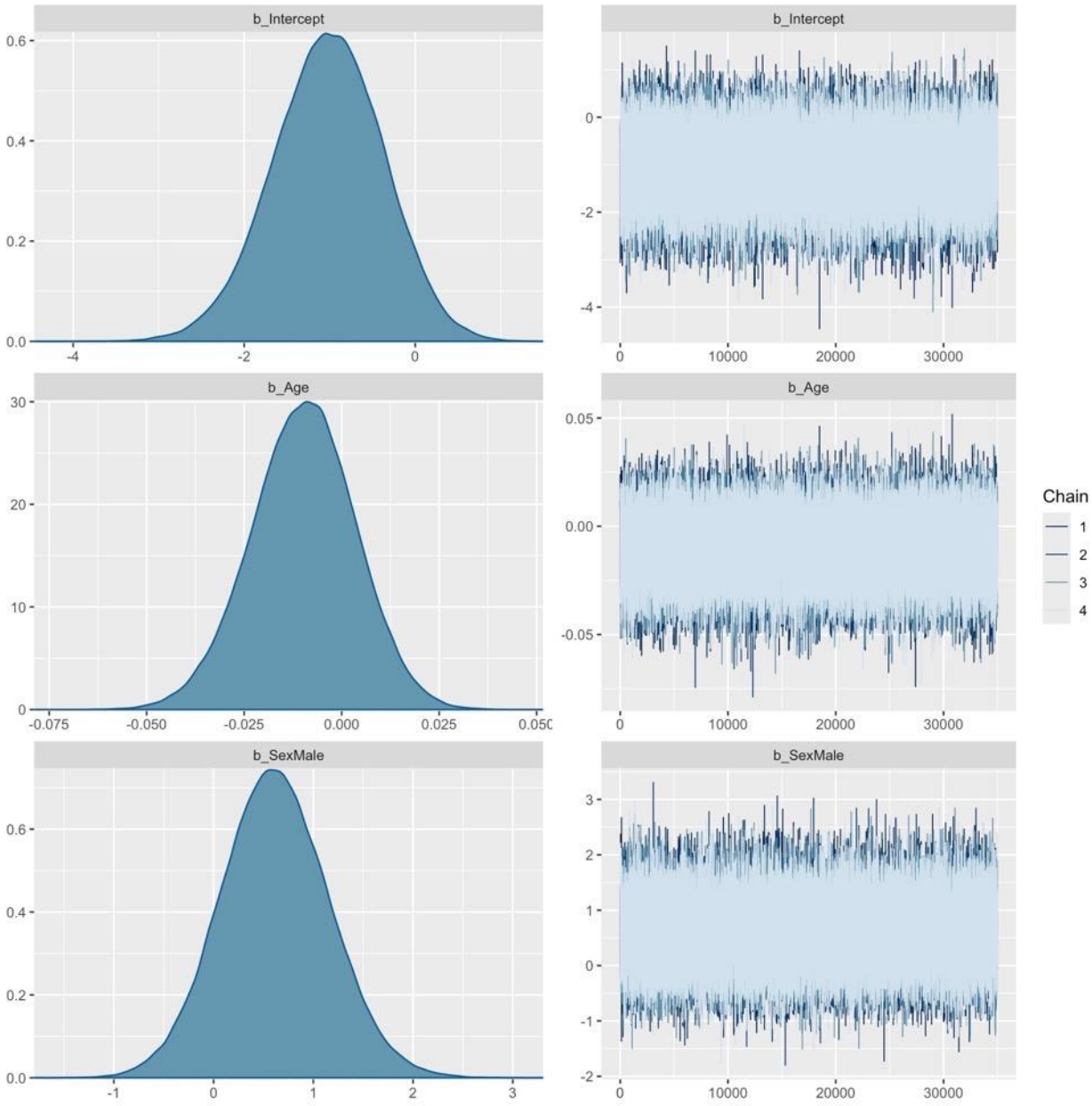


Figure 6.29. Posterior parameter distribution of the fit5 (Abscesses~Age+Sex) model parameters and HMC chains.

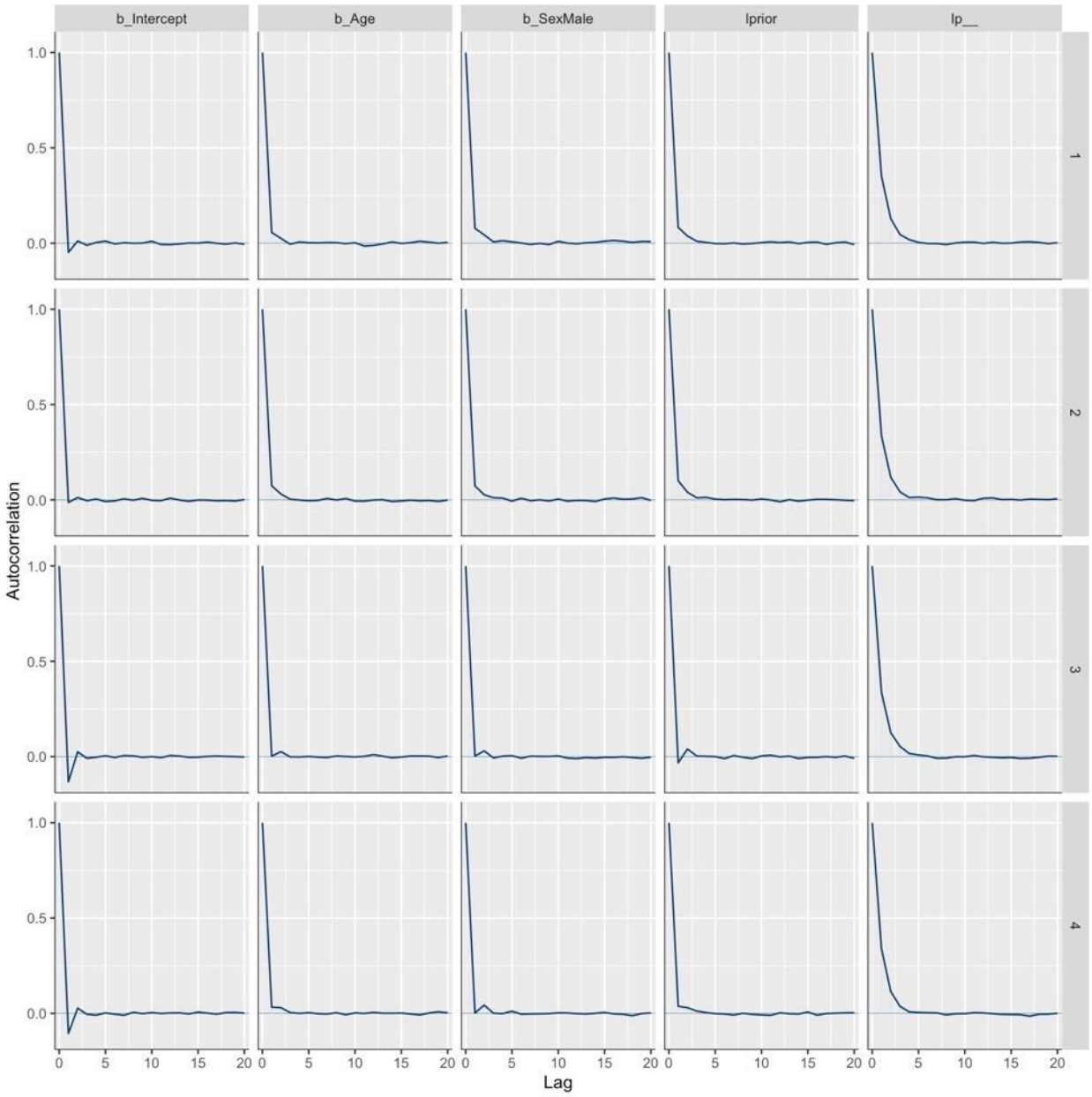


Figure 6.30. Autocorrelation plots for each fit5 (Abscesses~Age+Sex) parameter by HMC chain with flat priors that suggest negligible autocorrelation.

Model Summary. Model fit5 included age and sex predictor variables. The posterior predictive checks confirm this and show that posterior draws for this model are distributed symmetrically around the mean (Figure 6.31). Table 6.65 provides the parameters, the ORs, and 95% Credibility Interval. The posterior distributions for each estimate are depicted in Figure 6.29. Marginal effects plots are provided in Appendix Three.

Each parameter estimate represents a change in the log odds of presenting with abscesses given a change in the value associated with the predictor variable. For age, with each year of life, there is a slight decrease in the log odds of presenting with abscesses (log odds = -0.01, 95% CI = -0.04 – 0.02), and the odds of presenting with abscesses decreases for each year of age (OR = 0.99, 95% CI = 0.96– 1.02), but is not credibly different from chance. The probability of presenting with abscesses increases by 49.75% with each year of age.

By sex, the log odds of presenting with abscesses were higher among males than females (log odds = 0.62, 95% CI = -0.43 – 1.70), and males have increased odds of presenting with abscesses compared to females (OR = 1.85, 95% CI = 0.65 – 5.47), but it is not credibly different from chance. The probability of males presenting with abscesses compared to females is 64.91%.

Abscesses and Rib $\delta^{13}C$ and $\delta^{15}N$ values

Model Description. The model for abscesses and rib carbon and nitrogen isotope values used flat priors (Table 6.21). The full model summary is provided in Table 6.66. The Rhat values are all less than 1.01 and the Bulk and Tail ESS are all greater than 10,000, which indicates that the model converged.

Model Selection. A series of model fits with flat priors and different combinations of predictor variables were created to see which predictor variables from the full model best

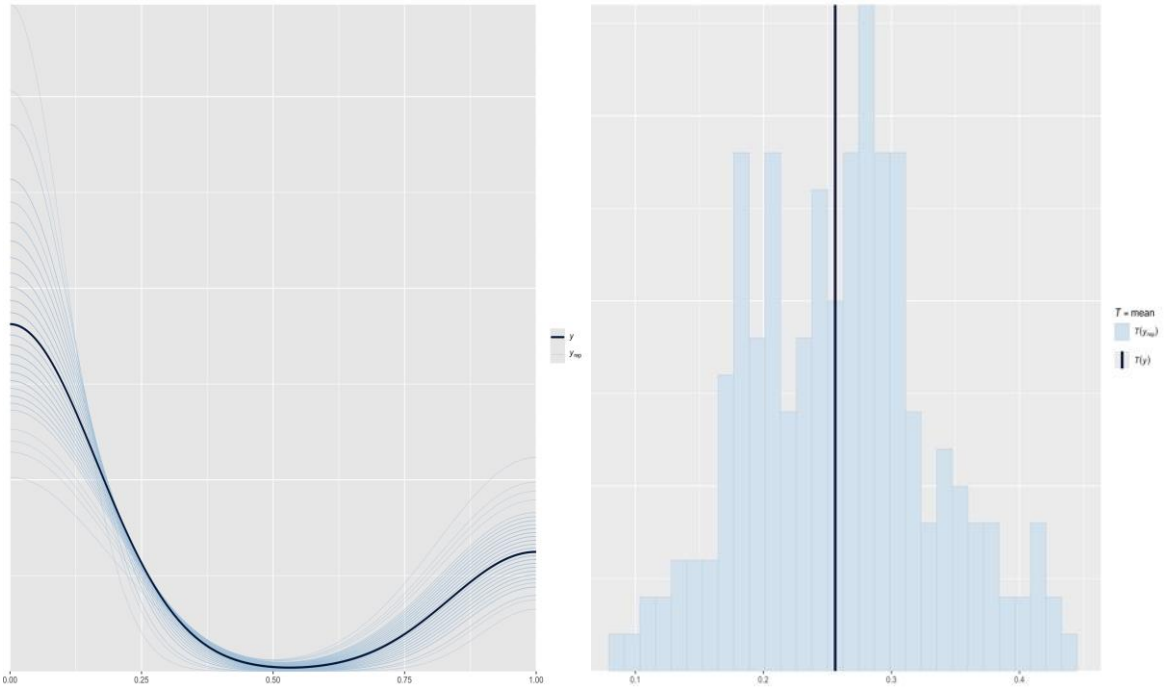


Figure 6.31. Density (left) and histogram (right) charts showing the posterior draws of the probability of presenting with abscesses based on fit5 (Abscesses~Age+Sex). Dark lines represent the mean and flat priors used. Light blue lines are the random draws from the posterior parameter space. The symmetrical distribution of the light blue lines around the mean suggests the model converged.

Table 6.65. Odds Ratios and 95% Credibility Interval for fit5.

		95% Credibility Interval	
	Odds Ratio (OR)	**Lower**	**Upper**
Intercept	6.36	1.17	5.98
Age	0.99	0.96	1.01
SexMale	1.31	0.49	3.52

Table 6.66. Log odds estimate, error, 95% Credibility Interval, Rhat values, and Bulk and Tail ESS for the full model.

			95% Credibility Interval				
	Estimate	**Error**	**Lower**	**Upper**	**Rhat**	**Bulk ESS**	**Tail ESS**
Intercept	-1.02	4.21	-9.26	7.32	1.00	142187	111425
Age	-0.00	0.01	-0.03	0.03	1.00	143128	103323
SexMale	0.47	0.61	-0.72	1.68	1.00	127631	104831
SiteSchitisor	-0.73	0.89	-2.52	1.00	1.00	109347	101638
SiteSuceava	-0.24	1.01	-2.17	1.79	1.00	92632	92472
δ^{13}C Rib	-0.02	0.14	-0.29	0.26	1.00	105576	100021
δ^{15}N Rib	-0.03	0.44	-0.90	0.81	1.00	121512	103849

explained the data and predicted the outcome of interest (presence or absence of a lesion). LOOIC was used for model selection.

Table 6.67 provides the LOOIC values for each. Model selection favored fit7 (Abscesses~1) which is the intercept or naïve model (Table 6.68) so the next best-fit model, fit5 (Abscesses~Age+Sex), is reported (Table 6.69). Fit5 Rhat values are less than 1.01 and the Bulk and Tail ESS are greater than 10,000, which indicates the model converged. This is visually confirmed by the Hamilton Monte Carlo (HMC) Chains (Figure 6.32) and no autocorrelation between the chains (Figure 6.33). This supports the conclusion that the Markov chains effectively explored the posterior parameter space and produced a representative sample of the posterior probability distribution for the fit5 model.

Model Summary. Model fit5 included age and sex predictor variables. The posterior predictive checks confirm this and show that posterior draws for this model are distributed symmetrically around the mean (Figure 6.34). Table 6.70 provides the parameters, the ORs, and 95% Credibility Interval. The posterior distributions for each estimate are depicted in Figure 6.32. Marginal effects plots are provided in Appendix Three.

Each parameter estimate represents a change in the log odds of presenting with abscesses given a change in the value associated with the predictor variable. For age, with each year of life, there is no change in the log odds of presenting with abscesses (log odds = -0.00, 95% CI = -0.03– 0.02), and the odds of presenting with abscesses does not change for each year of age (OR = 1.0, 95% CI = 0.97– 1.02), but it is not credibly different from chance. The probability of presenting with abscesses increases by 50% with each year of age.

Table 6.67. LOOIC values for each model fit.

Model fit	elpd_diff	se_diff	elpd_loo	se_elpd_loo	p_loo	se_p_loo	looic	se_looic
fit7	0.00	0.00	-45.11	4.13	1.01	0.13	90.23	8.27
fit5	-1.74	1.07	-46.85	4.45	3.06	0.42	93.71	8.90
fit6	-2.96	1.14	-48.07	4.61	4.30	0.60	96.14	9.23
fit4	-3.86	1.46	-48.97	4.78	5.44	0.72	97.95	9.56
fit3	-5.12	1.57	-50.24	4.92	6.68	0.86	100.47	9.83
fit2	-5.16	1.58	-50.27	4.94	6.69	0.94	100.54	9.87
fit	-6.42	1.72	-51.53	5.09	7.94	1.07	103.07	10.19

Table 6.68. The log odds estimate, 95% Credibility Interval, Rhat values, and Bulk and Tail ESS for fit7.

			95% Credibility Interval				
	Estimate	Error	Lower	Upper	Rhat	Bulk ESS	Tail ESS
Intercept	-1.05	0.26	-1.57	-0.55	1.00	51499	62094

Table 6.69. The log odds estimate, 95% Credibility Interval, Rhat values, and Bulk and Tail ESS for fit5.

			95% Credibility Interval				
	Estimate	Error	Lower	Upper	Rhat	Bulk ESS	Tail ESS
Intercept	-1.20	0.69	-2.58	0.10	1.00	151017	103520
Age	-0.00	0.01	-0.03	0.02	1.00	142584	107257
SexMale	0.47	0.54	-0.57	1.55	1.00	129582	101791

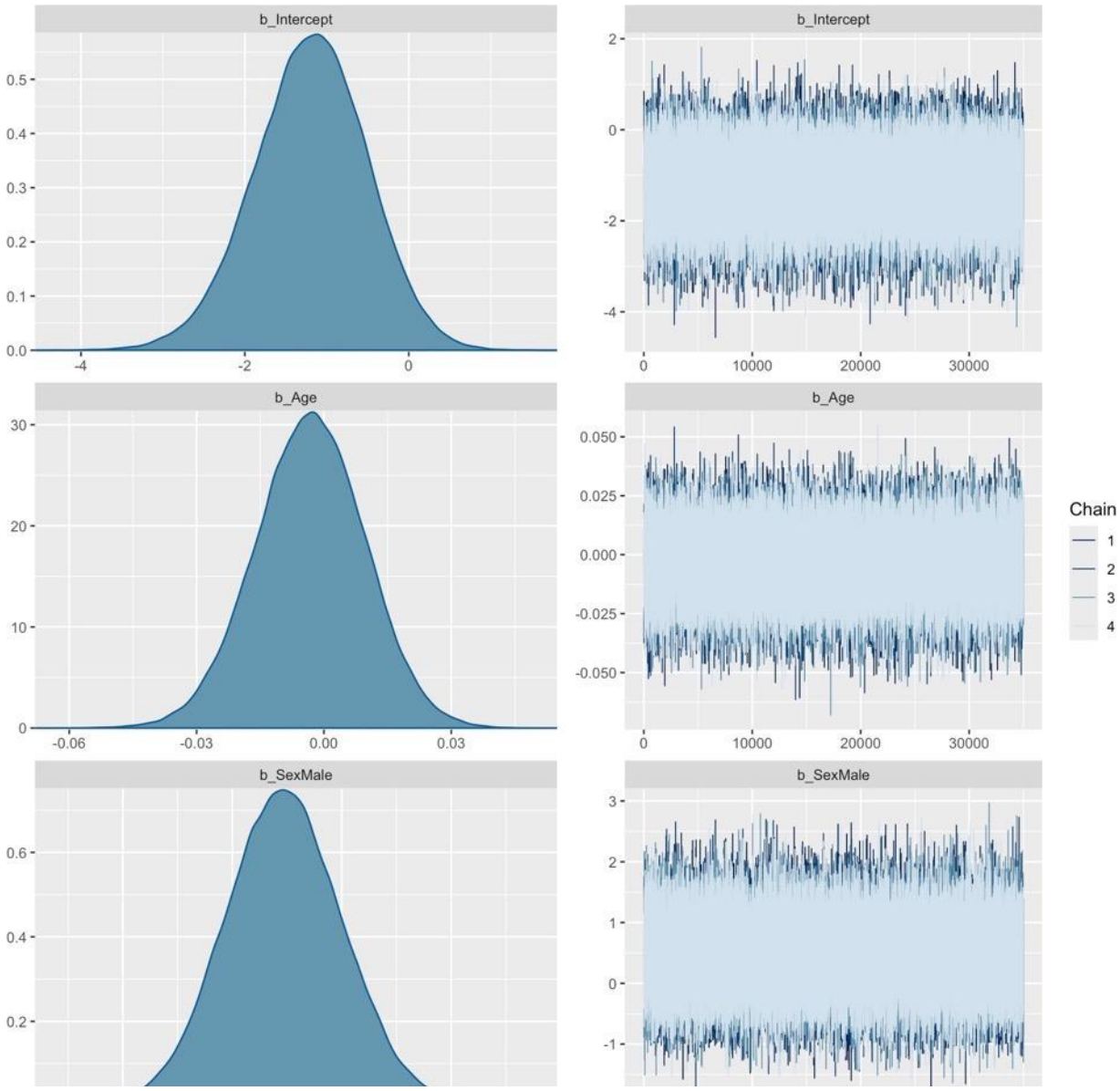


Figure 6.32. Posterior parameter distribution for the fit5 (Abscesses~Age+Sex) model parameters and HMC chains.

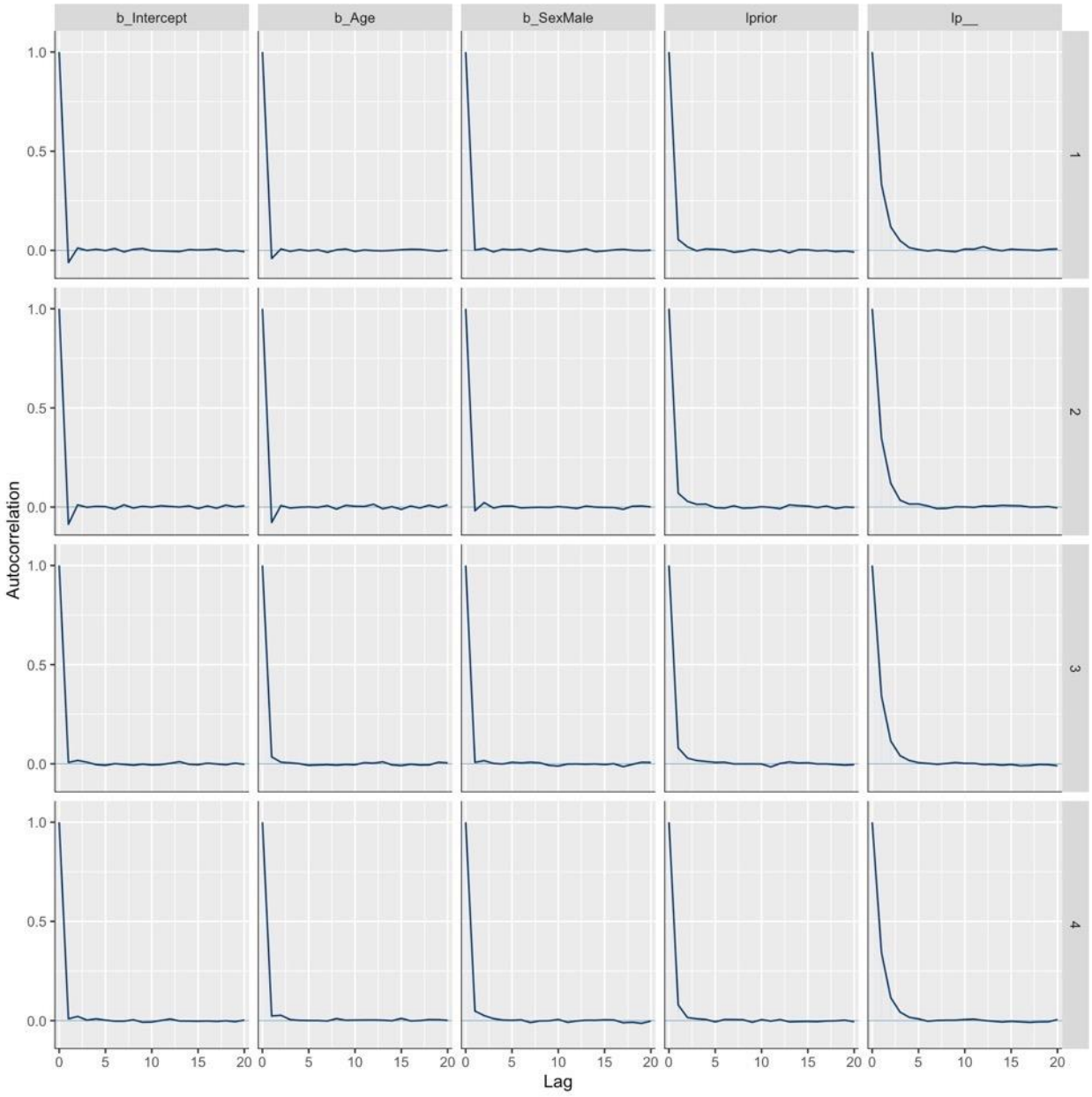


Figure 6.33. Autocorrelation plots for each fit5 (Abscesses~Age+Sex) parameter by HMC chain with flat priors that suggest negligible autocorrelation.

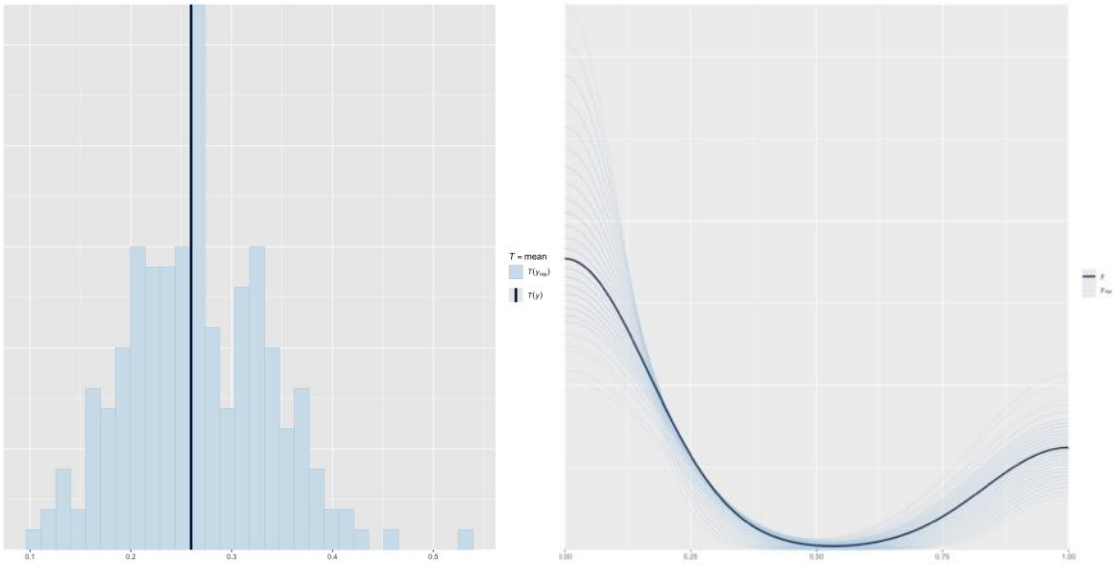


Figure 6.34. Density (left) and histogram (right) charts showing the posterior draws of the probability of presenting with abscesses based on fit5 (Abscesses~Age+Sex). Dark lines represent the mean and flat priors used. Light blue lines are the random draws from the posterior parameter space. The symmetrical distribution of the light blue lines around the mean suggests the model converged.

Table 6.70. Odds Ratios and 95% Credibility Interval for fit5.

		95% Credibility Interval	
	Odds Ratio (OR)	**Lower**	**Upper**
Intercept	0.30	0.07	1.10
Age	1.0	0.97	1.02
SexMale	1.6	0.56	4.71

By sex, the log odds of presenting with abscesses were higher among males than females (log odds = 0.47, 95% CI = -0.57 – 1.55), and males have increased odds of presenting with abscesses compared to females (OR = 1.6, 95% CI = 0.56 – 4.71), but it is not credibly different from chance. The probability of males presenting with abscesses compared to females is 61.54%.

PD and Femur $\delta^{13}C$ and $\delta^{15}N$ values

Model Description. The model for PD and femur carbon and nitrogen isotope values used flat priors (Table 6.21). The full model summary is provided in Table 6.71. The Rhat values are all less than 1.01 and the Bulk and Tail ESS are all greater than 10,000, which indicates that the model converged.

Model Selection. A series of model fits with flat priors and different combinations of predictor variables were created to see which predictor variables from the full model best explained the data and predicted the outcome of interest (presence or absence of a lesion). LOOIC was used for model selection. Table 6.72 provides the LOOIC values for each. Model selection favored fit7 (PD~1) which is the intercept or naïve model (Table 6.73) so the next best-fit model, fit5 (PD~Age+Sex), is reported (Table 6.74).

Fit5 Rhat values are less than 1.01 and the Bulk and Tail ESS are greater than 10,000, which indicates the model converged. This is visually confirmed by the Hamilton Monte Carlo (HMC) Chains (Figure 6.35) and no autocorrelation between the chains (Figure 6.36). This supports the conclusion that the Markov chains effectively explored the posterior parameter space and produced a representative sample of the posterior probability distribution for the fit5 model.

Model Summary. Model fit5 included age and sex predictor variables. The posterior predictive checks confirm this and show that posterior draws for this model are distributed

Table 6.71. Log odds estimate, error, 95% Credibility Interval, Rhat values, and Bulk and Tail ESS for full model.

			95% Credibility Interval				
	Estimate	**Error**	**Lower**	**Upper**	**Rhat**	**Bulk ESS**	**Tail ESS**
Intercept	-1.28	4.01	-9.17	6.56	1.00	146412	110740
Age	0.02	0.01	-0.01	0.04	1.00	159778	106493
SexMale	0.64	0.58	-0.49	1.79	1.00	145458	106598
SiteSchitisor	-0.03	0.91	-1.83	1.76	1.00	108909	102587
SiteSuceava	0.21	0.97	-1.67	2.17	1.00	85121	91786
δ^{13}C Femur	0.01	0.13	-0.25	0.26	1.00	116431	105413
δ^{15}N Femur	-0.05	0.39	-0.84	0.72	1.00	136980	107744

Table 6.72. LOOIC values for each model fit.

Model fit	**elpd_diff**	**se_diff**	**elpd_loo**	**se_elpd_loo**	**p_loo**	**se_p_loo**	**looic**	**se_looic**
fit7	0.00	0.00	-46.01	2.65	1.01	0.08	92.02	5.30
fit5	-0.58	1.82	-46.59	3.21	3.17	0.30	93.17	6.43
fit6	-2.32	1.48	-48.33	3.14	4.26	0.42	96.66	6.29
fit4	-3.04	1.93	-49.05	3.40	5.61	0.55	98.10	6.79
fit3	-4.43	2.06	-50.44	3.54	7.07	0.69	100.89	7.08
fit2	-4.52	2.05	-50.54	3.55	7.14	0.80	101.07	7.09
fit	-5.98	2.17	-52.00	3.69	8.66	0.92	103.99	7.38

Table 6.73. The log odds estimate, 95% Credibility Interval, Rhat values, and Bulk and Tail ESS for fit7.

			95% Credibility Interval				
	Estimate	**Error**	**Lower**	**Upper**	**Rhat**	**Bulk ESS**	**Tail ESS**
Intercept	-0.65	0.25	-1.16	-0.17	1.00	47245	69215

Table 6.74. The log odds estimate, 95% Credibility Interval, Rhat values, and Bulk and Tail ESS for fit5.

			95% Credibility Interval				
	Estimate	**Error**	**Lower**	**Upper**	**Rhat**	**Bulk ESS**	**Tail ESS**
Intercept	-1.67	0.65	-3.00	-0.43	1.00	125461	100173
Age	0.02	0.01	-0.01	0.04	1.00	122723	102516
SexMale	0.60	0.54	-0.44	1.67	1.00	120093	101860

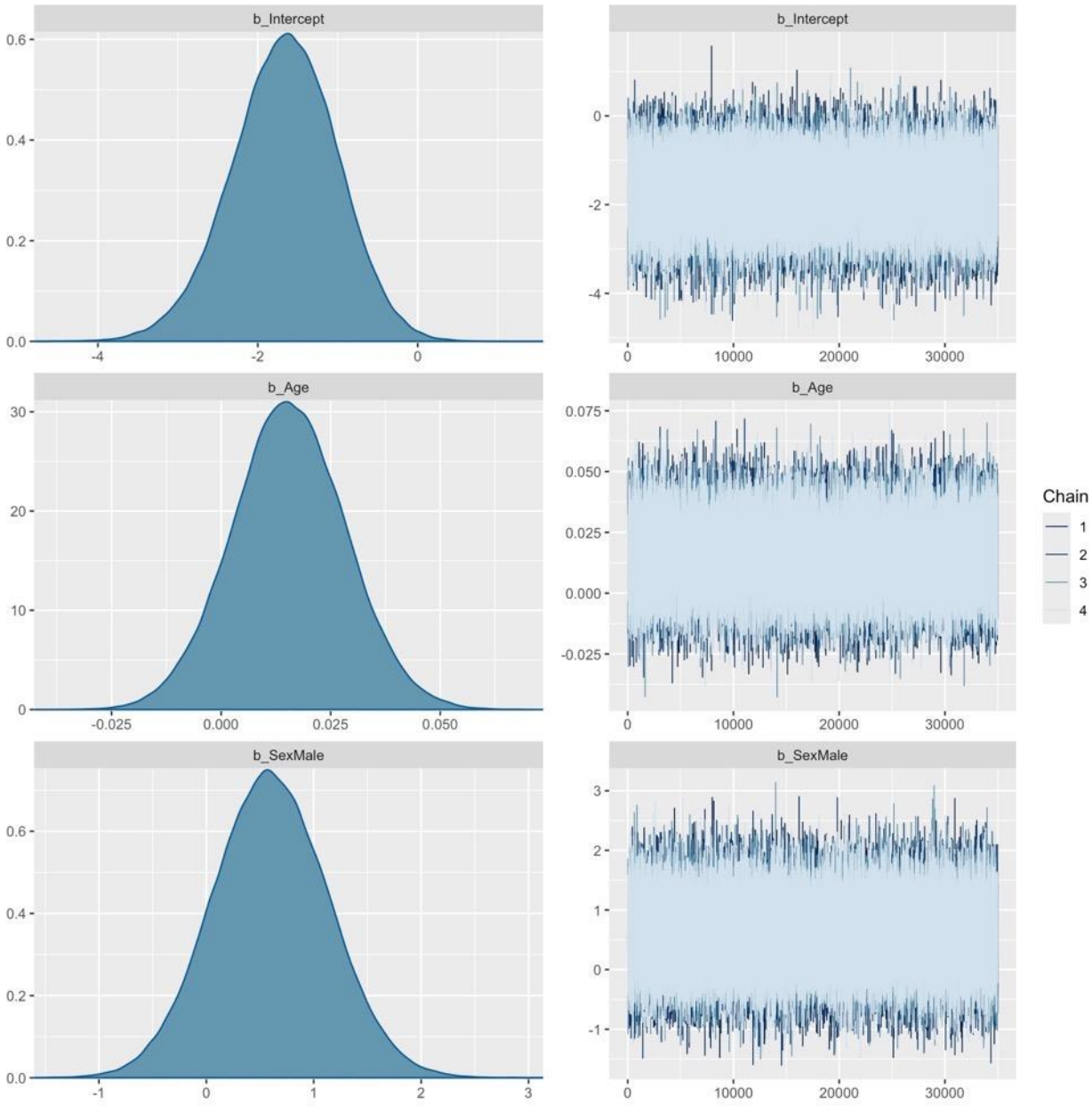


Figure 6.35. Posterior parameter distribution of the fit5 (PD~Age+Sex) model parameters and HMC chains.

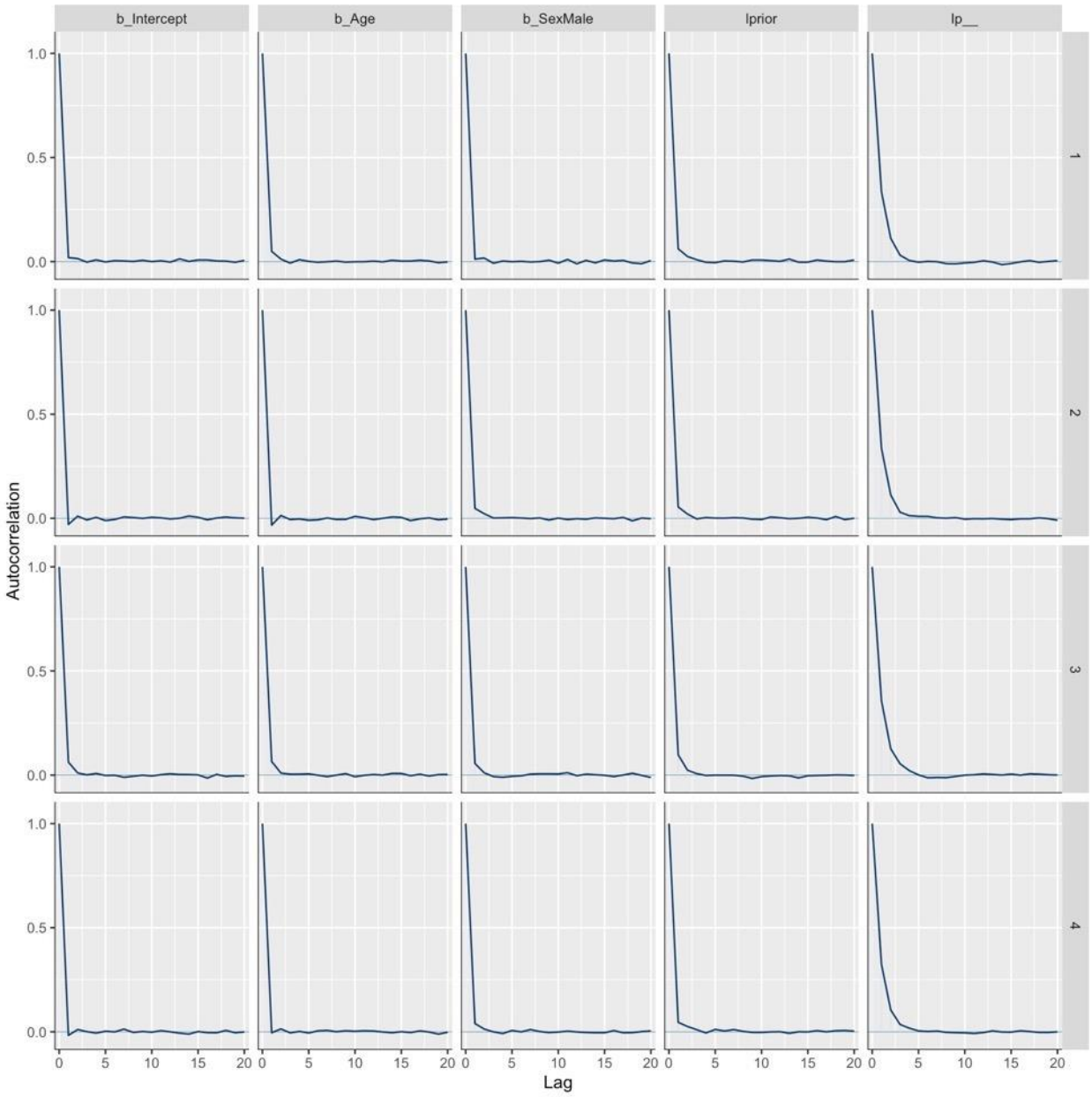


Figure 6.36. Autocorrelation plots for each fit5 (PD~Age+Sex) parameter by HMC chains with plat priors that suggest negligible autocorrelation.

symmetrically around the mean (Figure 6.37). Table 6.75 provides the parameters, the ORs, and 95% Credibility Interval. The posterior distributions for each estimate are depicted in Figure 6.35. Marginal effects plots are provided in Appendix Three.

Each parameter estimate represents a change in the log odds of presenting with PD given a change in the value associated with the predictor variable. For age, with each year of life, there is a slight increase in the log odds of presenting with PD (log odds = 0.02, 95% CI = -0.01– 0.04), and the odds of presenting with PD increases for each year of age (OR = 1.02, 95% CI = 0.99– 1.04), but it is not credibly different from chance. The probability of presenting with abscesses increases by 50.5% with each year of age.

By sex, the log odds of presenting with PD were higher among males than females (log odds = 0.60, 95% CI = -0.44 – 1.67), and males have increased odds of presenting with PD compared to females (OR = 1.82, 95% CI = 0.64 – 5.31), but it is not credibly different from chance. The probability of males presenting with PD compared to females is 64.57%.

PD and Rib $\delta^{13}C$ and $\delta^{15}N$ values

Model Description. The model for PD and rib carbon and nitrogen isotope values used flat priors (Table 6.21). The full model summary is provided in Table 6.76. The Rhat values are all less than 1.01 and the Bulk and Tail ESS are all greater than 10,000, which indicates that the model converged.

Model Selection. A series of model fits with flat priors and different combinations of predictor variables were created to see which predictor variables from the full model best explained the data and predicted the outcome of interest (presence or absence of a lesion). LOOIC was used for model selection. The model fit with the lowest LOOIC value was selected as the best-fit model. Table 6.77 provides the LOOIC values for each.

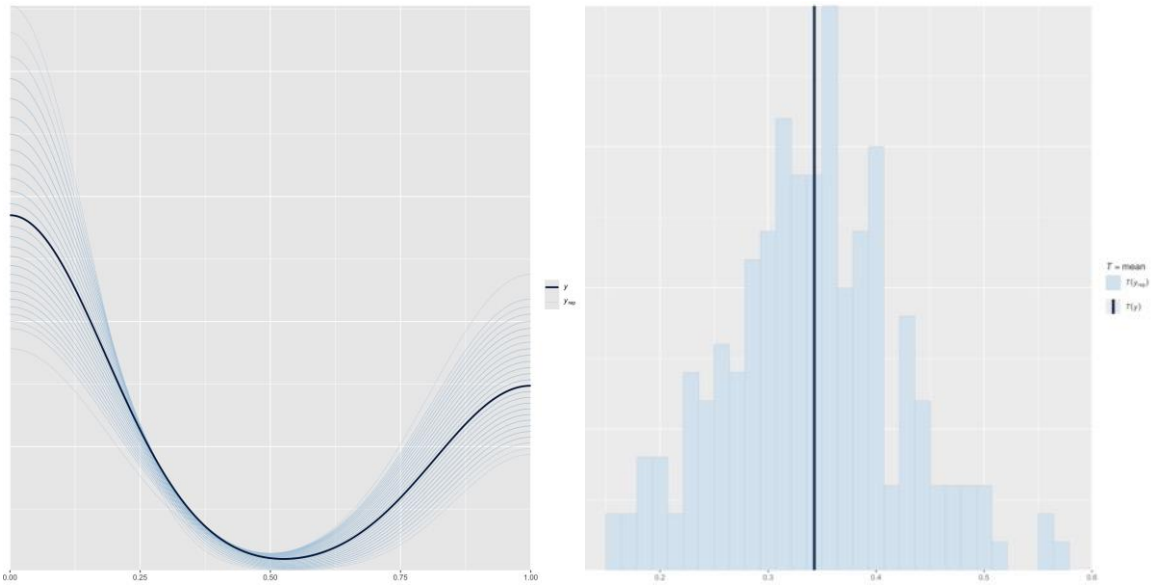


Figure 6.37. Density (left) and histogram (right) charts showing the posterior draws of the probability of presenting with abscesses based on fit5 (PD~Age+Sex). Dark lines represent the mean and flat priors used. Light blue lines are the random draws from the posterior parameter space. The symmetrical distribution of the light blue lines around the mean suggests the model converged.

Table 6.75. Odds Ratios and 95% Credibility Interval for fit5.

		95% Credibility Interval	
	Odds Ratio (OR)	**Lower**	**Upper**
Intercept	0.19	0.05	0.65
Age	1.02	0.99	1.04
SexMale	1.82	0.64	5.31

Table 6.76. Log odds estimate, error, 95% Credibility Interval, Rhat values, and Bulk and Tail ESS for the full model.

			95% Credibility Interval				
	Estimate	**Error**	**Lower**	**Upper**	**Rhat**	**Bulk ESS**	**Tail ESS**
Intercept	0.52	4.60	-8.45	9.64	1.00	137576	109992
Age	0.02	0.01	-0.01	0.04	1.00	148244	103861
SexMale	0.86	0.63	-0.34	2.12	1.00	123322	103482
SiteSchitisor	-0.20	0.94	-2.07	1.64	1.00	107529	101250
SiteSuceava	0.23	1.02	-1.73	2.27	1.00	89659	93353
δ^{13}C Rib	-0.07	0.14	-0.35	0.20	1.00	103958	103943
δ^{15}N Rib	-0.35	0.47	-1.31	0.55	1.00	117035	101227

Table 6.77. LOOIC values for each model fit.

Model fit	**elpd_diff**	**se_diff**	**elpd_loo**	**se_elpd_loo**	**p_loo**	**se_p_loo**	**looic**	**se_looic**
fit7	0.00	0.00	-43.25	2.38	1.01	0.08	86.50	4.76
fit5	-0.83	1.73	-44.07	2.96	3.15	0.28	88.15	5.93
fit6	-2.64	1.28	-45.89	2.82	4.32	0.40	91.78	5.65
fit4	-3.24	1.87	-46.49	3.16	5.59	0.53	92.98	6.32
fit3	-4.47	2.12	-47.72	3.40	7.00	0.71	95.44	6.81
fit2	-4.65	2.02	-47.90	3.31	7.03	0.75	95.79	6.63
fit	-5.90	2.41	-49.15	3.68	8.56	0.98	98.29	7.35

Model selection favored fit7 (PD~1) which is the intercept or naïve model (Table 6.78) so the next best-fit model, fit5 (PD~Age+Sex), is reported (Table 6.79). Fit5 Rhat values are less than 1.01 and the Bulk and Tail ESS are greater than 10,000, which indicates the model converged. This is visually confirmed by the Hamilton Monte Carlo (HMC) Chains (Figure 6.38) and no autocorrelation between the chains (Figure 6.39). This supports the conclusion that the Markov chains effectively explored the posterior parameter space and produced a representative sample of the posterior probability distribution for the fit5 model.

Model Summary. Model fit5 included age and sex predictor variables. The posterior predictive checks confirm this and show that posterior draws for this model are distributed symmetrically around the mean (Figure 6.40). Table 6.80 provides the parameters, the ORs, and 95% Credibility Interval. The posterior distributions for each estimate are depicted in Figure 6.38. Marginal effects plots are provided in Appendix Three.

Each parameter estimate represents a change in the log odds of presenting with PD given a change in the value associated with the predictor variable. For age, with each year of life, there is a slight increase in the log odds of presenting with PD (log odds = 0.01, 95% CI = -0.01– 0.04), and the odds of presenting with PD increases for each year of age (OR = 1.01, 95% CI = 0.99– 1.04), but it is not credibly different from chance. The probability of presenting with PD increases by 50.25% with each year of age.

By sex, the log odds of presenting with PD were higher among males than females (log odds = 0.62, 95% CI = -0.44 – 1.71), and males have increased odds of presenting with PD compared to females (OR = 1.86, 95% CI = 0.64 – 5.53), but it is not credibly different from chance. The probability of males presenting with abscesses compared to females is 65.02%.

Table 6.78. The log odds estimate, 95% Credibility Interval, Rhat values, and Bulk and Tail ESS for fit7.

			95% Credibility Interval				
	Estimate	**Error**	**Lower**	**Upper**	**Rhat**	**Bulk ESS**	**Tail ESS**
Intercept	-0.60	0.26	-1.12	-0.10	1.00	50988	62457

Table 6.79. The log odds estimate, 95% Credibility Interval, Rhat values, and Bulk and Tail ESS for fit5.

			95% Credibility Interval				
	Estimate	**Error**	**Lower**	**Upper**	**Rhat**	**Bulk ESS**	**Tail ESS**
Intercept	-1.59	0.69	-3.01	-0.28	1.00	139683	103565
Age	0.01	0.01	-0.01	0.04	1.00	148554	104122
SexMale	0.62	0.55	-0.44	1.71	1.00	145558	105473

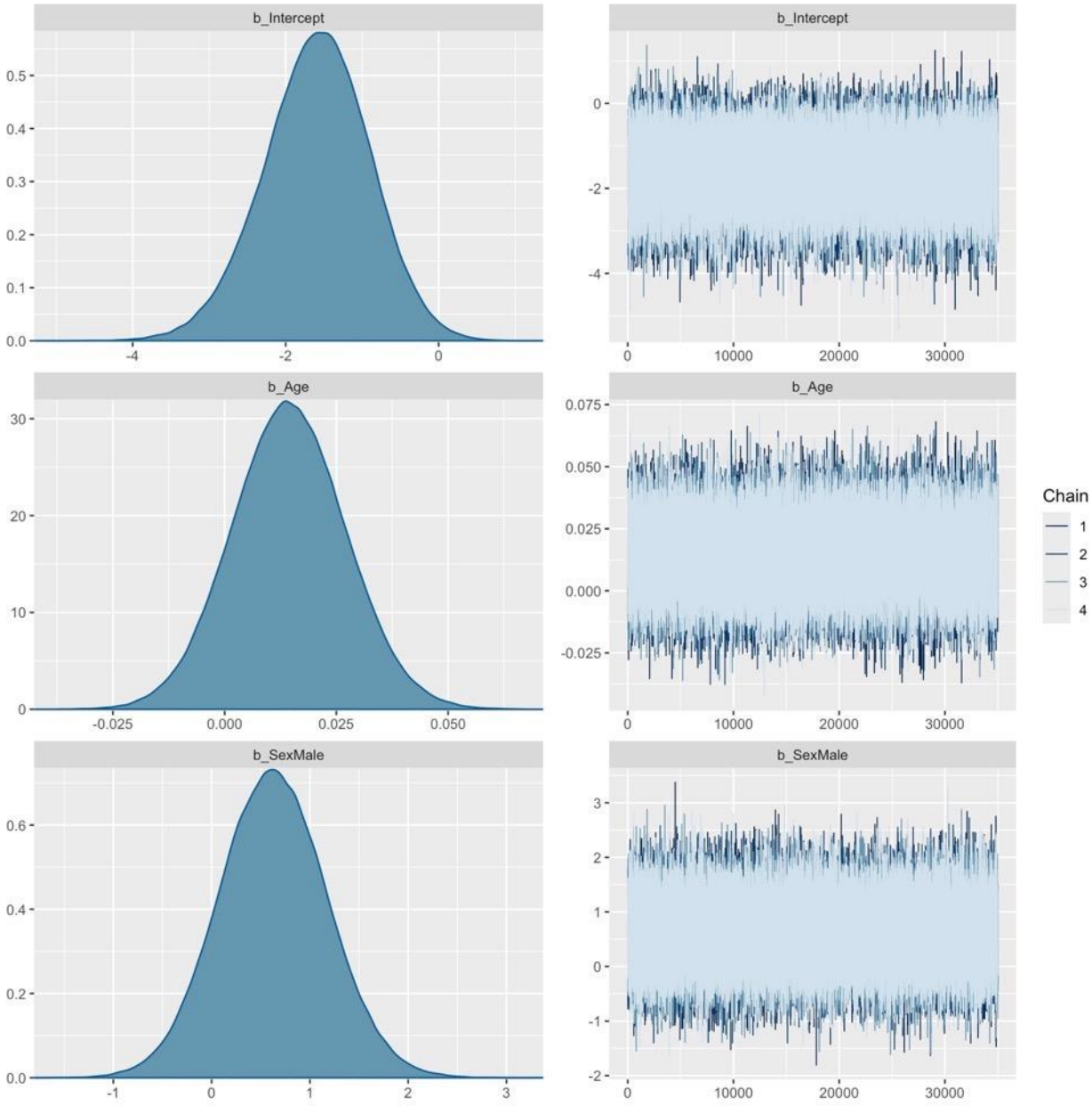


Figure 6.38. Posterior parameter distribution of the fit5 (PD~Age+Sex) model parameters and HMC chains.

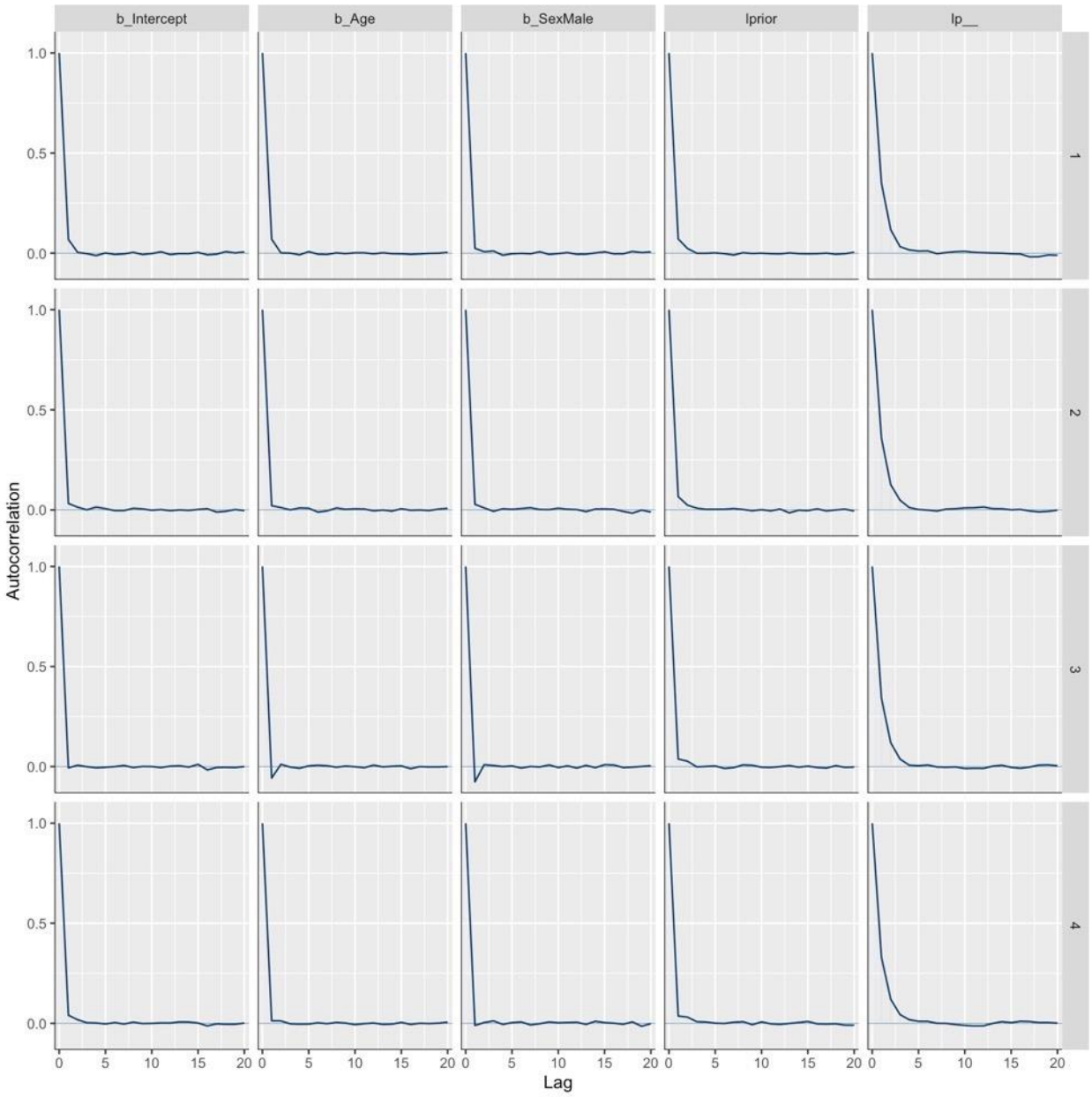


Figure 6.39. Autocorrelation plots for each fit5 (PD~Age+Sex) parameter by HMC chain with flat priors that suggest negligible autocorrelation.

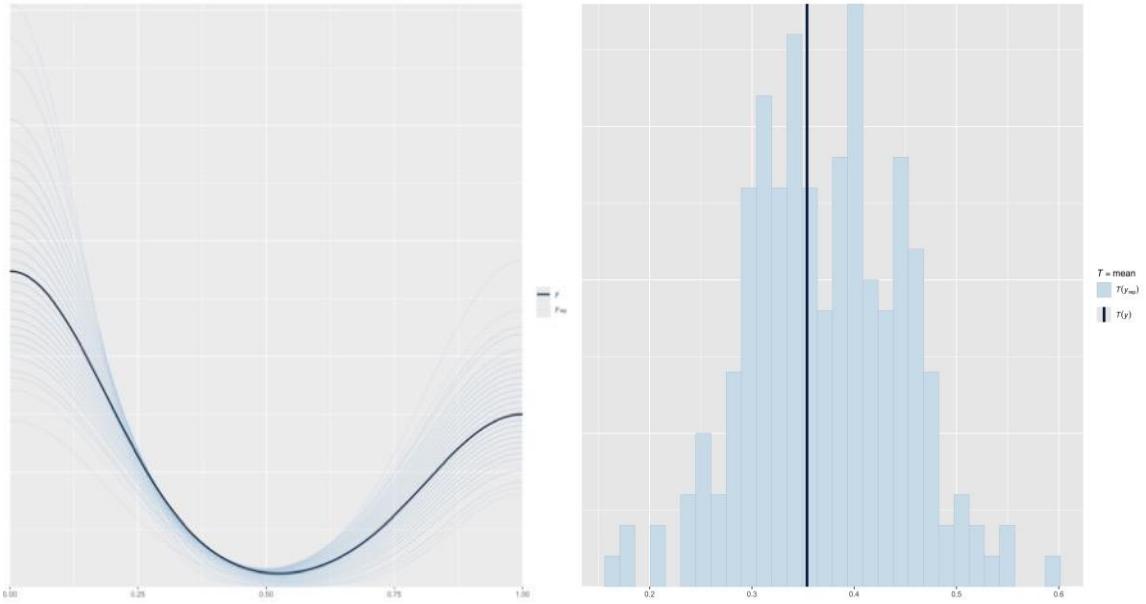


Figure 6.40. Density (left) and histogram (right) charts showing the posterior draws of the probability of presenting with abscesses based on fit5 (PD~Age+Sex). Dark lines represent the mean and flat priors used. Light blue lines are the random draws from the posterior parameter space. The symmetrical distribution of the light blue lines around the mean suggests the model converged.

Table 6.80. Odds Ratios and 95% Credibility Interval for fit5.

		95% Credibility Interval	
	Odds Ratio (OR)	**Lower**	**Upper**
Intercept	0.20	0.05	0.75
Age	1.01	0.99	1.04
SexMale	1.86	0.64	5.53

Post Hoc Analysis: Kaplan-Meier Survival Curves

Non-parametric Kaplan-Meier survival analysis with a log-rank test was performed *post hoc* to evaluate the effect of each lesion type on survival for individuals across all three sites. Kaplan-Meier survival analysis is a statistical method for analyzing time to an event between groups, in this case survival time for individuals with and without lesions (D'Arrigo et al. 2021).

Point age estimates and lesion presence or absence were used to both qualitatively and quantitatively test for an association between the presence/absence of a lesion and risk of death (DeWitte 2014). Significance was determined by the Log Rank (Chi-Square) test. Analyses were performed in SPSS (v.29.0.2.0(20)). The mean and median survival times tables for each lesion type are provided in Appendix Four.

PNBF

Of the 113 individuals observable for PNBF, 26.5% (30/113) presented with PNBF. The Kaplan-Meier Survival Functions for individuals with and without PNBF are provided in Figure 6.41. The median survival time for individuals without PNBF was 52.0 years (95% Confidence Interval (CI) = 38.31 – 65.69), and the median survival time for individuals with PNBF was 34.0 years (95% CI = 20.58 – 47.42). Despite the lower age-at-death for individuals with PNBF, the difference in survival time between those with and without PNBF was not significant ($p = 0.323$).

PH

Of the 87 individuals observable for PH, 18.4% (16/87) presented with PH. The Kaplan-Meier Survival Functions for individuals with and without PH are provided in Figure 6.42. The median survival time for individuals without PH was 37.8 years (95% CI = 32.76 – 42.84), and the median survival time for individuals with PH was 32.8 years (95% CI = 20.06 – 45.54).

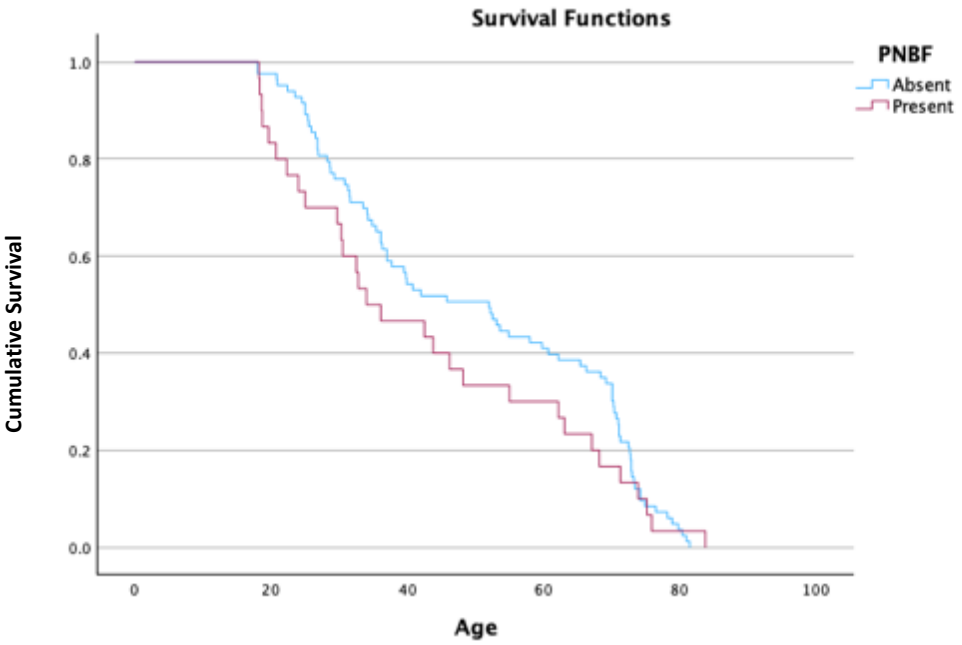


Figure 6.41. Kaplan-Meier survival functions for individuals with and without PNBF.

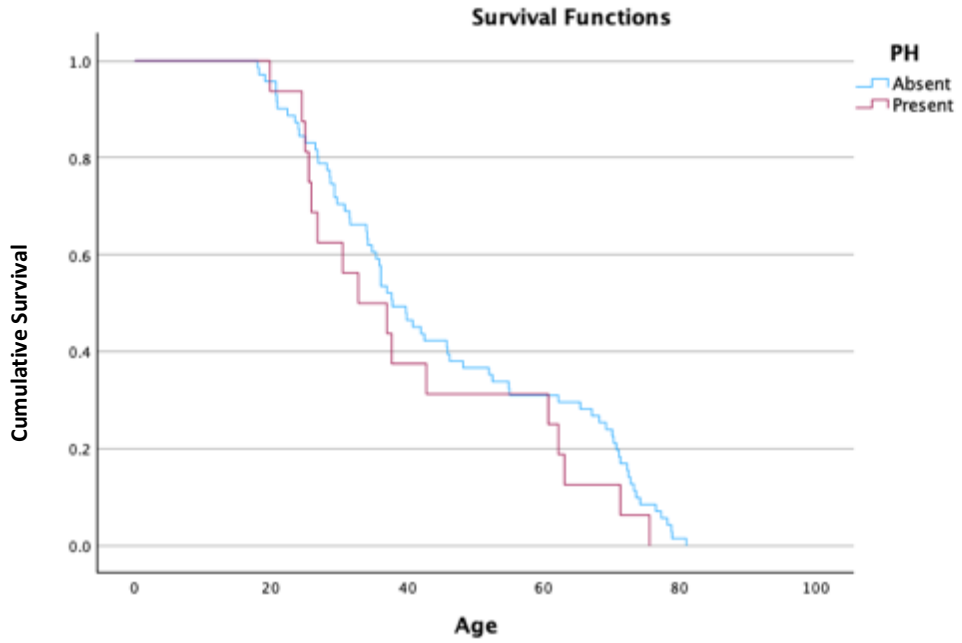


Figure 6.42. Kaplan-Meier survival functions for individuals with and without PH.

Despite the slightly lower age-at-death for individuals with PH, the difference in survival time between those with and without PH was not significant ($p = 0.266$).

CO

Of the 94 individuals observable for CO, 9.57% (9/94) presented with CO. The Kaplan-Meier Survival Functions for individuals with and without CO are provided in Figure 6.43. The median survival time for individuals without CO was 37.0 years (95% CI = 33.39 – 40.61), and the median survival time for individuals with CO was 32.8 years (95% CI =17.31 – 48.29). Despite the slightly lower age-at-death for individuals with CO, the difference in survival time between those with and without CO was not significant ($p = 0.853$).

Caries

Of the 97 individuals observable for caries, 40.20% (39/97) presented with caries. The Kaplan-Meier Survival Functions for individuals with and without caries are provided in Figure 6.44. The median survival time for individuals without caries was 37.0 years (95% CI =34.01 – 39.98), and the median survival time for individuals with caries was 45.8 years (95% CI =30.99 – 60.60). Despite the lower age-at-death for individuals without caries, the difference in survival time between those with and without caries was not significant ($p = 0.997$).

Abscesses

Of the 101 individuals observable for abscesses, 26.73% (27/101) presented with abscesses. The Kaplan-Meier Survival Functions for individuals with and without abscesses are provided in Figure 6.45. The median survival time for individuals without abscesses was 37.0 years (95% CI =19.51 – 54.49), and the median survival time for individuals with abscesses was 37.8 years (95% CI =32.97 – 42.63). The difference in survival time between those with and without abscesses was not significant ($p = 0.315$).

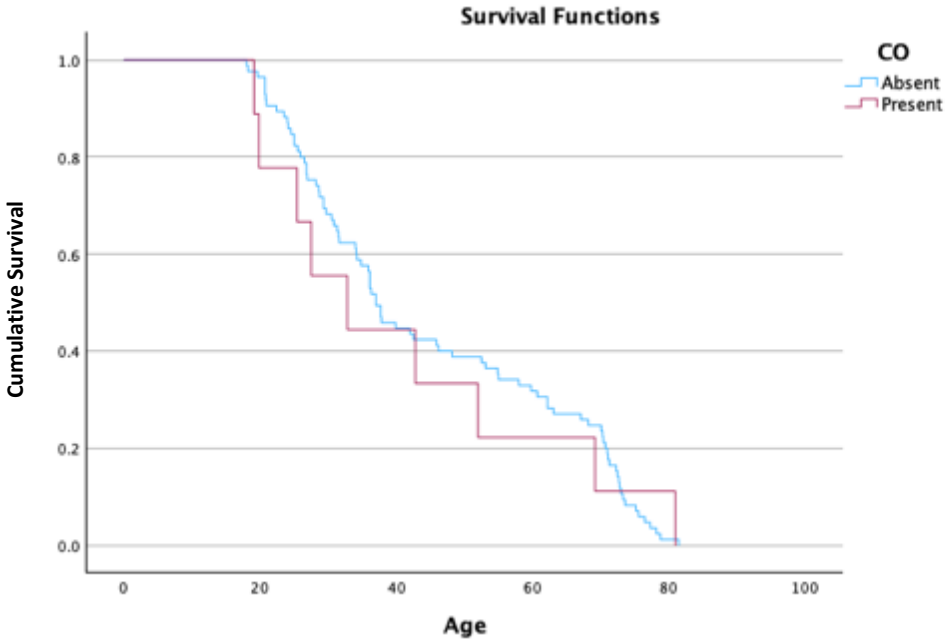


Figure 6.43. Kaplan-Meier survival functions for individuals with and without CO.

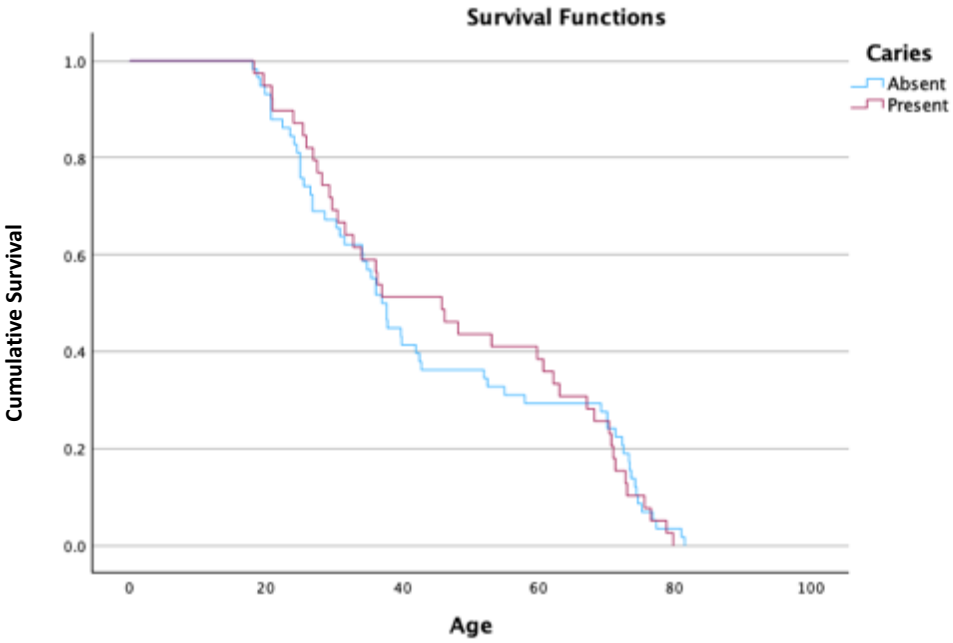


Figure 6.44. Kaplan-Meier survival functions for individuals with and without caries.

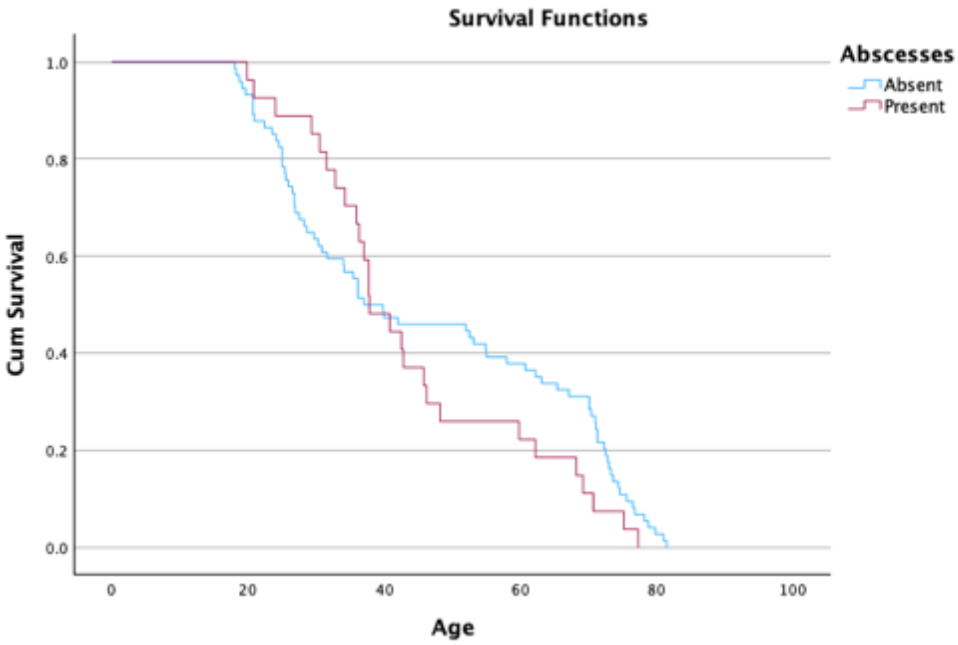


Figure 6.45. Kaplan-Meier survival functions for individuals with and without abscesses.

PD

Of the 88 individuals observable for PD, 28.4% (25/88) presented with PD. The Kaplan-Meier Survival Functions for individuals with and without PD are provided in Figure 6.46. The median survival time for individuals without PD was 36.1 years (95% CI =30.66 – 41.54), and the median survival time for individuals with PD was 39.8 years (95% CI =30.50 – 49.10). Despite the slightly lower age-at-death for individuals without PD, the difference in survival time between those with and without PD was not significant ($p = 0.150$).

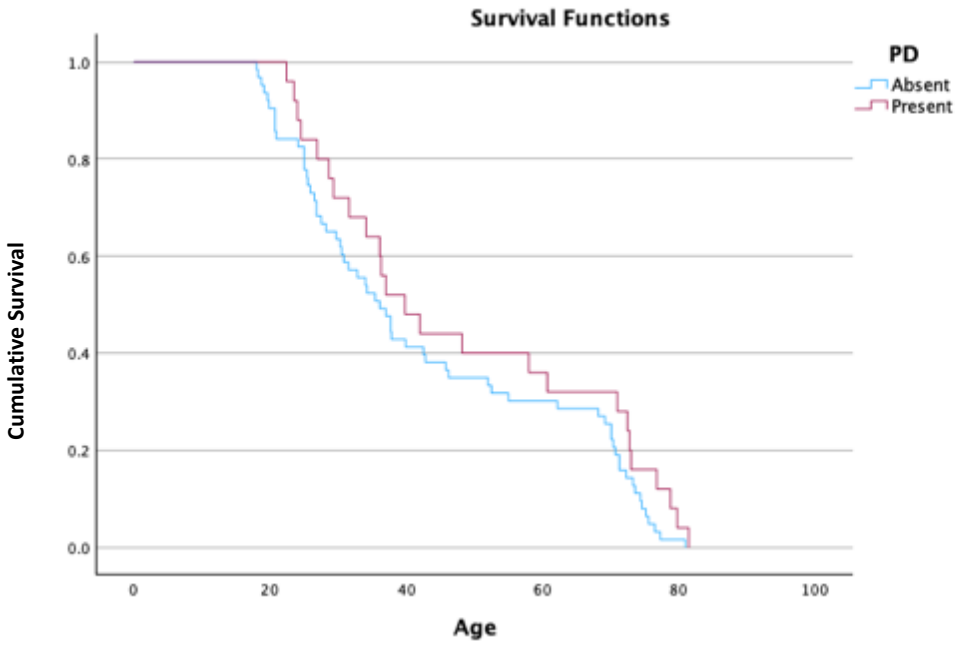


Figure 6.46. Kaplan-Meier survival functions for individuals with and without PD.

CHAPTER SEVEN: DISCUSSION

This research explored the effects of diet, social status, and demography on health, as understood by patterns of skeletal stress, in human populations from three cemetery sites in northeast Romania during the Late Medieval-Early Modern period (14^{th} – 18^{th} century). The goal was to better understand how social and environmental factors interact with biology to produce varying health experiences during a specific period of Romanian history and historical context that has previously been little studied. I hypothesized that:

1. Individuals at this time experienced a variety of different physiological stressors as indicated by the presence of non-specific stress lesions on the skeleton.
2. There will be a difference in physiological stress experiences between the sexes.
3. There will be a difference in physiological stress experiences between sites, with individuals from low-status sites experiencing a greater burden of stress than individuals at high status sites.
4. Romanians were consuming a majority C_3 plant and terrestrial protein diet, with some C_4 plant and aquatic protein inputs.
5. There will be dietary differences between sexes.
6. Dietary composition will be associated with burial site and there will be significant differences in diet between sites with higher-status individuals and sites with lower-status individuals.
7. Diet impacted patterns of physiological stress and dental disease.

The following sections of this chapter evaluate these hypotheses using the results from Chapter Six and provide a discussion about what these results tell us about diet and stress during Late Medieval-Early Modern Romania.

Dietary Composition

I hypothesized that 1) Romanians were consuming a majority C_3 plant and terrestrial protein diet, with some C_4 plant and aquatic protein inputs, 2) there would be dietary differences between sexes, and 3) dietary composition will be associated with burial site and there will be significant differences in diet between sites with higher-status individuals and sites with lower-status individuals.

Of these three hypotheses, the only one *not supported* was the hypothesis that there would be dietary differences between sexes. T-tests did not find a significant difference in $\delta^{13}C$ or $\delta^{15}N$ values between males and females. To check whether sample size was the issue, a power analysis was performed to see what sample size would be necessary to detect a moderate effect size with an 80% probability of correctly rejecting the null hypothesis (no difference). The sample size needed was 63 individuals in each group (males and females). My sample sizes were 62 males and 58 females. These are sufficient sample sizes and small sample size could be ruled out as a factor in the insignificant t-tests. For dietary protein, there is no evidence that males or females were consuming significantly different diets during this period of Romanian history.

The hypothesis that Romanians were consuming a majority C_3 plant and terrestrial protein diet, but some C_4 and aquatic inputs was *supported*. Figure 7.1 shows a scatter plot of $\delta^{13}C$ and $\delta^{15}N$ values color-coded by site. The overall spatial pattern of $\delta^{13}C$ and $\delta^{15}N$ values for individuals at Suceava, Schitişor, and Palatul Cnejilor suggests different sources of carbon between Suceava and both Schitişor and Palatul Cnejilor, with possibly more C_4 protein being consumed at the latter two sites. High $\delta^{15}N$ values (>11‰) combined with low $\delta^{13}C$ values at Suceava suggest possible consumption of freshwater fish by a subset of individuals. However, when interpreting diet, it is crucial to have faunal baseline data from animals, like livestock or

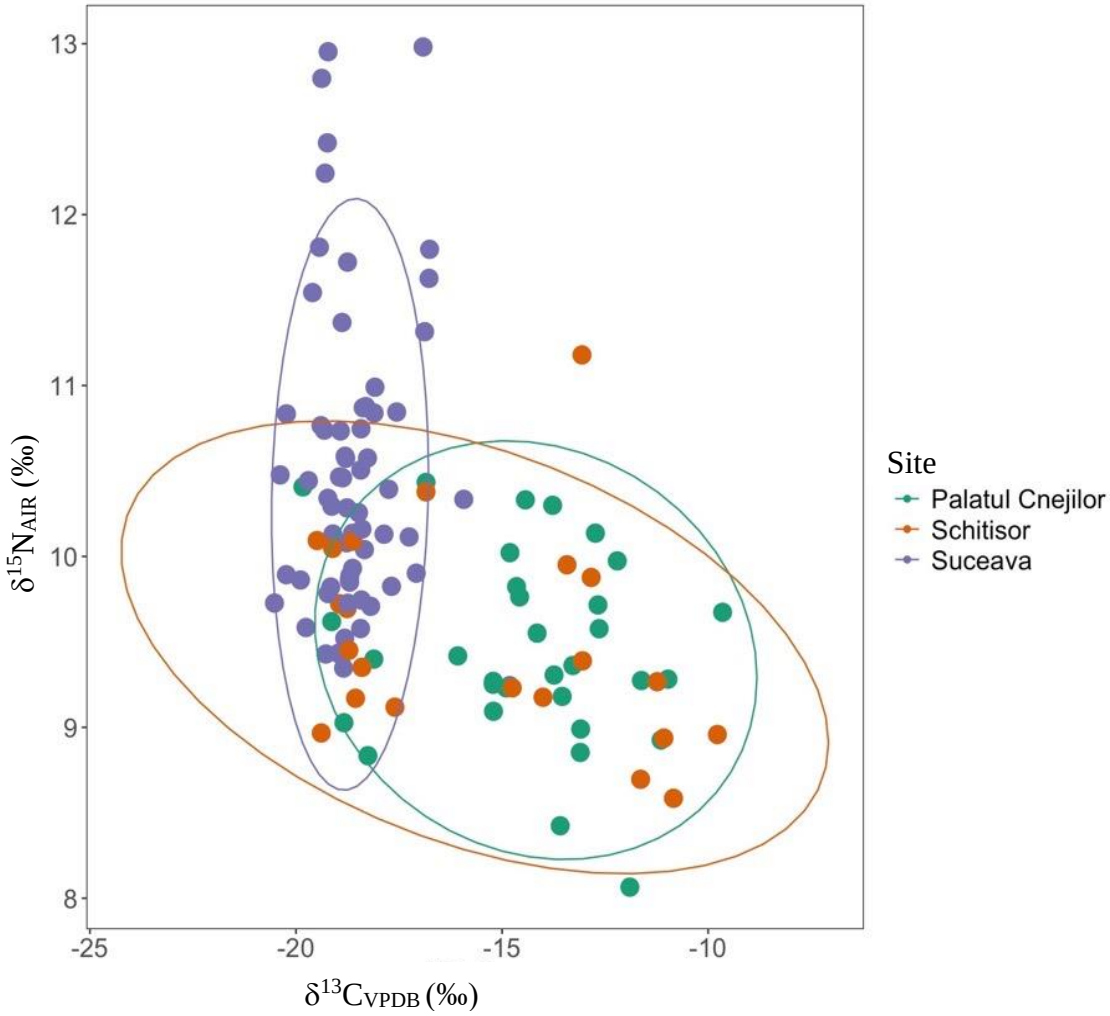


Figure 7.1. Biplot of $\delta^{13}C$ and $\delta^{15}N$ values for femur collagen by site.

wild game, that people at the time would have been consuming. Ideally, these remains come from the archaeological sites where the human remains were excavated. Unfortunately, no faunal remains were recovered and/or preserved for the three study sites and no faunal data from the same period or region in Romania currently exists. Thus, other faunal isotope data sets from similar periods or regions were used to help interpret the $\delta^{13}C$ and $\delta^{15}N$ values of human bone collagen from Suceava, Schitişor, and Palatul Cnejilor. Additionally, $\delta^{13}C$ values of enamel carbonate for 74 individuals across all three sites are also available from carbon and oxygen stable isotope analysis originally performed to assess these sites for evidence of migration. These data were not included in this dissertation because they did not address the questions and hypotheses that were explored. However, enamel apatite $\delta^{13}C$ values provide an additional dataset that can help interpret the $\delta^{13}C$ collagen values since enamel provides information about the whole diet, specifically carbohydrates and lipids (energy sources).

C_3 versus C_4 Animal Protein Consumption

Human bone collagen $\delta^{13}C$ and $\delta^{15}N$ values from all three study sites were plotted with terrestrial and aquatic faunal bone collagen $\delta^{13}C$ and $\delta^{15}N$ values from two medieval sites in north-central Poland (Reitsema et al. 2013; Reitsema et al. 2010) **(**Figure 7.2). Terrestrial fauna included cows, sheep, goats, deer, elk, chickens, and pigs. Aquatic fauna included freshwater fish including catfish, carp-bream, pike, pike-perch, tench, aspe, and sturgeon, all species found in Romania's rivers. The Romanian human $\delta^{13}C$ values from Suceava plot close to the terrestrial faunal $\delta^{13}C$ values. The $\delta^{13}C$ collagen to collagen spacing for humans consuming animal meat is about 1‰ (Ambrose and Norr 1993). The cluster of individuals from Suceava have an average

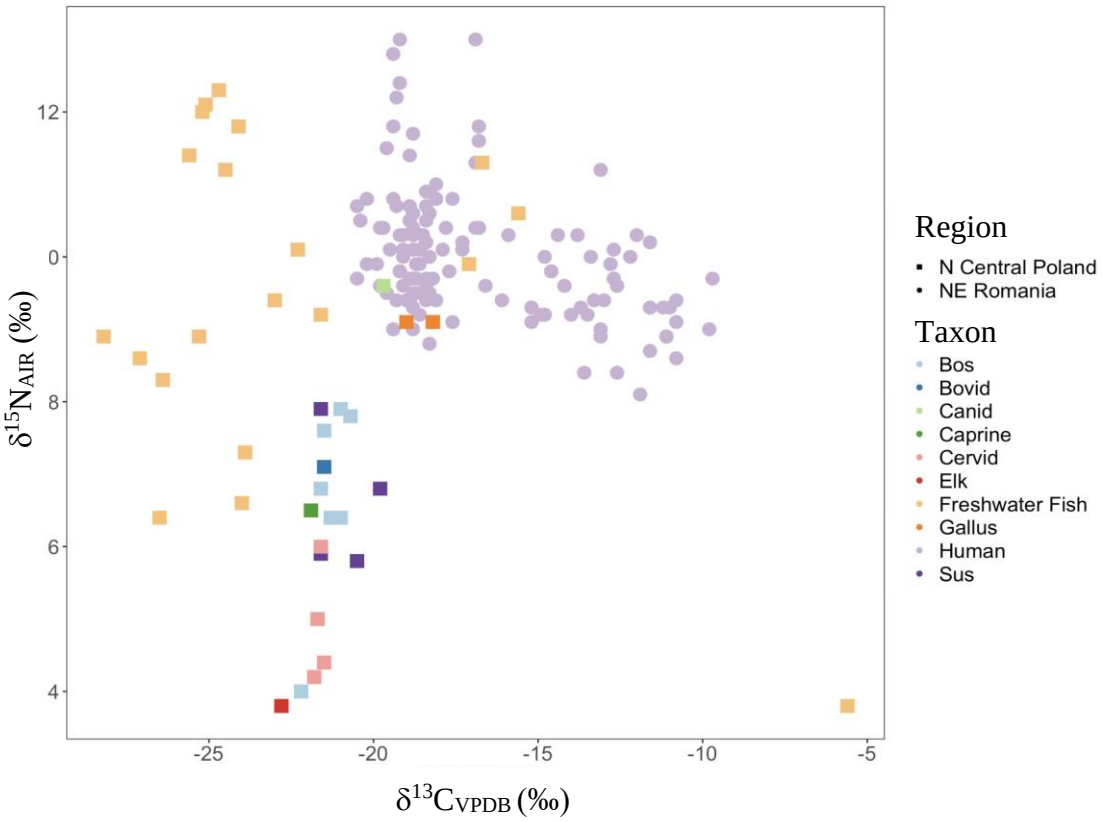


Figure 7.2. Scatter plot of faunal $\delta^{13}C$ and $\delta^{15}N$ collagen values from two medieval sites in north-central Poland, and human collagen (light purple) from Suceava, Palatul Cnejilor, and Schitişor.

$\delta^{13}C$ value of -18.6‰ and the terrestrial fauna have an average $\delta^{13}C$ value of -21‰. This is a 2.4‰ average difference suggesting these individuals were likely consuming terrestrial livestock foddered on C_3 crops. The >1‰ difference could be due to individuals at Suceava eating terrestrial livestock foddered on slightly different C_3 sources than the Polish livestock, with slightly higher $\delta^{13}C$ values due to differences in water-use efficiency (Farquhar et al. 1989; Petrík et al. 2023). Additionally, looking at the spread of individuals around the mean $\delta^{13}C$ value, several individuals are within 1‰ or overlap with the terrestrial faunal $\delta^{13}C$ values. The cluster of individuals from Schitişor and Palatul Cnejilor are plotting several ‰ higher than the terrestrial fauna and individuals from Suceava, with an average $\delta^{13}C$ value of -15.8‰ for Schitişor and -14.1‰ for Palatul Cnejilor. These values are 5.2‰ and 6.9‰ higher than the Polish terrestrial fauna and suggest C_4 protein consumption, likely animals that were foddered on C_4 crops like millet and maize.

However, no baseline faunal isotopic data exists for this region or period in Romania, so it is not possible to compare the $\delta^{13}C$ values of the humans at Suceava, Schitişor, and Palatul Cnejilor to the livestock they would have been consuming. From historical sources, it is known that cows, sheep, goats, and chickens were commonly raised livestock for consumption during the late medieval period (Székely 2018), so terrestrial animal protein was a known part of the diet. However, without isotopic data of these livestock, it is impossible to know where $\delta^{13}C$ values of those animals would plot relative to the humans from these sites and whether they were being foddered with more C_3 or C_4 crops.

Overall, individuals from Suceava are plotting consistent with individuals consuming C_3 animal protein, while individuals from Schitişor and Palatul Cnejilor are plotting consistent with individuals consuming C_4 animal protein. Having this baseline faunal isotopic data would further

strengthen these dietary interpretations. Stable isotopes make it possible to see how people were interacting with the environment at an atomic level, which includes the animals they were eating. However, without faunal remains for either isotopic or zooarchaeological analysis, it is difficult to get a complete picture of animal protein consumption at this time.

Terrestrial versus Aquatic Protein Consumption

Figure 7.2 also shows $\delta^{13}C$ and $\delta^{15}N$ bone collagen values for various freshwater fishes from north-central Poland (Reitsema 2010, Reitsema 2011). There is a large range of freshwater fish $\delta^{15}N$ values (6.4‰ to 12.3‰, excluding a tench with a very low $\delta^{15}N$ value of 3.8‰), but there is a cluster of individuals from Suceava with $\delta^{15}N$ values between 11‰ and 13‰. Considering the approximately 3-5‰ trophic level enrichment that occurs for $\delta^{15}N$ values of collagen with each trophic level, this cluster of individuals is one trophic level above the cluster of Polish freshwater fish with $\delta^{15}N$ values between about 6‰ and 10‰. Combined with low $\delta^{13}C$ values, this is consistent with freshwater fish consumption and suggests at least some individuals at Suceava were consuming freshwater fish in addition to terrestrial animal protein. These findings are consistent with historical sources that identify catfish, pike, carp, trout, and sturgeon as common fishes found in Romania's rivers and were consumed either fresh or dried (Székely 2018; Tița 2006).

Individuals from Schitişor and Palatul Cnejilor do not have $\delta^{15}N$ values high enough or $\delta^{13}C$ values low enough in the context of the Polish faunal data to suggest they were consuming freshwater fish. Anadromous and marine fish have $\delta^{15}N$ values that are higher than freshwater fish and $\delta^{13}C$ values that appear C_4. Thus, individuals with higher $\delta^{13}C$ values and high $\delta^{15}N$ values may be consuming anadromous or marine fish. However, the individuals at Schitişor and

Palatul Cnejilor do not have $\delta^{15}N$ collagen values that would suggest marine fish consumption, and instead were likely consuming terrestrial animals foddered on C_4 crops, as discussed above.

C_3 vs C_4 Plant Protein Consumption

Dietary protein also comes from plants, so $\delta^{13}C$ values of bone collagen are also representative, to a lesser extent, of the C_3 and C_4 plants that were consumed. To better interpret which individuals were likely consuming C_3 or C_4 plants, the average $\delta^{13}C$ values of archaeological rye from Romania (Golea et al. 2023) and wheat from medieval Czech Republic (Halffman and Velemínský 2015; Murray and Schoeninger 1988) were included in the carbon and nitrogen biplots of all individuals from Suceava, Palatul Cnejilor, and Schitişor (Figure 7.3). Both rye and wheat are C_3 crops that were grown and consumed in medieval Romania. Vertical solid lines indicate the average $\delta^{13}C$ value of rye (-21.3‰) and wheat (-25.5‰) and the dashed lines indicate the +5‰ diet to collagen spacing (Fernandes et al. 2015). Based on these values, individuals at Suceava, and a few individuals from Palatul Cnejilor and Schitişor were consuming C_3 crops. All these individuals are around -20‰, the expected bone collagen value for individuals consuming wheat, considering the +5‰ diet to collagen spacing. Rye has a higher average $\delta^{13}C$ value (-21.3‰), so individuals consuming all rye would have a bone collagen value of about -16.1‰. Thus, all individuals with values higher than -16.1‰ were likely consuming a majority C_4 diet, like millet or maize (Figure 7.4). -16.1‰ is close to the cut-off value of -18‰ or greater as an indication of the consumption of C_4 crops used by Lightfoot and colleagues (2013) in their study of prehistoric millet consumption in Eurasia. This cut-off value was based on research conducted by Pearson and colleagues (2007) into diet in neolithic Hungary. All individuals with a bone collagen $\delta^{13}C$ value > -16.1‰ are from Schitişor and Palatul Cnejilor so, in addition to consuming C_4 terrestrial protein, these individuals also seem to have been

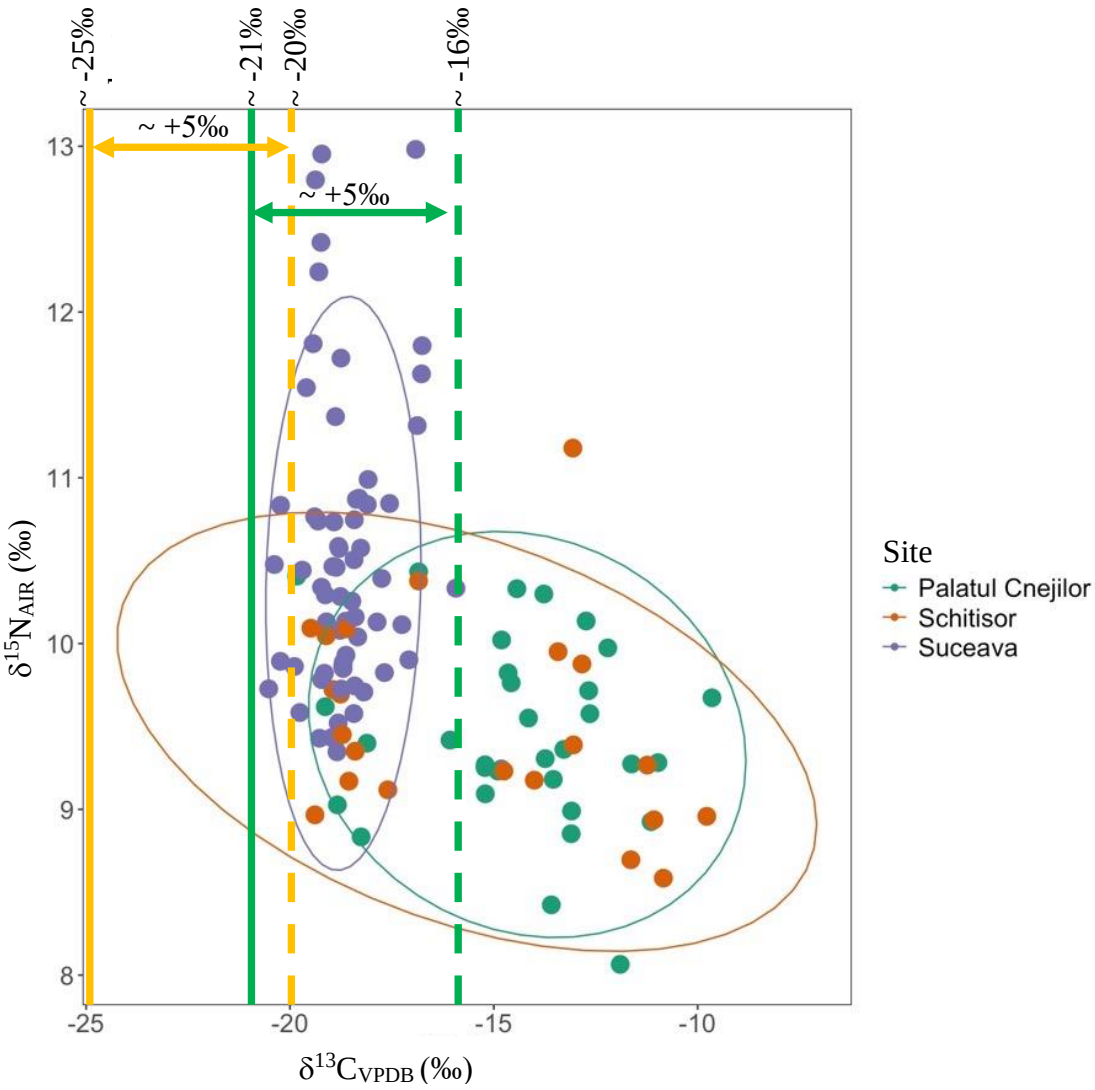


Figure 7.3. Human $\delta^{13}C$ and $\delta^{15}N$ collagen values with average $\delta^{13}C$ values for archaeological wheat (solid yellow line) and rye (solid green line). Dashed lines indicate the +5‰ diet to collagen enrichment for wheat (yellow) and rye (green).

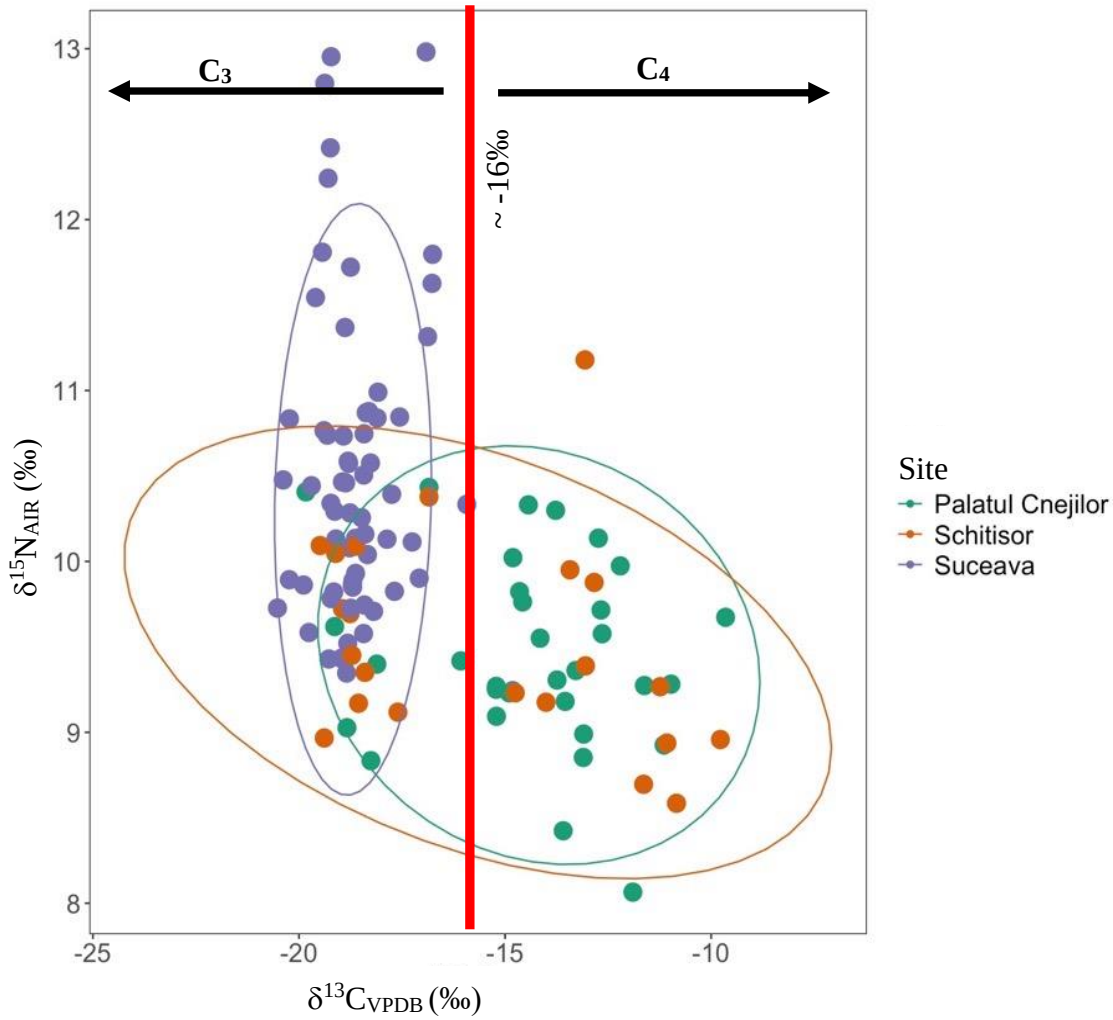


Figure 7.4. Biplot of $\delta^{13}C$ and $\delta^{15}N$ human collagen values with the solid red line indicating the cut off for a C_3 versus C_4 diet.

consuming C_4 plants, likely maize. This makes sense, as usually the staple crops that are being grown and consumed by humans are often also fed to livestock.

C_3 and C_4 Sources in the Bulk Diet versus Protein

In addition to bone collagen stable isotope data, enamel carbonate was also originally analyzed for oxygen and carbon stable isotopes to explore migration at the study sites. The enamel carbonate $\delta^{13}C$ values provide an additional data set to help interpret C_3 vs C_4 consumption at Suceava, Palatul Cnejilor, and Schitişor as enamel represents the whole diet, including carbohydrates and lipids from plants and/or animal fats. Enamel also records dietary composition from a different time in a person's life, specifically childhood. All samples used for comparison come from the second molar, which forms between the ages of two and eight years and represents the whole diet during this time. Sampling, pretreatment, and analysis protocols for tooth enamel carbon and oxygen stable isotope analysis, the enamel carbonate $\delta^{13}C$ values, the standards used, the standard's observed and expected values, and the international reference standards used to report $\delta^{13}C$ enamel values are all included in Appendix Five.

While dietary protein has a significant influence on bone collagen $\delta^{13}C$ values, strong correlations have been observed between collagen and whole diet $\delta^{13}C$ values (Froehle et al. 2010). This suggests that other components of the diet, such as carbohydrates and lipids also influence collagen $\delta^{13}C$ values (Froehle et al. 2010). Froehle and colleagues (2010) performed regression analysis on $\delta^{13}C$ apatite and collagen values from rats with 100% C_3 or 100% C_4/marine protein diets to produce C_3 and C_4 protein regression lines. These regression lines were then used to evaluate protein versus whole diet composition for swine based on how the swine $\delta^{13}C$ apatite and collagen values plotted around the regression lines. To better understand

dietary composition at Suceava, Palatul Cnejilor, and Schitişor, these regression lines were recreated in Excel using Froehle and colleagues' data set. Then the $\delta^{13}C$ apatite and collagen values for individuals from all three sites were plotted against these lines (Figure 7.5). The diet to enamel apatite spacing for humans is between 9‰ and 11‰ (Fernandes et al. 2015). For consistency and the purposes of interpreting the human enamel apatite $\delta^{13}C$ values, a diet to apatite spacing of 9‰ is used.

Suceava

Most individuals from Suceava plot close to the C_3 protein regression line. The majority have low $\delta^{13}C$ apatite values (between -9‰ and -13‰) and $\delta^{13}C$ collagen values (-19‰ to -20‰), so they plot along the left half of the C_3 protein line. This indicates they were consuming a mostly C_3 bulk diet (protein and energy sources) and C_3 protein. Since enamel records diet during childhood and bone collagen represents about a 20-year average of dietary composition, most individuals at Suceava were consuming a mostly C_3 diet across all macronutrients (protein, carbohydrates, and lipids) throughout their life.

There are also a few individuals from Suceava with low $\delta^{13}C$ apatite values (-11‰ to -13‰) and low collagen values (-15‰ to -17‰), but they are plotting between the C_3 protein and C_4 protein lines. This suggests these individuals were consuming a C_3 bulk diet, but were possibly consuming mixed C_3/C_4 protein sources as well (Froehle et al. 2010). There are also two outliers in the Suceava sample. One individual (Sample #87) has a high $\delta^{13}C$ apatite value (-5.5‰) but a low $\delta^{13}C$ collagen value (-17.9‰). This individual seems to have been consuming a bulk diet largely composed of C_4 foods and C_3 protein. The second outlier (Sample #110) has a very high $\delta^{13}C$ apatite value (-2.1‰) but plots close to the C_3 protein line. According to Froehle

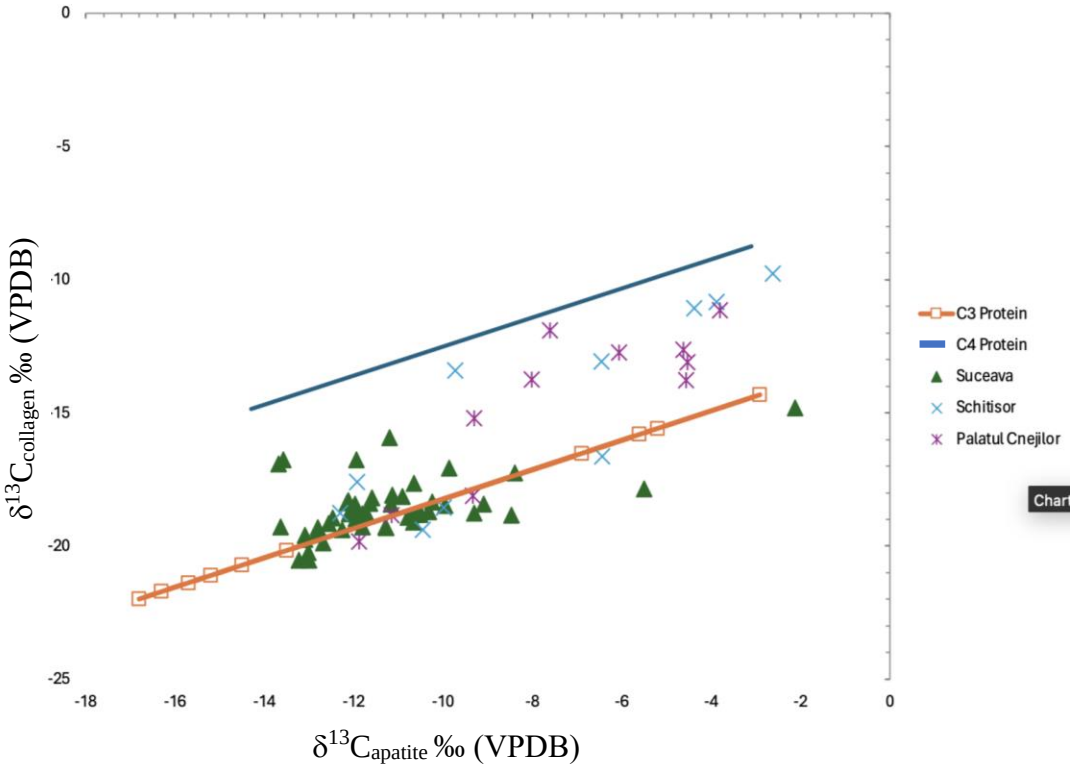


Figure 7.5. Scatter plot of human $\delta^{13}C$ apatite and collagen values plotted against C_3 and C_4 protein regression lines calculated from rat $\delta^{13}C$ collagen and apatite values by Froehle et al. (2010).

and colleagues (2010), the far end of the C_3 protein regression line indicates a 100% C_4 bulk diet (mostly carbohydrates and lipids). Accounting for the +9‰ enrichment between diet and enamel, this individual was likely consuming a bulk diet with a $\delta^{13}C$ value of around -11‰. Their relatively low $\delta^{13}C$ collagen value (-14.8‰) represents the average adulthood diet, and plots along the C_3 protein line indicating they were consuming C_3 protein in adulthood.

Palatul Cnejilor and Schitişor

There are individuals from both Palatul Cnejilor and Schitişor who, like most individuals from Suceava, fall on the C_3 protein line indicating they were also consuming a more C_3 bulk diet and C_3 protein. However, there are individuals from both sites plotting along the C_4 protein line with $\delta^{13}C$ collagen values as high as -9‰, indicating C_4 protein consumption. A few of these individuals also have high $\delta^{13}C$ apatite values (-4.3‰ to -2.6‰). According to Figure 5 in Froehle and colleagues (2010:2669) this indicates a 100% C_4 bulk diet. The high $\delta^{13}C$ collagen values (-14‰ to -9‰) along the C_4 protein line also indicate they were consuming C_4 protein. There are three individuals from Palatul Cnejilor that cluster together between the C_3 and C_4 protein lines with $\delta^{13}C$ collagen values between -12‰ and -13‰. They also have high $\delta^{13}C$ apatite values (around -4.5‰). This suggests they were consuming a bulk C_4 diet (mostly carbohydrates and lipids) but consuming mixed C_3/C_4 protein.

Overall, across all three sites, individuals are either plotting close to the C_3 protein line or the C_4 protein line. This mostly patterns by site with individuals from Suceava consuming more C_3 protein and individuals from Palatul Cnejilor and Schitişor consuming more C_4 protein. However, there is a wide range of $\delta^{13}C$ apatite values. Some individuals are on one side of the apatite spectrum consuming a majority or 100% C_4 bulk diet (mostly individuals from Palatul

Cnejilor and Schitişor) while others (mostly from Suceava) are consuming a majority C_3 bulk diet. Apart from the outliers, individuals at Suceava were consuming a C_3 bulk diet in childhood and continuing to consume mostly C_3 protein in adulthood. At Palatul Cnejilor and Schitişor, individuals that were consuming a majority or 100% C_4 bulk diet in childhood were also consuming C_4 protein in adulthood, with the exception of three individuals who were consuming C_3 and C_4 protein in adulthood. Finally, there were also individuals from Palatul Cnejilor and Schitişor who were consuming a C_3 bulk diet in childhood, and consuming C4, or mixed C_3/C_4 protein in adulthood.

From the $\delta^{13}C$ collagen values discussed previously and the Polish faunal $\delta^{13}C$ collagen data, there seemed to be a general trend of C_4 protein at Palatul Cnejilor and Schitişor and C_3 protein at Suceava. However, the contributions of bulk diet energy sources (carbohydrates and lipids) are not as visible in $\delta^{13}C$ collagen values. The inclusion of enamel apatite $\delta^{13}C$ values shows that while the protein consumption patterns observed from the $\delta^{13}C$ collagen data are maintained, the bulk diet that people at these sites were consuming in childhood, and possibly into adulthood, was somewhat more variable. For example, more C_3 inputs were observed for certain individuals at Palatul Cnejilor and Schitişor whose collagen showed mostly C_4 protein consumption, and a C_4 bulk diet for two individuals at Suceava whose collagen showed mostly C_3 protein. This provides an interesting snapshot into the dietary composition of medieval Romanians, and how it varied between these three sites. However, what was driving these dietary differences between sites?

Differences in Dietary Composition: Social Status or Temporal Change?

The hypothesis that dietary composition will be associated with burial site and there will be significant differences in diet between sites with higher-status individuals and sites with

lower-status individuals was also *supported*, but only for $\delta^{13}C$ values. An Analysis of Variance (ANOVA) showed significant differences in $\delta^{13}C$ values between Suceava and Palatul Cnejilor, and Suceava and Schitişor, but no significant difference in $\delta^{15}N$ values between the sites. Additionally, the mean difference in $\delta^{13}C$ values between Suceava and Palatul Cnejilor was ~5‰ and the mean difference between Suceava and Schitişor was ~3‰. The differences in $\delta^{13}C$ values between sites are statistically but also biologically meaningful as both mean differences are greater than a trophic level for $\delta^{13}C$ values between collagen. These results also correspond to the spatial patterns in $\delta^{13}C$ values seen in Figure 7.1, where individuals from both Palatul Cnejilor and Schitişor clustered away from individuals at Suceava in terms of $\delta^{13}C$ values.

Based on the dietary interpretations discussed above, individuals at Suceava were consuming mostly C_3 plant and animal protein, while individuals from Palatul Cnejilor and Schitişor were eating mostly C_4 plant and animal protein sources. So, what is driving these dietary differences? One possibility is social status. Overall, Suceava had more high-status individuals like nobles and palace rulers buried at the cemetery, while Palatul Cnejilor and Schitişor had more low-status individuals like monks and peasants.

The relationship between social status and diet is well documented in multiple contexts across time with higher-status individuals having access to better quality and more varied foods, while lower-status individuals are limited to lower quality protein, low protein diets (Crowder et al. 2019; Reitsema et al. 2017). Unequal access to food and economic resources by region and socioeconomic status persists in Romania today and influences the overall health of poorer, more rural communities (Gentilcore 2016; Pecican 2006). Historically, millet gruel (C_4) or porridge

was a staple food for medieval peasants and was likely consumed by medieval Romanian peasants as well (Crowder et al. 2019; Gugora et al. 2018; Hitchins 2014a; Voas et al. 2021).

Meat was also largely more accessible to higher-status individuals and men because access to plant and animal protein sources was historically not egalitarian in medieval societies. This was due to the strict social stratification of feudal society (Crowder et al. 2019; Gugora et al. 2018; Hitchins 2014a; Voas et al. 2021). It is likely that if people at Palatul Cnejilor and Schitişor were consuming C_4 crops, they were likely feeding those same crops to their livestock resulting in livestock with higher (more C_4) $\delta^{13}C$ body tissue values. Wheat (C_3) and an animal protein-rich diet, including consumption of freshwater fish, has been associated with higher-status individuals in the medieval period, and fish consumption has been associated with monastic individuals (Lightfoot et al. 2016; Pérez-Ramallo et al. 2022; Riddell et al. 2018; Živaljević et al. 2019).

Suceava having a more C_3 plant and terrestrial/aquatic protein diet is consistent with a study by Palincaş and colleagues (2019) that analyzed individuals from a $14^{th} – 17^{th}$ century site in Bărăşti, Romania, a small village in the Subcarpathian highlands in what was the principality of Wallachia, which was also periodically ruled by the Ottoman Empire. Stable carbon isotope analysis of three individuals showed that two individuals were consuming a mostly C_3 plant and animal protein diet, and one individual was consuming more C_4 sources. For this time period, the major C_4 resource would have been millet. Given the lack of dietary isotope data for medieval Romania, this one study, despite its small sample size, shows that individuals in the south were also consuming millet prior to the introduction of maize along with C_3 resources (Palincaş et al. 2019).

While social status may be driving dietary differences between the sites, diachronic changes in diet must also be considered, especially given the dates of the sites. Recall, the cemetery site at Suceava dates between the 14th and 16th centuries while the cemetery sites at Palatul Cnejilor and Schitişor date to the 17th – 18th/early 19th centuries. Maize, a C_4 crop, was introduced to Romania around the end of the 17th century and thus by the 18th century, maize was likely commonly cultivated and consumed. Food made from corn meal, notably polenta, is a staple part of Romanian cuisine today. The significant differences in $\delta^{13}C$ values between Suceava and Palatul Cnejilor and Schitişor may be due to diachronic changes in diet due to the availability of new crops i.e., maize, making C_4 a larger proportion for the diet regardless of social class. It is possible that individuals at Suceava had a more C_3 plant diet not only because higher status individuals meant greater access to and consumption of C_3 crops, but also because maize had not yet been introduced to Romania and become a significant part of the diet. When maize was introduced, during part of the time when the cemeteries and Schitişor and Palatul Cnejilor were in use, individuals had more access to and thus consumed more C_4 maize regardless of social status.

Patterns of Skeletal Stress and Dental Disease

I hypothesized that 1) individuals at this time experienced a variety of different physiological stressors as indicated by the presence of non-specific stress lesions on the skeleton, 2) there will be a difference in physiological stress experiences between the sexes, 3) there will be a difference in physiological stress experiences between sites, with individuals from low-status sites experiencing a greater burden of stress than individuals at high-status sites.

Demography

The age and sex structures of each site were not significantly different (Figures A.13-A.17 and A.20-A.24) so there was not a significantly different number of males or females between sites or an overrepresentation of younger or older individuals at each site. The average age-at-death for all three sites was between 43 and 57 years. Since these sites have no significant demographic differences, they are comparable in terms of the lesion frequencies observed.

The comparability of the sites is especially important for age-progressive lesions like caries, abscesses, and periodontal disease (PD) that require many years to accumulate, as you would not expect to see a high frequency of these lesions at a site with more young people. If the sites were significantly different in their age structures, then a greater burden of dental disease at a site with an older population could be the result of having more older individuals who had time to develop advanced dental lesions. As for *cribra orbitalia* (CO) and *porotic hyperostosis* (PH), these are not age-progressive lesions, and typically form in childhood. Thus, if the sites had significantly different age structures with more young people at one site compared to another, these lesion frequencies would not be comparable between sites.

Non-Specific Stress Lesions and Dental Disease

All lesions analyzed (PNBF, PH, CO, caries, abscesses, and PD) are present at all three sites. PNBF and PH are more frequent at Suceava, and CO is more frequent at Palatul Cnejilor. All three lesions are also more frequent among those who died young (18-25). PNBF is more frequent in males at Schitişor and Palatul Cnejilor, and in females at Suceava. PH is more frequent in males at Suceava and Palatul Cnejilor, and females at Schitişor. CO is more frequent in females at all three sites. For dental lesions, dental caries are more frequent at Schitişor, and abscesses and PD are more frequent at Palatul Cnejilor. Caries and abscesses are more frequent

in males at all three sites and in older individuals. PD is more frequent in males at Suceava and Palatul Cnejilor, and in females at Schitişor. PD was also more frequent in older individuals.

Usually, due to differences in mortality risk between lesions, raw lesion frequencies are not a reliable indicator of the true burden of a lesion in the living population from which skeletal samples are derived. This is due to selective mortality acting on populations that are heterogeneous in terms of their levels of frailty (susceptibility to disease and death) (Wood et al. 1992). Selection removes the frailest individuals from the population through death, contributing to the deceased population which in turn forms the skeletal assemblages used to construct health and disease in past populations. Selective mortality along with excavation bias and preservation issues can lead to an overrepresentation of lesions that increase the risk of death in a skeletal assemblage, making it seem like this lesion had a high prevalence in the living population (Wood et al. 1992).

For the three study sites, Kaplan-Meier survival curves found no significant difference in mortality risk for any of the lesion types. Thus, mortality does not seem to be selectively removing people from the living population at these sites based on non-specific stress lesions or dental disease. Thus, lesion frequencies at these sites are likely reflective of, to an extent, the burden of stress in the living populations from which these skeletal samples are derived (Wood et al. 1992).

Non-specific stress lesions and dental disease are ubiquitous in archaeological populations as they can be due to any number of causes, and lesions like PNBF do not take long to form on the bone surface. Thus, it was expected to see some level of physiological stress burden at all three sites, and this was observed across sites and sexes. The hypothesis that individuals at these sites were experiencing a variety of physiological stressors was *supported*.

Statistical tests yielded no significant difference between the presence/absence of any of the lesions analyzed (PNBF, PH, CO, caries, abscesses, and PD) and age, biological sex, or burial site (Appendix One). This suggests a similar burden of stress and dental disease between males and females and across sites. Thus, the hypotheses that physiological stress experiences will differ between sexes and high and low-status sites were not supported. It is possible that the sample size was too small for the statistical tests to detect meaningful patterns in the data between lesions and demography. However, the results indicate that everyone in this population was stressed to some extent, and it is likely that non-specific stress lesions did not pattern by biological sex or burial site. If that is truly the case, then increasing the sample size is not going to change the results. It is more likely that everyone at this time was experiencing stress from their environment due to the political and social climate of the time that manifested biologically in the form of skeletal stress lesions.

Stress that manifests skeletally is present in every population and may not pattern in any identifiable or meaningful way across age, sex, or social groups. Lesions like PNBF, particularly, can result from many possible conditions. Minor trauma, systemic inflammation, metabolic disease, and nutritional stress are just a few possible conditions that can disrupt skeletal homeostasis and throw off the balance between bone resorption and bone deposition by osteoclasts and osteoblasts that is required for normal bone turnover (Buikstra 2019; Matsuo and Irie 2008; Weston 2008). In PNBF specifically, osteoblasts in the periosteum are triggered by trauma or an inflammatory process to deposit woven bone on the cortical surface resulting in a lesion that can form in a matter of days but potentially persist for months or years due to sustained disruption to homeostasis (Ito et al. 2001; Klaus 2014). While not specific to any one disease process, and even without clear patterns in its presence between sexes, ages, or

individuals of different social statuses at the study sites, the presence of PNBF does reveal something about the physiology of an individual at or around the time of death and experiences of stress in the wider population that were likely ubiquitous and chronic due to their environment.

Non-Specific Stress in Medieval Romania

As discussed in Chapter Two, the 14th – 18th centuries were a period of significant social, cultural, and political change to the former principalities of Moldavia, Transylvania, and Wallachia with the Hungarian Empire ruling Transylvania in the west and the Ottoman Turkish Empire ruling Wallachia and Moldavia on and off for 500 years (Georgescu 1991a; Hitchins 2014a). My findings are consistent with research on past and modern populations that have found that increased physiological stress is associated with social, political, and climatic change (Kyle et al. 2020; Mewes et al. 2017; Rohleder et al. 2004).

Changes in political power and occupation by a foreign power inevitably affect the general population in terms of trade, access to food resources, the political and social structure of their communities, immigration, and exposure to disease and violence (Kyle et al. 2020). The Ottoman Empire repeatedly occupied Moldavia or demonstrated various levels of political power in Romania for hundreds of years. It follows that the individuals living in this region, specifically at the study sites, likely experienced social and political repercussions, both positive and negative, associated with Ottoman rule their entire lives (Georgescu 1991a; Hitchins 2014a). Occupation by a foreign power undoubtedly took a physical toll and resulted in populations experiencing variable degrees of social and political stress that may have triggered a biological stress response. The biological stress response leading to the formation of non-specific skeletal stress lesions could be due to several potential factors including mental, physical, or emotional

stress, and/or nutritional stress due to a change in access to sufficient food resources (Dent et al. 2020).

Regarding sex, the literature is varied on its conclusions about whether males or females are more susceptible to non-specific stress, infectious disease, metabolic disease, etc. (DeWitte 2010; Klein and Flanagan 2016; Kyle et al. 2018; Wilson 2014). This is not entirely surprising because the way biological sex interacts with environmental stressors to produce differential health outcomes is not consistent through time or across different social contexts. For example, during the Black Death in medieval England, males with stress lesions were found to have an increased risk of death compared to females while in the Pre-Columbian Illinois River Valley females with LEH had a higher mortality risk during their reproductive years (DeWitte 2010; Wilson 2014). In modern populations, females tend to live longer and be more resistant to environmental stressors than males (DeWitte 2010). Hormonal differences, the physiological cost of childbearing and rearing, exposure to physical labor or violence, and social systems that either buffer against or expose individuals to stressors or increase or decrease access to resources are all going to result in differential health outcomes for males and females (Temple and Goodman 2014). The relationship between sex and experiences of stress, morbidity, and mortality are unique to the place and time a person was living and the lived experiences of men and women. At Suceava, Palatul Cnejilor, and Schitişor, the data do not indicate that biological sex was a major driver of physiological stress experiences in these populations.

Dental Disease in Medieval Romania

In the context of each site and the social status of the individuals buried at each site, the patterns of dental disease are interesting. Both sites that are thought to have more low-status individuals buried there (Palatul Cnejilor and Schitişor) had the greatest frequencies of dental

disease. Schitişor, likely consisting of mostly peasants, had the greatest frequency of caries, and Palatul Cnejilor had the greatest frequencies of abscesses and PD. Overall, the lower-status sites seemed to have the greatest burden of dental disease. Given the dietary composition of these sites based on the stable carbon isotope data, greater consumption of C_4 sources at the lower status sites, possibly maize, may be driving greater dental disease burden, specifically dental caries which have been linked to consumption of higher carbohydrate, higher sugar foods like maize (Larsen 2006).

While not necessarily a stress lesion, dental disease, specifically abscesses and PD, is an inflammatory state, and poor dental health and hygiene have been linked to cardiovascular disease (DeStefano et al. 1993; Park et al. 2019) and other inflammatory issues. For example, an untreated dental abscess can introduce harmful bacteria directly into the bloodstream and given the proximity to the brain, can sometimes result in a fatal brain or systemic infection. Thus, poor dental health is often associated with co-morbidities that shape an individual's health experience and susceptibility to other diseases throughout life.

As discussed in Chapter Three, dental disease indicates an inflammatory state because of an imbalance between oral microflora and the body's immune response. This imbalance due to chronic inflammation can potentially lead to a shift in the homeostasis of an individual resulting in immune dysregulation (Dent et al. 2020). Individuals suffering from chronic dental diseases like caries, abscesses, and PD (all three often co-occur) are in an inflammatory state. If individuals are already stressed from other biological factors or social and cultural stressors, the stress response can result in a downregulated immune system leading to greater susceptibility to disease, including dental disease. Having any sort of disease has been shown to upregulate the immune response leading to this dysregulated immune activity. This has the potential to cause a

"spillover" effect leading to chronic systemic inflammation that may manifest as lesions in other parts of the skeleton (Crespo 2021; Dent et al. 2020). This creates a feedback loop of a depressed immune system due to stress and inflammation, increasing susceptibility to disease, and an increased immune response leading to further inflammation. The result is lesions like PNBF in other parts of the skeleton, and alveolar bone and tooth loss from abscesses and PD, which can be directly observed in archaeological populations.

It is also important to note that dental caries, abscesses, and PD take time to develop, with caries often being the first lesions to present and can then develop into an abscess over time. Chronic inflammation of the surrounding gingiva eventually results in alveolar bone loss and PD (Hillson 2018). Lesion frequencies and mean age-at-death at all three sites indicate that dental lesions were more frequent in older individuals, which makes sense given that dental disease often takes years to develop.

Diet, Demography, and Skeletal Stress

Burial Site as Predictors for Dental Caries?

I hypothesized that diet would impact patterns of physiological stress and dental disease. Table 7.1 shows all 12 Bayesian logistic regression models and which model fit was selected as the best fit. For all lesions except caries, model selection chose the intercept model as the best fit, meaning there was no patterning to the data. This is not informative to the purposes of this research so results were reported in Chapter Six for the next best-fit model, which was the model that selected Age and Sex as predictor variables. The caries model with femur $\delta^{13}C$ and $\delta^{15}N$ values was the only model that chose the Caries~Age+Sex model fit as the best-fit rather than the intercept. This is not a surprising finding as it makes sense there are demographic patterns in the

Table 7.1. Full Bayesian logistic regression models and best-fit model selected. The only model that selected Site as a predictor is highlighted in grey.

Full Model	Best Fit Model
PNBF ~ Age + Sex + Site + $\delta^{13}C_{Femur}$ + $\delta^{15}N_{Femur}$	PNBF~1
PNBF ~ Age + Sex + Site + $\delta^{13}C_{Rib}$ + $\delta^{15}N_{Rib}$	PNBF~1
PH ~ Age + Sex + Site + $\delta^{13}C_{Femur}$ + $\delta^{15}N_{Femur}$	PH~1
PH ~ Age + Sex + Site + $\delta^{13}C_{Rib}$ + $\delta^{15}N_{Rib}$	PH~1
CO ~ Age + Sex + Site + $\delta^{13}C_{Femur}$ + $\delta^{15}N_{Femur}$	CO~1
CO ~ Age + Sex + Site + $\delta^{13}C_{Rib}$ + $\delta^{15}N_{Rib}$	CO~1
Caries ~ Age + Sex + Site + $\delta^{13}C_{Femur}$ + $\delta^{15}N_{Femur}$	Caries~Age+Sex
Caries ~ Age + Sex + Site + $\delta^{13}C_{Rib}$ + $\delta^{15}N_{Rib}$	Caries~Age+Sex+Site
Abscesses ~ Age + Sex + Site + $\delta^{13}C_{Femur}$ + $\delta^{15}N_{Femur}$	Abscesses~1
Abscesses ~ Age + Sex + Site + $\delta^{13}C_{Rib}$ + $\delta^{15}N_{Rib}$	Abscesses~1
PD ~ Age + Sex + Site + $\delta^{13}C_{Femur}$ + $\delta^{15}N_{Femur}$	PD~1
PD ~ Age + Sex + Site + $\delta^{13}C_{Rib}$ + $\delta^{15}N_{Rib}$	PD~1

lesions, but overall these patterns were not meaningful or predictive of the odds of experiencing a stress or dental lesion.

Of note was the other caries model that used rib $\delta^{13}C$ and $\delta^{15}N$ values and selected Age, Sex, *and* Site as predictor variables for caries. The inclusion of Site as a predictor of dental caries is interesting considering that the t-tests showed a significant difference in $\delta^{13}C$ values between Suceava (a high-status C_3 site) and both Schitişor (a low-status C_4 site) with a mean difference of about 5‰, and Palatul Cnejilor (a low-status C_4 site) with a mean difference of about 3‰. This suggests that there is something about the burial site that is influencing $\delta^{13}C$ values between higher-status and lower-status sites.

Statistically, no significant difference was found in $\delta^{13}C$ values of those with and without caries, so a direct relationship between diet and caries was not observed. However, the Bayesian logistic regression model selection included Site as a predictor for caries. It is worth recalling here that the frequency of caries was highest at Schitişor and Palatul Cnejilor, sites where people were possibly consuming maize, a high carbohydrate, high sugar C_4 crop whose consumption has been linked to a greater burden of dental caries in archaeological populations (Jílková et al. 2019; Larsen 2006; Van Der Merwe and Vogel 1978).

The Bayesian model is saying Site is predictive of caries, and t-tests showed there is a significant difference in $\delta^{13}C$ values between the high-status C_3 site (Suceava) and both low-status C_4 sites (Schitişor and Palatul Cnejilor). Is this because social status, which is tied to site, was influencing access to food resources, specifically C_3 and C_4 plants, and since there were more low-status individuals at Palatul Cnejilor and Schitişor, people were consuming maize and that is why their odds of presenting with caries is higher compared to individuals at Suceava? Or, as previously discussed, is it that maize was available at Schitişor and Palatul Cnejilor after the

17th century, so individuals living at these sites between the 18th and 19th centuries were likely consuming maize regardless of sex or social status? Thus, it follows the odds of experiencing caries would be higher and the overall burden of caries would be greater at Schitişor and Palatul Cnejilor than for individuals at Suceava, who lived before the introduction of maize and were consuming more C_3 crops like wheat and rye.

Overall, these findings suggest there is something about where an individual lived and was buried that is predictive of experiencing caries. Site seems to be acting as an effect modifier on the relationship between diet ($\delta^{13}C$ values) and caries (Figure 7.6). However, it is not the site itself that is modifying this relationship but rather what site represents: social status. More specifically, the feudal system that is driving social stratification in medieval Romania and thus differential access to food resources. It is possible that feudalism is the variable that is modifying this relationship between diet and the experience of dental caries. Thus, the hypothesis that diet would impact patterns of physiological stress and dental disease, is *partially supported*.

Diet and Nutritional Stress

Neither femur nor rib $\delta^{13}C$ and $\delta^{15}N$ values were considered predictors of lesions based on the model selection process. It is possible this is because dietary protein sources were not driving experiences of stress in this population. People may have been sufficiently nourished throughout life and other factors, including the political and social factors discussed earlier like raids and violence from invading empires, and overall political instability associated with Ottoman rule were driving stress experiences in this population and access to proper nutrition as being malnourished can lead to decreased immune function. Some infections can also lead to malnourishment (Calder and Jackson 2000; Morgan 1997; Scrimshaw and SanGiovanni 1997).

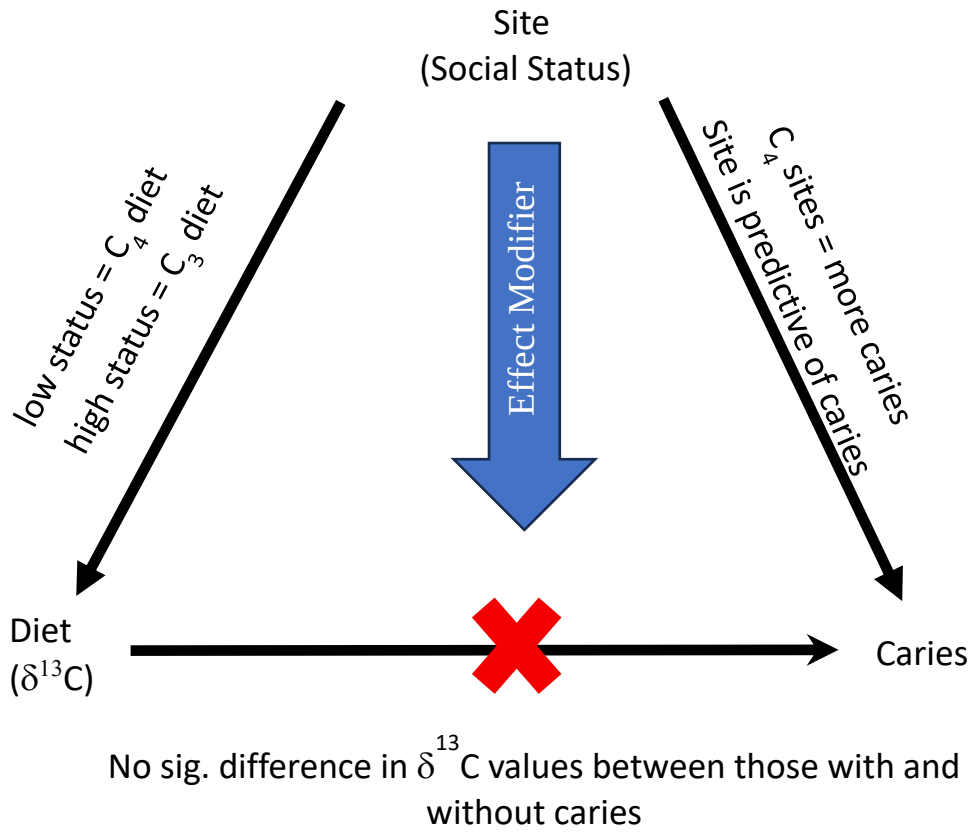


Figure 7.6. Diagram illustrating the relationship between diet and dental caries with effect modification from social status.

Thus, dietary isotope values not being predictive of stress lesions and no association found between $\delta^{13}C$ and $\delta^{15}N$ values and lesions suggests stress was likely not driven by dietary protein sources or nutritional stress.

CHAPTER EIGHT: CONCLUSION

The purpose of this research was to document the frequency of non-specific stress lesions in three late medieval cemetery sites from northeast Romania, determine the demographic makeup of these populations, reconstruct dietary composition, and analyze how demographic factors, historical context, and diet influenced patterns of physiological stress within the theoretical framework of isotope ecology and biocultural theory. Skeletal assemblages housed at the FRIA in Bucharest, Romania were analyzed for age-at-death, biological sex, non-specific stress lesions, and sampled bone collagen for carbon and nitrogen stable isotope analysis.

Age-at-death and biological sex were estimated with Transition Analysis 2 and Walker (2008) morphological sex estimation methods using traits of the pelvis and cranium. Non-specific stress lesions recorded included periosteal new bone formation (PNBF), *porotic hyperostosis* (PH), *cribra orbitalia* (CO), caries, abscesses, and periodontal disease (PD). Bone from both the femur and rib was sampled. Collagen extraction and carbon and nitrogen stable isotope analysis were performed in the Zooarchaeological Laboratory in the Department of Anthropology and the Stable Isotope Laboratory in the Department of Earth and Planetary Sciences.

Both frequentist tests of association and difference were performed to look for associations and significant differences in lesion frequencies and diet between males and females and sites. Bayesian modeling using Bayesian logistic regression was performed using 12 model iterations and flat priors to test which predictor variables (age, sex, site, $\delta^{13}C$ rib/femur, $\delta^{15}N$ rib/femur values) were most predictive for lesion presence/absence.

Based on the results of this research, the hypotheses that individuals would experience a variety of stress lesions and were consuming a mostly C_3 diet with some C_4 inputs were

supported. The hypothesis that diet would be associated with burial site (as a proxy for social status) was only partially supported. The hypothesis that lesion frequencies would differ between males and females and high and low-status individuals was not supported. The hypotheses that diet would differ between males and females and play an important role in physiological stress were also not supported.

The only significant finding was a significant difference between $\delta^{13}C$ rib values and burial site, and Age, Sex, and Site being predictive for dental caries. These findings show an interesting pattern in these populations where something about burial site is influencing experiences of dental caries, likely diet and/or social status. The stable isotope data shows that the sites with lower-status individuals (Palatul Cnejilor and Schitişor) also had more consumption of C_4 plant protein, likely maize given that these sites represent a period that overlaps with the introduction of maize to Romania. The consumption of maize and a greater probability of dental caries would not be a surprising relationship but is interesting, nonetheless. Further research with larger samples and assessing the co-occurrence of all dental disease indicators will provide a more nuanced understanding of the relationship between social status, diet, and dental health at these sites.

Limitations and Future Research

There are several limitations to this research that need to be addressed. These include sample size, baseline faunal data, site dating, limited historical information, lack of strontium/migration data, the Osteological Paradox, and the need for more complex ways of modeling the relationship between isotopes and pathology to better understand health in the past. While these limitations exist for this research, they also provide several avenues for future research that can build upon the findings of this dissertation.

Sample Size

As with most bioarchaeological research, small sample size was a limitation for this research. While upwards of 300 graves were excavated in the 1950s only about 244 adult and juvenile individuals were curated in the collections at the FRIA. Of those individuals there were cases of commingling due to the medieval practice of disinterring individuals and adding other individuals to the grave before reburial, as well as preservation issues including missing skeletal elements, and extensive taphonomic damage to the cortical surface which prohibited the assessment of PNBF. Poor preservation also affected the ability to score the traits for TA2 age estimation as well as metric and non-metric sex estimation methods. Overall, the preservation was fair/good, especially for a medieval cemetery, but the issues described above further reduced the sample size. Additionally, the Bayesian analyses require that individuals included in the analysis must have every available data point. This meant individuals with intermediate or undetermined sex, were too young or not sufficiently preserved for TA2 analysis, or were unobservable for the pathology of interest had to be eliminated.

While the analysis of only adult individuals in this sample further limited the sample size, this was an intentional choice. Since this is the first analysis of these cemetery sites, I decided it was important to first focus on adult demography, diet, and health as including juveniles opens other questions and considerations, particularly about early life stress and its effects on adulthood morbidity and mortality. This research was not testing the DOHaD (Developmental Origins of Health and Disease) hypothesis, but this is a future research question that can be considered with the data collected from juveniles in this sample to look at early life stress and how it affected adulthood PNBF and dental disease morbidity and mortality risk.

Additionally, other sites from a similar period in history were not available or present in the FRIA collection, and establishing connections with other collections in other countries takes time. Thus, adding additional samples from other regions and periods is something that will be pursued for future research to expand the sample size and allow cross-regional and temporal comparisons, something that was outside the scope of this dissertation given financial and time constraints.

Site Dates, Historical Background, and Baseline Isotopic Data

As previously discussed in Chapter Seven, all three sites do not date to the same time period. The individuals from Suceava are from burials that date between the 14th and 16th centuries while the individuals from Palatul Cnejilor and Schitișor are from burials that date from the 17th – 18th, possibly even early 19th centuries. Thus, drawing conclusions about health and diet at these sites is complicated by possible temporal changes in diet (particularly the introduction of maize by the late 17th century), changing social and political landscape over time, and comparing populations of individuals who likely did not coexist. Even between Palatul Cnejilor and Schitișor, which do share a date range, skeletal samples are complicated by the fact that not everyone in that cemetery died or lived at the same time. A 200-year time range is still several generations, and it cannot be reasonably expected that the stressors they experienced and their ability to face them were homogenous across time. This is a complication not unique to my dissertation, but rather bioarchaeological research as a whole. This is why true prevalence of a lesion cannot be known from skeletal samples. True prevalence, as calculated in epidemiology, requires an entire population to be randomly sampled and is expressed as a percentage or cases per 100,000. In bioarchaeology, we never have access to the entire living population from which a cemetery sample came from, and a cemetery sample cannot be considered a random

representative sample of that once-living population due to the biases of hidden heterogeneity in frailty and selective mortality discussed in Chapter Three. Instead, each individual represents a cross-sectional view of an individual's physiological state at the time of their death. Combining these cross-sectional data points to try to extrapolate patterns from the wider population is fraught.

This is not to say bioarchaeology is not worth doing, and we should just give up, but it does limit what we can know and conclude about this past. However, incorporating biomolecular and biogeochemical methods along with careful and purposeful consideration of how we try to model the relationship between skeletal stress, diet, and health can push bioarchaeology towards more robust conclusions about past health and disentangle some of the biases inherent in skeletal samples.

Since there was no baseline faunal isotopic data from the medieval period in Romania or the study sites, faunal data from other regions and similar time periods had to be used in the interpretations of human dietary composition. While this is helpful in interpreting carbon and nitrogen stable isotope values and what they are actually saying about plant and animal protein sources being consumed, having faunal data from the study sites would provide richer context and interpretation of human diet in medieval Romania.

Role of Migration: Demographic Non-Stationarity and Hidden Heterogeneity in Frailty

The original research design for this dissertation included strontium stable isotope data from tooth enamel and plant samples to create a strontium isoscape of the region where the cemetery sites are located and determine if any non-local/migrant individuals are present in the sample. Due to issues and delays with setting up a low metal clean lab at UTK and needing to find an external lab capable of doing strontium analysis, strontium stable isotope analysis could

not begin until January 2024. I was able to carry out the lab work at Arizona State University's Metals, Environmental, and Terrestrial Analytical Laboratory (METAL) in early January 2024, but on the third day of my visit, their Neptune MC-ICP-MS died after 20 years of use at METAL. While I was able to prepare all my samples for analysis in their new machine, the new machine would not be installed until the end of February. Installation occurred on schedule but a series of software glitches and over a month of troubleshooting with Thermo-Scientific meant my samples could not be analyzed until mid-April. This did not provide sufficient time to analyze and incorporate the strontium data into this dissertation.

As a result, I do not have migration data. The inclusion of migration data would have been an additional variable that could have been included in the Bayesian models to see how predictive migrant status was in the probability of an individual exhibiting a particular lesion. Researchers in recent years have been combining pathological and isotope data to look at the relationship between migration and health (Groves et al. 2013; Kendall et al. 2013; Redfern et al. 2018; Roberts et al. 2013). Thus, incorporating this approach was a key piece of the original research design and something that has not been explored in medieval Romania, a period that likely had significant population movement due to the presence of Ottoman soldiers. Additionally, migration data would be useful for addressing demographic non-stationarity as it would allow me to see how many individuals were present in this sample who spent their childhood elsewhere and migrated into this region of Romania during their lifetime, direct evidence of population movement, which would have contributed to the heterogeneity in frailty and health experiences in this population.

Future research will include the strontium and oxygen stable isotope data and I plan to create a strontium isoscape of this region of Romania to characterize local strontium ratios and

identify non-local individuals in this sample. This will allow me to address questions about migration and health in future publications. Additional research will also include analysis of juvenile dental enamel and further plant sampling in Romania to expand the isoscape. A strontium isoscape of Romania will be useful to multiple scientific fields beyond anthropology including paleoecology and geology. Currently, no strontium isoscape exists for Eastern Europe as the bulk of strontium isoscape work in Europe is focused on Western Europe (Bataille et al. 2018) so this is the first step in beginning to characterize strontium ratios for Eastern Europe which will facilitate future migration research in this region.

Modeling the Relationship between Isotopes and Pathology

While traditional frequentist approaches to analyzing bioarchaeological data can be informative, tests of association like Pearson's chi-square tests and Independent Samples t-tests can only say whether there is an association between variables or a significant difference. This is a good first step in understanding the patterns present in the data and relationships between variables, but it doesn't say anything about what these patterns and differences mean in the context of your research questions. The Bayesian logistic regression modeling approach used in this dissertation was a first attempt to move beyond basic tests of associations and difference, and get probabilistic outcomes to be able to say which variables of interest (age, sex, pathology, and isotopic dietary indicators) are most predictive for each lesion type and the probability of an individual exhibiting a lesion given these predictor variables. Instead of only being able to conclude whether a variable is associated with a lesion, and not really knowing what that means, this approach allows you to say whether a variable is predictive of experiencing lesions and how they influence the probability of exhibiting a specific lesion.

While this research suffered from limited sample size, which in turn affected the ability of the models to generate meaningful results, this approach was able to identify burial site as a predictor variable for dental caries. Combined with what the stable carbon isotope data indicated about C_3 vs C_4 dietary composition at each site (Suceava more C_3 and Palatul Cnejilor and Schitişor more C_4), and the independent samples t-tests identifying a significant difference in $\delta^{13}C$ rib values between Suceava and Palatul Cnejilor and Suceava and Schitisor, this is an interesting result. It shows that there is something meaningful occurring in the relationship between experiencing dental caries and the site where an individual was buried, possibly due to social status and sources of plant protein. While not reported, t-tests for pathology and carbon and nitrogen stable isotope values were run. There were no significant differences found, except for caries and rib $\delta^{13}C$ values. However, the difference in the isotope values between those with and without caries was not biologically meaningful as the mean difference was only 1.5‰. However, this is further support of something interesting occurring in this population regarding their diet, experience of dental caries and where they were buried.

Future research would benefit from the inclusion of co-occurrence data for caries, abscesses, and PD. These are all lesions that represent different stages of dental disease and are biologically associated. Thus, looking at how often they co-occur in this sample will provide a more nuanced look at dental health in these populations. However, this requires more nuanced and complex approaches for modeling the relationship between stable isotopes and lesions that we use to try to understand “health”.

A couple of potential future approaches are Structural Equation Modeling and incorporating intersectionality theory (Crenshaw 1989) and interaction effects. Structural Equation Modeling (SEM) is a multivariate statistical approach for examining linear causal

relationships between variables. It is well suited for analyzing complex relationships between variables, testing causal relationships, and accounting for measurement error and has been used more frequently in medical and epidemiological research in the last several years (Beran and Violato 2010; David et al. 2021; Fujii et al. 2022; Oyewola et al. 2021; Smid and Rosseel 2020).

Intersectionality theory originates in Black Feminist scholarship and theorizes how multiple identities interact to shape the experiences of an individual, particularly their experiences of marginalization and oppression (Crenshaw 1989). Intersectionality theory has been applied to several recent bioarchaeological works (Boyd 2022; DeWitte and Yaussy 2020; Knudson et al. 2020; Maass 2023; Ralston 2023; Torres-Rouff and Knudson 2017; Yaussy et al. 2016) to explore how social categories like age, sex, social status, occupation, region of burial, migrant status, etc. interact in complex and layered ways to produce differential morbidity and mortality risk. Intersectionality provides a framework to understand how these different social identities result in different experiences of marginalization or privilege that mediate an individual's exposure to pathogens, stressors, pollutants, violence, etc. (Boyd 2022; DeWitte and Yaussy 2020).

Future research at the medieval Romanian sites explored in this dissertation could incorporate demographic data, social status indicators, migrant status, and dietary isotopes within an intersectional framework. Using intersectionality theory and Bayesian approaches for looking at interaction effects between age, sex, social status, diet, and migrant status would make it possible to explore how these factors produce multiply-marginalized or multiply-privileged identities and how that influences the probability of experiencing physiological stress.

Additional Future Research

Dental calculus was also collected during data collection from all individuals who had sufficient dental calculus deposits. Dental calculus provides an opportunity to further look at dietary composition, but on a more recent timescale than bone provides. Stable carbon isotope analysis of dental calculus could elucidate whether C_3 or C_4 plants were consumed in the last few years of life. Paleoproteomic analysis can look at the presence of milk proteins which can elucidate the consumption of milk protein and the significance of dairy to the diet of medieval Romanians. It may also be possible to analyze dental calculus for amelogenin, a gene that encodes proteins in tooth enamel and is commonly used in forensic human identification (Watherston and Ward 2023). One form of this gene is on the X chromosome and the other is on the Y chromosome (Couwenhoven et al. 1993; Watherston and Ward 2023). This makes amelogenin a possible method for estimating sex from juvenile remains, which is not currently possible with current morphological methods. The ability to estimate the sex of juveniles would add an additional layer to research with juvenile remains. Sex-based differences often only explored in adults could be explored in juveniles. Particularly, sex-based differences in diet, pathology, and breastfeeding and weaning practices as understood through oxygen and nitrogen stable isotope analysis of tooth enamel and dentin. This would open many avenues of research in juvenile bioarchaeology and paleopathology, including in these medieval Romanian populations.

The addition of sulfur stable isotope analysis of bone collagen would provide additional insight into dietary composition, particularly freshwater versus terrestrial protein consumption. Given that the $\delta^{15}N$ and $\delta^{13}C$ values of some individuals at Suceava suggest possible freshwater fish consumption, the addition of sulfur stable isotope ($\delta^{34}S$) analysis could help to confirm or refute the presence of freshwater fish in the diet of individuals at Suceava (Florin et al. 2011;

Hyland et al. 2021; Privat et al. 2007; Richards et al. 2003). Additionally, sulfur isotopes reflect local geology, so combined with strontium and oxygen stable isotope data, sulfur isotopes can be an additional tool for identifying migrants in a sample. Sulfur stable isotopes can also be analyzed in bone collagen, which would provide data about mobility and migration during the last several years of life. Combined with strontium and oxygen isotopes from dental enamel, which records the childhood environment, the addition of sulfur isotopes can provide more detailed and nuanced information about how an individual was moving across the landscape into adulthood (Bataille et al. 2021; Ebert et al. 2021; Guo et al. 2018; Hyland et al. 2021; Richards et al. 2001). Finally, stable isotope analysis of faunal remains from Romania, especially faunal remains from the medieval period, would provide crucial baseline data to improve and deepen the interpretations about dietary composition at Suceava, Palatul Cnejilor, and Schitişor.

Broader Impacts and Final Reflections

This research will be one of the first to combine stable isotope and paleopathological analysis to characterize diet and patterns of stress and frailty in late medieval-early modern Romanian human populations. Characterizing the health and demography of these people will establish the significance of this region in the medieval period by illuminating the lived experiences of these people as individuals and as members of a larger population during a period of social, political, and cultural change. This study will provide baseline data for future comparative studies of health and mobility in Romania and surrounding regions and advance the field of stable isotope analysis in Romanian bioarchaeology.

Research on the biological and environmental processes that affected human health in the past can provide temporal depth and nuance to our understanding of how these processes continue to affect health today. This can potentially inform modern public health research and

policy aimed at improving the health of individuals in communities across the world. Regional disparities in income, education, health, and nutrition in Romania are systemic issues that have deep roots in historical processes of occupation, conflict, slavery, and social stratification experienced during the medieval period as well as the policies enacted under Communism in the 1940s and 1950s, as discussed in Chapter Two. The roots of modern health disparities extend deep into Romanian history. Thus, exploring how factors like age, sex, social status, migrant status, and access to nutritional resources impacted human health in Romania's past has the potential to provide an historically informed perspective of how these processes continue to play out in Romania today. This knowledge can be leveraged to address unequal access to resources and health disparities that affect Romanians today.

Bioarchaeological research has the potential to inform public health research by providing a deep time view of how human health has evolved and how the many factors that affect human health have changed depending on time period, region, social and political institutions, religious influences, environmental change, etc. The factors associated with health outcomes and how individual identity intersects with societal institutions and ideologies to shape health experiences vary across time and space. However, there are also many patterns and trends that we see in the past that persist with alarming similarity in the present. In particular, how those of marginalized identities experience greater risk of disease and death due to limited access to resources, barriers to care, discrimination, and the stress from experiencing daily oppression and marginalization. We see the toll this takes on modern people and there is no question it took a toll in past peoples too, even if it is difficult to observe through what is available in the archaeological record.

Conducting this research amid the COVID-19 pandemic and the constant discourse by news media around “co-morbidities” associated with the risk of COVID-19 disease and death and the groups most affected by and at risk of dying from Covid was a surreal experience. It forced me to think critically about my own research in a way that I may not have otherwise. It made the connections between studying health in the past and how it can (or cannot) inform the present, and vice versa, impossible to ignore. Witnessing firsthand how the elderly, people with disabilities, People of Color, gender-queer and LBGTQIA individuals, and those with several co-morbidities such as diabetes, hypertension, and obesity were disproportionality impacted by COVID-19 was eye-opening and forced me to put my own research in perspective. Specifically, how can my research articulate with and inform current medical and public health research on how people of marginalized identities are disproportionally impacted by chronic and infectious diseases, and how can changes to policy and societal norms combat this? It is my hope that this research is the first step in a larger research program that can work with researchers in medicine and public health to tackle these questions both in the distant past and the present.

REFERENCES

Achim, Viorel

2004a The Arrival of the Gypsies on the Territory of Romania. In *The Roma in Romanian History*, pp. 7-26. Central European University Press, Budapest.

2004b *The Roma in Romanian History*. Central European University Press, Budapest.

Adamson, Melitta Weiss

2004 *Food in medieval times*. Bloomsbury Publishing USA.

Allen, Kathryn Grow, Ryan D. Mills, Kelly J. Knudson, and Noreen von Cramon-Taubadel

2020 Biological diversity in an Islamic archaeological population: A radiogenic strontium isotope and craniometric analysis of affinity in Ottoman Romania. *American journal of physical anthropology* 171(4):569-583.

Ambrose, S.H. , and L. Norr

1993 Experimental evidence for the relationship of the carbon isotope ratios of whole diet and dietary protein to those of bone collagen and carbonate. In *Prehistoric Human Bone: Archaeology at the Molecular Level*, edited by J.B. Lambert, and G. Grupe, pp. 1-37. Springer-Verlag, New York.

Ambrose, Stanley H

1991 Effects of diet, climate and physiology on nitrogen isotope abundances in terrestrial foodwebs. *Journal of archaeological science* 18(3):293-317.

Armelagos, G.J., D.S. Carlson, and D.P. Van

1982 The Theoretical Foundations and Development of Skeletal Biology. In *A History of American physical anthropology, 1930-1980*, edited by Frank Spencer, pp. 305-329. Academic Press, New York, N.Y.

Balasse, Marie

2002 Reconstructing dietary and environmental history from enamel isotopic analysis: time resolution of intra-tooth sequential sampling. *International journal of osteoarchaeology* 12(3):155-165.

Bataille, Clément P, Klervia Jaouen, Stefania Milano, Manuel Trost, Sven Steinbrenner, Éric Crubézy, and Rozenn Colleter

2021 Triple sulfur-oxygen-strontium isotopes probabilistic geographic assignment of archaeological remains using a novel sulfur isoscape of western Europe. *PLoS One* 16(5):e0250383.

Bataille, Clement P., Isabella C. C. von Holstein, Jason E. Laffoon, Malte Willmes, Xiao-Ming Liu, and Gareth R. Davies

2018 A bioavailable strontium isoscape for Western Europe: A machine learning approach. *PloS one* 13(5):e0197386-e0197386.

Batariuc, Paraschiva-Victoria
1993 Necropola Medievala De La Suceava - Campul Santurilor. *Arhcologia Moldovei* XVI:229-249.

Beck, Jess, Horia Ciugudean, and Colin Quinn
2021 Bioarchaeology and Mountain Landscapes in Transylvania's Golden Quadrangle. *Bioarchaeology International* 4(2):89.

Beck, Sam
1989 The origins of Gypsy slavery in Romania. *Dialectical Anthropology* 14(1):53-61.

Ben-David, Merav , and Elizabeth A. Flaherty
2012 Stable isotopes in mammalian research: a beginner's guide. *Journal of mammalogy* 93(2):312-328.

Bentley, Alexander R.
2006 Strontium Isotopes from the Earth to the Archaeological Skeleton: A Review. *Journal of archaeological method and theory* 13(3):135-187.

Bentley, R. Alexander, T. Douglas Price, Jens Lning, Detlef Gronenborn, Joachim Wahl, and PaulD Fullagar
2002 Prehistoric Migration in Europe: Strontium Isotope Analysis of Early Neolithic Skeletons. *Current anthropology* 43(5):799-804.

Beran, Tanya N., and Claudio Violato
2010 Structural equation modeling in medical research: a primer. *BMC Research Notes* 3(1):267.

Berger, Steph M., Jacob S. Griffin, and Sophia C. Dent
2020 Phenotypes and pathways: Working toward an integrated skeletal biology in biological anthropology. *American journal of human biology*:e23450-e23450.

Bocherens, H., and D. Drucker
2003 Trophic level isotopic enrichment of carbon and nitrogen in bone collagen: case studies from recent and ancient terrestrial ecosystems. *International journal of osteoarchaeology* 13(1-2):46-53.

Bocherens, Hervé, Caroline Polet, and Michel Toussaint
2007 Palaeodiet of Mesolithic and Neolithic populations of Meuse Basin (Belgium): evidence from stable isotopes. *Journal of archaeological science* 34(1):10-27.

Bogaard, A., T. H. E. Heaton, P. Poulton, and I. Merbach
2007 The impact of manuring on nitrogen isotope ratios in cereals: archaeological implications for reconstruction of diet and crop management practices. *Journal of archaeological science* 34(3):335-343.

Boldsen, J. L., G. R. Milner, and R. Hylleberg
2016 ADBOU age estimator (2.1).

Boldsen, Jesper L., George R. Milner, Lyle W. Konigsberg, and James W. Wood
2002 Transition analysis: a new method for estimating age from skeletons. In *Paleodemography: Age distributions from skeletal samples*, edited by Robert D. Hoppa, and James W. Vaupel. Cambridge University Press, Cambridge, UK.

Borić, Dušan, and T. Douglas Price
2013 Strontium isotopes document greater human mobility at the start of the Balkan Neolithic. *Proceedings of the National Academy of Sciences - PNAS* 110(9):3298-3303.

Boyd, Derek A
2022 Morbidity, mortality, and marginalization: An intersectional investigation of respiratory stress and differential frailty in Industrial-Era England.

Bradley, Elizabeth W. , Jennifer J. Westendorf, Andre J. van Wijnen, and Amel Dudakovic
2018 Osteoblasts: Function, Development, and Regulation. In *Primer on the Metabolic Bone Diseases and Disorders of Mineral Metabolism*, edited by J. P. Bilezikian, pp. 31-37. 9th ed. John Wiley & Sons, Incorporated.

Budd, Paul, Janet Montgomery, Barbara Barreiro, and Richard G. Thomas
2000 Differential diagenesis of strontium in archaeological human dental tissues. *Applied geochemistry* 15(5):687-694.

Buikstra, J.E.
2019 *Ortner's identification of pathological conditions in human skeletal remains*. Third edition. ed. Identification of pathological conditions in human skeletal remains. Academic Press, London, United Kingdom.

Buikstra, J.E., and D.H. Ubelaker
1994 *Standards for Data Collection from Human Skeletal Remains*. Arkansas Archaeological Survey Research Series No. 44, Fayetteville, AR.

Buikstra, Jane E.
2006 A Historical Introduction. In *Bioarchaeology : the contextual analysis of human remains*, edited by Jane E. Buikstra, and Lane A. Beck, pp. 7-27. Academic Press, Amsterdam ;.

Bürkner, Paul-Christian
2017 brms: An R package for Bayesian multilevel models using Stan. *Journal of statistical software* 80:1-28.

Burns, Thomas S.
2003 *Rome and the Barbarians: 100 B.C.-A.D. 400*. The Johns Hopkins University Press, Baltimore, Maryland.

Calder, Philip C., and Alan A. Jackson
2000 Undernutrition, infection and immune function. *Nutrition Research Reviews* 13(1):3-29.

Cerling, Thure E, and John M Harris
1999 Carbon isotope fractionation between diet and bioapatite in ungulate mammals and implications for ecological and paleoecological studies. *Oecologia* 120:347-363.

Cerling, Thure E., John M. Harris, Bruce J. MacFadden, Meave G. Leakey, Jay Quade, Vera Eisenmann, and James R. Ehleringer
1997 Global vegetation change through the Miocene/Pliocene boundary. *Nature (London)* 389(6647):153-158.

Chen, Linlin, Huidan Deng, Hengmin Cui, Jing Fang, Zhicai Zuo, Junliang Deng, Yinglun Li, Xun Wang, and Ling Zhao
2018 Inflammatory responses and inflammation-associated diseases in organs. *Oncotarget* 9(6):7204.

Cheverko, Colleen M., Julia R. Prince-Buitenhuys, and Mark Hubbe
2021 Theory in bioarchaeology: An introduction. In *Theoretical approaches in bioarchaeology*, edited by Colleen M. Cheverko, Julia R. Prince-Buitenhuys, and Mark Hubbe, pp. 1-14. Routledge/Taylor & Francis Group, Abingdon, Oxon ;.

Choi, Woo-Jung, Sang-Mo Lee, Hee-Myong Ro, Kyoung-Cheol Kim, and Sun-Ho Yoo
2002 Natural 15N abundances of maize and soil amended with urea and composted pig manure. *Plant and soil* 245(2):223-232.

Chu, Wei
2018 The Danube Corridor Hypothesis and the Carpathian Basin: Geological, Environmental and Archaeological Approaches to Characterizing Aurignacian Dynamics. *Journal of world prehistory* 31(2):117-178.

Couwenhoven, RI, SA Schwartz, and ML Snead
1993 Arrest of amelogenin transcriptional activation in bromodeoxyuridine-treated developing mouse molars in vitro. *Journal of Craniofacial Genetics and Developmental Biology* 13(4):259-269.

Crenshaw, Kimberle
1989 Demarginalizing the intersection of race and sex: a black feminist critique of antidiscrimination doctrine, feminist theory and antiracist politics. *University of Chicago Legal Forum*.

Crespo, Fabian
2021 Reconstructing immune competence in skeletal samples. In *Theoretical approaches in bioarchaeology*, edited by Colleen M. Cheverko, Julia R. Prince-Buitenhuys, and Mark Hubbe, pp. 76-92. Routledge/Taylor & Francis Group, Abingdon, Oxon.

Crowder, Kayla D, Janet Montgomery, Darren R Gröcke, and Kori L Filipek
2019 Childhood "stress" and stable isotope life histories in Transylvania. *International Journal of Osteoarchaeology* 29(4):644-653.

Curto, Ana, Patrick Mahoney, Anne-France Maurer, Cristina Barrocas-Dias, Teresa Fernandes, and Geraldine E. Fahy
2019 Diet and disease in Tomar, Portugal: Comparing stable carbon and nitrogen isotope ratios between skeletons with and without signs of infectious disease. *Journal of archaeological science* 105:59-69.

D'Arrigo, Graziella, Daniela Leonardis, Samar Abd ElHafeez, Maria Fusaro, Giovanni Tripepi, and Stefanos Roumeliotis
2021 Methods to analyse time-to-event data: the Kaplan-Meier survival curve. *Oxidative medicine and cellular longevity* 2021.

David, OO, GD Emmanuel, JN Ndunagu, AU Terang, and SA Akinwumi
2021 COVID-19 Risk Factors, Economic Factors, and Epidemiological Factors nexus on Economic Impact: Machine Learning and Structural Equation Modelling Approaches.

Deniro, Michael J., and Samuel Epstein
1981 Influence of diet on the distribution of nitrogen isotopes in animals. *Geochimica et cosmochimica acta* 45(3):341-351.

Dent, Sophia C, Steph M Berger, and Jacob S Griffin
2020 Biocultural pathways linking periodontal disease expression to food insecurity, immune dysregulation, and nutrition. *American Journal of Human Biology* https://doi.org/10.1002/ajhb.23549.

DeStefano, F, R F Anda, H S Kahn, D F Williamson, and C M Russell
1993 Dental disease and risk of coronary heart disease and mortality. *British Medical Journal* 306(6879):688-691.

DeWitte, Sharon N, and Samantha L Yaussy
2020 Bioarchaeological applications of intersectionality. In *Theoretical approaches in bioarchaeology*, pp. 45-58. Routledge.

DeWitte, Sharon N.
2010 Sex differentials in frailty in medieval England. *American journal of physical anthropology* 143(2):285-297.

2014 Differential survival among individuals with active and healed periosteal new bone formation. *International journal of paleopathology* 7:38-44.

DeWitte, Sharon N., and Christopher M. Stojanowski
2015 The Osteological Paradox 20 Years Later: Past Perspectives, Future Directions. *Journal of archaeological research* 23(4):397-450.

Diaconu, G.
2003 The Middle Ages and the Early Modern Era. B. Archaeological research, e) Cnejilor Palace. In *Archaeological and historical research in the Bicaz reservoir area*, edited by M. Petrescu Dîmbovița, and V. Spinei, pp. 212-228.

Djuvara, Neagu
1995 *Between East and West: Romanian countries at the beginning of the modern era (1800-1848)*. Humanitas, Bucharest.

Dobos, Adrian, Andrei Soficaru, and Erik Trinkaus
2010 *The prehistory and paleontology of the Peştera Muierii, Romania*.

Ebert, Claire E, Asta J Rand, Kirsten Green-Mink, Julie A Hoggarth, Carolyn Freiwald, Jaime J Awe, Willa R Trask, Jason Yaeger, M Kathryn Brown, and Christophe Helmke
2021 Sulfur isotopes as a proxy for human diet and mobility from the preclassic through colonial periods in the Eastern Maya lowlands. *PLoS One* 16(8):e0254992.

Encyclopedia Britannica
Ottoman Empire, pp. https://www.britannica.com/place/Egypt/The-Ottomans-1517-1798#/media/1511/180382/194947. Encyclopedia Britannica.

Evans, R. D.
2007 Soil nitrogen isotope composition. In *Stable Isotopes in Ecology and Environmental Science*, edited by R.H. Michener, and K. Lajtha, pp. 83-98. 2nd ed. Blackwell Scientific Publications, Boston.

Evans, R. Dave
2001 Physiological mechanisms influencing plant nitrogen isotope composition. *Trends in plant science* 6(3):121-126.

Farquhar, G. D., J. R. Ehleringer, and K. T. Hubick
1989 Carbon Isotope Discrimination and Photosynthesis. *Annual review of plant physiology and plant molecular biology* 40(1):503-537.

Fernandes, Ricardo, Pieter Grootes, Marie-Josée Nadeau, and Olaf Nehlich
2015 Quantitative diet reconstruction of a Neolithic population using a Bayesian mixing model (FRUITS): The case study of Ostorf (Germany). *American journal of physical anthropology* 158(2):325-340.

Florin, Scott T, Laura A Felicetti, and Charles T Robbins
2011 The biological basis for understanding and predicting dietary-induced variation in nitrogen and sulphur isotope ratio discrimination. *Functional Ecology* 25(3):519-526.

Fraser, Rebecca A., Amy Bogaard, Tim Heaton, Michael Charles, Glynis Jones, Bent T. Christensen, Paul Halstead, Ines Merbach, Paul R. Poulton, Debbie Sparkes, and Amy K. Styring
2011 Manuring and stable nitrogen isotope ratios in cereals and pulses: towards a new archaeobotanical approach to the inference of land use and dietary practices. *Journal of archaeological science* 38(10):2790-2804.

Froehle, Andrew W, Corina M Kellner, and Margaret J Schoeninger
2010 FOCUS: effect of diet and protein source on carbon stable isotope ratios in collagen: follow up to. *Journal of Archaeological Science* 37(10):2662-2670.

Fry, B., and E. B. Sherr
1989 δ13C Measurements as Indicators of Carbon Flow in Marine and Freshwater Ecosystems, pp. 196-229. Ecological Studies. Springer New York, New York, NY.

Fujii, Ryosuke, Roberto Melotti, Martin Gögele, Laura Barin, D Ghasemi, Giulia Barbieri, Peter P Pramstaller, and Cristian Pattaro
2022 Epidemiology, Risk Factors, Prevention Structural Equation Modeling of Kidney Function Biomarkers Improves Incident Cardiovascular Risk Estimation: TH-PO624. *J Am Soc Nephrol 33, 2022*:224-224.

Fuller, Benjamin T, James L Fuller, David A Harris, and Robert EM Hedges
2006 Detection of breastfeeding and weaning in modern human infants with carbon and nitrogen stable isotope ratios. *American Journal of Physical Anthropology: The Official Publication of the American Association of Physical Anthropologists* 129(2):279-293.

Fuller, Benjamin T., James L. Fuller, Nancy E. Sage, David A. Harris, Tamsin C. O'Connell, and Robert E. M. Hedges
2004 Nitrogen balance and δN: Why you're not what you eat during pregnancy. *Rapid communications in mass spectrometry* 18(23):2889-2896.

2005 Nitrogen balance and δ15N: why you're not what you eat during nutritional stress. *Rapid communications in mass spectrometry* 19(18):2497-2506.

Gentilcore, David
2016 *Food and health in early modern Europe : diet, medicine and society, 1450-1800*. Bloomsbury Academic, an imprint of Bloomsbury Publishing Plc., London ;.

Georgescu, Vlad
1991a Medieval Civilization: Byzantium after Byzantium. In *The Romanians A History*, edited by Matei Calinescu, pp. 58-72. Ohio State University Press, Columbus.

1991b *The Romanians: A History*. Ohio State University Press, Columbus.

Gerling, Claudia
2015a A multi-isotopic pilot study of the burial mound of Boyanovo. *Praehistorische Zeitschrift* 90(1):172-184.

2015b *Prehistoric mobility and diet in the west Eurasian steppes 3500 to 300 BC : an isotopic approach*. Topoi.Berlin Studies of the Ancient World, Volume 25. De Gruyter, Berlin, [Germany] ;.

Gerling, Claudia, Eszter Bánffy, János Dani, Kitti Köhler, Gabriella Kulcsár, Alistair W. G. Pike, Vajk Szeverényi, and Volker Heyd
2012 Immigration and transhumance in the Early Bronze Age Carpathian Basin: the occupants of a kurgan. *Antiquity* 86(334):1097-1111.

Gerling, Claudia, and H. Ciugudean
2013 Insights into Transylvanian Early Bronze Age using Strontium and Oxygen Isotope Analysis - A Pilot Study. In *Transitions to the Bronze Age. Interregional Interaction and Socio-Cultural Change in the Third Millennium BC Carpathian Basin and Neighboring Regions*, edited by V Heyd, G Kulcsár, and V. Szeverenyi, pp. 181-202, Budapest.

Godde, Kanya, Valerie Pasillas, and America Sanchez
2020 Survival analysis of the Black Death: Social inequality of women and the perils of life and death in Medieval London. *American journal of physical anthropology* 173(1):168-178.

Golea, Mihaela, Ana García-Vázquez, Cristina Mircea, Marin Cârciumaru, Gabriela Sava, Johannes Mueller, Wiebke Kirleis, and Cătălin Lazăr
2023 Revisiting Archived Rye Grains Discovered at the Neolithic Site CUNEŞTI (romania). *Radiocarbon*:1-18.

Goodman, Alan H., J Lallo, G.J. Armelagos, and J.C. Rose
1984 Health changes at Dickson Mounds, Illinois (A.D. 950-1300). In *Paleopathology at the origins of agriculture: Bioarchaeological interpretations of the human past: Local, Regional, and Global*, edited by MN Cohen, and GH Armelagos, pp. 271-306. University Press of Florida, FL.

Groves, S. E., C. A. Roberts, S. Lucy, G. Pearson, D. R. Gröcke, G. Nowell, C. G. Macpherson, and G. Young
2013 Mobility histories of 7th–9th century AD people buried at early medieval Bamburgh, Northumberland, England. *American Journal of Physical Anthropology* 151(3):462-476.

Gugora, Ariana, Tosha L Dupras, and Erzsébet Fóthi
2018 Pre-dating paprika: Reconstructing childhood and adulthood diet at medieval (13th century CE) Solt-Tételhegy, Hungary from stable carbon and nitrogen isotope analyses. *Journal of Archaeological Science: Reports* 18:151-160.

Guo, Y, Y Fan, Y Hu, J Zhu, and Michael P Richards
2018 Diet transition or human migration in the Chinese Neolithic? Dietary and migration evidence from the stable isotope analysis of humans and animals from the Qinglongquan site, China. *International Journal of Osteoarchaeology* 28(2):85-94.

Hakenbeck, Susanne, Ellen McManus, Hans Geisler, Gisela Grupe, and Tamsin O'Connell
2010 Diet and mobility in Early Medieval Bavaria: A study of carbon and nitrogen stable isotopes. *American Journal of Physical Anthropology* 143(2):235-249.

Halffman, Carrin M, and Petr Velemínský
2015 Stable isotope evidence for diet in early medieval Great Moravia (Czech Republic). *Journal of Archaeological Science: Reports* 2:1-8.

Hankenson, K. D., K. Gagne, and M. Shaughnessy
2015 Extracellular signaling molecules to promote fracture healing and bone regeneration. *Advanced Drug Delivery Reviews* 94:3-12.

Hartnett, Kristen M.
2010 Analysis of Age-at-Death Estimation Using Data from a New, Modern Autopsy Sample—Part II: Sternal End of the Fourth Rib. *Journal of forensic sciences* 55(5):1152-1156.

Hillson, Simon
1996 *Dental anthropology*. Cambridge University Press, Cambridge.

2018 Dental pathology. *Biological anthropology of the human skeleton*:293-333.

Hitchins, Keith
2014a Between East to West, fourteenth century to 1774. In *A Concise History of Romania*, pp. 22-61. Cambrdige University Press, Cambridge.

2014b *A Concise History of Romania*. Cambridge Concise Histories. Cambridge University Press, Cambridge.

Hobbie, John E, and Erik A Hobbie
2006 15N in symbiotic fungi and plants estimates nitrogen and carbon flux rates in Arctic tundra. *Ecology* 87(4):816-822.

Houschyar, Khosrow S., Christian Tapking, Mimi R. Borrelli, Daniel Popp, Dominik Duscher, Zeshaan N. Maan, Malcolm P. Chelliah, Jingtao Li, Kamran Harati, Christoph Wallner, Susanne Rein, Dominik Pförringer, Georg Reumuth, Gerrit Grieb, Sylvain Mouraret, Mehran Dadras, Johannes M. Wagner, Jungul Y. Cha, Frank Siemers, Marcus Lehnhardt, and Björn Behr
2019 Wnt Pathway in Bone Repair and Regeneration – What Do We Know So Far. *Frontiers in cell and developmental biology* 6:170-170.

Hyland, Corrie, Jean-François Millaire, and Paul Szpak
2021 Migration and maize in the Virú Valley: Understanding life histories through multi-tissue carbon, nitrogen, sulfur, and strontium isotope analyses. *American Journal of Physical Anthropology* 176(1):21-35.

IBM Corp
2023 IBM SPSS Statistics for Macintosh. 29.0.2.0 ed. Vol. 27.0. IBM Corps, Armonk, NY.

Ion, Alexandra
2011 A brief overview of "Francisc J. Rainer" human osteological collection. *Ann Roum Anthropol* 48:24-32.

Iordachi, Constantin
2020 The Phanariot regime in the Romanian Principalities, 1711/1716–1821. In *The Routledge Handbook of Balkan and Southeast European History*, pp. 35-41. Routledge.

Ito, Y, JS Fitzsimmons, A Sanyal, MA Mello, N Mukherjee, and SW O'driscoll
2001 Localization of chondrocyte precursors in periosteum. *Osteoarthritis and Cartilage* 9(3):215-223.

Jílková, Michaela, Sylva Kaupová, Alena Černíková, Lumír Poláček, Jaroslav Brůžek, and Petr Velemínský
2019 Early medieval diet in childhood and adulthood and its reflection in the dental health of a Central European population (Mikulčice, 9th–10th centuries, Czech Republic). *Archives of oral biology* 107:104526.

Kaupová, Sylva, Petr Velemínský, Estelle Herrscher, Vladimír Sládek, Jiří Macháček, Lumír Poláček, and Jaroslav Brůžek
2018 Diet in transitory society: isotopic analysis of medieval population of Central Europe (ninth–eleventh century AD, Czech Republic). *Archaeological and Anthropological Sciences* 10:923-942.

Keeley, J. E., and D. R. Sandquist
1992 Carbon: freshwater plants. *Plant, cell and environment* 15(9):1021-1035.

Kendall, E. J., J. Montgomery, J. A. Evans, C. Stantis, and V. Mueller
2013 Mobility, mortality, and the middle ages: Identification of migrant individuals in a 14th century black death cemetery population. *American journal of physical anthropology* 150(2):210-222.

Kenyhercz, Michael W, Alexandra R Klales, Kyra E Stull, Kyle A McCormick, and Stephanie J Cole
2017 Worldwide population variation in pelvic sexual dimorphism: A validation and recalibration of the Klales et al. method. *Forensic Science International* 277:259. e251-259. e258.

Klales, Alexandra R., Stephen D. Ousley, and Jennifer M. Vollner
2012 A revised method of sexing the human innominate using Phenice's nonmetric traits and statistical methods. *American journal of physical anthropology* 149(1):104-114.

Klaus, Haagen D.
2014 Frontiers in the bioarchaeology of stress and disease: Cross-disciplinary perspectives from pathophysiology, human biology, and epidemiology. *American journal of physical anthropology* 155(2):294-308.

Klein, Sabra L, and Katie L Flanagan
2016 Sex differences in immune responses. *Nature Reviews Immunology* 16(10):626-638.

Knipper, Corina, Petra Held, Marc Fecher, Nicole Nicklisch, Christian Meyer, Hildrun Schreiber, Bernd Zich, Carola Metzner-Nebelsick, Vera Hubensack, and Leif Hansen
2015 Superior in life—superior in death: dietary distinction of central European prehistoric and medieval elites. *Current Anthropology* 56(4):579-589.

Knudson, Kelly J, Christina Torres-Rouff, and A Hoff
2020 Intersectionality and the multiplicity of identities in the Andean past. *Bioarchaeology and identity revisited*:185-198.

Knudson, Kelly J., Barra O'Donnabhain, Charisse Carver, Robin Cleland, and T. Douglas Price
2012 Migration and Viking Dublin: paleomobility and paleodiet through isotopic analyses. *Journal of archaeological science* 39(2):308-320.

Koch, Paul L
2007 Isotopic study of the biology of modern and fossil vertebrates. *Stable isotopes in ecology and environmental science*:99-154.

Koch, PL, ML Fogel, and N Tuross
1994 Tracing the diets of fossil animals using stable isotopes. In (K. Lajtha & B. Michener, Eds) Stable Isoptopes in Ecology and Environmental Science. Oxford: Blackwell Scientific Publications.

Kong, Young-Yun, Ulrich Feige, Iidiko Sarosi, Brad Bolon, Anna Tafuri, Sean Morony, Casey Capparelli, Ji Li, Robin Elliott, and Susan McCabe
1999 Activated T cells regulate bone loss and joint destruction in adjuvant arthritis through osteoprotegerin ligand. *Nature* 402(6759):304-309.

Kruschke, John
2015 *Doing Bayesian data analysis: A tutorial with R, JAGS, and STAN (2nd ed.)*. Academic Press, London, UK.

Kyle, Britney, Laurie J. Reitsema, Janelle Tyler, Pier Francesco Fabbri, and Stefano Vassallo
2018 Examining the osteological paradox: Skeletal stress in mass graves versus civilians at the Greek colony of Himera (Sicily). *American journal of physical anthropology* 167(1):161-172.

Kyle, Britney, Eduard Shehi, Marlon Koçi, and Laurie J Reitsema
2020 Bioarchaeological reconstruction of physiological stress during social transition in Albania. *International Journal of Paleopathology* 30:118-129.

Langley, Natalie R, L Meadows Jantz, Stephen D Ousley, Richard L Jantz, and George Milner
2016 Data collection procedures for forensic skeletal material 2.0. *University of Tennessee and Lincoln Memorial University*.

Larsen, Clark Spencer
2006 The agricultural revolution as environmental catastrophe: Implications for health and lifestyle in the Holocene. *Quaternary International* 150(1):12-20.

Lightfoot, Emma, Xinyi Liu, and Martin K. Jones
2013 Why move starchy cereals? A review of the isotopic evidence for prehistoric millet consumption across Eurasia. *World archaeology* 45(4):574-623.

Lightfoot, Emma, Magdalena Naum, Villu Kadakas, and Erki Russow
2016 The influence of social status and ethnicity on diet in mediaeval Tallinn as seen through stable isotope analysis. *Estonian Journal of Archaeology* 20(1):81.

Linderholm, Anna, and Anna Kjellström
2011 Stable isotope analysis of a medieval skeletal sample indicative of systemic disease from Sigtuna Sweden. *Journal of archaeological science* 38(4):925-933.

Maass, Claire K
2023 Race, Gender, and Intersectionality in the Bioarchaeology of the African Diaspora: Perspectives from Colonial Peru. *Journal of Archaeological Method and Theory* 30(3):805-827.

Maeda, Kazuhiro, Yasuhiro Kobayashi, Masanori Koide, Shunsuke Uehara, Masanori Okamoto, Akihiro Ishihara, Tomohiro Kayama, Mitsuru Saito, and Keishi Marumo
2019 The Regulation of Bone Metabolism and Disorders by Wnt Signaling. *International journal of molecular sciences* 20(22):5525.

Marcu Istrate, Daniela, and Annamaria Diana
2017 The Black Church Cemetery: Interdisciplinary approaches to the study of a medieval urban skeletal assemblage (Braşov, Romania). *Studies in Digital Heritage* 1(2):364-379.

Martinoia, Valentina, Stefano Benazzi, Mario Carić, and Siniša Radović
2021 Reconstructing the childhood diet of the individuals from the Middle Late Bronze Age Bezdanjača Cave, Croatia (ca. 1430 1290 BCE) using stable C and N isotope analysis of dentin collagen. *Journal of bioanthropology* 1(1):42-56.

Matsuo, Koichi, and Naoko Irie
2008 Osteoclast–osteoblast communication. *Archives of Biochemistry and Biophysics* 473(2):201-209.

McElreath, Richard
2018 *Statistical rethinking: A Bayesian course with examples in R and Stan*. Chapman and Hall/CRC.

McIlvaine, B. K.
2015 Implications of Reappraising the Iron-Deficiency Anemia Hypothesis. *International journal of osteoarchaeology* 25(6):997-1000.

McKinley, Jacqueline I
2004 Compiling a skeletal inventory: cremated human bone. In *Guidelines to the standards for recording human remains*, Vol 14, edited by Megan B. Brickley, and Jacqueline I McKinley, pp. 14-17. Southhampton & Reading: BABAO & IFA.

Mewes, R., H. Reich, N. Skoluda, F. Seele, and U. M. Nater
2017 Elevated hair cortisol concentrations in recently fled asylum seekers in comparison to permanently settled immigrants and non-immigrants. *Translational Psychiatry* 7(3):e1051-e1051.

Michener, R.H., and L. Kaufmnan
2007 Stable isotopes as tracers in marine food webs. In *Stable Isotopes in Ecology and Environmental Science*, edited by R. Michener, and Lajtha K., pp. 238-282. Blackwell Scientific Publiciations, Boston.

Minagawa, Masao, and Eitaro Wada
1984 Stepwise enrichment of 15N along food chains: Further evidence and the relation between δ15N and animal age. *Geochimica et cosmochimica acta* 48(5):1135-1140.

Ministry of Environment and Forests
2010 *Romania's Fifth National Communication on Climate Change under the United Nations Framework Convention on Climate Change*, www://unfccc.int.

Mitrea B. et al.
1955 Suceava-Cetatea Neamţului construction site. *Studies and researches of ancient history and archeology* 6(3-4):753-818.

Mitrea, B., and I. Nestor
1953 The Suceava Site. *Studies and researches of ancient history and archeology* 4(1-2):335-393.

Morgan, Gareth
1997 What, if any, is the effect of malnutrition on immunological competence? *The Lancet (British edition)* 349(9066):1693-1695.

Murphy, B.P., and D. M. J. S. Bowman
2006 Kangaroo Metabolism Does Not Cause the Relationship between Bone Collagen δ15N and Water Availability. *Functional ecology* 20(6):1062-1069.

Murray, Matthew L, and Margaret J Schoeninger
1988 Diet, status, and complex social structure in Iron Age Central Europe: some contributions of bone chemistry. In *Tribe and polity in Late Prehistoric Europe: Demography, production, and exchange in the evolution of complex social systems*, pp. 155-176. Springer.

Nesbitt, Mark, and G. D. Summers
1988 Some recent Discoveries of Millet (Panicum Miliaceum L. and Setaria italica (L.) P. Beauv.) at Excavations in Turkey and Iran. *Anatolian studies* 38(1):85-97.

Nestor, I.G. , M. Matei Diaconu, N. T. Martinovici, and Ş. Olteanu Constantinescu
1957 *Suceava archaeological site. Preliminary report on the excavations of the 1955 campaign*. Materiale şi cercetări arheologice

Nestor, I.G., T. Martinovici, M. Matei, G. Diaconu, S. Olteanu, and N. Constantinescu
1959 Suceava Archaeological Site. *Archaeological materials and research* 5:593-618.

O'Leary, Marion H
1981 Carbon isotope fractionation in plants. *Phytochemistry* 20(4):553-567.

O'Leary, Marion H.
1988 Carbon Isotopes in Photosynthesis. *Bioscience* 38(5):328-336.

Ogden, A
2008 Advances in the paleopathology of jaws and teeth. *Advances in Human Palaeopathology. New York: Wiley-Liss*:283-307.

Ortner, Donald J.
2003 *Identification of pathological conditions in human skeletal remains*. 2nd ed. ed. Academic, San Diego, Calif.

Oxenham, Marc Fredrick, and Ivor Cavill
2010 Porotic hyperostosis and cribra orbitalia: the erythropoietic response to iron-deficiency anaemia. *Anthropological Science* 118(3):199-200.

Oyewola, David Opeoluwa, Emmanuel Gbenga Dada, Juliana Ngozi Ndunagu, Terrang Abubakar Umar, and SA Akinwunmi
2021 COVID-19 risk factors, economic factors, and epidemiological factors nexus on economic impact: machine learning and structural equation modelling approaches. *Journal of the Nigerian Society of Physical Sciences*:395-405.

Palincaş, Nona, Corina Anca Simion, Gabriela Odilia Sava, Oana Gâza, Tiberiu Bogdan Sava, Bogdan Constantinescu, Daniela Stan, and Maria Mihaela Manea
2019 Archaeometry and Individual Biographies: Evidence from Radiocarbon Dating, Isotope-Based Diet Reconstruction and Metal Composition from the 14th-17th-Century Cemetery in Bărăşti (Southern Romania). *Bridging Science and Heritage in the Balkans*:16.

Pardo, L. H., P. H. Templer, C. L. Goodale, S. Duke, P. M. Groffman, M. B. Adams, P. Boeckx, J. Boggs, J. Campbell, B. Colman, J. Compton, B. Emmett, P. Gundersen, J. Kjønaas, G. Lovett, M. Mack, A. Magill, M. Mbila, M. J. Mitchell, G. McGee, S. McNulty, K. Nadelhoffer, S. Ollinger, D. Ross, H. Rueth, L. Rustad, P. Schaberg, S. Schiff, P. Schleppi, J. Spoelstra, and W. Wessel
2006 Regional Assessment of N Saturation Using Foliar and Root δ^{15}n. *Biogeochemistry* 80(2):143-171.

Pardo, Linda H., and Knute J. Nadelhoffer
2009 Using Nitrogen Isotope Ratios to Assess Terrestrial Ecosystems at Regional and Global Scales, pp. 221-249. Springer Netherlands, Dordrecht.

Park, Shin-Young, Sun-Hwa Kim, Si-Hyuck Kang, Chang-Hwan Yoon, Hyo-Jung Lee, Pil-Young Yun, Tae-Jin Youn, and In-Ho Chae

2019 Improved oral hygiene care attenuates the cardiovascular risk of oral health disease: a population-based study from Korea. *European heart journal* 40(14):1138-1145.

Pearson, JA, and REM Hedges
2007 Stable carbon and nitrogen analysis and the evidence for diet at Ecsegfalva and beyond. *The Early Neolithic on the Great Hungarian Plain: investigations of the Körös culture site of Ecsegfalva* 23:413-419.

Pecican, Ovidiu
2006 Between Magnanimitas and Blagorodia. Nobility in the Romanian Middle Ages. *Caietele Echinox* (10):282-285.

Pérez-Ramallo, Patxi, José Ignacio Lorenzo-Lizalde, Alexandra Staniewska, Belén Lopez, Michelle Alexander, Sara Marzo, Mary Lucas, Jana Ilgner, David Chivall, Aurora Grandal-d'Anglade, and Patrick Roberts
2022 Stable isotope analysis and differences in diet and social status in northern Medieval Christian Spain (9th–13th centuries CE). *Journal of Archaeological Science: Reports* 41:103325.

Petrík, Peter, Anja Petek-Petrik, Mohammad Mukarram, Bernhard Schuldt, and Laurent J Lamarque
2023 Leaf physiological and morphological constraints of water-use efficiency in C3 plants. *AoB PLANTS* 15(4).

Pilloud, Marin A, and Al W Schwitalla
2020 Re-evaluating traditional markers of stress in an archaeological sample from central California. *Journal of Archaeological Science* 116:105102.

Plecerová, Adéla, Sylva Kaupová Drtikolová, Jaromír Šmerda, Milan Stloukal, and Petr Velemínský
2020 Dietary reconstruction of the Moravian Lombard population (Kyjov, 5th–6th centuries AD, Czech Republic) through stable isotope analysis (δ13C, δ15N). *Journal of Archaeological Science: Reports* 29:102062.

Privat, Karen L, Tamsin C O'Connell, and Robert EM Hedges
2007 The distinction between freshwater-and terrestrial-based diets: methodological concerns and archaeological applications of sulphur stable isotope analysis. *Journal of Archaeological Science* 34(8):1197-1204.

Qin, Lei, Wen Liu, Huiling Cao, and Guozhi Xiao
2020 Molecular mechanosensors in osteocytes. *Bone research* 8(1):23-23.

Radu, C., L. Andreica, M. Constantinescu, and A. Soficaru
2016 Multiple Cases with Probable Treponemal Infection from 16th to 19th Centuries Romania: Multiple Cases with Probable Treponemal Infection. *International journal of osteoarchaeology* 26(4):563-573.

Ralston, Claira Elizabeth
2023 Gendered Bodies, Engendered Lives: Bioarchaeological Exploration of the Intersectionality of Gender, Health, and Trauma at Turkey Creek Pueblo, Arizona (AD 1225–1286), University of Nevada, Las Vegas.

Redfern, R. C., S. N. DeWitte, J. Beaumont, A. R. Millard, and C. Hamlin
2019 A new method for investigating the relationship between diet and mortality: hazard analysis using dietary isotopes. *Annals of human biology* 46(5):378-387.

Redfern, Rebecca, Sharon Dewitte, Janet Montgomery, and Rebecca Gowland
2018 A Novel Investigation into Migrant and Local Health-Statuses in the Past: A Case Study from Roman Britain.(Case study). *Bioarchaeology International* 2(1):20.

Reitsema, L. J., T. Kozłowski, and D. Makowiecki
2013 Human–environment interactions in medieval Poland: a perspective from the analysis of faunal stable isotope ratios. *Journal of Archaeological Science* 40(10):3636-3646.

Reitsema, Laurie, and Sammantha Holder
2018 Stable Isotope Analysis and the Study of Human Stress, Disease, and Nutrition. *Bioarchaeology international* 2(2):63-74.

Reitsema, Laurie J, Tomasz Kozłowski, Douglas E Crews, M Anne Katzenberg, and Wojciech Chudziak
2017 Resilience and local dietary adaptation in rural Poland, 1000–1400 CE. *Journal of Anthropological Archaeology* 45:38-52.

Reitsema, Laurie J., Douglas E. Crews, and Marek Polcyn
2010 Preliminary evidence for medieval Polish diet from carbon and nitrogen stable isotopes. *Journal of Archaeological Science* 37(7):1413-1423.

Richards, M. P., B. T. Fuller, and T. I. Molleson
2006 Stable isotope palaeodietary study of humans and fauna from the multi-period (Iron Age, Viking and Late Medieval) site of Newark Bay, Orkney. *Journal of Archaeological Science* 33(1):122-131.

Richards, M. P., and R. E. M. Hedges
1999 Stable Isotope Evidence for Similarities in the Types of Marine Foods Used by Late Mesolithic Humans at Sites Along the Atlantic Coast of Europe. *Journal of archaeological science* 26(6):717-722.

Richards, Michael P, Ben T Fuller, Matt Sponheimer, Todd Robinson, and Linda Ayliffe
2003 Sulphur isotopes in palaeodietary studies: a review and results from a controlled feeding experiment. *International Journal of Osteoarchaeology* 13(1-2):37-45.

Richards, Michael P, BT Fuller, and Robert EM Hedges
2001 Sulphur isotopic variation in ancient bone collagen from Europe: implications for human palaeodiet, residence mobility, and modern pollutant studies. *Earth and Planetary Science Letters* 191(3-4):185-190.

Riddell, Scott, Egill Erlendsson, Guðrún Gísladóttir, Kevin J Edwards, Jesse Byock, and Davide Zori
2018 Cereal cultivation as a correlate of high social status in medieval Iceland. *Vegetation History and Archaeobotany* 27:679-696.

Roberts, C. A., A. R. Millard, G. M. Nowell, D. R. Gröcke, C. G. Macpherson, D. G. Pearson, and D. H. Evans
2013 Isotopic tracing of the impact of mobility on infectious disease: The origin of people with treponematosis buried in hull, England, in the late medieval period. *American Journal of Physical Anthropology* 150(2):273-285.

Roberts, Patrick, Mary E Prendergast, Anneke Janzen, Ceri Shipton, James Blinkhorn, Jana Zech, Alison Crowther, Elizabeth A Sawchuk, Mathew Stewart, and Emmanuel Ndiema
2020 Late Pleistocene to Holocene human palaeoecology in the tropical environments of coastal eastern Africa. *Palaeogeography, Palaeoclimatology, Palaeoecology* 537:109438.

Rohleder, Nicolas, Ljiljana Joksimovic, Jutta M. Wolf, and Clemens Kirschbaum
2004 Hypocortisolism and increased glucocorticoid sensitivity of pro-Inflammatory cytokine production in Bosnian war refugees with posttraumatic stress disorder. *Biological Psychiatry* 55(7):745-751.

Roth, James D, and Keith A Hobson
2000 Stable carbon and nitrogen isotopic fractionation between diet and tissue of captive red fox: implications for dietary reconstruction. *Canadian Journal of zoology* 78(5):848-852.

Rüsz Fogarasi, Enikő
2009 Habitat, nutrition, crafts. In *The History of Transylvania, Vol. II (From 1541 to 1711)*, edited by Ioan-Aurel; Nägler In Pop, Thomas; Magyari, András pp. 181-197. Romanian Academy (Center for Transylvanian Studies.

Sattenspiel, Lisa, and Henry Harpending
1983 Stable Populations and Skeletal Age. *American antiquity* 48(3):489-498.

Schaefer, Maureen, Sue M Black, Maureen C Schaefer, and Louise Scheuer
2009 *Juvenile osteology*. Elsevier.

Schoeninger, Margaret J, and Michael J DeNiro
1984 Nitrogen and carbon isotopic composition of bone collagen from marine and terrestrial animals. *Geochimica et Cosmochimica acta* 48(4):625-639.

Scrimshaw, Nevin S, and John Paul SanGiovanni
1997 Synergism of nutrition, infection, and immunity: an overview. *The American journal of clinical nutrition* 66(2):464S-477S.

Sealy, Judith C., Nikolaas J. van der Merwe, Julia A. Lee Thorp, and John L. Lanham
1987 Nitrogen isotopic ecology in southern Africa: Implications for environmental and dietary tracing. *Geochimica et cosmochimica acta* 51(10):2707-2717.

Sharp, Z. D.
2007 Terminology, Standards, and Mass Spectrometry. In *Principles of stable isotope geochemistry*. Pearson education, Upper Saddle River, NJ.

Smid, Sanne C, and Yves Rosseel
2020 SEM with small samples: Two-step modeling and factor score regression versus Bayesian estimation with informative priors. In *Small sample size solutions*, pp. 239-254. Routledge.

Sponheimer, M., T. F. Robinson, B. L. Roeder, B. H. Passey, L. K. Ayliffe, T. E. Cerling, M. D. Dearing, and J. R. Ehleringer
2003 An experimental study of nitrogen flux in llamas: is 14N preferentially excreted? *Journal of archaeological science* 30(12):1649-1655.

Spradley, M. Katherine, and Richard L. Jantz
2011 Sex Estimation in Forensic Anthropology: Skull Versus Postcranial Elements: SEX ESTIMATION IN FORENSIC ANTHROPOLOGY. *Journal of forensic sciences* 56(2):289-296.

Steckel, Richard H, Clark Spencer Larsen, Paul W Sciulli, and Phillip L Walker
2006 Data collection codebook. *The global history of health project* 2006:1-41.

Sulzman, E.
2007 Stable isotope chemistry and measurement: a primer. In *Stable Isotopes in Ecology and Environmental Sciences*, edited by R. Michener, and K. Lajtha, pp. 1-21. 2nd ed. Blackwell Publishing, Malden, MA.

Székely, Maria Magdalena
2018 Food and Culinary Practices in 17th-Century Moldavia: Tastes, Techniques, Choices. In *Earthly delights: economies and cultures of food in Ottoman and Danubian*

Europe, c. 1500-1900, edited by Angela Jianu, and Violeta Barbu, pp. 170-216. Brill, Boston.

Szpak, P, K Krippner, and MP Richards
2017 Effects of sodium hydroxide treatment and ultrafiltration on the removal of humic contaminants from archaeological bone. *International Journal of Osteoarchaeology* 27(6):1070-1077.

Szpak, Paul
2014 Complexities of nitrogen isotope biogeochemistry in plant-soil systems: implications for the study of ancient agricultural and animal management practices. *Frontiers in plant science* 5:288-288.

Tafuri, Mary Anne, Oliver E. Craig, and Alessandro Canci
2009 Stable isotope evidence for the consumption of millet and other plants in Bronze Age Italy. *American journal of physical anthropology* 139(2):146-153.

Takayanagi, Hiroshi
2018 Osteoclast Biology and Bone Resorption. In *Primer on the Metabolic Bone Diseases and Disorders of Mineral Metabolism*, edited by J. P. Bilezikian, pp. 46-53. 9th ed. John Wiley & Sons, Incorporated.

Temple, Daniel H.
2019 Bioarchaeological evidence for adaptive plasticity and constraint: Exploring life-history trade-offs in the human past. *Evolutionary anthropology* 28(1):34-46.

Temple, Daniel H., and Alan H. Goodman
2014 Bioarcheology has a "health" problem: Conceptualizing "stress" and "health" in bioarcheological research. *American journal of physical anthropology* 155(2):186-191.

Tieszen, Larry L.
1991 Natural variations in the carbon isotope values of plants: Implications for archaeology, ecology, and paleoecology. *Journal of archaeological science* 18(3):227-248.

Tița, Claudia
2006 From various food to the food of Heaven. Voivode's guests and food codes in 16th-century Ungrovlahia. *Journal of Historical Anthropology* 8-9(13-22).

Torres-Rouff, Christina, and Kelly J. Knudson
2017 Integrating Identities: An Innovative Bioarchaeological and Biogeochemical Approach to Analyzing the Multiplicity of Identities in the Mortuary Record. *Current Anthropology* 58(3):381-409.

Treptow, Kurt W., Ioan Bolovan, Florin Constantiniu, Paul E. Michelson, Ioan Aurel Pop, Cristian Popa, Marcel Popa, Ioan Scurtu, Marcela Vultur, and Larry L. Watts
1997 *A History of Romania*. The Center for Romanian Studies.

Turner Tomaszewicz, Calandra N., Jeffrey A. Seminoff, Matthew D. Ramirez, and Carolyn M. Kurle
2015 Effects of demineralization on the stable isotope analysis of bone samples. *Rapid communications in mass spectrometry* 29(20):1879-1888.

Van Der Merwe, Nikolaas J., and J. C. Vogel
1978 13C Content of human collagen as a measure of prehistoric diet in woodland North America. *Nature (London)* 276(5690):815-816.

Ventresca Miller, Alicia R., James Johnson, Sergey Makhortykh, Claudia Gerling, Ludmilla Litvinova, Svetlana Andrukh, Gennady Toschev, Jana Zech, Petrus le Roux, Cheryl Makarewicz, Nicole Boivin, and Patrick Roberts
2021 Re-evaluating Scythian lifeways: Isotopic analysis of diet and mobility in Iron Age Ukraine. *PloS one* 16(3):e0245996-e0245996.

Ventresca Miller, Alicia R., and Cheryl A. Makarewicz
2019 Intensification in pastoralist cereal use coincides with the expansion of trans-regional networks in the Eurasian Steppe. *Scientific reports* 9(1):8363-8363.

Vidal-Ronchas, Rocio, Petra Rajić Šikanjić, Zrinka Premužić, Anita Rapan Papeša, and Emma Lightfoot
2019 Diet, sex, and social status in the Late Avar period: stable isotope investigations at Nuštar cemetery, Croatia. *Archaeological and Anthropological Sciences* 11:1727-1737.

Voas, Maddeline R., Kristina Killgrove, Robert H. Tykot, Zsolt Nyárádi, Andre Gonciar, and Jonathan D. Bethard
2021 Childhood in the Carpathians: An isotopic analysis of childhood diet and weaning in a medieval and Early Modern Transylvanian village. *Journal of archaeological science, reports* 38:103046.

Walker, Phillip L.
2008 Sexing skulls using discriminant function analysis of visually assessed traits. *American journal of physical anthropology* 136(1):39-50.

Walker, Phillip L., Rhonda R. Bathurst, Rebecca Richman, Thor Gjerdrum, and Valerie A. Andrushko
2009 The causes of porotic hyperostosis and cribra orbitalia: A reappraisal of the iron-deficiency-anemia hypothesis. *American journal of physical anthropology* 139(2):109-125.

Walter, Brittany S, Sharon N DeWitte, and Rebecca C Redfern
2016 Sex differentials in caries frequencies in Medieval London. *Archives of Oral Biology* 63:32-39.

Walter, Brittany S., Sharon N. DeWitte, Tosha Dupras, and Julia Beaumont
2020 Assessment of nutritional stress in famine burials using stable isotope analysis. *American journal of physical anthropology* 172(2):214-226.

Watanabe, Sumio
2010 Asymptotic Equivalence of Bayes Cross Validation and Widely Applicable Information Criterion in Singular Learning Theory. *arXiv.org*.

Watherston, Jeremy, and Jodie Ward
2023 Chapter 8 - Autosomal short tandem repeat (STR) profiling of human skeletal remains. In *Forensic Genetic Approaches for Identification of Human Skeletal Remains*, edited by Angie Ambers, pp. 167-197. Academic Press.

Weston, Darlene A.
2008 Investigating the specificity of periosteal reactions in pathology museum specimens. *American Journal of Physical Anthropology* 137:48-59.

2012 Nonspecific Infection in Paleopathology: Interpreting Periosteal Reactions. In *A companion to paleopathology*, edited by Anne L. Grauer. Wiley-Blackwell, Chichester, West Sussex.

Wilson, Jeremy J.
2014 Paradox and promise: Research on the role of recent advances in paleodemography and paleoepidemiology to the study of "health" in Precolumbian societies. *American journal of physical anthropology* 155(2):268-280.

Winner, William E., Sean C. Thomas, Joseph A. Berry, Barbara J. Bond, Clifton E. Cooper, Thomas M. Hinckley, James R. Ehleringer, Julianna E. Fessenden, Brian Lamb, Sarah McCarthy, Nate G. McDowell, Nathan Phillips, and Mathew Williams
2004 Canopy Carbon Gain and Water Use: Analysis of Old-growth Conifers in the Pacific Northwest. *Ecosystems* 7(5):482-497.

Wood, James W., George R. Milner, Henry C. Harpending, Kenneth M. Weiss, Mark N. Cohen, Leslie E. Eisenberg, Dale L. Hutchinson, Ramantas Jankauskas, Gintautas Cesnys, Gintautas Česnys, M. Anne Katzenberg, John R. Lukacs, Janet W. McGrath, Eric Abella Roth, Douglas H. Ubelaker, and Richard G. Wilkinson
1992 The Osteological Paradox: Problems of Inferring Prehistoric Health from Skeletal Samples. *Current Anthropology* 33(4):343-370.

World Health Organization
2023 Health and Wellbeing, accessed 2023.

Yaussy, Samantha L, Sharon N DeWitte, and Rebecca C Redfern
2016 Frailty and famine: Patterns of mortality and physiological stress among victims of famine in medieval London. *American Journal of Physical Anthropology* 160(2):272-283.

Zaharia, E., and N. Zaharia
2003
Middle Ages and the beginning of the modern era. B. Archaeological excavations, e) Schitisor. In *Archaeological and historical research in the Bicaz reservoir area*, edited by M. Petrescu Dîmbovița, and V. Spinei, pp. 229-241.

Zhu, Xiaomin, Wei Zhang, Hao Chen, and Jiangming Mo
2015 Impacts of nitrogen deposition on soil nitrogen cycle in forest ecosystems: A review. *Acta ecologica Sinica* 35(3):35-43.

Živaljević, Ivana, Nemanja Marković, and Milomir Maksimović
2019 Food worthy of kings and saints: fish consumption in the medieval monastery Studenica (Serbia). *Anthropozoologica* 54(1):179-201.

Zuckerman, Molly K, and John Crandall
2019 Reconsidering sex and gender in relation to health and disease in bioarchaeology. *Journal of Anthropological Archaeology* 54:161-171.

Zuckerman, Molly K., and George J. Armelagos
2011 The Origins of Biocultural Dimensions in Bioarchaeology. In *Social Bioarchaeology*, edited by Sabrina C. Agarwal, and Bonnie A. Glencross, pp. 13-43. Blackwell Publishing.

APPENDIX ONE: TESTS OF DIFFERENCE AND ASSOCIATION

Multiple Comparisons

Dependent Variable: Age

Scheffe

(I) Site	(J) Site	Mean Difference (I-J)	Std. Error	Sig.	95% Confidence Interval	
					Lower Bound	Upper Bound
1	2	2.34269	5.69320	.919	-11.7489	16.4343
	3	12.75060*	4.32084	.015	2.0558	23.4454
2	1	-2.34269	5.69320	.919	-16.4343	11.7489
	3	10.40791	4.94546	.113	-1.8329	22.6487
3	1	-12.75060*	4.32084	.015	-23.4454	-2.0558
	2	-10.40791	4.94546	.113	-22.6487	1.8329

*. The mean difference is significant at the 0.05 level.

Figure A.1. ANOVA with Scheffe's post hoc for differences in age structure between sites. Palatul Cnejilor (1), Schitișor (2), Suceava (3).

Chi-Square Tests

	Value	df	Asymptotic Significance (2-sided)
Pearson Chi-Square	4.403[a]	2	.111
Likelihood Ratio	4.495	2	.106
Linear-by-Linear Association	4.270	1	.039
N of Valid Cases	135		

a. 0 cells (.0%) have expected count less than 5. The minimum expected count is 11.20.

Figure A.2. Results of the Pearson Chi-Square Test for biological sex and site.

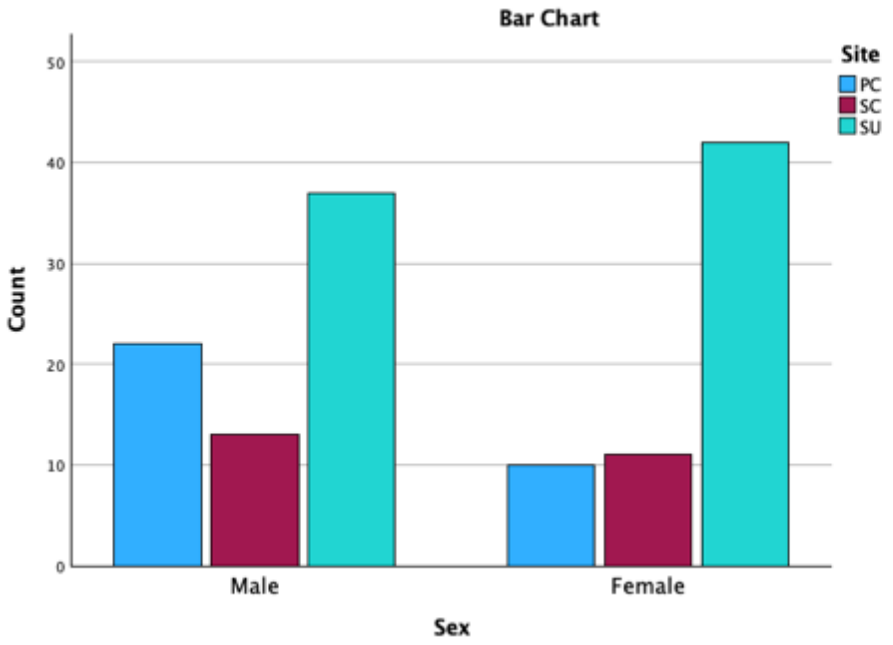


Figure A.3. Bar chart of the number of males and females at each site.

Chi-Square Tests

	Value	df	Asymptotic Significance (2-sided)
Pearson Chi-Square	5.594[a]	2	.061
Likelihood Ratio	6.102	2	.047
Linear-by-Linear Association	5.515	1	.019
N of Valid Cases	124		

a. 0 cells (.0%) have expected count less than 5. The minimum expected count is 5.48.

Figure A.4. Pearson Chi-Square Test for PNBF and preservation.

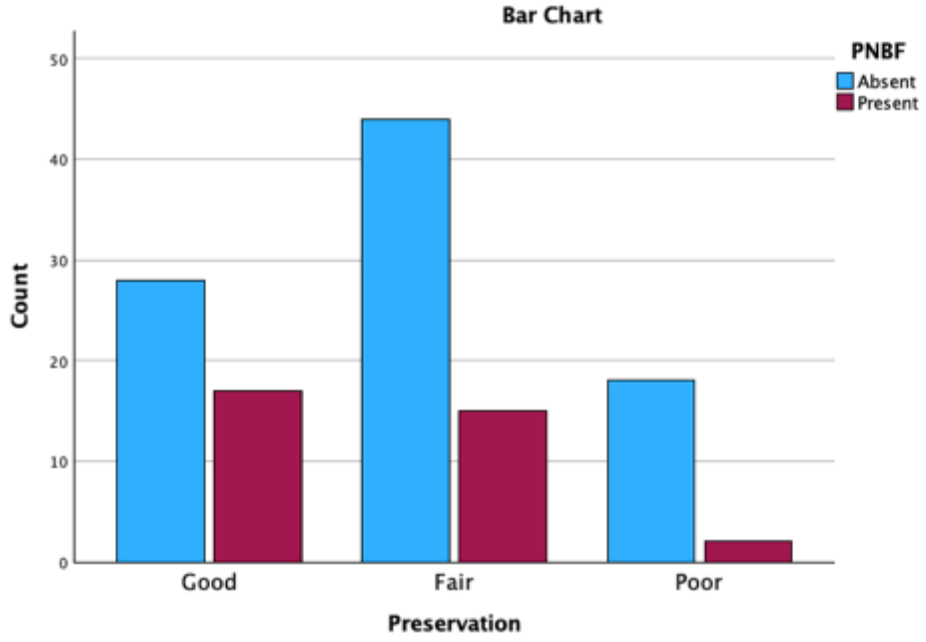


Figure A.5. Bar chart of presence/absence of PNBF by preservation.

Independent Samples Test

		Levene's Test for Equality of Variances		t-test for Equality of Means							
						Significance				95% Confidence Interval of the Difference	
		F	Sig.	t	df	One-Sided p	Two-Sided p	Mean Difference	Std. Error Difference	Lower	Upper
Age	Equal variances assumed	.160	.690	1.619	111	.054	.108	7.18912	4.43922	-1.60750	15.98574
	Equal variances not assumed			1.598	50.153	.058	.116	7.18912	4.49772	-1.84413	16.22238

Figure A.6. Levene's Test for Equality of Variances for PNBF and age-at-death.

Chi-Square Tests

	Value	df	Asymptotic Significance (2-sided)	Exact Sig. (2-sided)	Exact Sig. (1-sided)
Pearson Chi-Square	.750[a]	1	.386		
Continuity Correction[b]	.438	1	.508		
Likelihood Ratio	.754	1	.385		
Fisher's Exact Test				.420	.254
Linear-by-Linear Association	.744	1	.388		
N of Valid Cases	116				

a. 0 cells (.0%) have expected count less than 5. The minimum expected count is 16.12.

b. Computed only for a 2x2 table

Figure A.7. Pearson Chi-Square Test for PNBF and biological sex.

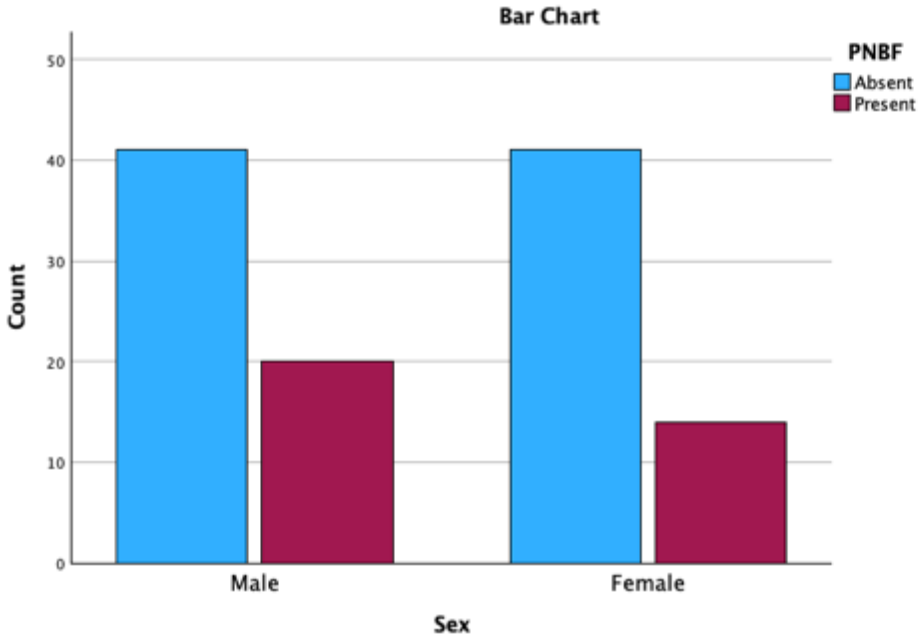


Figure A.8. Bar chart of presence/absence of PNBF for males and females.

Chi-Square Tests

	Value	df	Asymptotic Significance (2-sided)
Pearson Chi-Square	.437[a]	2	.804
Likelihood Ratio	.439	2	.803
Linear-by-Linear Association	.394	1	.530
N of Valid Cases	124		

a. 0 cells (.0%) have expected count less than 5. The minimum expected count is 6.58.

Figure A.9. Pearson Chi-Square Test for PNBF and site.

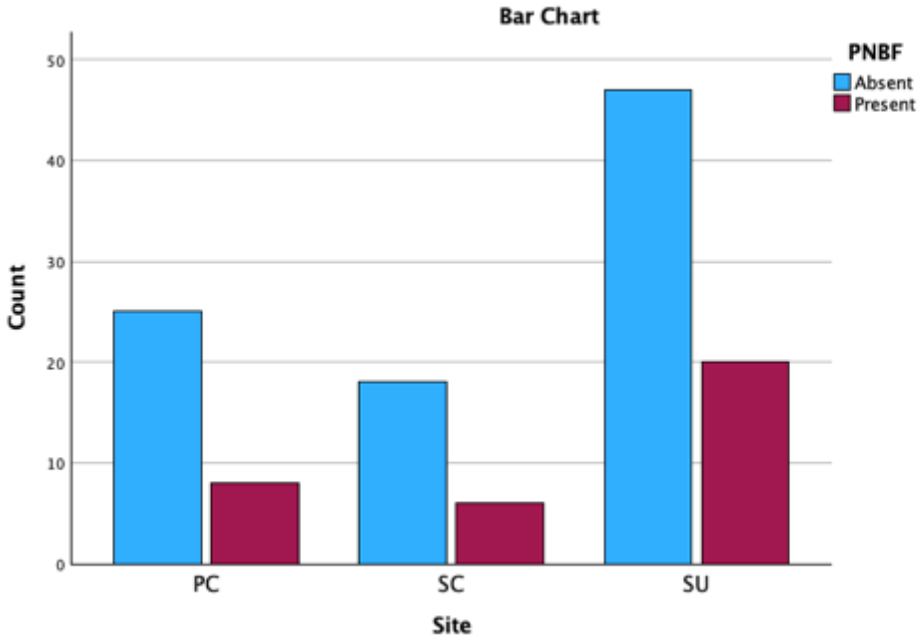


Figure A.10. Bar chart of presence/absence of PNBF for each site.

Chi-Square Tests

	Value	df	Asymptotic Significance (2-sided)
Pearson Chi-Square	4.829[a]	2	.089
Likelihood Ratio	7.903	2	.019
Linear-by-Linear Association	3.346	1	.067
N of Valid Cases	91		

a. 1 cells (16.7%) have expected count less than 5. The minimum expected count is 3.18.

Figure A.11. Pearson Chi-Square Test for PH and preservation.

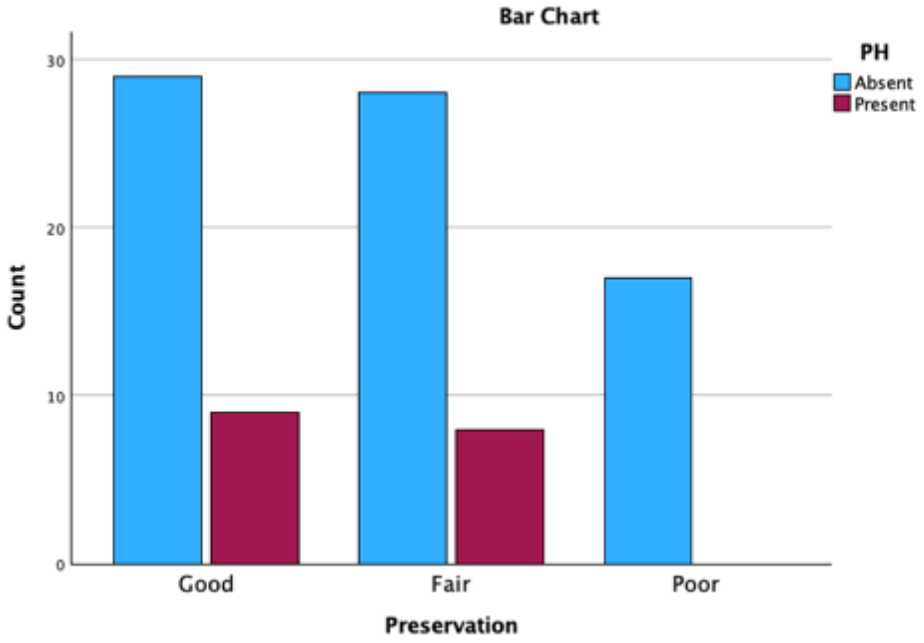


Figure A.12. Bar chart of presence/absence of PH by preservation.

Independent Samples Test

		Levene's Test for Equality of Variances		t-test for Equality of Means							
						Significance				95% Confidence Interval of the Difference	
		F	Sig.	t	df	One-Sided p	Two-Sided p	Mean Difference	Std. Error Difference	Lower	Upper
Age	Equal variances assumed	.461	.499	.769	85	.222	.444	4.23463	5.50529	-6.71136	15.18063
	Equal variances not assumed			.804	23.426	.215	.430	4.23463	5.26845	-6.65303	15.12229

Figure A.13. Levene's Test for Equality of Variances for PH and age-at-death.

Chi-Square Tests

	Value	df	Asymptotic Significance (2-sided)	Exact Sig. (2-sided)	Exact Sig. (1-sided)
Pearson Chi-Square	1.804[a]	1	.179		
Continuity Correction[b]	1.112	1	.292		
Likelihood Ratio	1.883	1	.170		
Fisher's Exact Test				.251	.146
Linear-by-Linear Association	1.782	1	.182		
N of Valid Cases	83				

a. 0 cells (.0%) have expected count less than 5. The minimum expected count is 6.33.

b. Computed only for a 2x2 table

Figure A.14. Pearson Chi-Square Test for PH and biological sex.

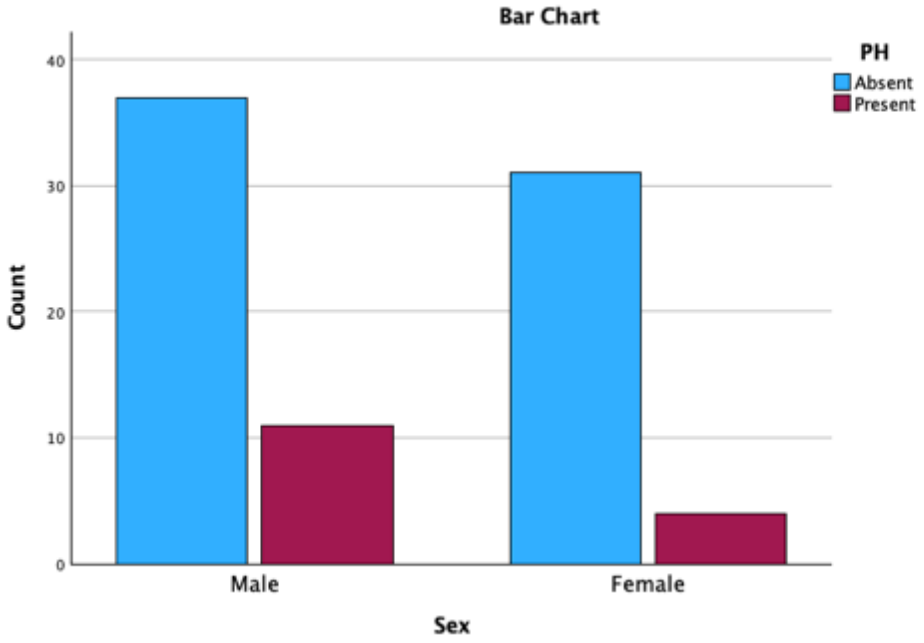


Figure A.15. Bar chart of presence/absence of PH for males and females.

Chi-Square Tests

	Value	df	Asymptotic Significance (2-sided)
Pearson Chi-Square	.094[a]	2	.954
Likelihood Ratio	.095	2	.953
Linear-by-Linear Association	.091	1	.763
N of Valid Cases	91		

a. 2 cells (33.3%) have expected count less than 5. The minimum expected count is 3.18.

Figure A.16. Pearson Chi-Square Test for PH and site.

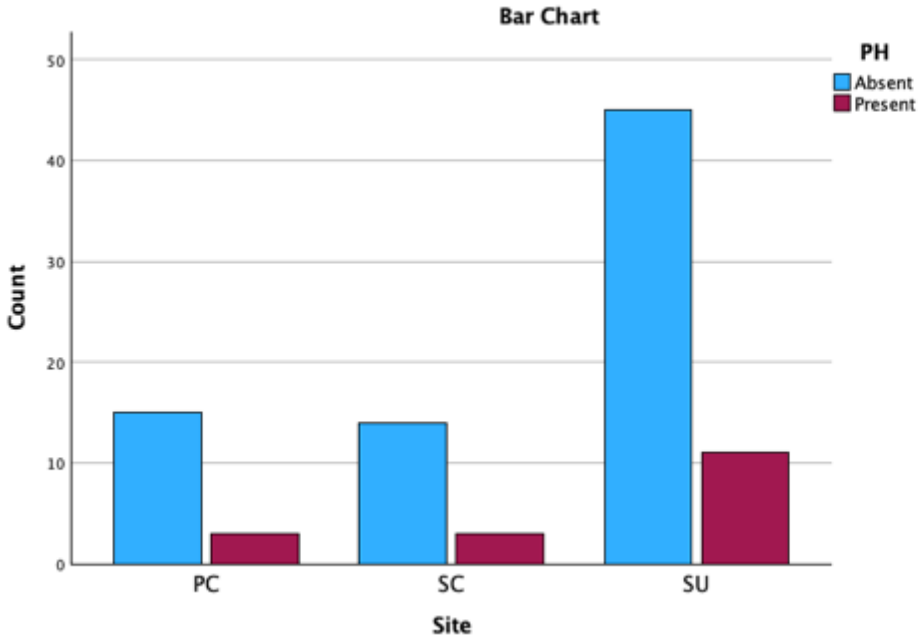


Figure A.17. Bar chart of presence/absence of PH for each site.

Chi-Square Tests

	Value	df	Asymptotic Significance (2-sided)
Pearson Chi-Square	4.035[a]	2	.133
Likelihood Ratio	3.885	2	.143
Linear-by-Linear Association	.560	1	.454
N of Valid Cases	98		

a. 3 cells (50.0%) have expected count less than 5. The minimum expected count is 1.94.

Figure A.18. Pearson Chi-Square Test for CO and preservation.

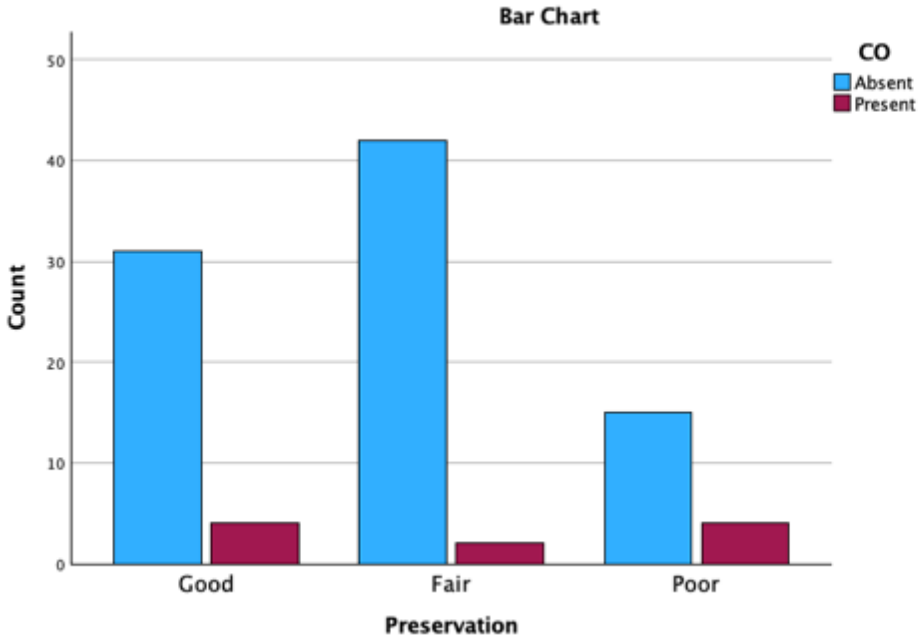


Figure A.19. Bar chart of presence/absence of CO by preservation.

Independent Samples Test

		Levene's Test for Equality of Variances		t-test for Equality of Means						
						Significance				95% Confidence Interval of the Difference
		F	Sig.	t	df	One-Sided p	Two-Sided p	Mean Difference	Std. Error Difference	Lower	Upper
Age	Equal variances assumed	.008	.927	.592	92	.278	.555	4.23404	7.14682	-9.96016	18.42824
	Equal variances not assumed			.549	9.459	.298	.596	4.23404	7.71654	-13.09375	21.56182

Figure A.20. Levene's Test for Equality of Variances for CO and age-at-death.

Chi-Square Tests

	Value	df	Asymptotic Significance (2-sided)	Exact Sig. (2-sided)	Exact Sig. (1-sided)
Pearson Chi-Square	1.174[a]	1	.279		
Continuity Correction[b]	.556	1	.456		
Likelihood Ratio	1.165	1	.280		
Fisher's Exact Test				.325	.227
Linear-by-Linear Association	1.161	1	.281		
N of Valid Cases	91				

a. 1 cells (25.0%) have expected count less than 5. The minimum expected count is 4.40.

b. Computed only for a 2x2 table

Figure A.21. Pearson Chi-Square Test for biological sex and CO.

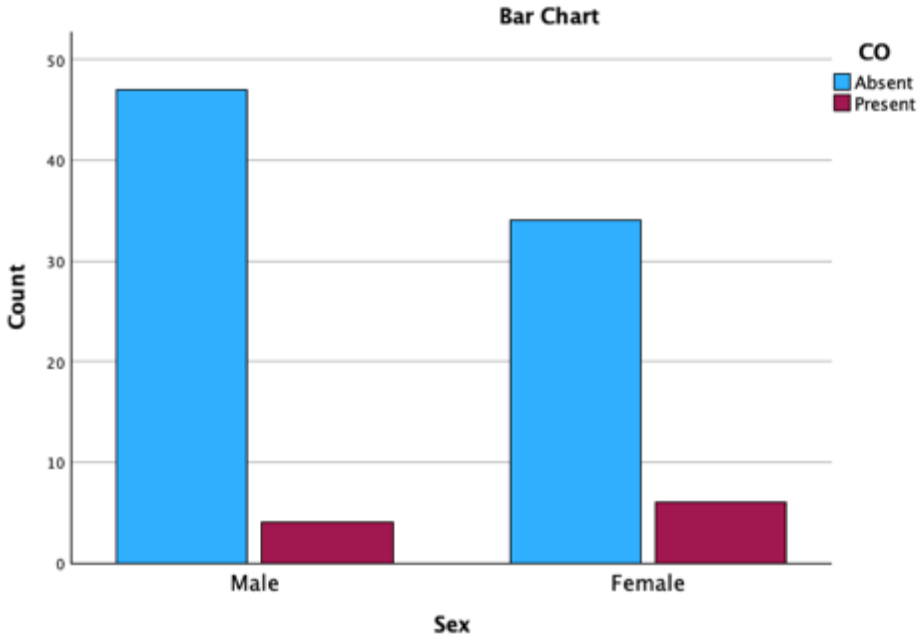


Figure A.22. Bar chart of presence/absence of CO for males and females.

Chi-Square Tests

	Value	df	Asymptotic Significance (2-sided)
Pearson Chi-Square	.419[a]	2	.811
Likelihood Ratio	.473	2	.789
Linear-by-Linear Association	.030	1	.863
N of Valid Cases	98		

a. 2 cells (33.3%) have expected count less than 5. The minimum expected count is 1.73.

Figure A.23. Pearson Chi-Square Test for CO and site.

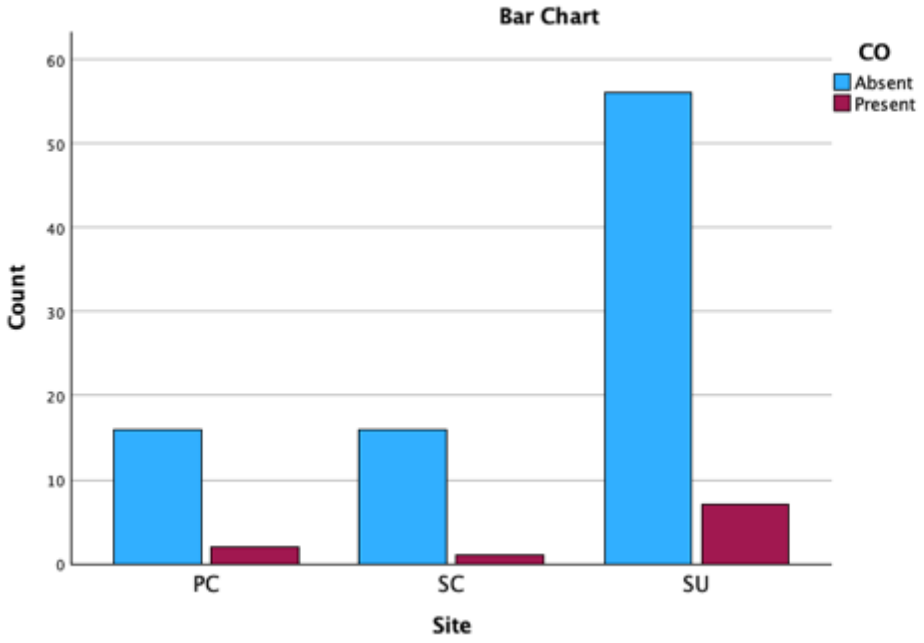


Figure A.24. Bar chart of presence/absence of CO for each site.

Chi-Square Tests

	Value	df	Asymptotic Significance (2-sided)
Pearson Chi-Square	.300[a]	2	.861
Likelihood Ratio	.305	2	.859
Linear-by-Linear Association	.155	1	.694
N of Valid Cases	105		

a. 0 cells (.0%) have expected count less than 5. The minimum expected count is 7.03.

Figure A.25. Pearson Chi-Square Test for caries and preservation.

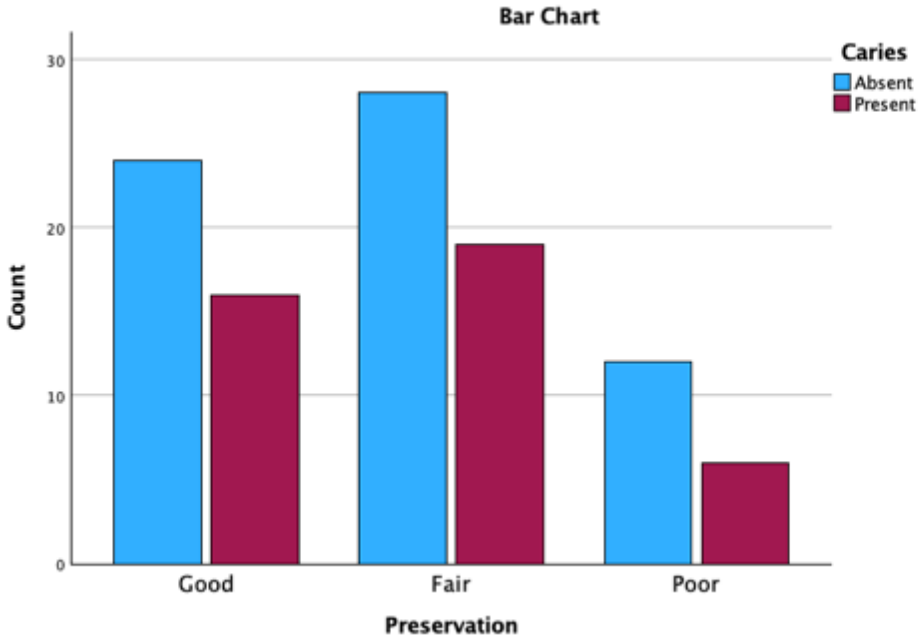


Figure A.26. Bar chart of presence/absence of caries by preservation.

Independent Samples Test

		Levene's Test for Equality of Variances		t-test for Equality of Means							
						Significance				95% Confidence Interval of the Difference	
		F	Sig.	t	df	One-Sided p	Two-Sided p	Mean Difference	Std. Error Difference	Lower	Upper
Age	Equal variances assumed	.007	.933	-.670	95	.252	.504	-2.92302	4.36195	-11.58258	5.73655
	Equal variances not assumed			-.673	82.727	.252	.503	-2.92302	4.34545	-11.56636	5.72033

Figure A.27. Levene's Test for Equality of Variances for caries and age-at-death.

Chi-Square Tests

	Value	df	Asymptotic Significance (2-sided)	Exact Sig. (2-sided)	Exact Sig. (1-sided)
Pearson Chi-Square	3.429[a]	1	.064		
Continuity Correction[b]	2.692	1	.101		
Likelihood Ratio	3.459	1	.063		
Fisher's Exact Test				.091	.050
Linear-by-Linear Association	3.392	1	.065		
N of Valid Cases	93				

a. 0 cells (.0%) have expected count less than 5. The minimum expected count is 18.39.

b. Computed only for a 2x2 table

Figure A.28. Pearson Chi-Square Test for biological sex and caries.

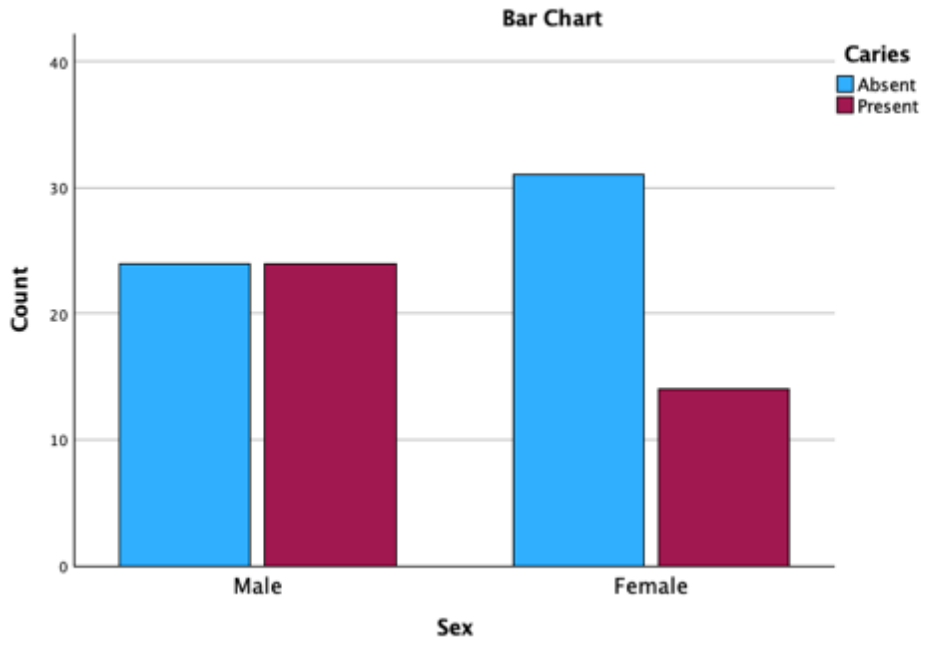


Figure A.29. Bar chart of presence/absence of caries for males and females.

Chi-Square Tests

	Value	df	Asymptotic Significance (2-sided)
Pearson Chi-Square	5.002[a]	2	.082
Likelihood Ratio	4.914	2	.086
Linear-by-Linear Association	1.669	1	.196
N of Valid Cases	105		

a. 0 cells (.0%) have expected count less than 5. The minimum expected count is 6.64.

Figure A.30. Pearson Chi-Square Test for caries and site.

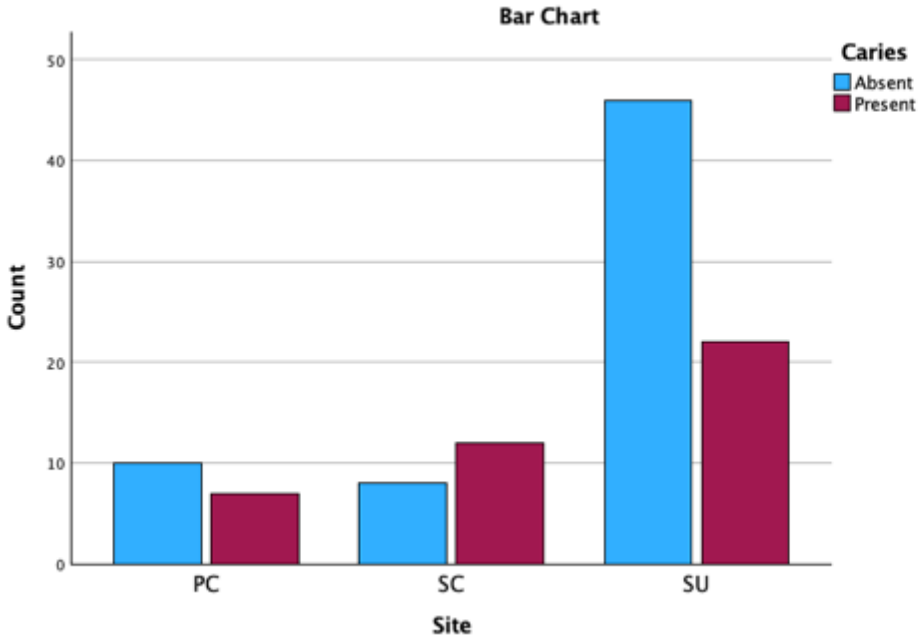


Figure A.31. Bar chart of presence/absence of caries for each site.

Chi-Square Tests

	Value	df	Asymptotic Significance (2-sided)
Pearson Chi-Square	2.369[a]	2	.306
Likelihood Ratio	2.426	2	.297
Linear-by-Linear Association	.033	1	.855
N of Valid Cases	110		

a. 1 cells (16.7%) have expected count less than 5. The minimum expected count is 4.91.

Figure A.32. Pearson Chi-Square Test for abscesses and preservation.

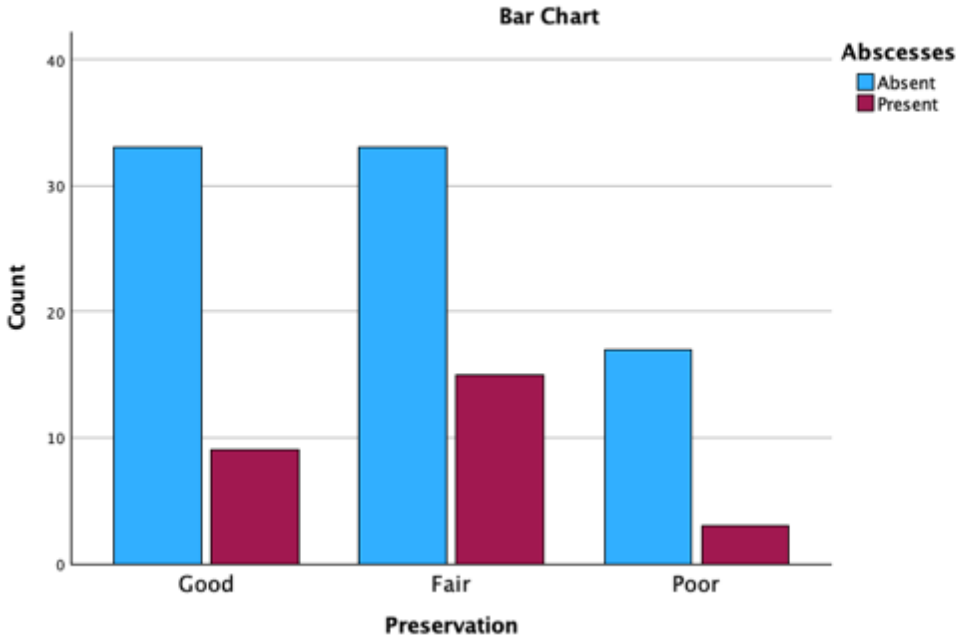


Figure A.33. Bar chart of presence/absence of abscesses by preservation.

Independent Samples Test

		Levene's Test for Equality of Variances		t-test for Equality of Means						
						Significance				95% Confidence Interval of the Difference
		F	Sig.	t	df	One-Sided p	Two-Sided p	Mean Difference	Std. Error Difference	Lower	Upper
Age	Equal variances assumed	15.410	<.001	.542	99	.294	.589	2.54280	4.68983	-6.76284	11.84844
	Equal variances not assumed			.618	61.259	.269	.539	2.54280	4.11467	-5.68428	10.76989

Figure A.34. Levene's Test for Equality of Variances for abscesses and age-at-death.

Chi-Square Tests

	Value	df	Asymptotic Significance (2-sided)	Exact Sig. (2-sided)	Exact Sig. (1-sided)
Pearson Chi-Square	1.981[a]	1	.159		
Continuity Correction[b]	1.387	1	.239		
Likelihood Ratio	2.010	1	.156		
Fisher's Exact Test				.176	.119
Linear-by-Linear Association	1.960	1	.161		
N of Valid Cases	97				

a. 0 cells (.0%) have expected count less than 5. The minimum expected count is 12.06.

b. Computed only for a 2x2 table

Figure A.35. Pearson Chi-Square Test for biological sex and abscesses.

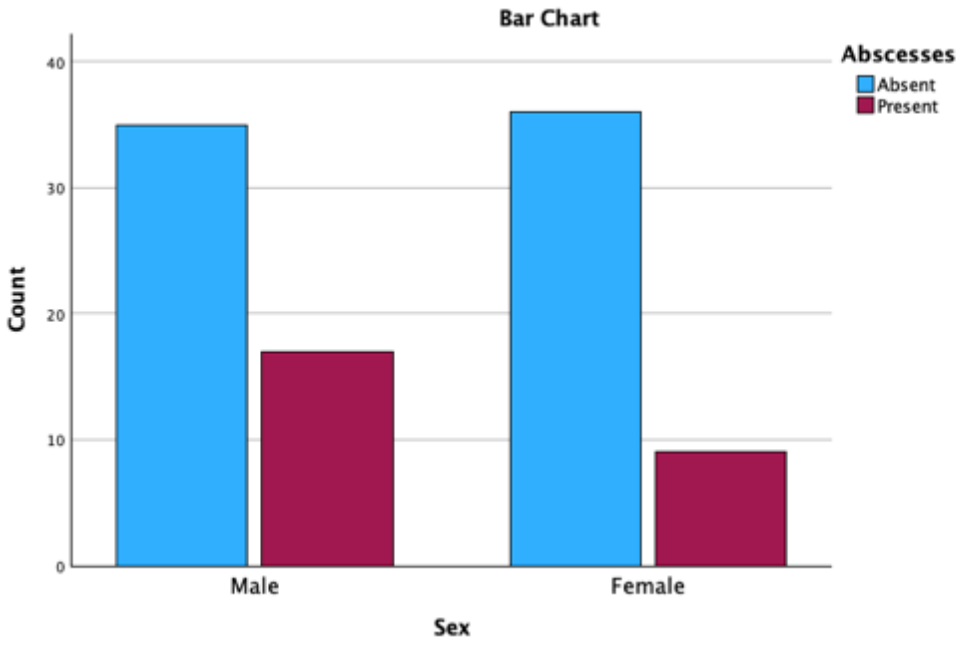


Figure A.36. Bar chart of presence/absence of abscesses for males and females.

Chi-Square Tests

	Value	df	Asymptotic Significance (2-sided)
Pearson Chi-Square	.318[a]	2	.853
Likelihood Ratio	.312	2	.856
Linear-by-Linear Association	.089	1	.766
N of Valid Cases	110		

a. 1 cells (16.7%) have expected count less than 5. The minimum expected count is 4.17.

Figure A.37. Pearson Chi-Square Test for abscesses and site.

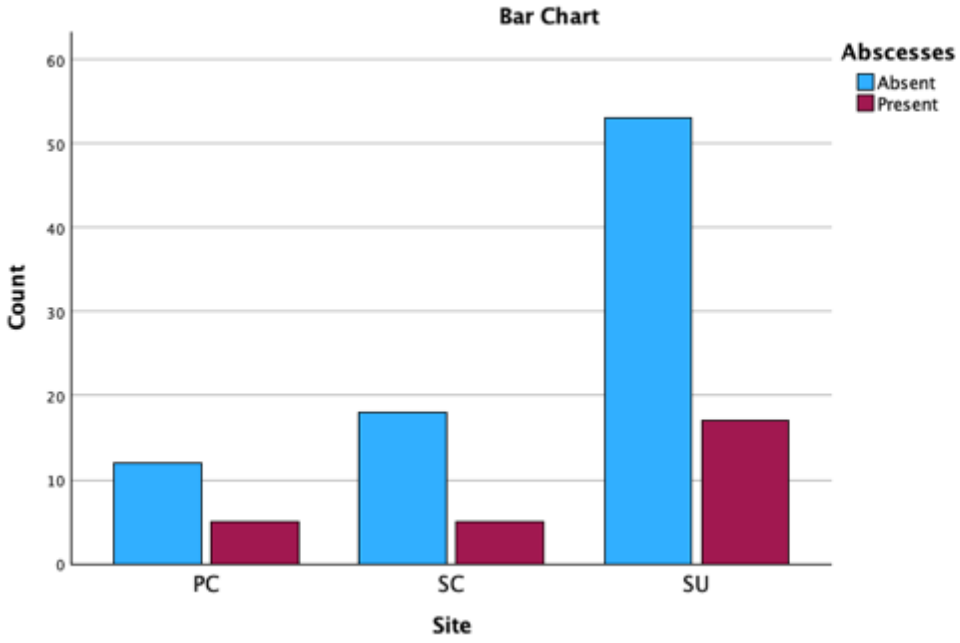


Figure A.38. Bar chart of presence/absence of abscesses for each site.

Chi-Square Tests

	Value	df	Asymptotic Significance (2-sided)
Pearson Chi-Square	5.422[a]	2	.066
Likelihood Ratio	6.431	2	.040
Linear-by-Linear Association	.840	1	.359
N of Valid Cases	97		

a. 1 cells (16.7%) have expected count less than 5. The minimum expected count is 4.38.

Figure A.39. Pearson Chi-Square Test for PD and preservation.

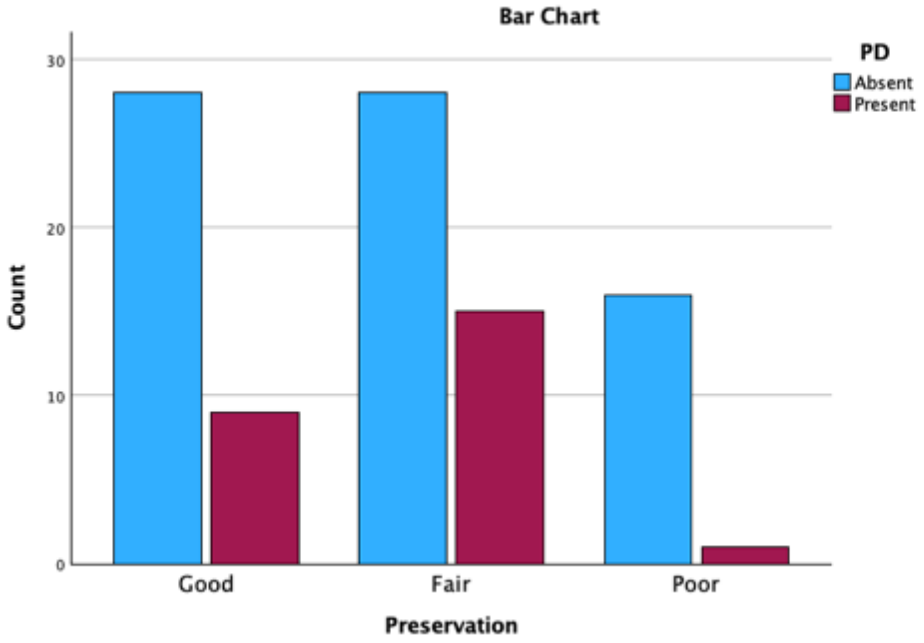


Figure A.40. Bar chart of presence/absence of PD by preservation.

Independent Samples Test

		Levene's Test for Equality of Variances		t-test for Equality of Means						
						Significance				95% Confidence Interval of the Difference
		F	Sig.	t	df	One-Sided p	Two-Sided p	Mean Difference	Std. Error Difference	Lower	Upper
Age	Equal variances assumed	.102	.750	-.983	86	.164	.328	-4.91308	4.99674	-14.84626	5.02010
	Equal variances not assumed			-.974	43.296	.168	.335	-4.91308	5.04369	-15.08265	5.25649

Figure A.41. Levene's Test for Equality of Variances for PD and age-at-death.

Chi-Square Tests

	Value	df	Asymptotic Significance (2-sided)	Exact Sig. (2-sided)	Exact Sig. (1-sided)
Pearson Chi-Square	1.227[a]	1	.268		
Continuity Correction[b]	.750	1	.386		
Likelihood Ratio	1.238	1	.266		
Fisher's Exact Test				.337	.194
Linear-by-Linear Association	1.212	1	.271		
N of Valid Cases	85				

a. 0 cells (.0%) have expected count less than 5. The minimum expected count is 11.29.

b. Computed only for a 2x2 table

Figure A.42. Pearson Chi-Square Test for biological sex and PD.

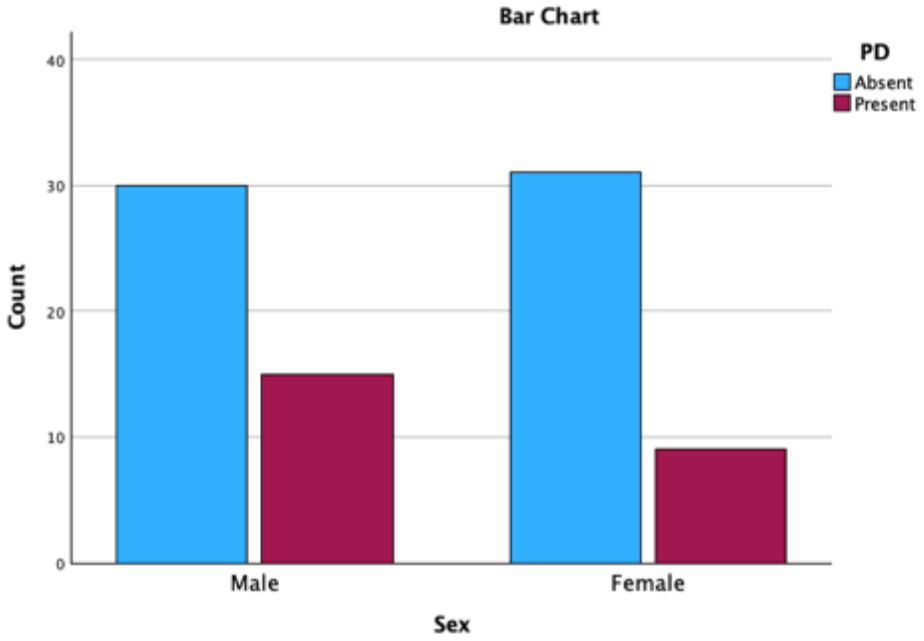


Figure A.43. Bar chart of presence/absence of PD for males and females.

Chi-Square Tests

	Value	df	Asymptotic Significance (2-sided)
Pearson Chi-Square	1.161[a]	2	.560
Likelihood Ratio	1.117	2	.572
Linear-by-Linear Association	1.149	1	.284
N of Valid Cases	97		

a. 2 cells (33.3%) have expected count less than 5. The minimum expected count is 3.61.

Figure A.44. Pearson Chi-Square Test for PD and site.

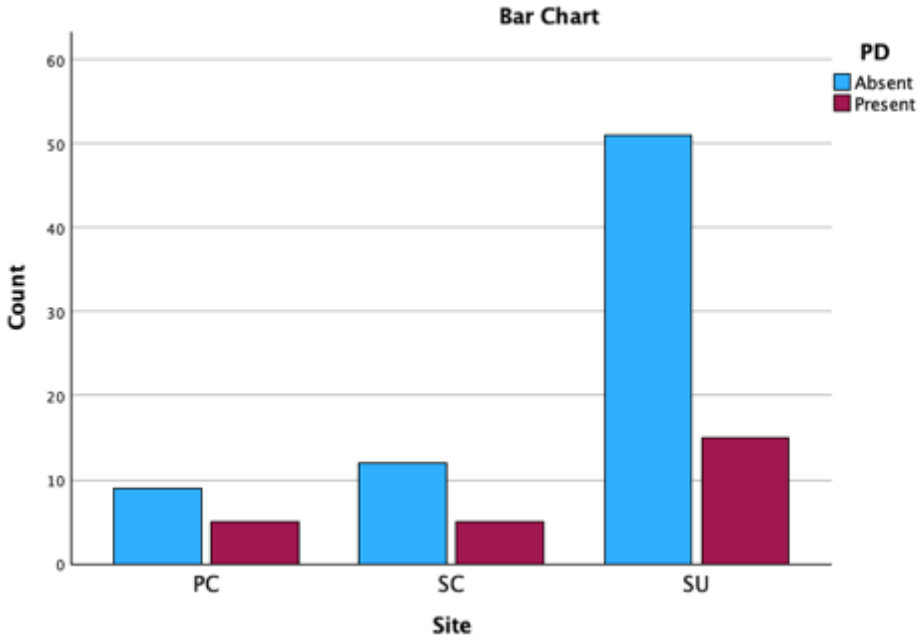


Figure A.45. Bar chart of presence/absence of PD for each site.

Group Statistics

	Sex	N	Mean	Std. Deviation	Std. Error Mean
d13C_Femur	Male	62	-16.42550	2.984751	.379064
	Female	56	-17.39659	2.619659	.350067

Figure A.46. Descriptive statistics for $\delta^{13}C$ femur values for males and females.

Independent Samples Test

		Levene's Test for Equality of Variances		t-test for Equality of Means							
						Significance				95% Confidence Interval of the Difference	
		F	Sig.	t	df	One-Sided p	Two-Sided p	Mean Difference	Std. Error Difference	Lower	Upper
d13C_Femur	Equal variances assumed	5.558	.020	1.870	116	.032	.064	.971089	.519425	-.057697	1.999876
	Equal variances not assumed			1.882	115.911	.031	.062	.971089	.515981	-.050884	1.993062

Figure A.47. Levene's Test for Equality of Variances for $\delta^{13}C$ femur values and sex.

Group Statistics

	Sex	N	Mean	Std. Deviation	Std. Error Mean
d13C_Rib	Male	55	-16.15878	3.255668	.438994
	Female	50	-17.51014	2.528756	.357620

Figure A.48. Descriptive statistics for $\delta^{13}C$ rib values for males and females.

Independent Samples Test

		Levene's Test for Equality of Variances		t-test for Equality of Means							
						Significance				95% Confidence Interval of the Difference	
		F	Sig.	t	df	One-Sided p	Two-Sided p	Mean Difference	Std. Error Difference	Lower	Upper
d13C_Rib	Equal variances assumed	11.882	<.001	2.358	103	.010	.020	1.351358	.572999	.214951	2.487766
	Equal variances not assumed			2.387	100.619	.009	.019	1.351358	.566223	.228073	2.474643

Figure A.49. Levene's Test for Equality of Variances for $\delta^{13}C$ rib and sex.

ANOVA

d13C_Femur

	Sum of Squares	df	Mean Square	F	Sig.
Between Groups	526.654	2	263.327	57.458	<.001
Within Groups	582.030	127	4.583		
Total	1108.684	129			

Figure A.50. One-Way ANOVA for $\delta^{13}C$ femur values and site.

Multiple Comparisons

Dependent Variable: d13C_Femur

Scheffe

(I) Site	(J) Site	Mean Difference (I-J)	Std. Error	Sig.	95% Confidence Interval	
					Lower Bound	Upper Bound
PC	SC	1.681329*	.558173	.013	.29879	3.06387
	SU	4.518285*	.433588	<.001	3.44433	5.59224
SC	PC	-1.681329*	.558173	.013	-3.06387	-.29879
	SU	2.836956*	.508282	<.001	1.57799	4.09592
SU	PC	-4.518285*	.433588	<.001	-5.59224	-3.44433
	SC	-2.836956*	.508282	<.001	-4.09592	-1.57799

*. The mean difference is significant at the 0.05 level.

Figure A.51. ANOVA with Scheffe's post hoc for differences in $\delta^{13}C$ femur values between sites.

ANOVA

d13C_Rib

	Sum of Squares	df	Mean Square	F	Sig.
Between Groups	536.413	2	268.206	59.321	<.001
Within Groups	501.857	111	4.521		
Total	1038.269	113			

Figure A.52. One-Way ANOVA for $\delta^{13}C$ rib values and site.

Multiple Comparisons

Dependent Variable: d13C_Rib

Scheffe

(I) Site	(J) Site	Mean Difference (I-J)	Std. Error	Sig.	95% Confidence Interval	
					Lower Bound	Upper Bound
PC	SC	2.045367*	.582316	.003	.60055	3.49018
	SU	5.021367*	.475459	<.001	3.84168	6.20105
SC	PC	-2.045367*	.582316	.003	-3.49018	-.60055
	SU	2.976000*	.513555	<.001	1.70179	4.25021
SU	PC	-5.021367*	.475459	<.001	-6.20105	-3.84168
	SC	-2.976000*	.513555	<.001	-4.25021	-1.70179

*. The mean difference is significant at the 0.05 level.

Figure A.53. ANOVA with Scheffe's post hoc for differences in $\delta^{13}C$ rib values between sites.

Group Statistics

	Sex	N	Mean	Std. Deviation	Std. Error Mean
d15N_Femur	Male	62	9.98794	1.045227	.132744
	Female	56	10.05786	.859466	.114851

Figure A.54. Descriptive statistics for $\delta^{15}N$ femur values for males and females.

Independent Samples Test

		Levene's Test for Equality of Variances		t-test for Equality of Means							
						Significance				95% Confidence Interval of the Difference	
		F	Sig.	t	df	One-Sided p	Two-Sided p	Mean Difference	Std. Error Difference	Lower	Upper
d15N_Femur	Equal variances assumed	2.055	.154	-.394	116	.347	.694	-.069922	.177281	-.421048	.281205
	Equal variances not assumed			-.398	115.023	.346	.691	-.069922	.175533	-.417617	.277774

Figure A.55. Levene's Test for Equality of Variances for $\delta^{15}N$ femur values and sex.

Group Statistics

	Sex	N	Mean	Std. Deviation	Std. Error Mean
d15N_Rib	Male	55	10.26698	.917754	.123750
	Female	50	10.09712	.772855	.109298

Figure A.56. Descriptive statistics for $\delta^{15}N$ rib values for males and females.

Independent Samples Test

		Levene's Test for Equality of Variances		t-test for Equality of Means							
						Significance				95% Confidence Interval of the Difference	
		F	Sig.	t	df	One-Sided p	Two-Sided p	Mean Difference	Std. Error Difference	Lower	Upper
d15N_Rib	Equal variances assumed	3.107	.081	1.020	103	.155	.310	.169862	.166463	-.160278	.500001
	Equal variances not assumed			1.029	102.422	.153	.306	.169862	.165106	-.157610	.497333

Figure A.57. Levene's Test for Equality of Variances for $\delta^{15}N$ rib values and sex.

ANOVA

d15N_Femur

	Sum of Squares	df	Mean Square	F	Sig.
Between Groups	34.545	2	17.272	28.082	<.001
Within Groups	78.113	127	.615		
Total	112.658	129			

Figure A.58. One-Way ANOVA for $\delta^{15}N$ femur values and site.

Multiple Comparisons

Dependent Variable: d15N_Femur

Scheffe

(I) Site	(J) Site	Mean Difference (I-J)	Std. Error	Sig.	95% Confidence Interval	
					Lower Bound	Upper Bound
PC	SC	-.100164	.204484	.887	-.60665	.40632
	SU	-1.068642*	.158843	<.001	-1.46208	-.67520
SC	PC	.100164	.204484	.887	-.40632	.60665
	SU	-.968478*	.186206	<.001	-1.42969	-.50726
SU	PC	1.068642*	.158843	<.001	.67520	1.46208
	SC	.968478*	.186206	<.001	.50726	1.42969

*. The mean difference is significant at the 0.05 level.

Figure A.59. ANOVA with Scheffe's post hoc for differences in $\delta^{15}N$ femur values between sites.

ANOVA

d15N_Rib

	Sum of Squares	df	Mean Square	F	Sig.
Between Groups	33.280	2	16.640	37.207	<.001
Within Groups	49.642	111	.447		
Total	82.922	113			

Figure A.60. One-Way ANOVA for δ^{15}N rib values and site.

Multiple Comparisons

Dependent Variable: d15N_Rib

Scheffe

(I) Site	(J) Site	Mean Difference (I-J)	Std. Error	Sig.	95% Confidence Interval Lower Bound	95% Confidence Interval Upper Bound
PC	SC	-.053983	.183145	.958	-.50839	.40043
	SU	-1.105467*	.149537	<.001	-1.47649	-.73444
SC	PC	.053983	.183145	.958	-.40043	.50839
	SU	-1.051483*	.161519	<.001	-1.45224	-.65073
SU	PC	1.105467*	.149537	<.001	.73444	1.47649
	SC	1.051483*	.161519	<.001	.65073	1.45224

*. The mean difference is significant at the 0.05 level.

Figure A.61. ANOVA with Scheffe's post hoc for differences in δ^{15}N rib values between sites.

APPENDIX TWO: CARBON AND NITROGEN STABLE ISOTOPE DATA SET AND BIPLOTS

Table A.1. Carbon and nitrogen stable isotope data set for all adult rib samples. Asterice* indicates samples with a C:N > 3.6 suggesting an unreliable value due to diagenesis.

Sample ID	$\delta^{15}N_{AIR}$	$\delta^{13}C_{VPDB}$	%N	%C	C:N
PC_Rib_#25	10.342	-13.790	13.615	42.386	3.6
PC_Rib_#26	8.695	-13.741	14.111	41.016	3.4
PC_Rib_#27	9.762	-14.872	14.350	40.920	3.3
PC_Rib_#28	10.539	-19.694	7.564	21.653	3.3
PC_Rib_#29	9.938	-11.767	13.768	41.103	3.5
PC_Rib_#31	9.329	-11.683	15.329	43.701	3.3
PC_Rib_#33	10.163	-12.647	13.723	39.859	3.4
PC_Rib_#34	10.562	-18.757	12.904	35.923	3.2
PC_Rib_#35	10.465	-17.492	13.958	41.215	3.4
PC_Rib_#36	8.909	-10.808	7.851	22.382	3.3
PC_Rib_#37	9.269	-11.827	14.329	41.773	3.4
SCHIT_Rib_#38	9.709	-11.666	11.079	35.692	3.8*
SCHIT_Rib_#39	9.335	-13.363	8.085	25.421	3.7*
SCHIT_Rib_#40	9.635	-19.206	13.644	39.330	3.4
SCHIT_Rib_#41	9.402	-18.378	12.175	38.064	3.6
SCHIT_Rib_#42	9.825	-20.394	11.981	34.880	3.4
SCHIT_Rib_#44	9.710	-16.626	7.708	25.578	3.9*
SCHIT_Rib_#45	8.943	-11.408	8.438	23.456	3.2
SCHIT_Rib_#46	9.450	-19.637	12.843	37.440	3.4
SCHIT_Rib_#47	11.065	-13.408	12.634	38.794	3.6
SCHIT_Rib_#48	9.638	-11.269	13.557	40.075	3.4
SCHIT_Rib_#49	8.723	-16.490	13.989	41.035	3.4
SUC_Rib_#53	9.251	-19.432	7.952	22.633	3.3
SUC_Rib_#54	9.798	-18.453	12.113	34.145	3.3
SUC_Rib_#57	9.520	-18.750	12.442	34.978	3.3
SUC_Rib_#63	12.083	-19.574	9.906	28.477	3.4
SUC_Rib_#67	11.338	-19.650	11.674	38.770	3.9*
SUC_Rib_#69	11.630	-19.299	14.761	42.365	3.3
SUC_Rib_#73	11.167	-19.537	14.518	41.683	3.3
SUC_Rib_#76	10.737	-19.254	14.631	42.343	3.4
SUC_Rib_#77	11.959	-17.723	14.134	41.001	3.4
SUC_Rib_#78	9.895	-19.210	13.892	40.338	3.4

Table A.1 Continued

SUC_Rib_#79	11.540	-19.034	14.336	41.122	3.3
SUC_Rib_#81	10.033	-19.998	14.559	41.597	3.3
SUC_Rib_#82	10.643	-19.146	14.676	42.760	3.4
SUC_Rib_#83	10.154	-19.077	16.434	45.221	3.2
SUC_Rib_#85	11.323	-17.087	14.026	40.948	3.4
SUC_Rib_#87	9.582	-18.906	14.507	41.220	3.3
SUC_Rib_#88	9.954	-18.996	16.235	44.936	3.2
SUC_Rib_#89	11.206	-20.048	11.998	37.508	3.6
SUC_Rib_#90	10.563	-18.167	16.085	43.946	3.2
SUC_Rib_#91	10.155	-19.404	14.993	42.892	3.3
SUC_Rib_#95	11.993	-19.010	14.734	41.950	3.3
SUC_Rib_#97	12.707	-19.284	14.839	41.364	3.3
SUC_Rib_#98	10.782	-19.183	15.612	43.772	3.3
SUC_Rib_#99	10.980	-19.366	13.404	39.503	3.4
SUC_Rib_#101	9.657	-18.924	15.298	42.644	3.3
SUC_Rib_#103	11.814	-17.395	14.621	41.503	3.3
SUC_Rib_#104	10.497	-17.473	14.641	41.809	3.3
SUC_Rib_#105	10.710	-19.989	13.801	38.292	3.2
SUC_Rib_#106	10.719	-21.160	10.497	35.384	3.9*
SUC_Rib_#107	10.831	-18.956	14.197	40.573	3.3
SUC_Rib_#108	9.787	-19.357	15.472	42.780	3.2
SUC_Rib_#110	10.651	-16.719	14.571	41.440	3.3
SUC_Rib_#111	10.832	-15.692	15.665	43.758	3.3
SUC_Rib_#112	10.769	-19.083	12.099	36.694	3.5
SUC_Rib_#113	10.021	-17.996	14.038	41.889	3.5
SUC_Rib_#114	10.377	-18.380	14.909	43.811	3.4
SUC_Rib_#115	10.594	-18.149	14.848	43.789	3.4
SUC_Rib_#116	10.568	-18.931	14.167	41.531	3.4
SUC_Rib_#118	11.096	-18.846	15.433	44.683	3.4
SUC_Rib_#120	10.367	-17.033	13.982	41.591	3.5
SUC_Rib_#121	9.872	-18.807	14.819	43.495	3.4
SUC_Rib_#123	9.934	-18.373	15.332	44.363	3.4
SUC_Rib_#124	11.634	-19.014	14.077	41.476	3.4
SUC_Rib_#127	11.244	-20.775	11.512	36.597	3.7*
SUC_Rib_#128	10.686	-17.636	12.956	36.715	3.3
SUC_Rib_#138	9.828	-19.111	14.596	43.035	3.4
PC_Rib_#141	9.635	-13.370	14.623	43.026	3.4

Table A.1 Continued

PC_Rib_#143	9.441	-11.952	14.663	42.869	3.4
PC_Rib_#147	9.413	-14.967	14.757	42.719	3.4
PC_Rib_#148	9.614	-13.773	14.296	41.251	3.4
PC_Rib_#150	9.833	-16.713	12.793	38.433	3.5
PC_Rib_#152	9.682	-10.611	14.656	42.805	3.4
PC_Rib_#154	9.609	-13.065	12.643	38.112	3.5
PC_Rib_#155	9.563	-19.528	12.517	37.490	3.5
PC_Rib_#156	9.741	-13.615	14.629	42.071	3.4
PC_Rib_#157	8.926	-13.901	15.920	44.299	3.2
PC_Rib_#158	9.032	-12.614	15.167	41.568	3.2
PC_Rib_#159	9.704	-14.382	15.286	41.871	3.2
PC_Rib_#160	10.275	-14.185	16.436	44.929	3.2
PC_Rib_#161	9.538	-11.997	15.060	41.460	3.2
PC_Rib_#162	8.726	-12.319	15.463	42.617	3.2
PC_Rib_#165	8.884	-13.780	10.918	30.019	3.2
PC_Rib_#167	9.521	-11.552	10.223	28.695	3.3
PC_Rib_#168	9.863	-11.497	15.580	43.477	3.3
PC_Rib_#169	8.603	-11.933	15.030	41.408	3.2
SCHIT_Rib_#170	9.529	-12.313	13.867	38.818	3.3
SCHIT_Rib_#171	9.476	-18.670	15.046	41.578	3.2
SCHIT_Rib_#172	9.134	-12.623	6.277	17.593	3.3
SCHIT_Rib_#173	9.855	-18.364	14.086	39.337	3.3
SCHIT_Rib_#174	9.078	-11.509	14.936	41.913	3.3
SCHIT_Rib_#175	9.402	-17.488	12.492	34.389	3.2
SCHIT_Rib_#176	11.182	-19.051	11.642	34.646	3.5
SCHIT_Rib_#178	9.343	-15.140	11.449	31.659	3.2
SCHIT_Rib_#179	9.261	-10.822	11.376	31.571	3.2
SCHIT_Rib_#180	9.875	-12.724	6.419	18.173	3.3
SCHIT_Rib_#181	10.170	-19.424	14.384	39.478	3.2
SCHIT_Rib_#182	10.234	-19.147	9.527	26.663	3.3
SCHIT_Rib_#183	9.440	-20.124	14.722	40.682	3.2
SUC_Rib_#184	10.569	-19.030	13.231	36.352	3.2
SUC_Rib_#185	10.409	-18.330	13.521	37.390	3.2
SUC_Rib_#192	10.640	-19.727	10.334	28.523	3.2
SUC_Rib_#194	10.527	-18.115	14.825	40.807	3.2
SUC_Rib_#196	9.923	-18.779	14.900	40.828	3.2
SUC_Rib_#198	9.784	-18.031	11.804	32.660	3.2

Table A.1 Continued

SUC_Rib_#199	12.080	-19.852	8.380	23.450	3.3
SUC_Rib_#200	11.933	-18.218	13.593	37.425	3.2
SUC_Rib_#201	10.973	-20.490	13.337	36.595	3.2
SUC_Rib_#202	11.098	-18.380	12.676	35.153	3.2
SUC_Rib_#203	10.838	-18.810	12.238	33.883	3.2
SUC_Rib_#204	9.914	-18.262	15.265	42.995	3.3
SUC_Rib_#206	10.773	-18.182	12.314	34.017	3.2
SUC_Rib_#208	10.805	-18.211	16.327	44.753	3.2
SUC_Rib_#211	11.549	-19.059	14.578	41.734	3.3
SUC_Rib_#213	12.318	-17.281	11.829	33.824	3.3

Table A.2. Carbon and nitrogen stable isotope data set for all adult femur samples. Asterice* indicates samples with a C:N > 3.6 suggesting an unreliable value due to diagenesis.

Sample ID	$\delta^{15}N_{AIR}$	$\delta^{13}C_{VPDB}$	%N	%C	C:N
PC_Femur_#25	10.136	-12.736	41.595	15.171	3.2
PC_Femur_#26	9.306	-13.739	45.660	16.349	3.3
PC_Femur_#27	9.269	-15.214	43.178	15.879	3.2
PC_Femur_#28	10.407	-19.833	43.058	15.835	3.2
PC_Femur_#29	9.577	-12.645	44.408	16.153	3.2
PC_Femur_#31	8.926	-11.143	42.093	15.450	3.2
PC_Femur_#33	10.299	-13.773	26.661	9.634	3.2
PC_Femur_#34	9.027	-18.837	39.529	14.503	3.2
PC_Femur_#35	9.399	-18.111	43.673	15.838	3.2
PC_Femur_#36	8.065	-11.900	39.845	14.624	3.2
PC_Femur_#37	8.853	-13.103	41.552	15.167	3.2
SCHIT_Femur_#38	8.937	-11.074	44.037	15.939	3.2
SCHIT_Femur_#39	9.951	-13.425	39.672	14.389	3.2
SCHIT_Femur_#40	9.723	-18.945	39.105	13.849	3.3
SCHIT_Femur_#41	9.695	-18.761	42.408	13.967	3.5
SCHIT_Femur_#42	8.967	-19.387	24.836	8.921	3.2
SCHIT_Femur_#45	8.585	-10.841	41.027	14.961	3.2
SCHIT_Femur_#46	9.170	-18.556	36.788	13.289	3.2
SCHIT_Femur_#47	11.179	-13.062	43.211	15.716	3.2
SCHIT_Femur_#48	8.958	-9.776	45.741	16.628	3.2
SCHIT_Femur_#49	9.118	-17.600	32.121	11.517	3.3
SUC_Femur_#50	10.765	-19.394	44.610	16.332	3.2
SUC_Femur_#51	10.080	-18.774	44.171	16.157	3.2
SUC_Femur_#53	9.578	-18.433	23.241	8.406	3.2
SUC_Femur_#54	9.864	-18.709	37.776	13.538	3.3
SUC_Femur_#57	10.135	-18.632	44.721	16.175	3.2
SUC_Femur_#63	11.809	-19.432	43.184	15.495	3.3
SUC_Femur_#68	11.544	-19.599	23.542	8.255	3.3
SUC_Femur_#70	11.627	-16.773	21.935	7.557	3.4
SUC_Femur_#71	10.387	-18.794	35.949	12.743	3.3
SUC_Femur_#72	10.990	-18.084	22.030	7.815	3.3
SUC_Femur_#73	10.574	-18.793	40.585	14.684	3.2
SUC_Femur_#76	10.506	-18.429	43.650	15.617	3.3
SUC_Femur_#77	11.797	-16.759	42.562	15.441	3.2
SUC_Femur_#78	9.888	-18.693	40.405	14.752	3.2

Table A.2 Continued

SUC_Femur_#79	10.460	-18.868	44.643	15.938	3.3
SUC_Femur_#80	9.521	-18.818	37.200	13.120	3.3
SUC_Femur_#81	10.688	-20.527	37.416	11.904	3.7*
SUC_Femur_#82	10.340	-19.226	28.934	10.131	3.3
SUC_Femur_#83	10.284	-18.763	26.450	9.102	3.4
SUC_Femur_#85	10.423	-16.910	39.918	14.267	3.3
SUC_Femur_#86	9.371	-18.907	42.028	15.003	3.3
SUC_Femur_#87	9.347	-18.847	40.082	14.035	3.3
SUC_Femur_#88	9.850	-18.697	29.625	10.461	3.3
SUC_Femur_#89	12.242	-19.293	34.942	12.272	3.3
SUC_Femur_#90	10.130	-17.865	42.666	15.066	3.3
SUC_Femur_#91	9.821	-19.156	43.004	15.265	3.3
SUC_Femur_#94	9.584	-19.758	24.174	8.501	3.3
SUC_Femur_#95	11.722	-18.750	42.124	15.002	3.3
SUC_Femur_#96	9.638	-16.629	39.784	14.304	3.2
SUC_Femur_#98	9.428	-18.863	42.098	15.088	3.3
SUC_Femur_#99	10.739	-19.313	33.065	11.771	3.3
SUC_Femur_#100	9.727	-20.522	35.121	12.525	3.3
SUC_Femur_#101	10.131	-19.106	28.772	10.211	3.3
SUC_Femur_#102	9.726	-18.743	40.063	14.284	3.3
SUC_Femur_#103	12.981	-16.917	43.680	15.695	3.2
SUC_Femur_#104	10.114	-17.255	42.493	15.321	3.2
SUC_Femur_#105	9.862	-19.891	34.121	12.211	3.3
SUC_Femur_#106	9.893	-20.235	27.879	9.891	3.3
SUC_Femur_#107	10.040	-18.339	33.187	11.925	3.2
SUC_Femur_#108	9.429	-19.275	30.925	10.950	3.3
SUC_Femur_#110	9.244	-14.817	31.703	11.236	3.3
SUC_Femur_#111	10.334	-15.930	39.889	14.228	3.3
SUC_Femur_#112	10.465	-18.947	36.839	13.088	3.3
SUC_Femur_#113	9.433	-18.974	43.825	15.849	3.2
SUC_Femur_#114	9.745	-18.412	41.576	15.122	3.2
SUC_Femur_#118	10.877	-18.307	40.510	14.645	3.2
SUC_Femur_#119	10.870	-18.371	41.127	15.158	3.2
SUC_Femur_#120	9.902	-17.083	42.806	15.603	3.2
SUC_Femur_#123	9.708	-18.189	43.319	15.984	3.2
SUC_Femur_#124	10.747	-18.423	41.300	14.862	3.2
SUC_Femur_#130	10.256	-18.482	42.545	15.812	3.1

Table A.2 Continued

PC_Femur_#141	9.362	-13.283	40.556	14.933	3.2
PC_Femur_#143	9.716	-12.674	43.155	15.873	3.2
PC_Femur_#144	10.160	-11.578	43.492	15.113	3.4
PC_Femur_#146	10.252	-11.967	42.246	14.209	3.5
PC_Femur_#147	10.433	-16.845	42.931	13.763	3.6
PC_Femur_#148	9.823	-14.649	31.528	11.014	3.3
PC_Femur_#149	9.673	-9.650	42.123	14.957	3.3
PC_Femur_#150	10.173	-17.296	45.737	16.046	3.3
PC_Femur_#151	9.145	-10.790	42.703	15.091	3.3
PC_Femur_#152	9.363	-10.753	46.005	16.176	3.3
PC_Femur_#153	9.094	-15.209	46.664	16.531	3.3
PC_Femur_#154	9.974	-12.205	43.269	15.236	3.3
PC_Femur_#155	9.619	-19.134	44.528	15.654	3.3
PC_Femur_#156	9.551	-14.150	44.187	15.728	3.3
PC_Femur_#157	9.231	-14.899	43.365	15.281	3.3
PC_Femur_#158	8.990	-13.094	43.019	15.226	3.3
PC_Femur_#159	9.418	-16.075	46.380	16.274	3.3
PC_Femur_#160	9.252	-15.216	44.252	15.757	3.3
PC_Femur_#161	9.181	-13.541	41.889	14.854	3.3
PC_Femur_#162	8.424	-13.590	41.013	15.005	3.2
PC_Femur_#163	9.763	-14.574	45.378	16.069	3.3
PC_Femur_#164	10.331	-14.434	45.959	16.244	3.3
PC_Femur_#165	10.022	-14.809	39.162	12.724	3.6
PC_Femur_#166	8.834	-18.256	42.309	15.390	3.2
PC_Femur_#167	9.274	-11.620	41.075	14.488	3.3
PC_Femur_#168	9.282	-10.975	37.578	13.239	3.3
PC_Femur_#169	8.393	-12.626	40.887	14.239	3.3
SCHIT_Femur_#170	9.176	-14.007	45.713	15.954	3.3
SCHIT_Femur_#171	9.451	-18.716	35.584	12.492	3.3
SCHIT_Femur_#172	9.389	-13.049	34.619	12.180	3.3
SCHIT_Femur_#173	9.521	-18.300	44.605	15.398	3.4
SCHIT_Femur_#174	8.696	-11.639	42.747	15.073	3.3
SCHIT_Femur_#175	9.351	-18.400	42.254	14.641	3.4
SCHIT_Femur_#176	10.090	-18.619	41.324	14.454	3.3
SCHIT_Femur_#177	9.231	-14.753	43.127	13.837	3.6
SCHIT_Femur_#178	10.378	-16.846	35.818	12.908	3.2
SCHIT_Femur_#179	9.267	-11.237	40.712	14.807	3.2

Table A.2 Continued

SCHIT_Femur_#180	9.877	-12.838	37.170	13.458	3.2
SCHIT_Femur_#181	10.093	-19.489	39.824	14.338	3.2
SCHIT_Femur_#182	10.047	-19.112	27.626	9.761	3.3
SCHIT_Femur_#183	9.471	-19.610	29.977	10.561	3.3
SUC_Femur_#184	10.294	-19.132	43.138	15.532	3.2
SUC_Femur_#185	10.160	-18.400	36.183	12.920	3.3
SUC_Femur_#190	12.797	-19.375	34.715	12.366	3.3
SUC_Femur_#191	12.953	-19.221	25.973	9.192	3.3
SUC_Femur_#192	10.443	-19.698	33.225	11.886	3.3
SUC_Femur_#193	10.586	-18.809	32.522	11.556	3.3
SUC_Femur_#194	10.845	-17.557	26.429	9.382	3.3
SUC_Femur_#196	9.930	-18.627	43.002	15.451	3.2
SUC_Femur_#198	12.420	-19.239	36.417	13.081	3.2
SUC_Femur_#199	10.834	-20.231	13.874	4.885	3.3
SUC_Femur_#200	11.315	-16.880	35.579	12.653	3.3
SUC_Femur_#201	10.477	-20.384	38.546	13.803	3.3
SUC_Femur_#202	10.576	-18.265	32.859	11.789	3.3
SUC_Femur_#203	10.734	-18.922	26.254	9.232	3.3
SUC_Femur_#204	9.825	-17.683	30.449	10.831	3.3
SUC_Femur_#206	10.839	-18.104	26.563	9.284	3.3
SUC_Femur_#208	10.393	-17.750	42.267	15.301	3.2
SUC_Femur_#209	9.783	-19.224	34.738	12.672	3.2
SUC_Femur_#211	11.369	-18.883	29.138	10.355	3.3

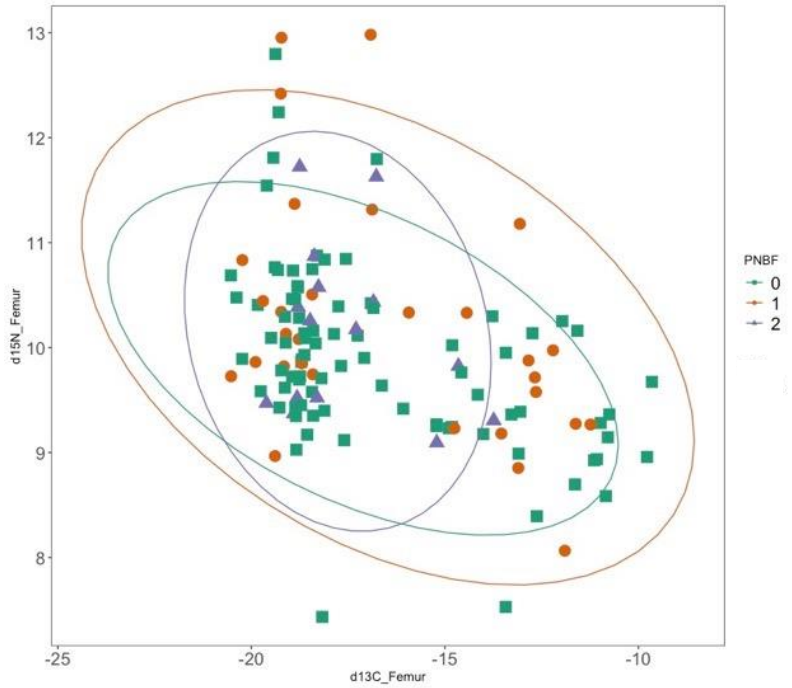


Figure A.62. $\delta^{13}C$ and $\delta^{15}N$ femur values for individuals that are absent (0), present (1), and unobservable (2) for PNBF with 95% confidence ellipses.

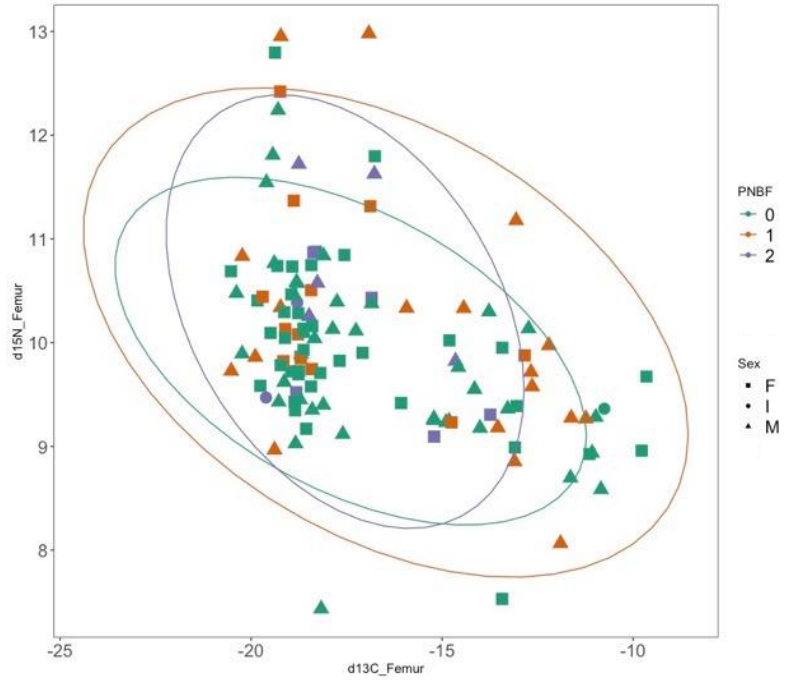


Figure A.63. $\delta^{13}C$ and $\delta^{15}N$ femur values those absent (0), present (1), and unobservable (2) for PNBF by site and sex with 95% confidence ellipses.

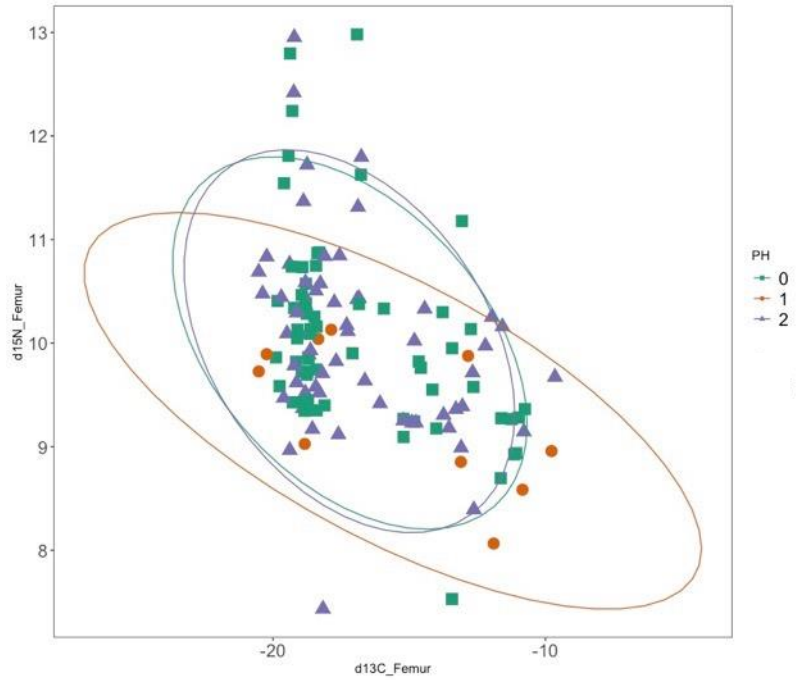


Figure A.64. $\delta^{13}C$ and $\delta^{15}N$ femur values for individuals that are absent (0), present (1), and unobservable (2) for PH with 95% confidence ellipses.

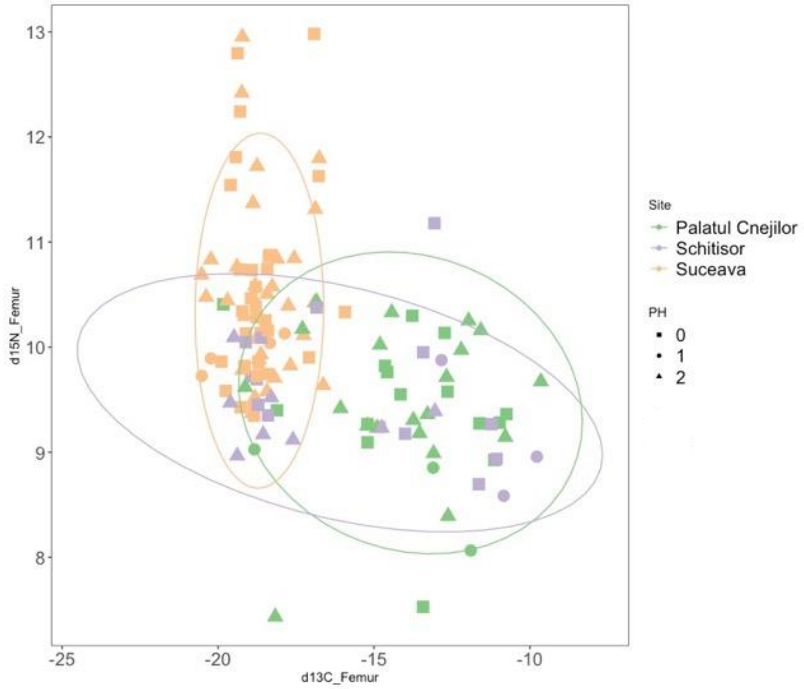


Figure A.65. $\delta^{13}C$ and $\delta^{15}N$ femur values for individuals that are absent (0), present (1), and unobservable (2) for PH by site with 95% confidence ellipses.

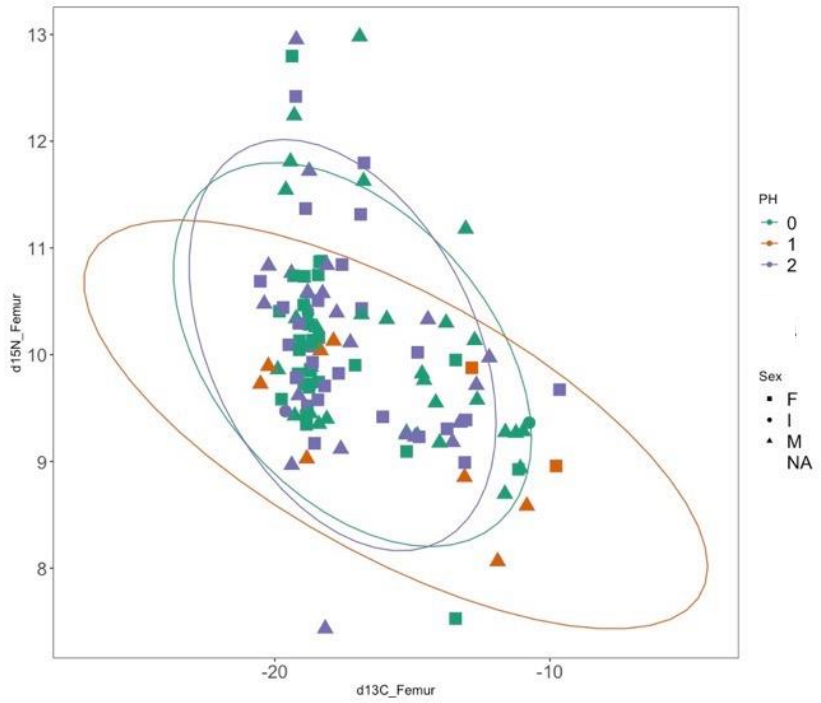


Figure A.66. $\delta^{13}C$ and $\delta^{15}N$ femur values for individuals that are absent (0), present (1), and unobservable (2) for PH by sex with 95% confidence ellipses.

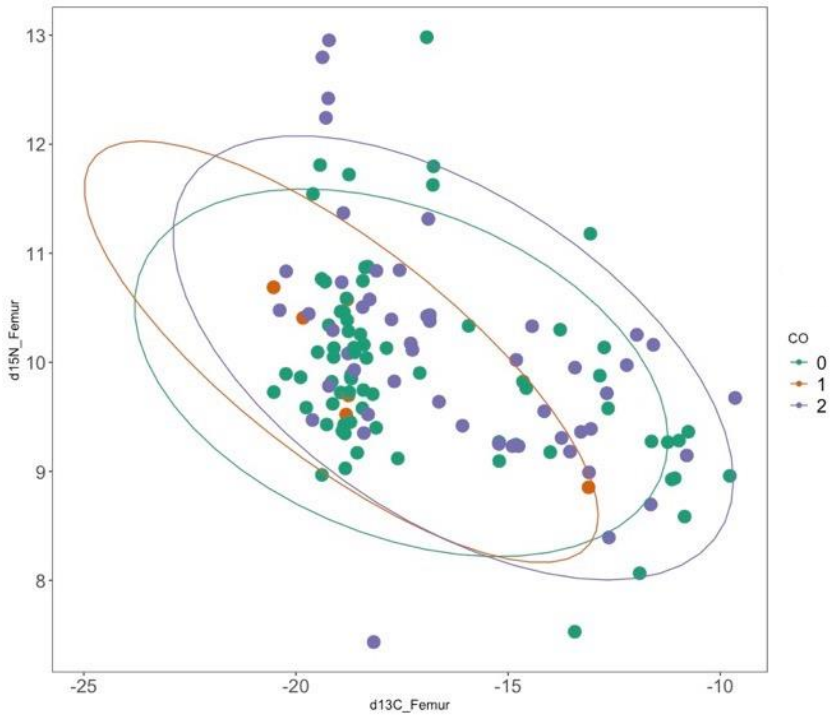


Figure A.67. $\delta^{13}C$ and $\delta^{15}N$ femur values for individuals that are absent (0), present (1), and unobservable (2) for CO with 95% confidence ellipses.

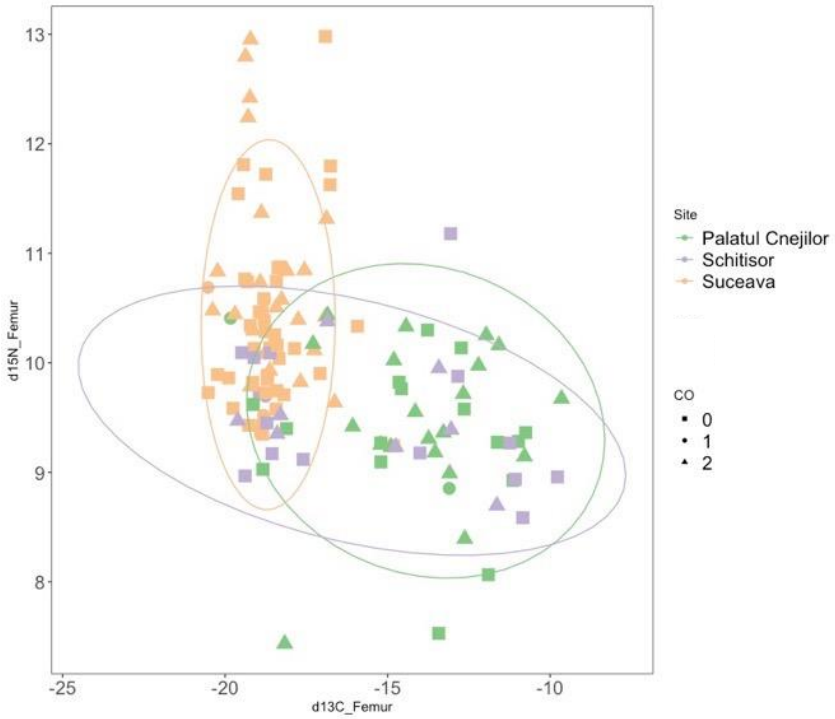


Figure A.68. $\delta^{13}C$ and $\delta^{15}N$ femur values for individuals that are absent (0), present (1), and unobservable (2) for CO by site with 95% confidence ellipses.

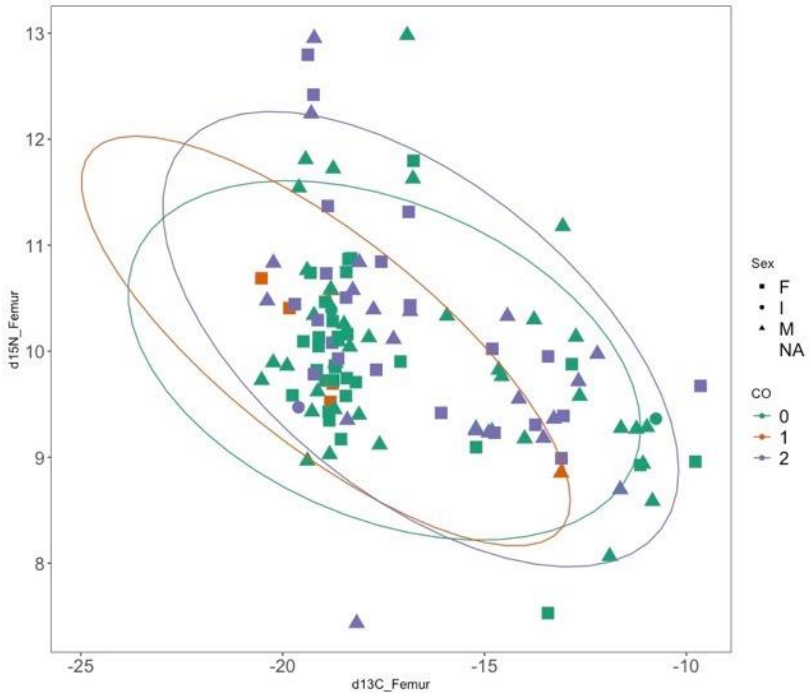


Figure A.69. $\delta^{13}C$ and $\delta^{15}N$ femur values for individuals that are absent (0), present (1), and unobservable (2) for CO by sex with 95% confidence ellipses.

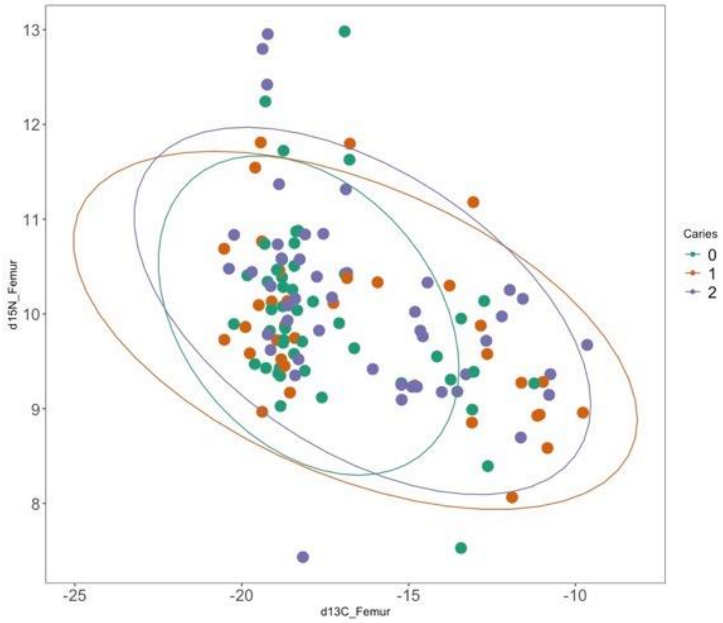


Figure A.70. $\delta^{13}C$ and $\delta^{15}N$ femur values for individuals that are absent (0), present (1), and unobservable (2) for caries with 95% confidence ellipses.

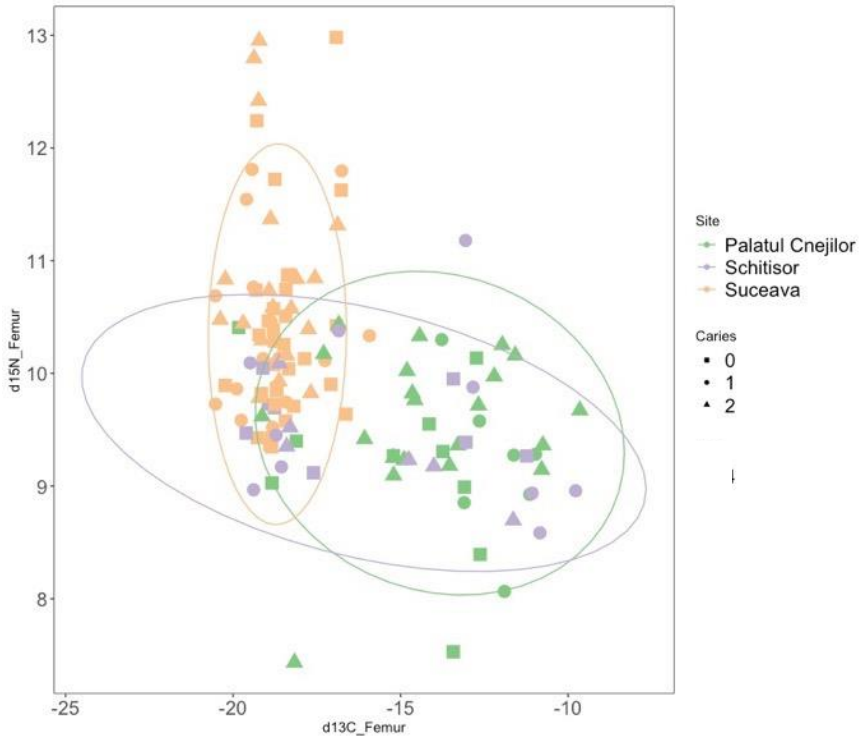


Figure A.71. $\delta^{13}C$ and $\delta^{15}N$ femur values for individuals that are absent (0), present (1), and unobservable (2) for caries by site with 95% confidence ellipses.

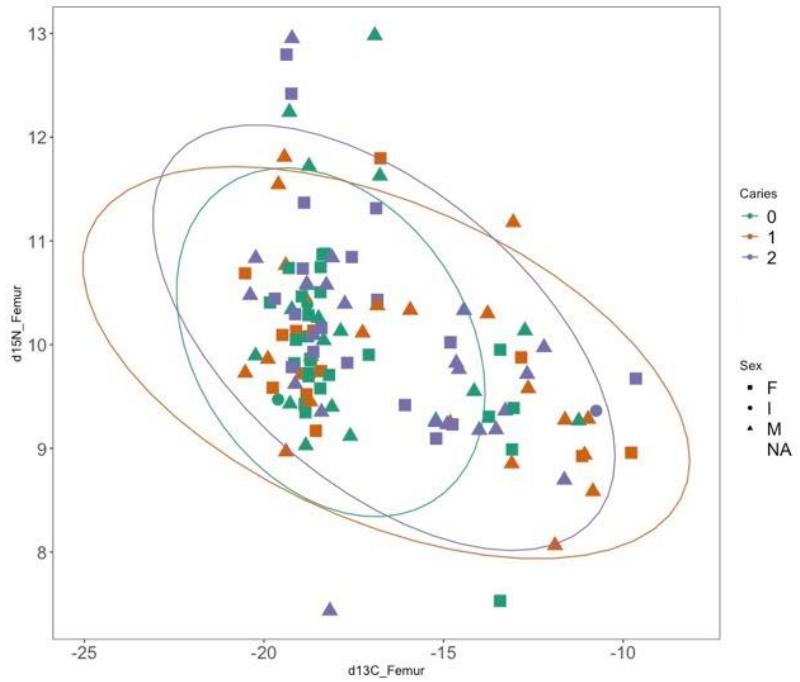


Figure A.72. $\delta^{13}C$ and $\delta^{15}N$ femur values for individuals that are absent (0), present (1), and unobservable (2) for caries by sex with 95% confidence ellipses.

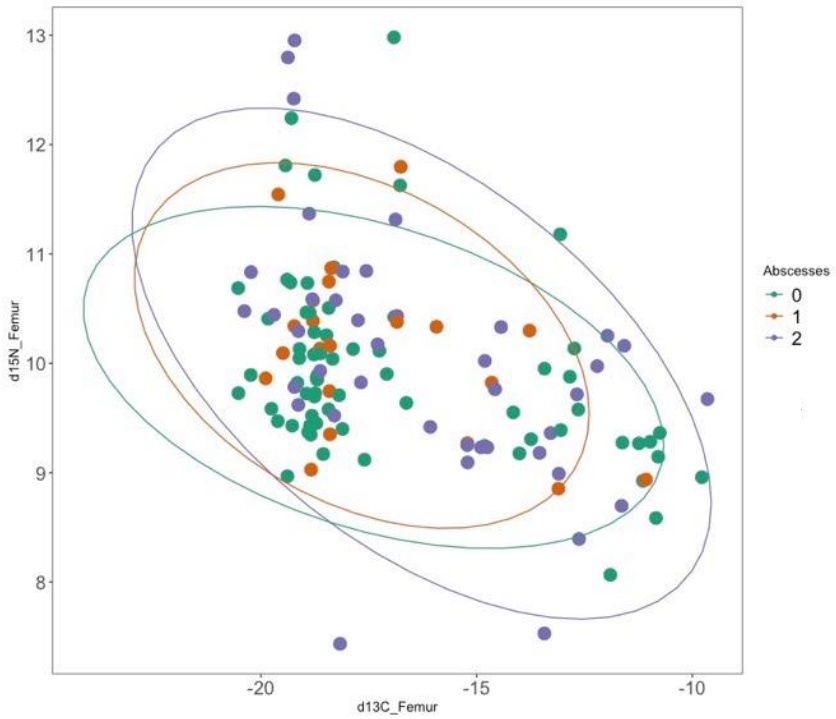


Figure A.73. $\delta^{13}C$ and $\delta^{15}N$ femur values for individuals that are absent (0), present (1), and unobservable (2) for abscesses with 95% confidence ellipses.

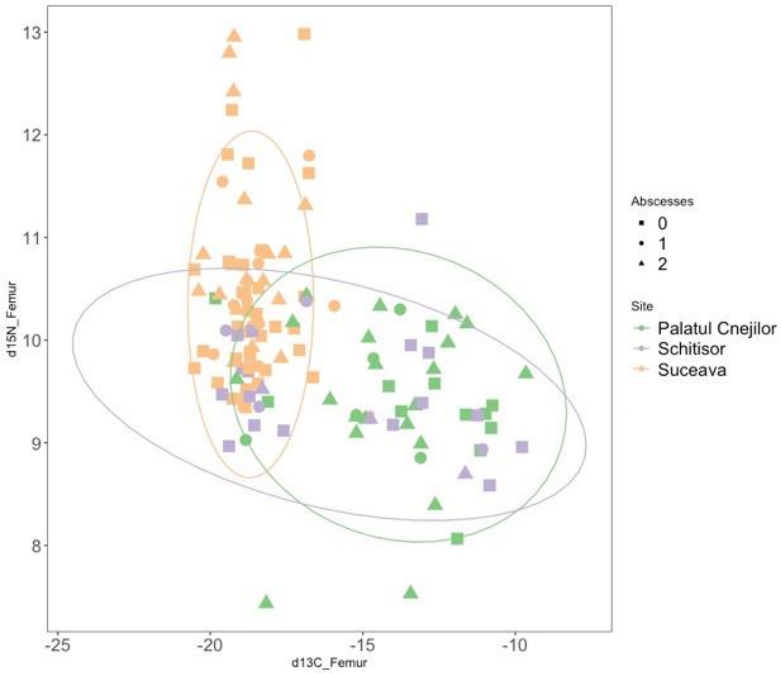


Figure A.74. $\delta^{13}C$ and $\delta^{15}N$ femur values for individuals that are absent (0), present (1), and unobservable (2) for abscesses by site with 95% confidence ellipses.

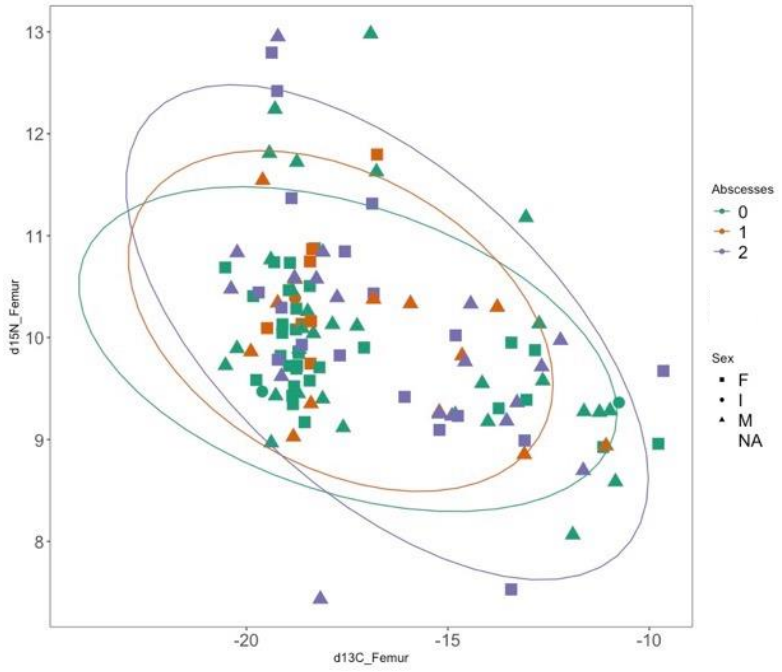


Figure A.75. $\delta^{13}C$ and $\delta^{15}N$ femur values for individuals that are absent (0), present (1), and unobservable (2) for abscesses by sex with 95% confidence ellipses.

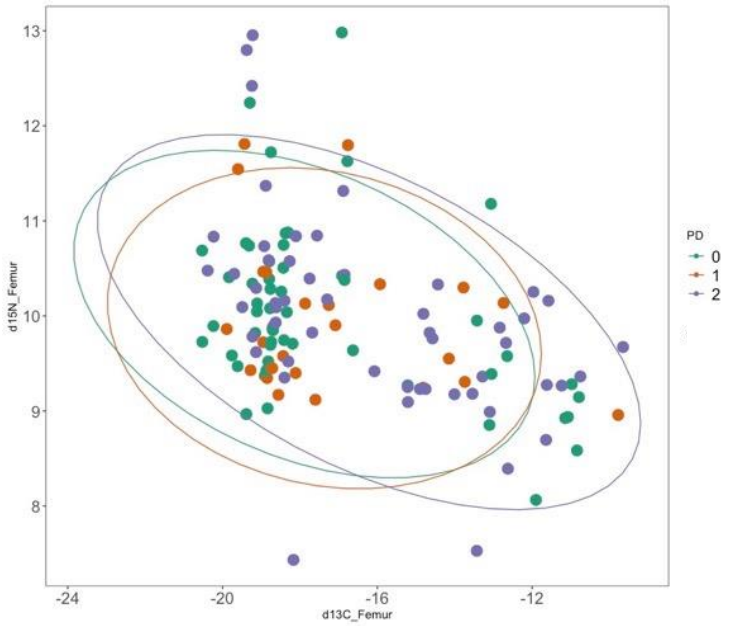


Figure A.76. $\delta^{13}C$ and $\delta^{15}N$ femur values for individuals that are absent (0), present (1), and unobservable (2) for PD with 95% confidence ellipses.

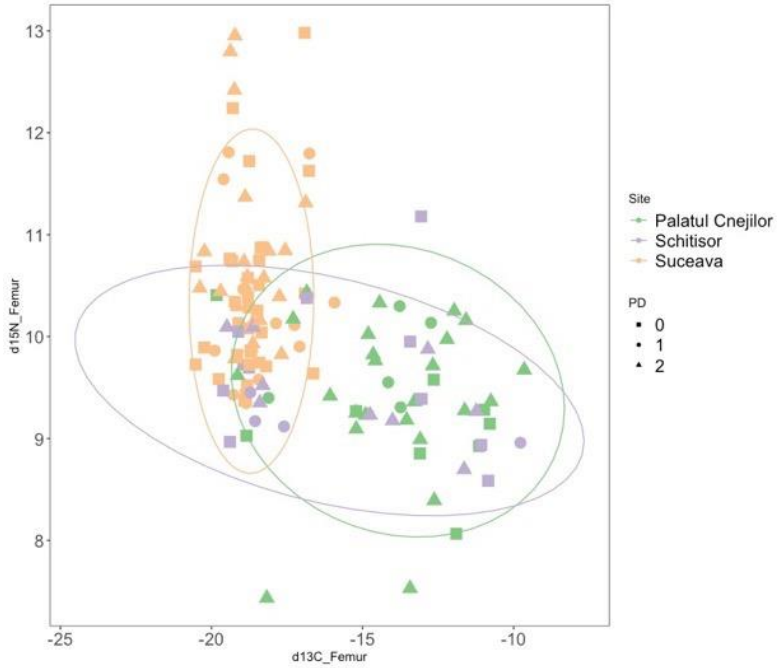


Figure A.77. $\delta^{13}C$ and $\delta^{15}N$ femur values for individuals that are absent (0), present (1), and unobservable (2) for PD by site with 95% confidence ellipses.

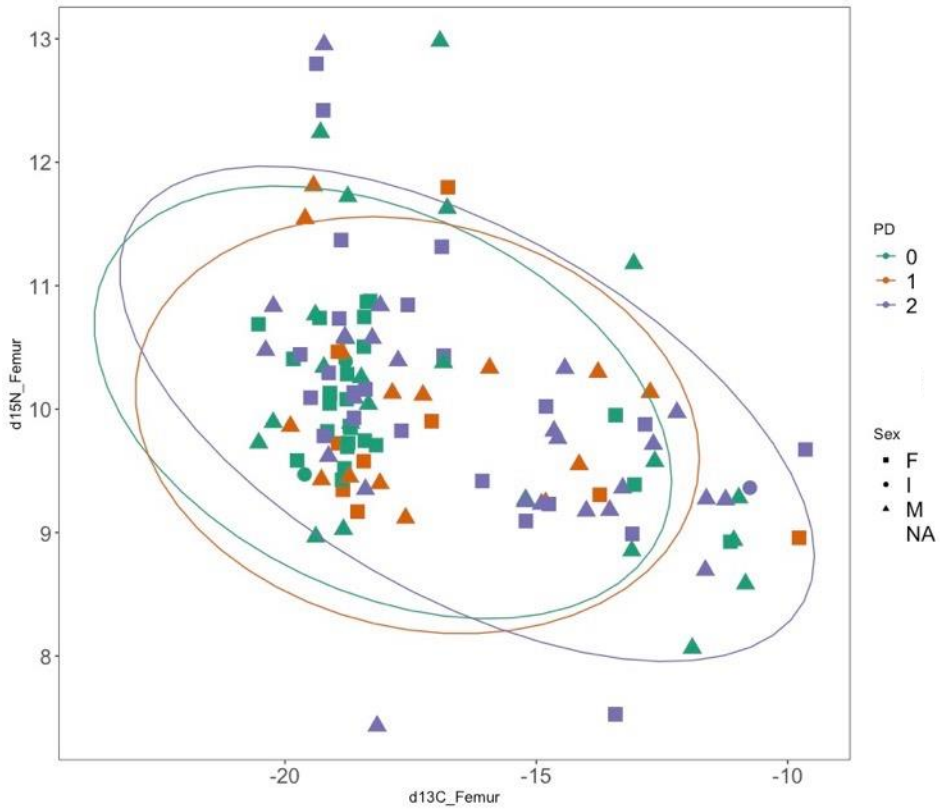


Figure A.78. $\delta^{13}C$ and $\delta^{15}N$ femur values for individuals that are absent (0), present (1), and unobservable (2) for PD by sex with 95% confidence ellipses.

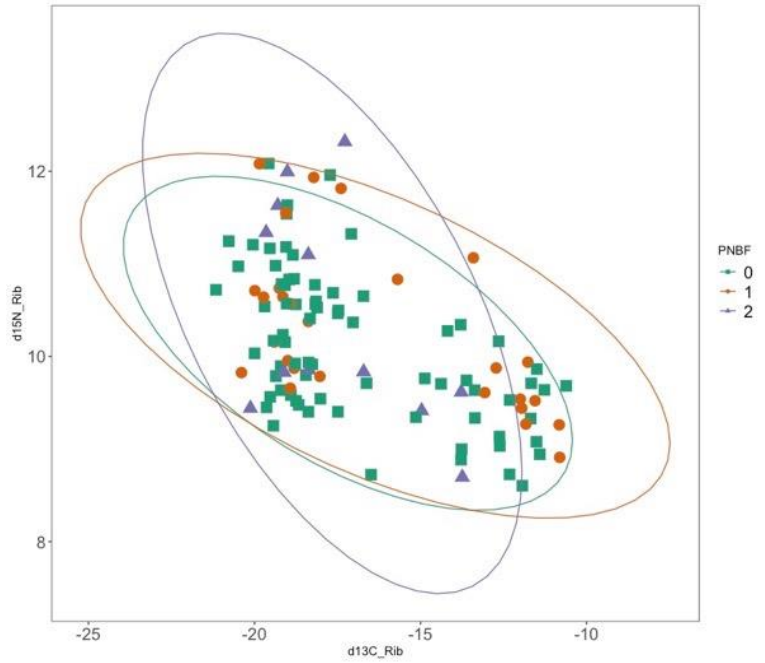


Figure A.79. $\delta^{13}C$ and $\delta^{15}N$ rib values for individuals that are absent (0), present (1), and unobservable (2) for PNBF with 95% confidence ellipses.

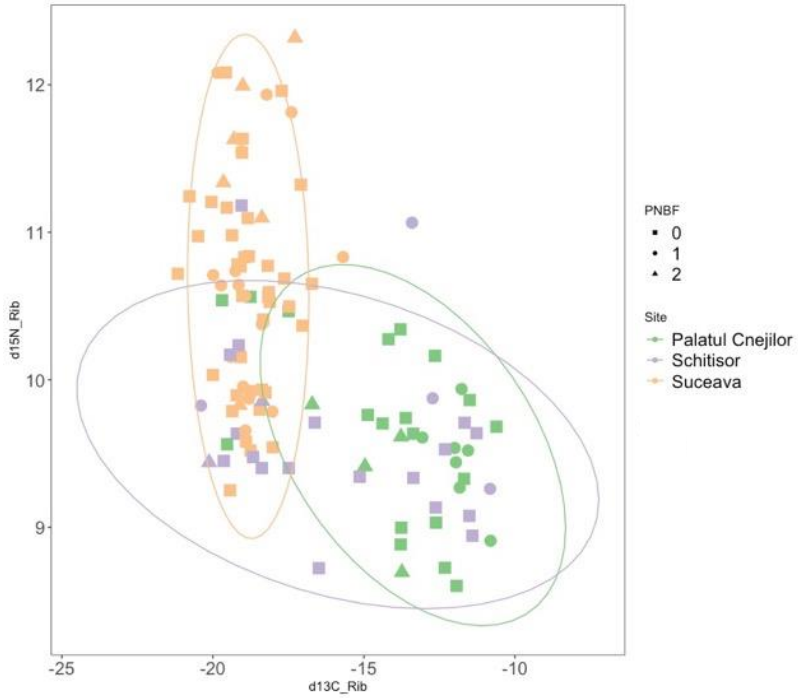


Figure A.80. $\delta^{13}C$ and $\delta^{15}N$ rib values for individuals that are absent (0), present (1), and unobservable (2) for PNBF by site with 95% confidence ellipses.

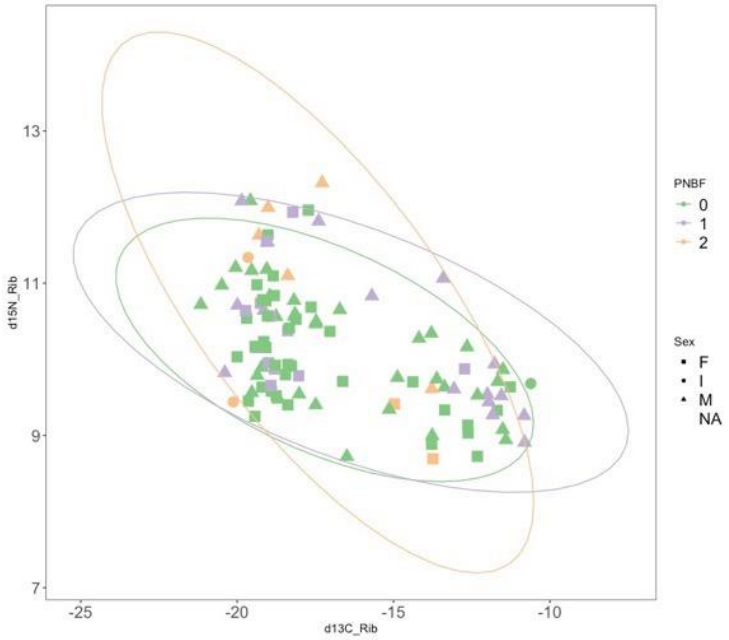


Figure A.81. $\delta^{13}C$ and $\delta^{15}N$ rib values for individuals that are absent (0), present (1), and unobservable (2) for PNBF by sex with 95% confidence ellipses.

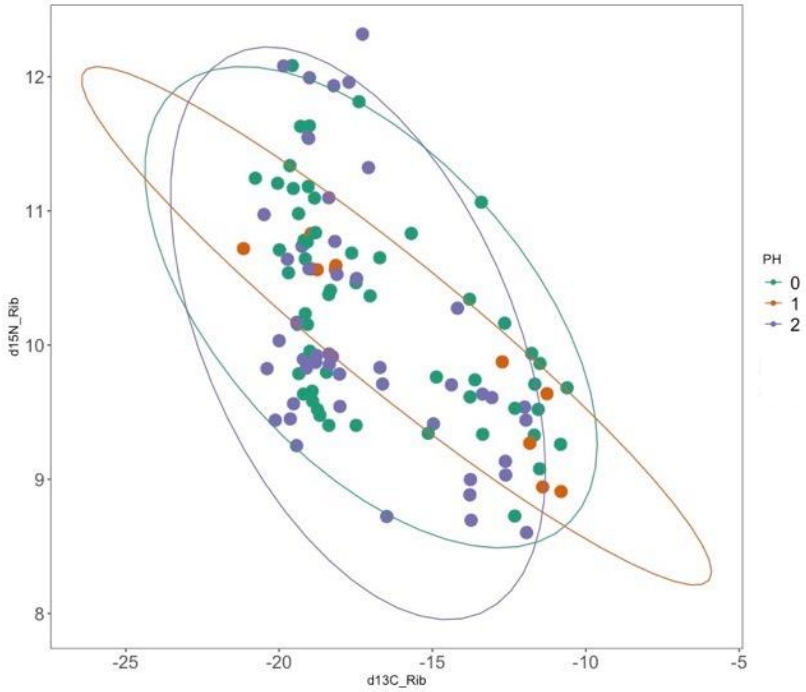


Figure A.82. $\delta^{13}C$ and $\delta^{15}N$ rib values for individuals that are absent (0), present (1), and unobservable (2) for PH with 95% confidence ellipses.

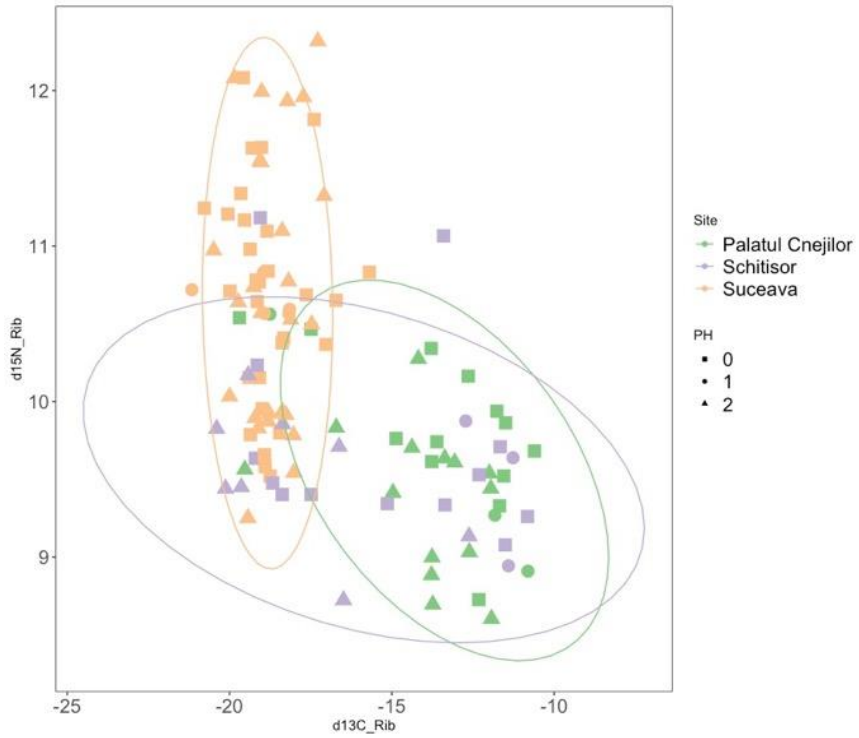


Figure A.83. $\delta^{13}C$ and $\delta^{15}N$ rib values for individuals that are absent (0), present (1), and unobservable (2) for PH by site with 95% confidence ellipses.

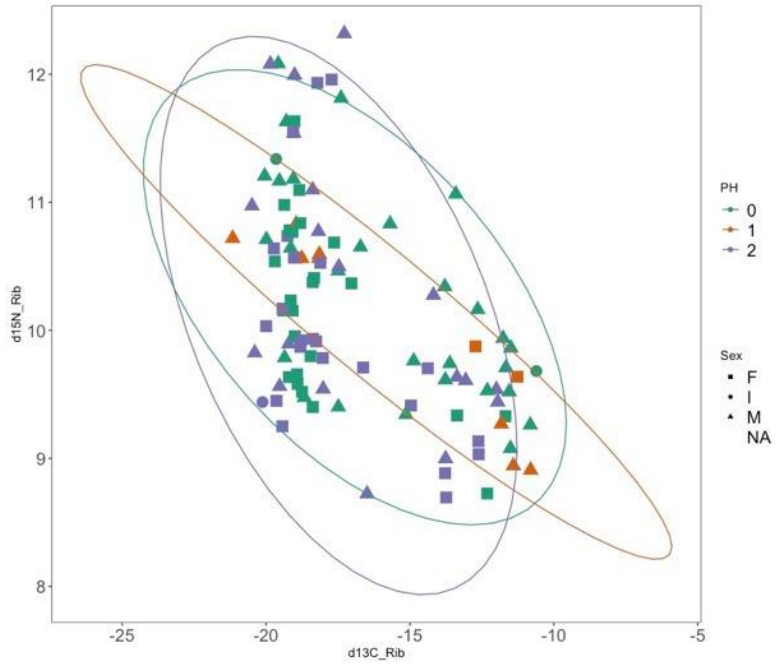


Figure A.84. $\delta^{13}C$ and $\delta^{15}N$ rib values for individuals that are absent (0), present (1), and unobservable (2) for PH by sex with 95% confidence ellipses.

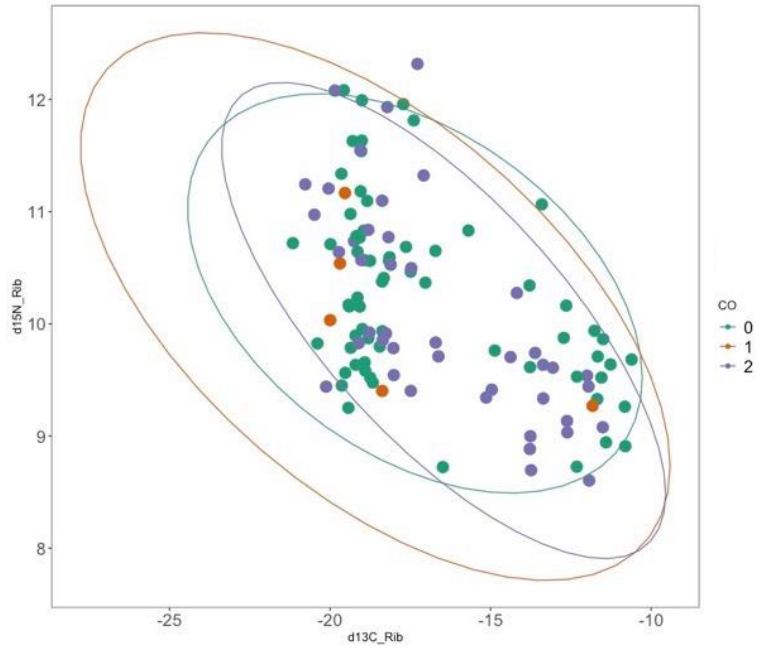


Figure A.85. $\delta^{13}C$ and $\delta^{15}N$ rib values for individuals that are absent (0), present (1), and unobservable (2) for CO with 95% confidence ellipses.

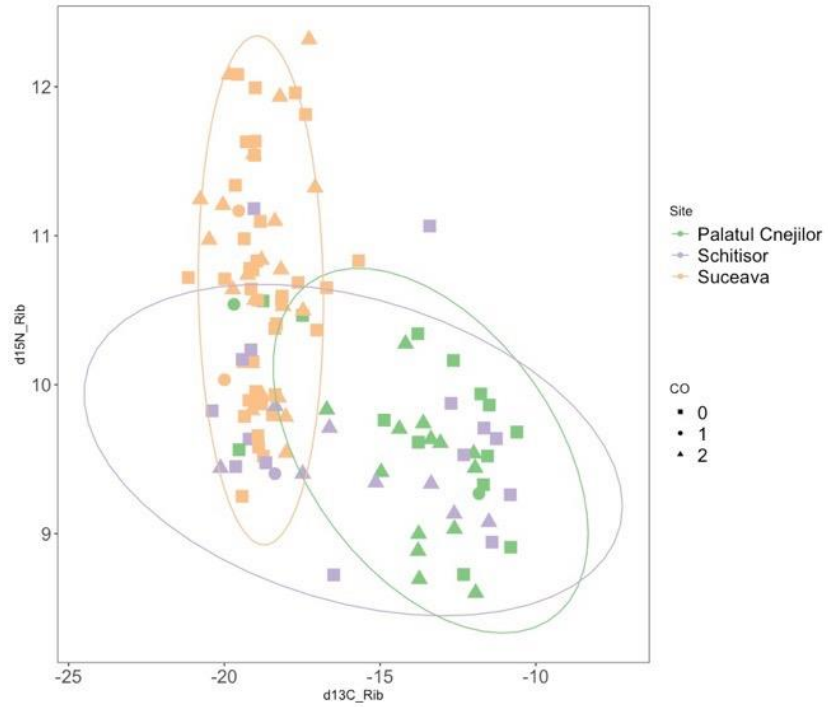


Figure A.86. $\delta^{13}C$ and $\delta^{15}N$ rib values for individuals that are absent (0), present (1), and unobservable (2) for CO by site with 95% confidence ellipses.

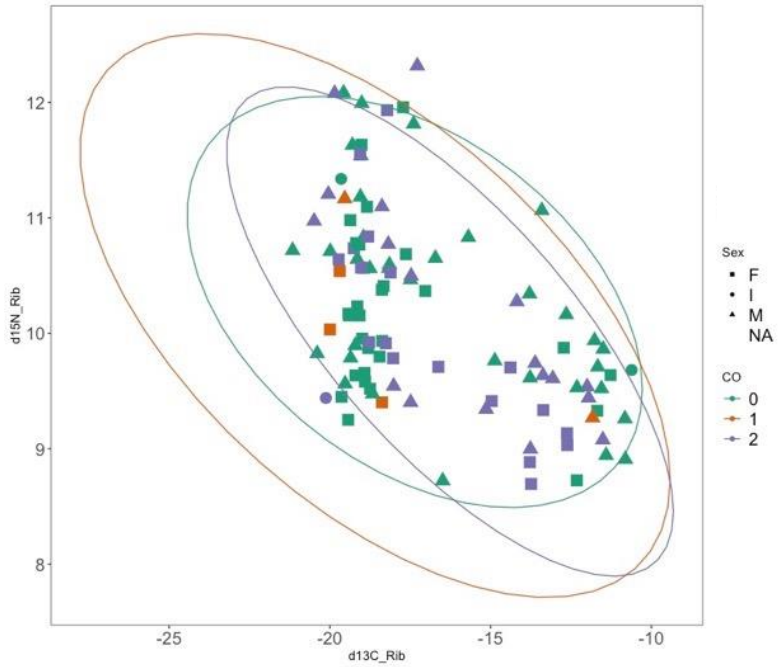


Figure A.87. $\delta^{13}C$ and $\delta^{15}N$ rib values for individuals that are absent (0), present (1), and unobservable (2) for CO by sex with 95% confidence ellipses.

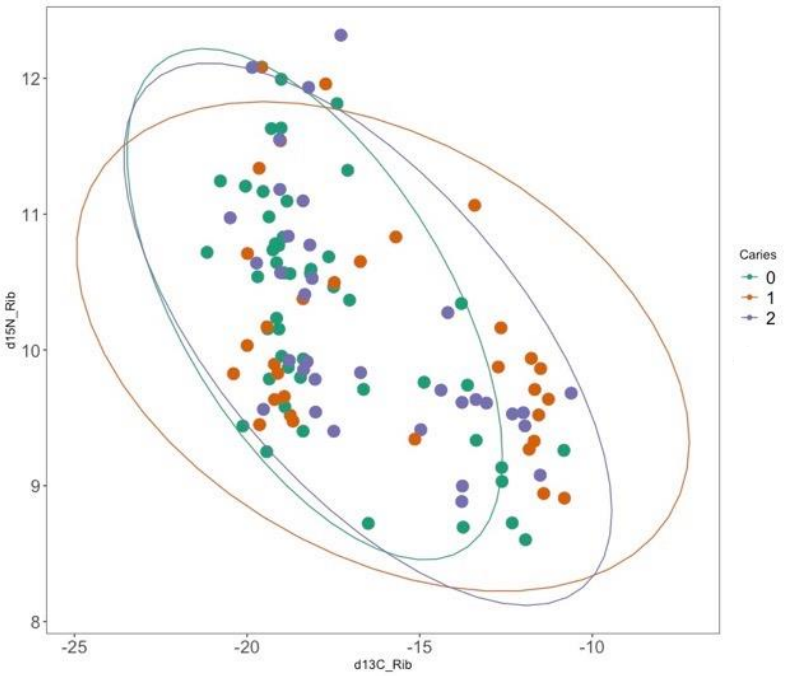


Figure A.88. $\delta^{13}C$ and $\delta^{15}N$ rib values for individuals that are absent (0), present (1), and unobservable (2) for caries with 95% confidence ellipses.

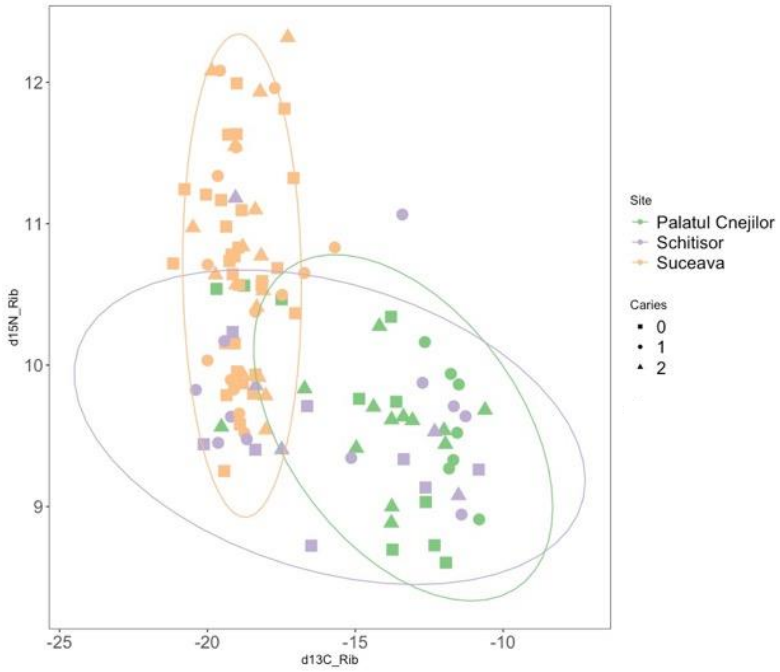


Figure A.89. $\delta^{13}C$ and $\delta^{15}N$ rib values for individuals that are absent (0), present (1), and unobservable (2) for caries by site with 95% confidence ellipses.

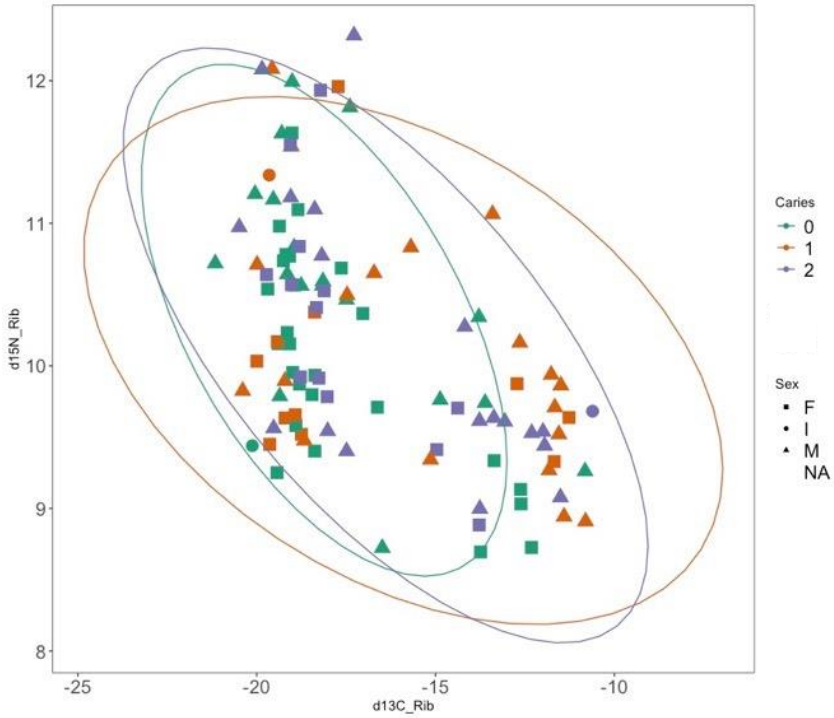


Figure A.90. $\delta^{13}C$ and $\delta^{15}N$ rib values for individuals that are absent (0), present (1), and unobservable (2) for caries by sex with 95% confidence ellipses.

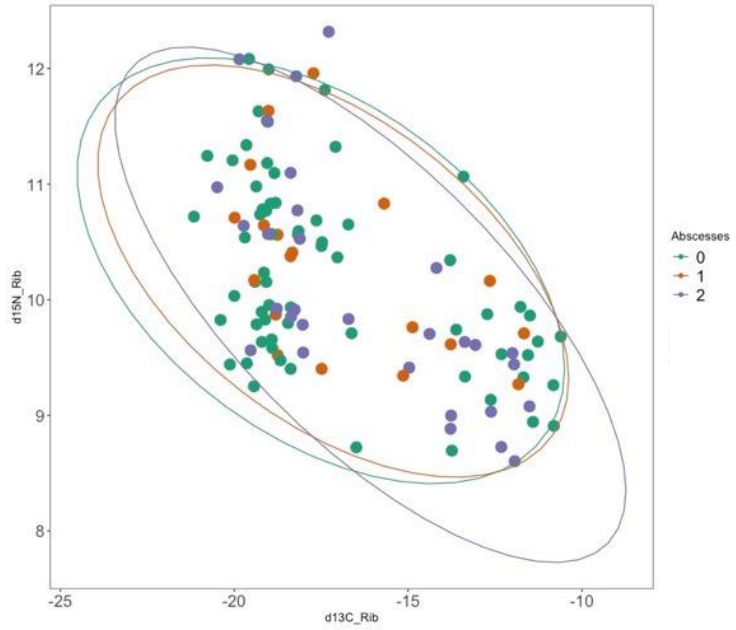


Figure A.91. $\delta^{13}C$ and $\delta^{15}N$ rib values for individuals that are absent (0), present (1), and unobservable (2) for abscesses with 95% confidence ellipses.

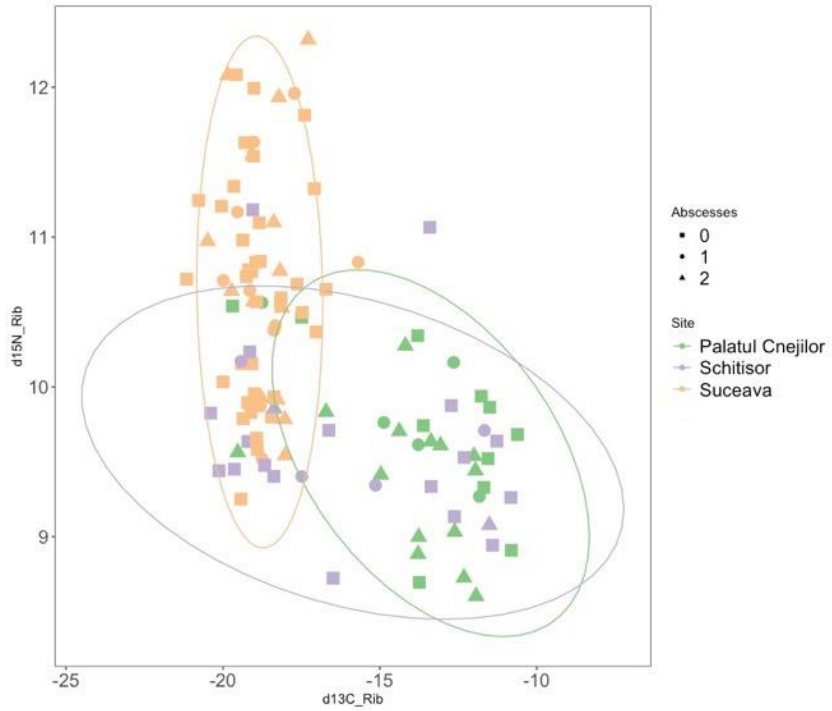


Figure A.92. $\delta^{13}C$ and $\delta^{15}N$ rib values for individuals that are absent (0), present (1), and unobservable (2) for abscesses by site with 95% confidence ellipses.

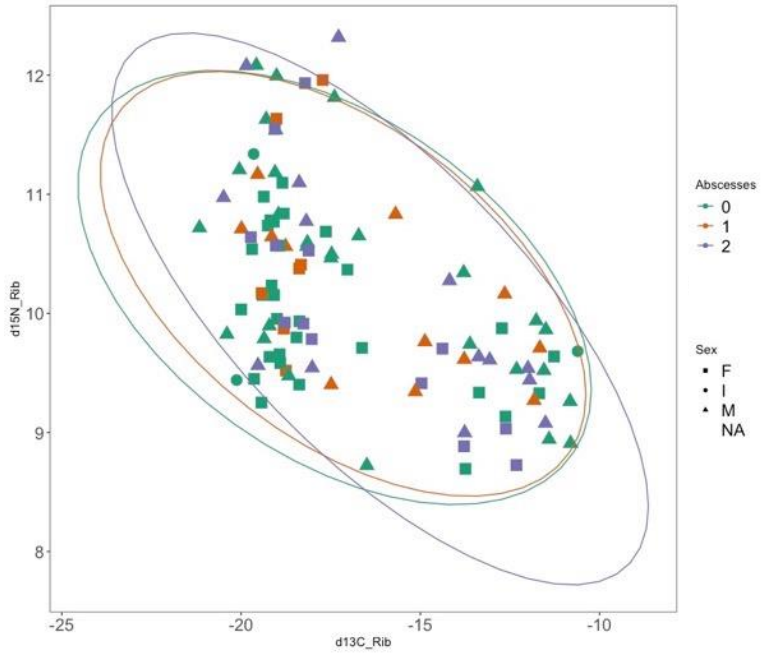


Figure A.93. $\delta^{13}C$ and $\delta^{15}N$ rib values for individuals that are absent (0), present (1), and unobservable (2) for abscesses by sex with 95% confidence ellipses.

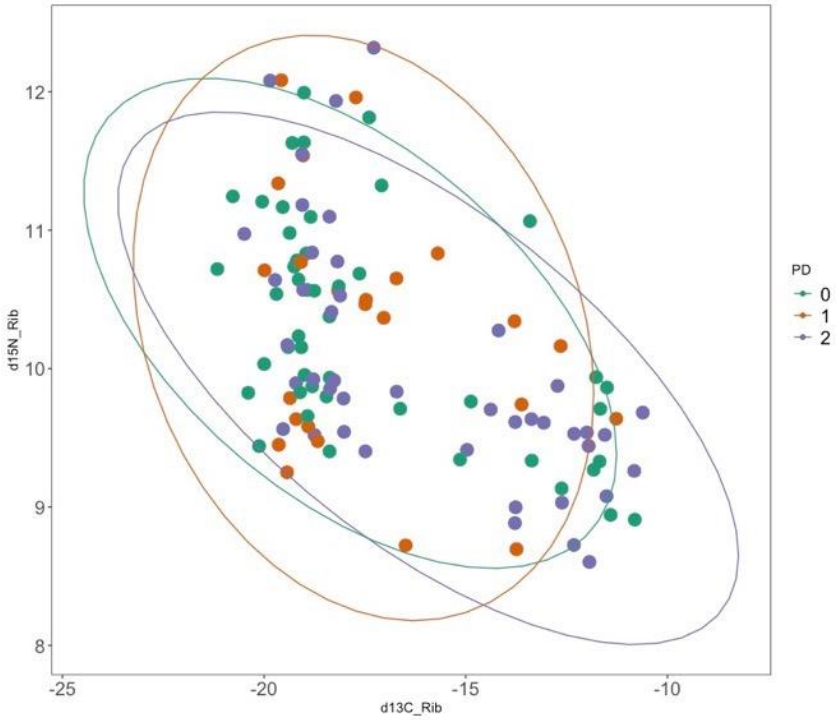


Figure A.94. $\delta^{13}C$ and $\delta^{15}N$ rib values for individuals that are absent (0), present (1), and unobservable (2) for PD with 95% confidence ellipses.

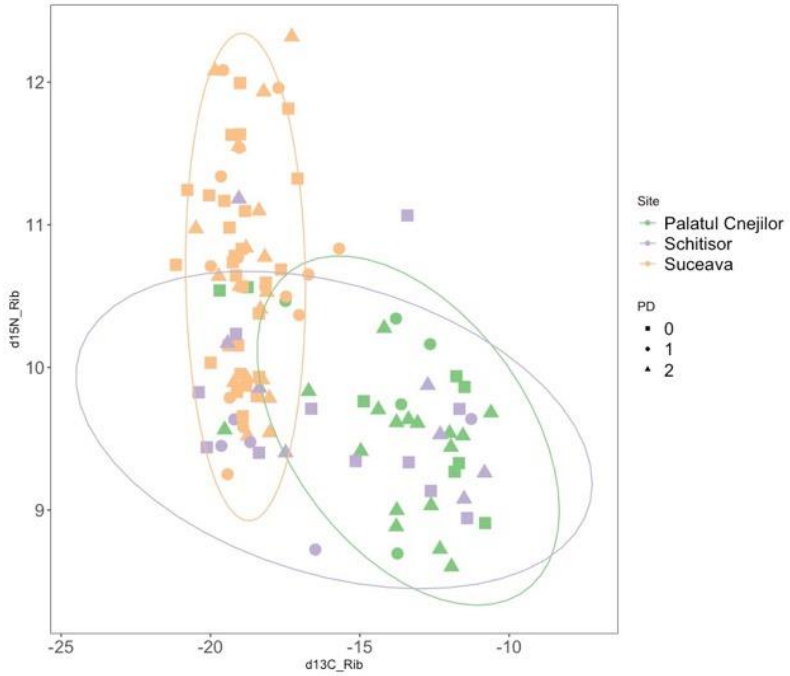


Figure A.95. $\delta^{13}C$ and $\delta^{15}N$ rib values for individuals that are absent (0), present (1), and unobservable (2) for PD by site with 95% confidence ellipses.

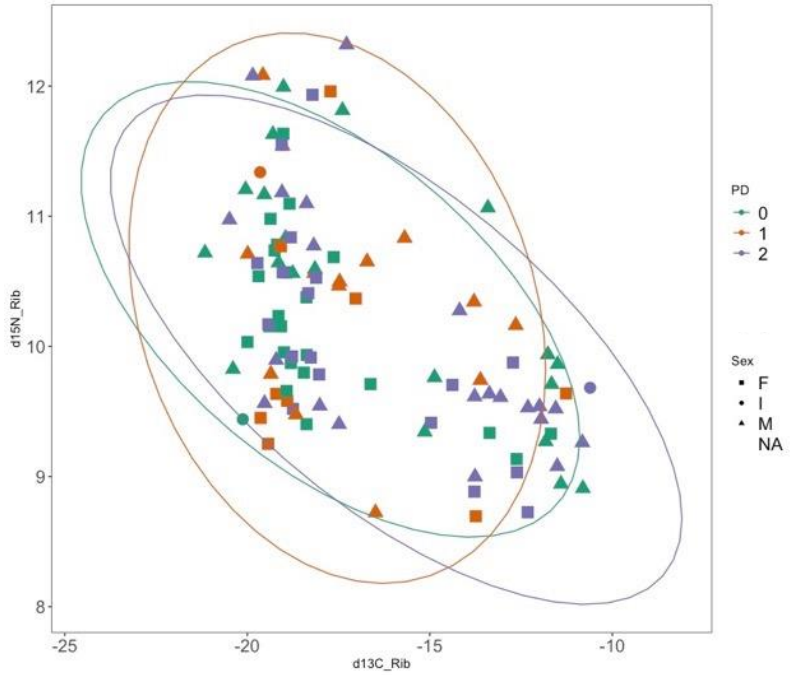


Figure A.96. $\delta^{13}C$ and $\delta^{15}N$ rib values for individuals that are absent (0), present (1), and unobservable (2) for PD by sex with 95% confidence ellipses.

APPENDIX THREE: BAYESIAN MODEL FITS AND MARGINAL EFFECTS PLOTS

Table A.3. All seven model fits for PNBF using different combinations of predictor variables and only femur carbon and nitrogen isotope values.

Model Fit Name	Model Fit for PNBF
fit	PNBF ~ Age + Sex + Site + $\delta^{13}C_{femur}$ + $\delta^{15}N_{femur}$
fit2	PNBF ~ Age + Sex + Site + $\delta^{13}C_{femur}$
fit3	PNBF ~ Age + Sex + Site + $\delta^{15}N_{femur}$
fit4	PNBF ~ Age + Sex + Site
fit5	PNBF ~ Age + Sex
fit6	PNBF ~ Age + Site
fit7	PNBF ~ 1

Table A.4. All seven model fits for PNBF using different combinations of predictor variables and only rib carbon and nitrogen isotope values.

Model Fit Name	Model Fit for PNBF
fit	PNBF ~ Age + Sex + Site + $\delta^{13}C_{rib}$ + $\delta^{15}N_{rib}$
fit2	PNBF ~ Age + Sex + Site + $\delta^{13}C_{rib}$
fit3	PNBF ~ Age + Sex + Site + $\delta^{15}N_{rib}$
fit4	PNBF ~ Age + Sex + Site
fit5	PNBF ~ Age + Sex
fit6	PNBF ~ Age + Site
fit7	PNBF ~ 1

Table A.5. All seven model fits for PH using different combinations of predictor variables and only femur carbon and nitrogen isotope values.

Model Fit Name	Model Fit for PH
fit	PH ~ Age + Sex + Site + $\delta^{13}C_{femur}$ + $\delta^{15}N_{femur}$
fit2	PH ~ Age + Sex + Site + $\delta^{13}C_{femur}$
fit3	PH ~ Age + Sex + Site + $\delta^{15}N_{femur}$
fit4	PH ~ Age + Sex + Site
fit5	PH ~ Age + Sex
fit6	PH ~ Age + Site
fit7	PH ~ 1

Table A.6. All seven model fits for PH using different combinations of predictor variables and only rib carbon and nitrogen isotope values.

Model Fit Name	Model Fit for PH
fit	PH ~ Age + Sex + Site + $\delta^{13}C_{rib}$ + $\delta^{15}N_{rib}$
fit2	PH ~ Age + Sex + Site + $\delta^{13}C_{rib}$
fit3	PH ~ Age + Sex + Site + $\delta^{15}N_{rib}$
fit4	PH ~ Age + Sex + Site
fit5	PH ~ Age + Sex
fit6	PH ~ Age + Site
fit7	PH ~ 1

Table A.7. All seven model fits for CO using different combinations of predictor variables and only femur carbon and nitrogen isotope values.

Model Fit Name	Model Fit for CO
fit	CO ~ Age + Sex + Site + $\delta^{13}C_{femur}$ + $\delta^{15}N_{femur}$
fit2	CO ~ Age + Sex + Site + $\delta^{13}C_{femur}$
fit3	CO ~ Age + Sex + Site + $\delta^{15}N_{femur}$
fit4	CO ~ Age + Sex + Site
fit5	CO ~ Age + Sex
fit6	CO ~ Age + Site
fit7	CO ~ 1

Table A.8. All seven model fits for CO using different combinations of predictor variables and only rib carbon and nitrogen isotope values.

Model Fit Name	Model Fit for CO
fit	CO ~ Age + Sex + Site + $\delta^{13}C_{rib}$ + $\delta^{15}N_{rib}$
fit2	CO ~ Age + Sex + Site + $\delta^{13}C_{rib}$
fit3	CO ~ Age + Sex + Site + $\delta^{15}N_{rib}$
fit4	CO ~ Age + Sex + Site
fit5	CO ~ Age + Sex
fit6	CO ~ Age + Site
fit7	CO ~ 1

Table A.9. All seven model fits for caries using different combinations of predictor variables and only femur carbon and nitrogen isotope values.

Model Fit Name	Model Fit for Caries
fit	Caries ~ Age + Sex + Site + $\delta^{13}C_{femur}$ + $\delta^{15}N_{femur}$
fit2	Caries ~ Age + Sex + Site + $\delta^{13}C_{femur}$
fit3	Caries ~ Age + Sex + Site + $\delta^{15}N_{femur}$
fit4	Caries ~ Age + Sex + Site
fit5	Caries ~ Age + Sex
fit6	Caries ~ Age + Site
fit7	Caries ~ 1

Table A.10. All seven model fits for caries using different combinations of predictor variables and only rib carbon and nitrogen isotope values.

Model Fit Name	Model Fit for Caries
fit	Caries ~ Age + Sex + Site + $\delta^{13}C_{rib}$ + $\delta^{15}N_{rib}$
fit2	Caries ~ Age + Sex + Site + $\delta^{13}C_{rib}$
fit3	Caries ~ Age + Sex + Site + $\delta^{15}N_{rib}$
fit4	Caries ~ Age + Sex + Site
fit5	Caries ~ Age + Sex
fit6	Caries ~ Age + Site
fit7	Caries ~ 1

Table A.11. All seven model fits for abscesses using different combinations of predictor variables and only femur carbon and nitrogen isotope values.

Model Fit Name	Model Fit for Abscesses
fit	Abscesses ~ Age + Sex + Site + $\delta^{13}C_{femur}$ + $\delta^{15}N_{femur}$
fit2	Abscesses ~ Age + Sex + Site + $\delta^{13}C_{femur}$
fit3	Abscesses ~ Age + Sex + Site + $\delta^{15}N_{femur}$
fit4	Abscesses ~ Age + Sex + Site
fit5	Abscesses ~ Age + Sex
fit6	Abscesses ~ Age + Site
fit7	Abscesses ~ 1

Table A.12. All seven model fits for abscesses using different combinations of predictor variables and only rib carbon and nitrogen isotope values.

Model Fit Name	Model Fit for Abscesses
fit	Abscesses ~ Age + Sex + Site + $\delta^{13}C_{rib}$ + $\delta^{15}N_{rib}$
fit2	Abscesses ~ Age + Sex + Site + $\delta^{13}C_{rib}$
fit3	Abscesses ~ Age + Sex + Site + $\delta^{15}N_{rib}$
fit4	Abscesses ~ Age + Sex + Site
fit5	Abscesses ~ Age + Sex
fit6	Abscesses ~ Age + Site
fit7	Abscesses ~ 1

Table A.13. All seven model fits for PD using different combinations of predictor variables and only femur carbon and nitrogen isotope values.

Model Fit Name	Model Fit for PD
fit	PD ~ Age + Sex + Site + $\delta^{13}C_{femur}$ + $\delta^{15}N_{femur}$
fit2	PD ~ Age + Sex + Site + $\delta^{13}C_{femur}$
fit3	PD ~ Age + Sex + Site + $\delta^{15}N_{femur}$
fit4	PD ~ Age + Sex + Site
fit5	PD ~ Age + Sex
fit6	PD ~ Age + Site
fit7	PD ~ 1

Table A.14. All seven model fits for PD using different combinations of predictor variables and only rib carbon and nitrogen isotope values.

Model Fit Name	Model Fit for PD
fit	PD ~ Age + Sex + Site + $\delta^{13}C_{rib}$ + $\delta^{15}N_{rib}$
fit2	PD ~ Age + Sex + Site + $\delta^{13}C_{rib}$
fit3	PD ~ Age + Sex + Site + $\delta^{15}N_{rib}$
fit4	PD ~ Age + Sex + Site
fit5	PD ~ Age + Sex
fit6	PD ~ Age + Site
fit7	PD ~ 1

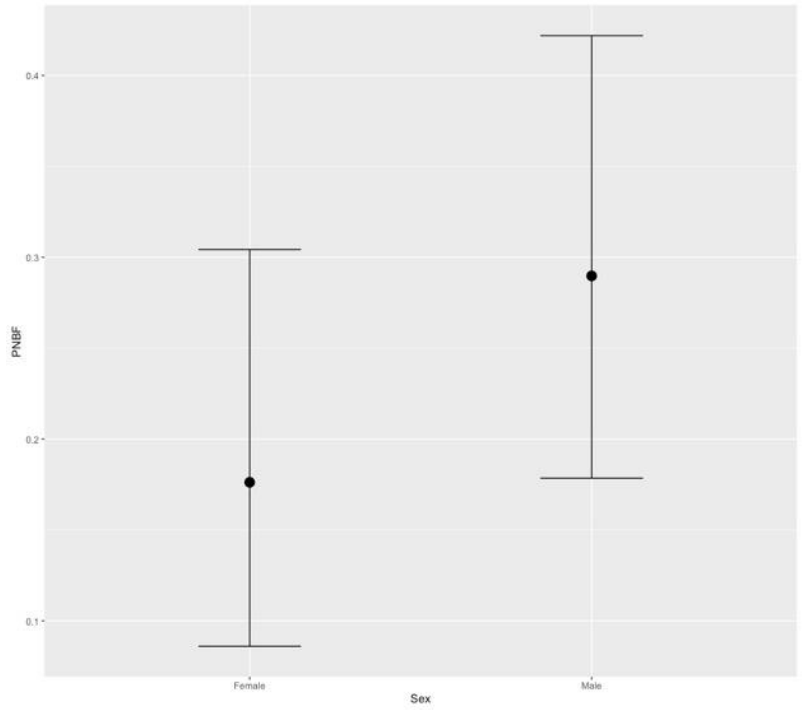


Figure A.97. Marginal effect of sex on PNBF frequency for femur $\delta^{13}C$ and $\delta^{15}N$ values.

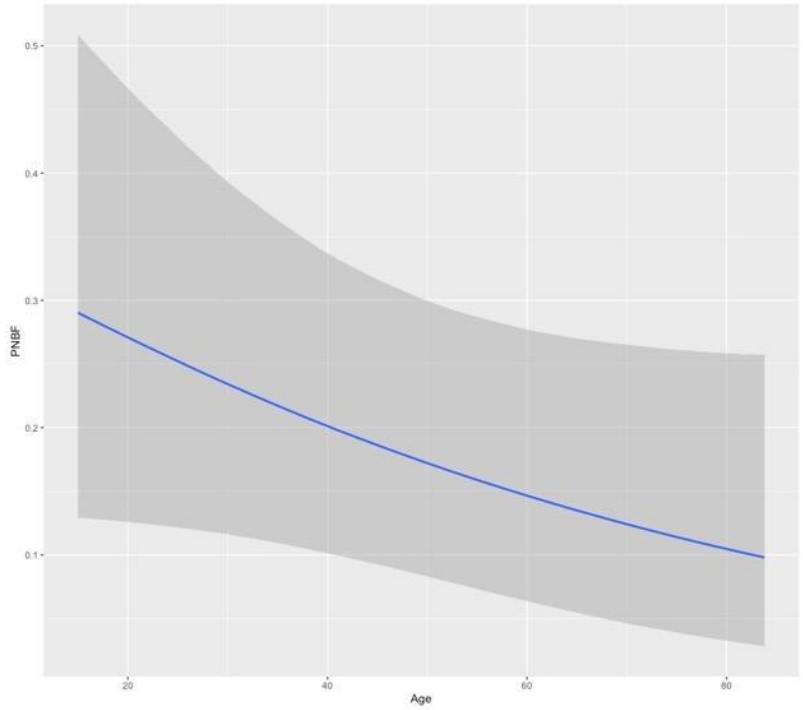


Figure A.98. Marginal effect of age on PNBF frequency for femur $\delta^{13}C$ and $\delta^{15}N$ values.

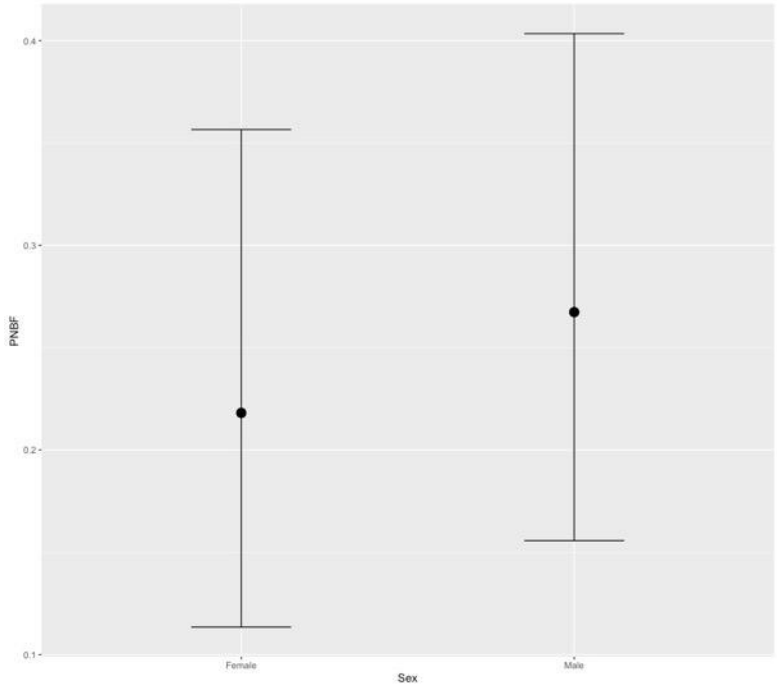


Figure A.99. Marginal effect of sex on PNBF frequency for rib $\delta^{13}C$ and $\delta^{15}N$ values.

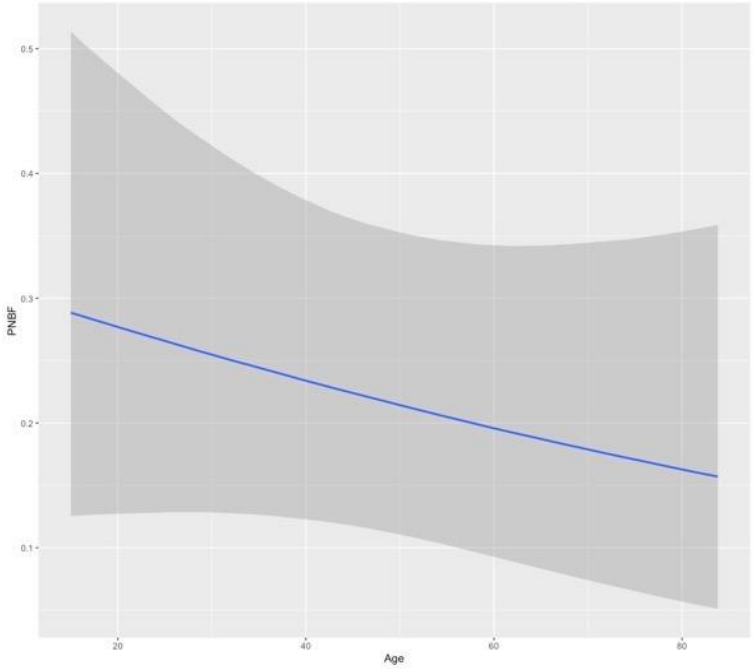


Figure A.100. Marginal effect of age on PNBF frequency for rib $\delta^{13}C$ and $\delta^{15}N$ values.

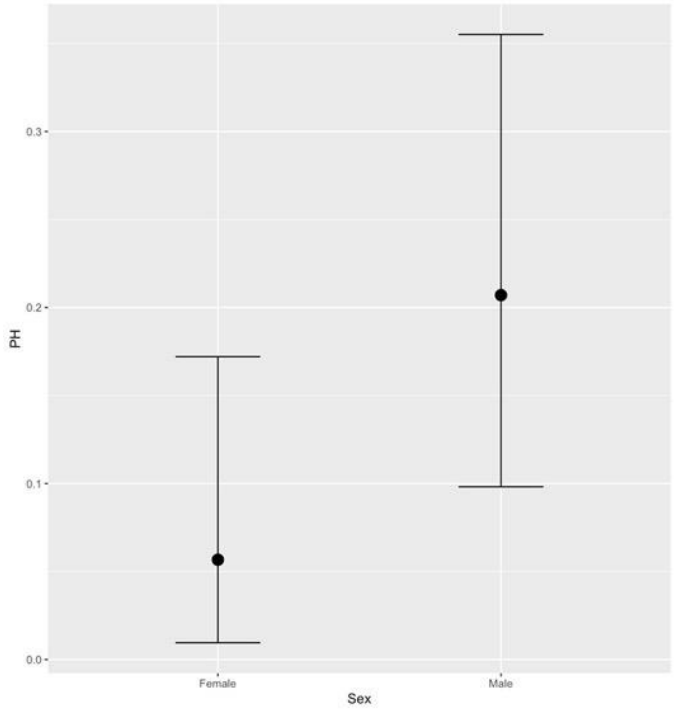


Figure A.101. Marginal effect of sex on PH frequency for femur $\delta^{13}C$ and $\delta^{15}N$ values.

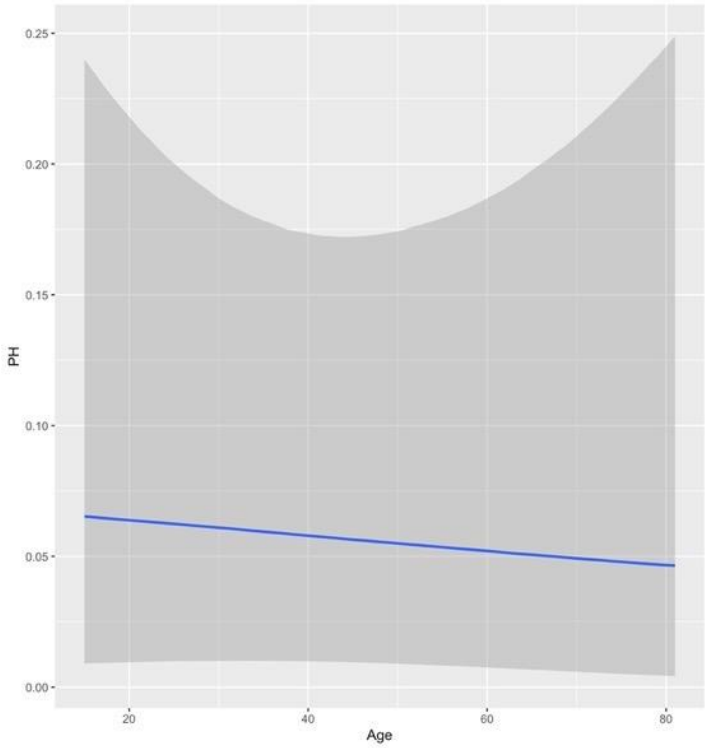


Figure A.102. Marginal effect of age on PH frequency for femur $\delta^{13}C$ and $\delta^{15}N$ values.

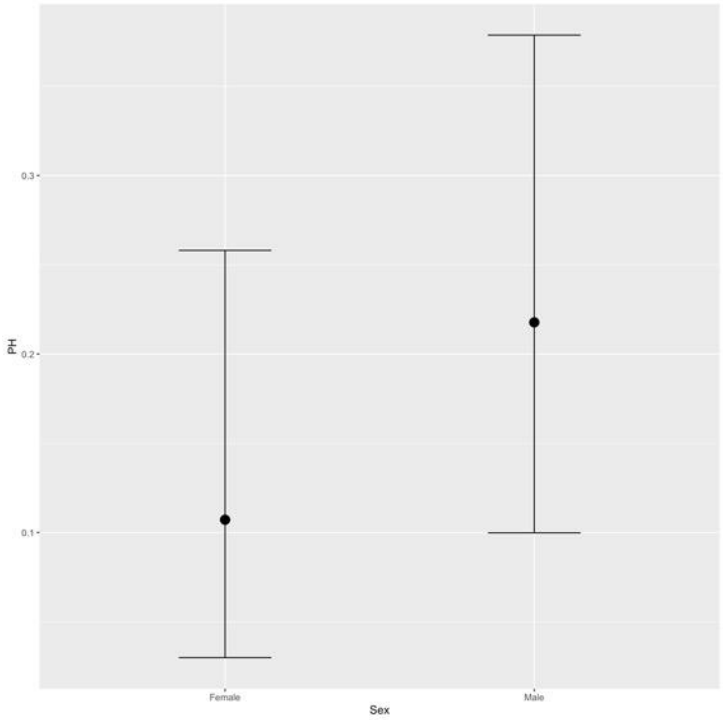


Figure A.103. Marginal effect of sex on PH frequency for rib $\delta^{13}C$ and $\delta^{15}N$ values.

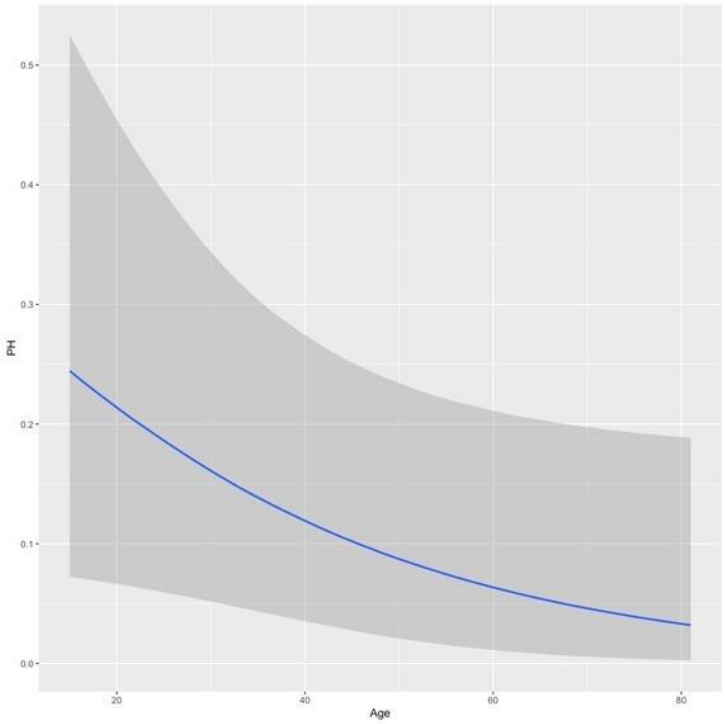


Figure A.104. Marginal effect of age on PH frequency for rib $\delta^{13}C$ and $\delta^{15}N$ values.

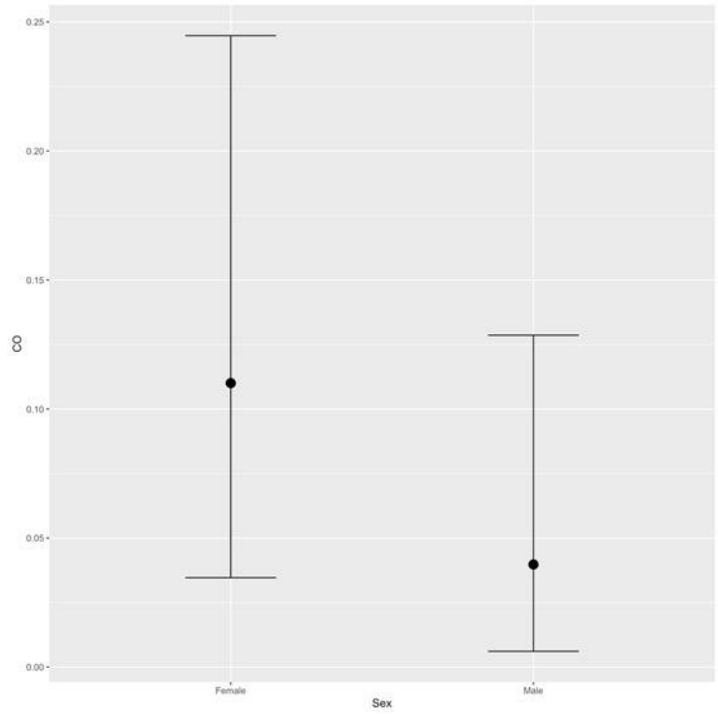


Figure A.105. Marginal effect of sex on CO frequency for femur $\delta^{13}C$ and $\delta^{15}N$ values.

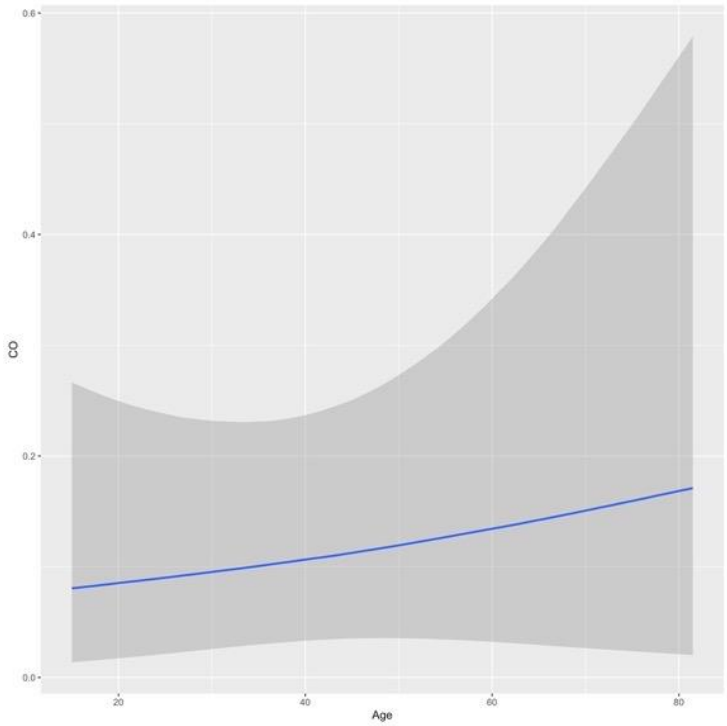


Figure A.106. Marginal effect of age on CO frequency for femur $\delta^{13}C$ and $\delta^{15}N$ values.

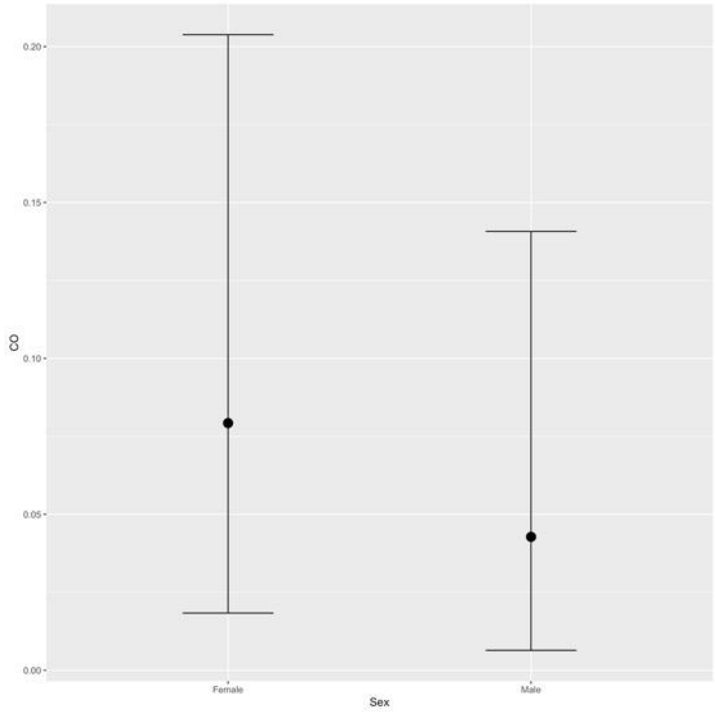


Figure A.107. Marginal effect of sex on CO frequency for rib $\delta^{13}C$ and $\delta^{15}N$ values.

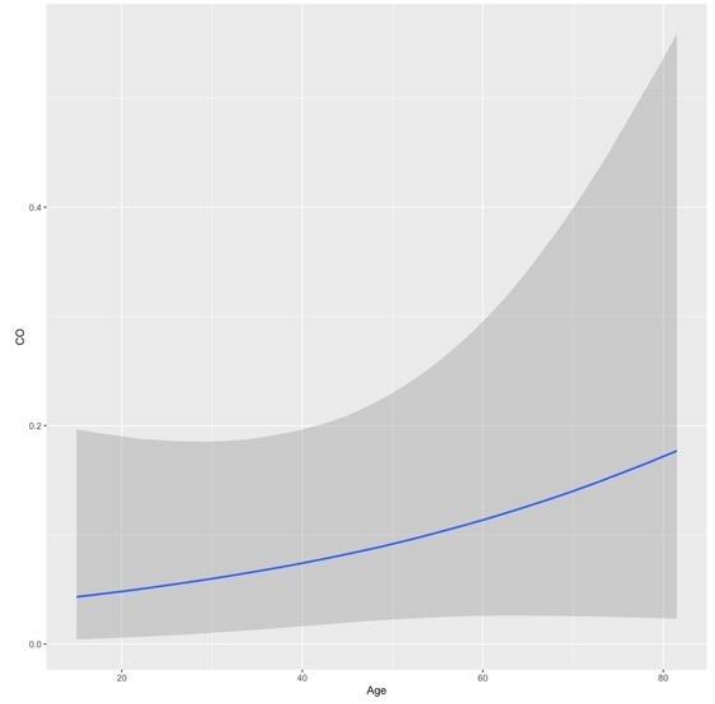


Figure A.108. Marginal effect of age on CO frequency for rib $\delta^{13}C$ and $\delta^{15}N$ values.

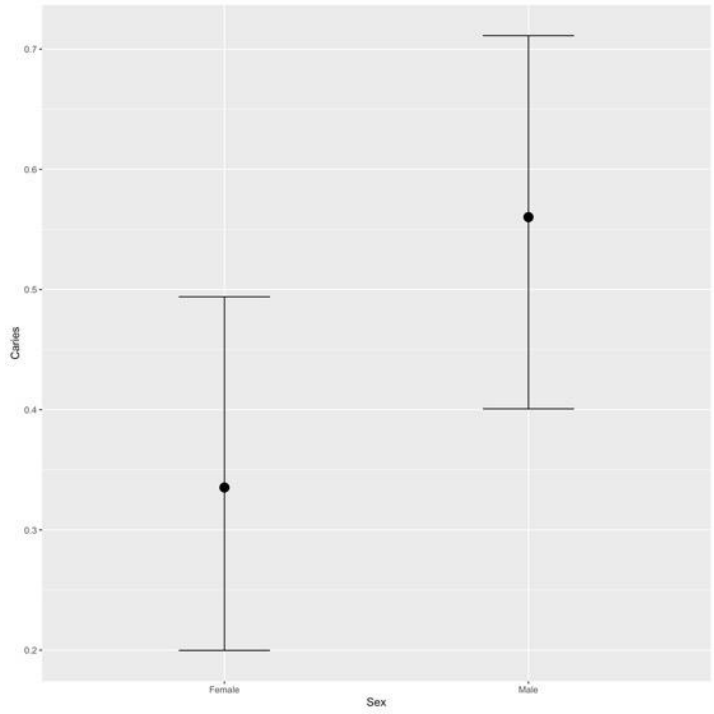


Figure A.109. Marginal effect of sex on caries frequency for femur $\delta^{13}C$ and $\delta^{15}N$ values.

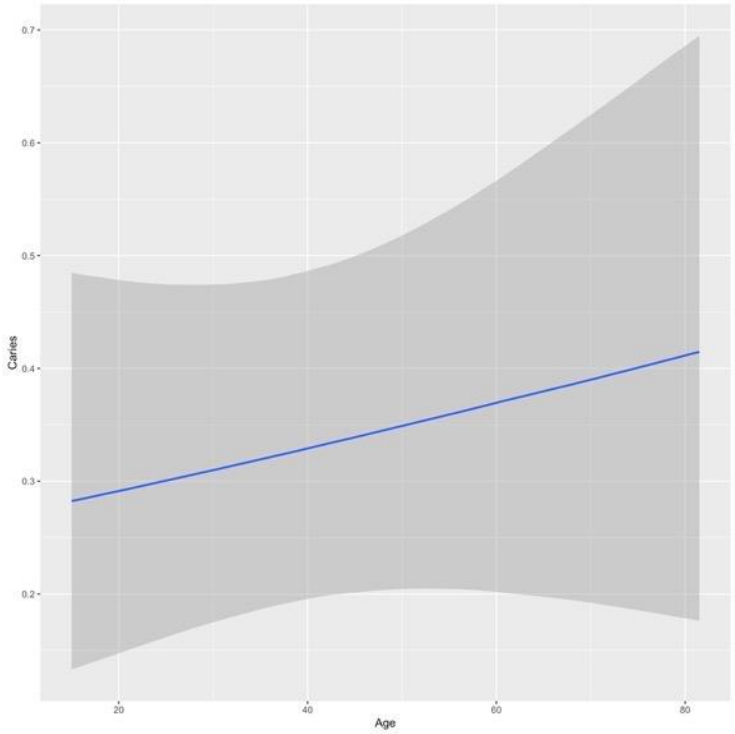


Figure A.110. Marginal effect of age on caries frequency for femur $\delta^{13}C$ and $\delta^{15}N$ values.

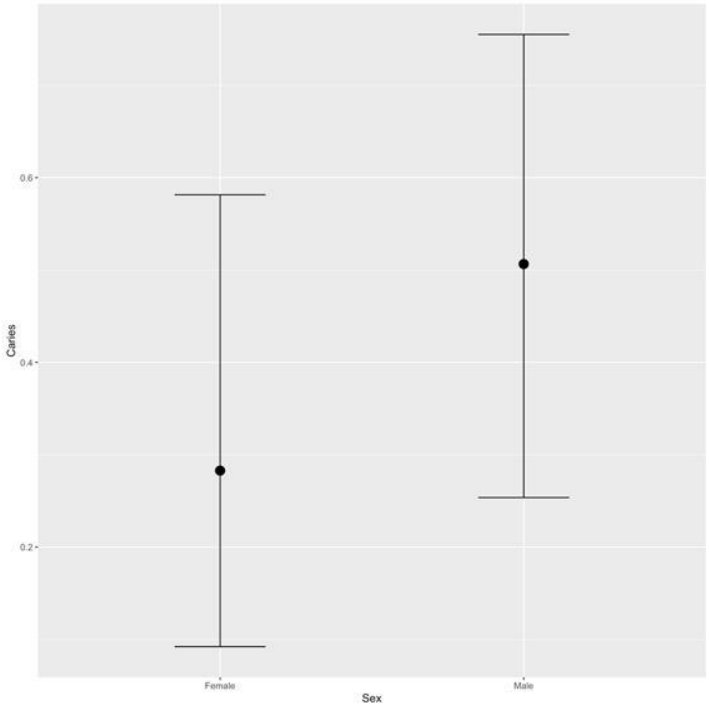


Figure A.111. Marginal effect of sex on caries frequency for rib $\delta^{13}C$ and $\delta^{15}N$ values.

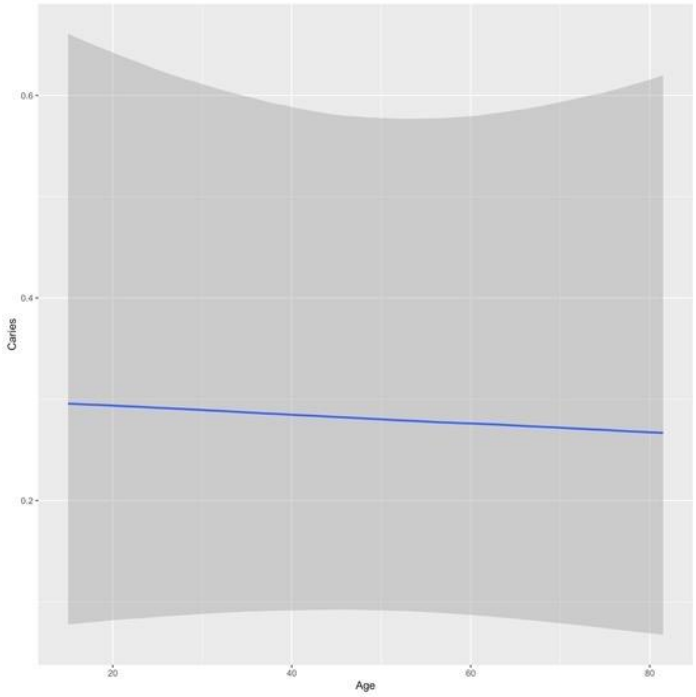


Figure A.112. Marginal effect of age on caries frequency for rib $\delta^{13}C$ and $\delta^{15}N$ values.

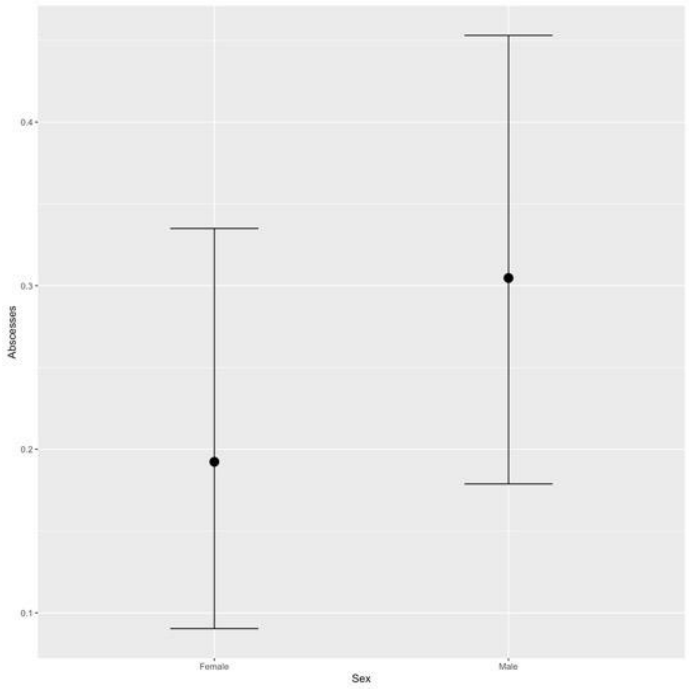


Figure A.113. Marginal effect of sex on abscesses frequency for femur $\delta^{13}C$ and $\delta^{15}N$ values.

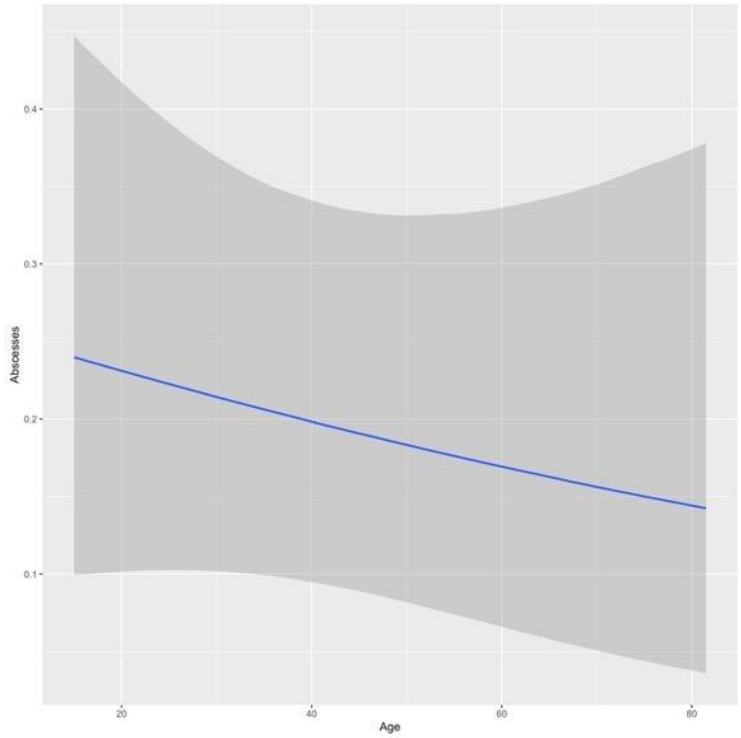


Figure A.114. Marginal effect of age on abscesses frequency for femur $\delta^{13}C$ and $\delta^{15}N$ values.

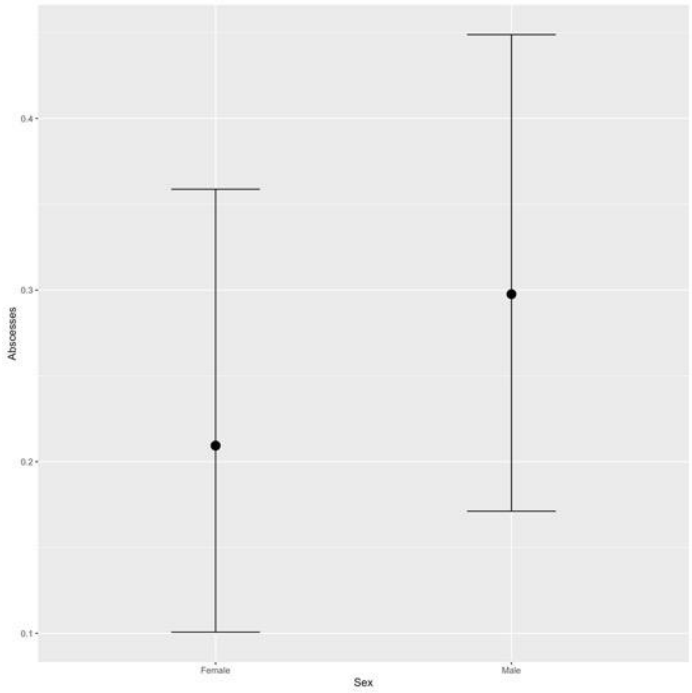


Figure A.115. Marginal effect of sex on abscesses frequency for rib $\delta^{13}C$ and $\delta^{15}N$ values.

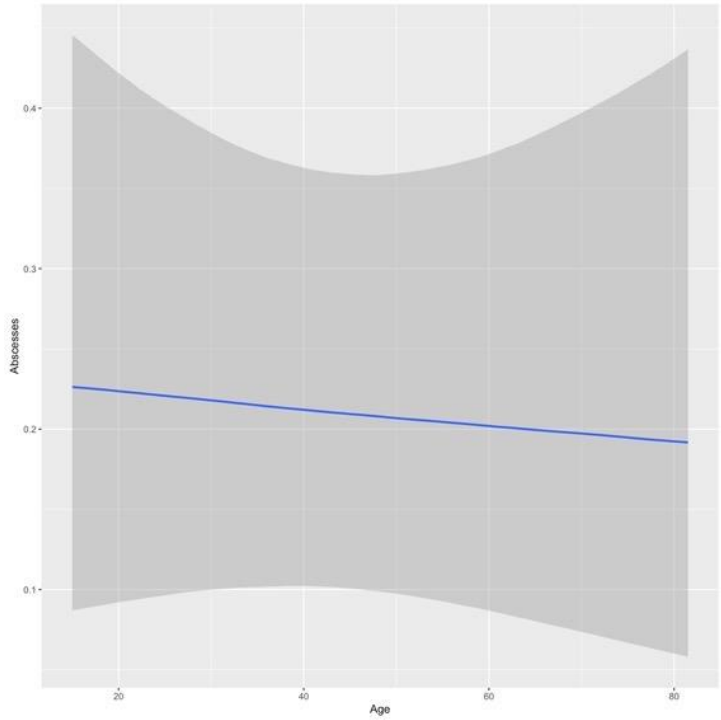


Figure A.116. Marginal effect of age on abscesses frequency for rib $\delta^{13}C$ and $\delta^{15}N$ values.

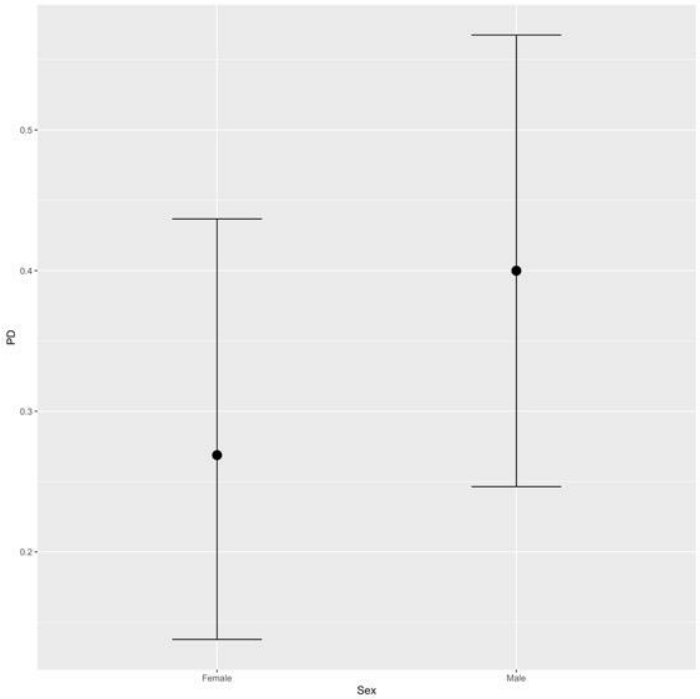


Figure A.117. Marginal effect of sex on PD frequency for femur $\delta^{13}C$ and $\delta^{15}N$ values.

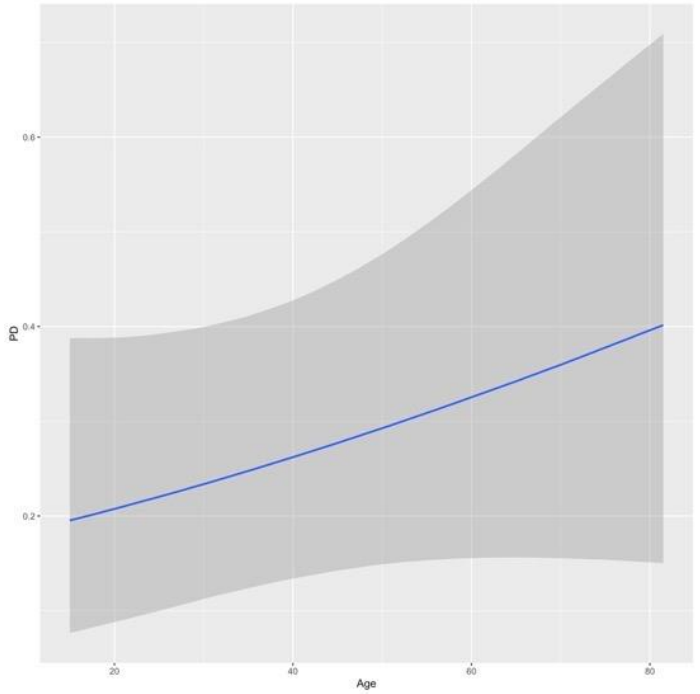


Figure A.118. Marginal effect of age on PD frequency for femur $\delta^{13}C$ and $\delta^{15}N$ values.

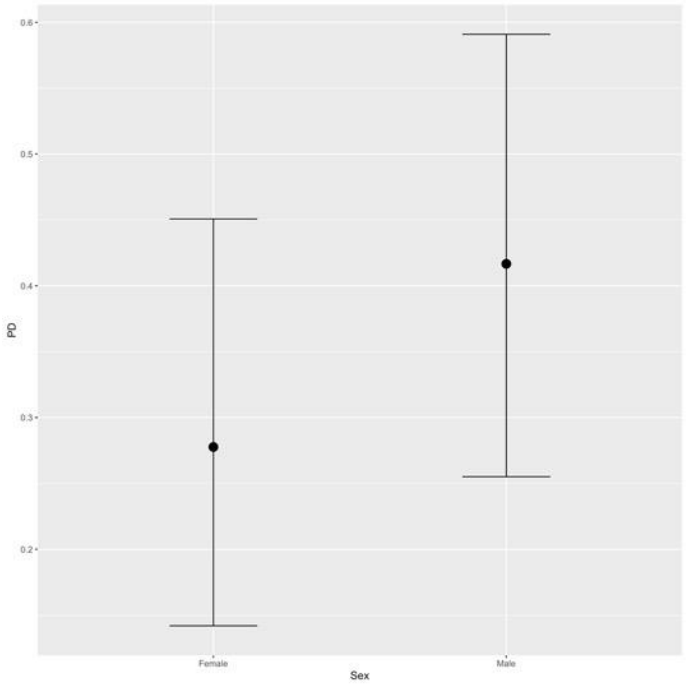


Figure A.119. Marginal effect of sex on PD frequency for rib $\delta^{13}C$ and $\delta^{15}N$ values.

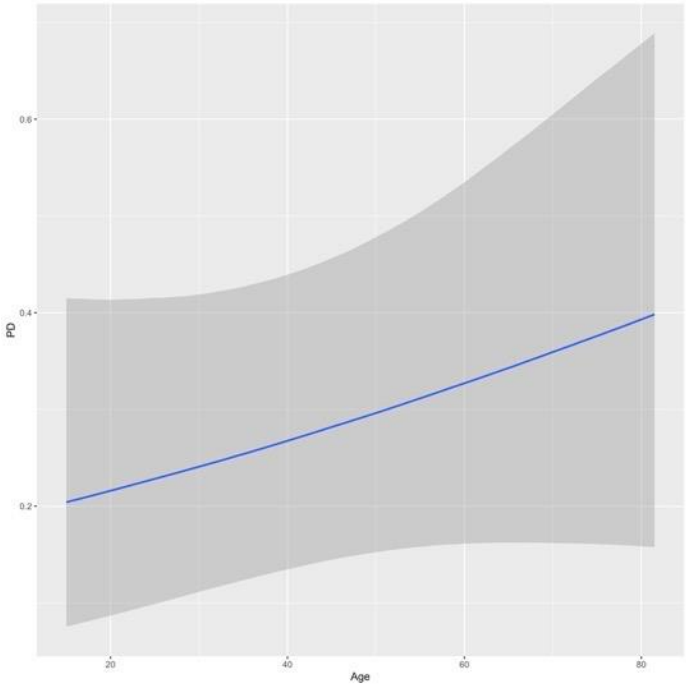


Figure A.120. Marginal effect of age on PD frequency for rib $\delta^{13}C$ and $\delta^{15}N$ values.

APPENDIX FOUR: SURVIVAL TABLES

Means and Medians for Survival Time

	Mean[a]				Median			
			95% Confidence Interval				95% Confidence Interval	
PNBF	Estimate	Std. Error	Lower Bound	Upper Bound	Estimate	Std. Error	Lower Bound	Upper Bound
Absent	50.114	2.271	45.664	54.565	52.000	6.984	38.311	65.689
Present	42.923	3.883	35.313	50.534	34.000	6.847	20.581	47.419
Overall	48.205	1.975	44.335	52.075	42.500	6.214	30.320	54.680

a. Estimation is limited to the largest survival time if it is censored.

Figure A.121. Mean and median survival estimates for individuals with and without PNBF.

Means and Medians for Survival Time

	Mean[a]				Median			
			95% Confidence Interval				95% Confidence Interval	
PH	Estimate	Std. Error	Lower Bound	Upper Bound	Estimate	Std. Error	Lower Bound	Upper Bound
Absent	45.563	2.388	40.883	50.244	37.800	2.570	32.763	42.837
Present	41.325	4.697	32.119	50.531	32.800	6.500	20.060	45.540
Overall	44.784	2.128	40.613	48.954	37.700	1.864	34.046	41.354

a. Estimation is limited to the largest survival time if it is censored.

Figure A.122. Mean and median survival estimates for individuals with and without PH.

Means and Medians for Survival Time

	Mean[a]				Median			
			95% Confidence Interval				95% Confidence Interval	
CO	Estimate	Std. Error	Lower Bound	Upper Bound	Estimate	Std. Error	Lower Bound	Upper Bound
Absent	45.300	2.192	41.004	49.596	37.000	1.844	33.386	40.614
Present	41.067	7.399	26.565	55.568	32.800	7.901	17.314	48.286
Overall	44.895	2.096	40.787	49.002	37.000	1.939	33.200	40.800

a. Estimation is limited to the largest survival time if it is censored.

Figure A.123. Mean and median survival estimates for individuals with and without CO.

Means and Medians for Survival Time

	Mean[a]				Median			
			95% Confidence Interval				95% Confidence Interval	
Caries	Estimate	Std. Error	Lower Bound	Upper Bound	Estimate	Std. Error	Lower Bound	Upper Bound
Absent	44.486	2.787	39.024	49.949	37.000	1.523	34.015	39.985
Present	47.410	3.334	40.875	53.945	45.800	7.554	30.994	60.606
Overall	45.662	2.133	41.482	49.842	37.700	2.707	32.394	43.006

a. Estimation is limited to the largest survival time if it is censored.

Figure A.124. Mean and median survival estimates for individuals with and without caries.

Means and Medians for Survival Time

	Mean[a]				Median			
			95% Confidence Interval				95% Confidence Interval	
Abscesses	Estimate	Std. Error	Lower Bound	Upper Bound	Estimate	Std. Error	Lower Bound	Upper Bound
Absent	46.772	2.576	41.722	51.821	37.000	8.925	19.507	54.493
Present	44.230	3.208	37.941	50.518	37.800	2.466	32.966	42.634
Overall	46.092	2.068	42.038	50.146	37.800	2.923	32.070	43.530

a. Estimation is limited to the largest survival time if it is censored.

Figure A.125. Mean and median survival estimates for individuals with and without abscesses.

Means and Medians for Survival Time

	Mean[a]				Median			
			95% Confidence Interval				95% Confidence Interval	
PD	Estimate	Std. Error	Lower Bound	Upper Bound	Estimate	Std. Error	Lower Bound	Upper Bound
Absent	43.454	2.647	38.265	48.643	36.100	2.778	30.656	41.544
Present	48.368	4.293	39.953	56.783	39.800	4.746	30.497	49.103
Overall	44.850	2.253	40.434	49.266	37.000	2.626	31.853	42.147

a. Estimation is limited to the largest survival time if it is censored.

Figure A.126. Mean and median survival estimates for individuals with and without PD.

APPENDIX FIVE: ENAMEL CARBON STABLE ISOTOPE DATA, STANDARDS, AND METHODS

Table A.15. Carbon stable isotope data of bone collagen and enamel apatite.

Sample ID	δ^{13}Cvpdb_coll	δ^{13}Cvpdb_apa
PC_M2_#25	-12.736	-6.055
PC_M2_#26	-13.739	-8.013
PC_M2_#27	-15.214	-9.304
PC_M2_#28	-19.833	-11.880
PC_M2_#29	-12.645	-4.614
PC_M2_#31	-11.143	-3.798
PC_M2_#33	-13.773	-4.558
PC_M2_#34	-18.837	-11.158
PC_M2_#35	-18.111	-9.328
PC_M2_#36	-11.900	-7.612
PC_M2_#37	-13.103	-4.529
SCHIT_M2_#38	-11.074	-4.379
SCHIT_M2_#39	-13.425	-9.723
SCHIT_M2_#41	-18.761	-12.299
SCHIT_M2_#42	-19.387	-10.451
SCHIT_M2_#44	-16.626	-6.435
SCHIT_M2_#45	-10.841	-3.872
SCHIT_M2_#46	-18.556	-9.983
SCHIT_M2_#47	-13.062	-6.454
SCHIT_M2_#48	-9.776	-2.625
SCHIT_M2_#49	-17.600	-11.925
SUC_M2_#50	-19.394	-12.253
SUC_M2_#51	-18.774	-9.308
SUC_M2_#53	-18.433	-9.084
SUC_M2_#54	-18.709	-10.326
SUC_M2_#63	-19.432	-12.806
SUC_M2_#68	-19.599	-13.095
SUC_M2_#69	-19.299	-12.799
SUC_M2_#70	-16.773	-11.940
SUC_M2_#71	-18.794	-12.103
SUC_M2_#72	-18.084	-11.143
SUC_M2_#73	-18.793	-11.804
SUC_M2_#76	-18.429	-11.971

Table A.15 Continued

SUC_M2_#77	-16.759	-13.584
SUC_M2_#78	-18.693	-11.949
SUC_M2_#79	-18.868	-11.703
SUC_M2_#80	-18.818	-10.615
SUC_M2_#81	-20.527	-13.231
SUC_M2_#83	-18.763	-10.554
SUC_M2_#87	-18.847	-8.463
SUC_M2_#88	-18.697	-12.078
SUC_M2_#89	-19.293	-11.283
SUC_M2_#90	-17.865	-5.506
SUC_M2_#91	-19.156	-12.559
SUC_M2_#94	-19.758	-13.098
SUC_M2_#95	-18.750	-10.514
SUC_M2_#97	-19.284	-13.634
SUC_M2_#98	-18.863	-10.739
SUC_M2_#99	-19.313	-11.274
SUC_M2_#100	-20.522	-12.994
SUC_M2_#101	-19.106	-10.670
SUC_M2_#102	-18.743	-11.734
SUC_M2_#103	-16.917	-13.686
SUC_M2_#104	-17.255	-8.397
SUC_M2_#105	-19.891	-12.684
SUC_M2_#106	-20.235	-13.017
SUC_M2_#107	-18.339	-10.246
SUC_M2_#108	-19.275	-11.809
SUC_M2_#110	-14.817	-2.120
SUC_M2_#111	-15.930	-11.194
SUC_M2_#112	-18.947	-12.472
SUC_M2_#113	-18.974	-11.961
SUC_M2_#114	-18.412	-11.636
SUC_M2_#115	-18.149	-10.906
SUC_M2_#116	-18.931	-10.783
SUC_M2_#118	-18.307	-12.118
SUC_M2_#119	-18.371	-12.150
SUC_M2_#120	-17.083	-9.864
SUC_M2_#121	-18.807	-10.515
SUC_M2_#123	-18.189	-11.594

Table A.15 Continued

SUC_M2_#124	-18.423	-11.165
SUC_M2_#128	-17.636	-10.649
SUC_M2_#130	-18.482	-9.957

Enamel Pre-Treatment Protocol and Analysis

A total of 74 enamel samples from the permanent second molar were pre-treated and analyzed for carbon and oxygen stable isotope analysis. Enamel pre-treatment occurred at the University of Tennessee in the Zooarchaeology Laboratory in the Department of Anthropology and stable isotope analysis occurred in the Department of Earth, Environmental, and Planetary Sciences Stable Isotope Laboratory.

Pretreatment Protocol

At least 5 mg of enamel powder was weighed out on a micro-balance and collected in a pre-labeled and weighed 1.5 mL microcentrifuge tube. Pre-treatment of enamel samples followed the protocol in (Roberts et al. 2020). 5% sodium hypochlorite (NaClO) was diluted to 2.5% NaClO, and 100 μL of NaClO per mg of enamel sample was pipetted into each sample following the protocol from Balasse (2002).

Each sample was vortexed and left to sit for 60 minutes. Samples were placed in a centrifuge for at least four minutes to fully separate the enamel powder from the NaClO. The NaClO was pipetted out, rinsing the pipette tip twice in ultra-purified water in between each sample. Each sample was rinsed with ultra-purified water: ultra-purified water was pipetted in, samples were vortexed, centrifuged for at least 4 minutes, and water was pipetted out. This process was repeated three times to ensure the NaClO was completely removed.

To remove exogenous carbonates from the enamel samples, 0.1 M acetic acid combined with buffered sodium acetate was added to each enamel sample (100 μL per mg of sample). Each sample was vortexed and left to sit for 10 minutes. The buffered acetic acid was pipetted out and then each sample was rinsed three times with ultra-purified water using the same rinsing protocol

as the NaOCl. Samples were then placed in a lab oven, with caps open, at 33˚C overnight. Final sample weights were recorded.

Analysis and Standards

Between 2-3 mg of the pretreated enamel was weighed on a micro-balance and collected in glass vials. The samples were analyzed for $\delta^{13}C$ and $_{d}{}^{18}O$ on a Gas Bench II and Thermo-Finnigan Delta+XL Mass Spectrometer. For every 12 samples, two in-house standards were used, ANUM1 and CALSED, and samples were corrected to these standards. Isotopic ratios ($\delta^{13}C$ and $\delta^{18}O$) of these in-house standards were calibrated against two international standards, LSVEC and NBS 19 with $\delta^{13}C$ values of -46.6‰ and 1.95‰, respectively, and $\delta^{18}O$ values of -26.41‰ and -2.2‰, respectively. Across six runs, the in-house standard ANUM1 yielded a mean $\delta^{13}C$ value of 1.27‰ (expected value 1.27‰), and a mean $\delta^{18}O$ value of -6.07‰ (expected value -6.07‰). The in-house standard CALSED yielded a mean $\delta^{13}C$ value of -40.28‰ (expected value -40.28‰), and a mean $\delta^{18}O$ value of -22.72‰ (expected value -22.72‰). All isotopic results were scale normalized to the expected values of the in-house standards.

Stable isotope ratios of enamel apatite were reported as delta (δ) values relative to an international standard. For both carbon and oxygen ratios in apatite, this was Vienna Pee Dee Belemnite (VPDB). Values are reported using the (‰) notation, where d(‰) = (Rsample/Rstandard)-1, and R is the heavy/light isotope ratio for a particular element.

VITA

Jenna Mackenzie Spears Watson was born on October 15, 1990 in Tucson, AZ. She and her family moved to Vancouver, WA in 1997 and she graduated from Skyview High School in 2009. After high school, she attended Wellesley College in Wellesley, MA, and graduated with a B.A. in Anthropology in 2013. After college, Jenna spent 10 months serving as a Corps Member with AmeriCorps National Civilian Community Corps (NCCC)-FEMA Corps providing administrative support to FEMA's disaster preparedness, response, and recovery projects at FEMA regional offices in Kansas City, MO and Denton, TX, and FEMA headquarters in Washington D.C. After graduating from the program in 2014, she moved to New York City where she worked as the office manager and executive assistant to the executive director of Physicians for Human Rights (PHR). In 2016 Jenna began graduate school at the University of Tennessee (UT)-Knoxville, earning her M.A. in anthropology in 2018. As a master's student at UT Knoxville, Jenna worked as a research assistant on a Department of Defense grant-funded research project assessing different techniques for locating clandestine graves, and as the communications and correspondence manager for the Forensic Anthropology Center's (FAC) Body Donation Program. In the fall of 2018, Jenna began the Ph.D. program at UT Knoxville where she taught courses on introduction to biological anthropology, human osteology, human anatomy, and hominin paleobiology in the Department of Anthropology as well as a dissection-based human gross anatomy course to students in the Physician Assistant (PA) program at High Point University in High Point, NC. At the FAC, she assisted with forensic casework, assisted with various grant-funded research projects on rapid DNA for Disaster Victim Identification (DVI) and estimating the post-mortem interval, taught laboratory and field-based forensic anthropology methods courses to students and medicolegal professionals, and completed an

internship at the West Tennessee Regional Forensic Center in Memphis, TN. Jenna was also involved with the Anthropology Graduate Student Association (AGSA) as the biological subfield and carrel representative and assisted with coordinating professional development programs with the Undergraduate Anthropology Association (UAA). In 2021 Jenna received a Fulbright Research Grant to Romania from the Fulbright U.S. Student program to complete her dissertation data collection. She spent nine months in Bucharest, Romania analyzing and sampling three skeletal assemblages at the Francisc I. Rainer Institute of Anthropology (FRIA). She received her Ph.D. in anthropology from UT Knoxville in 2024. In August 2024, she joined the anatomy faculty at the University of Massachusetts (UMass) Chan Medical School as an Assistant Professor of Radiology in the Department of Radiology, Division of Translational Anatomy.